



NATIONAL AERONAUTICS AND SPACE ADMINISTRATION

1418

EARTH RESOURCES AIRCRAFT PROGRAM

STATUS REVIEW

VOLUME II

AGRICULTURE, FORESTRY, AND SENSOR STUDIES

Presented at the

NASA Manned Spacecraft Center
Houston, Texas

September 16 to 18, 1968

N71-16147

(ACCESSION NUMBER)

452 G3

(PAGES)

TMX 602565

(NASA CR OR TMX OR AD NUMBER)

FACILITY FORM 602

N71-16165

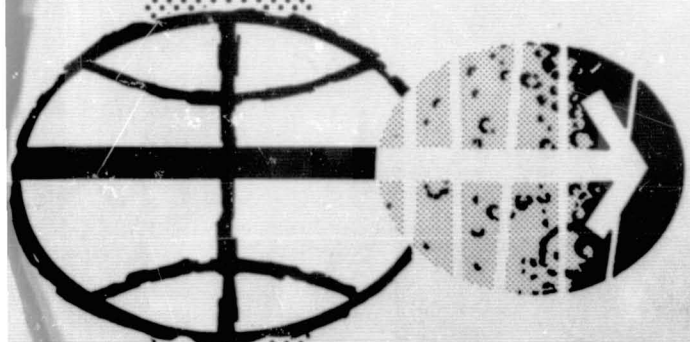
(CODE)

14

(CATEGORY)



MANNED SPACECRAFT CENTER
HOUSTON, TEXAS



PRECEDING PAGE BLANK NOT FILMED

iii

CONTENTS

Section	Page
1 INTRODUCTION	1-1
28 PHOTOGRAPHIC STUDIES AND APPLICATIONS OF THE NASA EARTH RESOURCES SURVEY PROGRAM	28-1 ✓
By Robert N. Colwell	
29 INTEGRATION OF DETAILED LABORATORY AND FIELD STUDIES WITH THE AIRCRAFT PROGRAM	29-1 ✓
By Victor I. Myers and Ross W. Leamer	
30A CROP AND SOIL IDENTIFICATION FROM AERIAL PHOTOGRAPHS	30A-1 ✓
By R. W. Leamer and D. A. Weber	
30B REFLECTANCE AND STRUCTURE OF CYCOCEL-TREATED COTTON LEAVES, <u>Gossypium hirsutum</u> L.	30B-1 ✓
By H. W. Gausman, R. Cardenas, W. A. Allen, V. I. Myers, and R. W. Leamer	
30C REFLECTANCE PRODUCED BY A PLANT LEAF	30C-1 ✓
By W. A. Allen, A. J. Richardson, and H. W. Gausman	
31 BIOPHYSICAL RESEARCH AT LARS-PURDUE	31-1 ✓
By Roger M. Hoffer	
32 DATA PROCESSING PROGRAMS AT LARS-PURDUE	32-1 ✓
By D. A. Landgrebe	
33 PHYSICAL MEASUREMENTS PROGRAMS AT LARS-PURDUE	33-1 ✓
By Roger A. Holmes	
34 RADAR AS A SENSOR IN AGRICULTURE	34-1 ✓
By D. S. Simonett	

Section

Page

- 35 WILDLAND RESOURCE INVENTORIES UNDER THE NASA EARTH
RESOURCES SURVEY PROGRAM 35-1 ✓
By William C. Draeger
- 36 DEVELOPING SPECTROSIGNATURE INDICATORS OF ROOT DISEASE
ON LARGE FOREST AREAS 36-1 ✓
By John F. Wear
- 37 DETECTION OF FOREST INSECT OUTBREAKS BY REMOTE
SENSING 37-1 ✓
By R. C. Heller
- 38 THE IDENTIFICATION OF WESTERN FOREST SPECIES BY MEANS OF
REMOTE SENSING 38-1 ✓
By Donald T. Lauer
- 39 REMOTE-SENSING APPLICATIONS FOR THE INVENTORY OF RANGE
RESOURCES 39-1 ✓
By David M. Carnegie
- 40 THE FEASIBILITY OF INVENTORYING NATIVE VEGETATION AND
RELATED RESOURCES FROM SPACE PHOTOGRAPHY 40-1 ✓
By Charles E. Poulton
- 41 RESULTS OF EARTH RESOURCE INVESTIGATIONS 41-1 ✓
By Marvin R. Holter
- 50 RADAR PROGRESS IN THE NASA EARTH RESOURCES AIRCRAFT
PROGRAM 50-1 ✓
By R. K. Moore
- 51 INFRARED STUDIES 51-1 ✓
By D. S. Lowe

TABLES

Table		Page
28-I	FEASIBILITY OF IDENTIFYING VARIOUS NATURAL RESOURCE FEATURES IN AERIAL AND SPACE PHOTOGRAPHY, BASED ON STUDIES CONDUCTED AT NASA TEST SITES IN CALIFORNIA AND ARIZONA	28-16
28-II	MAJOR TERRAIN-VEGETATION TYPES	28-18
28-III	DISCREPANCY ANALYSIS FOR MAJOR GEOLOGIC TYPES	28-18
28-IV	A TABULAR SUMMARY OF CHARACTERISTICS GOVERNING THE FEASIBILITY OF REMOTE SENSING IN VARIOUS PARTS OF THE ELECTROMAGNETIC SPECTRUM	28-19
29-I	DATA MEANS FOR THE MICRODENSITOMETER TRACES OF FIGURES 29-11 TO 29-13	29-9
34-I	REPORT ON STUDIES AT GARDEN CITY, KANSAS, TEST SITE 76	34-19
34-II	REPORT ON STUDIES AT HORSEFLY MOUNTAIN, OREGON, TEST SITE 159 USING NASA/MSO AND NASA-FUNDED AIRCRAFT DATA	34-21
37-I	EMITTANCE TEMPERATURES (IN DEGREES KELVIN) OF GRASS AND A RESOLUTION TARGET MEASURED WITH A BARNES PRT-5 RADIOMETER — 8.0 μ TO 14.0 μ	37-29
37-II	EMITTANCE TEMPERATURES (IN DEGREES KELVIN) OF TREE FOLIAGE AND FOREST FLOOR IN SUN AND SHADE AS MEASURED WITH A STOLL-HARDY HL-4 — SPECTRAL BANDPASS > 3.5 μ	37-30
37-III	GROUND RESOLUTION FOR THE HRB SINGER RECONOFAX XI AT 1500 TO 2000 FEET ABOVE THE TERRAIN DURING THREE DAYLIGHT TIME PERIODS — JUNE 16 TO 18, 1967	37-31
37-IV	GROUND RESOLUTION FOR THE TEXAS INSTRUMENTS RS-7 AT 2000 FEET ABOVE THE TERRAIN DURING TWO DAY LIGHT TIME PERIODS — JUNE 16 AND 18, 1967	37-32
39-I	FEASIBILITY OF INTERPRETING SIGNIFICANT RANGE FEATURES AND CONDITIONS	39-10

Table		Page
39-II	REMOTE SENSORS OPERATED OVER RANGELAND	39-11
39-III	GROUND INFORMATION COLLECTED TO ANALYZE REMOTE- SENSING DATA	39-12
40-I	COMPARATIVE VALUE OF LIVESTOCK PRODUCTS FROM THE NATIONAL FORESTS	40-19
51-I	SCANNER-SPECTROGRAPH SPECIFICATIONS	51-4

FIGURES

Figure		Page
28-1	These two panchromatic aerial photographs of an Alaskan streambed illustrate the use of sequential photography to detect changes which occur in a period of several seconds	28-20
28-2	These two IR aerial photographs of a cereal crop nursery on the Davis campus of the University of California illustrate the use of sequential photography to detect changes which occur in the development of black stem rust on wheat and oats in a period of several days	28-21
28-3	These two space photographs of the agricultural lands surrounding Willcox Dry Lake in Arizona illustrate the use of sequential photography spanning a period of several weeks to differentiate perennial crops such as alfalfa from annual crops such as wheat . . .	28-22
28-4	These two panchromatic aerial photographs of a forested area in Oregon illustrate the use of sequential photography spanning a period of several months for determining the location and areal extent of timber harvesting operations, as explained in the text . . .	28-23
28-5	The purpose of this sequential photography is to demonstrate the extent to which previsual symptoms of loss of vigor in plants can be made manifest through use of the proper wavelengths of radiant energy when taking the photographs. Shown here is a mangrove swamp near Brisbane, Australia	
	a. Comparison of panchromatic and IR photographs taken in December 1966 by Australian Bureau of Mineral Resources	28-24
	b. This photograph taken by Colwell in September 1968 shows, consistent with our predictions that had been made from a study of the earlier photography, virtually all of the trees on the left of the levee have died in the interim, whereas those on the right of the levee remain vigorous	28-25

Figure		Page
28-6	These two panchromatic aerial photographs of an area in the Sierra Nevada Mountains of California illustrate the usefulness of sequential photography to detect changes which occur in a period of several years	
a.	1944	28-26
b.	1968. From a comparison of the two photographs, it is evident that part of the grassland area has been invaded by brush and that part of the brushland area has been invaded by conifers during the intervening 24-year period	28-27
28-7	The two members comprising this pair of sequential photographs are separated by a time interval of 100 years. Both were taken from exactly the same spot on Glacier Point, Yosemite National Park, and with the same camera orientation. Since the process of plant succession occurs very slowly on sites such as the one shown here, a time span of this length is highly desirable	28-28
28-8	An oblique aerial photograph taken from the point indicated on the Gemini photograph of figure 28-10	28-29
28-9	Characteristic Central Australian topography appears in this photograph taken from the Gemini V spacecraft on August 27, 1965, from an altitude of 165 miles . . .	28-30
28-10	Essentially the same tone values are exhibited by the aerial photograph on the left as on the matching space photograph on the right	28-31
28-11	These two maps permit a determination to be made of the accuracy with which boundaries of major vegetation types can be interpreted and delineated on space photography	
a.	Interpretation of major vegetation types on Gemini photography	28-32
b.	Ground truth for major vegetation types	28-33

Figure		Page
28-12	These two maps permit a determination to be made of the accuracy with which boundaries of major geographic types can be interpreted and delineated on space photography	
a.	Interpretation of major geologic types on Gemini photography	28-34
b.	Ground truth for major geologic types	28-35
29-1	Apollo mission 502 color photography of areas in north Texas (April 4, 1968)	
a.	AS6-2-1454	29-10
b.	AS6-2-1460	29-10
c.	AS6-2-1462	29-11
d.	AS6-2-1483	29-11
29-2	Spectrophotometer scans of color transparencies from Apollo mission 502. See figure 29-1 for identification of areas scanned. Trace no. 4 was made with a 3× magnification	29-12
29-3	Spectrophotometer scans of color transparencies from Apollo mission 502. See figure 29-1 for identification of areas scanned	29-13
29-4	Spectrophotometer scans of color transparencies from NASA aircraft mission 75, Site 32, Weslaco, Texas	29-14
29-5	Double-row planted cotton, showing total illumination of soil. Flight line 13, time 14:18 hours, July 25, 1968	29-15
29-6	Black and white print from an Ektachrome infrared aerial transparency of cotton field shown in figure 29-5. Flight altitude 3000 feet, 15:28 hours, scale 1:18 000. (Circled area is site of detailed studies.)	29-15
29-7	Variable sun elevation study — 15:28 hours, showing partial shading of soil. (Compare with figures 29-5 and 29-8.)	29-16

Figure		Page
29-8	Variable sun elevation study — 16:14 hours, showing total shading of soil. (Compare with figures 29-5 and 29-7.)	29-16
29-9	Microdensitometer traces of the no. 2 scan line shown in figure 29-6 (red and blue filters at the 14:18 hours flight time)	29-17
29-10	Microdensitometer traces of the no. 2 scan line shown in figure 29-6 (green filter and no filter at the 14:18 hours flight time)	29-18
29-11	Microdensitometer traces of cotton field, 100-percent plant cover. Ektachrome IR film, G-15 filter, elevation 3000 feet	29-19
29-12	Microdensitometer traces of cotton field, 60-percent plant cover. Ektachrome IR film, G-15 filter, elevation 3000 feet	29-20
29-13	Microdensitometer traces of bare soil. Ektachrome IR film, G-15 filter, elevation 3000 feet	29-21
29-14	Change in optical density of transparencies with change in sun angle (time), measured by a microdensitometer. Ektachrome IR film, G-15 filter, elevation 3000 feet	29-22
30B-1	Total light reflectance of cotton leaves from 100-g/ha Cycocel-treated and untreated plants; each spectrum is an average value for five leaves	30B-7
30B-2	Transmittance of cotton leaves from 100-g/ha Cycocel-treated and untreated plants; each spectra is an average value for five leaves	30B-8
30B-3	Internal structure of cotton leaves from untreated and 100-g/ha Cycocel-treated plants	
	a. Untreated plants	30B-9
	b. 100-g/ha Cycocel-treated plants	30B-9
30C-1	Simulated leaf of total thickness D. The leaf is composed of N subplates separated by air spaces of infinitesimal thickness. The quantity N, equal to 3 in this figure, does not need to be an integer	30C-7

Figure		Page
30C-2	Multiple reflections produced by a transparent plate with rough surfaces	30C-8
30C-3	Reflectance and transmittance curves	
	a. Reflectance curves of citrus leaves	30C-9
	b. Transmittance curves of citrus leaves	30C-10
	c. Theoretical reflectance curves based upon optical constants for pure water	30C-11
	d. Theoretical transmittance curves based upon optical constants for pure water	30C-12
30C-4	Effective refractive index of a citrus leaf compared with that of water	30C-13
31-1	Organization diagram for the Laboratory for Agricultural Remote Sensing, Purdue University. The relationship between LARS and the other facilities involved in agricultural remote sensing is also indicated	31-15
31-2	Location of a 70-mile flight line in south-central Indiana. Multispectral scanner data for this entire flight line were automatically classified into basic cover types	31-16
31-3	Comparison of a photo mosaic and automatic classification results for the same area. A photograph of a computer print-out showing only the points identified as water is shown on the right	31-17
31-4	Closeup of classification results	31-18
31-5	Closeup of automatic classification results for basic cover types	31-19
31-6	Automatic classification results for new crops and cereal grains. The lines and crop species identification symbols were manually added to the computer print-outs	31-20
31-7	Closeup of the computer print-out of crop species identification results and corresponding aerial photograph	31-21

Figure		Page
31-8	Photo mosaic and corresponding computer print-out indicating the test areas (outlined by rectangles) within which quantitative classification results were summarized	31-22
31-9	Graph of quantitative classification results for the areas indicated in figure 31-8	31-23
31-10	Table of computer output showing the quantitative classification results and the numbers of samples used to obtain the percentage correct recognition figures indicated here and in figure 31-9	31-24
31-11	Color photographs obtained by the NASA Convair 240 aircraft on June 18 and July 30, 1968 to show distinct changes that have taken place for various types of vegetation	31-25
31-12	Adjacent frames of color photography obtained by NASA on July 30, 1968 to show the marked effects of look angle and the row direction of the crop upon the tone recorded on an aerial photograph . . .	31-26
31-13	Color photograph of an agricultural area showing three fields of red clover	31-27
31-14	Color photograph of wheat breeding plots on the Purdue Agronomy Farm, showing the marked differences in appearance that can be found on the same date for different varieties and crosses of a single crop species	31-28
32-1	Diagram of earth-observational system	32-11
32-2	Block diagram of a pattern-recognition device	32-12
32-3	Example of categorizer decision boundaries in two-dimensional feature space	32-13
32-4	Organization of the LARSYS programing system	32-14
32-5	Use of LARSYS in categorizer design	32-15
32-6	Organization of LARSYSAA	32-16

Figure		Page
32-7	Panchromatic aerial photo mosaic of Tippecanoe County, Indiana (21 by 24 miles)	32-17
32-8	Lineprinter print-outs of July 1968 scanner data showing the effects of cloud shadows and processing to minimize it	32-18
32-9	Example print-out from the feature selection processor of LARSYSAA	32-19
32-10	Results in one specific case to the problem of choosing optimum feature sets of optimum dimensionality	32-20
32-11	Visible and thermal infrared print-outs of data to be overlaid. A panchromatic photograph is shown for comparison	32-21
32-12	Data overlay steps	32-22
32-13	Example print-outs of visible and reflective infrared data before and after border enhancement	32-23
32-14	Typical overlay geometry illustrating the manner in which manual supervision of the automated overlay can be used to improve system performance	32-24
33-1	The fundamental hypothesis of remote sensing is that radiance measurements on ground-scene resolution elements will contain information on the natural objects in the ground scene	33-8
33-2	Field instrumentation van behind the cherrypicker-mounted Michelson interferometer spectrometer	33-9
33-3	Panchromatic photograph, University of Michigan scanner data print-out, and NASA thermal mapper image	33-10
33-4	A photograph (NASA aircraft) and 8 μ to 14 μ thermal print-out (University of Michigan aircraft) from the July 30, 1968, mission	33-11
33-5	Blackbody equivalent temperature spectra	33-12
33-6	Blackbody equivalent temperature spectra	33-13
33-7	Blackbody equivalent temperature spectra	33-14

Figure		Page
33-8	Blackbody equivalent temperature spectra	33-15
33-9	Composite radiance spectra of soil, water, and green vegetation based on field spectral measurements at LARS	33-16
33-10	Typical field radiance spectra in the 0.4- to 1.05- μ m wavelength region	33-17
33-11	Typical field radiance spectra in the 0.7- to 1.9- μ m wavelength region	33-18
33-12	Typical field radiance spectra in the 1.9- to 2.8- μ m wavelength region	33-19
33-13	Typical field radiance spectra in the 4- to 16- μ m wavelength region	33-20
33-14	Interior view of the LARS leaf-scattering appa- ratus	33-21
33-15	Polar plot of leaf-scattering radiance as presented on the storage oscilloscope	33-22
33-16	Leaf-scattering data, corn leaf	33-23
33-17	Leaf-scattering data, soybean leaf	33-24
34-1	The K-band image of Garden City, Kansas, Test Site 76	34-22
34-2	Information available at Garden City, Kansas, in September 1965 on HH- and HV-polarization K-band radar	34-23
34-3	Crop-type categorization of July radar image densi- ties	34-24
34-4	Comparison of actual land use with the classes derived- from clustering image densities from four K-band polarizations	34-25
34-5	Relative radar return curves for a series of crops at Garden City, Kansas, based on HH-polarization K-band imagery densities	34-26 //

Figure		Page
34-6	Color-combined HH-HV radar image of a portion of the Garden City, Kansas, Test Site in September 1965	34-27
35-1	Multispectral black and white Ektachrome Aero IR and color-enhanced images of an area in the Bucks Lake Test Site	35-3
35-2	A comparison of the ease of discrimination of terrain and vegetation features as imaged on conventional color and color IR films	35-4
35-3	A Gemini photograph of the Orizaba region of Mexico, upon which broad natural vegetation types can easily be distinguished	35-5
35-4	A portion of the Bucks Lake Test Site	35-6
35-5	Graph of data that result from classification of timber types in figure 35-4	35-7
35-6	Sequential small-scale imagery, as illustrated above, can serve as a valuable guide to hydrologists in their determinations of both surface and subsurface runoff that can be expected during a particular period	35-8
35-7	These two photographs show the set of six projectors used to enhance multispectral black and white images	35-9
35-8	Four color-enhanced multiband images as obtained using the equipment pictured in figure 35-7	35-10
36-1	Dense stand of Douglas fir in the center of which an area infested with the fungus <u>Poria weirii</u> can be discerned	36-7
36-2	A special pole pruner permits the efficient collection of treetop foliage samples from which to make spectrometric analysis	36-8
36-3	Operation of a PRT-5 radiometer from a hovering helicopter permits the investigator to determine how much energy is being emitted from the upper 30 percent of a tree crown	36-9

Figure		Page
36-4	Photograph of a single frame of the tape recording from the Ampex 7500	36-10
36-5	This new remote-sensing technique incorporates a non-imaging IR radiometer with an instant-replay video-scan tape-recording system that can be used either in a helicopter or fixed-wing aircraft	36-11
37-1	Study areas I and II near Lead, South Dakota	37-33
37-2	Oblique photograph of bark beetle-induced tree mortality of ponderosa pine, Lead, South Dakota	37-34
37-3	Screen cage on attractant pine tree. Screen wire cage stapled to ponderosa pine trunk. The cage is charged with live beetles to induce attack by indigenous beetles on a normally healthy tree	37-35
37-4	Ground plot of infested trees	37-36
37-5	Spectral reflectance from pine foliage (0.4 μ to 22.0 μ)	
	a. Foliage reflectance from 0.4 μ to 1.08 μ	37-37
	b. Foliage reflectance from 0.4 μ to 2.2 μ	37-37
	c. Foliage reflectance from 2.5 μ to 22.0 μ	37-37
37-6	Needle temperature and wind velocity recorders and sap flow instrument	
	a. Brown Electronic Model 152 by 60 P16 multipoint temperature recorder on left and Esterline-Angus 20-channel event recorder on right	37-38
	b. Portable microvoltmeter, Medistor Model A-60-C, is used with two heat detectors and a heat source to measure relative transpiration rates between healthy and dying ponderosa pine	37-39
37-7	Barnes PRT-10 radiation thermometer and Stoll-Hardy IR radiometer	
	a. A Barnes PRT-10 portable radiation thermometer was used at the resolution target to record apparent emitted temperatures	37-40
	b. Stoll-Hardy IR radiometer being used to measure apparent needle temperature in the upper crown of a ponderosa pine tree	37-41

Figure

Page

- 37-8 Instrument tower and soil moisture instrument
- a. Stationary 60-foot tower erected to record wind velocity at four levels in the tree crown, to record solar radiation, and to provide a platform for making emitted foliage temperature measurements in the tree tops 37-42
 - b. Colman Soil Moisture Meter being used to measure soil moisture and temperature from probes buried in the soil profile 37-43
- 37-9 Pyrlieliograph and needle tension instrument
- a. Weather cabinet housing hygrothermograph in opening near healthy and infested trees. Recording pyrlieliograph (resting on roof of weather cabinet) measures total solar radiation 37-44
 - b. Scholander bomb for measuring needle moisture tension 37-45
- 37-10 Microscopic cross sections of ponderosa pine needle tissue 37-46
- 37-11 Field thermal resolution target. Resolution target under construction at Black Hills Test Site. Panels were 8 feet long and in one of three widths: 2, 4, and 8 feet. They alternated between aluminum painted with black velvet paint and aluminum. Stereographic pair shown in lower photograph is from Anscochrome D/200 transparency, scale 1:1584 37-47
- 37-12 Interior view of multispectral electronic equipment used by the Willow Run Laboratories, University of Michigan, and mounted in a C-47 type aircraft. Both optical-mechanical scanners are mounted in the floor opening — lower right of picture. All scanner voltage signals are fed to the two magnetic tape recorders shown in the right forward section of the cabin 37-48

Figure		Page
37-13	Four wavebands of line-scan imagery. Sample imagery from optical-mechanical scanners. Warm objects on this imagery appear light in tone; cold objects such as water of the aluminum target appear dark in tone	
	a. Reconofax XI — no filter, mostly reflected energy	37-49
	b. Reconofax XI — 2.0μ to 2.6μ , some reflected, some thermal energy	37-49
	c. Reconofax XI — thermal energy, 4.5μ to 5.5μ	37-49
	d. RS-7 — thermal energy, 8.0μ to 14.0μ	37-49
37-14	G.A.F. Model 650 microdensitometer permits microanalysis of black and white and color film densities. Density is recorded on chart at right in analog form from density values of 0.0 to 4.0	37-50
37-15	Microdensitometer traces across and along scan lines. Microdensitometer traces across Reconofax XI thermal IR imagery in the 4.5μ to 5.5μ band shown below. Flight made at approximately 14:00 hours, June 16, 1967	
	a. Traces diagonally across scan lines. Note regularly spaced low-density readings caused by gaps between scan lines	37-51
	b. Trace along scan line. Note the reduced amplitude between the coolest (forest canopy) and warmest (forest opening) objects	37-51
	c. Also, note distortion in outlined figure surrounding dying trees; it was roughly square but, because of changes in V/H with respect to scanning speed, is distorted on the thermal imagery	37-51
37-16	Microdensitometer traces of four wavebands across resolution target	37-52
37-17	Microdensitometer trace of target on pan film. A microdensitometer trace across the resolution target photographed on Plus-X Aerographic film. The photograph shows the target image at four times the original 1:4400 scale	37-53
37-18	Munsell notations made in the field of 209 infested and 47 healthy ponderosa pine trees in May, June, July, and August 1967	37-54

Figure		Page
37-19	Photointerpretation results	37-55
37-20	Ground estimate of dying pines versus photointerpreter	37-56
37-21	Munsell hue notations by three methods	37-57
37-22	Change in foliage color	37-58
37-23	Pilot study area enlarged from 1:116 000 scale Kodak Aero Ektachrome IR transparency. Adjoining base map shows infestation locations as plotted on ground . . .	37-59
37-24	Stereographic example of prints made from very small-scale (1:116 000) and normal-scale (1:7920) transparencies (Kodak Aero Ektachrome IR) of Black Hills beetle infestations near Lead, South Dakota	37-60
37-25	Detection success (mean of three interpreters) expressed as a percent for four infestation size classes (in feet), five photograph scales, and two films	37-61
37-26	Comparison of ground temperatures obtained with a Barnes PRT-5 instrument related to thermal image density on film determined by G.A.F. microdensitometer	37-62
38-1	Brazilian and Mexican representatives were cordially invited to observe and participate in forest remote-sensing activities for a combined period of 1 month (May 12 through June 8)	38-6
38-2	Photography taken in a combination of bands of the spectrum	38-7
38-3	Increased accuracy can be obtained when distinguishing deciduous from evergreen species if care is taken in selecting the optimum season of photography	38-8
38-4	Seasonal variations in the reflectance characteristics of different terrain features and conditions can be observed on high-quality sequential imagery	38-9

Figure		Page
38-5	Species composition: <u>Quercus garryana</u> (Oregon oak) at A, <u>Acre macrophyllum</u> (bigleaf maple) at B, and <u>Pseudotsuga menziesii</u> (Douglas fir) — a young stand at C and a mature stand at D	
	a. Film: Panchromatic Filter: Wratten 15 Scale: 1:20 000	38-10
	b. Film: Aerial Ektachrome Filter: None Scale: 1:3500	38-11
	c. Film: Ektachrome Aero IR Filter: Wratten 12 plus EF 2200 Scale: 1:3500	38-11
38-6	<u>Pinus lambertiana</u> (sugar pine), squared, and <u>Abies concolor</u> (white fir), circled, can easily be identified on the larger scale aerial photograph shown above by virtue of such crown characteristics as branching habit and shape of crown apex	
	a. Film: Aerial Ektachrome Scale: 1:10 000	38-12
	b. Film: Aerial Ektachrome Scale: 1:2500	38-12
	c. Comparison of <u>Pinus lambertiana</u> and <u>Abies concolor</u>	38-13
38-7	Spectrozoal imagery offers unique advantages in determining forest species composition and mapping vegetation types	38-14
38-8	A three-diameter enlargement of an Ekta Aero IR duplicate transparency taken from Gemini VII on December 7, 1965, over the southeastern United States	38-15
38-9	Mosaic form of conventional aerial photographs required to cover a portion of the area shown on the Gemini photograph	38-16
39-1	NASA Harvey Valley Range Test Site 135	39-13

Figure

Page

- 39-2 These aerial photographs (scale 1:8500) of Harvey Valley Range illustrate a variety of vegetation types associated with changes in soil type and moisture regime
- a. Panchromatic (Plus X Aerographic) 39-14
 - b. Aerographic IR 39-15
 - c. Ektachrome Aero 39-15
 - d. Ektachrome Aero IR 39-16
- 39-3 Vegetation types
- a. Blue grass (Poa nevadensis)-silver sagebrush (Artemisia cana) community 39-17
 - b. Wet meadow site at Cone Spring. The dominant species in this type are sedges (Carex sp.) and forbs 39-17
 - c. Low sagebrush community 39-18
 - d. Sharp vegetation boundary between wet meadow site and big sagebrush site, caused by an abrupt change in soil type, topography, and moisture regime . . . 39-18
 - e. Big sagebrush (Artemisia tridentata) community . . . 39-19
- 39-4 Portion of the Harvey Valley Test Site, taken June 11, 1966. Scale approximately 1:30 000
- a. Ektachrome Aero 39-20
 - b. Ektachrome Aero IR 39-20
- 39-5 Ektachrome Aero IR photograph. Scale 1:30 000 39-21
- 39-6 Large-scale 70-mm color (Anscochrome D-200, top) and color IR (Ektachrome Aero IR, bottom) photographs. Scale ranges from 1:900 to 1:640 39-22
- 39-7 Ektachrome Aero IR photograph, taken October 18, 1967, by NASA-Houston aircraft 39-23
- 39-8 Ektachrome Aero IR photographs
- a. Taken in early May 39-24
 - b. Taken in late August 39-24

Figure		Page
39-9	The two images were taken simultaneously on October 18, 1967	
	a. Thermal IR imagery (8 μ to 14 μ), Reconofax IV	39-25
	b. Ektachrome Aero IR photograph	39-25
39-10	Multiband line-scan imagery obtained by an optical-mechanical scanner (May 18, 1966) showing range resources	39-26
39-11	Seasonal stage when range foliage is near maximum development	39-27
40-1	Chart of work flow for the use of space photography in the inventory and analysis of rangeland vegetation and related resources	40-20
40-2	Range vegetation provides a critical part of the feed base	40-21
40-3	Part of a Gemini photograph enlarged and rectified to a topographic map	40-22
40-4	A preliminary vegetation resource map prepared on Gemini IV color photography	40-23
40-5	A comparative example of vegetation mapping with the same information as in figure 40-4 on high-resolution aerial photography	40-24
41-1	Panchromatic photomosaics of Davis, California, agriculture area	
	a. Photomosaic with annotations	41-10
	b. Photomosaic without annotations	41-11
41-2	Eighteen multispectral images of Davis, California, agricultural area	
	a. Imagery from 0.32 μ to 0.62 μ	41-12
	b. Imagery from 0.62 μ to 13.5 μ	41-13
41-3	Simulated panchromatic film imagery of Davis, California, agricultural area	41-14
41-4	Simulated IR Aerographic imagery of Davis, California, agricultural area	41-15

Figure		Page
41-5	Color imagery of Davis, California, agricultural area	41-16
41-6	The ways to code the amplitude of the signal within a single band (8μ to 14μ)	
	a. Thermal contours	41-17
	b. Quantized levels assigned density levels, with entire region within a quantized level presented at same density	41-17
	c. Quantized levels color coded	41-17
41-7	Recognition pictures, Davis, California, agricultural area	41-18
41-8	Color recognition in picture, Davis, California, agricultural area (red, relatively mature green rice; blue, immature rice; green, safflower; black, bare earth)	41-19
41-9	Digital recognition map, Davis, California, agricultural area	41-20
41-10	Crop acreage of Davis, California, agricultural area	41-21
50-1	Curves of radar differential scattering coefficient versus angle of incidence compared with photograph showing regions from which the data were obtained using the 13.3-gigahertz scatterometer	50-24
50-2	Curves of difference between radar differential scattering coefficient and values for a mean curve compared with photograph of Pisgah Crater area from which the data were obtained by the 13.3-gigahertz scatterometer	50-25
50-3	Color codes for the information obtained by scatterometer from the Pisgah Crater area, compared with a photograph of the area	50-26
50-4	Curves of radar differential scattering coefficient versus angle of incidence compared with a line map of the Garden City Test Site area from which the data were obtained with the 13.3-gigahertz scatterometer	50-27

Figure		Page
50-5	Curves of difference between radar differential scattering coefficient and values for a mean curve compared with a line map of the Garden City Test Site area from which the data were obtained with the 13.3-gigahertz scatterometer	50-28
50-6	Variation of radar differential scattering cross section with frequency as reported by Daley of NRL (horizontal polarization). The parametric angle is the elevation angle, the complement of the angle of incidence	50-29
50-7	Variation of radar differential scattering cross section with frequency as reported by Daley of NRL (vertical polarization). The parametric angle is the elevation angle, the complement of the angle of incidence	50-30
50-8	Frequency dependence of scattering coefficient obtained by ultrasonic simulation (undulating surface)	50-31
50-9	Frequency dependence of scattering coefficient obtained by ultrasonic simulation (undulating surface roughened with sand particles)	50-32
50-10	Effect of frequency average on image of sphere targets	
	a. Monochromatic image of two spheres ($f = 1.5 \text{ MHz}$)	50-33
	b. Swept frequency image of two spheres ($f = 1.5 \text{ MHz} \pm 10\%$)	50-33
50-11	Monochromatic images of the same target made at nearby frequencies compared with panchromatic images with ± 3 -percent and ± 6 -percent frequency variation. These images were produced in the ultrasonic simulator	50-34
50-12	Example of possible spectral-response-separated trichromatic radar	50-35
50-13	Block diagram of the IDECS and associated equipment	50-36
50-14	False color IDECS-enhanced image of Bucks Lake Test Site. Original data multispectral photographs from NASA aircraft 926 overflight	50-37

Figure		Page
50-15	False-color IDECS-enhanced image of Bucks Lake Test Site. Original data multispectral photographs from NASA aircraft 926 overflight	50-38
50-16	False-color IDECS-enhanced image of Bucks Lake Test Site. Original data multispectral photographs from NASA aircraft 926 overflight	50-39
50-17	False-color IDECS-enhanced image of Bucks Lake Test Site. Original data multispectral photographs from NASA aircraft 926 overflight	50-40
50-18	False-color IDECS-enhanced image of Bucks Lake Test Site. Original data multispectral photographs from NASA aircraft 926 overflight	50-41
50-19	Identification accuracy for August-September 1965 radar imagery	50-42
50-20	Identification accuracy for July 1966 radar imagery	50-43
50-21	Identification accuracy for Pisgah Crater scatterometer data	50-44
50-22	Scattergram of July 1966 Garden City radar image data projected on its first two principal axes	50-45
50-23	Scattergram of August 1965 to September 1965 Garden City radar image data projected on its first two principal axes	50-46
50-24	Image 1 of made-up data	50-47
50-25	Image 2 of made-up data	50-48
50-26	Image 3 of made-up data	50-49
50-27	Classified image of made-up data using spatial clustering	50-50
50-28	Classified image of made-up data using measurement space clustering	50-51
51-1	Schematic of multispectral scanner and data processor	51-7

Figure		Page
51-2	Typical spectrometer video data	51-8
51-3	Typical x-y scope pictures	51-9
51-4	Raw spectrum of green paint	51-10
51-5	Light-green standard reflectance panel	51-11
51-6	Illustrative plots of relative signal versus scan angle for wheat field	51-12
51-7	Signal variation as a function of scan angle and direction	51-13
51-8	Distribution of wheat-field signals data	51-14
51-9	Typical signal relationships of dwell time on land to water changes	51-15
51-10	Tonal variations arising from ac coupling	51-16
51-11	Thermal stripmap with gain set to observe thermal patterns in water	51-17

VOLUME II

AGRICULTURE AND FORESTRY

SECTION I

INTRODUCTION

On September 16, 17, and 18, a review of various aspects of the Earth Resources Program was held at the Manned Spacecraft Center, Houston, Texas. Particular emphasis was placed on the results of analysis of data obtained with the Manned Spacecraft Center and other aircraft which have contributed data to the program.

The review was arranged in conjunction with the Department of Interior, Department of Agriculture and the Department of the Navy. Attendees and participants at the meeting included program investigators, their immediate associates, and program representatives from the above named agencies and ESSA and NASA.

The review was divided into the disciplinary areas of Geology, Geography, Hydrology, Agriculture and Forestry, and Oceanography. An additional session was held on instrumentation. Program investigators presented the results of their work in each of these areas. The material presented is being published in three volumes:

Vol I — GEOLOGY, GEOGRAPHY, AND SENSOR STUDIES

Vol II — AGRICULTURE, FORESTRY, AND SENSOR STUDIES

Vol III — HYDROLOGY, OCEANOGRAPHY, AND SENSOR STUDIES

It should be noted that the instrumentation section is repeated in all three volumes as much of this material is of interest to more than one discipline.

The review provided a current assessment of the program for both management and technical personnel. It is important to note that the material presented represented the current status on ongoing programs and consequently complete technical analyses will be available at a later date.

N71-16148

PHOTOGRAPHIC STUDIES AND APPLICATIONS
OF THE NASA EARTH RESOURCES SURVEY PROGRAM

By Robert N. Colwell
Forestry Remote Sensing Laboratory, University of California

INTRODUCTION

The conveners of this conference have asked me to describe the various photographic studies which have been performed and the applications found by investigators who have been working on the NASA Earth Resources Survey Program in the fields of agriculture, forestry, and range management.

RESULTS ACQUIRED THROUGH THE USE OF DATA
FROM NASA AIRCRAFT

On numerous occasions during the past 3 years, multiband photography has been obtained by NASA aircraft of (1) NASA agricultural test sites at Lafayette, Indiana; Weslaco, Texas; and Davis, California, and (2) NASA forest and range test sites at Bucks Lake, Harvey Valley, and San Pablo Reservoir in California. Of the many uses which the NASA agriculture/forestry team has made of that photography, an especially important one has been the preparation of feasibility summaries such as those appearing in table 28-I. This table is based primarily on a study of all photography of these test sites flown to date by NASA aircraft. However, the table also is based on a study of (1) all other available aerial photography of these test sites and adjacent areas and (2) Gemini space photography of agricultural, forest, and rangeland sites, regardless of locality. In order that values might be assigned to all of the squares appearing in the table, interpolations have been made in those few instances in which no examples were available of the film-filter/photographic-scale combinations indicated.

If vertical photography is taken from a spacecraft at an altitude of 100 miles, using a camera of 6-inch focal length, the photographic scale is approximately 1:1 000 000. This is one of the most commonly mentioned scales in discussions of future space photography. Consequently, based on our studies of Gemini photography, entries for a

scale of 1:1 000 000 have been included in the feasibility study reported in table 28-I. A study of those entries will indicate (1) which of the agriculture/forestry resource features listed might be identified on space photography and (2) the extent to which resource inventories based primarily on space photography might be improved by the flying of limited amounts of supplementary large-scale aerial photography — a process known as "double sampling."

In table 28-I, the features pertaining to the vegetation resource are shown. Feasibility ratings are given for the four film-filter combinations currently considered as most promising: panchromatic-25A, infrared-89B, Ektachrome with appropriate haze-cutting filter, and Ektachrome infrared (IR) with a minus-blue (Wratten 12) filter. The interpretability of water, soil, and geologic features at the same three photographic scales are also indicated.

Anyone can be a "square filler." In approximately 4 minutes, a grammar school student or a great-grandmother could have completed table 28-I in one fashion or another without ever bothering to look at a single frame of NASA photography. Therefore, it is important to emphasize that many man-days of detailed photointerpretation work on the part of some of the best and most dedicated photointerpreters in the world will be found summarized in table 28-I. During the past 3 years (each time that a NASA aircraft has flown a photographic mission over one of the agricultural, forest, or rangeland test sites in California), these experts have carefully interpreted the photography to determine the feasibility of identifying the various resource features indicated in the table. To a lesser extent, the same photointerpreters and their colleagues elsewhere on the NASA agriculture/forestry team have evaluated NASA aerial photography of the other test sites mentioned previously.

Of necessity, even more energy has been expended in rigorously establishing ground truth at these test sites than in making detailed interpretations of the photography. For example, the task of establishing detailed accurate ground truth at the NASA Bucks Lake Forestry Test Site is a very sizable one. The total area occupied by that test site is 120 square miles, and elevations range from 3900 to 7200 feet. However, when making feasibility studies designed to determine the photointerpretability of wildland resources (as at the Bucks Lake Test Site), it is important that a carefully selected area of approximately this size be used and that accurate ground truth be maintained for it. Otherwise, there is no standard against which to compare the photointerpretations and hence no basis for assigning feasibility ratings of the types shown in table 28-I.

Since the determination of feasibility constitutes a major objective of our work under the NASA Earth Resources Survey Program, my

colleagues and I feel certain that table 28-I summarizes some highly significant "results acquired through the use of data from the NASA aircraft." Other tables of similar content and significance appear in certain of our NASA progress reports and in the paper which David Carnegie presented. Other valuable uses which our group has made of data from the NASA aircraft are described throughout the remainder of this paper.

AGRICULTURAL AND FORESTRY USES OF SEQUENTIAL PHOTOGRAPHY

The term "sequential photography" pertains to photography taken of any given area at two or more different times. From a comparative analysis of sequential photographs, certain time-dependent features may be identified or evaluated, even though it would have been impossible to do so on any single set of photographs. In some instances, the diagnostic changes will occur within a few seconds, and in other instances, in a period of several days, weeks, or years. Figures 28-1 to 28-7 illustrate some time-dependent phenomena that are best interpreted through the use of sequential photographs taken over a suitable time span.

The Detection of Changes Which Occur in a Period of Several Seconds

Typically, a forester, as one who manages all of the resources of a wildland area, is interested in the inventory of fish and wildlife as well as timber, forage, soils, and water. Figure 28-1 shows two sequential panchromatic aerial photographs taken of a streambed in Alaska. During the brief time interval that separated these two exposures, schools of salmon swam a short distance upstream toward their spawning beds. If only one of these photographs were available, the photointerpreter could not differentiate salmon from rocks. From a comparison of the two photographs, however, he can readily differentiate the moving salmon from the stationary rocks despite their tonal similarities and the low spatial resolution of the photography, analogous to that anticipated on space photography in the near future. A determination of the areal extent and density of each school of fish from a study of space photography should be of great value in making salmon inventories, provided that a few representative schools of fish are studied on large-scale aerial photographs and directly on the ground.

In similar studies, my colleagues and I have found that cattle, sheep, and big game animals on the open range frequently are confused with rocks, stumps, and bushes when only a single exposure is studied.

This is true whether the animals are studied individually as on large-scale photography, or in herds and flocks as in small-scale, simulated satellite photography. When overlapping photographs taken only a few seconds apart are studied stereoscopically, however, animals usually can be differentiated from inanimate objects by evidence that the animals have moved.

In both previous examples, the most suitable time interval corresponds very closely to the interval separating two overlapping space photographs taken in any given orbital pass around the earth.

The Detection of Changes Which Occur in a Period of Several Days

Some enthusiasts have hailed space photography as the means by which crop diseases will be detected in the future and crop yield estimates made. Figure 28-2 shows two sequential IR aerial photographs of a cereal crop nursery on the Davis campus of the University of California. During the 21-day interval that separated these two exposures, black stem rust was able to spread to each of several spots that previously were healthy. If only one of these photographs were available, the photointerpreter probably could not differentiate the dark-toned foliage, indicative of disease, from the dark-toned soil, indicative merely of sparse stands. In attempting to make an accurate prediction of crop yield, the photointerpreter must make this distinction. From a comparison of these two photographs, he can readily differentiate the spreading disease from the unchanging sparse stands despite their tonal similarities and the low resolution of the photography. Also, from a comparison of these two photographs, together with others that were taken at suitably earlier and later dates, the photointerpreter is able to establish the time when each area became diseased, in relation to the state of development of the crop. This additional information must be known in order to assess accurately the reduction in crop yield caused by the disease. In one of the tests, it was determined that wheat fields infested with rust 3 weeks before maturing will suffer a 90-percent reduction in yield, whereas those infested 1 week before maturing will suffer only a 10-percent reduction in yield. This is true even though the severity of disease, as estimated in the conventional manner in terms of the amount of leaf and stem area covered by pustules of the pathogen, may eventually become the same in the two fields.

In similar studies, it was found that the identification of hardwood tree species from a determination of the dates when they leaf out in the spring, or change color in the fall, frequently is possible from a comparative analysis of sequential small-scale aerial photographs taken over a period of several days. In most instances, from a study

of sequential photographs, it also is possible to distinguish trees which, because of an unhealthy condition, turn yellow, red, or brown at some unusual time of year from trees which turn these colors as part of their normal seasonal change.

The Detection of Changes Which Occur in a Period of Several Weeks

The inference was given in figure 28-2 that not only crop vigor but also crop type might be determinable from a study of small-scale sequential photography. In figure 28-3 are two sequential space photographs taken in June and August, respectively, of an area centered around Willcox Dry Lake, Arizona. During the time interval that separated these two exposures, the perennial crops (mainly alfalfa) remained green, and the annuals (mainly wheat) grew from seedlings to vegetative maturity. If only one of these photographs were available, the photointerpreter could not determine acreage by major crop type. From a comparison of these two photographs, however, he usually can make this determination despite tonal similarities of the crop types and poor spatial resolution of the photography.

In similar studies, our group has been able, from a comparative study of sequential high-altitude, small-scale aerial photographs, to trace the rate and extent of improvement or deterioration of rangelands under various management practices. As in most of the other examples cited in this paper, some on-the-ground observation is required, but conditions are found to be so similar in areas having a homogeneous appearance on the photographs that stratified sampling techniques can be used to great advantage, sometimes reducing by a thousandfold the amount of ground observation required to achieve a desired standard of accuracy.

The Detection of Changes Which Occur in a Period of Several Months

Another claim that has been made for small-scale sequential photography is that the progress of timber-harvesting operations and the volume of timber cut during specified periods of time may be determinable by such means. Figure 28-4 shows two sequential panchromatic aerial photographic mosaics (simulated satellite photographs) of a sizable area in the state of Oregon that is being logged in blocks by a clear-cutting process. During the time interval that separated these two exposures, several blocks of timber were harvested. If only one of these photographs were available, the photointerpreter could not determine the rate at which timber was being harvested. From a comparison of these two photographs, however, he can readily determine the

acreage that has been logged, despite the poor spatial resolution. Detailed inventories of timber volume by species are made, block by block, in this entire area every 10 years, using a combination of aerial photointerpretation and detailed on-the-ground timber-cruising techniques. Consequently, at various intermediate dates, the photointerpreter should be able to use the most recent of these inventories to determine, with the aid of satellite photography, the volume of timber by species that has been cut within each block during the intervening time period. Given comparable space photography at specified time periods, the photointerpreter eventually might be able to determine the rate at which timber is being harvested on a national or even on a global basis. Such a determination could prove invaluable to those who seek to maintain an intelligent timber cutting budget that will insure the wise use of timber resources in perpetuity.

From similar photography of vast wild-land areas, our group has been able to determine the location and cumulative areal extent of forest fire burns, brushfield clearing activities, and range reseeding or forest planting operations.

Figure 28-5 provides another example of how change detection over a period of several months can be useful. Only by having "before" and "after" photographs such as these can one make a valid appraisal of the extent to which previsual symptoms of vigor loss in plants can be discerned on IR photography.

The Detection of Changes Which Occur in a Period of Several Years

The example shown in figure 28-6 relates to the claim that plant successional trends might be determined from a study of sequential photography. Shown in the figure are two sequential panchromatic aerial photographs of an area in the Sierra Nevada Mountains of California within which plant succession is being studied by our group by use of high-altitude, small-scale aerial photography. During the 24-year time interval that separated these two photographs, grasslands have been invaded by brush, and brushlands have been invaded by coniferous trees during the same period. If only one of these photographs were available, the photointerpreter could not determine area by area the nature of plant succession and the rate at which it is progressing. However, from a comparison of these two photographs, supplemented as necessary with a few on-the-ground determinations of species composition, vigor, and foliage density, the photointerpreter can make such determinations. A more adequate understanding of the nature, direction, and rate of plant succession under different types of resource management is prerequisite to the more intelligent management of these resources.

As evidenced by this example, an improved understanding of such phenomena may be achievable through the interpretation of sequential space photographs which, in the future, should be of a quality comparable to that shown in the aerial photographs of figure 28-6.

In similar studies, our group has found that the rate at which gully erosion is causing the deterioration of an area, or the rate at which improved range management practices are promoting the improvement of an area, can be detected through a comparative analysis of sequential aerial photographs that are separated by a time interval of several years. Similar determinations can be made of the rate at which agricultural activity is encroaching on wild lands, urbanization activity is encroaching on agricultural lands, and filling operations are decreasing the areal extent of bays and harbors. In each instance, the spatial resolution required for the making of the comparative analyses is compatible with that which routinely will be available in the near future in space photography. Yet, in each instance, a limited amount of large-scale, high-resolution photography should be obtained, and a few selected spots should be visited on the ground.

The longer the elapsed time, the better some successional trends can be studied, particularly when the changes occur very slowly. This fact is evident from a study of the sequential photographs in figure 28-7, in which the time spanned is 100 years.

Mindful of the potential value of using sequential space photography in the inventory of agricultural, forest, and rangeland resources, our group is making maximum use of repetitive coverage that is being obtained by spacecraft across the southern portion of the original 48 states. For example, the area shown in figure 28-3 already has been photographed on two Gemini missions and one Apollo mission and, in all probability, will be photographed on another Apollo mission the next month after this meeting. As in the past, we plan to have personnel vigorously collecting ground truth for that area at the time when the space photography is being taken. Furthermore, we have been assured that a maximum effort will be made by NASA aircraft to obtain simultaneous aerial photographic coverage of the same area in order to better establish the true condition of crops and wild-land vegetation at the time of the space flight and to test the applicability of triple sampling techniques for inventorying earth resources in such an area. The triple sampling in this case pertains to the use of (1) complete coverage with space photography of a vast area within which the resources are to be inventoried (the initial photographic classifications being made on this coverage in an effort to subdivide the area into homogeneous "strata"), (2) limited coverage with conventional aerial photography of selected portions of each stratum to acquire certain detailed information not derivable directly from the space photographs, and (3) still more limited coverage by ground-truth survey teams who

will study, in each stratum, areas that have been carefully selected from an interpretation of aerial and space photography. In so doing, the teams will acquire more detailed information pertinent to the resource survey and applicable, stratum by stratum, to the entire area being inventoried. Further details relative to the concept and validity of stratified sampling with the aid of space photography appear in the following section.

FEASIBILITY OF DELINEATING MEANINGFUL RESOURCE BOUNDARIES ON SPACE PHOTOGRAPHY

In the NASA Earth Resources Survey Program, too much emphasis sometimes is placed on the making of accurate identifications, when in reality most of the benefit accrues merely from making accurate discriminations. In order to delineate meaningful boundaries, we may need merely to discriminate between earth resource features — a task which is usually far more feasible than that of making positive identifications of the features themselves. Accurate identifications may ultimately be required, but they can be made through the intelligent use of double and triple sampling techniques (i.e., those which supplement the boundary delineations made of a vast area in space photography with object identifications made in large-scale aerial photographs and/or ground observations of selected areas within these boundaries). Of the numerous examples which might be used to document this important point, only the example in the following discussion needs to be given here.

Persons charged with making periodic inventories of the timber resources of the United States have been using aerial photographs effectively for many years. Of major importance in the making of such inventories is an accurate determination of timber volume by species in each portion of the forest. It is quite generally recognized, however, that neither timber volume nor tree species can be determined consistently on the 1:20 000-scale panchromatic aerial photographs which the photointerpreters are obliged to use for forest inventory purposes. Nevertheless, using such characteristics as tree size, timber stand density, and photographic tone and texture, photointerpreters are able to discriminate each homogeneous portion of the forest from all others and to recognize any given homogeneous class in each of the many places where such a class occurs throughout the forest. Since the photointerpreter is able to draw boundaries between classes, he can delineate all portions of the forest into meaningful strata. However, only by on-the-ground timber-cruising methods is he able to determine the volume by species in each stratum.

The tremendous increase in efficiency that results from the ability of the photointerpreter to discriminate, even though he cannot identify, is indicated by the findings in one representative state (California) which contains 16 million acres of commercial conifer. Through use of aerial photographs, the amount of on-the-ground sampling of timber volume by species is reduced in this vast area to less than one-tenth of 1 percent of what it would otherwise have to be in order to achieve the same accuracy in the forest inventory. This is despite the fact that (1) the ultimate objective is to obtain an inventory of timber volume by species and (2) on the photographs, it is not possible to determine consistently either volume or species.

In relation to the potential usefulness of satellite photography for inventorying earth resources, the importance of the foregoing example can scarcely be overemphasized. Boundary delineations frequently are made more easily with the medium-resolution photography obtainable from spacecraft than with the high-resolution photography obtainable from aircraft. This fact is well illustrated by comparing the vegetation-soils boundary appearing in the aerial photograph of figure 28-8 with the corresponding boundary as seen in the space photograph of figure 28-9. For stratified sampling techniques to be employed, photointerpreters, who participate in the photographic stratification of resources in a vast area, must draw the stratification boundaries in a fashion which is consistent with the stratification boundary techniques employed by all the other photointerpreters. As shown by comparing figures 28-8 and 28-9, more consistency is likely to result from their delineating these boundaries on space photographs than on aerial photographs.

The feasibility of drawing accurate stratification boundaries depends on both spatial resolution and tonal characteristics of the photography. By using NASA photography of the agricultural, forest, and rangeland test sites in California, our group has done a great deal of work to determine the photographic "tone signature" of each important earth resource stratum. The question logically arises: To what extent can these same tone signatures be used eventually in the interpretation of space photography? As indicated by figure 28-10, which is representative of a large number of examples tested, a highly optimistic answer to that question appears to be justified.

The example (shown in figs. 28-9, 28-11, and 28-12) is one taken from central Australia — a part of the world where earth resource inventories currently are being made by conventional means. The area has been selected by our group for study because (1) accurate ground truth already is available for a very sizable portion of this area, (2) the ground truth has been compiled in a highly meaningful form, since the resource classifications used are those which the local resource management experts have agreed would be most meaningful in relation to resource development and land management, (3) representative space

photography covering a portion of the area is available, and (4) virtually every type of vegetation, soil, and geologic resource encountered in the 70 percent of Australia which is arid occurs in each of several spots within this single Gemini photograph.

The photograph shown in figure 28-9 was taken from the Gemini V spacecraft on August 27, 1965, and covers an area of nearly 15 000 square miles (120 miles on a side). The spacecraft was at an altitude of 165 miles. A second photograph, overlapping the first one by approximately 60 percent, was taken on the same orbit. This permitted our photointerpreters to determine the extent to which image interpretation might be improved through binocular viewing of conjugate images. (It was recognized that stereoscopic parallax would be virtually indiscernible in this imagery because of the adverse ratio of terrain height to flight altitude.) In addition, the photography was studied in both transparency and print forms, using first-generation reproductions that were made by personnel at NASA, Houston, as five-diameter enlargements of the original. The area covered in figure 28-9 falls almost exactly in the geographic center of Australia. For many years, personnel of the Land Research Division, CSIRO, in Australia, have been studying this area and its immediate surroundings.

With a view to testing the accuracy with which meaningful boundary delineations might be made on space photography, and mindful that most of the benefits of such a process result merely from discriminating rather than identifying major features, some of our photointerpreters have attempted to delineate the major vegetation, soils, and geologic boundaries from a study of the space photography. Figures 28-11 and 28-12 show two representative results of this effort. In each instance, the map on the left portrays the boundaries as drawn on the space photography, and the map on the right portrays the ground truth as obtained during the past several years by Australian scientists working in the area. In most instances, the discrepancies represent errors in photointerpretation, but my field checking of the area, in company with the Australian scientists who had been doing the field work, revealed several instances in which the boundaries had been more accurately delineated by interpretation of the space photography than by on-the-ground observations.

Assuming the ground-truth maps to be correct in all respects, two types of analyses were made of errors made by the photointerpreters. The first analysis, as exemplified by table 28-II was merely a comparison of total areas class by class as determined by interpretation of the space photography and by ground observation. This permitted a determination of the extent to which, through compensating errors, accurate area totals of the various classes might be obtained by the photointerpreter. In some contexts, such compensating errors are quite

acceptable because the initial consideration may be merely to determine whether there is likely to be enough of some particular type of commercially important resource to merit possible development. In this way, vast areas can be quickly eliminated from further study, since it is known with considerable confidence that such study would be fruitless; also, in this way, a few areas can be highlighted as showing sufficient promise, in terms of the resource being sought, to merit more detailed, costly, and time-consuming surveys.

The second type of analysis is exemplified in table 28-III. The objective in this instance has been to express in accurate, quantitative terms the feasibility of inventorying various important earth resources on space photography. The presumption in this second type of analysis is that compensating errors are not tolerable, since each area must be accurately classified. Through analysis of the types of errors being made (as shown in table 28-III), improvement in future space photo-interpretations may be possible.

The example which has just been considered has purposely dealt with only the extremely broad classification of the vegetation and geologic features of an area. The results are sufficiently encouraging, however, to merit studies as to the feasibility of making more detailed classification of these resources. Such studies presently are being undertaken.

MULTIBAND PHOTOGRAPHIC EXPERIMENTS

As an additional example of our photographic studies and applications, reference will be made to a variety of multiband photographic experiments which our group is conducting. These studies seek to determine (1) the optimum spectral bands for use in taking several photographs of a given grouping of earth resource features at the same time and (2) the interpretability of the resulting multiband photography, as compared with various kinds of color photography (Ektachrome, IR Ektachrome, Anscochrome, etc.). Interpretability is expressed in two ways, namely, the ease and accuracy with which the various important earth resources exhibited in the test area can be (1) identified and (2) discriminated between.

In one series of studies, the multiband black and white photographs are reconstituted with a "color combiner" to form various composite color images. An example of this work is presented by Bill Draeger, principal investigator for the NASA Bucks Lake Forestry Test Site. In related studies, another of the principal investigators, Philip Langley, obtains an alphanumeric record of each of the multiband photographs that cover a given area and seeks to identify resource features of

interest through computer analyses of tone signatures. In other work (as will be reported by personnel from Purdue University, Michigan, and Kansas University), the multiband magnetic tape records obtained initially with an optical-mechanical scanner can be subjected to computer analyses either in analog or digital form in an effort to use spectral-matching or pattern-recognition techniques in the automatic identification of earth resource features.

Because of the promise that already has been shown in these various approaches, our group currently is compiling for NASA, in rough draft form, a manual of multiband photography which seeks to summarize the present state of the art in this important area, with special reference to the inventory of earth resources. The first review of this document by NASA authorities was conducted in Houston in the week preceding the earth resources symposium.

Optical-mechanical scanners normally acquire imagery, not only in the spectral regions in which photographic emulsions might have recorded the image directly, but also in various other parts of the electromagnetic spectrum. Consequently, as a logical extension of our multiband photographic research, we have sought to compare the usefulness of imagery obtained in conventional photographic bands with that from various nonphotographic bands of the electromagnetic spectrum. One of the products of these studies has been the preparation of table 28-IV, which summarizes a few of the more important capabilities and limitations of the many spectral bands in which remote sensing is being performed.

THE CONSTRUCTION OF PHOTOINTERPRETATION KEYS

Whether the objective is to identify various resource features on aerial or space photography or merely to discriminate between them, properly constructed photointerpretation keys can be very useful. Since a significant amount of the effort of our group is devoted to the construction of such keys, some information regarding that activity should be included in this paper.

A photointerpretation key is reference material designed to facilitate the rapid and accurate identification of features from a study of their photographic images. The key usually consists of the two following parts:

1. Photographic examples of each class, stratum, or resource feature that is to be identified. Each example used in the key should have been ground checked to insure its accuracy. In using the key, a

photointerpreter seeks to identify a resource feature by determining which of these examples has image characteristics that most closely resemble those of the feature he is attempting to identify on operational photography. Obviously, if the examples are to be of maximum usefulness, the photography from which they are taken must have been flown to essentially the same specifications as were used in obtaining the photography that is being interpreted operationally.

2. Word descriptions which set forth in some systematic fashion the photorecognition features (in terms of tone, texture, pattern, topographic site, etc.) for each such class, stratum, or feature. For each type of resource feature that is illustrated in the key, a great many image characteristics are discernible. However, only a few of these characteristics may be of maximum diagnostic value in differentiating this type of feature from all other types with which it might be confused. This second part of the key describes in words each of these salient recognition features.

Many of the activities previously described in this paper (including those summarized in table 28-I) must be performed concurrently with the preparation of these photointerpretation keys. Numerous examples of such keys for use with aerial or space photography already have been published in NASA progress reports by our group.

PRELIMINARY TESTS OF OPERATIONAL FEASIBILITY

Our group believes that the NASA Earth Resources Survey Program can soon lead to the making of meaningful surveys of earth resources through the use of aerial and space photography. Many competent photointerpreters will be required to assist in the task, however. This is true even if the present efforts toward automatic photointerpretation by means of pattern recognition, spectral matching, and tone-signature analysis (alternate terms for essentially the same process) should prove to be phenomenally successful. Mindful of this fact, our group frequently convenes a class of 20 to 30 trainees for the purpose of submitting to them simulated operational tests from which the feasibility of making earth resource inventories from photography can be determined. Collectively, the individuals comprising such a class exhibit a wide range of backgrounds, visual acuities, and degrees of motivation toward the photointerpretation task.

Our training session for any such class usually lasts for 2 or 3 days and is followed immediately by 2 or 3 days of operational feasibility tests. In the tests, each student is equipped with photointerpretation keys and is provided with representative examples of aerial and/or space photography flown to specifications which have been

derived in our earlier studies. Ground truth is accurately known for each photointerpretation problem included in the test.

In some portions of the test, emphasis is placed on the identification of earth resource features. In other portions, emphasis is placed on the delineation of significant earth resource boundaries. In both instances, a subsequent determination of the average performance of these trainees can be quite discouraging, since the average usually is too low to be operationally acceptable. However, a highly encouraging result is obtained when results from only the top few students are considered. Herein lies an important inference regarding the manner in which a capability should be developed in the future for making resource inventories of large areas from aerial and space photography: We should be prepared to train and test four or five times as many individuals as will eventually be needed. Then, depending on student performance during the testing phase, perhaps only the top 20 to 25 percent of them will be retained for the operational phase.

SUMMARY AND CONCLUSIONS

This paper has attempted to demonstrate the following facts:

1. Thorough and effective use is being made of the photography and related data obtained on agricultural, forest, and rangeland test sites by NASA aircraft.
2. Similar use also is being made of selected space photographs which cover areas that are accessible to us.
3. From our studies, the following kinds of products are obtained and are included, project by project, in our annual reports:
 - a. Feasibility ratings indicating the accuracy and consistency with which earth resource survey features can be either identified or discriminated between on aerial and space photography flown to various specifications in terms of photographic film, filter, scale, season, et cetera
 - b. Based on these ratings, specifications for the type or types of aerial and space photography which we consider as optimum for making each of the several types of earth resource surveys
 - c. Photointerpretation keys illustrated with examples taken from photographs that have been flown to the preferred specifications and that set forth the image-recognition features discernible on such photography

d. Feasibility ratings based on the administering of simulated full-scale operational tests to a large group of trainees

For more than a century, man has been taking aerial photographs of one kind or another from which to inventory certain earth resources. Only within the last decade or so have important developments occurred which promise to make such resource inventories feasible for the first time on a national or global basis. Most of these developments have been in three interrelated areas: (a) improved capabilities of the aerial camera or other remote-sensing devices, (b) improved capabilities of the vehicles from which these sensors are operated (ranging from the hovering helicopter to the earth-orbiting spacecraft), and (c) improved capabilities in image analysis by both human and mechanical means.

As a result of these recent developments, we find ourselves, after a century of relatively slow progress, on the threshold of a new and important operational capability — that of making national or even global inventories of earth resources. Such a development is, indeed, very timely; for as the population of the world increases and the supply of natural resources of the world dwindles, the need for more intelligent management of these resources becomes all the more compelling. An important first step leading to such management is that of obtaining an accurate inventory of resources.

It was Victor Hugo, the famous French author and philosopher, who said: "There is nothing in this world as powerful as an idea whose time has come." I suspect that everyone in this audience would be in full agreement with that statement.

TABLE 28-I.- FEASIBILITY OF IDENTIFYING VARIOUS NATURAL RESOURCE FEATURES IN AERIAL AND SPACE PHOTOGRAPHY,
BASED ON STUDIES CONDUCTED AT NASA TEST SITES IN CALIFORNIA AND ARIZONA

28-16

Type of resource feature	Photographic scale and film-filter combination (a)											
	Scale 1:10 000				Scale 1:30 000				Scale 1:1 000 000			
	Pan- chromatic 12	IR- 89B	Ekta- chrome HF-1	Ekta- chrome IR-12	Pan- chromatic 12	IR- 89B	Ekta- chrome HF-1	Ekta- chrome IR-12	Pan- chromatic 12	IR- 89B	Ekta- chrome HF-1	Ekta- chrome IR-12
Vegetation resources												
Vegetated or nonvegetated	++	++	++	++	++	++	++	++	+	+	+	++
Wild or cultivated	++	++	++	++	++	++	++	++	+	+	+	++
Fields with crops	++	++	++	++	++	++	++	++	+	+	++	++
Fallow fields	++	++	++	++	++	++	++	++	-	+	+	+
Mature conifers	++	++	++	++	+	+	++	++	-	+	-	+
Mature hardwoods	+	++	++	++	-	+	+	++	-	+	-	++
Open brushfields	++	+	++	++	++	+	++	++	+	+	+	+
Riparian vegetation	+	++	++	++	+	+	+	++	+	+	+	++
Aquatic vegetation	+	++	++	++	+	++	++	++	-	+	+	+
Meadow or grassland	++	++	++	++	+	+	+	++	+	+	+	+
Sparse or drying vegetation less than 3 feet high	-	-	+	++	-	-	-	+	-	-	-	+
Vegetation not yet in leaf	-	-	+	++	--	--	+	++	--	--	--	--
Herbaceous vegetation in standing water	-	++	+	++	-	+	+	++	-	-	-	+
Sprayed brushfields	+	+	++	++	+	-	++	++	-	-	-	-
Dead or dying vegetation greater than 3 feet high	-	+	+	++	-	-	+	++	-	-	+	+
Snags or other downed timber	+	--	++	++	+	--	+	++	-	-	-	-
Burned areas	+	++	+	++	-	+	+	++	+	+	+	++
Windrowed brush	++	++	++	++	++	++	++	++	-	-	-	-

^aThe notation ++ signifies that the feature is readily and consistently identifiable, even by people with limited photointerpretation training and experience. The notation + signifies that the feature usually is identifiable, but only through careful study by photointerpreters who, by virtue of training, experience, and motivation are expert in identifying such features. The notation - signifies that the feature is not consistently identifiable even though expert photointerpreters are able to identify such features occasionally on photography of the film-filter/photographic-scale combination indicated. The notation -- signifies that, although the feature is an important one from the earth resources standpoint, it is almost never identifiable, even by expert photointerpreters.

TABLE 28-I.- FEASIBILITY OF IDENTIFYING VARIOUS NATURAL RESOURCE FEATURES IN AERIAL AND SPACE PHOTOGRAPHY,
 BASED ON STUDIES CONDUCTED AT NASA TEST SITES IN CALIFORNIA AND ARIZONA - Concluded

Type of resource feature	Photographic scale and film-filter combination (a)											
	Scale 1:10 000				Scale 1:30 000				Scale 1:1 000 000			
	Pan- chromatic 12	IR- 89B	Ekta- chrome HF-1	Ekta- chrome IR-12	Pan- chromatic 12	IR- 89B	Ekta- chrome HF-1	Ekta- chrome IR-12	Pan- chromatic 12	IR- 89B	Ekta- chrome HF-1	Ekta- chrome IR-12
Water resources												
Deep ponds or lakes	++	++	++	++	+	++	++	++	+	+	+	++
Shallow ponds or lakes	+	++	+	++	+	++	+	++	-	-	-	+
Streams and rivers	+	++	+	++	+	++	+	++	+	+	+	++
Waterweeds and algae	+	++	++	++	+	++	++	++	-	+	+	+
Degree of turbidity	+	+	+	++	+	+	+	++	-	-	-	+
Geologic resources												
Gross landforms	++	++	++	++	++	++	++	++	++	++	++	++
Igneous rock masses	+	+	+	+	+	+	+	+	+	+	+	+
Sedimentary rock masses	+	+	+	+	+	+	+	+	+	+	+	+
Metamorphic rock masses	+	+	+	+	+	+	+	+	+	+	+	+
Granitic outcrop covered with lichens	+	++	+	++	-	+	-	++	-	-	-	+
Granitic outcrop without lichen cover	++	-	++	++	+	-	++	++	-	-	+	+
Granitic talus	++	-	++	++	+	-	+	++	-	-	-	-
Serpentine rock	+	-	+	++	-	-	-	+	-	-	-	-
Soils resources												
Alluvial soils	++	++	++	++	++	++	++	++	+	+	+	+
Eolian soils	+	+	+	+	+	+	+	+	+	+	+	+
Glacier-derived soils	+	+	+	+	+	+	+	+	-	+	+	+
Residual soils	+	+	+	+	+	+	+	+	-	-	-	-
Serpentine-derived soils	+	-	+	++	-	-	-	+	-	-	-	+

^aThe notation ++ signifies that the feature is readily and consistently identifiable, even by people with limited photointerpretation training and experience. The notation + signifies that the feature usually is identifiable, but only through careful study by photointerpreters who, by virtue of training, experience, and motivation are expert in identifying such features. The notation - signifies that the feature is not consistently identifiable even though expert photointerpreters are able to identify such features occasionally on photography of the film-filter/photographic-scale combination indicated. The notation — signifies that, although the feature is an important one from the earth resources standpoint, it is almost never identifiable, even by expert photointerpreters.

TABLE 28-II.- MAJOR TERRAIN-VEGETATION TYPES

Type	Number of Areas for -	
	Ground truth	Gemini interpretation
Mountains and hills	654	629
Salt lakes	51	34
Alternating hills and lowlands	421	343
Forb pastures on flat country	679	828
Mitchell grass	17	20
Spinifex	930	928
Forb pastures on alluvium	253	253
Total	3015	3015

TABLE 28-III.- DISCREPANCY ANALYSIS FOR MAJOR GEOLOGIC TYPES

Type	Number in agreement	Number in disagreement	Percent accuracy	Type of misinterpretation
Cainozoic	1336	344	80	229 areas called Paleozoic 115 areas called Precambrian
Paleozoic	498	10	98	10 areas called Precambrian
Precambrian	506	162	75	132 areas called Cainozoic 30 areas called Paleozoic

TABLE 28-IV.- A TABULAR SUMMARY OF CHARACTERISTICS GOVERNING THE FEASIBILITY OF REMOTE SENSING IN VARIOUS PARTS OF THE ELECTROMAGNETIC SPECTRUM

	Wavelength, μ						
	10^{-6} (a)	10^{-4} (a)	10^{-2} (a)	10^{-1}	10^0 (b)	10^2 (b)	10^4 (b)
Spectral region	Gamma ray	X-ray	Ultraviolet	Visible	Photo IR	Thermal IR	Microwave
Properties sensed	Dissociation electron shifts	Dissociation electron shifts	Dissociation electron shifts	Molecular effects	Molecular effects	Macromolecular effects	Macromolecular effects
Detectors used	Ionization detectors	Phosphors	Phosphors	Photographic films	Quantum detectors	Quantum detectors	Antennas and circuits
Atmospheric con- straints	Clear weather only	Clear weather only	Clear weather only, hazy at- mosphere	Clear weather only, hazy at- mosphere	Clear weather only, hazy at- mosphere	Clear weather only, hazy at- mosphere, smoky atmosphere	Clear weather only, hazy at- mosphere, smoky atmosphere, foggy or cloudy
Maximum subsurface sensing depth, in milli- microns	10^8	10^4	10^2	10^1	10^2	10^4	10^8
Spatial resolution at- tainable in millira- dians	500	500	0.01 to 0.1	0.01 to 0.001	0.01 to 0.1	1.0	10

^aResolution in these short wavelengths is limited primarily by atmospheric scattering; $S = k_1 \cdot (1/\lambda^4)$, where S = scattering.

^bResolution in these long wavelengths is limited primarily by aperture of the sensor $R = k_2 \cdot (\lambda/D)$, where R = resolution and D = diameter of the "collection optics."

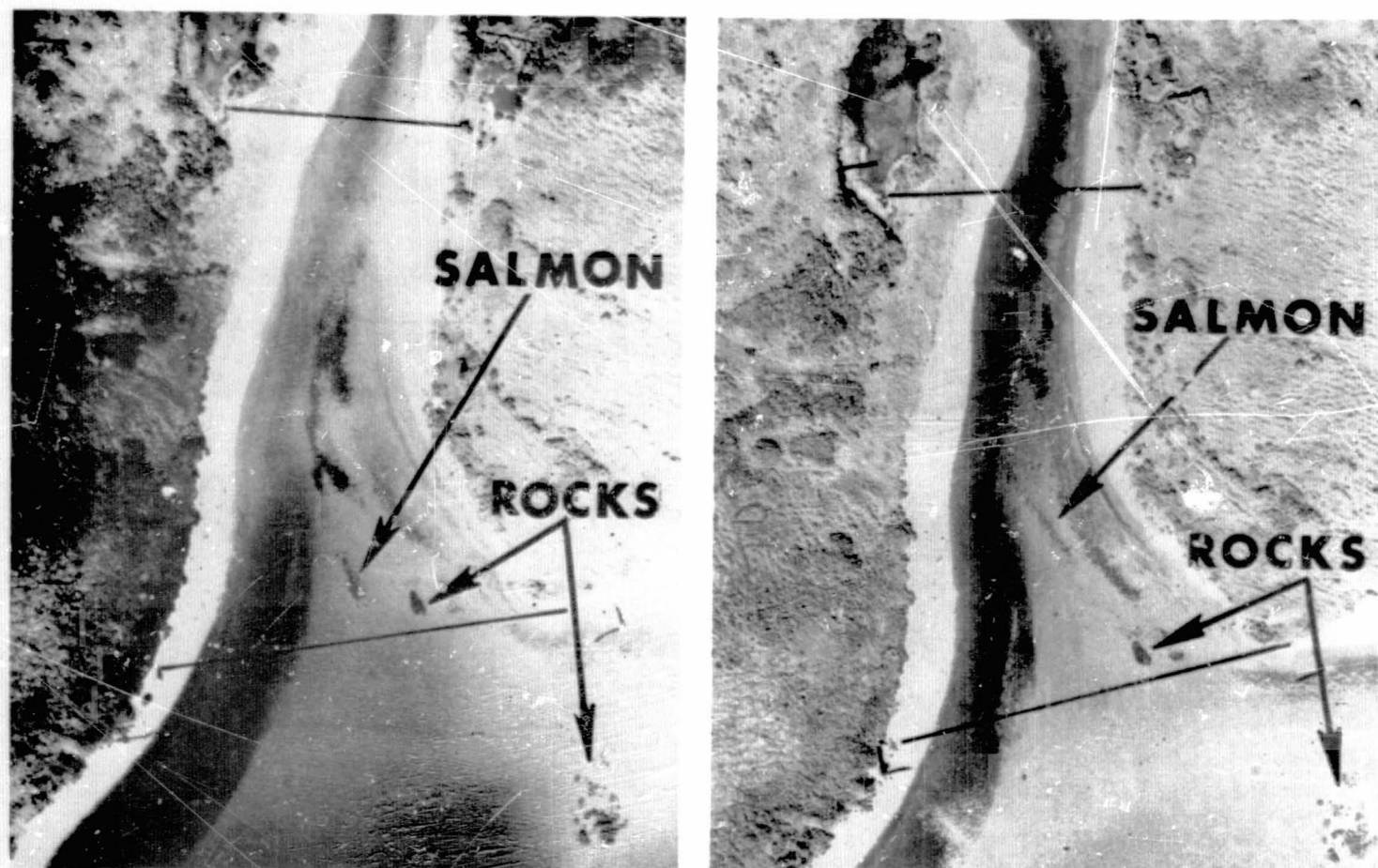


Figure 28-1.- These two panchromatic aerial photographs of an Alaskan streambed illustrate the use of sequential photography to detect changes which occur in a period of several seconds. Note from a comparison of the two photographs how easily the moving salmon can be differentiated from the stationary rocks. When the objective is to inventory salmon runs over very large geographic areas and in short periods of time, the large synoptic view obtainable from space platforms is desirable. Furthermore, the spatial resolution requirements probably are not excessively high since the inventory might be based on schools rather than on individual fish (photographs courtesy U.S. Fish and Wildlife Service).

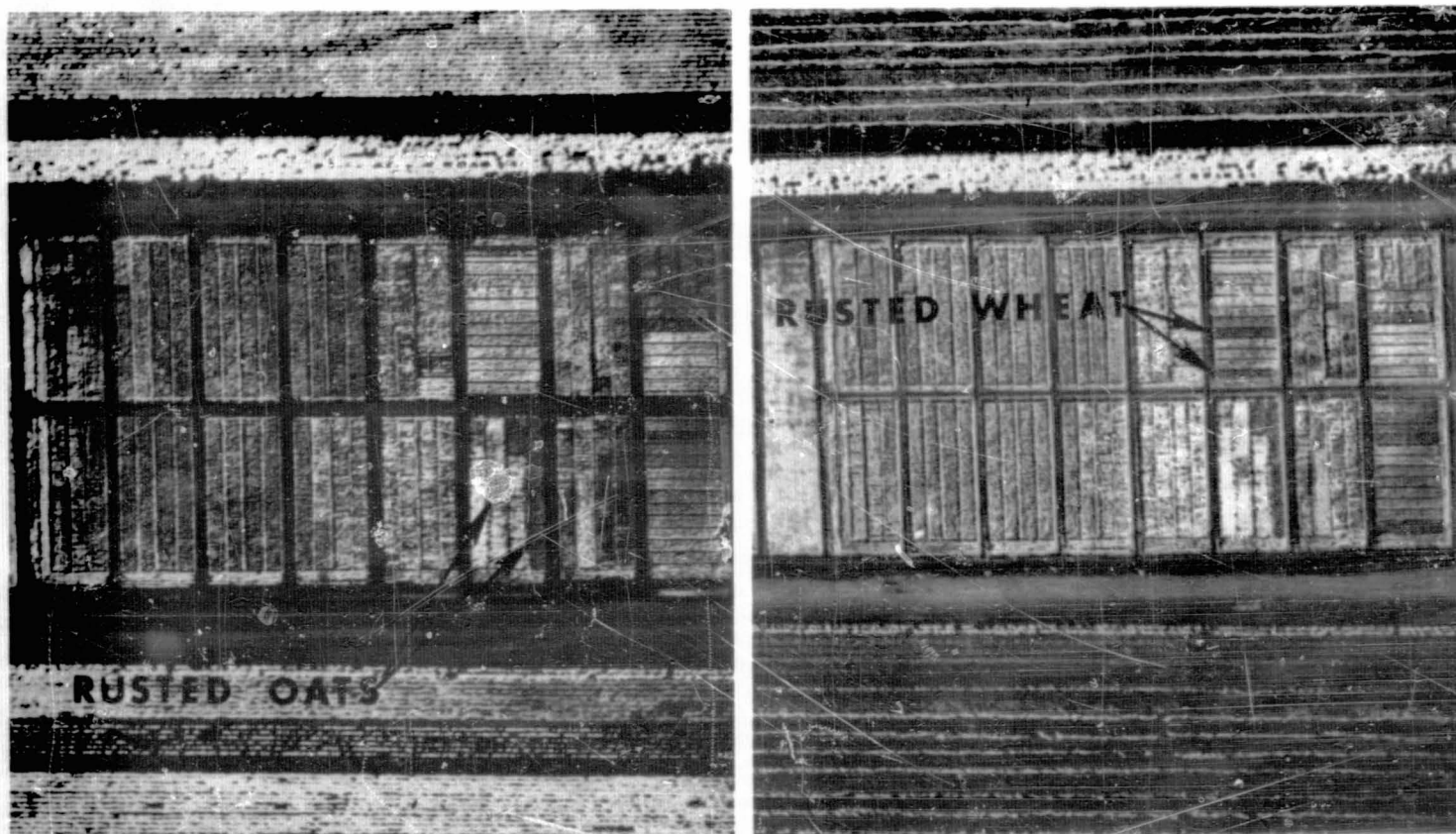


Figure 28-2.- These two IR aerial photographs of a cereal crop nursery on the Davis campus of the University of California illustrate the use of sequential photography to detect changes which occur in the development of black stem rust on wheat and oats in a period of several days. The left photograph was taken 21 days earlier than the right photograph. For an explanation of the value of making a comparative analysis of these sequential photographs, see the text. It is probable that the same distinctions could be made on space photography.

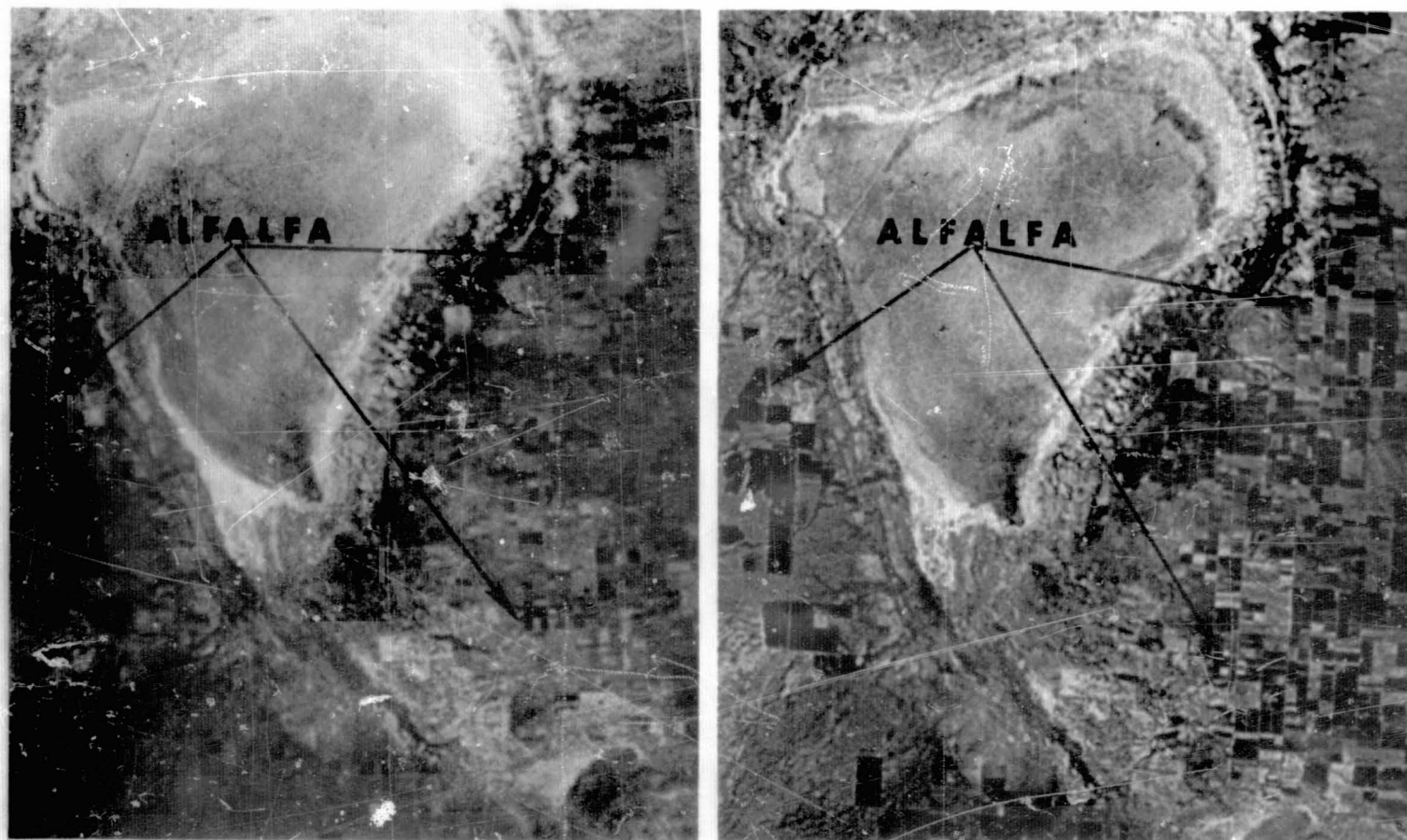


Figure 28-3.- These two space photographs of the agricultural lands surrounding Willcox Dry Lake in Arizona illustrate the use of sequential photography spanning a period of several weeks to differentiate perennial crops such as alfalfa from annual crops such as wheat. In the left photograph (taken in June), virtually all of the dark-tones fields are alfalfa; the additional fields which are dark-toned on the right photograph (taken in August) are, for the most part, annual crops.

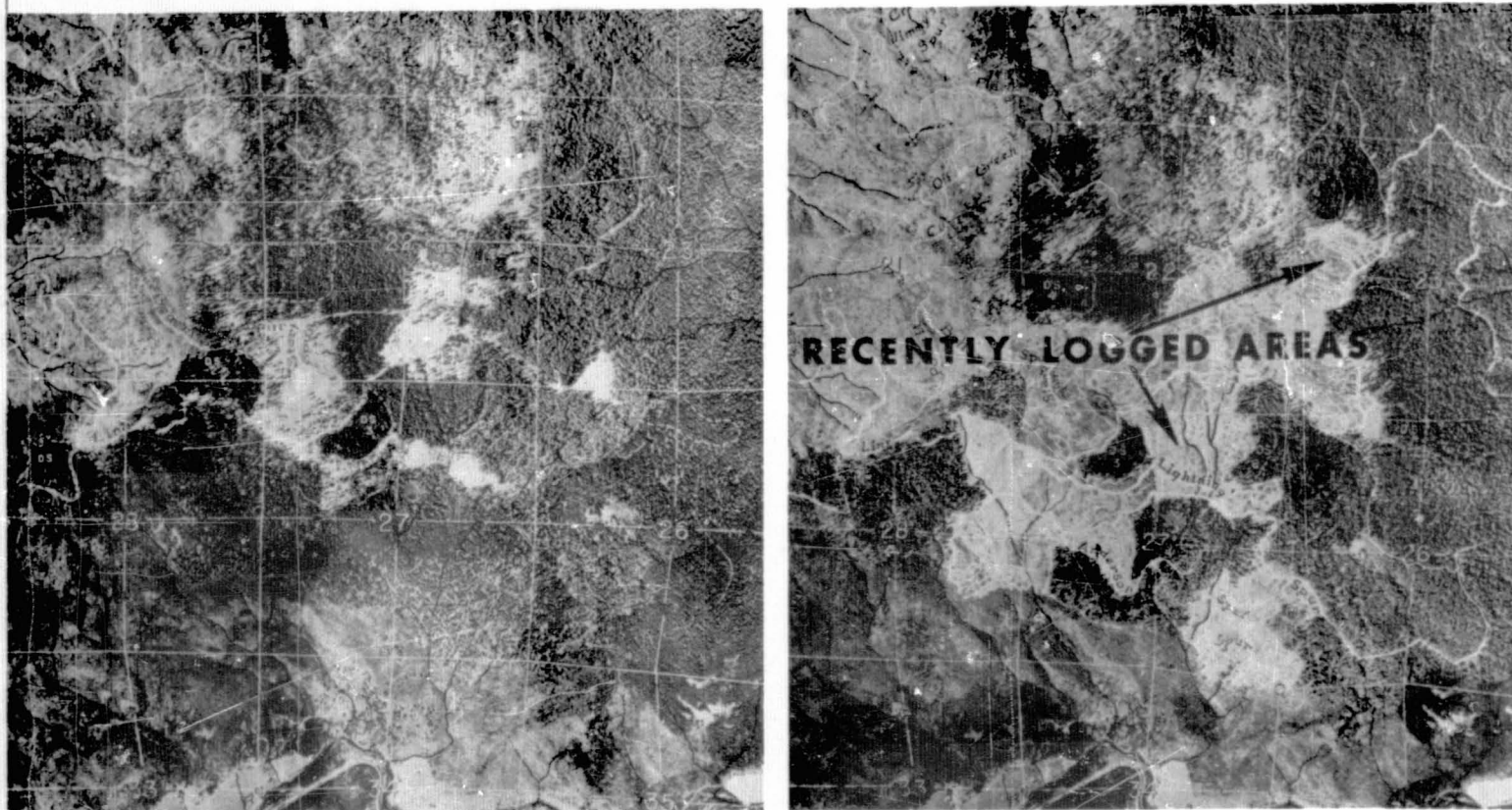
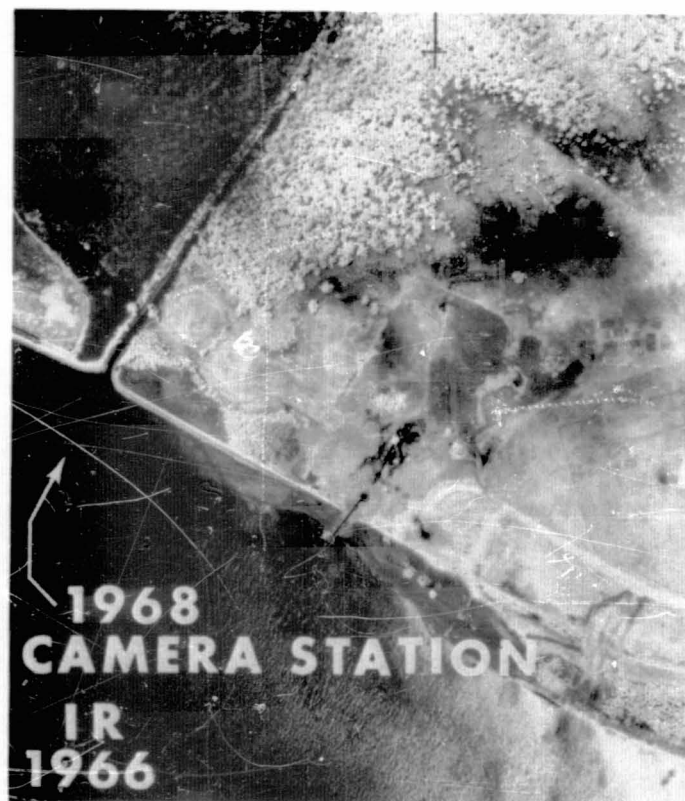
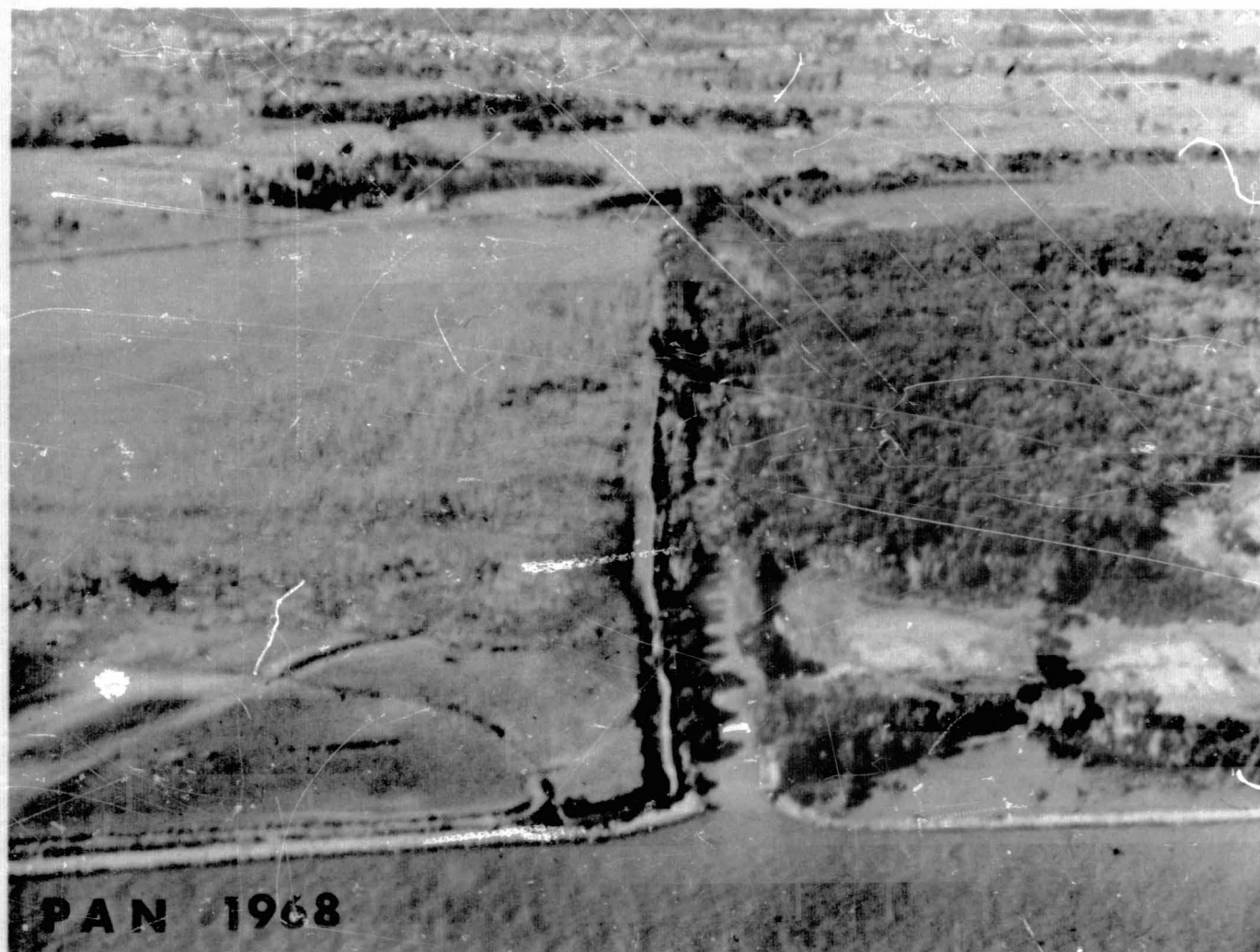


Figure 28-4.- These two panchromatic aerial photographs of a forested area in Oregon illustrate the use of sequential photography spanning a period of several months for determining the location and areal extent of timber harvesting operations, as explained in the text.



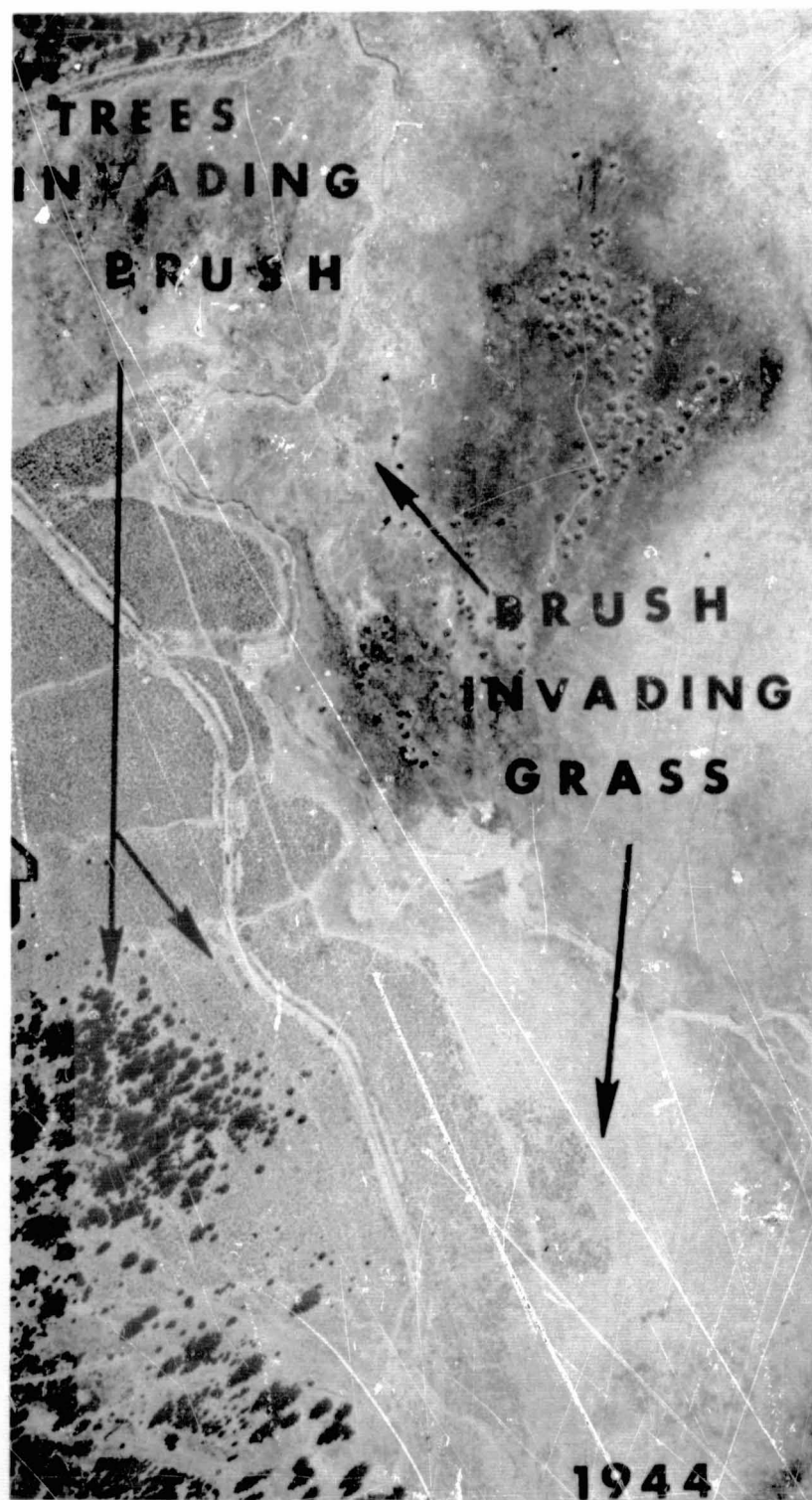
- a. Both the panchromatic and IR photographs were taken in December 1966 by the Australian Bureau of Mineral Resources (photographs courtesy of Ed Polak). Cloud shadows have affected somewhat the tone values of these two photographs. Nevertheless, on the panchromatic photograph there is essentially the same photographic tone for mangrove trees to left and right of the levee. On the IR photograph, however, the trees on the left of the levee are decidedly darker than those on the right, thereby providing previsual indications that they have lost vigor. In this case, the loss of vigor is the result of reclamation work which has resulted in the pumping of mud fill into the basin on the left of the levee (but not on the right), thereby causing inadequate aeration of the roots and consequent damage to the trees.

Figure 28-5.- The purpose of this sequential photography is to demonstrate the extent to which previsual symptoms of loss of vigor in plants can be made manifest through use of the proper wavelengths of radiant energy when taking the photographs. Shown here is a mangrove swamp near Brisbane, Australia.



- b. This photograph taken by Colwell in September 1968 shows, consistent with our predictions that had been made from a study of the earlier photography, virtually all of the trees on the left of the levee have died in the interim, whereas those on the right of the levee remain vigorous.

Figure 28-5.- Concluded.



a. 1944.

Figure 28-6.- These two panchromatic aerial photographs of an area in the Sierra Nevada Mountains of California illustrate the usefulness of sequential photography to detect changes which occur in a period of several years. Even from space photography, it should be possible to improve our understanding of the rate and direction of plant successional processes, provided that double or triple sampling techniques, employing large-scale aerial photographs and limited on-the-ground observation, are employed.



- b. 1968. From a comparison of the two photographs, it is evident that part of the grassland area has been invaded by brush and that part of the brushland area has been invaded by conifers during the intervening 24-year period.

Figure 28-6.- Concluded.

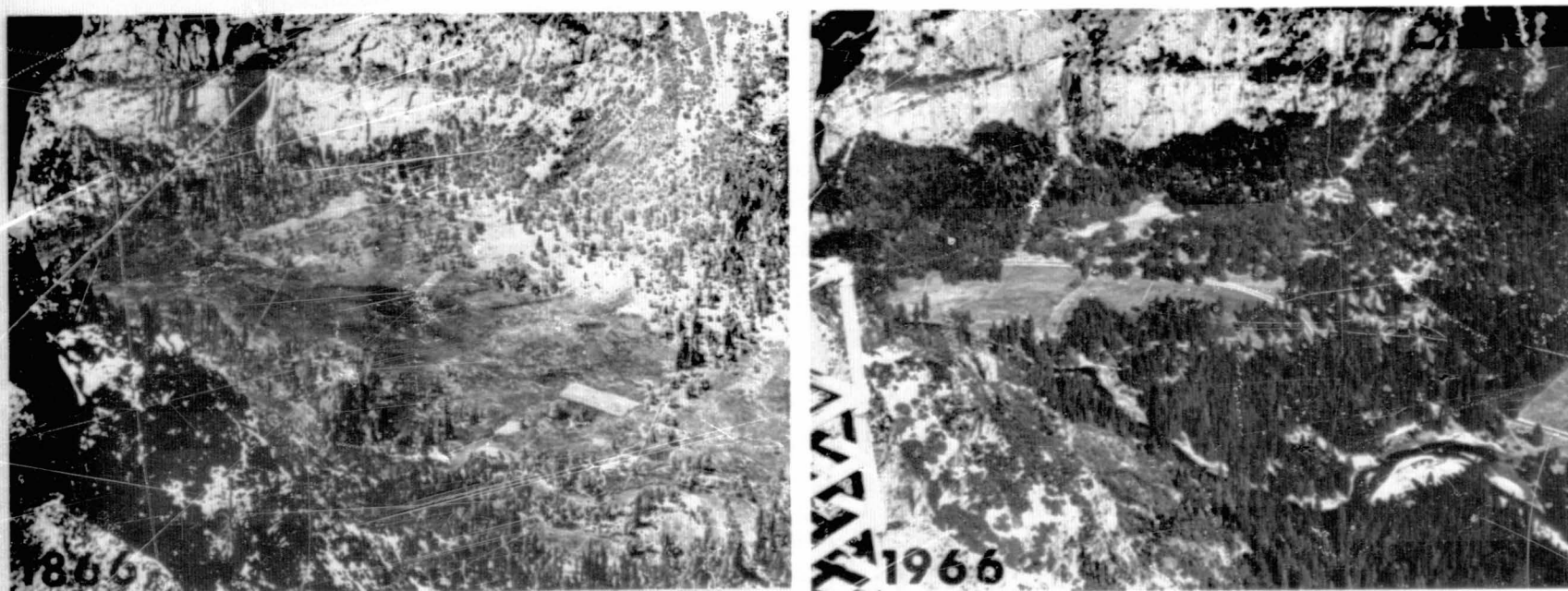


Figure 28-7.- The two members comprising this pair of sequential photographs are separated by a time interval of 100 years. Both were taken from exactly the same spot on Glacier Point, Yosemite National Park, and with the same camera orientation. Since the process of plant succession occurs very slowly on sites such as the one shown here, a time span of this length is highly desirable. Within 50 to 75 years, when sequential photography covering such a time span will be routinely available for most parts of the world, earth resource scientists will be able to acquire a much better understanding of plant successional trends that result from various kinds of land management.

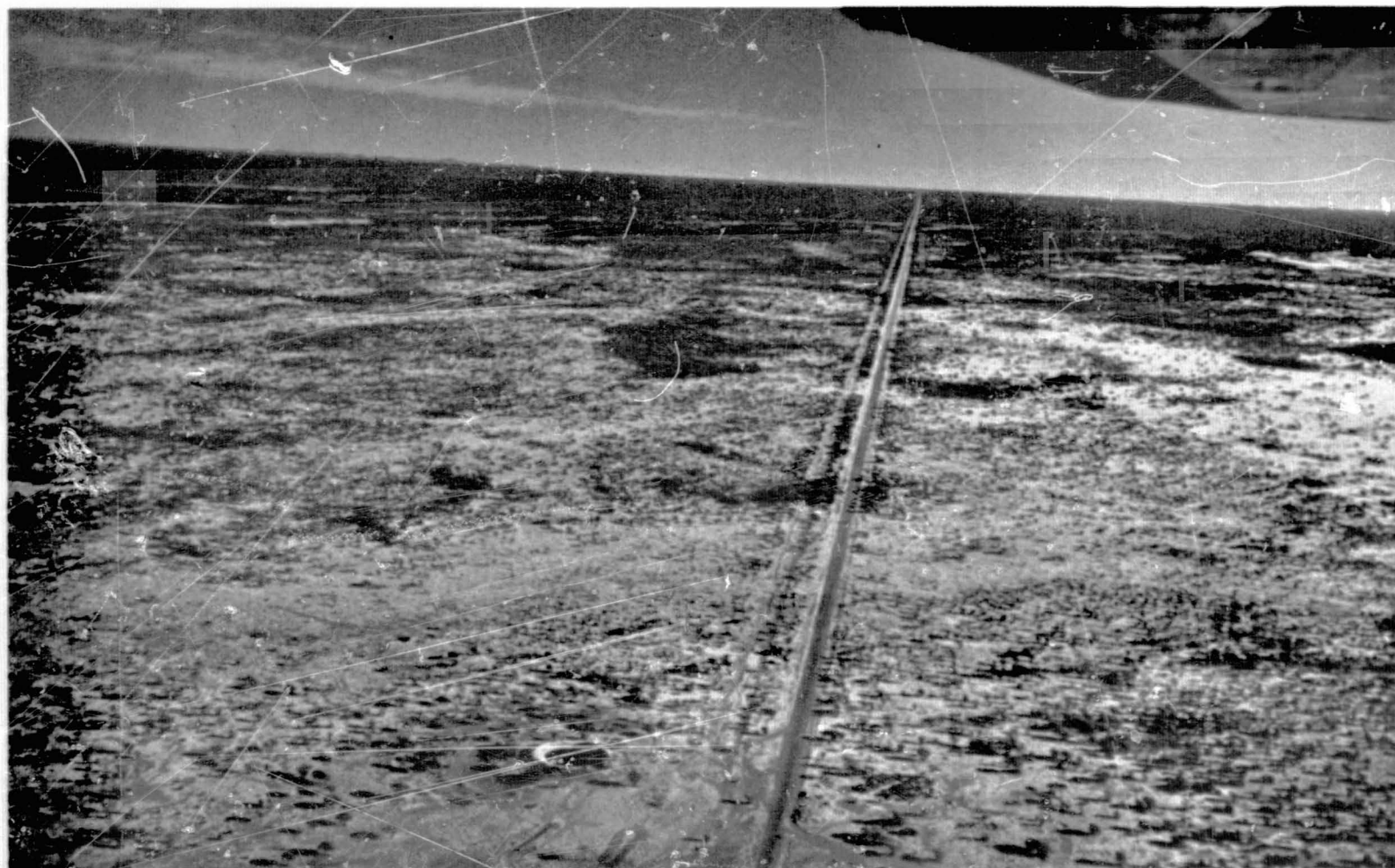


Figure 28-8.- An oblique aerial photograph taken from the point indicated on the Gemini photograph of figure 28-10. Note that the vegetation boundary separating mulga (a type of acacia tree, seen in the background) from spinifex (a type of grass seen in the foreground) is more difficult to draw consistently on this high-resolution photograph than on the low-resolution space photograph of figure 28-19.

28-29

28-30

NASA
S-65-45588



Figure 28-9.- Characteristic Central Australian topography appears in this photograph taken from the Gemini V spacecraft on August 27, 1965, from an altitude of 165 miles. For an indication of the accuracy with which resource boundaries can be delineated on photographs such as this, refer to the text.

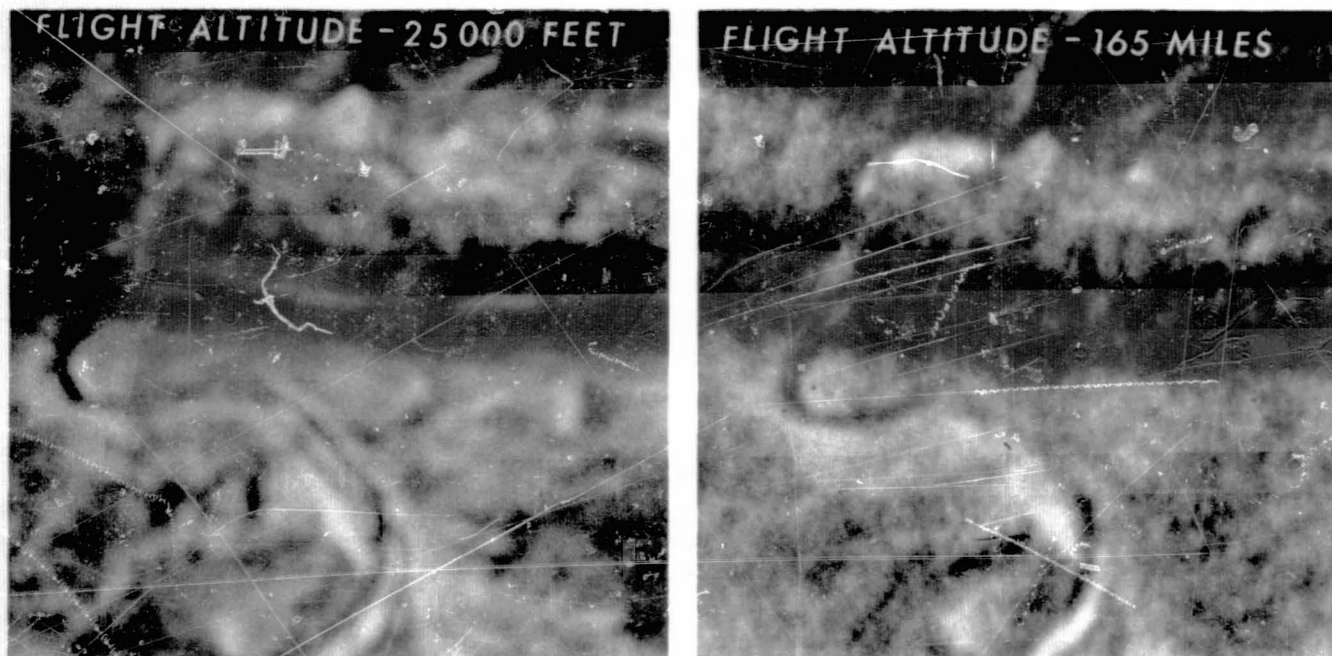
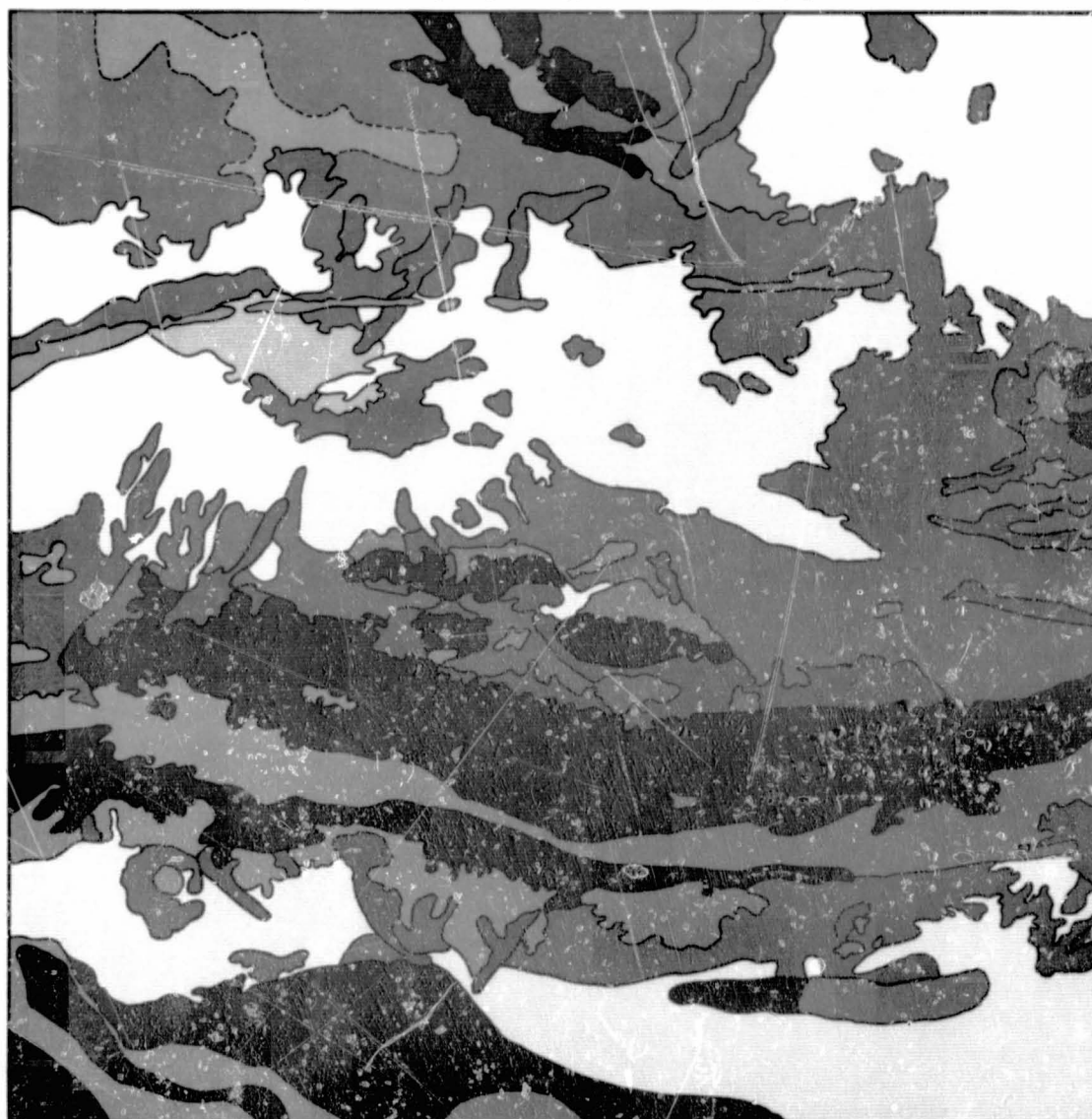


Figure 28-10.- Essentially the same tone values are exhibited by the aerial photograph on the left as on the matching space photograph on the right. This and numerous other examples being studied under the NASA Earth Resources Survey Program indicate that tone signatures derived from a study of the multiband aerial photographs currently being flown by NASA aircraft can be applied, with only moderate correction, to the interpretation of space photography. Spatial resolution on the aerial photograph has been purposely degraded to facilitate tonal comparisons.

28-32

Interpretation of major vegetation types on Gemini photography

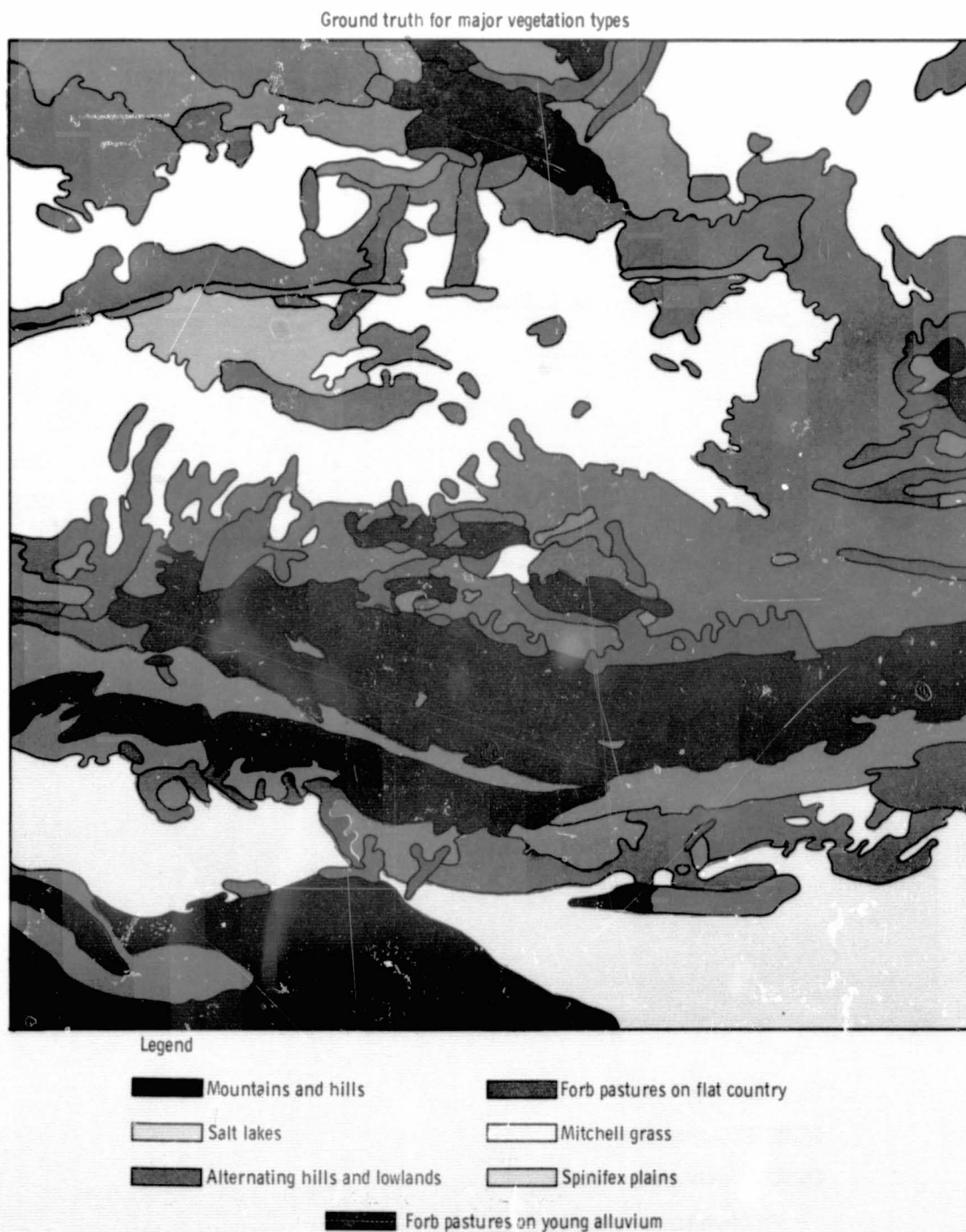


Legend

- | | |
|---|-------------------------------|
| Mountains and hills | Forb pastures on flat country |
| Salt lakes | Mitchell grass |
| Alternating hills and lowlands | Spinifex plains |
| Forb pastures on young alluvium | |
| ----- Boundary not seen on photo, but on ground survey. | |

a. Interpretation of major vegetation types on Gemini photography.

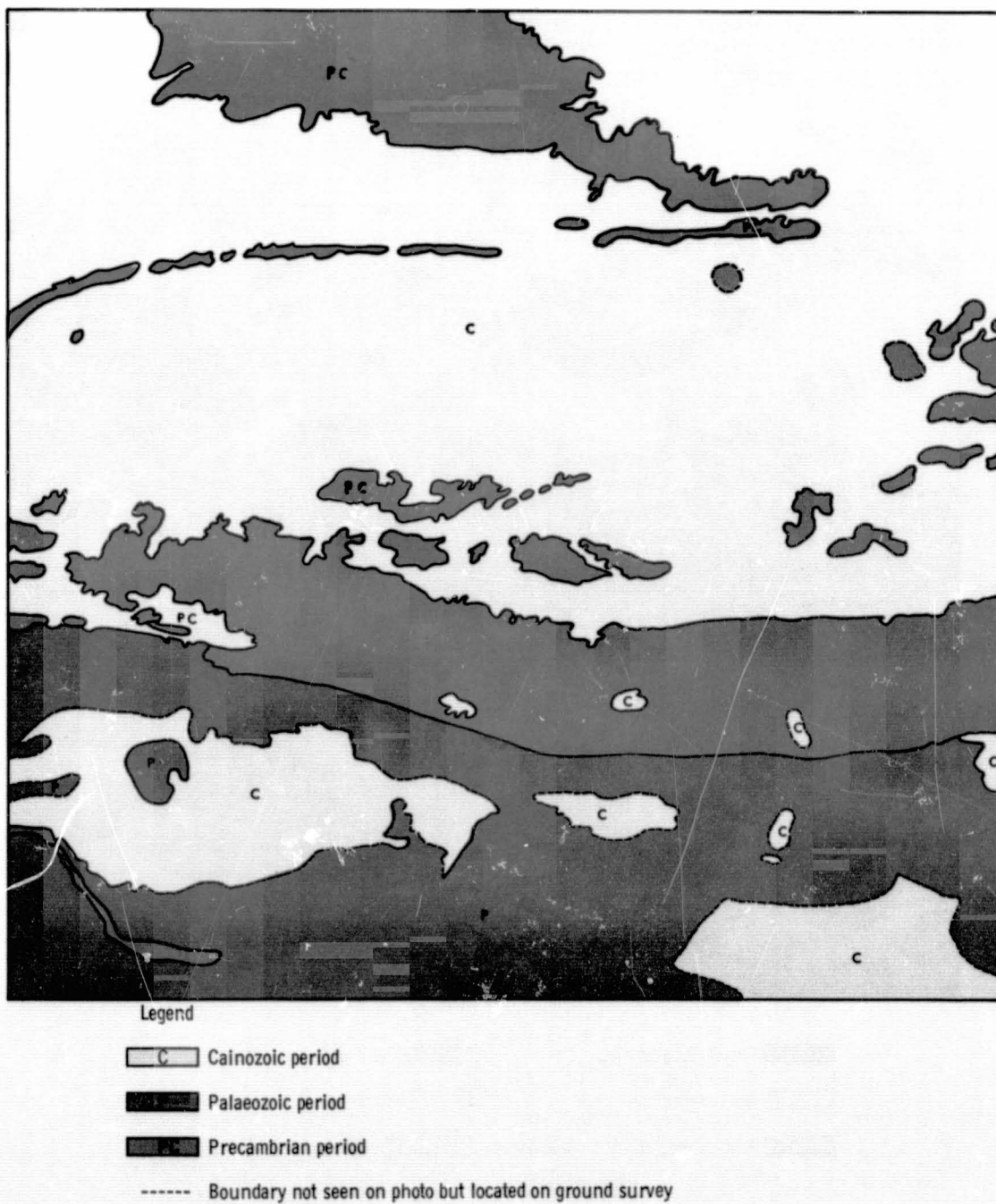
Figure 28-11.- These two maps permit a determination to be made of the accuracy with which boundaries of major vegetation types can be interpreted and delineated on space photography.



b. Ground truth for major vegetation types.

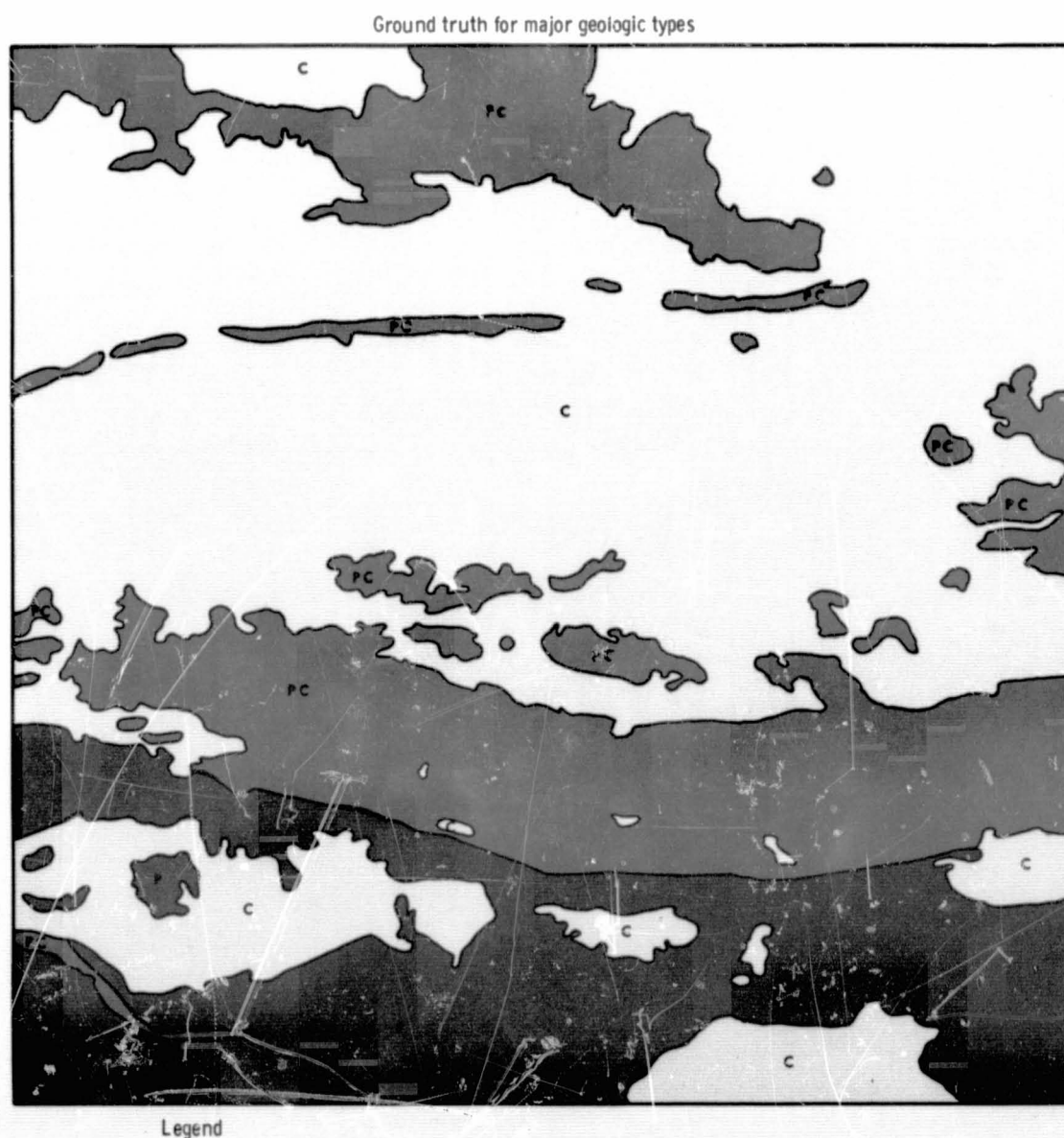
Figure 28-11.- Concluded.

Interpretation of major geologic types on Gemini photography



a. Interpretation of major geologic types on Gemini photography.

Figure 28-12.- These two maps permit a determination to be made of the accuracy with which boundaries of major geologic types can be interpreted and delineated on space photography.



b. Ground truth for major geologic types.

Figure 28-12.- Concluded.

N71-16149

INTEGRATION OF DETAILED LABORATORY AND FIELD

STUDIES WITH THE AIRCRAFT PROGRAM

By Victor I. Myers and Ross W. Leamer
U.S. Department of Agriculture

CHARACTERISTIC SIGNATURES OF EARTH OBJECTS FROM
SPECTROPHOTOMETER TRACES OF COLOR TRANSPARENCIES —
APOLLO MISSION 502 AND NASA AIRCRAFT MISSION 75

Introduction

The feasibility of performing earth-resource studies from space has been under study for some time. The National Aeronautics and Space Administration is supporting numerous research projects in various scientific disciplines to establish the feasibility of earth sensing from space and, even more important, to establish guidelines and principles which will permit interpretation of space imagery when Apollo applications missions become a reality.

Without any doubt, the initial earth-resources spacecraft will have photographic cameras as their prime sensing equipment. Much has been written recently concerning the advantages of multispectral remote-sensing techniques, including narrowband photography and scanning multichannel radiometers. While photographic systems have greater spatial fidelity, the scanning multichannel radiometer has outputs available for electronic processing in real time. Also the radiometer is not limited to wavelengths in the sensitive regions of photographic film and has other advantages beyond the scope of this discussion.

The human eye, as well as electronic instrumentation, has a much greater sensitivity to color differences than to shades of gray. As a result, there has been a considerable increase in the use of color photography. Black and white photography, especially multiband photography, has been projected as having certain advantages over color because of better resolution, exposure latitude, processing control, and others. However, there have been recent improvements in color fidelity, resolution, and cost which make the use of color very attractive for general usage for aerial photography.

It appears that, for determining plant and soil signatures, certain characteristics of color transparencies have not been fully exploited. Extraction of hue, value, and chroma can yield signatures of earth resources with tremendous potential for identifying earth objects from spacecraft or aircraft.

The Experiment

The objective of this study was to subject NASA spacecraft and aircraft photographic imagery to spectrophotometric analysis and to extract signatures of earth objects.

Apollo Mission 502 color photography was used for selection of areas to be scanned with a spectrophotometer. Figure 29-1 shows the sites where scans were made. The areas represented in the four photos are in North Texas. Frame AS6-2-1462 shows the cities of Dallas and Fort Worth. The spectrophotometer aperture, of 4 millimeters in diameter, was placed over the center of each circle. The light source, from a tungsten lamp, was transmitted through the aperture and transparency in each case. The 4-millimeter-diameter aperture represents an area on the ground of 425 meters.

A photoelectric detector was used to measure light transmittance. In a recording spectrophotometer, the results are plotted automatically to give a continuous record of the variation of transmission with wavelength, from which values of hue, value, and chroma, or CIE tristimulus values of X, Y, and Z can be obtained by integration or summation.

Figures 29-2 and 29-3 show the spectrophotometer scans with relative transmittance plotted against wavelength. Scans 1 and 2 are of the downtown areas of Dallas and Fort Worth. Scans 3, 4, 5, 6, and 7 are of agricultural areas, with variations in soil color and percent of scanned area cultivated. Rain had fallen over the entire area several days prior to the space flight.

NASA aircraft mission 75 over Weslaco, Texas, Site 32, provided photography for spectrophotometer scans of transmitted light through Ektachrome infrared (IR) transparencies. The scans are shown in figure 29-4. Some of the sites included in the study were cotton, sorghum stubble, pasture, bare soil, citrus, and ponded water. Scans for only cotton, pasture, bare soil, and water are shown in figure 29-4. The aperture diameter used in this case was 2 millimeters, representing 36 meters on the ground.

Discussion

Spectrophotometer scans of light transmitted through color transparencies, shown in figures 29-2 to 29-4, result in distinctive traces for earth-resource sites representing specific conditions. The wavelengths scanned include the visible spectrum. The possible variation in the shape of the traces is almost infinite because characteristics of hue, value, and chroma determine the shape of the curve in each case.

In addition to the influence of color on the shape of the curves in figures 29-2 to 29-4, characteristics of the spectrophotometer interference-filter wedge influence the shape. Normally a series of wavelength-dependent correction factors is applied to generate a corrected curve with true energy units. Corrections were not made for the traces included in this study.

In anticipation of the usual criticisms of color photography, it should be pointed out that many of the same criticisms can be leveled against any remote-sensing data-gathering system. There is one very important advantage that color photography has over electronic recording of narrowband energy, over recording of imagery using multispectral black and white photography, or over measuring densities of color transparencies through interference filters. The elements of wavelength (hue), strength of signal (value), and chroma are all recorded on color photography, but only wavelength and signal strength are recorded (or extracted) using the other analysis systems.

It is well known that in black and white photography, the limitation inherent in reproductions of only monochromatic gray tones can be only partly overcome by specific film-filter combinations that increase tonal contrast between conditions being compared in an earth-resources study. Even with this increased tonal contrast, the final result will be registered in a relatively limited range of black, gray, and white tones of which the human eye can distinguish only about 100 to 300. It is possible to make accurate distinctions between about 200 000 colors on the basis of hue, value, and chroma in using color aerial photography.

The suitable procedure for rapid analysis of space photography would be a scanning mechanism capable of recording information from color transparencies and color prints as well as from black and white transparencies and picture material.

The procedure described here can also be used for examining resolution elements of any size and for establishing the effect of spatial resolution on the accuracy of interpretation of space imagery.

Conclusions

Current plans for early Apollo missions, as well as NASA aircraft earth-resources missions, include photography as the prime sensor in visible and near-IR wavelengths. Automatic analysis of photography, particularly color photography, will be essential in taking advantage of the tremendous amounts of data contained in a single transparency. Procedures (of spectral scanning of specific points on a transparency with a spectrophotometer) described in this study demonstrate the fundamentals involved in generating scans having characteristic signatures that can be related to distinctive ground-cover conditions. The procedure uses the hue, value, and chroma characteristics of color photography which are not present in multispectral black and white photography or in electronic sensing. Ultimately, a suitable procedure for rapid analysis of space photography would be a rapid spatial-scanning mechanism capable of recording hue, value, and chroma from each resolution element of a color transparency. A computer, with a memory storage of characteristic scans such as those shown in this study, would then be able to automatically identify earth-resource features from the transparency.

EFFECT OF PARTIAL CROP CANOPY AND VARIABLE SUN ELEVATION ON REFLECTED RADIANCE

Purpose of Study

The purpose of this study was to determine the effect of time of day (sun elevation) on total illumination and shading of exposed soil between cotton rows and their effect on radiance as measured by a remote sensor. The study site was a field of double-row planted cotton with a 90-percent plant cover (fig. 29-5).

Data runs by the remote-sensing aircraft were made over the ground-study site at 14:18, 15:28, and 16:14 hours (central standard time) on July 25, 1968. Ground data were taken at the same times.

Ektachrome IR film (color IR) was used in the study because of the relative high film-density contrast between vegetation and soils on that film compared to others. Figure 29-6 is a black and white print, from an Ektachrome IR aerial transparency, of the cotton field shown in figure 29-5. It is the second of a series of three photos taken at the three flight times. The study site, where photos were taken and other related studies were conducted, is shown in figure 29-6.

Figures 29-7 and 29-8, taken at 15:28 hours and 16:14 hours, respectively, are pictures taken of the cotton field on the ground. Figures 29-5, 29-7, and 29-8 show, respectively, total illumination,

partial shading, and total shading of the soil between rows of cotton plants.

Ektachrome IR film has the unique capability of recording the high near-IR reflectance characteristic of plants. One layer of the film is sensitive to green, one layer is sensitive to red, and the third layer is sensitive to IR light. After processing, the colors blue, green, and red are formed, but the blue has resulted from green exposure, the green has resulted from red exposure, and the red has resulted from IR exposure.

Because plants and soils have contrasting exposure values on the three film layers, analytical densities of the layers, measured by inserting filters in the optical train of a microdensitometer, produce a trace that is meaningful in terms of vegetation and soil. The microdensitometer traces of figures 29-9 and 29-10 were produced by a scanning mechanism that has a resolution on the film of only a few microns. With that capability, crops in rows, and soil between rows in partial-plant canopies, can be resolved.

Microdensitometer traces were made on four scan lines across the cotton field on the color IR transparencies. The positions of the four scan lines are shown in figure 29-6. The traces are always made perpendicular to the planted rows. In making traces, four filters were used: (1) red, (2) green, (3) blue, and (4) no filter.

Figures 29-9 and 29-10 show microdensitometer traces for the four filters at the 14:18 hours flight time (for the no. 2 scan line). In each scan, highest densities are those of crops, and the lowest densities are those of soils.

Variable crop cover — 100, 60, and 0 percent — on Ektachrome IR transparencies was scanned on the microdensitometer. The results are shown in figures 29-11 to 29-13. Data means were computed for each of the filter-microdensitometer traces and standard deviations computed for some of the traces which were made for partial-crop-cover conditions. These data, except for the standard deviations, are shown in table 29-I.

The average optical density was measured for each scan line on the three transparencies representing the three sun angles at 14:18, 15:28, and 16:14 hours. The densities were measured using red, green, and blue filters, and no filter, as previously described.

The variability of reflectance from the cotton-crop canopy, as represented by optical density of the scan lines on the transparencies,

is shown in figure 29-14, plotted against time of day. The data are presented for average densities measured with the filters inserted in the microdensitometer.

Figure 29-14 shows in another way the variability of cotton-crop reflectance with increasing sun angle. Increasing optical density of the film transparency means less reflected light. The means computed for the microdensitometer traces at the three flight times were plotted in the figure for the blue and red filters and for no filter. The greatest change of optical density with time of day occurred using the blue filter.

Discussion

It is known that natural surfaces have widely varying reflection properties, the variation being dependent on total incoming radiation, dependence of reflectance on wavelength, angle of incidence, angle at which the surface is viewed, and the character of the surface of the material viewed. The variation of reflectance from partial-crop canopies where soil is showing between the rows is dependent on angle of incidence of the sun and results in substantial differences in radiance from crop-canopy radiances.

Figures 29-5, 29-7, and 29-8 show the progression of shading with time at three flight times. Similar shading of soil between crop rows might also result from the combination of east-west crop rows and a depressed sun angle in a more northerly latitude, in late summer or early fall when crops are maturing. The Ektachrome IR aerial photograph of figure 29-6 and those for the other flight times (not shown) also reveal very substantial contrasts in reflectance at the three flight times because of the progressive shading of the soil and a portion of the plants.

The cotton crop in this particular study is double-row planted, which results in a larger percentage of ground cover than would be the case if it were single-row planted.

The graphic technique of using a microdensitometer for scanning photographic film to measure color density changes, as seen in figures 29-9 and 29-10, provides accurate quantitative information. The microdensitometer operates as a flying-spot scanner and combines the speed and rapid coverage of a reconnaissance-oriented system, and the coordinate accuracy and optical-density responsiveness of a precision instrument.

Areas of mixed crops and soils on a photograph are greatly magnified at a ratio of 50:1 by the scanning process. Figures 29-9 and 29-10 illustrate the visual advantage gained by graphic magnification with

respect to clarification of the film-contained information. In addition to the graphical output, the microdensitometer wedge is coupled to an encoder which gives digital read-out on punched tape. The coded tape is fed into a computer which converts the coded values to optical density and makes other computations as described later.

The characteristic signatures of the microdensitometer traces are useful for identifying unique crop and soil patterns. The most useful of these signatures is the amplitude of the microdensitometer trace. Narrowband- or broadband-filtered light transmitted through a color transparency fluctuates in optical density when an area of alternating plants and soil is scanned.

The characteristic high IR reflectance from healthy crops registers on the IR-sensitive layer as bright red. The red, green, and IR-sensitive layers of the false-color film register soils as white, in shades of gray, or as some color other than red. Filtered red light is usually transmitted through the soil image on the transparency as readily as through the red plant image. The amplitude of the signal from the red layer, therefore, gives little clue to contrasts between plants and soil. Scanning a color IR transparency using white light (no filter) results in a trace similar to using filtered red light, although the amplitude of the trace is increased somewhat. The absence of almost all green and blue light in the red-plant-image layer, along with the presence of these colors in the soil image layer, results in an amplitude of the microdensitometer trace which is indicative of the plant-soil contrast.

An ideal uniform crop with uniform open soil between rows gives a sinusoidal pattern of transmittance, varying regularly and symmetrically between a minimum and a maximum. Departures from this ideal pattern are caused by irregularities in crop and soil conditions.

The microdensitometer traces of figures 29-9 and 29-10 are a set of traces made along a single scan line and thus are considered a family of curves. The statistical parameters shown in table 29-I, for figures 29-11 to 29-13, were computed, also, for the traces of figures 29-9 and 29-10.

The standard deviation computed for traces, representative of partial plant cover, can be interpreted as representing plants and soils. Because the highest values of optical density on each microdensitometer trace (made for a partial-crop-cover transparency) represent plants, and because lowest densities represent soils, the high and low limits of the standard deviation represent plants and soils, respectively. It is obvious that one cannot indiscriminantly use the standard deviation values, as in the case of 100- or 0-percent plant cover. Also, when soils are shaded by crops, the flying spot would measure higher optical densities for soils than for the case in which soils are sunlit.

There are two criteria, however, which help to establish the plant-cover condition. They are (1) the absence or presence of signal amplitude for the blue filter and (2) some computation such as Student's T test or an analysis of variance which would establish the extent of the spread in the means of the filter data in each case. The computations for item (2) have not been made as yet.

Figure 29-14 shows in another way the variability of reflectance from the cotton-crop canopy, with increasing sun angle. Plotted means for the blue filter show the greatest change of film optical density or change of reflectance. Part of the change in reflected energy from the crop with time of day was caused by a decrease in incoming solar radiation. The measured values of incoming and reflected radiance are shown in another part of this report.

Conclusions

Many of the problems associated with color photography and other forms of remote sensing have been and will continue to be solved as intensive research effort is brought to bear on them. The study described in this part of this paper is one that is representative of a number of studies at Weslaco.

The study showed that there was a substantial effect of sun elevation (time of day) on total illumination and shading of exposed soil between cotton rows. Partial shading of plants and shading of soil between planted rows caused by sun angle can result in radiance contrasts from crop canopies larger than differences in radiance that should be expected between crop varieties and conditions.

The combination of microdensitometer and statistical procedures used in this study should greatly enhance the opportunity for intelligent interpretation of aircraft and spacecraft photographic imagery. It should be emphasized that the use of microdensitometer traces for study and interpretation of detailed crop and soil background phenomena are essential to understanding the basic principles of interaction between the variables which make up the composite radiance signal in the larger resolution elements that will be typical of spacecraft imagery or optical-mechanical scanner imagery.

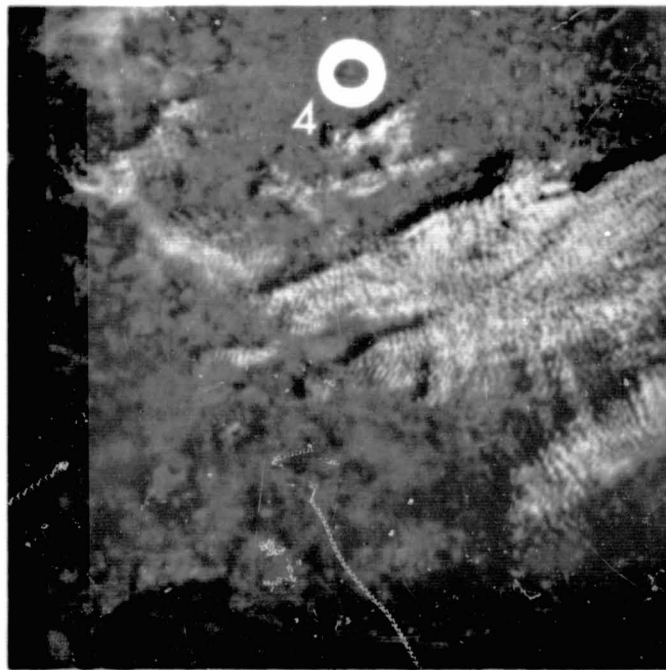
The microdensitometer and spectrophotometer instrumentation for studying imagery, although relatively slow for automatic interpretation of imagery, are useful research tools and have already identified the techniques that must be integrated in equipment that will be necessary for rapid interpretation of aircraft and spacecraft photographic imagery.

Table 29-I.- DATA MEANS FOR THE MICRODENSITOMETER TRACES
OF FIGURES 29-11 TO 29-13

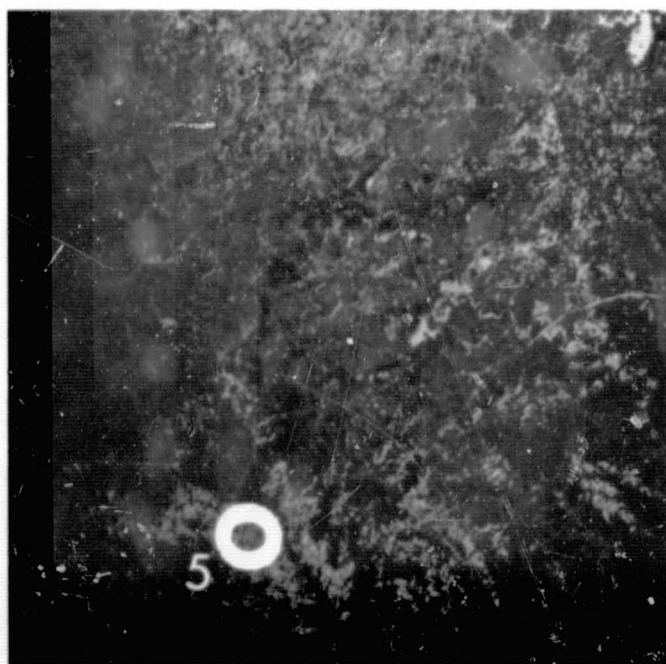
Crop cover and microdensitometer filter	Mean, \bar{x}
Cotton, 100-percent cover	
Red	0.48
None	1.18
Green	1.43
Blue	1.96
Cotton, 60-percent cover	
Red44
None93
Green	1.00
Blue	1.58
Bare Soil	
Red43
None57
Green61
Blue82

REPRODUCIBILITY OF THE ORIGINAL PAGE IS POOR.

29-10



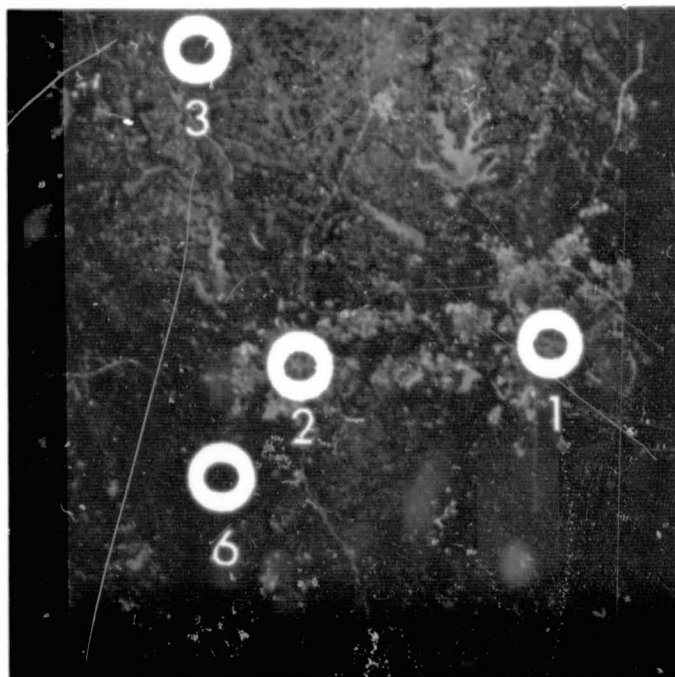
a. AS6-2-1454



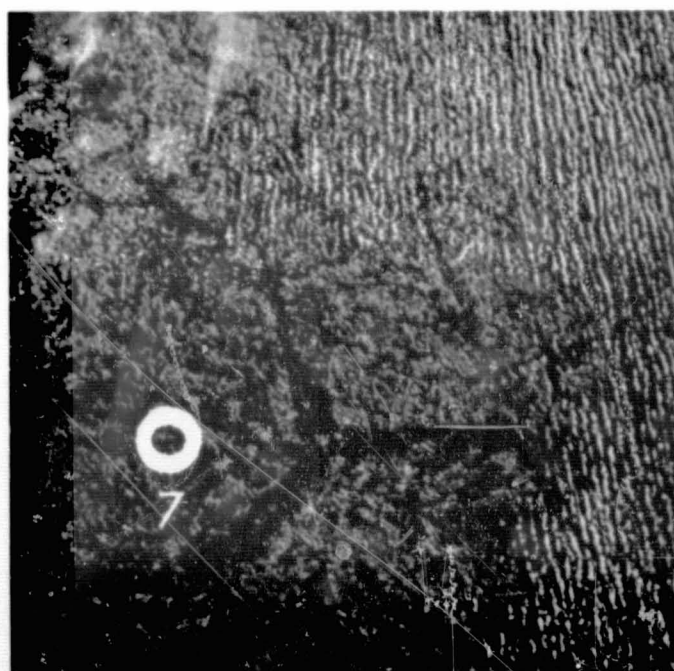
b. AS6-2-1460

Figure 29-1.- Apollo mission 502 color photography of areas in north Texas (April 4, 1968). Circles are of locations where scans, shown in figures 29-2 and 29-3, were made. Scale 1:3 600 000 — spacecraft altitude 128 statute miles.

29-11



c. AS6-2-1462



d. AS6-2-1483.

Figure 29-1.- Concluded.

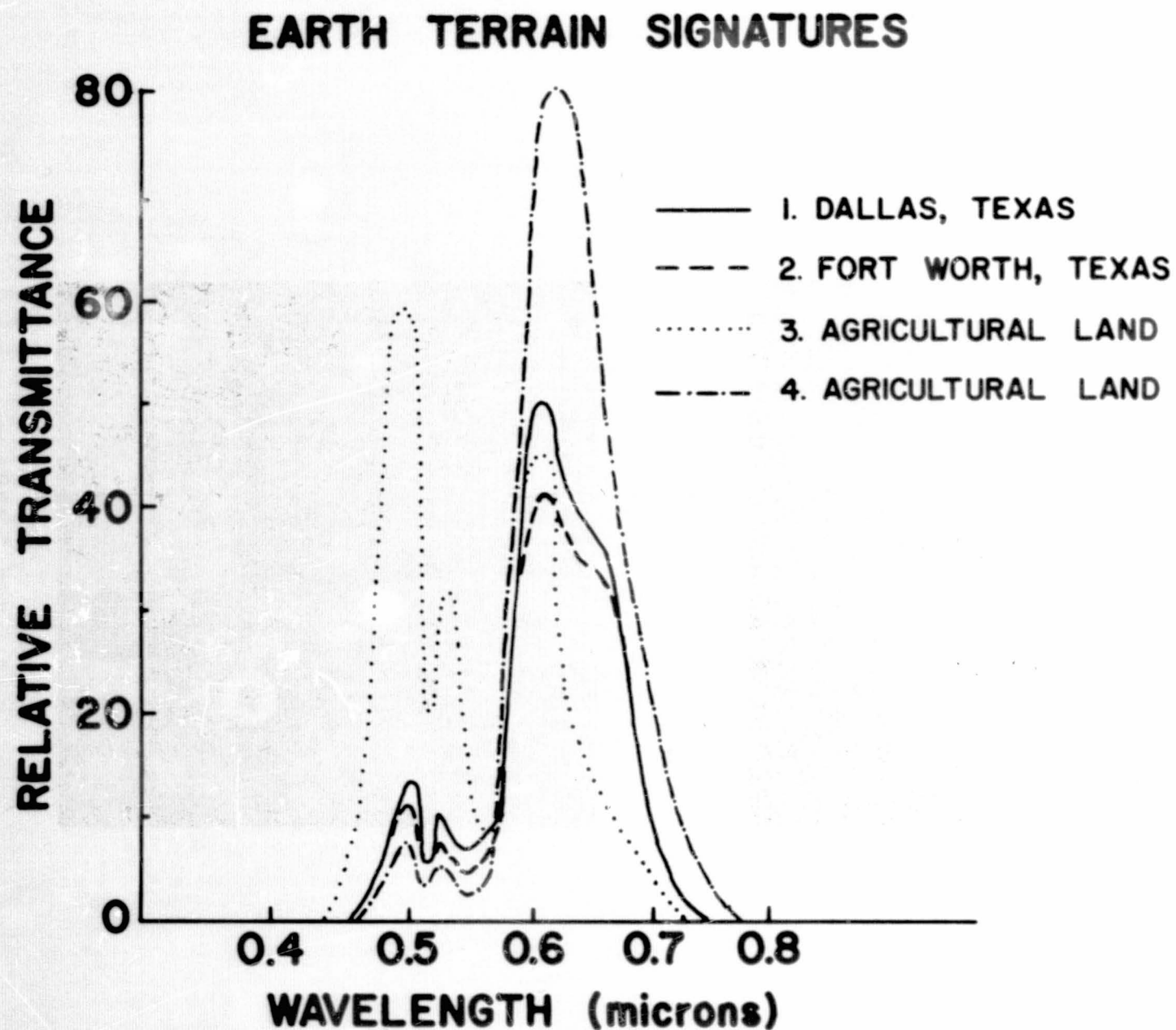


Figure 29-2.- Spectrophotometer scans of color transparencies from Apollo mission 502. See figure 29-1 for identification of areas scanned. Trace no. 4 was made with a 3 \times magnification.

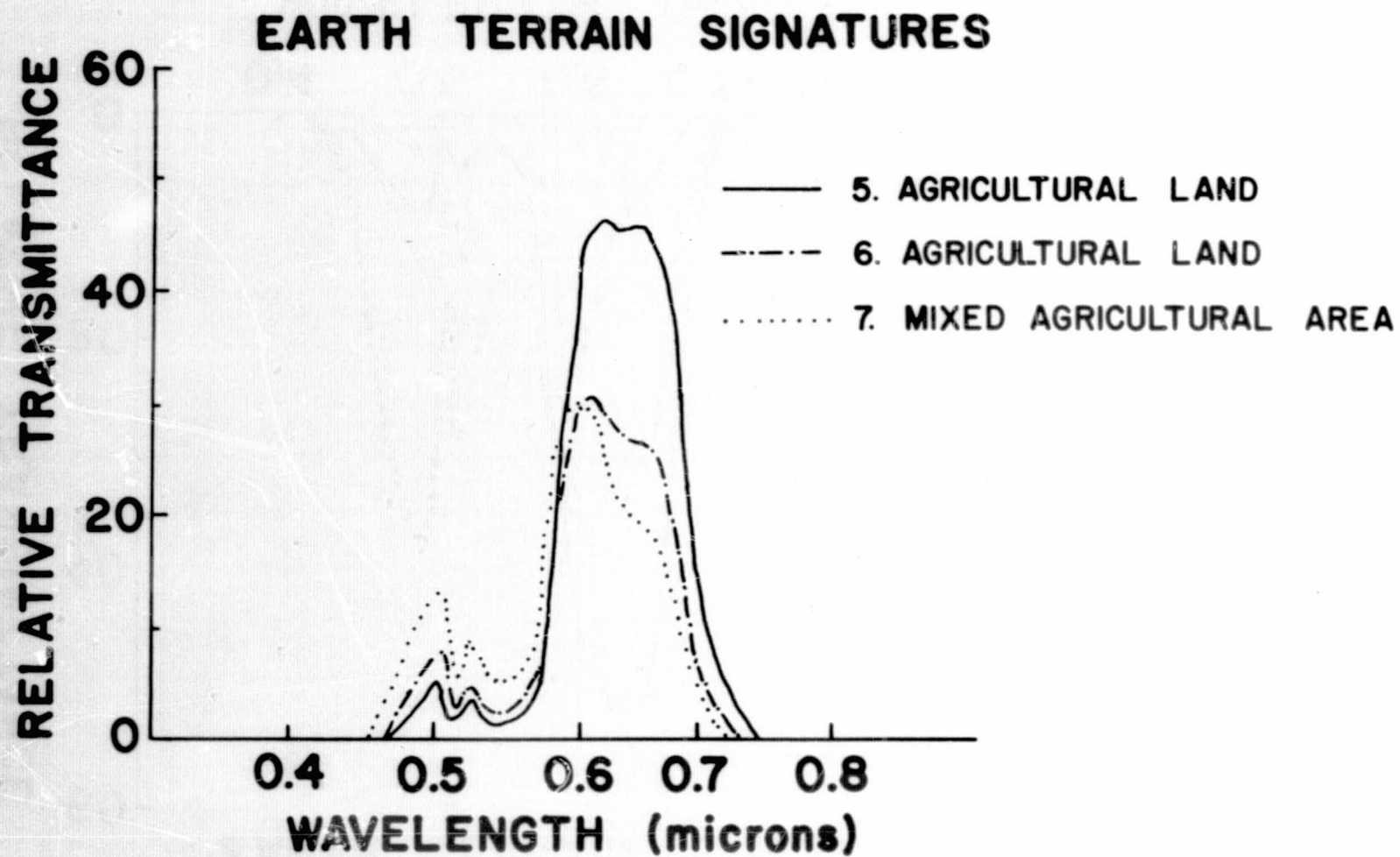


Figure 29-3.- Spectrophotometer scans of color transparencies from Apollo mission 502.
See figure 29-1 for identification of areas scanned.

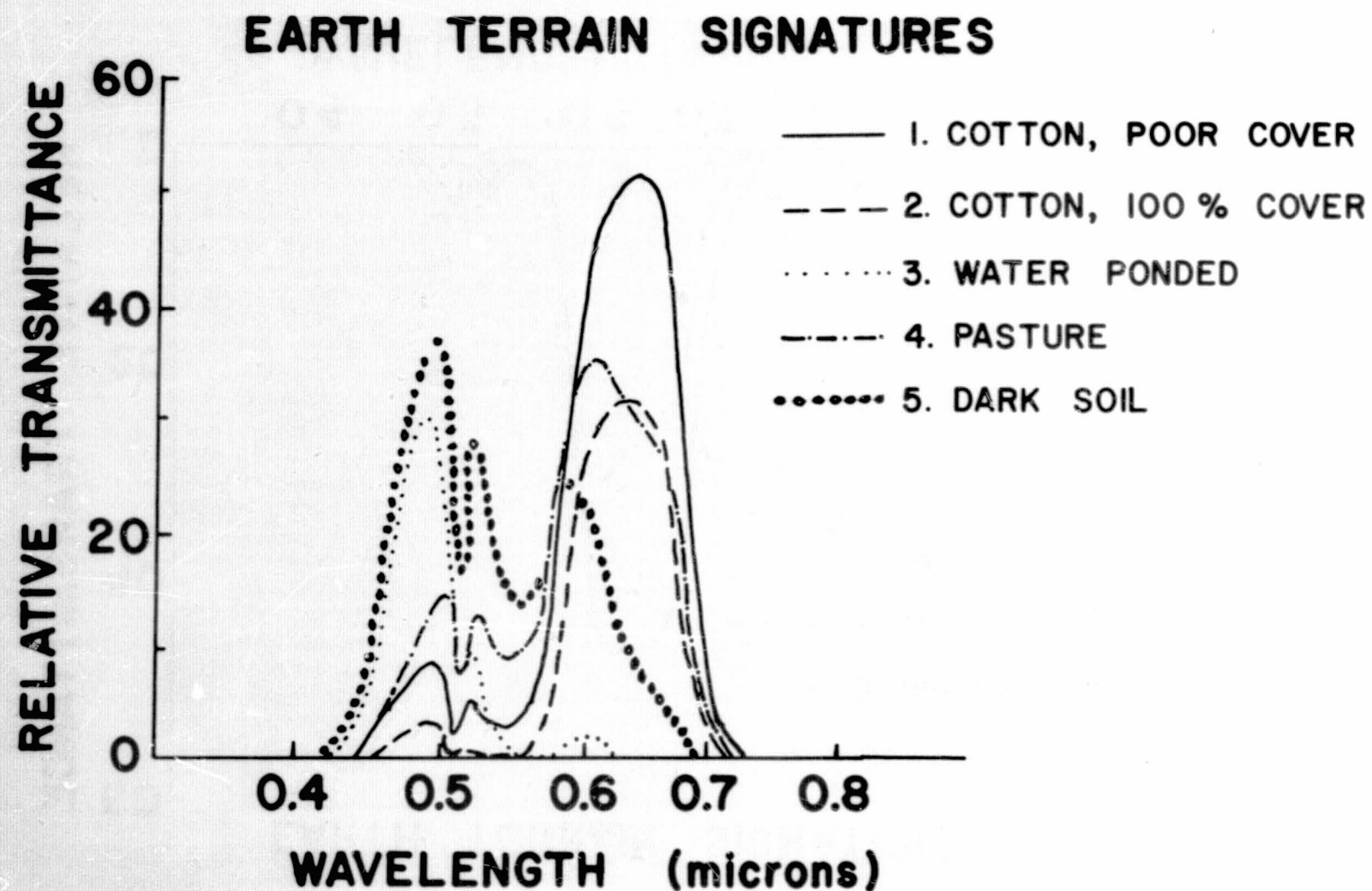
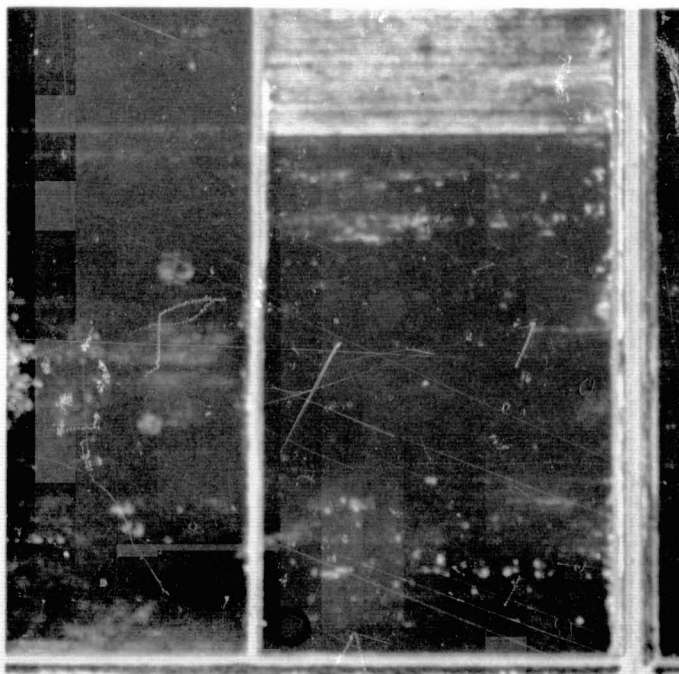


Figure 29-4.- Spectrophotometer scans of color transparencies from NASA aircraft mission 75, Site 32, Weslaco, Texas.



Figure 29-5.- Double-row planted cotton, showing total illumination of soil. Flight line 13, time 14:18 hours, July 25, 1968.



4321

Figure 29-6.- Black and white print from an Ektachrome infrared aerial transparency of cotton field shown in figure 29-5. Flight altitude 3000 feet, 15:28 hours, scale 1:18 000. (Circled area is site of detailed studies.)

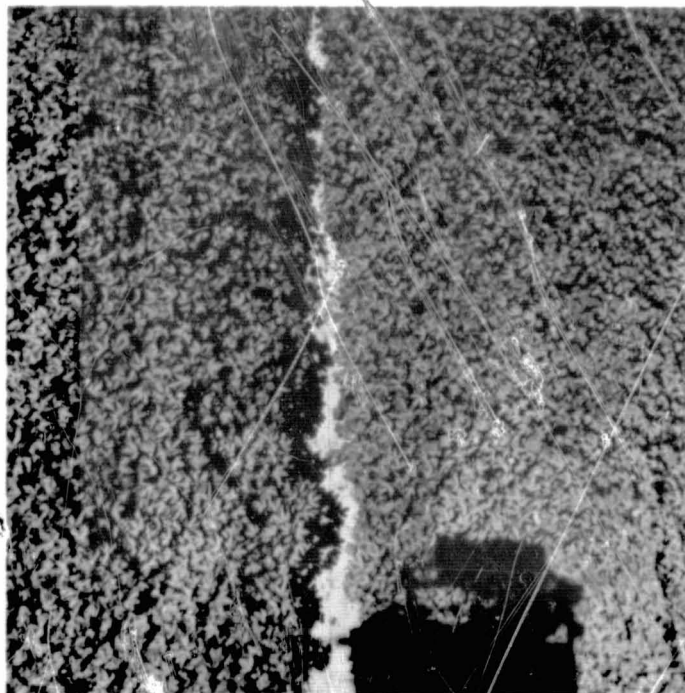


Figure 29-7.- Variable sun elevation study —
15:28 hours, showing partial shading of soil.
(Compare with figures 29-5 and 29-8.)



Figure 29-8.- Variable sun elevation study —
16:14 hours, showing total shading of soil.
(Compare with figures 29-5 and 29-7.)

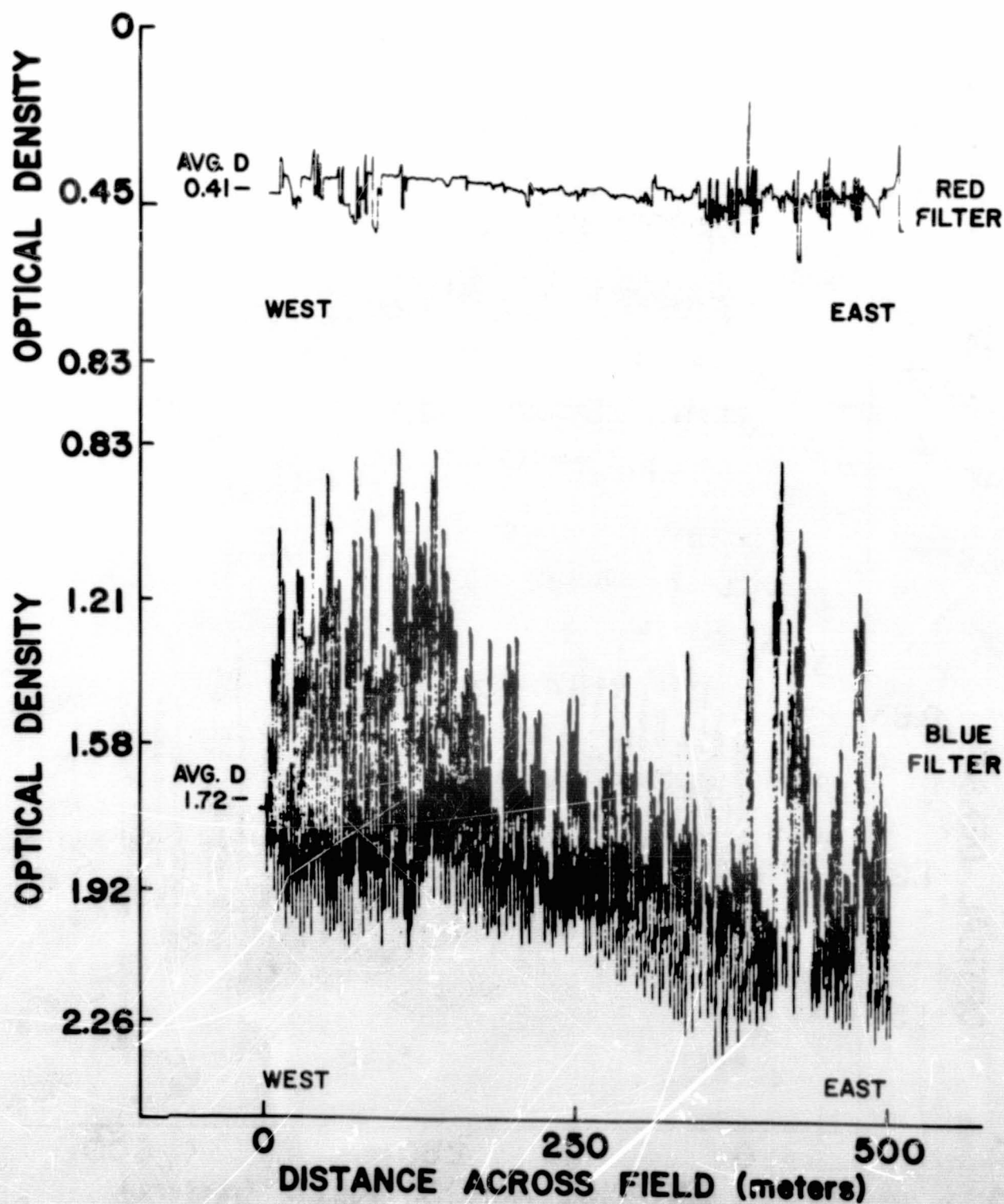


Figure 29-9.- Microdensitometer traces of the no. 2 scan line shown in figure 29-6 (red and blue filters at the 14:18 hours flight time).

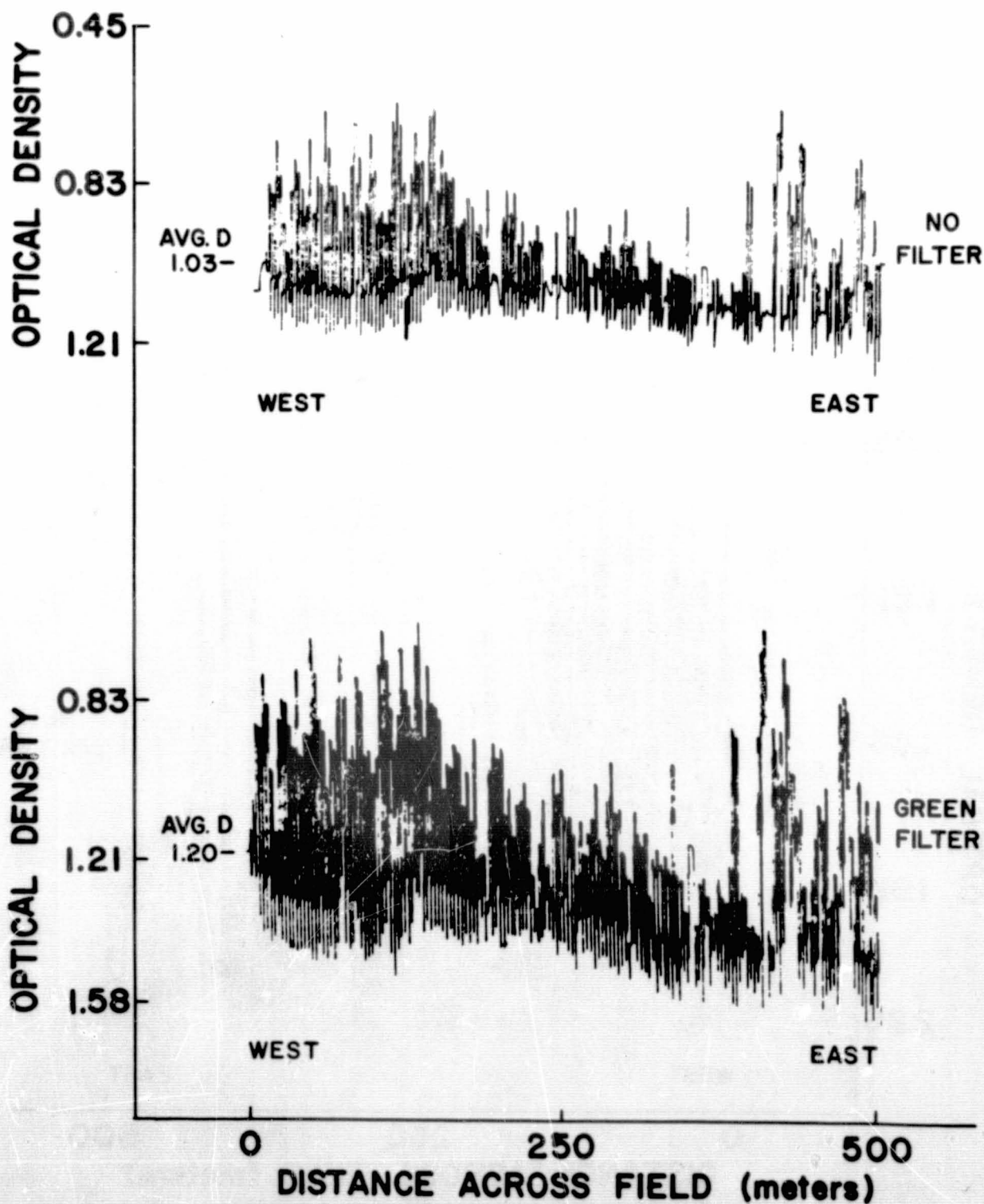


Figure 29-10.- Microdensitometer traces of the no. 2 scan line shown in figure 29-6 (green filter and no filter at the 14:18 hours flight time).

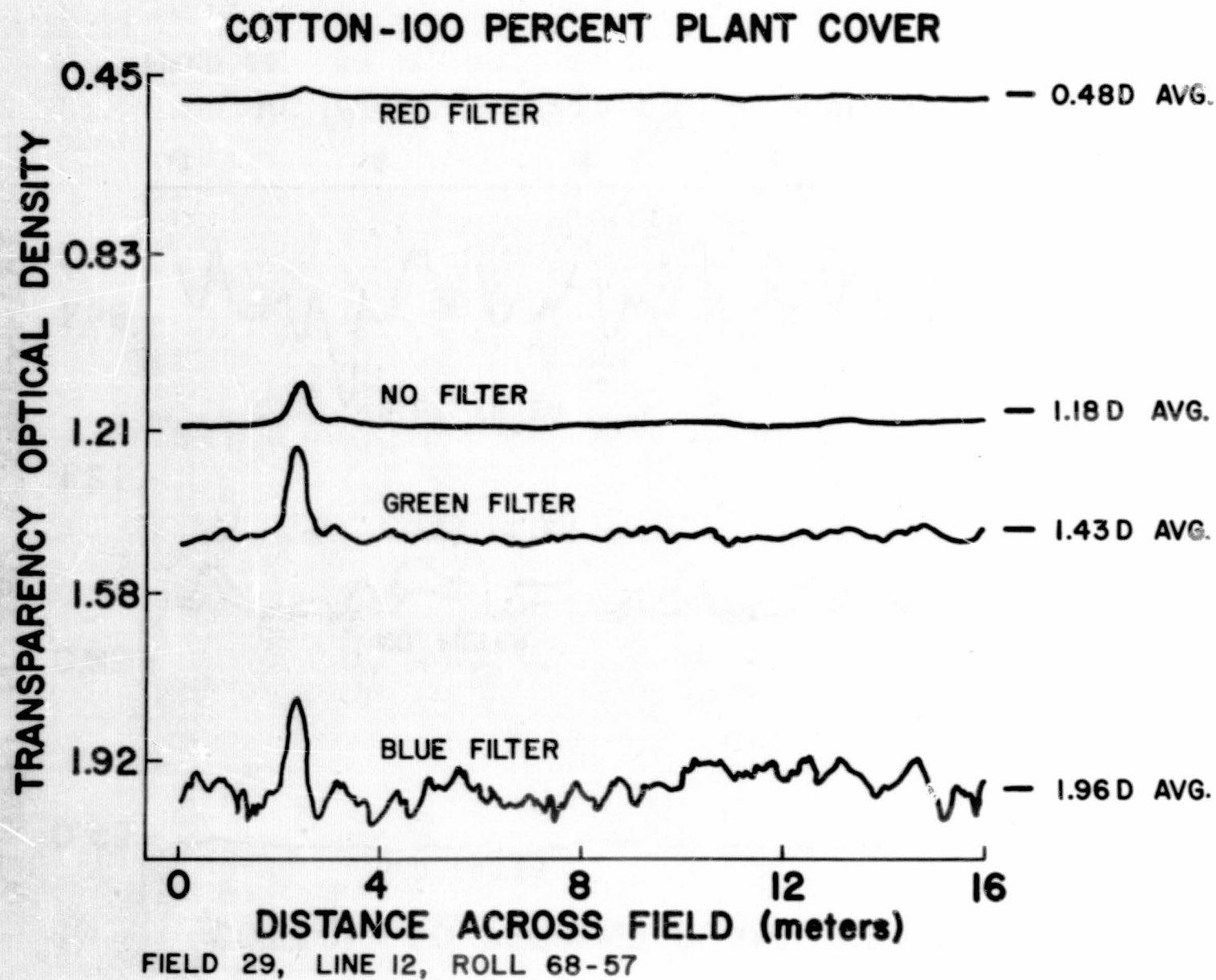
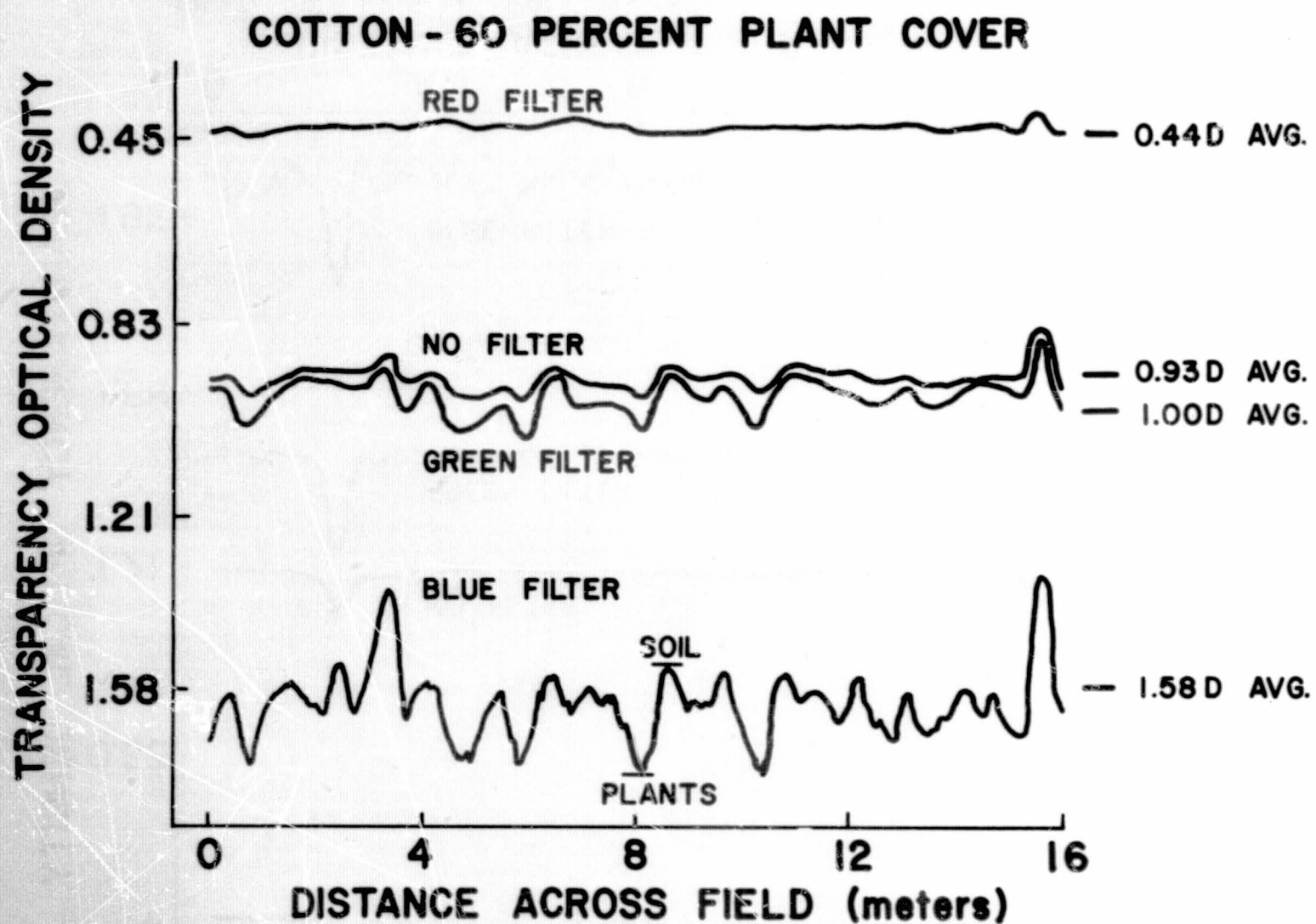


Figure 29-11.- Microdensitometer traces of cotton field, 100-percent plant cover.
Ektachrome IR film, G-15 filter, elevation 3000 feet.

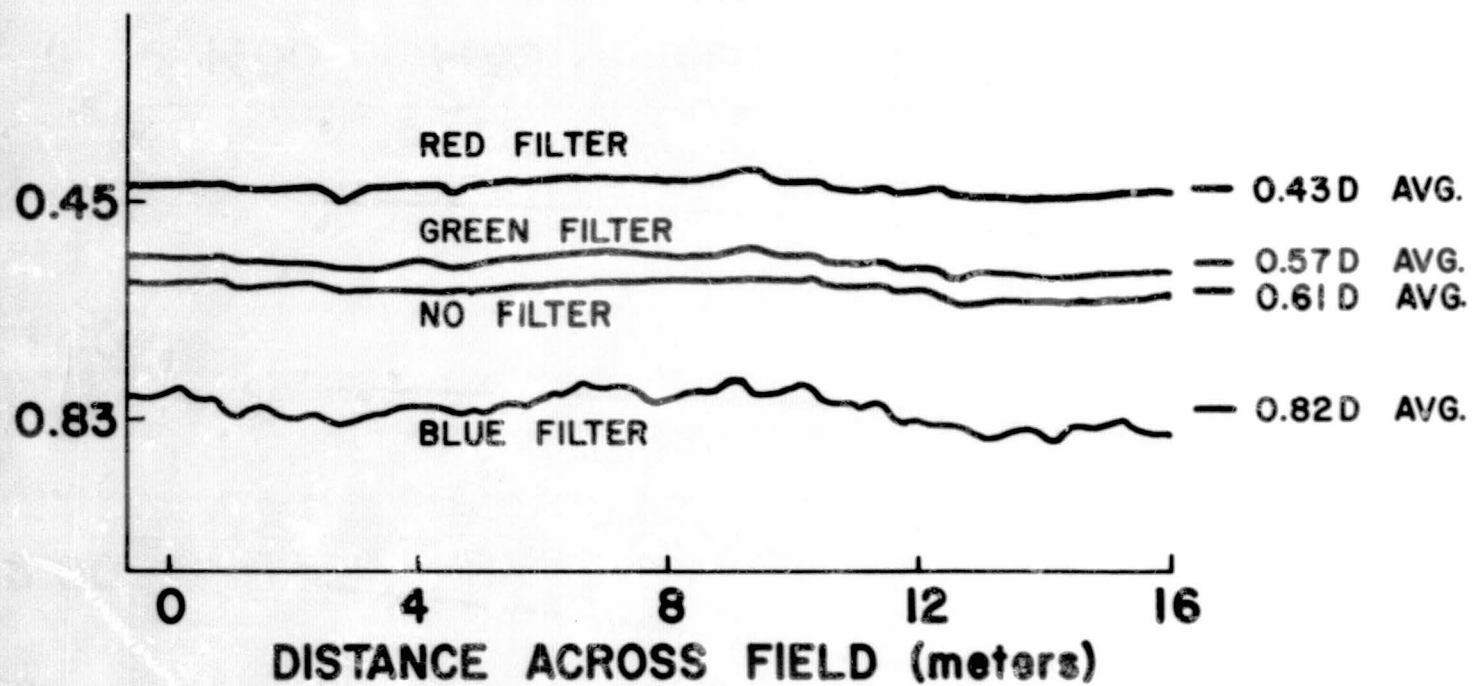


FIELD 53, LINE 12, ROLL 68-57

Figure 29-12.- Microdensitometer traces of cotton field, 60-percent plant cover.
Ektachrome IR film, G-15 filter, elevation 3000 feet.

TRANSPARENCY OPTICAL DENSITY

BARE SOIL



FIELD 52, LINE 12, ROLL 68-57

Figure 29-13.- Microdensitometer traces of bare soil. Ektachrome IR film, G-15 filter, elevation 3000 feet.

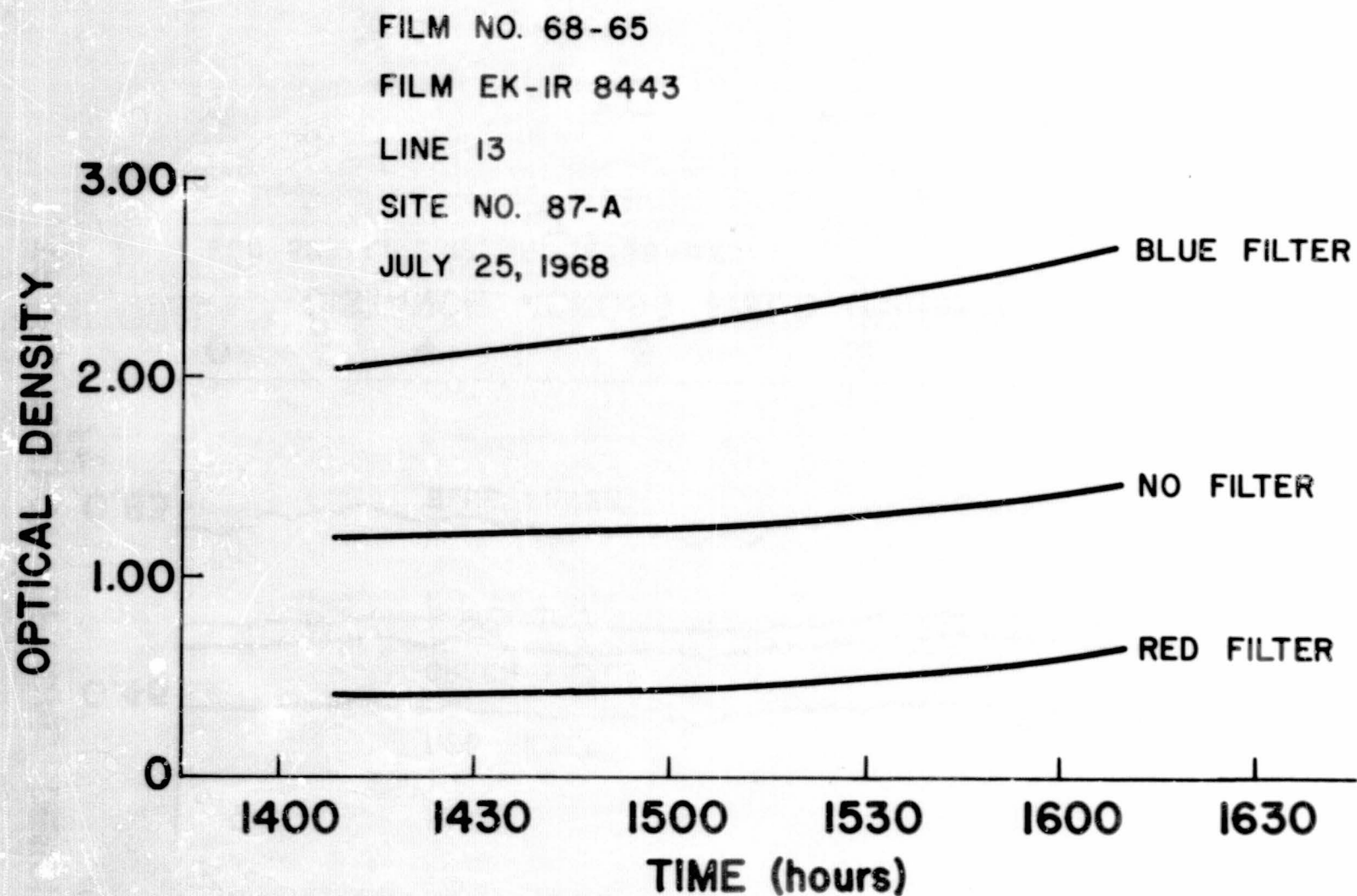


Figure 29-14.- Change in optical density of transparencies with change in sun angle (time), measured by a microdensitometer. Ektachrome IR film, G-15 filter, elevation 3000 feet.

N71-1615

CROP AND SOIL IDENTIFICATION FROM
AERIAL PHOTOGRAPHS*

By R. W. Leamer, Research Soil Scientist
and D. A. Weber, Physical Sciences Technician
U.S. Department of Agriculture, Weslaco, Texas

RESULTS ACQUIRED FROM THE USE OF DATA
FROM NASA AIRCRAFT

The purpose of this paper is to present a summary of preliminary examinations of aerial photographs taken in midsummer 1968 at Weslaco, Texas. NASA flight 75 flew the Weslaco flight lines during this time. The photographic imagery received to date from this mission was not adequate for the studies reported herein. Duplicate copies of the film have been requested but not yet received.

INTRODUCTION

The U.S. Department of Agriculture research program in remote sensing at Weslaco has, as one of its objectives, the determination of distinctive crop signatures and the identification of crops and crop conditions through the use of these crop signatures.

Crop signatures are a representation, in any of a number of forms, of the energy of the electromagnetic spectrum reflected from the crop or soil surface. The reflected energy may be measured in a number of ways; as analog voltage signals from sensors, as digital recordings of signals, or as densities on various photographic films.

*These studies were aided by contributions from the Soil and Water Conservation Research Division, Agricultural Research Service, U.S. Department of Agriculture, in cooperation with the Texas Agricultural Experiment Station, Texas Agricultural and Mechanical University. These studies were supported in part by the National Aeronautics and Space Administration under contract number 160-75-01-07-10.

This paper deals with the measurement of information on photographic film. This method, in common with most other analysis systems, is designed for development into an automated system by which desired information can be extracted by automatic data-handling equipment.

MATERIALS AND METHODS

Ground-truth information must be available to correlate the response of photographic film to ground conditions. At Weslaco, complete seasonal records are maintained of the actual conditions on the ground for all fields along the established flight lines. Ground observations are made periodically, as necessary, to maintain an up-to-date record of crop and crop conditions. These periodic records are updated as necessary to give information on crop height, crop condition, percent soil cover, soil moisture, and plant appearance at the time of an overflight by an instrumented plane. The same ground-truth information is required for calibrating remote sensors other than photographic film.

Measurement and interpretation of photographic film at Weslaco is being automated by use of a Joyce, Loebel isodensitracer¹ with a digital encoder and a paper-tape punch attached. The current operation is to have the exact areas from which ground-truth data were collected marked on each frame of each film. A scan representing from 20 to 50 feet on the ground is run on the isodensitracer. The film density is read along this scan line, and the digital values are punched in the paper tape.

The Joyce, Loebel isodensitracer is a dual-beam instrument with one beam going through the film and the other through a standard wedge with uniform variation of density from end to end. The two beams impinge on a pair of photoelectric cells connected to potentiometers. The photoelectric cell, measuring the light through the standard wedge, controls a motor which moves the wedge to the point where the density of the wedge equals the density of the film. The position of the standard wedge when the two beams are balanced is the measurement recorded as the density of the film.

For black and white film, densities are measured with unfiltered white tungsten light. Densities of colored films are measured with red,

¹Trade names and company names are included for the benefit of the reader and do not imply an endorsement or preferential treatment of the product listed by the U.S. Department of Agriculture.

green, and blue, as well as with white light. The colored beams are produced by passing each beam through identical colored filters. The readings produced are thus measurements of color densities on the film. The wavelengths of the peak transmission of the filters match closely the peak sensitivity of the three layers in the colored film.

The readings from the isodensitracer are coded in digital form on-to paper tape. The paper tape containing scans from several fields in one or more frames of the film is read into a computer. The data may then be manipulated at will to produce the information available on the film.

The intensity of selected wavelength bands of light reflected from target areas is determined by measuring the densities of the colors in colored film and by using multilens cameras with a variety of film/filter combinations. The spectra thus developed form the basis for identifying crop signatures. Photographs taken at various times through the growing season, as crops expand, fruit, mature, and are harvested, form a seasonal crop signature that helps identify each crop and crop conditions.

RESULTS AND DISCUSSION

The main crops growing at Weslaco on July 1, 1968, when NASA flight 75 flew that area were cotton and sorghum. At that time, both crops had developed so that ground cover, as measured by the ground-truth crews, was 50 percent or more. Both crops were green and showed very little difference in color or cover. Each crop occupied enough fields of the established flight lines to give a statistical measure of the variation within each.

Results have been obtained from Ektachrome infrared (IR) film and from a cluster of four Hasselblad cameras. The Hasselblads contained the following film/filter combinations:

<u>Camera</u>	<u>Film</u>	<u>Filter</u>
1	Ektachrome IR	None
2	Black and white IR	None
3	Tri-X Aerochrome	Green
4	Tri-X Aerochrome	Red

From these combinations, black and white IR film gave the clearest separation of the two crops. Optical density of this black and white film of the cotton fields averaged 1.7152 with a standard deviation of 0.2068. Sorghum fields averaged 1.1875 with a standard deviation of 0.1734. There was no overlapping of ranges; either actual or normal distribution measured as mean ± 1 standard deviation. The highest sorghum density was lower than the lowest cotton reading. The normal distribution ranges were separated by almost a full standard deviation. The ratio of mean cotton density to mean sorghum density is 1.44 to 1.00.

Infrared color film densities measured with no filter, or with a red filter, did not distinguish between cotton and sorghum in early July. The ranges on different fields and different films overlapped so that the differences in averages are of doubtful value in distinguishing between cotton and sorghum when both are in full vegetative stage of growth.

CONCLUSION

This information is not presented as an argument against the use of color IR film in remote sensing. The inference is that any information available should be used and that very simple sensors such as black and white IR film can produce useful information.

An understanding of the basic factors causing various wavelength bands to be reflected as they are is necessary to get a reliable crop signature. An understanding of the reflection spectra also aids in the development of new sensors by pointing out the wavelength bands in which crops or crop conditions can be identified.

W71-16151

REFLECTANCE AND STRUCTURE OF CYCOCCEL-TREATED

COTTON LEAVES, Gossypium hirsutum L.*

By H. W. Gausman, Research Plant Physiologist
R. Cardenas, Biologist
W. A. Allen, Research Physicist
V. I. Myers, Research Agricultural Engineer
and R. W. Leamer, Research Soil Scientist
U.S. Department of Agriculture, Weslaco, Texas

RESULTS ACQUIRED FROM THE USE OF DATA
FROM NASA AIRCRAFT

The purpose of this paper is to relate Cycocel-induced changes in internal structure of cotton leaves to reflectance, transmittance, and absorptance of near-infrared light. A further understanding of the relation of light reflectance to the internal structure of leaves will help interpret the data obtained from NASA aircraft.

INTRODUCTION

Tolbert (refs. 30B-1 and 30B-2) first reported the plant-growth-regulating properties of CCC or Cycocel ((2-chloroethyl) trimethylammonium chloride). The chemical formula is $(\text{CH}_3)_3\text{N}^+-\text{CH}_2-\text{CH}_2\text{Cl}\cdot\text{Cl}^-$.

Cycocel induces wider, greener, thicker leaves and shorter internodes on several plant species (refs. 30B-3 to 30B-7). Anatomically, Cycocel increased cell wall thickness and number of vascular bundles in the wheat stem (ref. 30B-8). Cycocel has been tested on cotton

*These studies were aided by contribution from the Soil and Water Conservation Research Division, Agricultural Research Service, U.S. Department of Agriculture, in cooperation with the Texas Agricultural Experiment Station, Texas Agricultural and Mechanical University. These studies were supported, in part, by the National Aeronautics and Space Administration under contract number 160-75-01-07-10.

(ref. 30B-9), with the objective of dwarfing plants to facilitate defoliant application and mechanical harvesting.

MATERIALS AND METHODS

Cotton leaves, variety Stoneville A, were obtained from a replicated field trial with Cycocel¹. The three treatments used were (1) two rates of Cycocel, 100 and 200 g/ha (0.545 and 1.090 lb/A), applied as a spray in enough water for runoff, and (2) a control treatment in which plants were sprayed with only the amount of water used for applying the Cycocel treatments. Treatments were applied 76 days after planting, at the bloom stage of plant growth. Ten leaves from the fourth node down from the top of the cotton plants were harvested for each treatment 92 days after planting. The leaves were wrapped immediately in Saran Wrap² to minimize water loss. The leaves were the same age, since treated and untreated plants had an equal number of nodes. In the laboratory, five leaves were randomly selected from each of the three groups of 10 leaves for reflectance and transmittance measurements. Spectra presented herein represent mean values for each set of five leaves.

The thickness of each leaf was measured at three locations, utilizing a linear displacement transducer and digital voltmeter (ref. 30B-10). The area of leaves was calculated using the method recommended by Johnson (ref. 30B-11).

Spectral diffuse reflectance on upper (adaxial) surfaces of single leaves and transmittance were measured with a Beckman Model DK-2A spectrophotometer with the reflectance attachment over the wavelength interval 500 μ to 2500 μ . Data have been corrected for a decrease in spectral diffuse reflectance of the MgO reference caused by deterioration during aging (ref. 30B-12).

¹The field experiment was conducted by M. D. Heilman and C. E. Gonzalez.

²Trade names and company names are included for the benefit of the reader and do not imply an endorsement or preferential treatment of the product listed by the U.S. Department of Agriculture.

Pieces of tissue taken near the center of leaves approximately one-half inch on either side of the midrib were fixed in formalin-acetic-acid-alcohol (ref. 30B-13). Tissues were dehydrated with tertiary butyl alcohol, infiltrated and embedded with paraffin (melting point about 52° C), and stained with safranin-fast green. Transverse sections were obtained with a rotary microtome. Photomicrographs were made with a Zeiss Standard Universal Photomicroscope at a magnification of 79. Enlargements of photomicrographs presented in this paper represent transverse sections having a thickness of 12 μ .

Analysis of variance (ref. 30B-14) was conducted on data.

RESULTS AND DISCUSSION

Cycocel-treated cotton plants had shorter internodes and thicker, larger leaves. Heights of untreated plants and Cycocel-treated plants at 100 and 200 g/ha were 108, 86, and 82 centimeters, respectively. Leaf thickness and area per leaf will be considered later.

Cycocel treatments, 200 versus 100 g/ha, had essentially the same influence on the reflectance and transmittance of cotton leaves with the largest differences approximated at 1 percent. Thus, this discussion will be generally limited to a comparison of results for the 100-g/ha Cycocel application to the control treatment. Further, the 750 μ to 1350 μ spectral range will be emphasized because it is affected by leaf structure; absorptance by pigments and water is negligible. Absorptance by pigments dominates the range of 500 μ to 750 μ , and the region above 1350 μ is greatly influenced by the amount of water in the tissue. The strongest water absorption bands occur at approximately 1450 μ and 1950 μ .

Figure 30B-1 shows that treatment with 100 g/ha of Cycocel increased the reflectance of cotton leaves approximately 5 percent (statistically significant, $p = 0.01$) over the wavelength range 750 μ to 1350 μ , compared to results for untreated leaves. As indicated later, increased reflectance was correlated with more intercellular spaces in the mesophyll of Cycocel-treated leaves which increased scattering. Increased scattering for Cycocel-treated leaves also seems apparent between 1600 μ and 1900 μ . However, beyond 1900 μ , light absorption by water apparently offset the effects of scattering, and the two spectra coincide. In this respect, Cycocel treatments significantly increased the percentage ($p = 0.01$) of moisture in leaves. Average values were 59.1, 67.1, and 69.8 percent for the control, 100-g/ha, and 200-g/ha treatments, respectively.

The 100-g/ha Cycocel treatment significantly decreased transmittance ($p = 0.01$) over the entire wavelength range of 500μ to 2500μ (fig. 30B-2). The decrease over the range of 500μ to 750μ was probably caused by internal structural changes in leaves and by increased plastid content, although chlorophyll determinations were not made in this study. The decrease over the range of 750μ to 1350μ was caused by changes in the internal structure of leaves which enhanced scattering, thereby increasing reflectance and decreasing transmittance. Beyond 1350μ , the decrease in transmittance may be accredited to additive effects of water absorption and scattering.

Absorptance was calculated according to the following formula: percent absorptance = $100 - (\text{percent reflectance} + \text{percent transmittance})$. The 100-g/ha Cycocel treatment increased absorptance 10 percent at 550μ , 2 to 3 percent over the range of 750μ to 1350μ , and 10 and 11 percent at water absorption bands of 1450μ and 1950μ , respectively.

Figure 30B-3 shows photomicrographs of transverse sections of cotton leaves from 100-g/ha Cycocel-treated and untreated plants. Untreated leaves had a more compact cellular arrangement in the leaf mesophyll with fewer and smaller intercellular spaces in the spongy parenchyma. This type of structure was associated with lower reflectance and higher transmittance over the 750μ to 1350μ wavelength range (figs. 30B-1 and 30B-2). Treatment with Cycocel induced statistically significant expansion and thickening ($p = 0.01$) of the leaf which gave more and larger intercellular spaces in the spongy parenchyma. This type of structure gave higher reflectance and lower transmittance over the 750μ to 1350μ wavelength range (figs. 30B-1 and 30B-2). Average areas per leaf were 77 and 96 cm^2 , and average thicknesses were 0.18 and 0.25 millimeter for untreated and 100-g/ha Cycocel-treated leaves, respectively.

CONCLUSION

Cycocel-treated leaves had more intercellular spaces in the spongy parenchyma. These caused increased reflectance and decreased transmittance, particularly over the 750μ to 1350μ range in which the influence of internal leaf structure is highly important. Results support the theory of Willstätter and Stoll (ref. 30B-15) in that reflectance was increased because light passed more often from a high (water, 1.33) to a low (air, 1.0) refractive index, and light was reflected at critical angles.

REFERENCES

- 30B-1. Tolbert, N. E.: (2-Chloroethyl) Trimethylammonium Chloride and Related Compounds as Plant Growth Substances, I. Chemical structure and bioassay. J. Biol. Chem. 235:475-479, 1960.
- 30B-2. Tolbert, N. E.: (2-Chloroethyl) Trimethylammonium Chloride and Related Compounds as Plant Growth Substances, II. Effect on Growth of Wheat. Plant Physiol. 35:380-385, 1960.
- 30B-3. Humphries, E. C.; and Wheeler, A. W.: The Physiology of Leaf Growth. In: Ann. Rev. Plant Physiol. 14:385-410, 1963.
- 30B-4. Appleby, A. P.; Kronstad, W. E.; and Rohde, C. R.: Influence of 2-Chloroethyltrimethylammonium Chloride (CCC) on Wheat (*Triticum aestivum* L.) When Applied as a Seed Treatment. Agron. J. 58:435-437, 1966.
- 30B-5. Goodin, J. R.; McKell, C. M.; and Webb, F. L.: Influence of CCC on Water Use and Growth Characteristics of Barley. Agron. J. 58:453-454, 1966.
- 30B-6. Larter, E. N.: The Effect of (2-Chloroethyl) Trimethylammonium Chloride (CCC) on Certain Agronomic Traits of Barley. Can. J. Plant Sci. 47:413-421, 1967.
- 30B-7. Adedipe, N. O.; Ormrod, D. P.; and Maurer, A. R.: Response of Pea Plant to Soil and Foliar Applications of Cycocel ((2-Chloroethyl) Trimethylammonium Chloride). Can. J. Plant Sci. 48:323-325, 1968.
- 30B-8. Mayr, H. H.; and Presoly, E.: Investigations with Chlorcholin-chloride (CCC)-treated Wheat Plants. Anatomical-morphological Results. Z. Acker. u-Pflanzenbau 118(2):109-124, 1963. Cited by Goodin et al. (1966).
- 30B-9. Thomas, R. O.: Effects of Application Timing and Concentration of 2-Chloroethyltrimethylammonium Chloride on Plant Size and Fruiting Responses of Cotton. Crop Sci. 4:403-406, 1964.
- 30B-10. Heilman, M. D.; Gonzalez, C. L.; Swanson, W. A.; and Rippert, W. J.: Adaption of a Linear Transducer for Measuring Leaf Thickness. Scheduled for publication in Sept.-Oct. Issue of Agron. J., 1968.
- 30B-11. Johnson, R. E.: Comparison of Methods for Estimating Cotton Leaf Area. Agron. J. 59:493-494, 1967.

30B-6

- 30B-12. Sanders, C. L.; and Middleton, E. E. K.: The Absolute Spectral Diffuse Reflectance of Magnesium Oxide in the Near Infrared. J. Opt. Soc. Am. 43:58, 1953.
- 30B-13. Jensen, W. A.: Botanical Histochemistry. W. H. Freeman & Co., San Francisco, Calif., 1962.
- 30B-14. Steel, R. G. D.; and Torrie, J. H.: Principles and Procedures of Statistics. McGraw-Hill Book Co., New York, 1960.
- 30B-15. Willstätter, R.; and Stoll, A.: Untersuchungen über die Assimilation der Kohlensäure. Springer-Verlag, Berlin, 1918. After Sinclair, T. R.: Pathway of Solar Radiation Through Leaves. M. S. Thesis, Purdue University Library, Lafayette, Indiana, 1968.

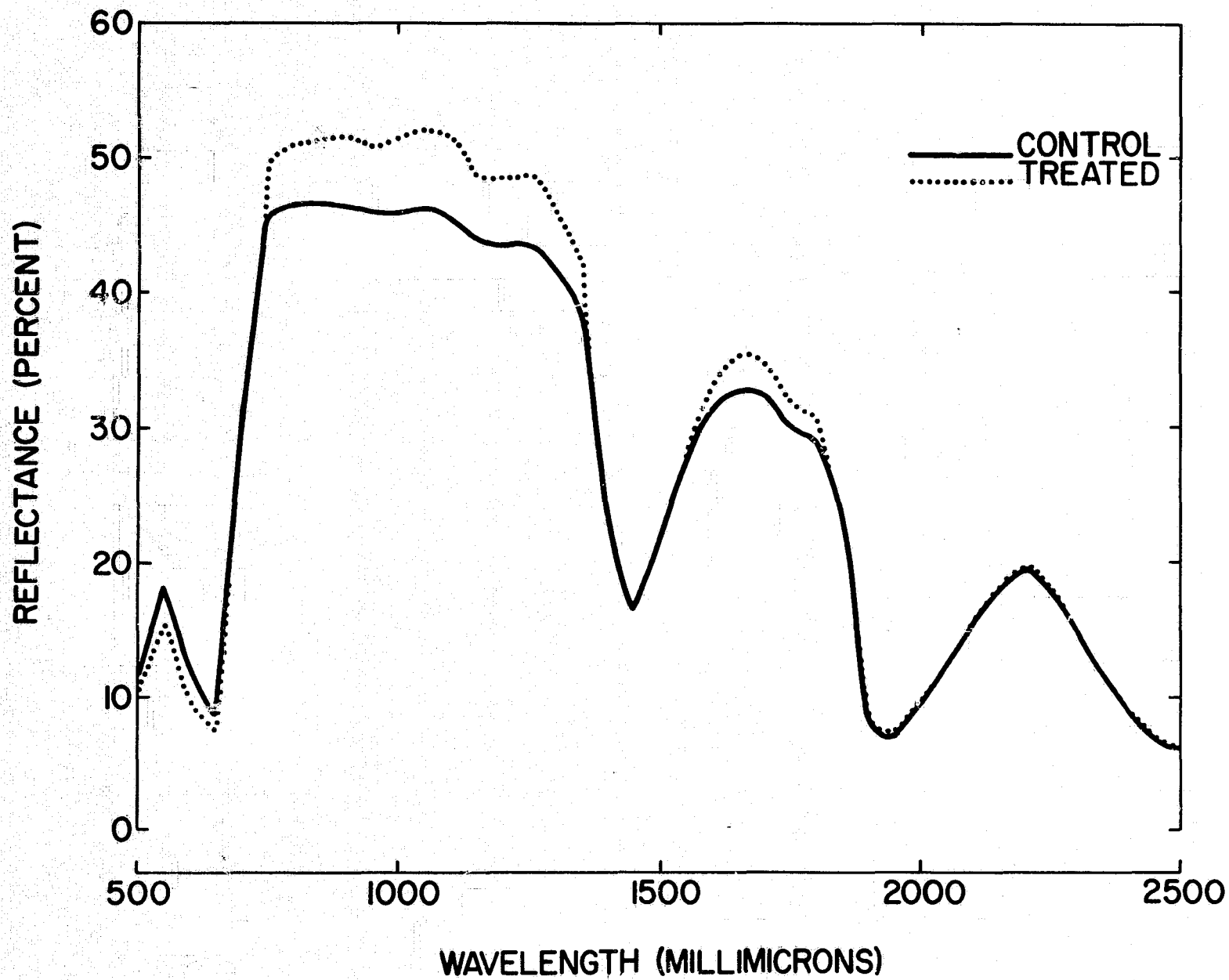


Figure 30B-1.- Total light reflectance of cotton leaves from 100-g/ha Cycocel-treated and untreated plants; each spectrum is an average value for five leaves.

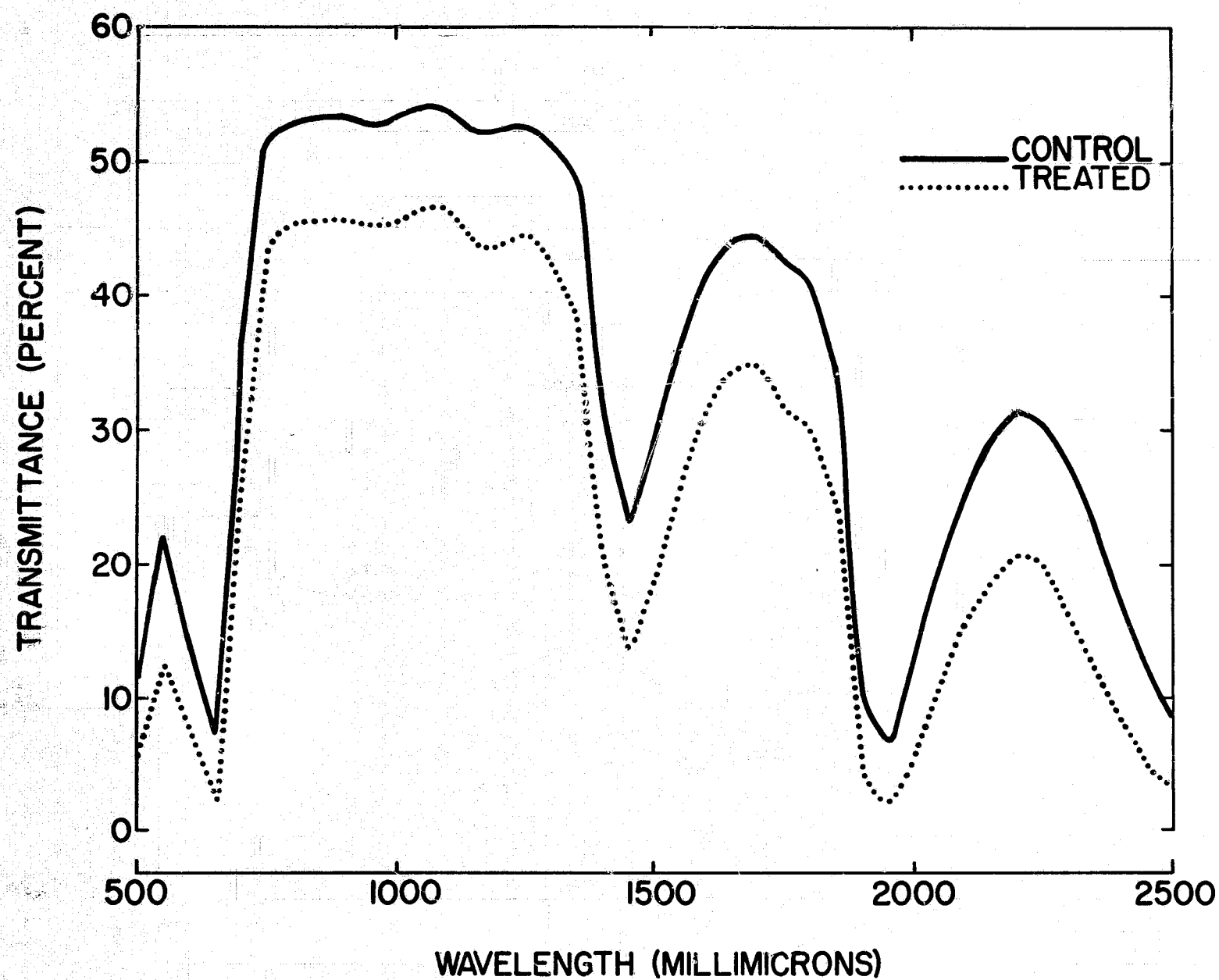
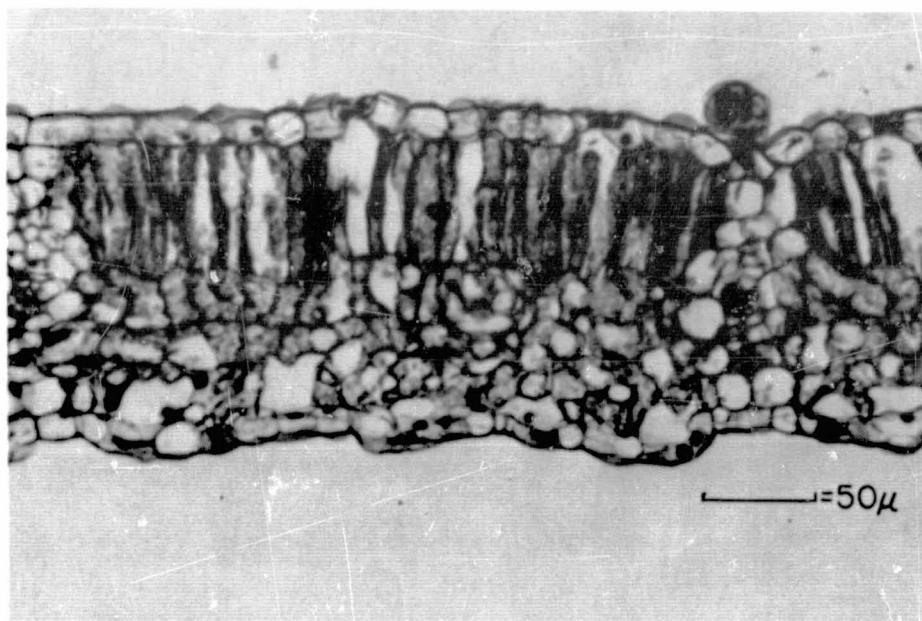
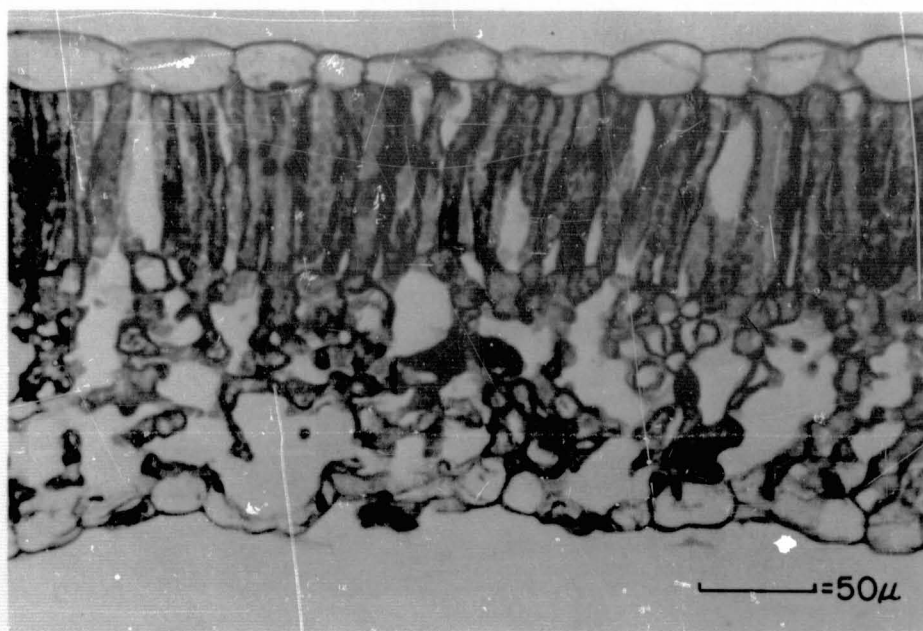


Figure 30B-2.- Transmittance of cotton leaves from 100-g/ha Cycocel-treated and untreated plants; each spectra is an average value for five leaves.



89

a. Untreated plants.



b. 100-g/ha Cycocel-treated plants.

Figure 30B-3.- Internal structure of cotton leaves
from untreated and 100-g/ha Cycocel-treated plants.

N71-16152

REFLECTANCE PRODUCED BY A PLANT LEAF*

By W. A. Allen, Research Physicist
A. J. Richardson, Physicist
and H. W. Gausman, Research Plant Physiologist
U.S. Department of Agriculture, Weslaco, Texas

RESULTS ACQUIRED FROM THE USE OF DATA
FROM NASA AIRCRAFT

Proper interpretation of multispectral imagery acquired from the NASA aircraft depends upon reliable ground-truth information. In the case of vegetation, ground-truth information can be reduced, in part, to effective optical parameters determined from individual leaves. Correlations can be, and have been, made between multispectral imagery acquired from the NASA aircraft and effective optical parameters measured in the laboratory.

INTRODUCTION

To interpret reflectance measured from space, the physics of light interaction with terrestrial features must be understood. The principal problem in agriculture is interpretation of reflectance caused by vegetation growing on a soil background. Reflectance from vegetation is the cumulative effects produced by leaves, stems, fruit, dust, dew, insecticide residue, and other attributes of a plant. Reflectance from the soil background is even more complicated. Reflectance differs, depending upon whether the incident light is specular or diffuse. Specular light emanates directly from the sun. Diffuse light is scattered from the rest of the sky. Polarization and atmospheric attenuation effects are important. The overall problem of reflectance from vegetation, therefore, is very complicated. Fortunately, the problem of reflectance from

*These studies were aided by contributions from the Soil and Water Conservation Research Division, Agricultural Research Service, U.S. Department of Agriculture, in cooperation with the Texas Agricultural Experiment Station, Texas Agricultural and Mechanical University. These studies were supported in part by the National Aeronautics and Space Administration under contract number 160-75-01-07-10.

vegetation can be broken down into manageable segments. We consider first the interaction of diffuse light with an individual leaf.

A paper (ref. 30C-1) has appeared in which the near-infrared reflectance and transmittance of a plant canopy and leaves stacked in a spectrophotometer was described by the Kubelka-Munk (K-M) theory for propagation of light through a diffusing medium. A basic entity in application of the K-M theory is the reflectance and transmittance of a single leaf. The purpose of the present paper is to synthesize, from fundamental considerations, the reflectance and transmittance of this single typical plant leaf.

The reflectance and transmittance spectrum of a typical plant leaf can be simulated with considerable accuracy by propagation of isotropic light through transparent plates with plane-parallel, but rough, surfaces. The leaf model advanced in this paper is based upon a stack of N transparent plates with rough surfaces, as illustrated in figure 30C-1. This simulated leaf will be characterized by two numbers, a cumulative void presentation area index $N - 1(\text{VAI})$ and an equivalent water path $D(\text{EWP})$. The VAI can be regarded as the average number of intercellular spaces intersected by a typical ray passing through a leaf. The EWP for a leaf can be regarded as the thickness of pure liquid water that will produce the observed absorption of a leaf. In addition, the reflectance properties of a leaf will depend upon effective optical constants, that is, an effective index of refraction n and an effective absorption coefficient k . These optical constants will be regarded provisionally as those of pure liquid water. Subsequently, deviation between experimental results and calculations based upon the properties of pure liquid water will be used to obtain the actual effective optical constants for a leaf.

The reflectance and transmittance of a leaf has been explained previously by Willstätter and Stoll (ref. 30C-2) on the basis of critical, that is, total reflection of light at the cell wall (air interface of spongy mesophyll tissue). A more recent paper by Sinclair (ref. 30C-3) advances the hypothesis that leaf reflectance derives from the diffusive characteristics of the plant cell walls. The concepts of Willstätter, Stoll, and Sinclair emerge naturally without additional special assumptions from the leaf model introduced in this paper.

The requirement that light passing through a leaf must be isotropic, or diffuse, is equivalent to the assumption that surfaces of the leaves are rough, that is, Lambertian. The reflectivity of the interface between two dielectrics for diffuse light can be calculated for any polarization state from the Fresnel relations (ref. 30C-4). The reflectance of a plate, consisting of two interfaces and intervening medium, can also be calculated, provided that an expression can be obtained for the transmissivity of a plate with respect to diffuse light.

TRANSMISSIVITY OF A PLATE WITH RESPECT TO ISOTROPIC LIGHT

The transmissivity of the plate illustrated in figure 30C-2 with respect to isotropic light is defined as the ratio of the light that reaches the second surface relative to the light that left the first surface where reflections have been neglected. The length of a typical slant ray through this plate is given by $D \sec \theta$ where D is the plate thickness and θ is measured from the plate normal. The transmissivity of the plate with respect to this particular slant ray is given by $\exp(-kD \sec \theta)$ where k is the absorption coefficient of the plate. Flux emerging from unit area on the first plate surface varies by definition as $\cos \theta$. The total flux emanating from unit area on the first surface that reaches the second surface is obtained by integration of all flux over the hemisphere $0 \leq \theta \leq \pi/2$. The average transmissivity τ for isotropic light passing through a plate with rough surfaces of thickness D , obtained by straightforward integration, can be written in the form

$$\tau = (1 - kD)e^{-kD} + (kD)^2 \int_{kD}^{\infty} x^{-1} e^{-x} dx \quad (30C-1)$$

REFLECTANCE OF A PLATE IN ISOTROPIC LIGHT

A typical leaf will be simulated by a single transparent plate, or a pile of N such plates, with a total thickness D . The distance D , the EWP, will be comparable to, and less than, the actual leaf thickness. The EWP corresponds to the actual amount of water that can be extracted from the leaf. Isotropic radiation I_0 emanates from medium 1, interacts with the interface between mediums 1 and 2, passes through medium of thickness D , interacts with the interface between mediums 2 and 3, and emerges into both mediums 1 and 3. Light emergence into medium 1 is termed reflectance, and light emergence into medium 3 is termed transmittance. Mediums 1 and 3 will be regarded provisionally as air, and medium 2 will be considered provisionally as pure liquid water characterized by the index of refraction n and by the absorption coefficient k . Transmissivity at an interface between mediums i and j will be designated T_{ij} ; the corresponding reflectivity is designated $R_{ij} = 1 - T_{ij}$. The irradiance associated with multiple reflections

within the plate are designated in figure 30C-2 by regions labeled 2, 6, 8, 12, ..., and 3, 5, 9, 11, Reflectance R is determined by contributions from regions 1, 7, 13, ...; transmittance is determined by contributions from regions 4, 10, Reflectance R and transmittance T are obtained by summing the appropriate power series. Diffuse light is essentially trapped by the second interface for those rays that exceed the critical angle; thus, $T_{12} \neq T_{23}$. The transmissivity T_{23} of the second interface can be either measured or calculated by means of the relation $T_{23} = n^{-2}T_{12}$. Reflectance R and transmittance T of the transparent plate of figure 30C-2 can be written in the forms

$$r = (1 - T_{12}) + \frac{\tau^2 T_{12}^2 (n^2 - T_{12})}{n^4 - \tau^2 (n^2 - T_{12})^2} \quad (30C-2)$$

and

$$t = \frac{\tau n^2 T_{12}^2}{n^4 - \tau^2 (n^2 - T_{12})^2} \quad (30C-3)$$

EXPERIMENTAL VERIFICATION

The theory developed in this paper for the reflectance and transmittance of a typical plant leaf has been applied to citrus leaves. Young leaves were taken from seedling plants. Reflectance and transmittance curves reproduced in figures 30C-3a and figure 30C-3b were obtained by means of a DK-2A ratio recording spectrophotometer with a reflectance attachment. Each normal leaf curve is an average for four leaves of average thickness 185μ . The normal leaves were measured essentially in their natural conditions. The dashed curves in figures 30C-3a and 30C-3b correspond to an average of five citrus leaves infiltrated with water. The average final leaf thickness was 188μ . The infiltration treatment consisted of placing the leaves under water and removing the intercellular air by means of a vacuum.

Figures 30C-3c and 30C-3d are theoretical curves based upon the optical constants for pure liquid water (ref. 30C-5). The VAI for the

untreated leaves was assumed to be 1.3, and the VAI for the treated leaves was assumed to be zero. The EWP for the untreated leaves was assumed to be 120μ , and the EWP for the treated leaves was assumed to be 160μ .

Deviations of reflectance and transmittance between the real and theoretical data of figure 30C-2 can be used to obtain effective optical constants that yield exact values of reflectance and transmittance for a leaf. Deviations between the optical constants for leaves and water can be regarded as differential spectra of leaves relative to water and as uncertainties in the fundamental optical constants of pure liquid water.

Figure 30C-4 is a plot of the effective index of refraction for the citrus leaves. The index of refraction for pure liquid water is also displayed in figure 30C-4a for comparison purposes. Anomalous behavior of the leaf dispersion curve occurs at wavelengths 0.68μ , 0.76μ , 0.97μ , 1.21μ , 1.45μ , and 1.95μ , that is, at those wavelengths that correspond to absorption bands for water. The maximum values of the index of refraction for the leaf (that is, $n = 1.4$) is not inconsistent with that of the epicuticular wax common to many leaves. The effective absorption coefficient of a typical leaf such as citrus is similar to that of pure liquid water except in the region of chlorophyll absorption.

CONCLUSIONS

The reflectance theory presented for a typical leaf is based upon determination of effective optical constants for that leaf. These effective optical constants n and k do not differ substantially from those of water over much of the spectrum 0.5μ to 2.5μ . Certain deviations that do exist can be regarded as differential spectra resulting from leaf materials other than water and as uncertainties in the corresponding fundamental constants for pure liquid water. Although the effective optical constants were obtained for citrus leaves, these values have been applied successfully to other leaves such as corn and cotton. Deviations between different leaves are to be expected and were found, especially in the chlorophyll absorption regions. However, the considerable role of air and water in a typical leaf appears to be described with considerable accuracy by the theory. While the concept of effective optical constants of a leaf is recognized as a device to make the theory exact, it is comforting to note that the relations obtained are reasonable.

REFERENCES

- 30C-1. Allen, W. A.; and Richardson, A. J.: Interaction of Light With a Plant Canopy. J. Opt. Soc. Am. 58, 1023, 1968.
- 30C-2. Willstätter, R.; and Stoll, A.: Untersuchungen über die Assimilation der Kohlensäure. Springer, Berlin, 1918.
- 30C-3. Sinclair, T. R.; Schreiber, M. M.; and Hoffer, R. M.: Pathway of Solar Radiation through Leaves. In press.
- 30C-4. Stern, Frank: Transmission of Isotropic Radiation Across an Interface Between Two Dielectrics. Applied Optics 3, 111-113, 1964.
- 30C-5. List, R. J.: Smithsonian Meteorological Tables. 6th ed., Sec. 10, Smithsonian Institution, Washington, D.C., 1963.

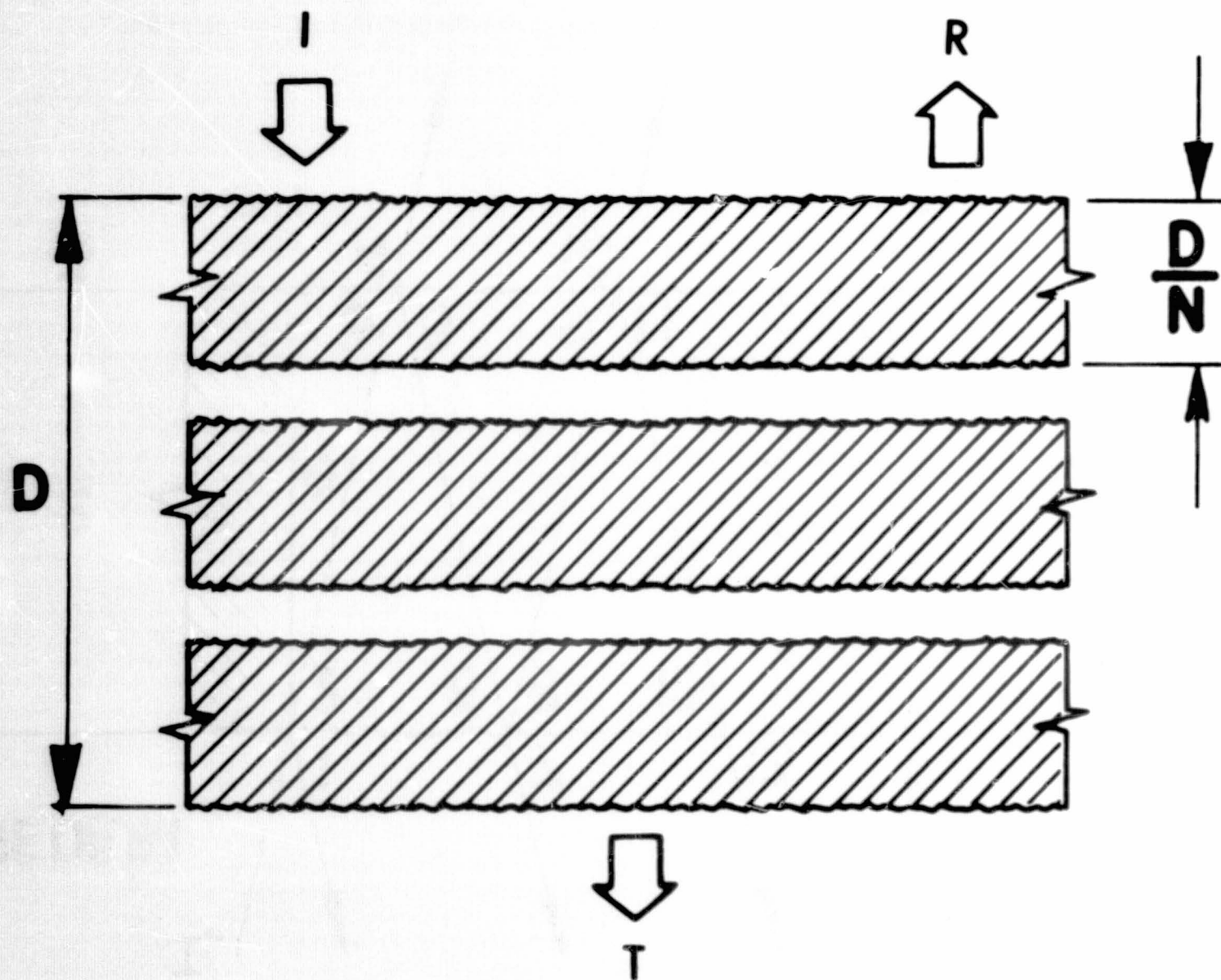
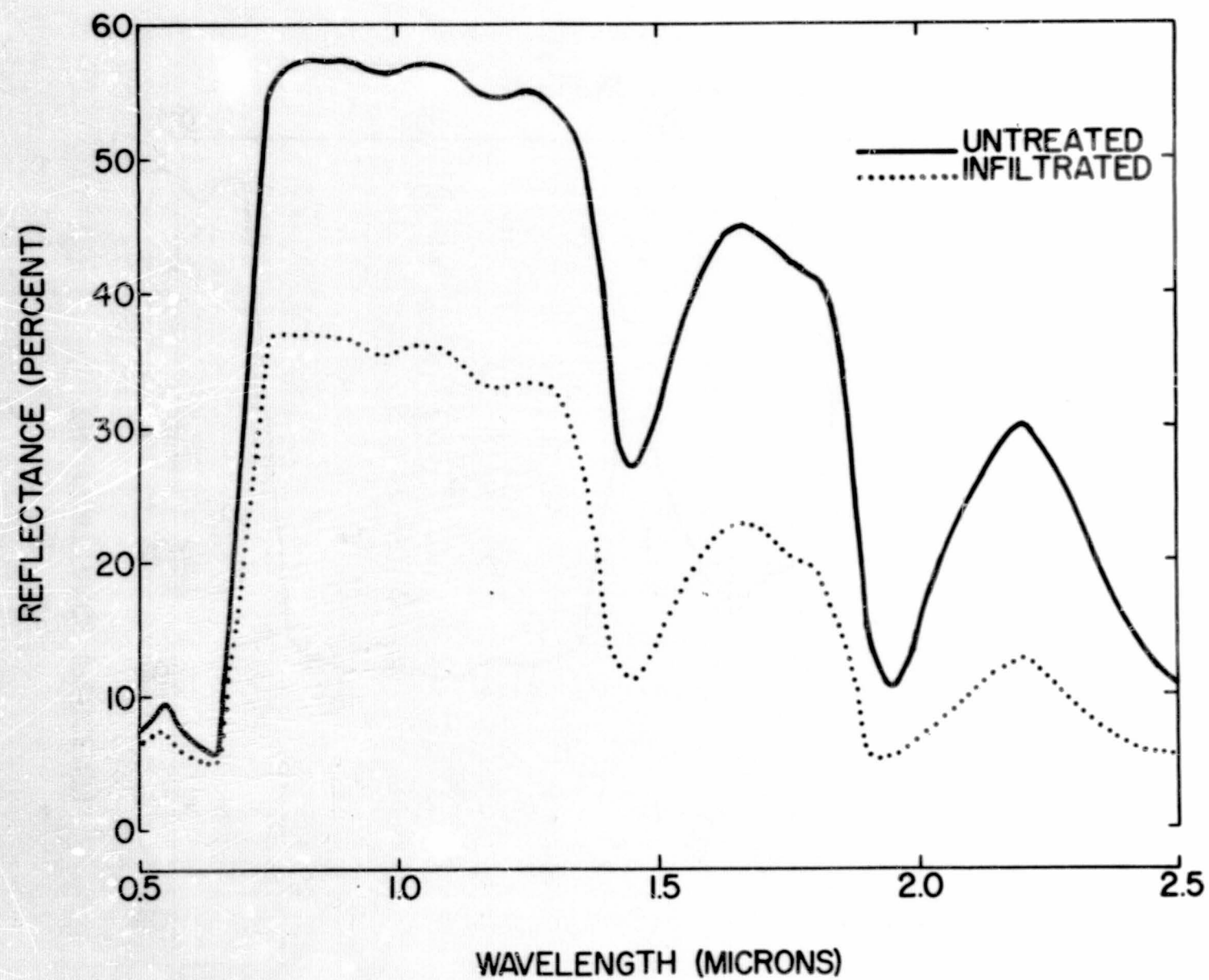


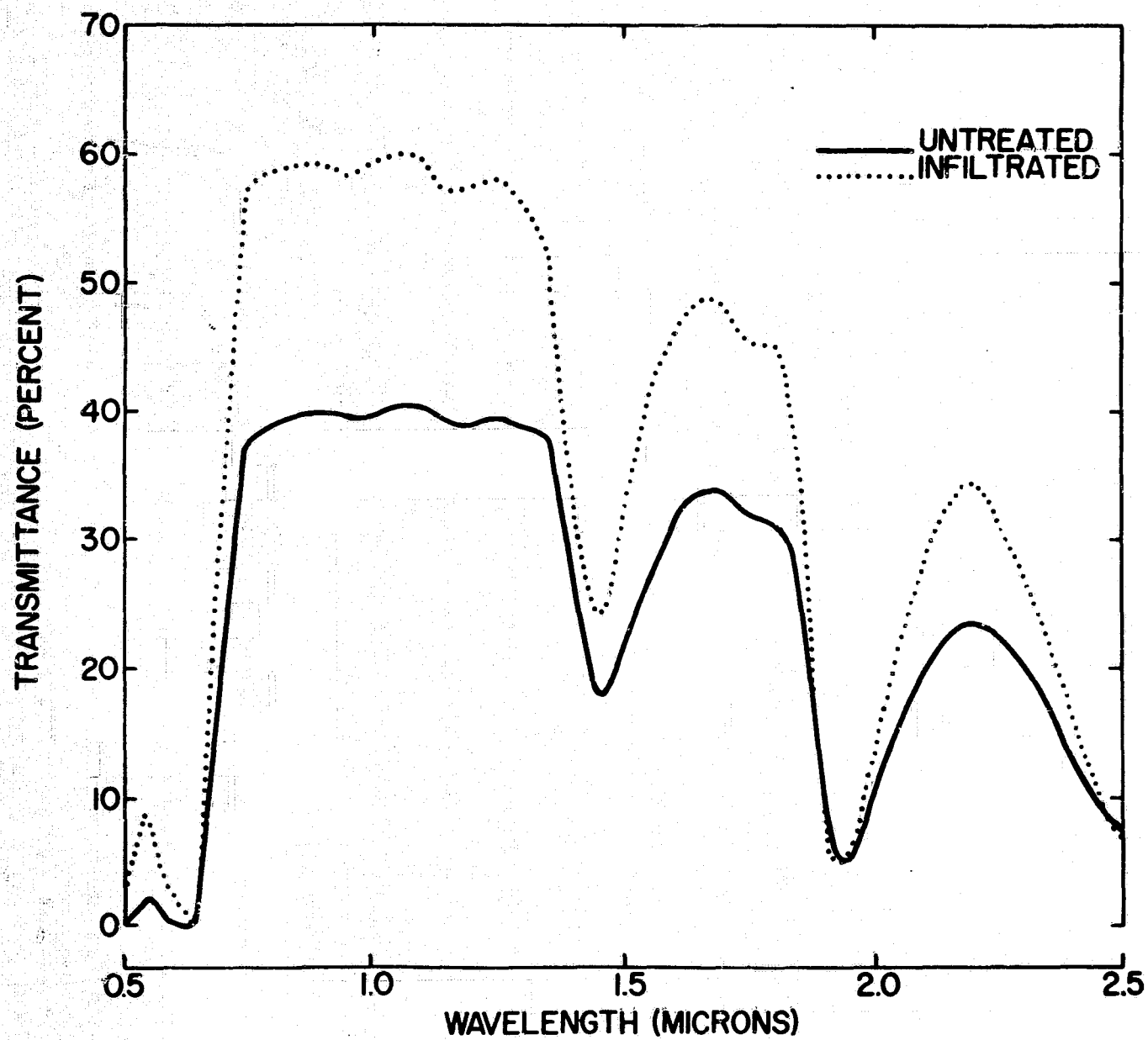
Figure 30C-1.- Simulated leaf of total thickness D . The leaf is composed of N subplates separated by air spaces of infinitesimal thickness. The quantity N , equal to 3 in this figure, does not need to be an integer.

Figure 30C-2.- Multiple reflections produced by a transparent plate with rough surfaces.



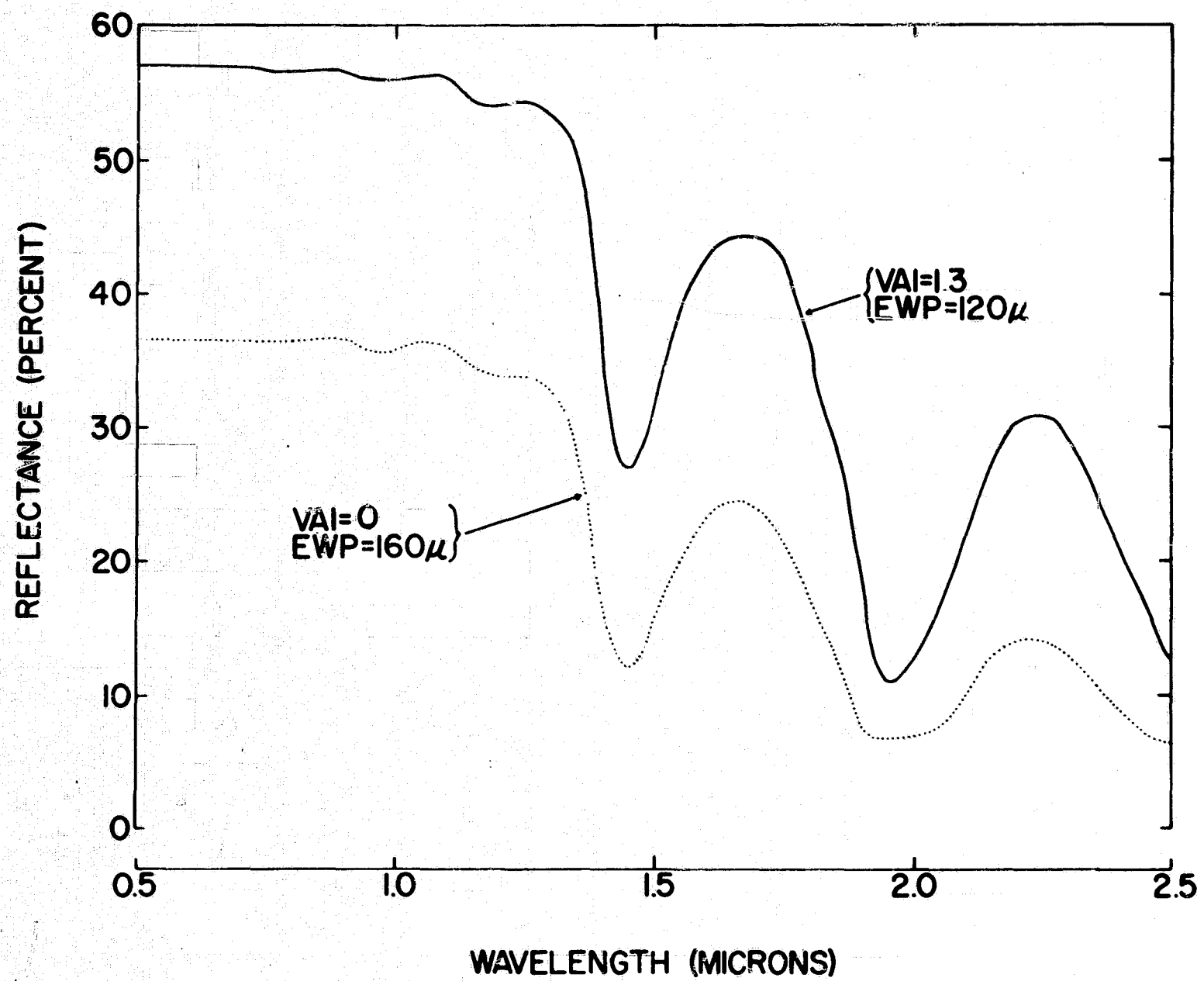
a. Reflectance curves of citrus leaves.

Figure 30C-3.- Reflectance and transmittance curves.



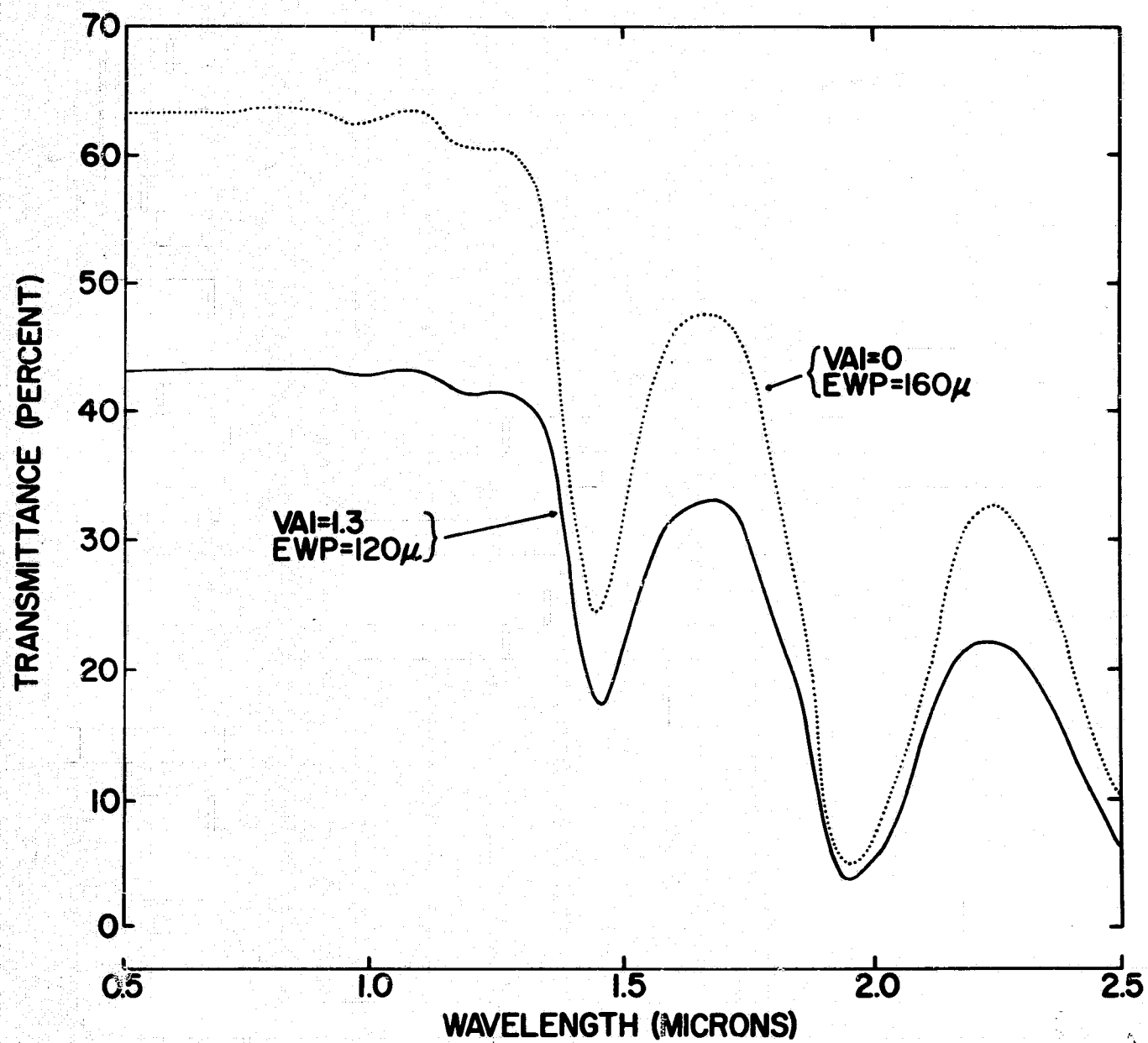
b. Transmittance curves of citrus leaves.

Figure 30C-3.- Continued.



c. Theoretical reflectance curves based upon optical constants for pure water.

Figure 30C-3.- Continued.



d. Theoretical transmittance curves based upon optical constants for pure water.

Figure 30C-3.- Concluded.

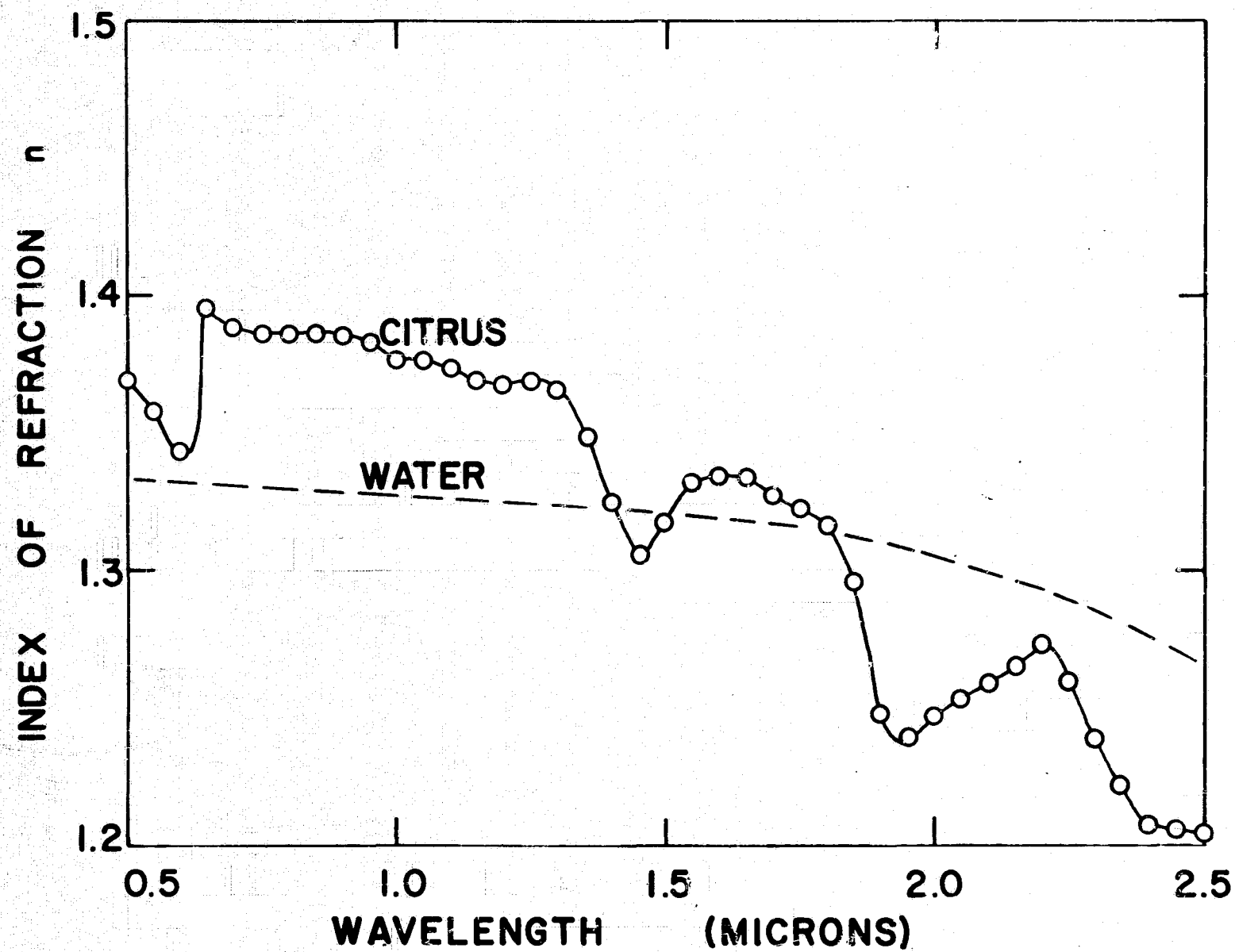


Figure 30C-4.- Effective refractive index of a citrus leaf compared with that of water.

N71-16153**BIOPHYSICAL RESEARCH AT LARS-PURDUE***

By Roger M. Hoffer
Program Leader, Laboratory for Agricultural Remote Sensing,
and Associate Professor, Purdue University

INTRODUCTION

The Laboratory for Agricultural Remote Sensing (LARS) was founded in 1966 at Purdue University by the National Aeronautics and Space Administration, in cooperation with the U.S. Department of Agriculture to plan and conduct research on data-collection, data-processing, and data-distribution techniques which permit the rapid collection of accurate information important to the management of agricultural resources.

The research effort at LARS is organized into the following five interreacting program areas, as shown in figure 31-1:

1. Measurements
2. Data processing
3. Agricultural requirements and applications
4. Aerospace agricultural programs
5. Agricultural research (biophysical research)

RESEARCH PROGRAMS**Measurements Program**

The measurements program is concerned with a task of defining procedures and equipment required to collect accurate and timely measurements and observations of pertinent agricultural phenomena.

*This report is based upon work sponsored jointly by the National Aeronautics and Space Administration and the U.S. Department of Agriculture, in cooperation with Purdue University.

Data-Processing Program

The data-processing program is developing analysis methods and data-handling systems to permit user-oriented scientists to adapt automatic data-processing techniques to agricultural applications.

Agricultural Remote-Sensing Program

A primary objective of the agricultural remote-sensing program is to conduct biophysical research to establish existing relationships between measurable and/or observable time, space, and frequency characteristics of electromagnetic energy radiating from agricultural situations. Also, it is here that user-oriented applications people adapt automatic data-processing techniques to specific agricultural problems.

Agricultural Requirements and Applications

In the agricultural requirements and applications area, we are working to define specific information requirements by various agricultural users and potential applications of remote sensing and automatic data processing in obtaining agricultural data.

Aerospace Agricultural Program

In the aerospace agricultural program, our objective is to integrate research work results into aerospace application experiment plans.

After approximately 30 months in the remote-sensing program, we would summarize our results as follows:

1. The feasibility of automatic data processing (ADP) for certain agricultural applications has been established.
2. We feel that for select applications, ADP is rather straightforward.
3. Many applications require further attention, but we believe they are feasible.
4. A host of other important agricultural situations require more sophisticated techniques before acceptable performance specifications can be met with automatic data processing.

It is our belief that in the next few years a pilot program should be established to demonstrate the utility of some of the new capabilities that have come out of the Earth Resources Program, as well as to further investigate important applications involving techniques requiring higher order sophistication.

In this and the following two papers, we will present some of the results which lead us to these conclusions.

Biophysical Research Program

The biophysical research program at LARS is involved in three primary tasks: signature studies, macrophysical studies, and microphysical studies. The objectives and some of our results of the research in these three areas are briefly as follows.

Signature Studies

In the signature studies program, we are attempting to determine those agricultural materials that can be uniquely identified on the basis of multispectral response signatures. In other words, what are the capabilities and limitations of remote multispectral sensing and ADP, as applied to agricultural situations? For example, can wheat be uniquely identified, as compared to all other crop species, through the use of remote multispectral sensing and ADP? On the basis of spectral response alone, is it possible to identify a field of corn, soybeans, or some other crop species? Is it possible to identify, or only to detect, wheat rust from a remote location?

Primary emphasis on the identification phase of the program thus far has been on crop species identification and on identification of primary ground cover such as bare soil, water, and vegetation. It is important to note that in the use of multispectral data for automatic identification of agricultural crops, many of the principles of photointerpretation such as size, shape, pattern, shadow, and texture of a target area can no longer be applied. Only the spectral response, which is the reflected or emitted energy from a small area on the ground, is used to identify a particular material when using remote multispectral sensing and ADP techniques.

Results Acquired from the Use of Data from NASA Aircraft

Flight missions have been conducted at different selected times during the growing season. The photographic (color and color infrared

(IR)) data and ultraviolet and thermal IR data have been studied to determine the following:

1. The utility of the different types of imagery for purposes of crop species identification
2. The utility of the different types of imagery for purposes of determining crop conditions of health and maturity
3. The utility of different scales of imagery for the previously discussed purposes
4. The utility of the different types of imagery for determining soil type and soil conditions of moisture and cultivation
5. The utility of good-quality color and color IR photographs in the analysis of multispectral scanner data
6. Look-angle and sun-angle effects upon the spectral characteristics of photographic data of various agricultural situations

Our results thus far can be summarized as follows:

1. Color photography is the easiest to use for purposes of crop species identification.
2. For fields of low-percentage vegetative cover, color IR photographs are superior to color photographs in determining the presence of vegetation. It is extremely difficult to differentiate between completely bare soil and a low percentage of vegetative cover on color photographs.
3. The ultraviolet imagery from the NASA aircraft is of little use in any of the previously discussed analysis tasks.
4. Thermal IR imagery is very useful in soil moisture studies and also for purposes of locating bodies of water partially obscured by vegetation.
5. Color IR photography is more useful than color photography for determining the presence of bare soil as opposed to dry, dead vegetation in spot locations within a canopy of green vegetation.
6. Conditions of crop health and maturity can best be studied using both color and color IR photographs in combination with each other. Color photographs are easier and more reliable for interpretation purposes, but often, subtle differences in spectral reflectance that would

be overlooked on color photographs are much more apparent on color IR photographs.

7. Sixty-percent overlap is necessary for studying angular effects of various agricultural situations. Twenty-percent overlap is not sufficient.

8. Crop canopy conditions can be grossly misinterpreted at view angles away from nadir. This is largely a function of row direction in conjunction with look angle. Crop height and row width also play a part. Precise limitations on allowable look angle have not yet been determined.

9. Scales of 1:14 000 are very useful for purposes of aiding in the analysis of multispectral scanner data. Many crop species identifications can be made from photography at this scale. However, 1:4000-scale photographs are required in many instances for positive identification. Therefore, both 1:14 000- and 1:4000-scale photographs are useful for many purposes of crop species and condition identification.

10. Color photographs are useful for purposes of soil type and condition classification. However, in many instances, color IR photographs were required to differentiate (a) between bare soil and dead vegetation, or (b) between completely bare soil and fields containing recently germinated crops (about 90 percent bare soil and 10 percent green vegetation).

11. Color and color IR photographs were equally useful in locating fields containing drainage tiles and in mapping out the location and pattern of the tiles. On the 1:4000-scale photographs, inferences could be drawn about the age of the tile system in many instances.

12. NASA photographic coverage is most useful if obtained over the same flight lines several times throughout the growing season.

Summary

Evaluation of NASA imagery for several purposes, outlined previously, has indicated that the NASA ultraviolet imagery is of little use. Thermal IR imagery is of value in certain situations. More work needs to be done with calibrated imagery in the future. Color and color IR photographs provide one of the best sources of "ground truth" information available. Many items of information that would be nearly impossible to obtain on the ground can be obtained easily from these aerial photographs.

Both color and color IR photographs are necessary and should be used together. Scales of both 1:14 000 and 1:4000 are useful for certain purposes, although the scale of 1:4000 could probably be changed to a scale of 1:6000 for most purposes. Sixty-percent overlap on the photographic coverage is essential. Examples of the utility of NASA photography are shown in the text of this report.

HIGHWAY 37 RESULTS

One of the analysis tasks undertaken this past summer has been the classification of a set of multispectral scanner data obtained in central Indiana. This involved over 70 miles of data flown at an altitude of 3200 feet in the area shown in figure 31-2. These data were obtained by the University of Michigan Institute of Science and Technology using their multispectral scanning system, collecting data in 18 discrete wavelength bands. As can be seen, this area involves a substantial length of flight line. Our first analysis task was to identify green vegetation, bare soil, and water automatically. Training samples were selected from approximately a 3-mile segment of the data, and the entire flight line was then automatically classified into one of these three categories. Figure 31-3 shows typical results for approximately a 4-mile segment of the data. On the left is a photo mosaic of the area, these photographs having been obtained 10 days before the scanner flight. They were obtained for planning purposes. In the center is the computer print-out showing the automatic classification results for the same area. The darker tones indicate areas of green vegetation; the light tones are bare soil; and the medium tones are water. On the right is a computer print-out of only the sample points identified as water. Many of these points appear very small and scattered, but aerial photographs reveal that these are actually areas of ponded water and drainage ditches. It is of interest to note that there were several instances in which water was identified correctly automatically but which had previously been overlooked on the aerial photographs. Several of these water areas were very difficult to see on color aerial photographs because of the lack of distinct color differences between the water and other materials in the vicinity. I would like to point out that because the black and white aerial photographs shown on the left were obtained 10 days before the multispectral scanner data were collected, in several areas, the ground conditions at the time of the scanner flight and as they appear on this photo mosaic were quite different. Figures 31-4 and 31-5 show closeups of small typical areas in the data. In figure 31-4, at point 1, a hedgerow is shown on the color photograph and can also be seen to have been correctly identified on the computer print-out on the right. Point 2 is a field of winter wheat, which is at a very green stage of maturation, as shown by the color photograph.

The symbol "I" used to identify green vegetation on the computer print-out indicates that this area was accurately classified. The dry brown vegetation shown at point 3 has been "thresholded" in the automatic classification process, which means that the multispectral response in this area was unlike the response for green vegetation, bare soil, or water. Therefore, this area of dry brown vegetation was not classified into any one of the designated categories and was left blank on the computer print-out. As may be seen in this figure, the roads and houses were also "thresholded" and are shown as blank areas in these automatic classification results. Point 4 is a pond of water which was correctly classified and is indicated by M (simply because M is a relatively "dark" symbol) on the print-out.

In figure 31-5, point 1 (at the corner of a field of green vegetation and two fields of bare soil) and point 2 (in the river) are indicated for purposes of orientation. Point 3 shows a small hedgerow between two areas of bare soil, which was accurately identified on the print-out. A tributary which was correctly identified is indicated at point 4. Point 5 is a very small pond of water that is almost indistinguishable on the color photograph. These results indicate a rather good capability for automatic identification of these cover types.

In order to automatically identify these cover types over the entire 70-mile flight line, pattern-recognition techniques were applied to the multispectral response data. The optical-mechanical scanner, which was used to obtain the data, measured the radiance of small areas on the ground simultaneously in several wavelength bands. By ordering the measured response values for each of the wavelength bands, one can obtain a measurement vector for each of the materials of interest. On the basis of these vectors, the pattern-recognition categorizer is programmed to determine spectral differences among the various materials. At this point, the categorizer is "trained" using known target materials. Then, the measurement vectors of unknown target materials or test samples can be examined and classified. The automatic classification shown in figures 31-3, 31-4, and 31-5 was carried out using the 0.48μ to 0.50μ , 0.58μ to 0.62μ , 0.66μ to 0.72μ , and 0.8μ to 1.0μ wavelength bands. Thus, all of the wavelength bands used for this classification were in the visible or near-reflective IR region.

In this particular analysis task, one of the primary objectives was to select approximately 30 training sample areas in a region about 3 miles long and to determine whether this same set of training samples could be used reliably throughout the entire 70-mile flight line. We feel that the results were satisfactory in demonstrating a capability to classify large geographic areas automatically, based upon relatively small training sample regions.

In order to quantitatively check at least a portion of these classification results, a total of 107 test sample areas were selected at random from the computer data. In 96 of the 107 test areas, a 97-percent or higher classification accuracy had been obtained, and in 106 of the 107 test areas a correct classification of over 83 percent of the sample points had been achieved. The average classification accuracy was 99 percent for green vegetation, 98 percent for soil, and 97 percent for water. It is the differences that exist in the spectral signatures of these materials which allow this capability for automatic identification. We feel that these and other results obtained have definitely established the feasibility for ADP for certain tasks where the spectral characteristics of the materials involved are quite different.

The significance of a procedure to apply pattern-recognition techniques to multispectral scanner data is that it offers a capability to obtain data rapidly over very large geographic areas, followed by rapid automatic processing of the data to a reasonable degree of accuracy, to produce useful information in a timely manner. There are many situations in which the current capability could advantageously be put to use.

CROP SPECIES IDENTIFICATION

Another step in sophistication above such simple cover-type identification would be to identify crop species groupings or various individual crop species of major importance such as corn, soybeans, wheat, and oats. In one such effort, we analyzed data from an agricultural farmland region southwest from Lafayette, Indiana. On the left of figure 31-6 is an annotated aerial photo mosaic of the flight-line area. In the center is a computer print-out identifying all the areas of row crops, which would be comprised of either corn or soybeans. The fields in the flight-line area for which ground truth was obtained and which were positively identified as being either corn or soybeans were outlined by hand and designated with a C or an S. One can see that these results are generally very good, although there are a couple of areas which were not corn or soybeans, but which were largely identified as row crop. One field of soybeans had very few sample points in the field that were automatically identified as such. An area at the very bottom of the computer print-outs was out of the designated flight-line area, and no ground truth was obtained. One might speculate, however, that the fields in question were indeed fields of corn or soybeans, based upon the results shown. In the print-out on the right, the computer printed out an L for each sample point which was automatically identified as a small grain (either wheat or oats). Again, one sees that all fields in the flight-line area which were small grains were largely identified as such. There are a few sample points in some of the fields that were

apparently not correctly classified. Likewise, there are a few scattered points throughout other areas of the flight line which were erroneously classified into the small-grain category. Figure 31-7 shows a closeup of the individual crop species identifications. On the black and white aerial photograph, it is extremely difficult to differentiate between, much less to identify, the individual crop species. By combining several wavelength bands of data simultaneously, it is possible to identify the individual species, as indicated by the computer print-out. In this figure, W stands for wheat, O for oats, S for soybeans, C for corn, P for pasture, and R for red clover hay. Since no attempt was made to classify diverted acres, this field was not classified into any particular crop species category.

As seen in these figures, the classification results appear to be quite good. Such an evaluation, however, is very qualitative and leads one to speculate about how accurate or inaccurate some of these results really are for the various categories of crop materials. Figure 31-8 shows the aerial photo mosaic of this flight-line area, and next to it is a computer print-out designating specific areas in the flight line for which the classification results were summarized in a quantitative fashion. One sees from this photograph that a large portion of the entire flight line was included in the quantitative classification results. There are a few areas which are not included because they consist of diverted acres. Because of extreme difficulty in classification of diverted acres as a result of natural variation which one finds in this land-use category, we did not automatically attempt to identify diverted acres, and they were, therefore, not included in the quantitative analysis results.

Figure 31-9 shows the summarization of the quantitative results in a graphical format indicating the percentage of correct classification for each cover type. One sees that the accuracy ranges from 100 percent for water to 80.7 percent for hay. Figure 31-10 shows how these figures were obtained. This figure is an actual computer print-out, which is why "wheat" is spelled "WHET," and "water" is spelled "WATE," since the program allowed only four-letter headings for each column. On the left, the ground-cover class is designated; and the number of samples which were known to belong to that class is indicated. On the right are the tabular results showing the number of samples which are actually classified into the various cover types. Thus, of 15 185 sample points designated as belonging to the row crop category, 14 035 were actually identified as row crops. This results in a percentage correct recognition of 92.4 percent. One can follow the various percentage figures down the column and see that they correspond to those shown in figure 31-9. The overall performance for these classification results was 89.7 percent. If one takes all categories and weighs each category equally, we get an average accuracy of 90.2 percent. I believe, however,

0

that the overall performance is a more meaningful figure in that this weights each cover type according to the portion of the total area which is covered by that material. Thus, in figure 31-10, of the total 27 312 samples classified, more than one-half of these, or 15 185, belong to the row crop category. This gives row crops over 50 percent of the weight in the overall performance figure of 89.7 percent.

Let us examine these classification results in another manner. Figure 31-10 represents the results from a total of 66 test areas outlined in figure 31-8. These 66 test areas were quantitatively analyzed on an individual basis. Of these areas, 60 out of the 66 had a percentage-correct recognition of over 75 percent. Thus, if one could assume that a 75-percent or better classification of the sample points in any field would identify that field as being a certain crop species or cover type, then in this case, 60 out of the 66 test areas of this flight line were correctly identified according to the ground cover. Of the six remaining fields, one field of soybeans would have been incorrectly identified as a pasture area. The other five fields did not have 75 percent of the sample points classified into any particular cover type and, therefore, could not be identified by this method.

One of the more difficult problems involved in automatic classification of agricultural materials is the proper selection of an adequate training set of data. The difficulty lies in the spectral variability of agricultural materials. To examine the problems which might be encountered for data obtained from widely separated geographical areas, we have done preliminary analysis work with data collected at the Weslaco, Texas, and California Test Sites. We found that the problems of agricultural variability and training sample selection were very similar to those encountered for data obtained in Indiana. On the basis of this work, we believe that the ADP approach will be applicable to various geographical areas.

A second area of endeavor within the signature studies program of biophysical research is to define the optimum portions of the electromagnetic spectrum for various identification tasks when using multispectral response data. In some instances, it appears possible to identify a crop species using only two or perhaps three wavelength bands. In other situations, a particular material may require five or six wavelength bands for correct identification, but these are not necessarily the same wavelength bands as were required for identification of the first crop. Thus, it is essential to determine, for each task at hand, which wavelength bands are necessary to identify a particular object or crop type and which wavelength bands yield little additional information. This will vary from crop to crop and from season to season. This type of research on wavelength-band determinations is one of the largest areas in which integrated laboratory, field, and aerospace endeavors are essential.

The third area of endeavor within the signature studies program is to determine the amount of seasonal variation in multispectral response patterns for the various crop species and soil conditions. We know, for example, that the spectral response for most crops will change throughout the growing season as the crops mature, and there may be greater or smaller amounts of variation at any particular time during the growing season. Photographic and other sensor data from the NASA aircraft program has proven very useful for study of the seasonal and year-to-year variations of agricultural situations. Figure 31-11 shows a comparison of color photographs taken by the NASA Convair 240 at 7000 feet above terrain in an area in Tippecanoe County, Indiana. The photograph on the left was taken on June 18, 1968 on mission 74. At this time of the year, there were many fields that appeared to be bare soil. At points 1 and 2, for example, the fields appear to be bare soil, but are actually planted to soybeans and corn, respectively. The crops have germinated, but are still small and have only a small percentage of ground cover. In the photograph on the right, these fields have changed drastically during the 6-week period between June 18 and July 30. One would have seen almost this much change had there only been a 4-week difference. At point 1 on the July 30 photograph, the soybeans are much greener than the corn, which had tasseled; yet these same two fields looked alike a few weeks earlier. On the June 18 photograph at point 3, a field of wheat is starting to ripen and is more yellow than the deep-green oat field at point 5. On the July 30 photograph, the oat field is oat stubble, and the wheat field is a combination of wheat stubble and an undergrowth of alfalfa. At point 4 is a field of red clover which can be seen to have changed considerably between June 18 and July 30.

Macrophysical Studies

The macrophysical studies in our program have the following goals: (1) to determine the agricultural causes of variations in multispectral response patterns and (2) to determine the significant items of ground truth that must be obtained and how best to obtain such data. Knowing that a certain amount of variation does exist in the multispectral response signature does not explain why this variation in spectral response exists. We have found, for example, that the variety of a crop species, the date of planting, the soil type, the row direction, the row width, and the soil moisture all cause significant differences in multispectral response signatures of a given crop species. These data then become items of importance in obtaining ground-truth information at the time of remote-sensing flights. We feel that it is extremely important to determine the causes of variations within crop species so that we may be able to predict the portion of the growing season when minimum variation in spectral response will exist and, therefore, to predict when the probability for correct automatic identification of crop species is greatest. Knowledge as to the agricultural variations

within a crop species is essential in order to determine the capabilities and limitations of such automatic processing of multispectral data for an operational remote-sensing system.

Figure 31-12 shows adjacent frames of color photography which include some of the same fields. These photographs were taken on July 30 of this year on NASA mission 77. In the photograph on the right is seen a field of soybeans that is near the center of the frame. The view is directly downward; therefore, a large portion of the field of view that is seen is bare soil. In the photograph on the left, which is the adjacent frame, the angle of view is not directly down on top of the field, but rather off to the side. In this case, the view is through the crop canopy and no bare soil is seen, but rather, the less illuminated sides of the plants and the shadow area on the inside of the crop canopy. There is little, if any, soil seen. Therefore, the entire field appears to be dark green. Row direction, as well as look angle, has a marked effect on the appearance of these soybeans in these photographs. This is illustrated vividly in the small areas in which the farmer had planted in a sequence of changing row directions. At point 1, the row direction is north-south (up and down on these photographs), whereas at point 2 it is east-west. The soybean field designated at point 3 also has a north-south row direction, and again the change in tone from green (left photograph) to mostly brown (right photograph) is very striking.

Figure 31-13 was obtained on July 27, 1966. In the center portion of the photograph, we see three fields, all of which contain red clover. However, the use of each of these fields is different. The closest field is being used as pastureland and presents a rather medium-brown appearance. Immediately behind this field is red clover being used for hay and having a rather greenish appearance. Behind that is a field of red clover in the diverted-acres program, which gives a brownish-black coloration. These differences will cause differences in the multispectral response signature. This points out the need in our ground-truth program to not only identify a field as to the crop species present in the field, but also to determine the use being made of a particular agricultural field. In many cases, we must try to identify the cover type in a field on the basis of use and crop species, not simply crop species identification alone.

A test area used for wheat variety trials at the Purdue Agronomy Farm is shown in figure 31-14. This indicates the wide variety of spectral signatures that one might encounter for a single crop species at the same time during the growing season. Because this photograph was obtained in an experimental area, the differences encountered are rather extreme, but it does serve to indicate the differences which might possibly be encountered for a single crop species in a given geographical area and at a given point in time.

The agricultural scene changes greatly throughout the entire growing season. Each crop species has a different rate of maturing. Corn, for example, takes about 180 days to mature; soybeans, on the other hand, mature in about approximately 100 days. Wheat is planted in the fall and matures in the spring, whereas most crops are planted in the spring and mature late in the fall. These differences in maturity rates and maturity cycle can work toward our advantage. We can be selective in the time of the growing season when we can conduct remote-sensing flights, such that we can observe the crop species of interest at a time when it has a distinct characteristic signature, different from all other crop species.

Some other agricultural variabilities may work to our advantage. For example, we know that row width will cause differences in multispectral response signatures. The signature for a field of corn planted in 20-inch row widths will be different from that planted in 40-inch row widths, at least during certain portions of the growing season. Agricultural industries, or "agribusiness," would like very much to know how many acres of corn are being planted in narrow row widths as opposed to the acreage that is planted in normal row widths. These data would allow revision of machinery designs to adapt to changing agricultural cultivation practices. This type of situation again points out the need for us to design an operational remote-sensing system around the information requirements of the user groups. It is the user groups, be it either agribusiness, the individual farmer, Government agencies, or international agencies who must offer guidelines as to the types of information which they would like to be able to obtain and which are of a nature that could be obtained with remote-sensing techniques.

Microphysical Studies

The microphysical studies area of the biophysical program at IARS-Purdue relates spectral response signatures to the physical and chemical properties of plants and soils. This involves the study of individual plants and leaves under controlled conditions in an attempt to become more knowledgeable about interactions between the plants and soils and the reflected or emitted energy which we are measuring remotely. For example, how does moisture content of plants affect the reflectance or emittance characteristic of the plant? In which wavelength bands does one find the best correlation between reflectance and various factors affecting the plant? For plants in various disease situations, is there a difference in reflectance? If so, why? Is it a change in pigmentation, a collapse of the spongy mesophyll, perhaps a change in the gross geometry of the plant allowing more soil to be viewed from above, or a complex combination of these factors? These are the kinds of questions which must be answered for many crop materials under carefully controlled field and greenhouse situations.

Summary

The research to date at LARS has indicated a great deal of promise for automatic assessment of various agricultural situations. There is still a great deal to be learned. There are some specialized items of field and aircraft equipment which need to be built.

Much of the work at LARS has centered around photographic and multispectral optical-mechanical scanner data. Although the multispectral scanner data cannot be obtained in any condition of weather, as is the case with radar, there are some advantages to this type of data in terms of resolution, power requirements, and data handling. Photography offers much better resolution than scanner data but only covers a narrow portion of the optical spectrum — 0.4μ to 0.9μ , whereas the scanner capability extends from 0.3μ to 15μ . The primary advantage of optical-mechanical scanner data is in the ease and accuracy with which the data can be quantized and then processed and analyzed by computer. It would appear to us that an operational remote-sensing system of the future should incorporate the unique advantages of several instrument systems, including photographic sensors, optical-mechanical scanners, radar, and perhaps laser altimeters and other instruments. We must not seal ourselves to the advantages of one instrument system and overlook the advantages of others that could and should be used in a remote-sensing program.

We believe that automatic data processing of remotely sensed data has a great deal of potential, both in this country and in developing countries. The major benefits of an operational remote-sensing information system in agriculture would be the capability of obtaining data rapidly over large geographical areas and the timely processing of such data to useful information with accompanying benefits in improved accuracy, timeliness, and perhaps economy of agricultural surveys.

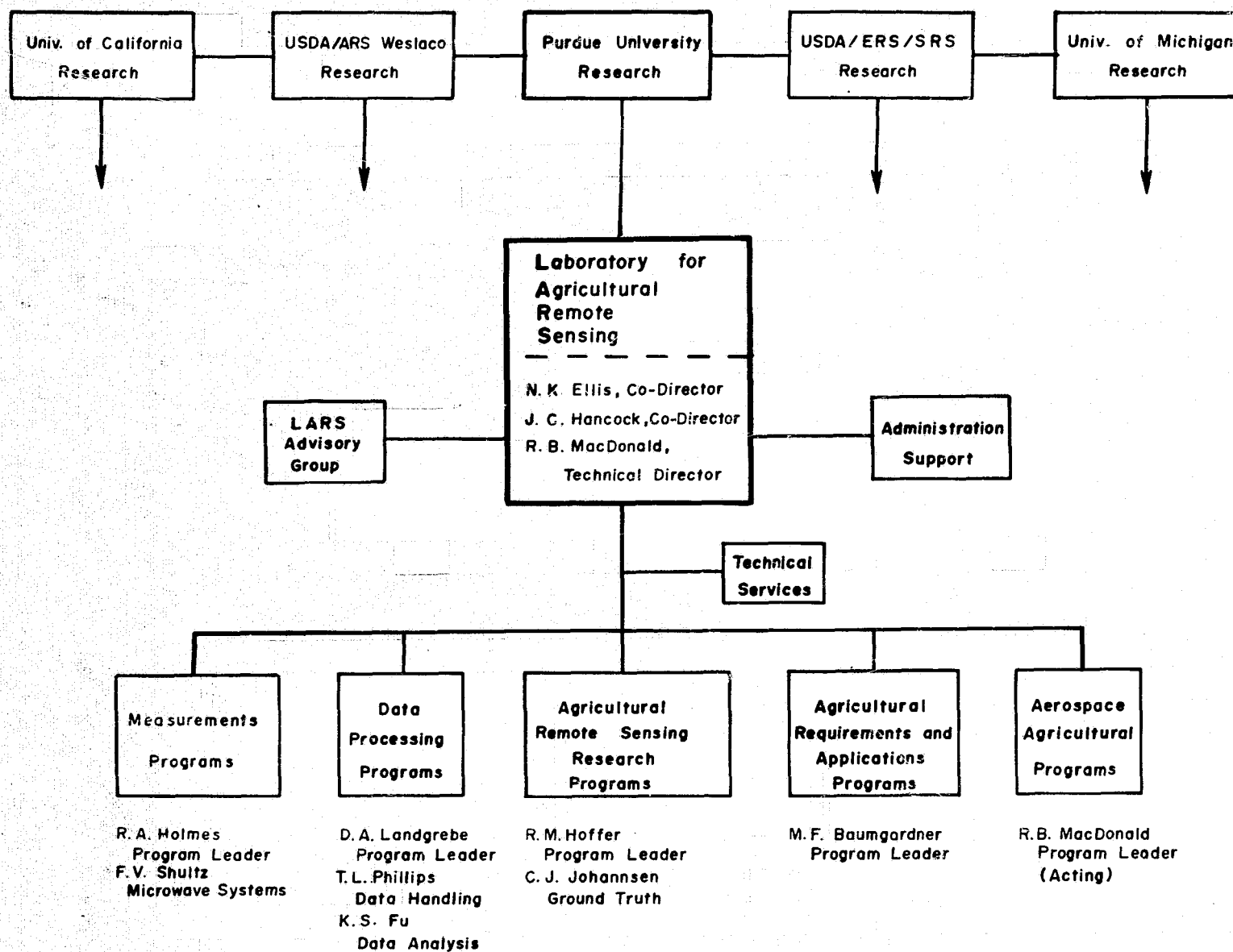


Figure 31-1.- Organization diagram for the Laboratory for Agricultural Remote Sensing, Purdue University. The relationship between LARS and the other facilities involved in agricultural remote sensing is also indicated.

HIGHWAY 37 FLIGHT-LINE LOCATION

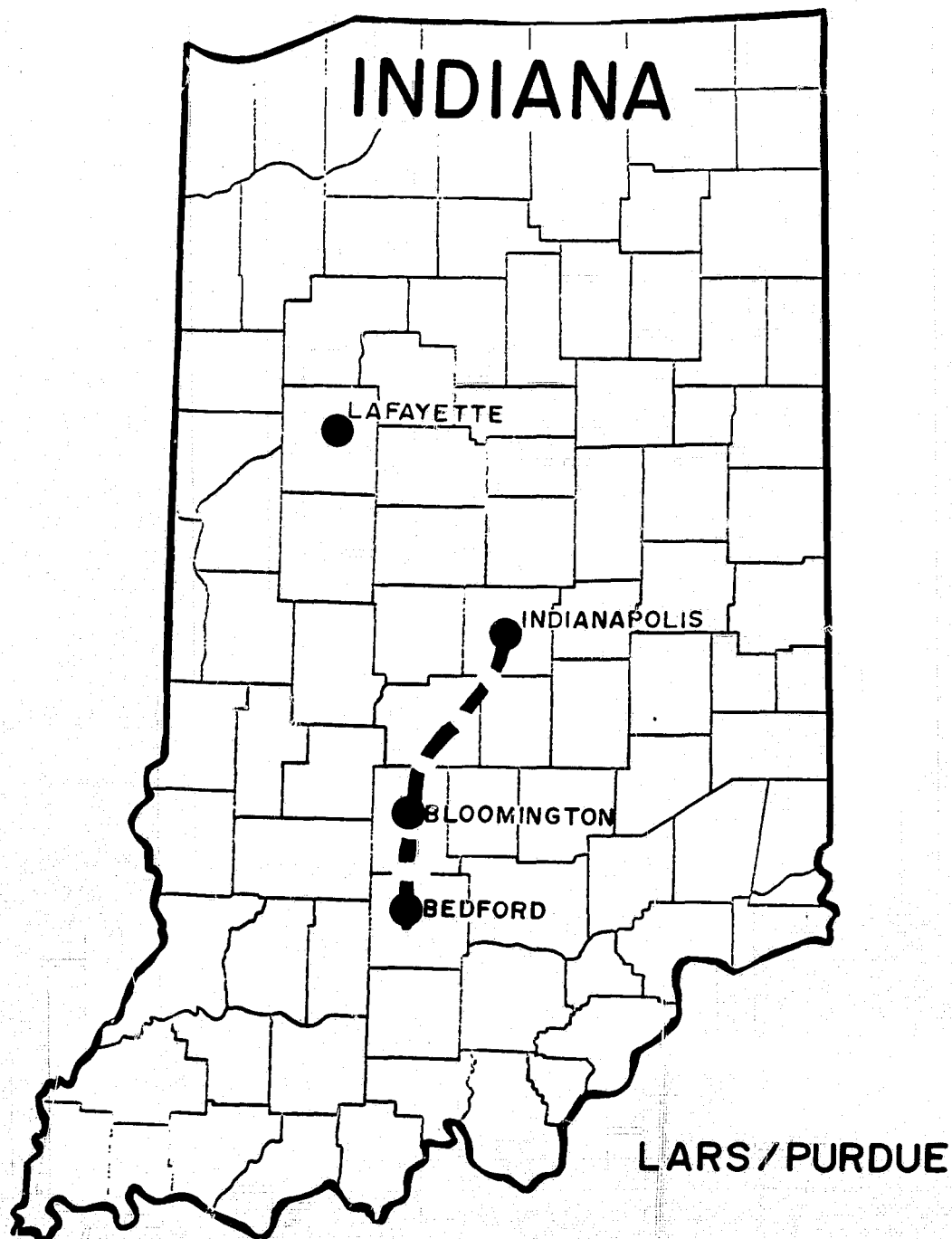


Figure 31-2.- Location of a 70-mile flight line in south-central Indiana. Multispectral scanner data for this entire flight line were automatically classified into basic cover types.

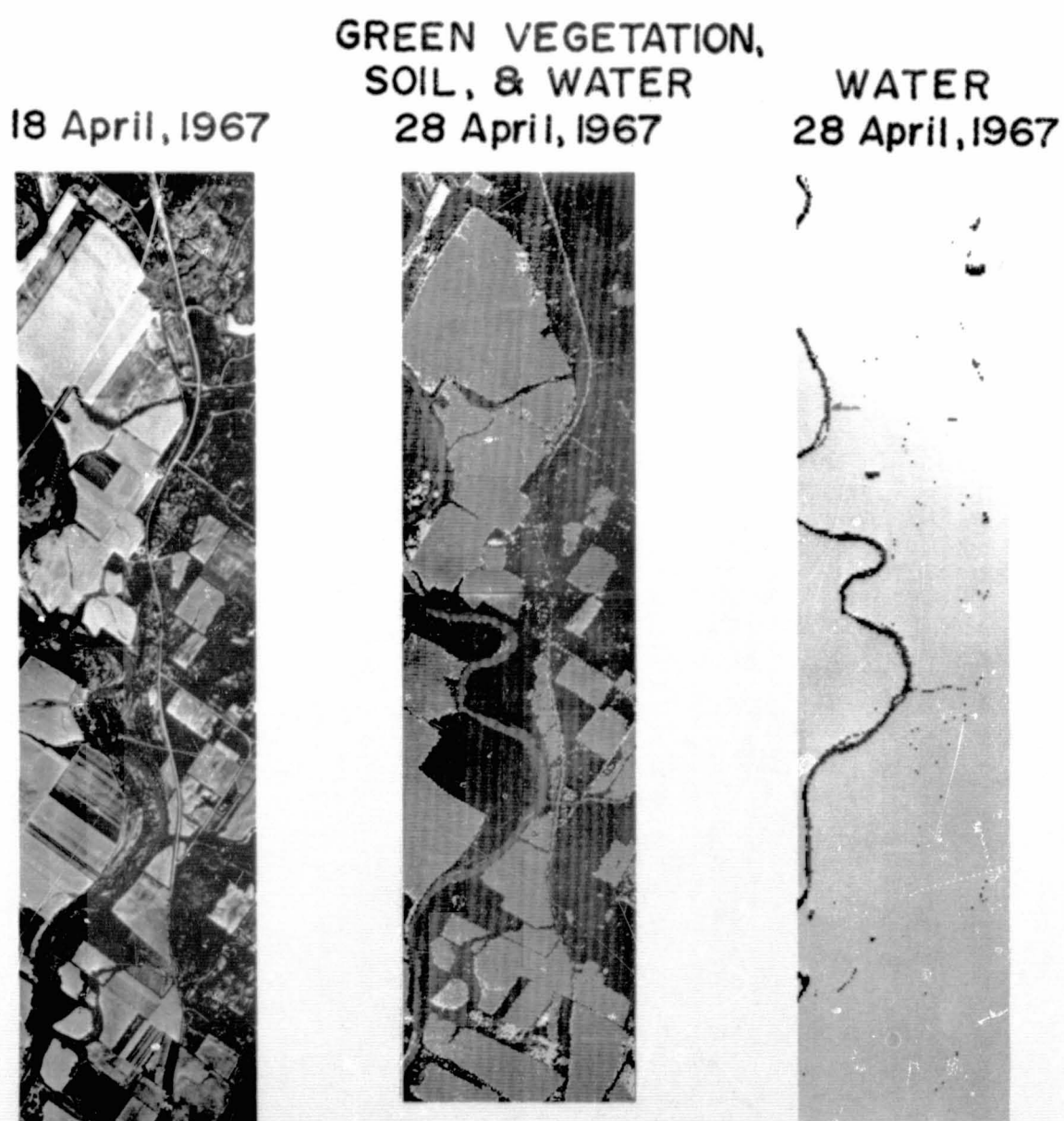


Figure 31-3.- Comparison of a photo mosaic and automatic classification results for the same area. A photograph of a computer print-out showing only the points identified as water is shown on the right.

31-18

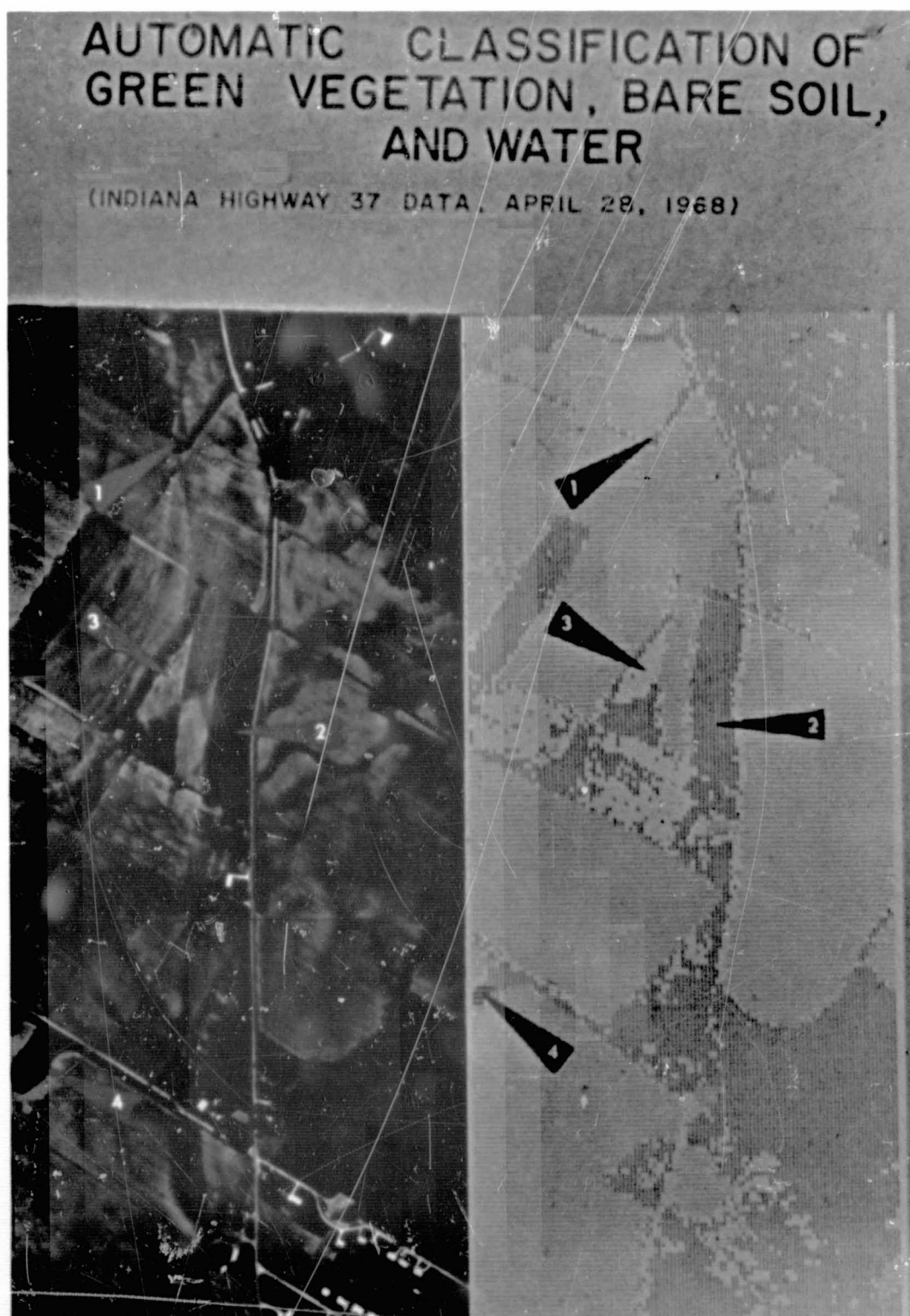


Figure 31-4.- Closeup of classification results. On the computer print-out on the right, I represents points classified as green vegetation, - represents bare soil, and M represents water. Dry, dead vegetation, houses, roads, and other points not classified into one of these three categories have been "thresholded" and are displayed as a blank.

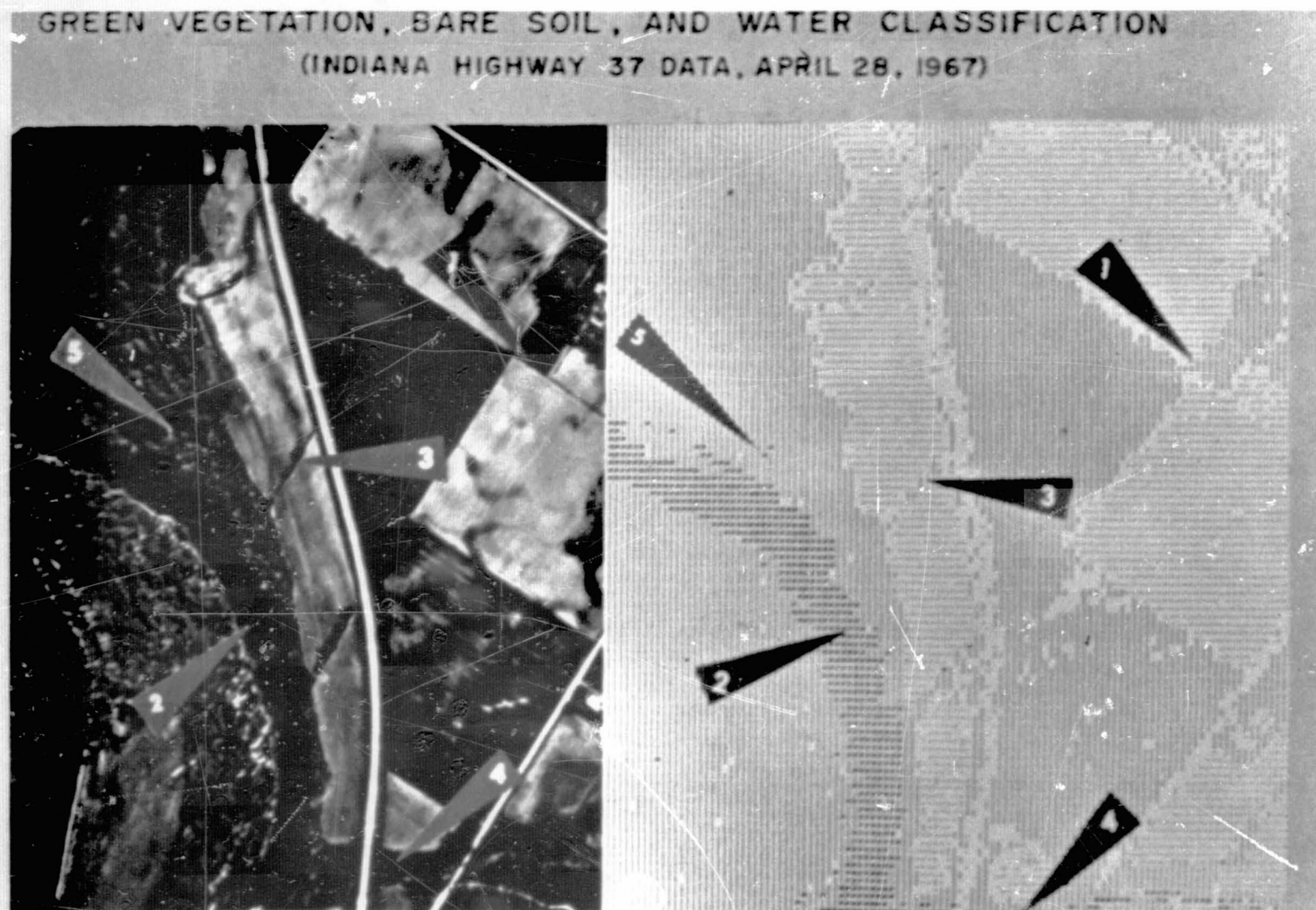


Figure 31-5.- Closeup of automatic classification results for basic cover types. The symbols used in the computer print-out are the same as those used in figure 31-4. Note the difficulty required in identifying the water at point 5 on the color photograph and note that this water was accurately classified by the computer.

31-19

ROW	CROPS	CEREAL	GRAINS
1	WHEAT	WHEAT	WHEAT
2	BARLEY	BARLEY	BARLEY
3	RYE	RYE	RYE
4	OATS	OATS	OATS
5	MAIZE	MAIZE	MAIZE
6	RICE	RICE	RICE
7	SOYBEANS	SOYBEANS	SOYBEANS
8	PEANUTS	PEANUTS	PEANUTS
9	CORN	CORN	CORN
10	WHEAT	WHEAT	WHEAT
11	BARLEY	BARLEY	BARLEY
12	RYE	RYE	RYE
13	OATS	OATS	OATS
14	MAIZE	MAIZE	MAIZE
15	RICE	RICE	RICE
16	SOYBEANS	SOYBEANS	SOYBEANS
17	PEANUTS	PEANUTS	PEANUTS
18	CORN	CORN	CORN
19	WHEAT	WHEAT	WHEAT
20	BARLEY	BARLEY	BARLEY
21	RYE	RYE	RYE
22	OATS	OATS	OATS
23	MAIZE	MAIZE	MAIZE
24	RICE	RICE	RICE
25	SOYBEANS	SOYBEANS	SOYBEANS
26	PEANUTS	PEANUTS	PEANUTS
27	CORN	CORN	CORN
28	WHEAT	WHEAT	WHEAT
29	BARLEY	BARLEY	BARLEY
30	RYE	RYE	RYE
31	OATS	OATS	OATS
32	MAIZE	MAIZE	MAIZE
33	RICE	RICE	RICE
34	SOYBEANS	SOYBEANS	SOYBEANS
35	PEANUTS	PEANUTS	PEANUTS
36	CORN	CORN	CORN
37	WHEAT	WHEAT	WHEAT
38	BARLEY	BARLEY	BARLEY
39	RYE	RYE	RYE
40	OATS	OATS	OATS
41	MAIZE	MAIZE	MAIZE
42	RICE	RICE	RICE
43	SOYBEANS	SOYBEANS	SOYBEANS
44	PEANUTS	PEANUTS	PEANUTS
45	CORN	CORN	CORN
46	WHEAT	WHEAT	WHEAT
47	BARLEY	BARLEY	BARLEY
48	RYE	RYE	RYE
49	OATS	OATS	OATS
50	MAIZE	MAIZE	MAIZE
51	RICE	RICE	RICE
52	SOYBEANS	SOYBEANS	SOYBEANS
53	PEANUTS	PEANUTS	PEANUTS
54	CORN	CORN	CORN
55	WHEAT	WHEAT	WHEAT
56	BARLEY	BARLEY	BARLEY
57	RYE	RYE	RYE
58	OATS	OATS	OATS
59	MAIZE	MAIZE	MAIZE
60	RICE	RICE	RICE
61	SOYBEANS	SOYBEANS	SOYBEANS
62	PEANUTS	PEANUTS	PEANUTS
63	CORN	CORN	CORN
64	WHEAT	WHEAT	WHEAT
65	BARLEY	BARLEY	BARLEY
66	RYE	RYE	RYE
67	OATS	OATS	OATS
68	MAIZE	MAIZE	MAIZE
69	RICE	RICE	RICE
70	SOYBEANS	SOYBEANS	SOYBEANS
71	PEANUTS	PEANUTS	PEANUTS
72	CORN	CORN	CORN
73	WHEAT	WHEAT	WHEAT
74	BARLEY	BARLEY	BARLEY
75	RYE	RYE	RYE
76	OATS	OATS	OATS
77	MAIZE	MAIZE	MAIZE
78	RICE	RICE	RICE
79	SOYBEANS	SOYBEANS	SOYBEANS
80	PEANUTS	PEANUTS	PEANUTS
81	CORN	CORN	CORN
82	WHEAT	WHEAT	WHEAT
83	BARLEY	BARLEY	BARLEY
84	RYE	RYE	RYE
85	OATS	OATS	OATS
86	MAIZE	MAIZE	MAIZE
87	RICE	RICE	RICE
88	SOYBEANS	SOYBEANS	SOYBEANS
89	PEANUTS	PEANUTS	PEANUTS
90	CORN	CORN	CORN
91	WHEAT	WHEAT	WHEAT
92	BARLEY	BARLEY	BARLEY
93	RYE	RYE	RYE
94	OATS	OATS	OATS
95	MAIZE	MAIZE	MAIZE
96	RICE	RICE	RICE
97	SOYBEANS	SOYBEANS	SOYBEANS
98	PEANUTS	PEANUTS	PEANUTS
99	CORN	CORN	CORN
100	WHEAT	WHEAT	WHEAT

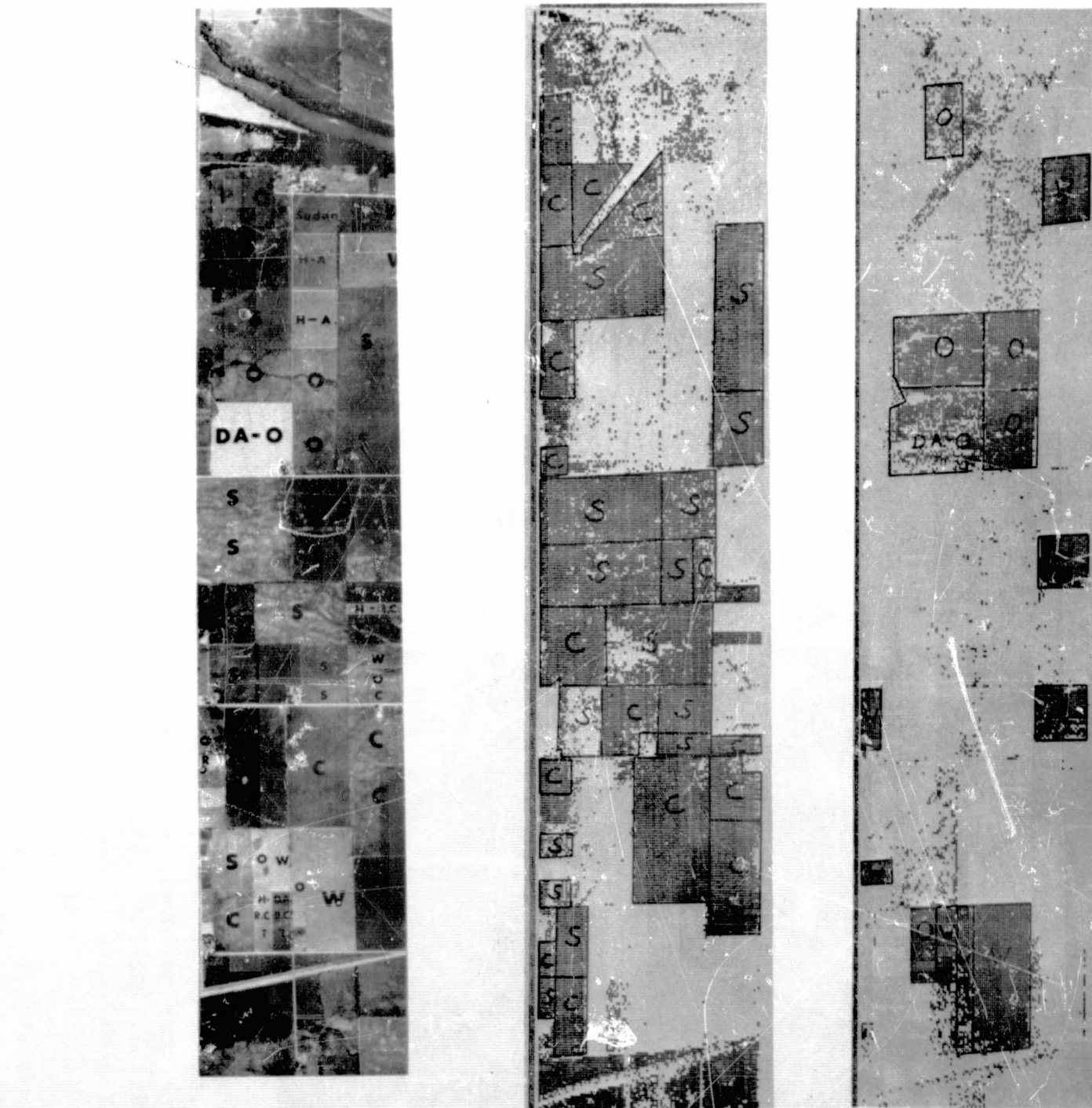


Figure 31-6.- Automatic classification results for new crops and cereal grains. The lines and crop species identification symbols were manually added to the computer print-outs. The symbols on the photo mosaic represent the following crop species or land use: S is soybeans, C is corn, O is oats, W is wheat, A is alfalfa, T is timothy, RC is red clover, R is rye, Sudan is sudan grass, P is pasture, DA is diverted acres, and H is hay.

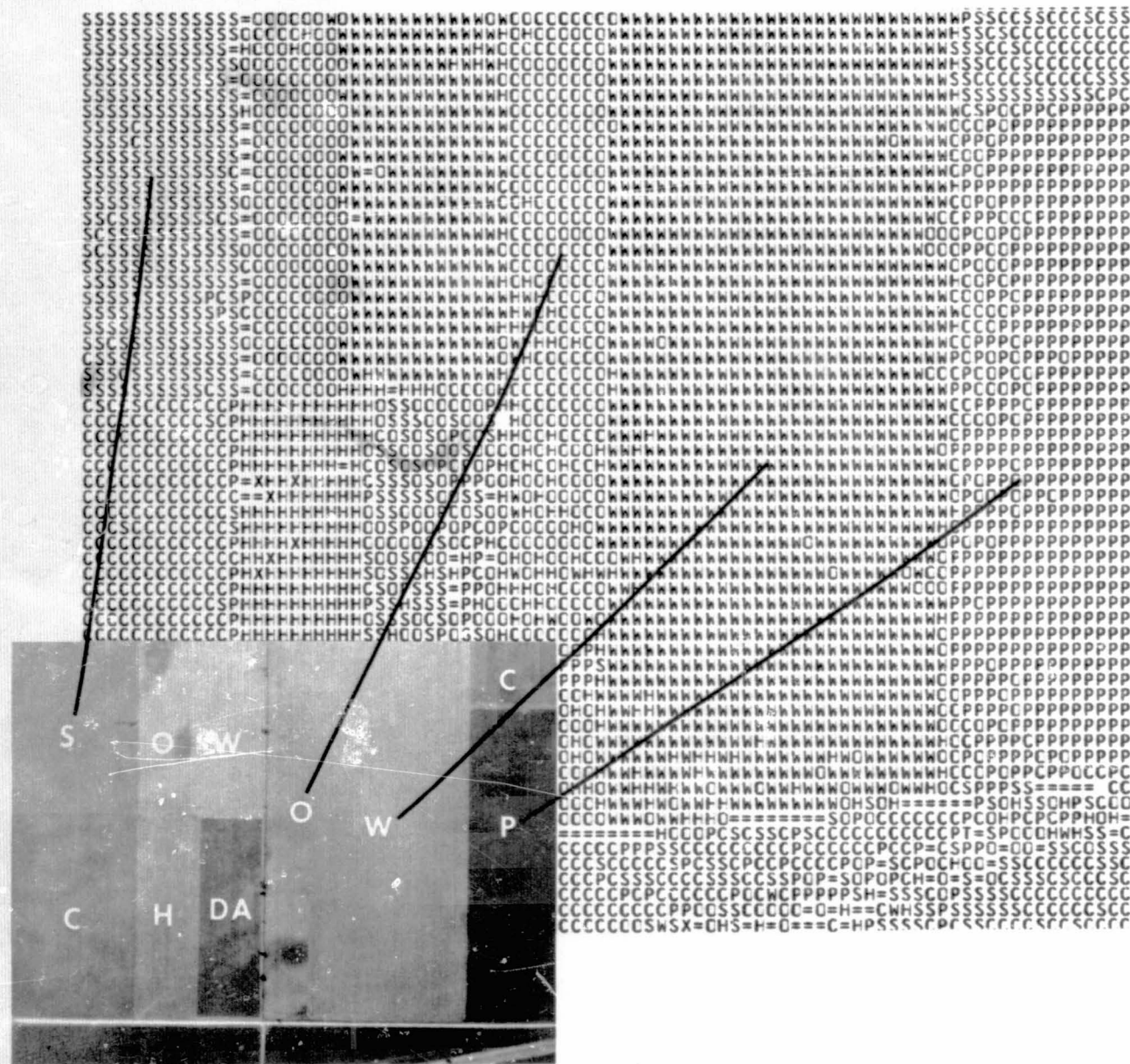


Figure 31-7.- Closeup of the computer print-out of crop species identification results and corresponding aerial photograph. Notice how difficult it is to locate some of the field boundaries on the Plus-X aerial photograph (wheat versus cats, corn versus soybeans), yet the automatic identification of the crop species allows the field boundaries to be distinctly displayed.

TEST SAMPLE AREAS

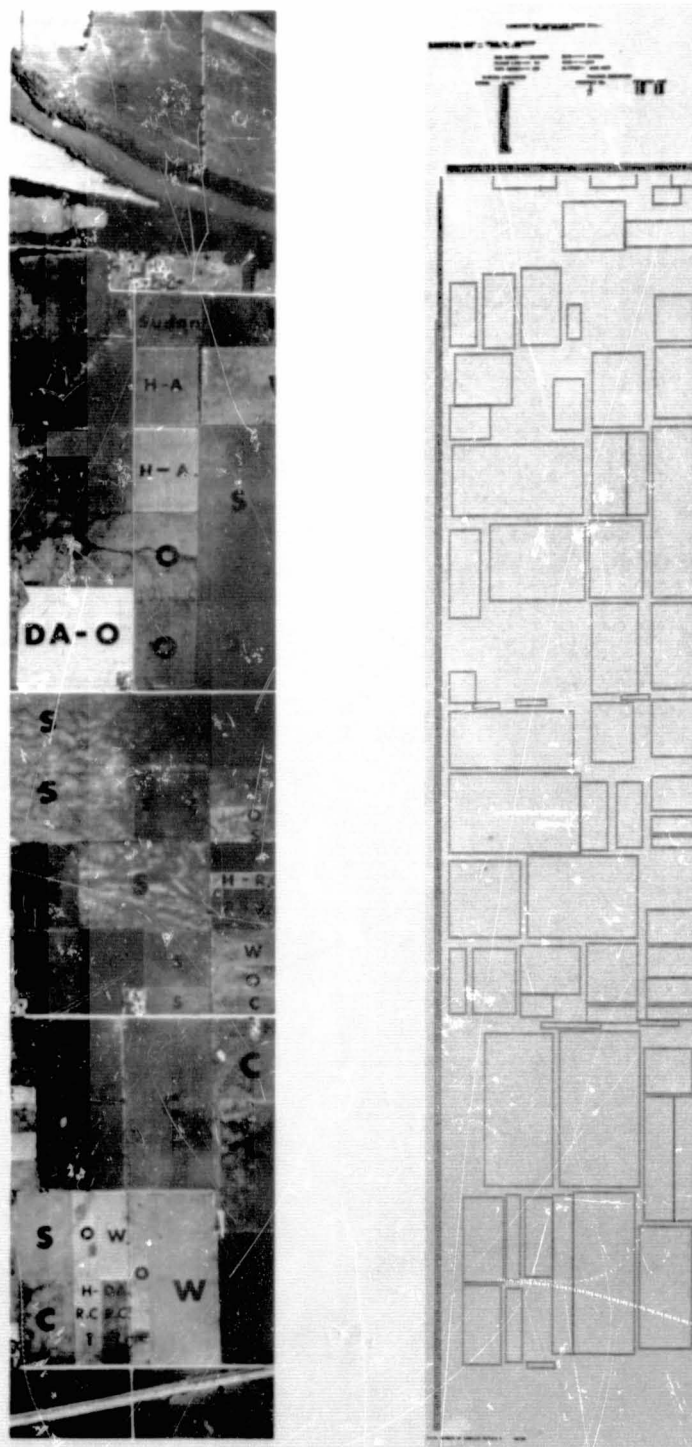


Figure 31-8.- Photo mosaic and corresponding computer print-out indicating the test areas (outlined by rectangles) within which quantitative classification results were summarized.

Classification Results For Test Samples

(Flight Line C-2; 28 June 1966; 4 Wavelength Bands Used)

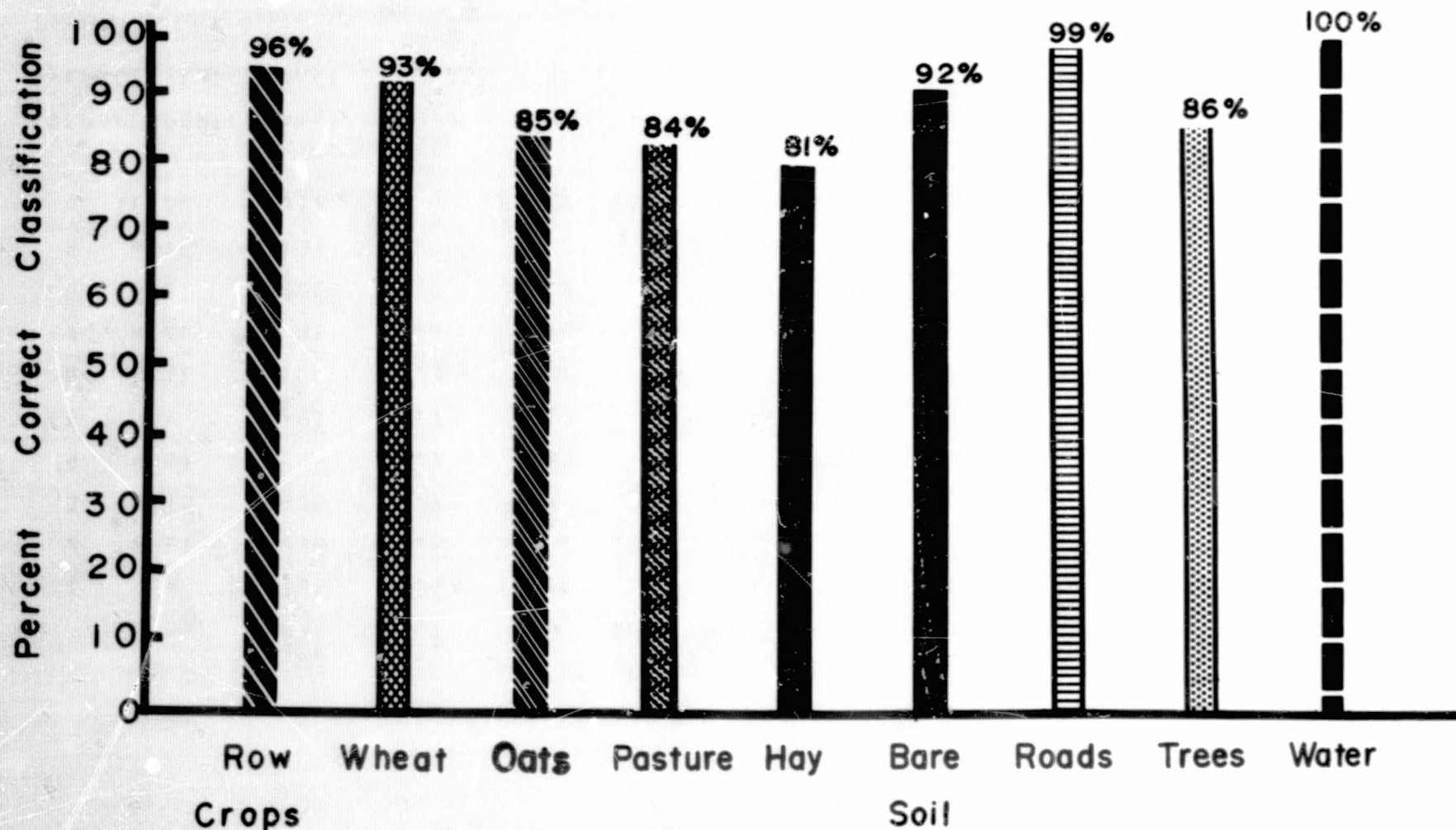


Figure 31-9.- Graph of quantitative classification results for the areas indicated in figure 31-8.

CLASSIFICATION SUMMARY BY TEST CLASSES

		NC OF SAMPLES CLASSIFIED INTO											
CLASS	NC OF SAMPS	PCT. CCRCT	ROW	WHET	DATS	PAST	HAY	SCIL	RCAC	TREE	WATE	THRS	
1	ROW	15185	92.4	14035	3	55	956	119	2	10	4	1	0
2	WHET	2736	92.6	2	2540	168	0	24	0	1	1	0	0
3	DATS	3465	84.7	175	21	2934	184	128	0	1	21	0	1
4	PAST	3595	83.7	159	1	260	3010	2	0	0	161	0	2
5	HAY	1291	80.7	17	2	226	0	1042	4	0	0	0	0
6	SCIL	104	92.3	6	0	0	0	1	96	1	0	0	0
7	RCAC	85	98.8	0	0	0	0	0	1	84	0	0	0
8	TREE	720	86.0	8	0	18	75	0	0	0	619	0	0
9	WATE	131	100.0	0	0	0	0	0	0	0	0	131	0
TOTAL		27312		14402	2567	3661	4225	1316	103	97	806	132	3

OVERALL PERFORMANCE = 89.7

AVERAGE PERFORMANCE BY CLASS = 90.2

Figure 31-10.- Table of computer output showing the quantitative classification results and the numbers of samples used to obtain the percentage correct recognition figures indicated here and in figure 31-9. This tabular format also allows examination of misclassification errors.



Figure 31-11.- Color photographs obtained by the NASA Convair 240 aircraft on June 18 and July 30, 1968. These photographs show distinct changes that have taken place for soybeans (1), corn (2), wheat (3), red clover (4), and oats (5) between these two dates. The wheat and oats were harvested in early July, and only stubble and mixture of stubble and alfalfa are seen on the July 30 photograph in fields 5 and 3, respectively.

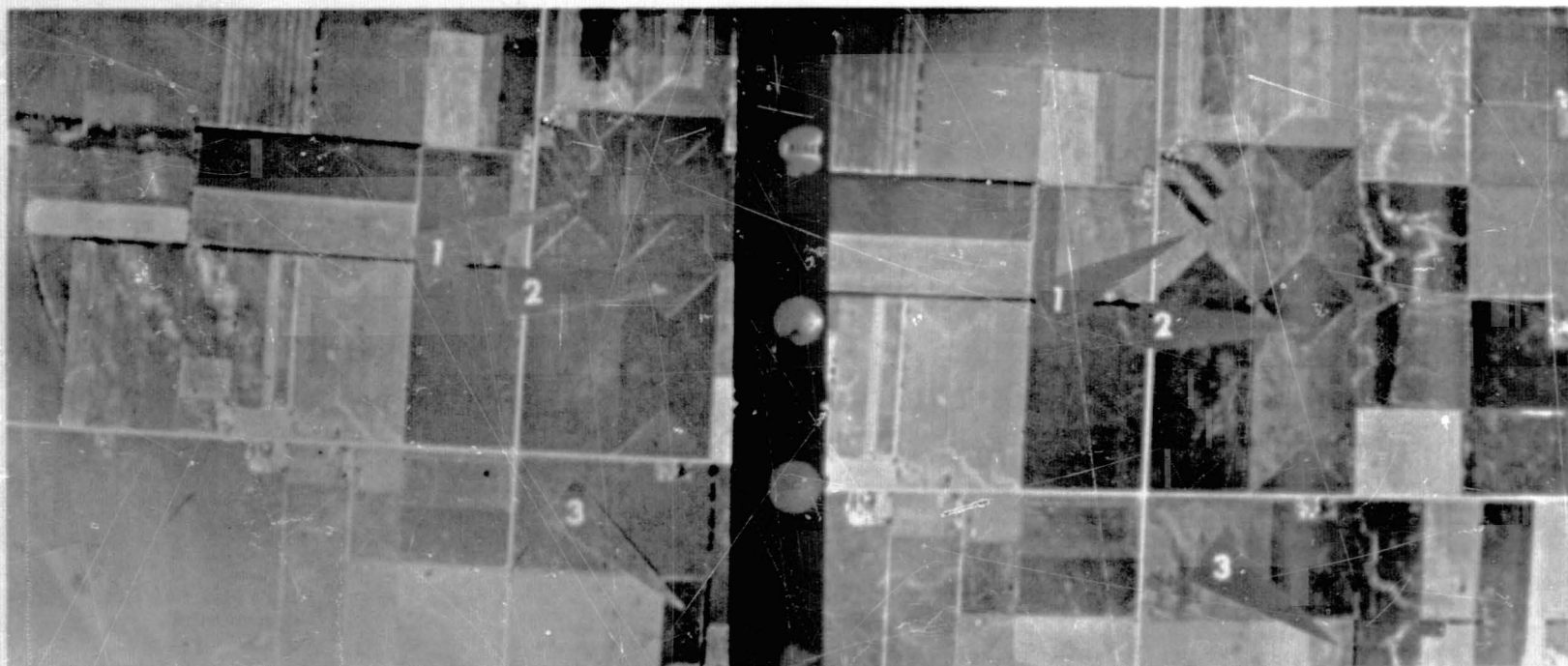


Figure 31-12.- Adjacent frames of color photography obtained by NASA on July 30, 1968. These frames show the marked effects of look angle and the row direction of the crop upon the tone recorded on an aerial photograph. Soybeans at points 1 and 3 were planted in a north-south orientation and at point 2 in an east-west direction.

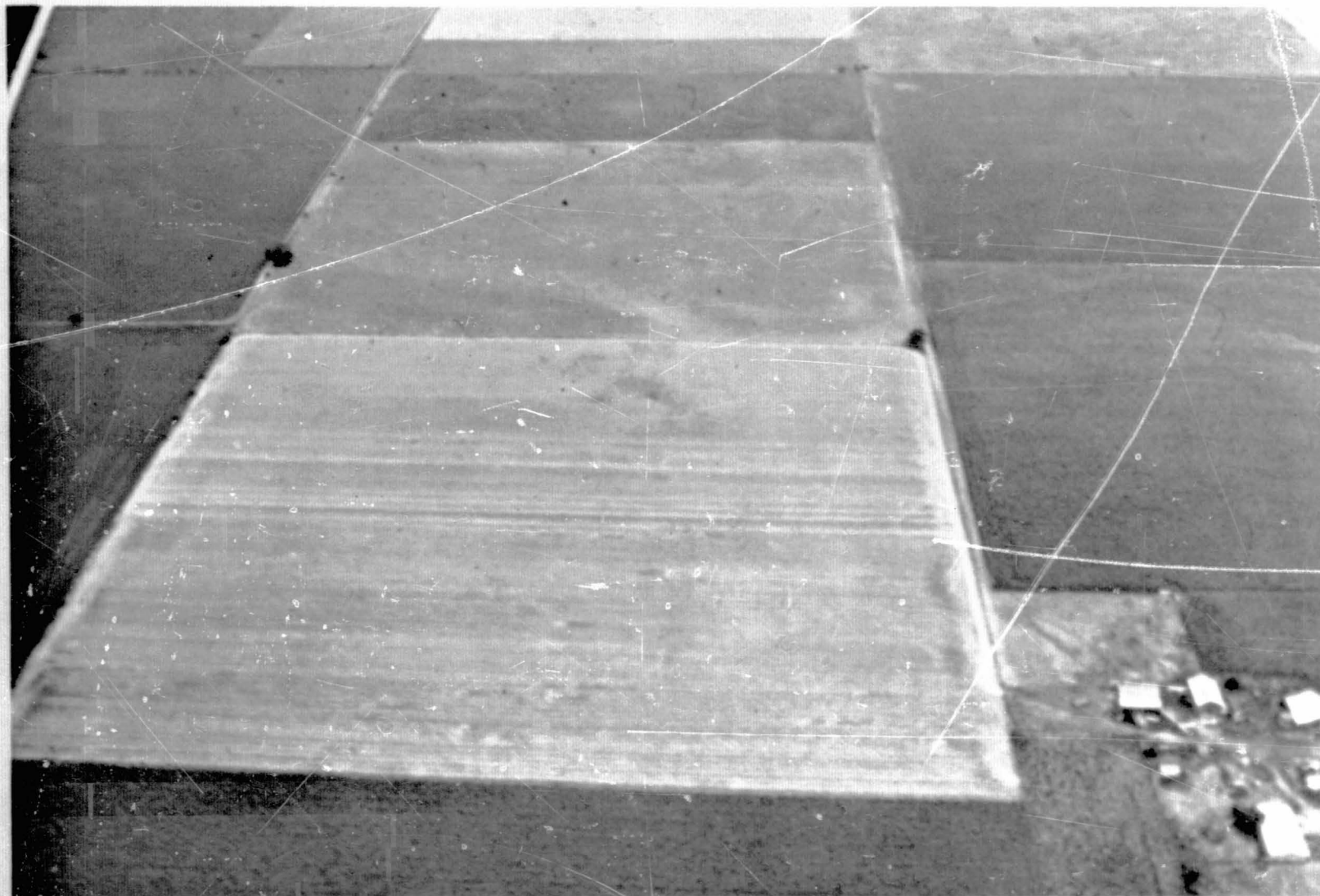


Figure 31-13.- Color photograph of an agricultural area showing three fields of red clover. The first field (medium brown area, center of photograph just beyond the yellowish stubble field) is red clover being used for hay. The second field (light green area just in front of the dark brown area) is red clover being used as pasture. The third field (just beyond second field) is very dark brown and is red clover in the diverted acres program. In each field, the crop species is the same, but the use of the field is different and creates marked differences in spectral reflectance. Ground-truth data should therefore include use of each field, as well as the identification of the species.

31-27

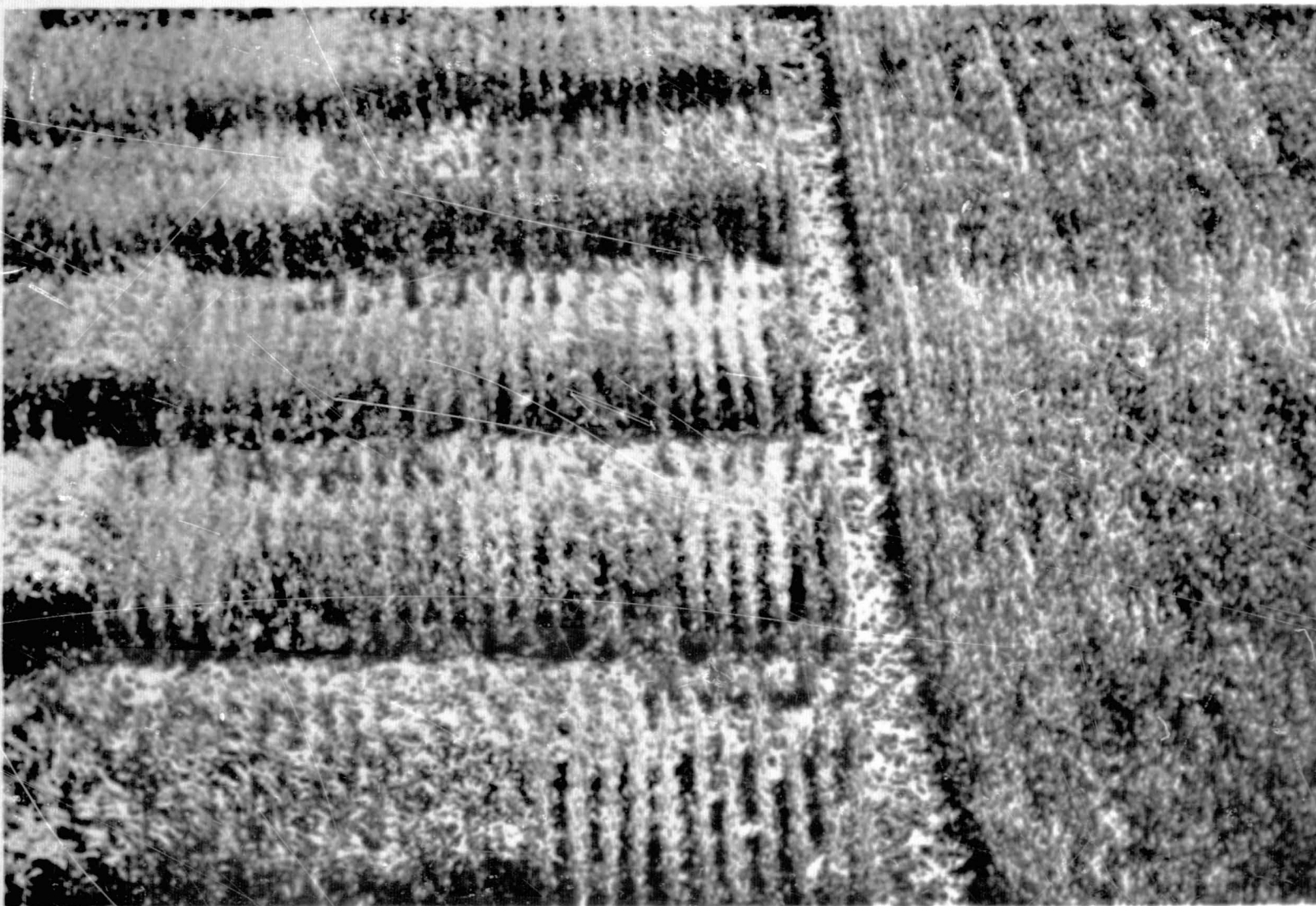


Figure 31-14.- Color photograph of wheat breeding plots on the Purdue Agronomy Farm, showing the marked differences in appearance that can be found on the same date for different varieties and crosses of a single crop species.

N71-16154

DATA PROCESSING PROGRAMS AT LARS-PURDUE*

By D. A. Landgrebe

Program Leader, Laboratory for Agricultural Remote Sensing,
and Associate Professor, Purdue University

SUMMARY

A primary objective of the Data Processing Programs Group, working in concert with the other four Laboratory for Agricultural Remote Sensing program areas, is to establish the existence of uniquely characteristic earth surface features of importance to agriculture. Initial efforts have concentrated on developing such a capability for the identification and measurement of important crop types in temperate zones. Other identification tasks of economic importance include soil mapping, identification of water bodies, detection of stressed vegetation conditions, general landscape mapping, et cetera. Feasibility studies to date indicate that the most promising set of characterizing features include stable, precise measurements of radiance of each scene-resolution element simultaneously in multiple-wavelength bands.

An appropriate instrument to obtain such measurements is a multispectral, object plane scanning radiometer. Unfortunately, this equipment is not yet available on a NASA aircraft; for this reason, NASA has funded data collection with a multispectral scanner developed under U.S. Army contract by the University of Michigan, mounted in a University of Michigan DC-3 aircraft. While this system has shortcomings, it has permitted feasibility research to be conducted. Laboratory for Agricultural Remote Sensing researchers look forward to the availability of a state-of-the-art multispectral sensing system on the NASA aircraft in the not too distant future. Such an instrument would be calibrated with state-of-the-art techniques and would be a single-aperture instrument, as opposed to the two-scanner, four-aperture system developed at Michigan. A state-of-the-art scanner of this type will greatly facilitate the handling and processing of data and permit investigations which are difficult, if not impossible, with existing equipment.

*This report is based upon work sponsored jointly by the National Aeronautics and Space Administration and the U.S. Department of Agriculture, in cooperation with Purdue University.

The work reported herein, therefore, utilized as prime data those data gathered by the University of Michigan under contract to NASA and other agencies. All pictorial computer print-outs, data overlays, and feature extraction studies reported herein utilized these data as prime-data inputs.

Critical to the success of research on automatic processing methods is the availability of extensive, high-quality, detailed ground truth. Extremely useful ground truth is collected with large-scale, high-quality color, color infrared, and black and white panchromatic aerial photography. The NASA aircraft has provided much of this type of data for the Laboratory for Agricultural Remote Sensing program. Panchromatic photography is utilized for the compilation of up-to-date base map materials. Field boundaries, color types, crop conditions, et cetera, are collected in the field and noted on panchromatic photography. The large-scale color and color infrared photography is invaluable in the selection of training samples and in the evaluation of classification trials with multispectral data in the research phases of our programs. Photography provided by the NASA aircraft has also been collected for use in temporal analysis of agricultural scenes and is permitting definition of the point in the calendar year at which certain agricultural conditions of importance can best be identified. The photography has also indicated effects of various sun-angle effects and hot-spot effects. Exemplary of the results with the photographic data was the observation of irrigation tile lines under given soil moisture conditions. Photography at a later date in a dry condition did not reveal these irrigation lines. We believe that high-quality photography is an invaluable input in our research to develop automatic recognition capabilities with multispectral data. In the future, as research data are collected over large areas, the use of photographic material will take on added importance.

INTRODUCTION

In addition to participating in the pattern recognition studies discussed by R. Hoffer in another report, the Laboratory for Agricultural Remote Sensing Data Processing Programs Group is engaged in several other activities. Three of these activities will be briefly described at this time. We begin with a discussion of the computer software system which has been developed to carry out research, and with, more importantly, the manner in which a system of this type can be used in an operational earth-observational satellite system. The work of the Group in developing techniques for optimal spectral band selection is discussed next. This is followed by a brief discussion of the studies and of the resulting system to overlay non-time-coincident scanner channels upon one another.

A MODE OF OPERATION FOR AN OPERATIONAL SYSTEM

Figure 32-1 shows a block diagram of an operational earth-observational information system. In this system, data are gathered by the sensor and then pass through onboard processing in which data are prepared for transmission to ground read-out stations. There must of course be a data link, and this is followed by ground-based processing. In this step, the remaining preprocessing of the data necessary prior to analysis is carried out. Following preprocessing, an appropriate analysis algorithm is applied to the data in order to convert data to information. This step is followed by distribution to consumers. At Purdue University, research is being carried out which is applicable to each of the six blocks illustrated in this report. This work is concentrated on a system which relies upon an automated analysis algorithm. Shortly after the Laboratory for Agricultural Remote Sensing (LARS) was founded, approximately 30 months ago, the use of pattern-recognition techniques (as compared to the spectral-matching techniques under research at that time) was proposed as an approach to finding a specific analysis algorithm. Let us briefly review the significant features of this type of approach.

Figure 32-2 shows a diagram of the manner in which pattern-recognition systems are typically described and designed. One sees that such systems are divided into two main steps. These are indicated here as the receptor and the categorizer. It is the job of the receptor to extract from the pattern certain characteristic measurements indicated here as a feature vector or measurement vector. In the case of our system, the components of this vector may consist of samples from the radiance-versus-wavelength curve of the electromagnetic energy, as measured by the sensor. In addition to simply making these measurements, the receptor is sometimes called upon to preprocess these measurements in an appropriate manner to place in greater evidence the significant properties of the pattern.

It is the job of the categorizer, then, with the feature vector as an input, to classify the vector as being a member of one of several preestablished categories. Figure 32-3 illustrates briefly how this might be done. This figure shows a hypothetical two-dimensional feature plot, a plot, for example, of radiance in spectral band 1 versus radiance in spectral band 2. Points have been plotted here to illustrate how three categories of crops might distribute themselves. Given the categories and training samples for the crops, the task of designing the categorizer becomes one of deciding upon decision boundaries which divide this two-dimensional space into regions belonging exclusively to each of the three crops expected. Note that while it was necessary here to restrict ourselves to two dimensions (i.e., spectral bands), no such restriction is necessary in designing a categorizer, and any number of

spectral bands (i.e., a feature vector of any number of components) is permitted. Furthermore, components of the feature vector need not be spectral measurements, but may be other types of information such as time of day, sun angle, or any other component.

We must point out two important facts about automated classification systems. First, note that in designing such a system, a region of N-dimensional space must be assigned for each type of surface cover which is expected to be encountered in observing the surface of the earth. This illustrates why the definition of categories is a key problem in designing such a system. Categories must be established which are in this sense all inclusive, which are of interest to the information consumer, and of course which are separable (i.e., nonoverlapping).

The second point is that desirable categories are generally not as separable as they have been made to appear in this hypothetical feature space (fig. 32-2), and they certainly vary greatly with time of day, view angle, geographical location, and many other variables. In short, it is naive to assume, for example, that a unique spectral signature can be determined for any of the major crop species which will be valid over an extended geographical area and over an extended period of time. It is for this reason that we were led from the beginning to attempt to establish that at any one time and in any one geographical area, differences in N-space between the desirable categories exist, rather than to attempt to determine what the differences are. As we have said in other reports, we are attempting to establish the existence of signatures rather than to determine what they are. The reason for this approach is that because of the great variability of the agricultural scene from season to season, from week to week, and geographical area to area, the approach to be taken is to reestablish the correct decision boundaries each time data from a new area at a new time are received.

Thus, in figure 32-1, what is significant to this discussion about such a system is indicated more by what is not present in the figure than by what is. These missing parts of figure 32-1 are all the other information inputs, such as ground truth of the area just observed from space, which will be input into the ground processing and data-reduction phases of this system. By retraining the system each time data are gathered, that is, by redefining the precise location of the decision boundaries, one will most certainly increase the performance of such a system. In addition, one greatly simplifies the job of the sensor designer and compensates for the difficulty in achieving precise absolute calibration. One can, by this mode of operation, normalize out many variables such as season-to-season variations which under other circumstances would prevent a high performance for the system.

It seems likely at this time that the amount and cost of ground truth necessary for operation of such a system in the agriculturally

significant parts of the U.S. will not be prohibitively great, certainly not so great as the amount of ground truthing which is now being done to carry out the surveys by less powerful methods by the U.S. Department of Agriculture.

In summary, then, what we have suggested over the past 2-1/2 years is that as a result of the high data loads, an automated analysis algorithm will be necessary for many survey tasks, and that the mode of system operation will be to gather a limited amount of ground truth by manual means and to use the satellite-gathered data to extrapolate from this small amount of ground truth to a much broader area of earth. The question of whether this can be done, then, rests upon the ability to design a system which can both discriminate between significant categories and be redesigned simply and easily in short periods of time.

An affirmative answer to this question is beginning to emerge. Figure 32-4 shows the programming system developed by LARS for carrying out pattern-recognition research. This system called LARSYS has been designed with this operational (extrapolation) mode in mind. Though all parts of this system are necessary in research and will be required in an operational system, we wish to draw attention now to only three parts. These are LARSYSAH, in which the aircraft data handling and preprocessing operations are carried out; LARSYSAA, in which the actual analysis algorithm is implemented; the LARSYSGT, the ground-truth-data processor. Figure 32-5 shows how these three parts are used to carry out classification attempts. One sees that the researcher receives inputs from LARSYSAH, presently in the form of gray-scale print-outs, and ground-truth information for LARSYSGT. He uses these to achieve the proper operation of the analysis algorithm carried out in LARSYSAA. A more detailed diagram of LARSYSAA is illustrated in figure 32-6. One sees here that this subsystem contains four processors, each under the control of its own supervisor. The first, the statistics processor, is used by the researcher to determine various statistical parameters of proposed classes in order to establish, a priori, the probable degree of separability of the proposed classes. The second processor, the feature-selection processor, is used to select the optimum set of features for the proposed classification and, in addition, serves to further indicate the degree of separability of the proposed classes a priori. The classification itself is carried out by the third processor with the results (in this research phase) being written immediately onto digital magnetic tape. This tape may then be read by the display processor for display and evaluation of the classification result. The print-outs seen in R. Hoffer's presentation were results of this display processor.

The system, as it now stands, has really been designed with a research mode of operation in mind. However, on a recent data-gathering mission, it was decided to attempt to test this extrapolation mode of

operation to further establish the practicality of this approach and to determine if it is reasonable to expect classifications in a short period of time.

Figure 32-7 shows a photo mosaic of Tippecanoe County within which the LARS test areas are presently located. The area shown here is approximately 21 by 24 miles, and we mention parenthetically that it is occasionally helpful to us to view this mosaic, simply to remind us of the quantity of data which will need to be processed by a space system. This county, 501 square miles, is approximately 1-1/2 percent of the land area in the state of Indiana and a very small portion of the agriculturally significant parts of the United States.

The primary purpose of the flight mission carried out by the University of Michigan aircraft was to reestablish the capability between the scanner system and our software system. It has been approximately 2 years since a data-gathering mission for LARS had been flown by this system. However, as previously mentioned, it was decided to make the test of this extrapolation mode a secondary objective. Two flight lines were flown, one north-south, extending the length of the county approximately 3 miles east of the western boundary. The second one was an east-west flight line running the width of the county approximately 4 miles from the northern boundary of the county. Thus, there were about 45 miles of data in all. The data were flown at 5000 feet. The mission was flown on Tuesday, July 30, 1968, under less than ideal conditions of cloud cover.

It was not possible for us to obtain analog magnetic tapes of the data until Wednesday night at approximately 10:30 p.m. Between that time and 4:30 p.m. the next afternoon, the tapes were converted from analog to digital, calibrated, and reformatted; some modifications in the system caused by modifications in the aircraft system were accomplished; categories were selected; training samples for those categories were determined; and the first classification result became available. The categories in this test were soybeans, corn, water, trees, and a mixed category made up of oat stubble, wheat stubble, diverted acres, and pasture. The overall accuracy, including test samples and training samples, was of the order of 75 to 80 percent on this first classification.

Figure 32-8 shows the effect of the cloud conditions on the data and illustrates a very simple type of preprocessing which LARSYSAH can carry out to improve the appearance of the data. The print-out on the left in figure 32-8 shows a portion of the east-west flight line with west at the top of the print-out. It is seen that as the flight proceeded to the east, that is towards the bottom of the print-out, a cloud condition developed which greatly reduced the contrast scale in the data. The line printer symbol to relative radiance correspondence for

the print-out was determined by histogramming the first 1000 scan lines. The center print-out shows the result of using the last 500 scan lines (i.e., in the dark region) for this purpose.

A change made in the University of Michigan system since previous flights for LARS included the addition of a sun sensor which makes available an electrical signal proportional to the amount of solar radiation present on the top of the aircraft. By using this input, it is possible to normalize out to some extent the variation insolation energy. The third print-out of figure 32-8 was obtained from this same data using the histogram of the first 1000 lines but calibrating to this sun sensor. The graph on the right shows the relative output of the sun sensor as a function of scan-line number (radiance increasing to the left).

FEATURE SELECTION STUDIES

We turn now to a brief description of the studies to determine an algorithm for finding the optimum set of spectral bands (features) for any given classification task. Consider again the two-dimensional space shown in figure 32-3. The problem of optimum feature selection reduces to determining the degree of separability of the various defined classes in terms of the proposed set of features. Then, by determining this degree of separability for all possible sets of features, one can determine the best set to use. The key to the success of this approach lies in having a suitable statistical distance measure which indicates the distance between two point sets in N-dimensional space. Figure 32-9 shows an example print-out from the feature selection processor of LARSYSAA. In this processor, such a statistical distance measure, called divergence, has been implemented. The program has been written in a mode highly interactive with the researcher so that he may make judgments and supervise the calculations as they proceed. The program also has many options, not all of which can be illustrated here.

In the example presented in this report, five classes were designated for study, as follows:

<u>Class name</u>	<u>Symbols</u>
Soybeans	S
Corn	C
Oats	O
Wheat I	W
Wheat II	M

There are 12 channels from which to pick optimum sets. The program was instructed to determine the 30 best sets of four channels (features) for separating (i.e., correctively classifying) these five classes. In addition, it was specified that the separability of the four-tuple of channels 1, 5, 10, and 12 should be displayed, even if it were not in the top 30 sets.

The results are as shown. The best four-tuple of channels is seen to be 1, 6, 10, and 12. To the right of the column labeled D(TOT) are listed the interclass distances. For example, for channels 1, 6, 10, and 12, that of soybeans and corn (S and C) is 36, while that for soybeans and oats (S and O) is 84. This means that a classifier will have less difficulty separating soybeans from oats than soybeans from corn. It is inappropriate in the space available here to say much about the meaning of the size of these numbers beyond the general statement that a distance of about 400 indicates very good separability, while a distance below about 20 would be marginal.

The entries in the column labeled D(TOT) are the sum of the interclass distances, and it is on the basis of these numbers that the feature sets are ordered. The column labeled DIJ(MIN) gives the minimum interclass distance of each feature set for easy reference. Other options illustrated include the following: If desired, one may apply a maximum distance to be considered in ordering the feature sets. This is desirable in order to prevent one highly separable pair of classes from unduly influencing the ordering of feature sets. The maximum set in this example is 350, and the entries indicated by three dots are those exceeding this maximum.

One may also set a minimum distance. If any interclass distance does not exceed this minimum for a given feature set, that feature set will be deemed unacceptable and not considered further. This is indicated by the blank lines in the interclass distance table. Furthermore, it is possible to apply varying weights to the interclass distances, as indicated by the numbers in parenthesis under the symbols. In this example, even though it is necessary to define two wheat categories, it is not desired to separate them from each other. Therefore, a weight of zero has been specified for the WM interclass distance. Note also that the feature set specifically called for (1, 5, 10, and 12) is displayed and marked by ***. Its rank was found to be 34.

Figure 32-10 shows the result of using this feature selection method on a specific classification task. In choosing the best set of features, one not only has the problem of finding the best set for a given size (e.g., the best four features or the best five), but one must also determine what size feature set to use. Figure 32-10 shows the result of such a study. In this case, the feature selection algorithm was used to determine the best set of features of each size

from one to 12. It is of interest to note that better accuracy is obtained by using the best three features than by using any other set of any size including all 12. In short, it is not always better to continue to add features.

ON OVERLAYING NON-TIME-COINCIDENT MULTISPECTRAL DATA

While the University of Michigan multispectral scanner system can gather data in 18 spectral bands, it does not gather all of this data through the same aperture; therefore, all of the data are not time coincident. It is seen from the previous discussion that in the application of pattern-recognition techniques, classifications of points on the ground are made from an N-dimensional feature vector, and the components of this vector consist of the radiance values in the various spectral bands from that point on the ground. In order to be able to use this approach, then, one must be assured that the components of each vector represent the radiance coming from the same point on the ground. Figure 32-11 shows two print-outs from two regions of the spectrum, together with a photo mosaic of the area for comparison. The print-outs are from two channels which are not gathered through the same aperture. The print-out in the middle is from the 0.62μ to 0.66μ region of the visible spectrum, while the print-out on the right is from the 8μ to 14μ region of the thermal spectrum.

If one wishes to carry out a classification in which these two channels are to be components of the feature vector, one must be assured that the address on the digital tape on which these data are contained for the visible and the thermal data are the same. We refer to establishing this commonality of addresses as "overlaying of channels" as it amounts to overlaying of the right print-out exactly upon top of the print-out shown in the middle of this figure.

One reason for undertaking this task for finding an overlaying procedure was to simulate a single-aperture instrument from the 18-channel data of the University of Michigan system. However, even after a single-aperture scanner has been built and is in operation, the ability to do this will still be of critical importance to the program because, for example, valuable information could be obtained by composing feature vectors which have as one component the radiance from the 8μ to 14μ portion of the spectrum gathered in the daytime and, as another component, the radiance from the same portion of the spectrum gathered at night. The feature vector in this fashion could contain information about the thermal variation as a function of time of the area overflown, and this information would be extremely helpful, especially in classifications involving the geology of the area. Another example might be to use in this manner data which have been gathered at two times several weeks apart.

In addition, there will always be images from portions of spectra which cannot be gathered through a single aperture, for example, images from the microwave region and the optical region. Thus, if these two regions of the electromagnetic spectrum are to be used as components in the same feature vector, one is forced to devise an overlay procedure.

The first attempt at carrying out an overlay procedure involved simply attempting two-dimensional correlation of the two images. This proved not entirely effective since the accuracy with which the overlay must take place must be to within one resolution element. Figure 32-12 shows a block diagram of the steps of the LARS overlay system recently placed in operation. It was found necessary to add, as a first step, a border enhancement process in which the boundaries evident in the data are greatly enhanced. This is followed by a two-dimensional correlation process between the two edge-enhanced images. Once this correlation process has been completed, the actual overlaying itself for alining of the data in the two channels can take place. Figure 32-13 shows print-outs of the two channels of data and the resulting print-outs after border enhancement.

Again, in this calculation as well as in the previous ones, it is found helpful to have human participation in the calculations as they proceed. In this case, it is convenient and helpful to system performance if checkpoints along the way can be established. This is illustrated in figure 32-14. These checkpoints are features which are obvious in the imagery as being points of commonality in the two images.

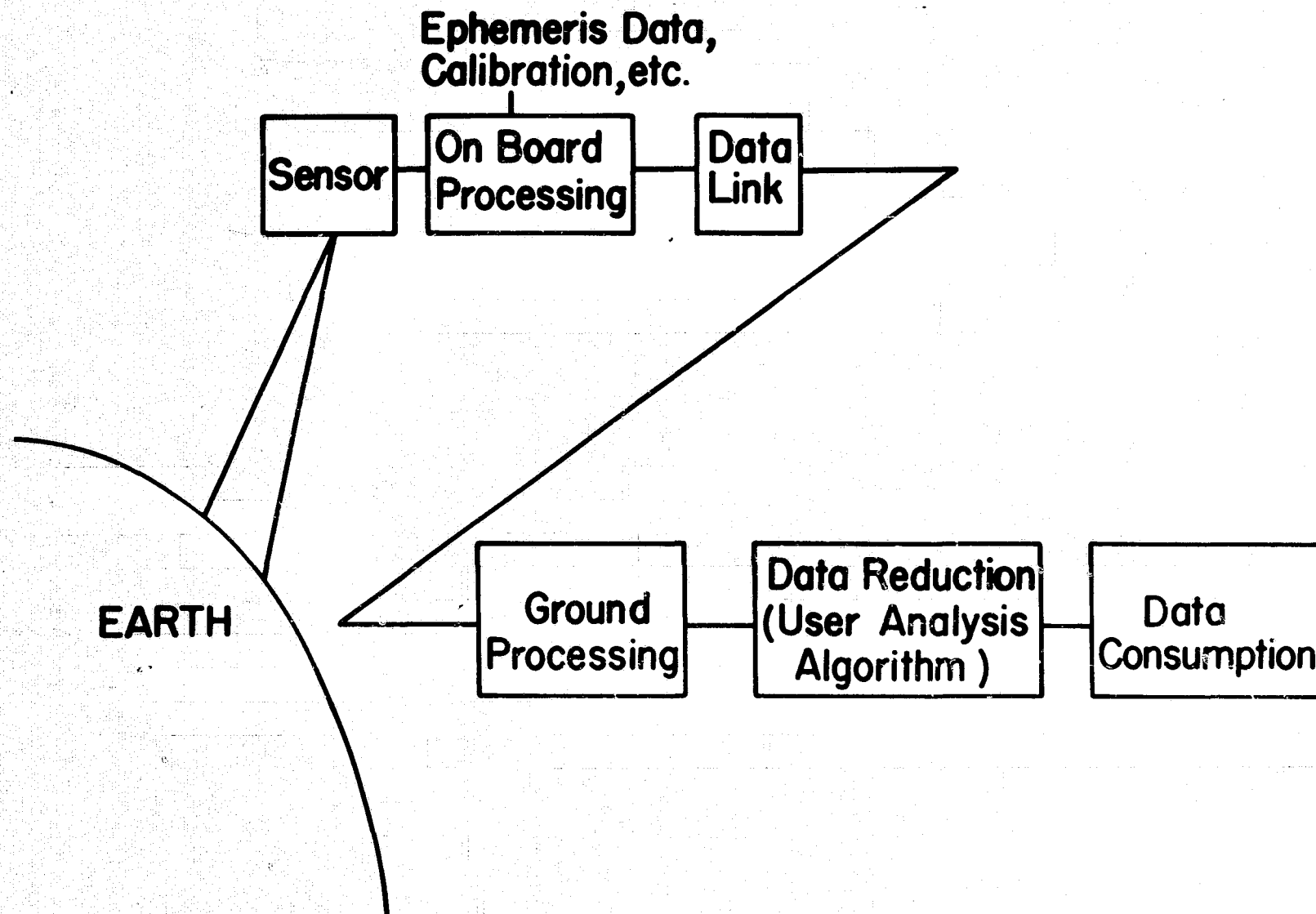


Figure 32-1.- Diagram of earth-observational system.

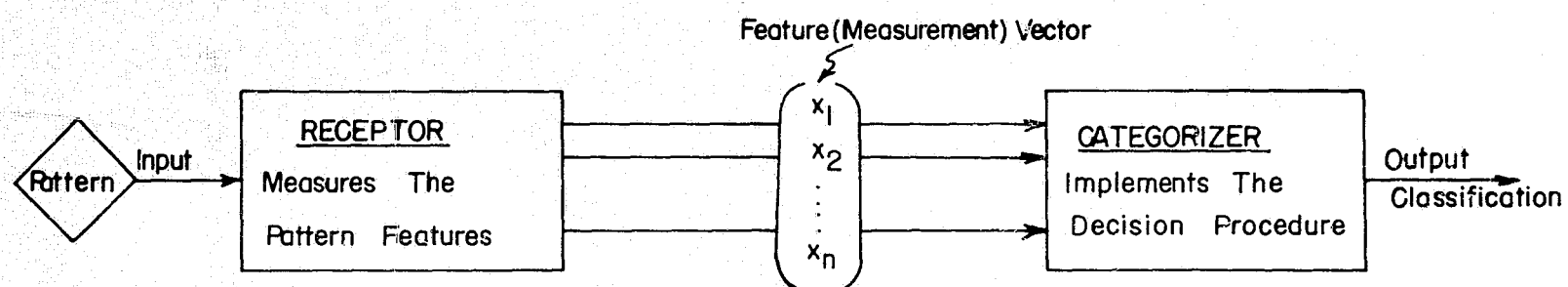


Figure 32-2.- Block diagram of a pattern-recognition device.

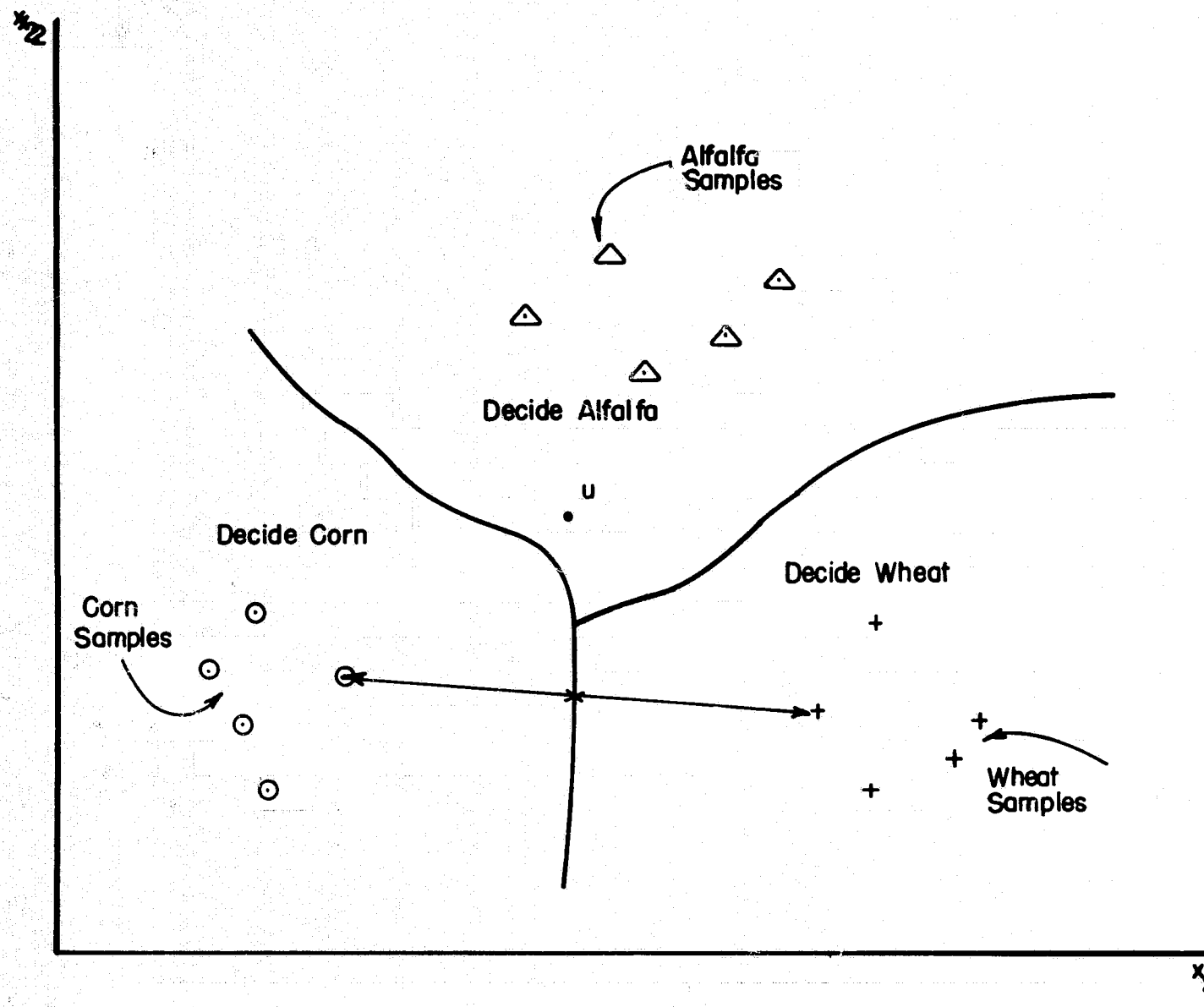


Figure 32-3.- Example of categorizer decision boundaries in two-dimensional feature space.

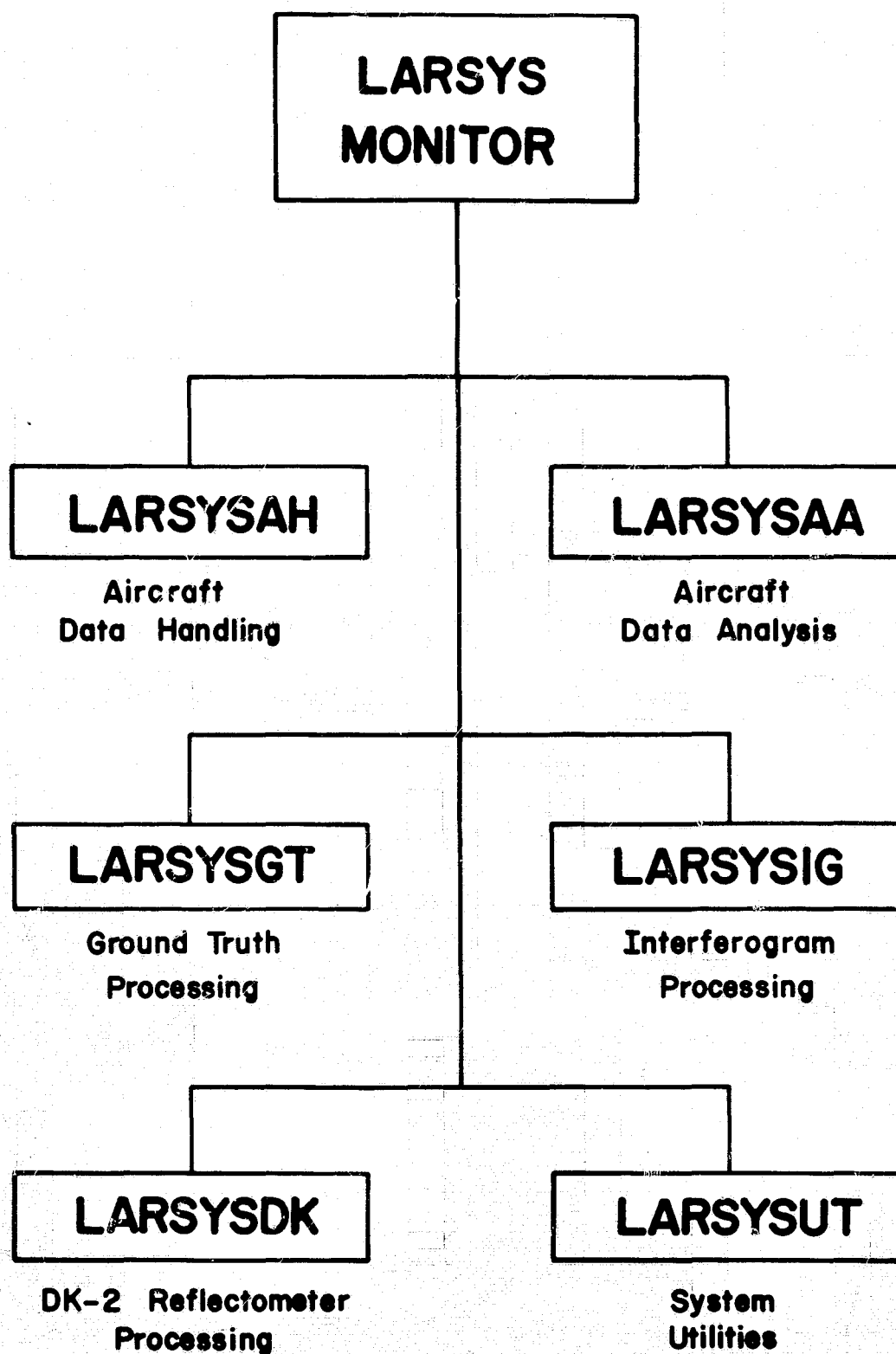


Figure 32-4.- Organization of the LARSYS programming system.

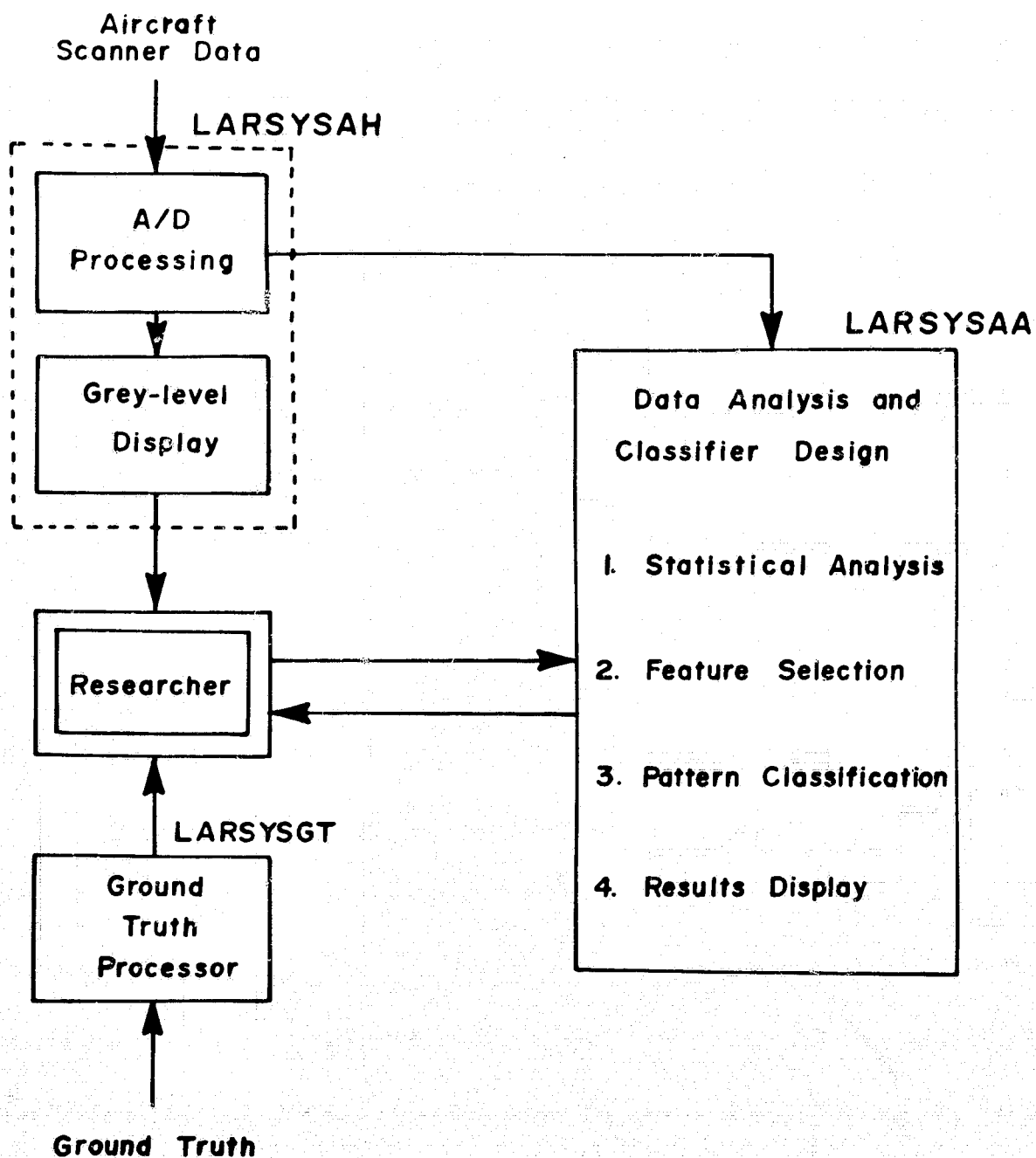
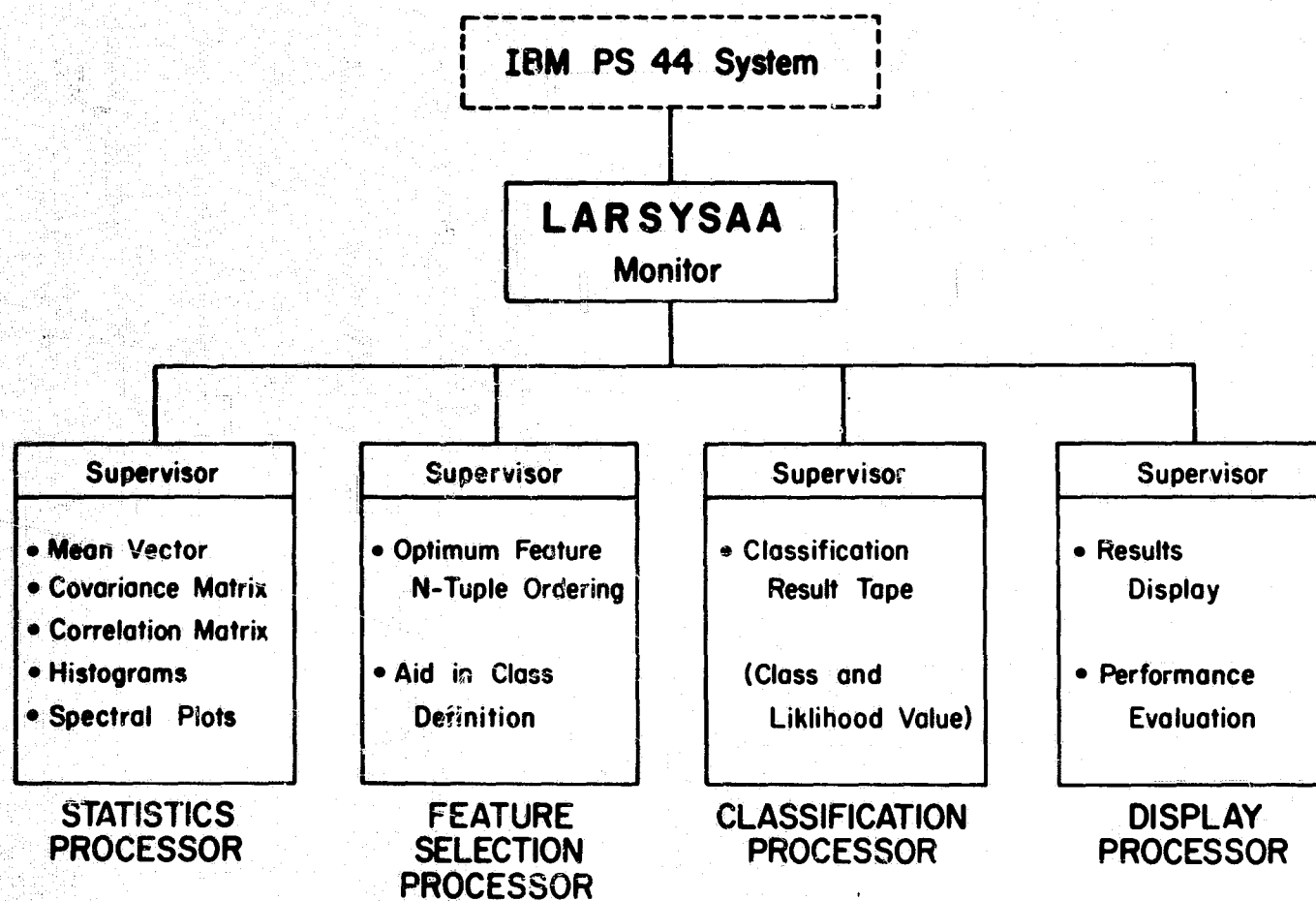
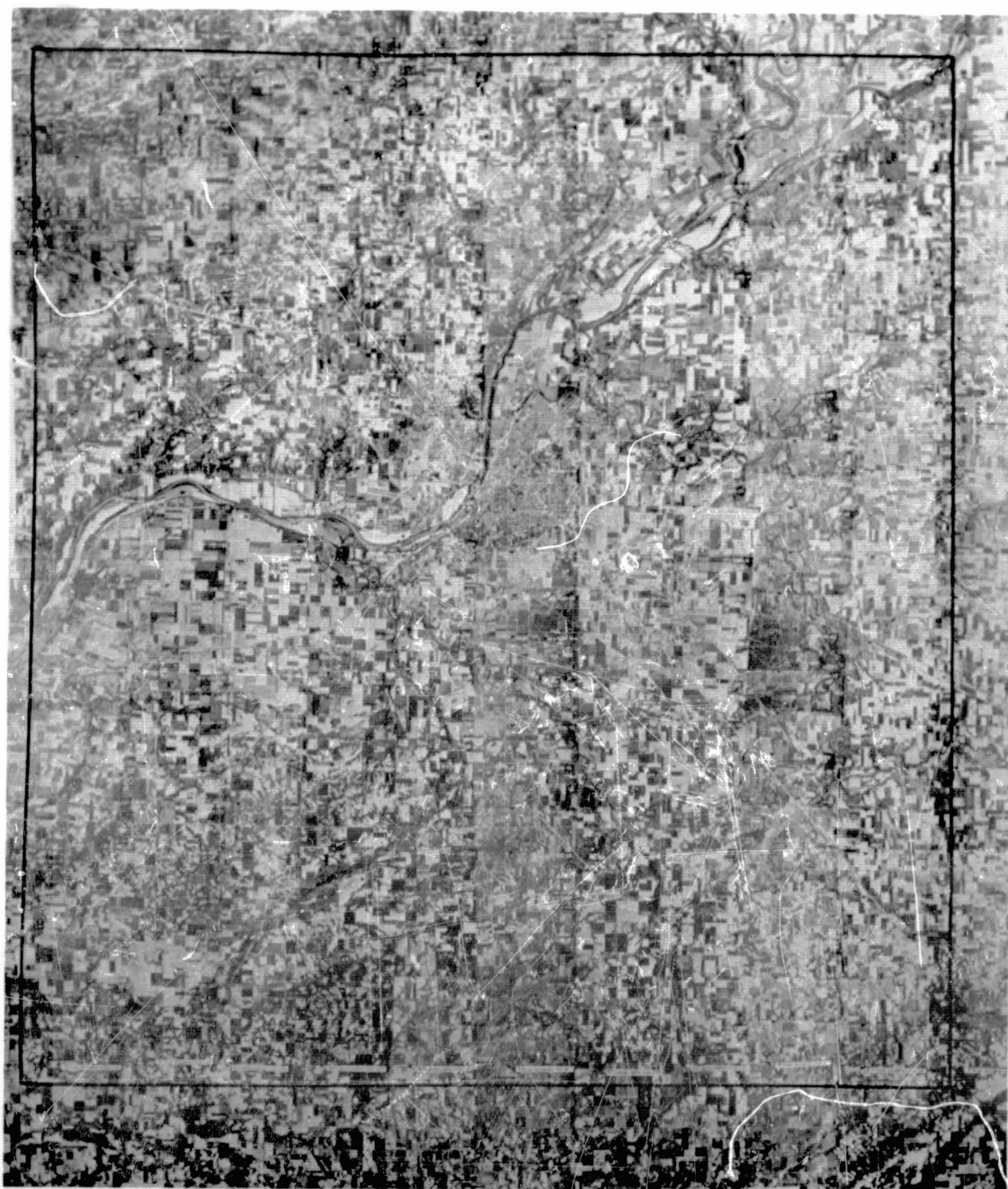


Figure 32-5.- Use of LARSYS in categorizer design.



LARS/PURDUE

Figure 32-6.- Organization of LARSYSAA.



Tippecanoe County
(501 sq. miles)

Figure 32-7.- Panchromatic aerial photo mosaic of
Tippecanoe County, Indiana (21 by 24 miles).

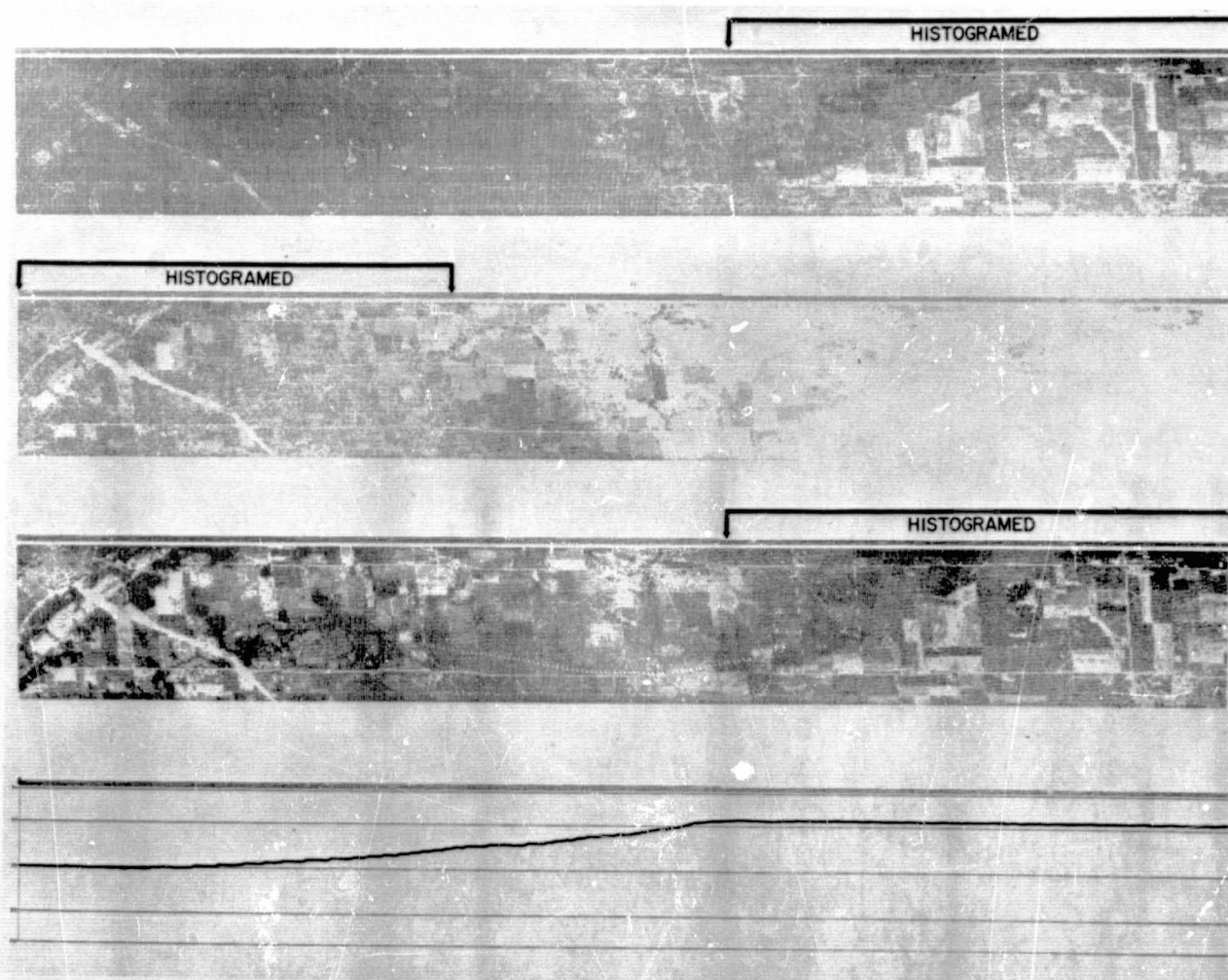


Figure 32-8.- Lineprinter print-outs of July 1968 scanner data showing the effects of cloud shadows and processing to minimize it.

LABORATORY FOR AGRICULTURAL REMOTE SENSING
Purdue University

*** LARSYSAA ILLUSTRATION ***

RESTORED DATA
RETENTION LEVEL .. 325
MINIMUM 25
MAXIMUM 350

	FEATURES	DIJ(MIN)	D(TOT)	INTERCLASS DIVERGENCE									
				SC (10)	SO (10)	SW (10)	SM (10)	CU (10)	CW (10)	CM (10)	OW (10)	OM (10)	WM (10)
1.	1 6 10 12	36.	1538.	36	84	194	179	120	...	347	95	133	0
2.	1 6 10 11	33.	1534.	33	81	196	184	120	90	130	0
3.	1 6 8 11												
4.	1 6 9 11	27.	1509.	27	69	201	189	83	104	136	0
5.	1 6 9 12	29.	1501.	29	73	200	175	82	...	343	111	138	0
6.	1 6 8 12	26.	1495.	26	82	170	206	93	311	...	98	159	0
7.	6 9 10 12	35.	1484.	35	66	175	153	108	116	131	0
8.	6 8 10 12	35.	1483.	35	67	160	164	109	108	140	0
9.	6 8 10 11	33.	1477.	33	60	166	183	105	104	126	0
10.	6 9 10 11	33.	1474.	33	58	179	168	105	108	123	0
11.	1 6 9 10	31.	1469.	31	54	220	192	112	71	89	0
12.	1 8 10 11	20.	1461.	28	71	166	212	95	295	...	93	151	0
13.	2 6 10 12	35.	1448.	35	76	166	194	114	...	325	95	133	0
14.	1 9 10 11												
15.	1 7 10 11	29.	1447.	29	74	174	183	101	310	...	87	139	0
16.	1 8 9 11												
17.	2 6 10 11	32.	1438.	32	69	169	158	112	...	332	90	126	0
18.	1 6 8 10	29.	1437.	29	47	206	209	106	52	88	0
19.	1 8 10 12	30.	1436.	30	70	160	208	92	274	...	95	157	0
20.	1 7 9 11												
21.	6 8 9 11	26.	1433.	26	51	164	176	71	113	132	0
22.	1 8 9 12	26.	1432.	26	70	162	205	79	279	...	102	159	0
23.	6 8 9 12	27.	1429.	27	59	158	151	76	...	344	119	145	0
24.	1 9 10 12	27.	1428.	31	67	171	193	92	299	...	100	125	0
25.	6 10 11 12	35.	1427.	35	72	152	147	106	...	326	111	128	0
26.	2 6 9 11	26.	1426.	26	55	175	159	72	105	134	0
27.	2 6 9 12	28.	1419.	28	63	172	144	74	...	336	112	140	0
28.	1 7 10 12	32.	1413.	32	75	169	179	99	290	343	89	137	0
29.	2 6 8 11												
30.	1 10 11 12	28.	1407.	32	74	166	174	94	300	343	107	117	0
*** 34.	1 5 10 12	31.	1403.	31	72	170	161	91	279	...	89	140	0

Figure 32-9.- Example print-out from the feature selection processor of LARSYSAA. The categories and their symbols are soybeans (S), corn (C), oats (O), wheat I (W), and wheat II (M). Feature numbers refer to spectral bands between 0.4 μ and 1.0 μ .

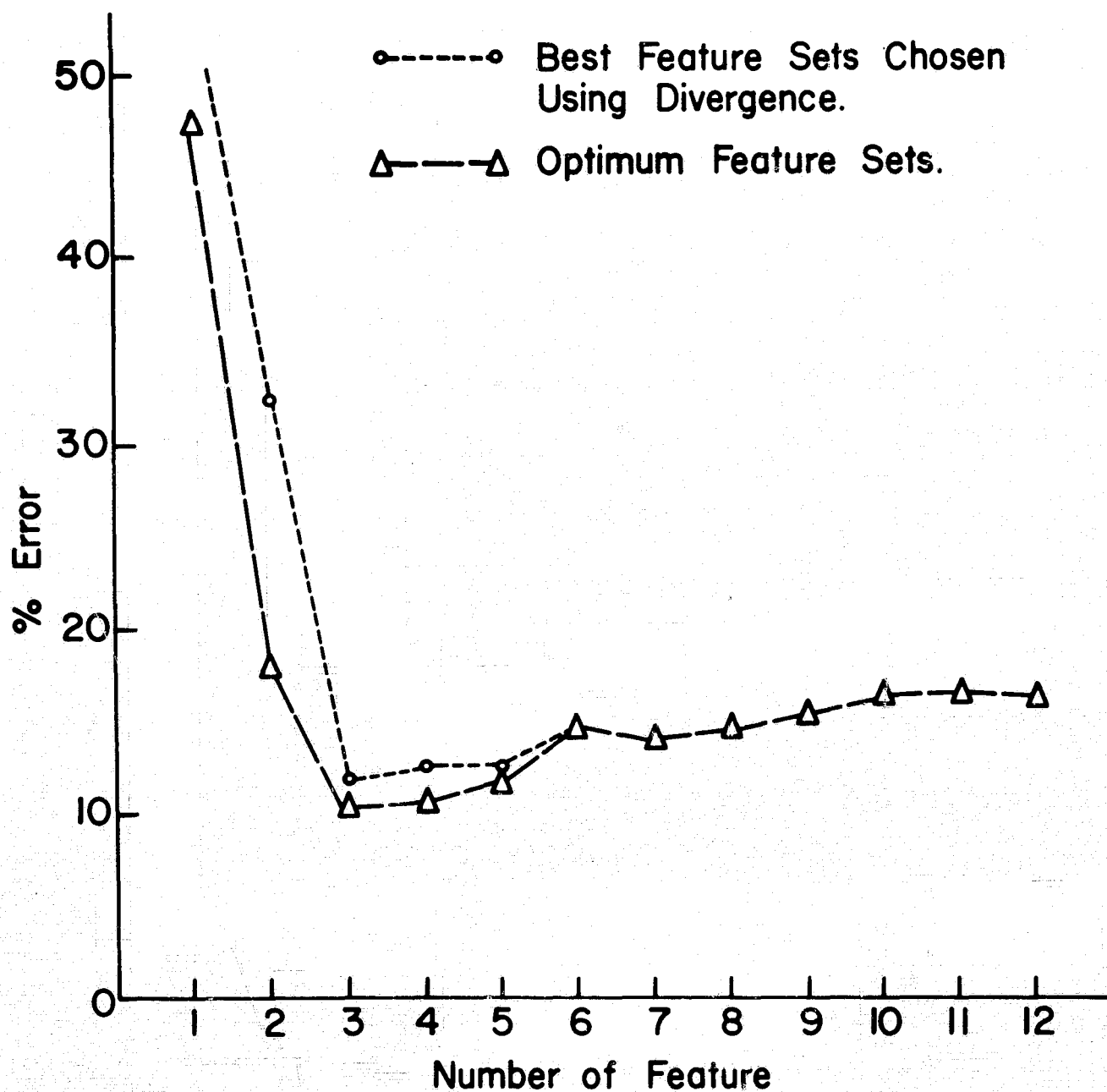


Figure 32-10.- Results in one specific case to the problem of choosing optimum feature sets of optimum dimensionality.



Figure 32-11.- Visible and thermal infrared print-outs of data to be overlaid. A panchromatic photograph is shown for comparison.

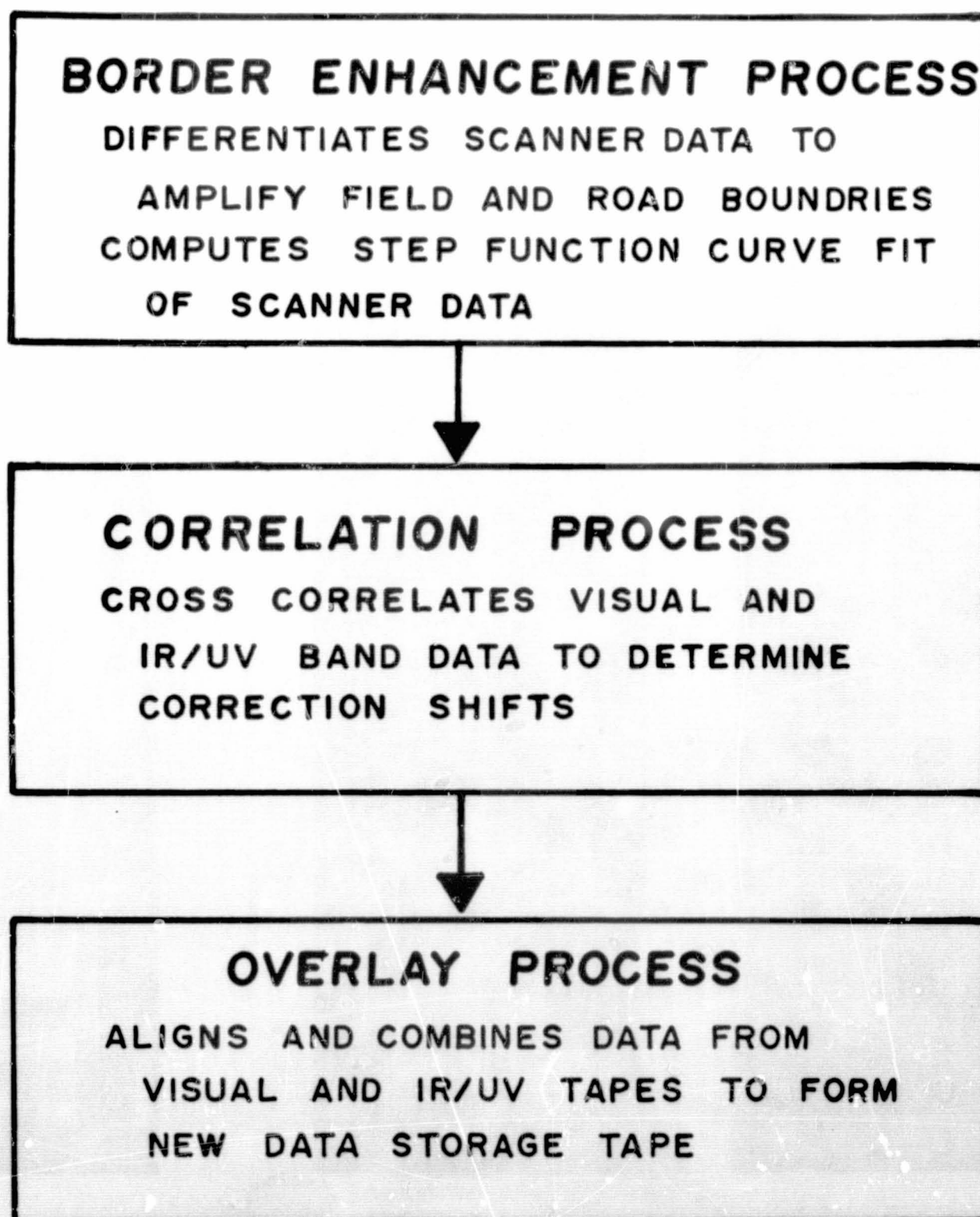


Figure 32-12.- Data overlay steps.

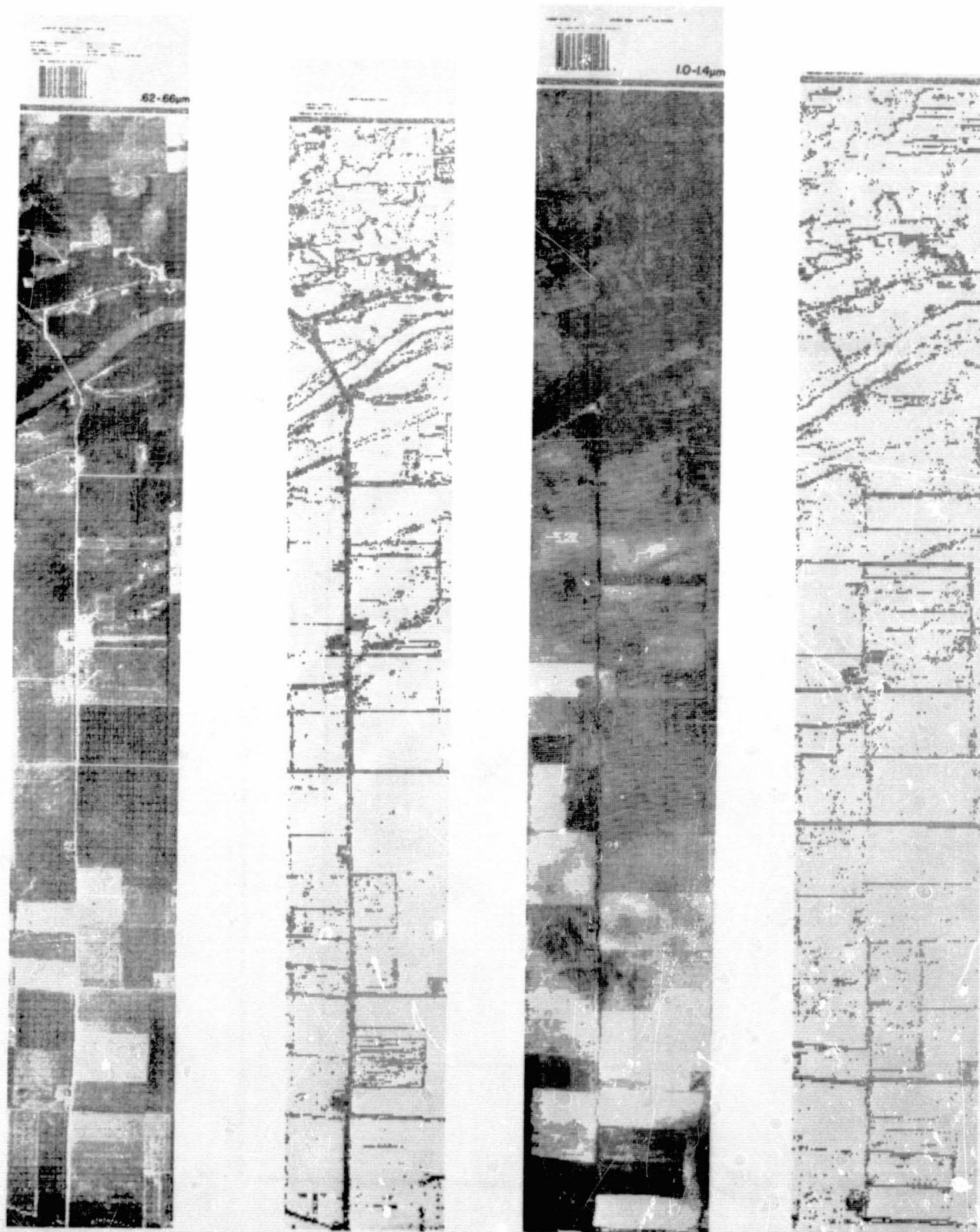


Figure 32-13.- Example print-outs of visible and reflective infrared data before and after border enhancement.

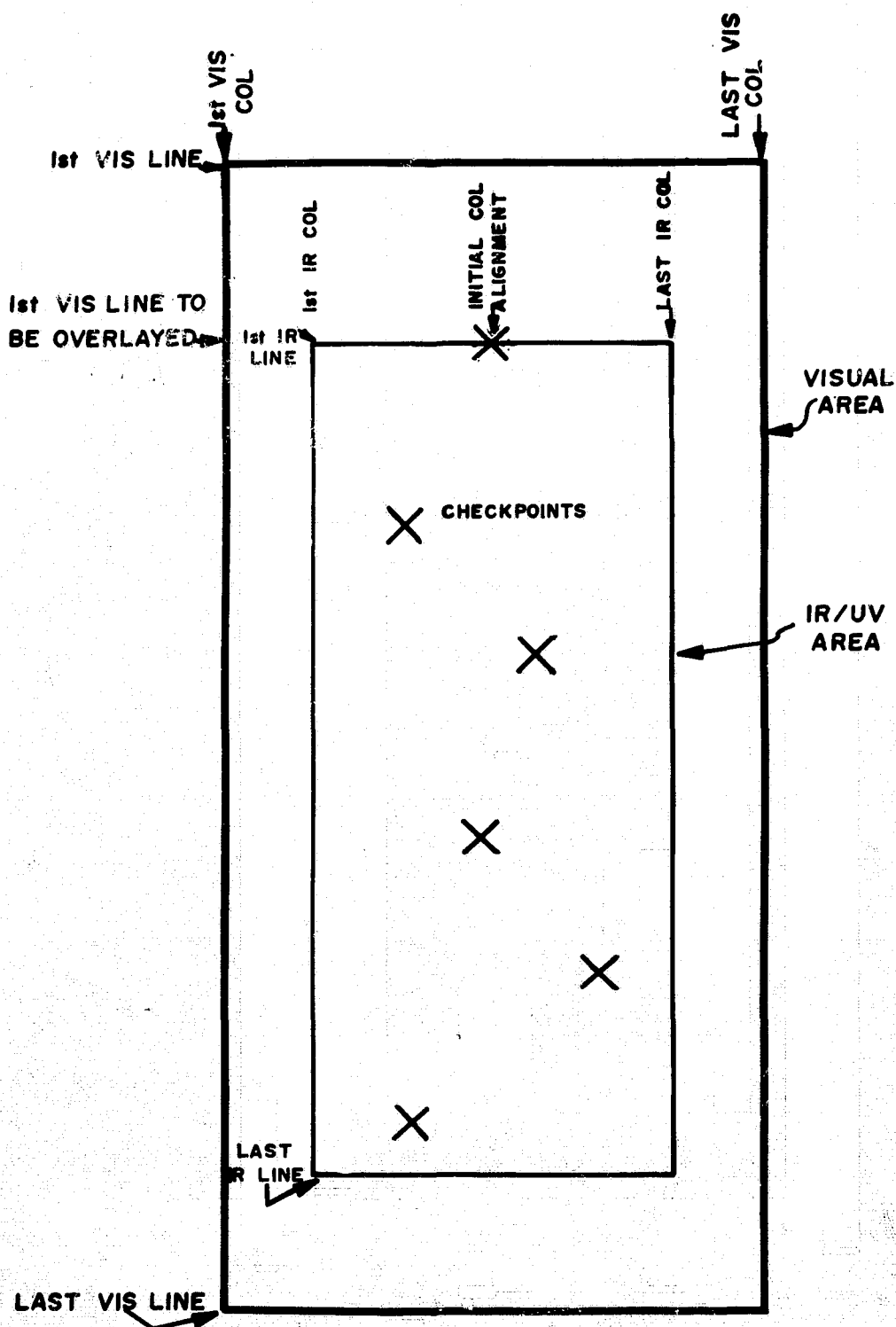


Figure 32-14.- Typical overlay geometry illustrating the manner in which manual supervision of the automated overlay can be used to improve system performance.

N71-16155

PHYSICAL MEASUREMENTS PROGRAMS AT LARS-PURDUE*

By Roger A. Holmes

Program Leader, Laboratory for Agricultural Remote Sensing
and Associate Professor, Department of Electrical
Engineering, Purdue University

INTRODUCTION

The Laboratory for Agricultural Remote Sensing (LARS) Physical Measurements Group has the general responsibility for the conception, experimental design, calibration, and operation of instruments for the measurement of physical observables of the natural environment. The scope of the measurements program includes laboratory, field, aircraft, and satellite experiments seeking to define, measure, and utilize electromagnetic radiation phenomena in timely quantitative identity of agricultural and vegetative conditions. These aspects are depicted in figure 33-1, except for the obvious laboratory phase. In this general sense, the following are the specific tasks of the Physical Measurements Group:

1. To continue to seek design proposals from industry for measurement apparatus, particularly for multichannel single-aperture scanners and field spectrometers of compatible data format
2. To continue to make known agricultural, aircraft, and satellite requirements to NASA and industry, with regard to bandwidth and resolution choices in photographic and electro-optic sensing instruments
3. To continue the development of a mobile ground-truth data-collection system, complete with field spectroscopy instrumentation
4. To construct laboratory apparatus capable of determining plant-part directional reflectance and transmittance variations caused by various induced plant conditions such as moisture and nutrient stress

*This report is based upon work sponsored jointly by the National Aeronautics and Space Administration and the U.S. Department of Agriculture, in cooperation with Purdue University.

5. To develop photoemulsion calibration techniques and requirements sufficient to insure consistent photointerpretation of black and white and color imagery

6. To maintain close liaison with life scientists to ascertain specific measurement needs as they arise

7. To maintain close liaison with the Data Processing Group concerning instrument calibration and reliability

RESULTS ACQUIRED FROM THE USE OF DATA FROM NASA AIRCRAFT

Work to date with NASA-gathered flight data is concentrated on quantitative results from optical-mechanical scanners flown in the University of Michigan aircraft with qualitative correlation to the uncalibrated best-contrast thermal imagery from the Reconofax IV scanner in the NASA aircraft. The NASA Ektachrome (and occasionally Ektachrome infrared (IR)) photographs are used as qualitative aids in the interpretation of thermal data by inference of solar irradiance input to the thermal balances which influence radiance in the emission IR region. The concentration of effort on thermal data is based on four facts:

1. Most thermal imagery is on integrated 8- to 14- μ m radiance, and concurrent radiance spectra indicate whether the target scene is essentially without spectral structure or not; if so, as is the case with soils, field spectra provide basic data for new scanner design.

2. The LARS field spectra instrumentation works routinely and conveniently from 4 to 16 μ m; figure 33-2 shows the field instrumentation van behind the cherry-picker-mounted Michelson interferometer spectrometer.

3. Field spectroscopy capability below 2 μ m has not been available since the summer of 1966, when a borrowed spectrometer was returned to NASA, Huntsville, Alabama.

4. The LARS is currently engaged in a research program on the possible measurement of thermal diffusivity through inference from temporal surface radiance development over soil types and the interpretation of moisture content thereby; this work is the doctoral research of Ronald Becker, a civil engineer on leave from Texas Instruments, Inc.

Figure 33-3 shows a panchromatic photograph, NASA thermal imagery, and University of Michigan thermal scanner data in print-out form. Controlled-calibration hot-and-cold plates in the University of Michigan scanner make possible direct correlation between print-out symbols and radiant temperature. The Reconofax IV thermal mapper has an unrecorded AGC system to give the best contrast on the emulsion imagery. Even so, the rank ordering of gray tone on the NASA mapper imagery is consistent with that of the calibrated print-out.

Figure 33-4 shows a photograph of an east-west flight line area in Tippecanoe County, together with a thermal print-out of the same area from the University of Michigan scanner, both from the July 30, 1968, mission. The arrows show the location of the LARS field van in the scene. Soybean, tasseled corn, and untasseled corn showed nearly blackbody radiance spectra at the scene with radiative temperatures of 21° to 24° C. At the same time, the University of Michigan scanner data showed radiative temperature measurements between 18° and 20.5° C from a 5000-foot altitude. There appears to be approximately 3° C of radiative temperature loss because of atmospheric H₂O and CO₂ absorption at the edges of the 8- to 14-μm region as measured by the scanner. This trend is similar to that reported by W. A. Hovis, Jr.; L. R. Blaine; and W. R. Callahan (ref. 33-1).

Figures 33-5 to 33-8 show blackbody equivalent temperature spectra for natural scenes from the July 30, 1968, NASA-University of Michigan flight and the May 7, 1968, NASA flight. In the process of these flights, Fourier spectroscopy interferograms are recorded on analog tape, and each tape includes at least two blackbody calibration runs viewing a known-temperature conical blackbody source carried in the field van. On inverse Fourier transformation and calibration, absolute radiance spectra are achieved. Finally, a blackbody equivalent temperature (BET) is found from each spectral radiance N_λ by

$$N_{\lambda \text{ scene}} = \frac{1.19 \times 10^4}{\lambda^5 [\exp 14388/\lambda(\text{BET}) - 1]} \left(\frac{W}{\text{cm}^2\text{-sr-}\mu\text{m}} \right) \quad (33-1)$$

Turning to the graphs, note that vegetative canopy such as corn and soybeans has flat, blackbody-like character between 8.5 and 13.5 μm. Stubble fields and water spectra are similar. Whenever soil, gravel, or sandy-road spectra are taken, the silica restrahlen or optical phonon absorption causes an increased reflectance at the resonance location of the ion lattice, about 8.5 to 9.3 μm. For the polycrystalline target generally found in nature, the drop in emissivity or increase in reflectance is less pronounced than one might generally find, for example, on

the surface of an oxidized silicon wafer in semiconductor technology. The effect results in a radiance reduction at the appropriate resonance region of about 2 to 5 percent, corresponding to a blackbody equivalent temperature dip of 1° to 3° C. Other absorption regions on the spectra arise for H_2O from about 5 to 7 μm and for CO_2 around 15 μm . The spectrometer resolving capability at 15 μm is about 0.9 μm ; thus, the depth or peak of the CO_2 absorption or emission cannot be interpreted as average ambient air temperature between scene and spectrometer, but does serve to show trends.

These spectra, taken in conjunction with NASA flights, have been helpful in guiding LARS recommendations on thermal portions of proposed optical-mechanical scanner designs. They have indicated the signal-to-noise ratio problems with regard to restrahlen soil identification. The physical measurements group will call for NASA flight missions with calibrated thermal scanners in harmony with Becker's field instrumentation to test the feasibility of thermal diffusivity measurements on bare soil fields.

SPECTRAL RADIANCE DATA AND FIELD SPECTROSCOPY

A composite spectral radiance graph for soil, water, and vegetation is shown in figure 33-9. This graph was compiled from field data from 0.4 to 4 μm in the summer of 1966 with a Perkin-Elmer SG-4 spectrometer and from field data from 4 to 16 μm in 1967 and 1968 with a Block 195-T Michelson interferometer spectrometer.

Figures 33-10 to 33-13 show typical field spectra employed in arriving at figure 33-9. While data have been gathered with borrowed spectrometers originally designed for other than field spectral measurements, the experience has proved extremely valuable in efforts to induce industry to propose a broad range (0.35 to 16 μm) field spectrometer for general use in gathering ground truth. While it seems obvious that the most meaningful kind of ground truth would consist of spectral radiance data from selected ground scenes (fig. 33-1), a truly adequate field spectrometer has yet to be acquired in the program. At LARS, one doctoral student, John Clevenger, is working on a design thesis on an inexpensive spectrometer for the range 0.35 to 2.4 μm that would be of particular value to those workers concentrating on photographic data and consistent calibration of photo emulsions. The requirements placed on such a spectrometer are unusual to the optical instrumentation industry. Solar irradiance varies rapidly enough (within a second or two) to require a rapid spectral scan and calibration or reference to solar input spectral irradiance, rather than the conventional standard lamp.

Spectral resolution can be traded for rapid-scan capability for the same signal-to-noise ratio. The spectrometer should have a 1° field of view for detail studies (plant leaves in the field scene, for example), but it should also have approximately a 15° field of view to integrate scene radiance over a ground patch of a few meters on a side to correlate with aircraft instrumentation spatial resolution patches. A Perkin-Elmer Model 98 monochromator is being modified to provide engineering tests for the inexpensive spectrometer design.

LABORATORY LEAF-SCATTERING STUDY

The question is often put forth, "Can you detect this or that kind of stress condition in vegetation?" The answer often averages out to, "Perhaps." If the stress can be detected as a change in radiance, it can come out in two forms from a physical point of view. First, there may be essentially geometric changes: leaves droop or turn over (soybeans), showing more soil or the silvery underside of a leaf; or the stressed plant simply fails to put out full secondary growth, as in mint verticillium wilt when lodged wheat shows the shiny stalk instead of the grain head. These aspects must be studied in the field environment and would be done best with a field spectrometer (when one is developed), as described in the previous section. However, biological changes may occur in the plant leaves per se: chemical abnormalities cause pigmentation changes; moisture stress alters the detailed scattering geometry of the cell structure; and so on. Some leaf analysis can be done, and has been done, on a spectroreflectometer with normal or near-normal beam incidence and hemispherical reflectance or hemispherical transmittance measured by the integrating sphere technique. However, the leaf is usually cut from the plant in this process, and the severe goniometric restrictions limit the experimenter's ability to use angles as experimentally adjustable parameters.

At LARS, a leaf-scattering apparatus has been constructed as part of the doctoral research of Harry Breece. A leaf is held gently in a holder while it is still on the plant. The angle of an incident monochromatic beam with respect to the leaf is set by choice, and a photomultiplier is driven in a plane on a concentric ring around the leaf. The chopped and synchronously demodulated beam signal is displayed on a storage oscilloscope in polar plot form. The apparatus interior is shown in figure 33-14, while a typical polar plot scope presentation is shown in figure 33-15.

The data taken thus far include over 400 runs on corn and soybean normal leaves in vivo to establish the unstressed base-line conditions. Scattering data were taken every 25 nautical miles from 400 to 675 nautical miles and every 50 nautical miles from 750 to 1000 nautical miles. The resulting data have several fascinating features concerning the

degree of Lambertian character of leaf scattering versus several parameters, points which will be discussed fully in the Breece thesis. Figures 33-16 and 33-17 show limited portions of scattering data for corn and soybean leaves, respectively.

With normal data established, it is now possible for the life scientist of the Agricultural Research Group to subject plants to specific stress conditions and measure the spectral scattering changes of the leaves of the plant, correlating these with observation and color photographs. This work is the next task of the leaf-scattering study.

DATA ACQUISITION/DATA PROCESSING LIAISON

The Physical Measurements Group interfaces with both the Data Processing Group and the Agricultural Research Group at LARS. The life scientist brings biophysical reasons for band choices in multispectral data to the fore, while the data processor displays a concern over the calibration, consistency, and noise level of data from acquisition instrumentation. These facets have been brought together in discussions with industry on scanner and other instrumentation requirements and in recommendations to NASA concerning data-acquisition instruments in a scanner sketchbook.

There is one major area which was studied briefly by the Physical Measurements Group leader in 1965 that has been of constant concern at LARS (though work with scanner data suppressed efforts) — photographic emulsion calibration. The photograph is deceptive in that some degree of success in obtaining an image from relatively inexpensive instruments is virtually guaranteed, even at the local drugstore. However, remote-sensing experimenters are using emulsion detectors, at least in part, as radiance measurement devices. In this sense, the film should be subjected to the same sort of usage philosophy that makes decent radiance detectors of the solid-state scanner devices. Spectral sensitometric wedges should be placed on film in any attempt to measure radiance by film.

The utilization of large amounts of photographs at LARS has made it necessary to reemphasize photograph calibration problems and acceptable solutions. This will be a major project this coming year for the Physical Measurements Group at LARS, interfacing with workers at Berkeley who are well aware of the problems.

REFERENCE

- 33-1. Hovis, W. A., Jr.; Blaine, L. R.; and Callahan, W. R.: Infrared Aircraft Spectra Over Desert Terrain 8.5μ to 16μ . Applied Optics, vol. 7, no. 6, June 1968, pp. 1137-1140.

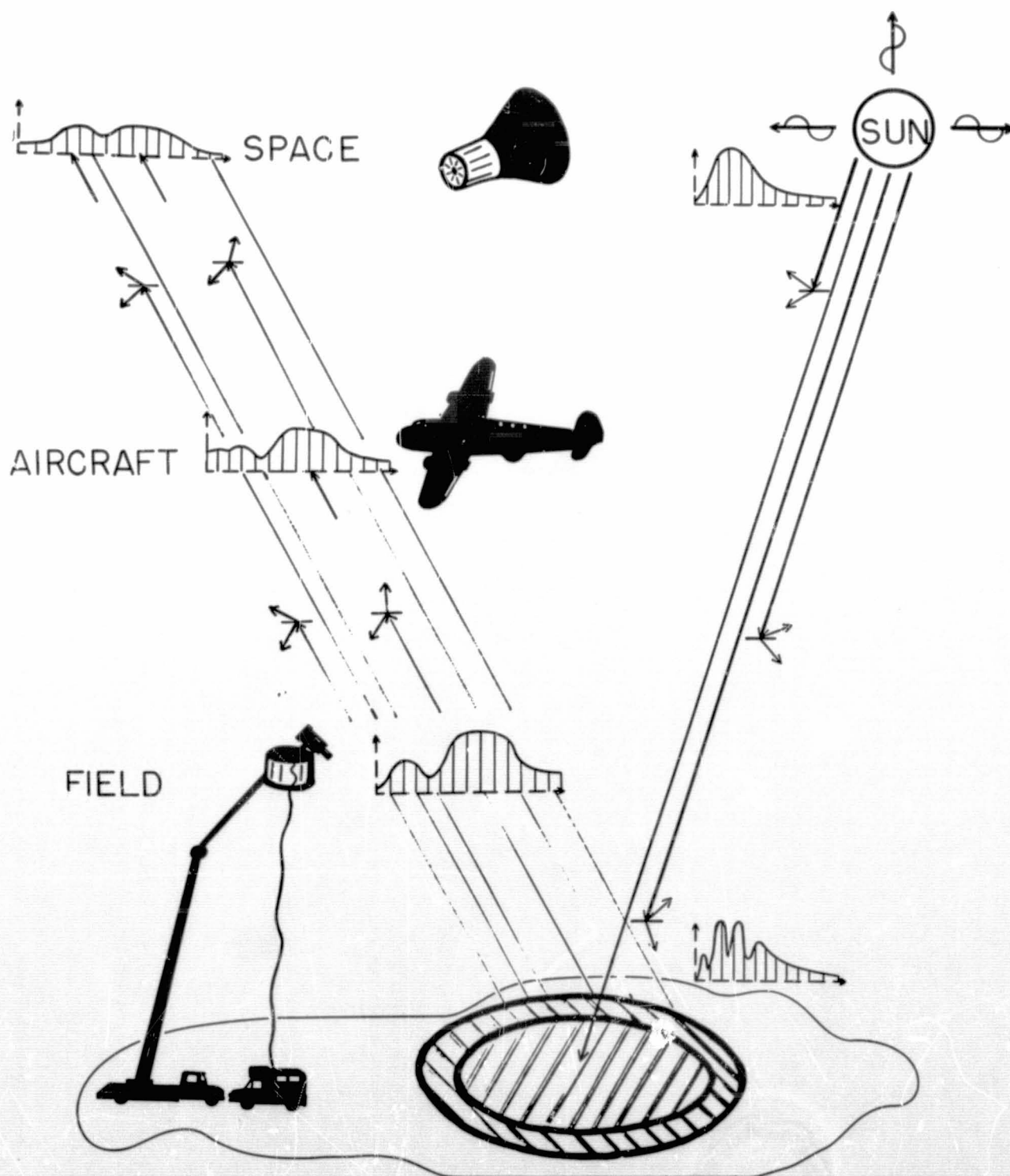


Figure 33-1.- The fundamental hypothesis of remote sensing is that radiance measurements on ground-scene resolution elements will contain information on the natural objects in the ground scene. This can be measured from cherry-picker, aircraft, or spacecraft altitudes.

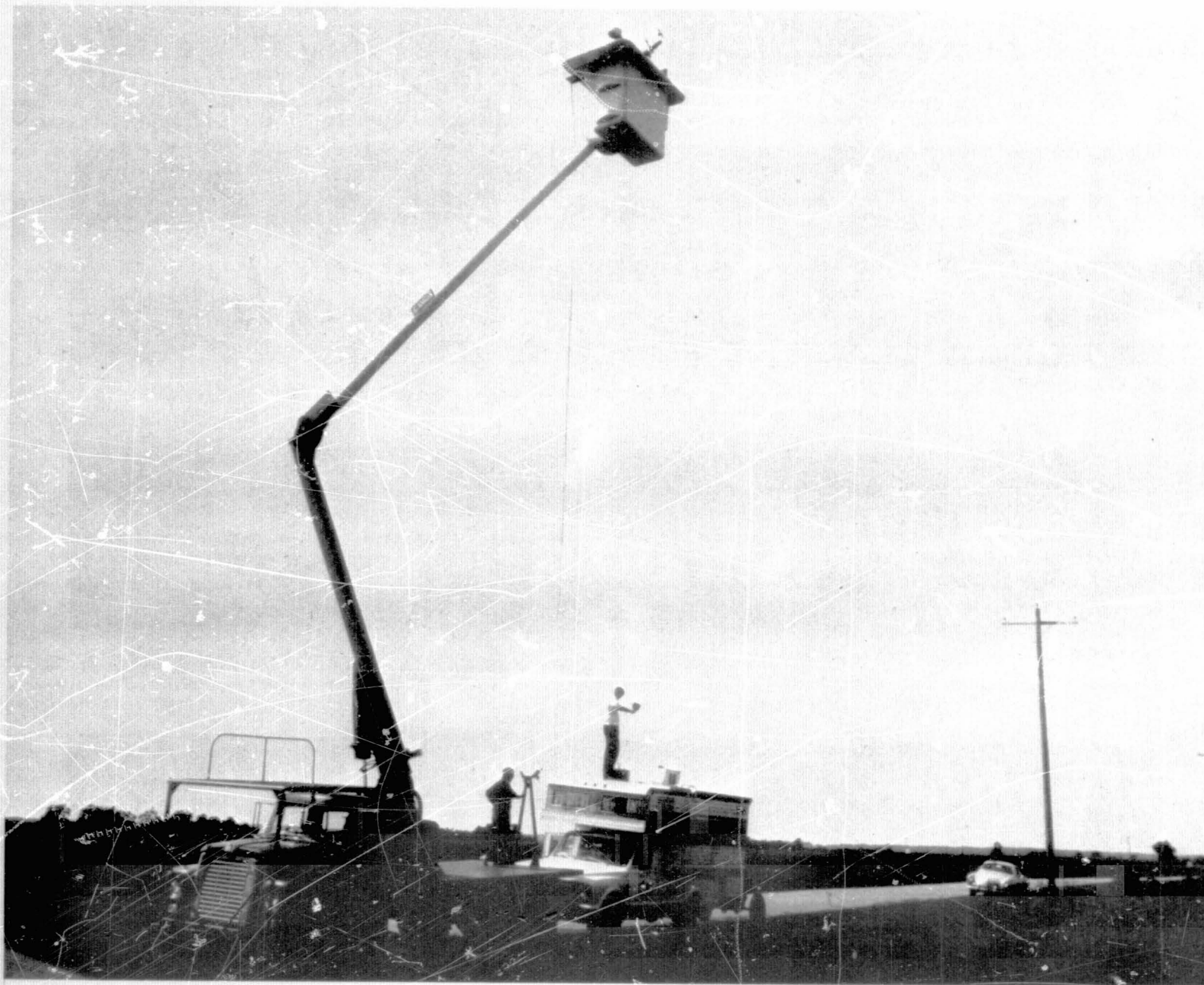
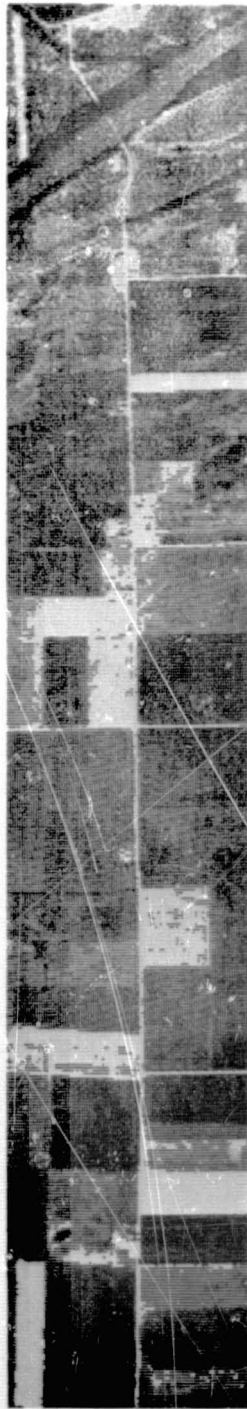


Figure 33-2.- Field instrumentation van behind the cherry-picker-mounted Michelson interferometer spectrometer.

Panchromatic
Film



8-14 μ m Scanner
Printout



8-14 μ m Scanner
Image



Figure 33-3.- Panchromatic photograph, University of Michigan scanner data print-out and NASA thermal mapper image from the July 30, 1968, mission over C-1 flight line in Tippecanoe County.

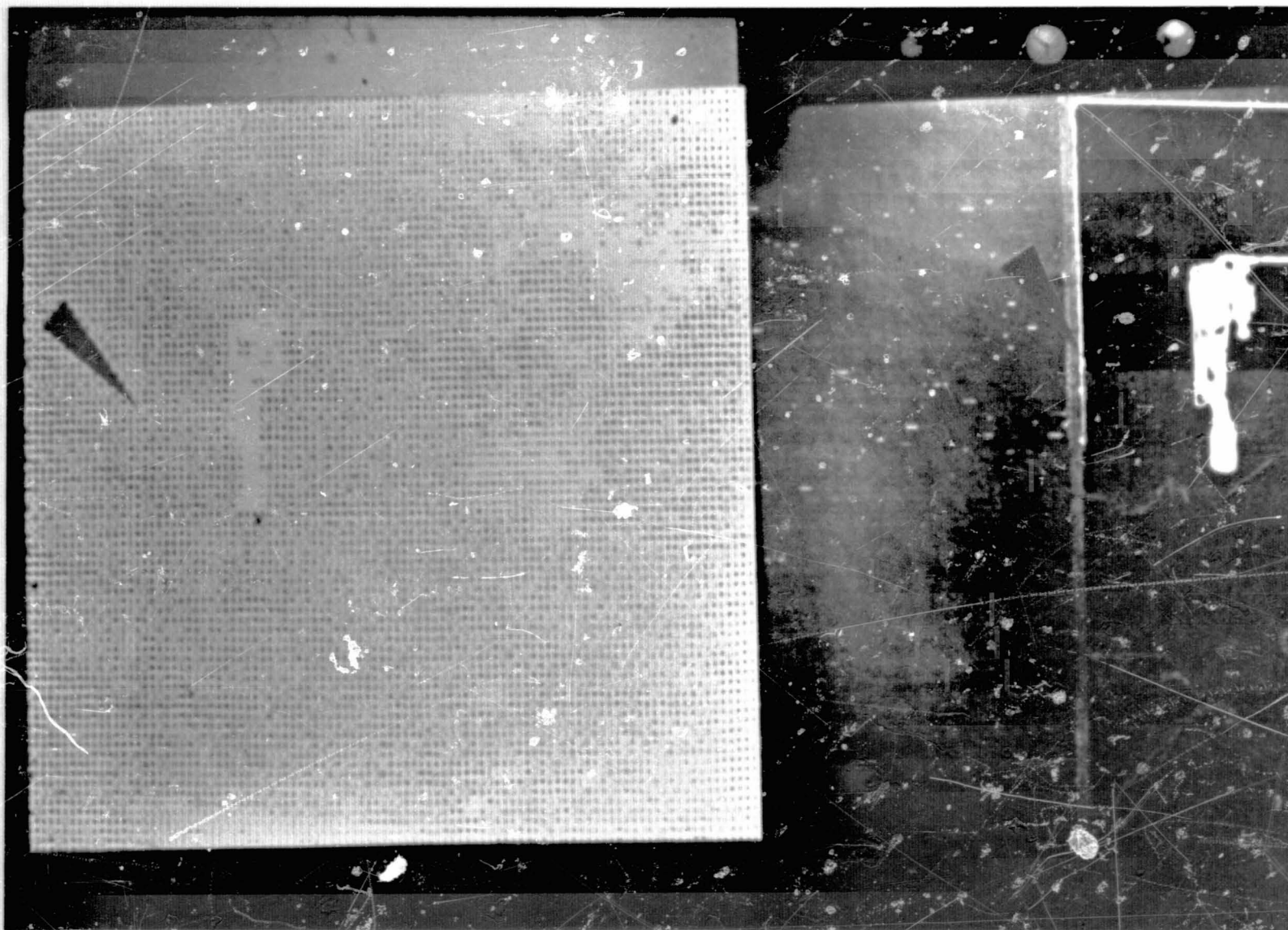


Figure 33-4.- A photograph (NASA aircraft) and 8μ to 14μ thermal print-out (University of Michigan aircraft) from the July 30, 1968, mission. Blank areas of the print-out are hotter than 25°C ; darkest areas are colder than 19°C . There are eight symbols on the print-out between these limits, each of which is associated with a calibrated radiative temperature scale.

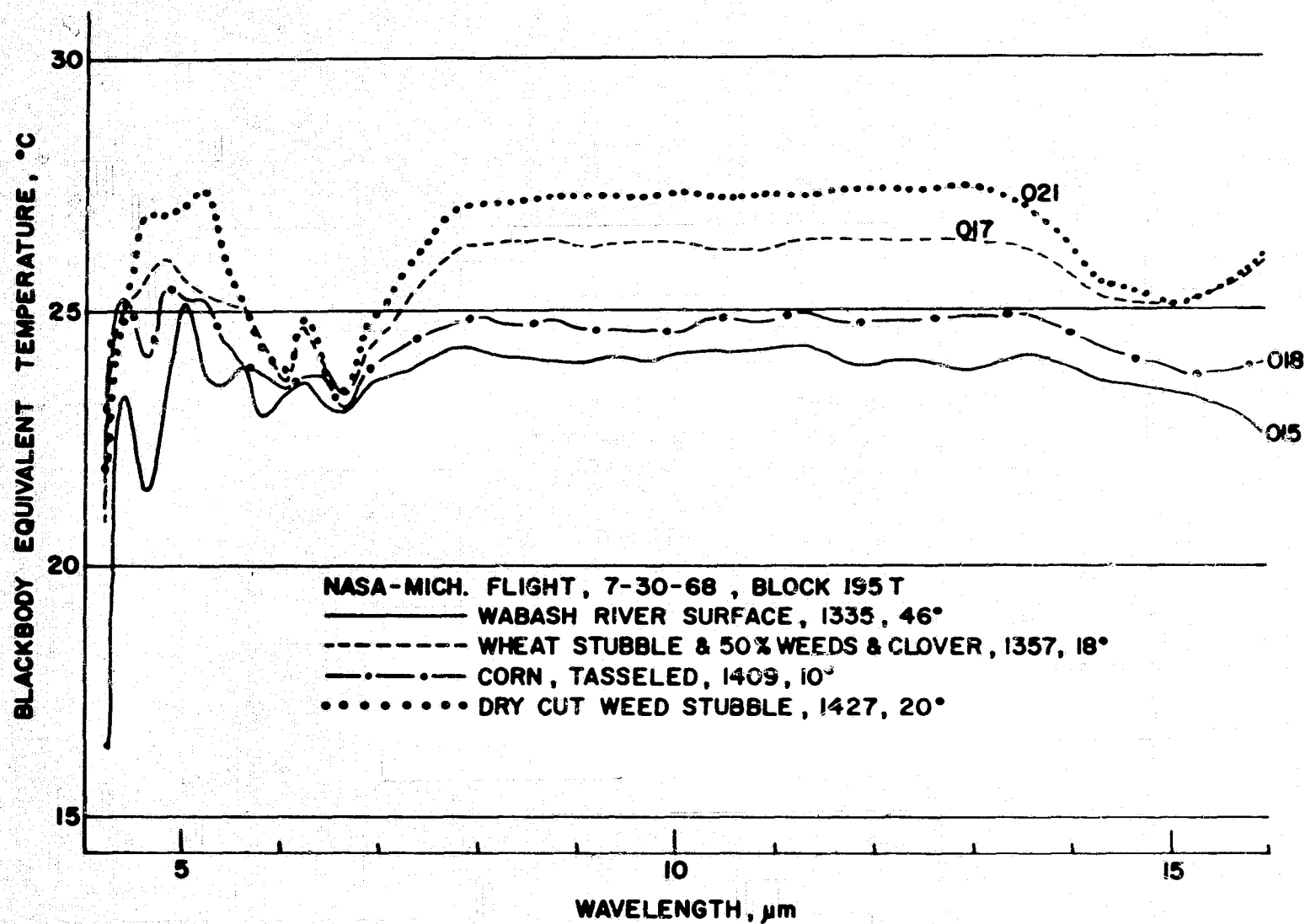


Figure 33-5.- Blackbody equivalent temperature spectra, July 30, 1968, NASA-University of Michigan flight.

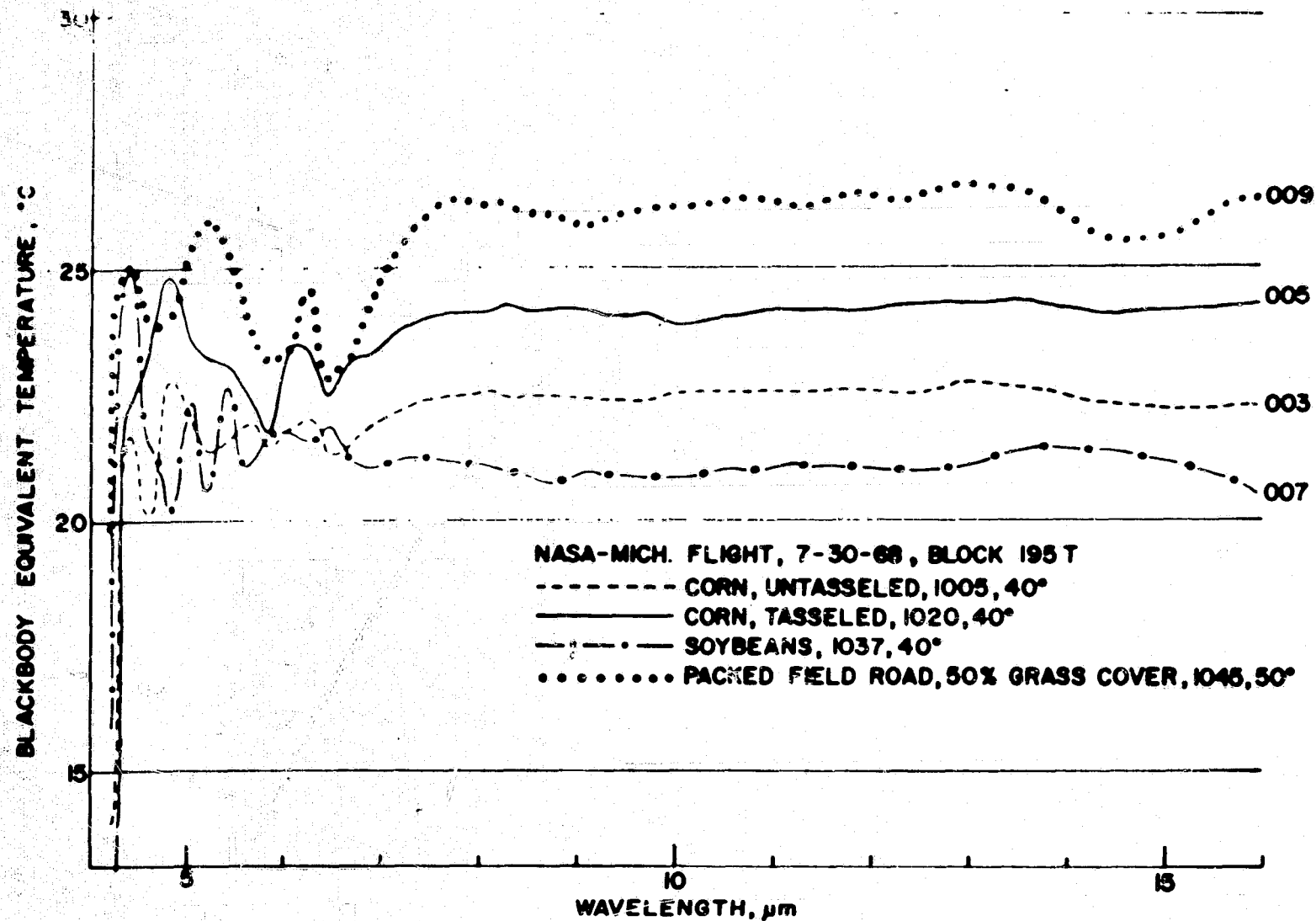


Figure 33-6.- Blackbody equivalent temperature spectra, July 30, 1968, NASA-University of Michigan flight.

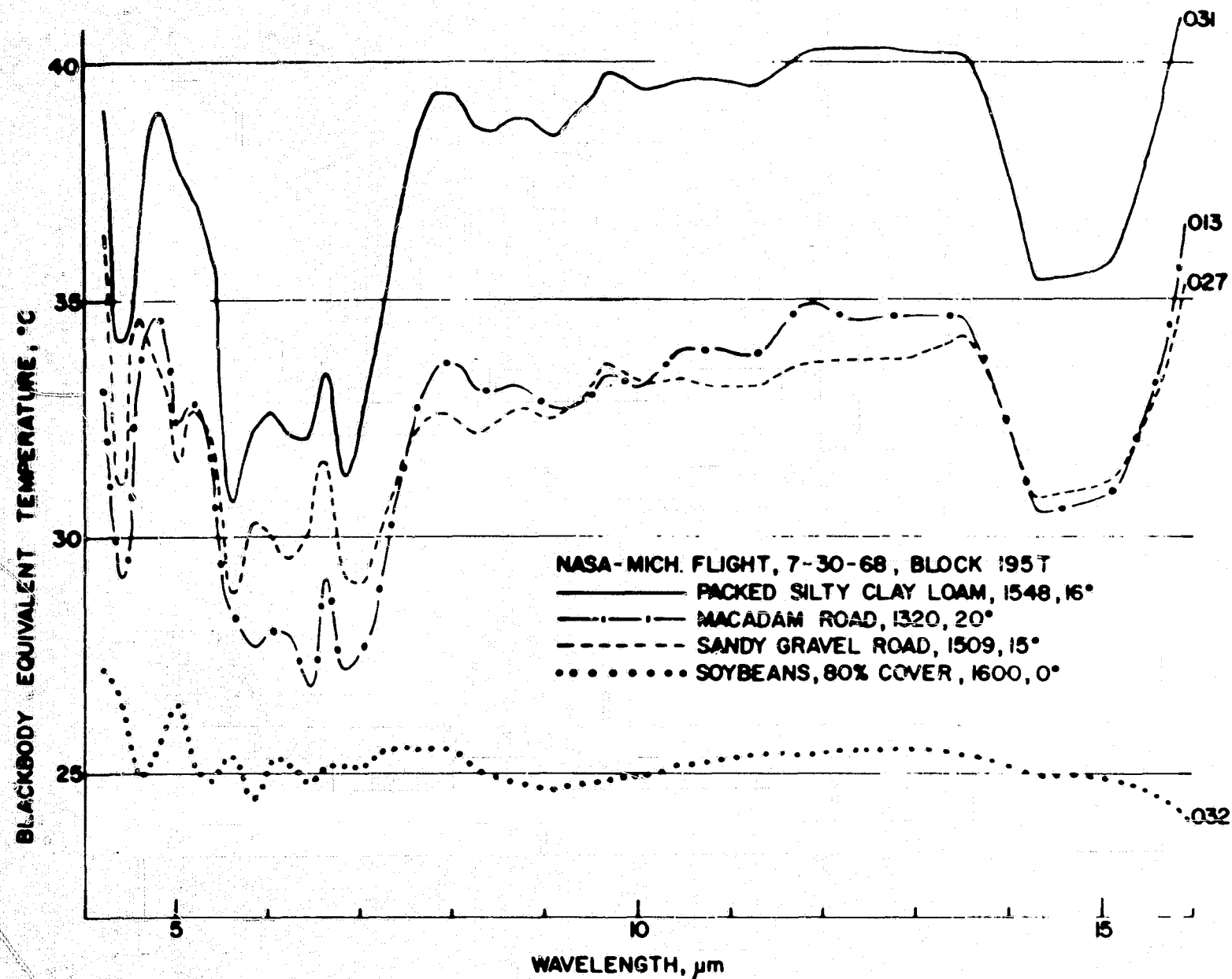


Figure 33-7.- Blackbody equivalent temperature spectra, July 30, 1968, NASA-University of Michigan flight.

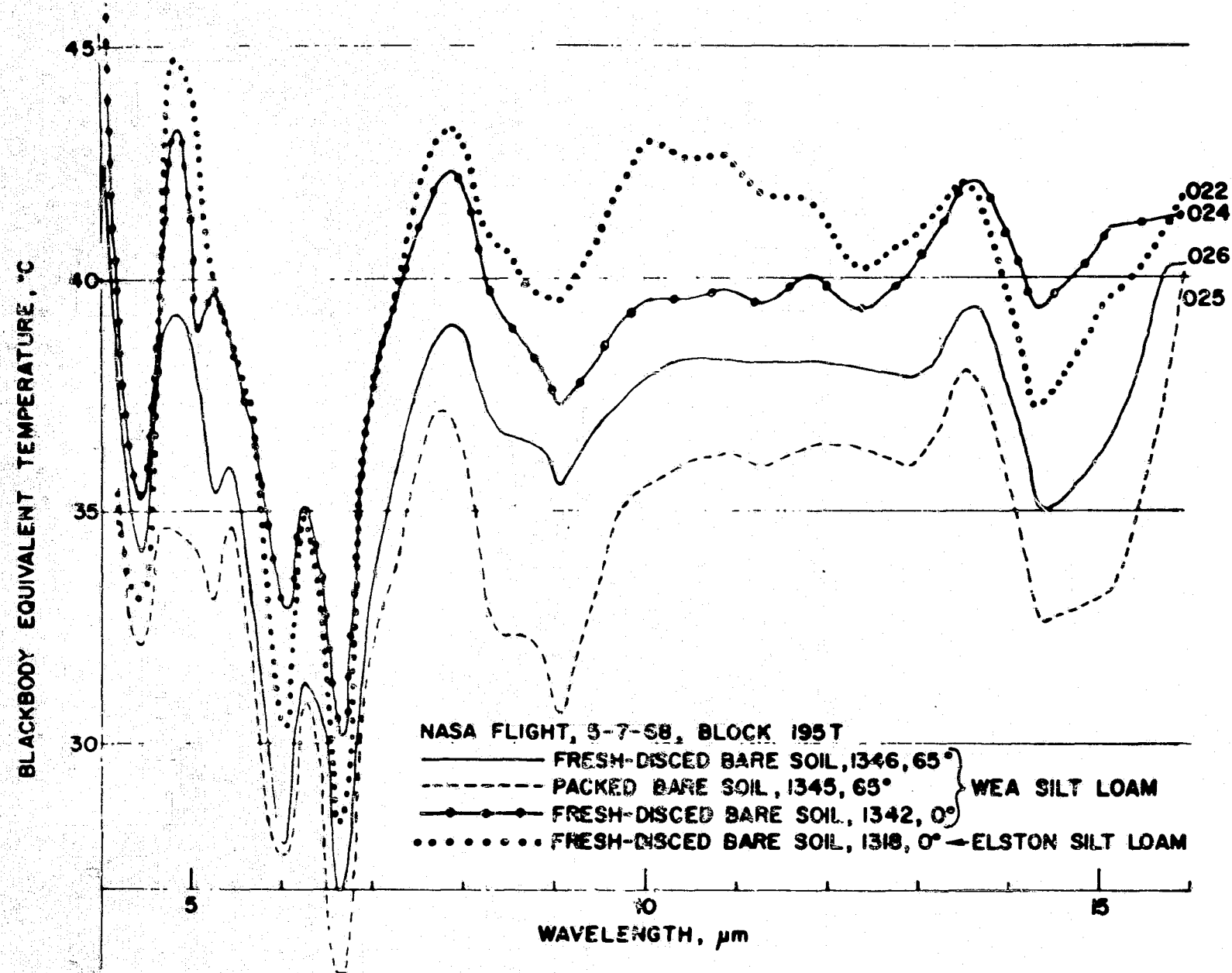


Figure 33-8.- Blackbody equivalent temperature spectra, May 7, 1968, NASA flight.

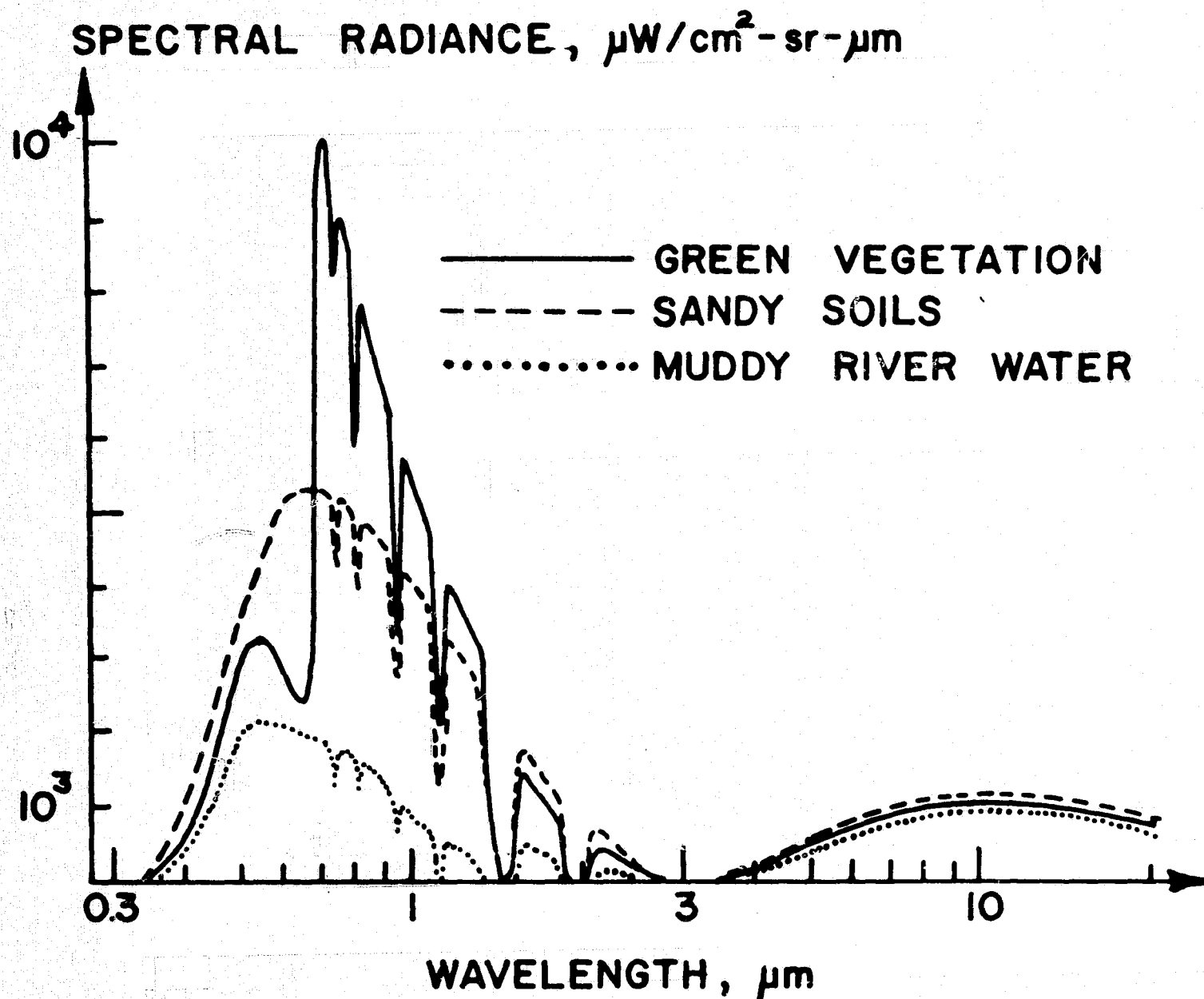


Figure 33-9.- Composite radiance spectra of soil, water, and green vegetation based on field spectral measurements at LARS. A clear day is assumed in the reflective region.

8-30-66, 1335, PERKIN-ELMER SG-4

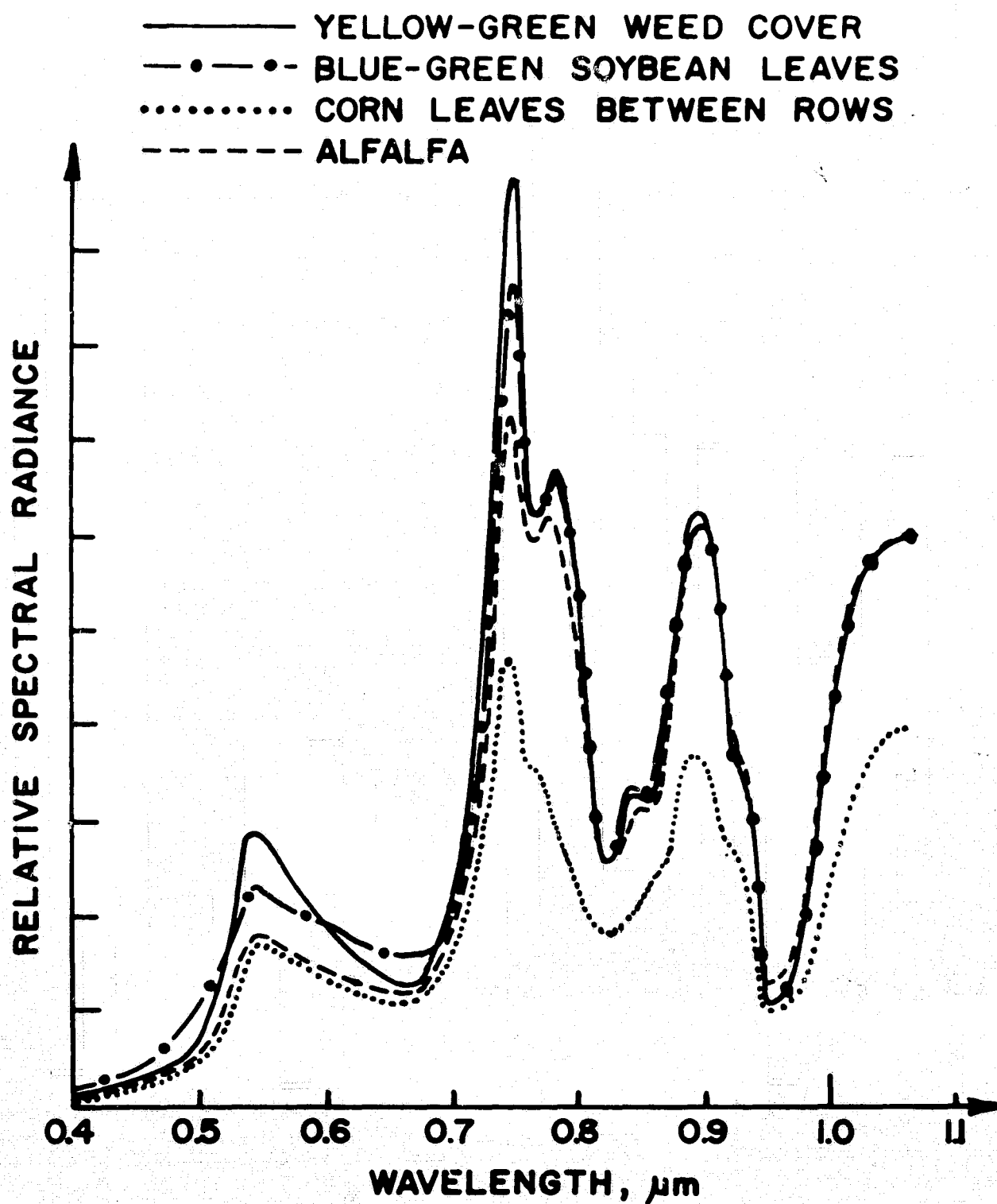


Figure 33-10.- Typical field radiance spectra in the 0.4- to 1.05- μm wavelength region.

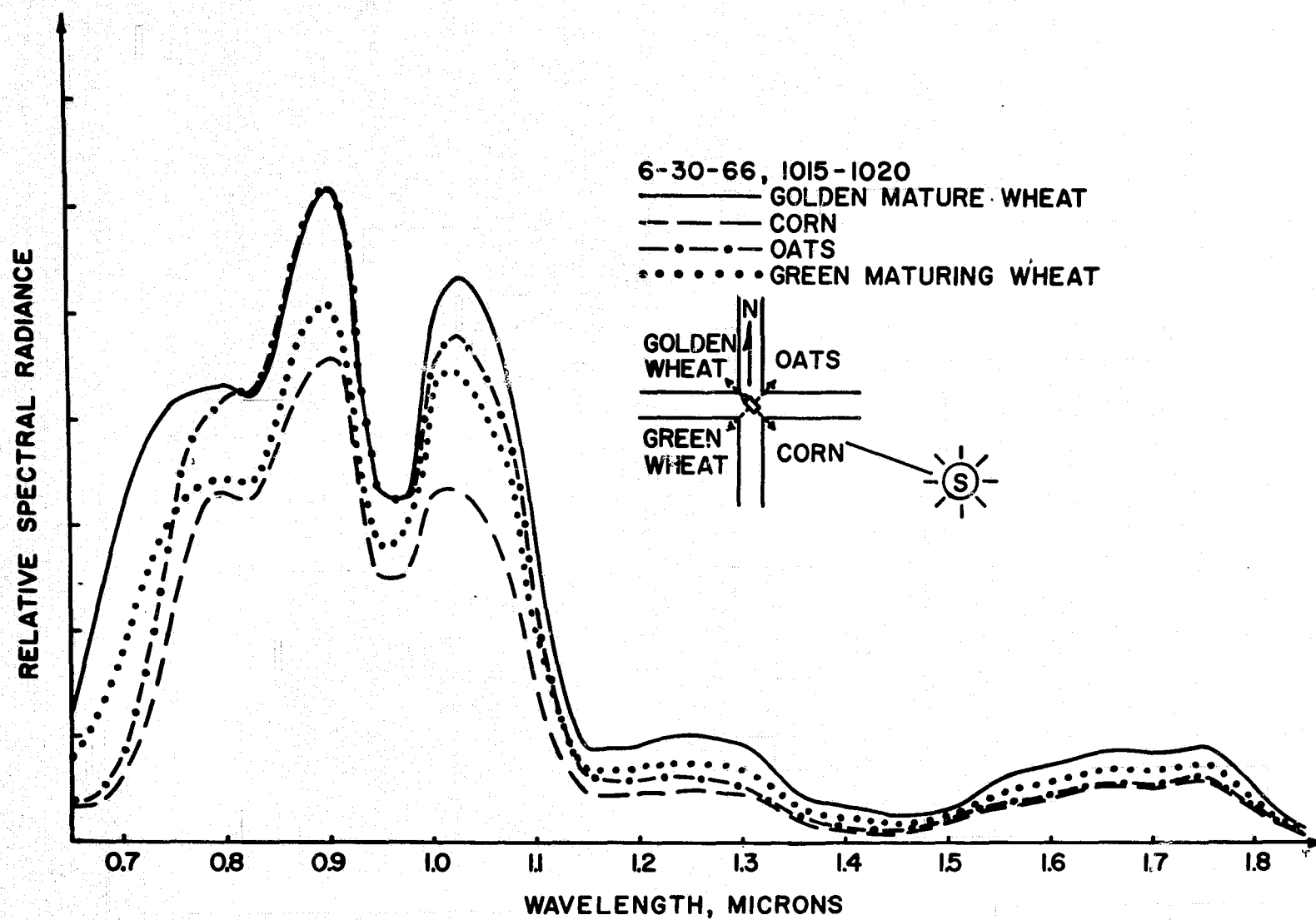


Figure 33-11.- Typical field radiance spectra in the 0.7- to 1.9- μ m wavelength region.

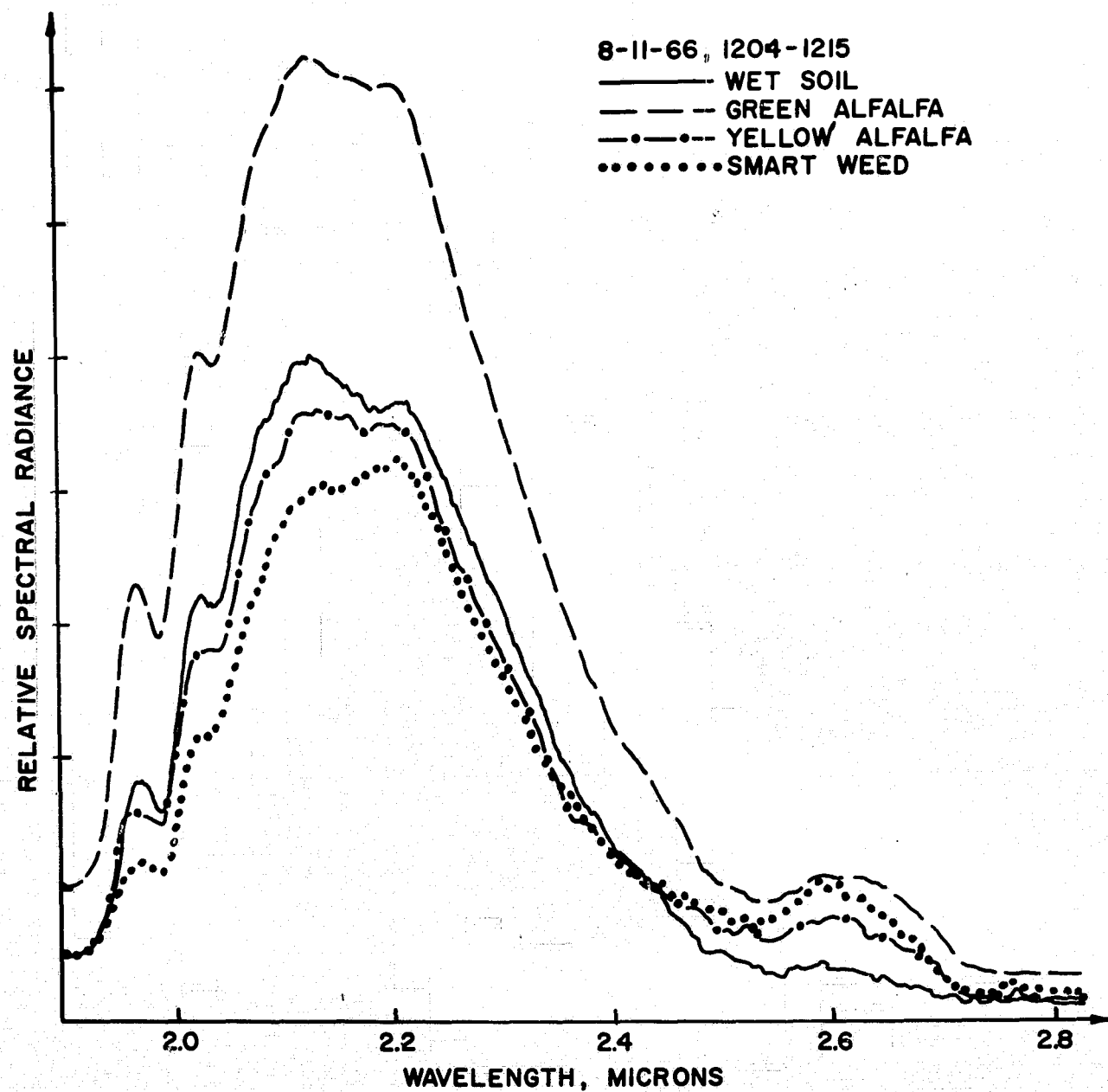


Figure 33-12.- Typical field radiance spectra in the 1.9- to 2.8- μ m wavelength region. Curves should be compared in functional form only, since gain settings were changed from run to run.

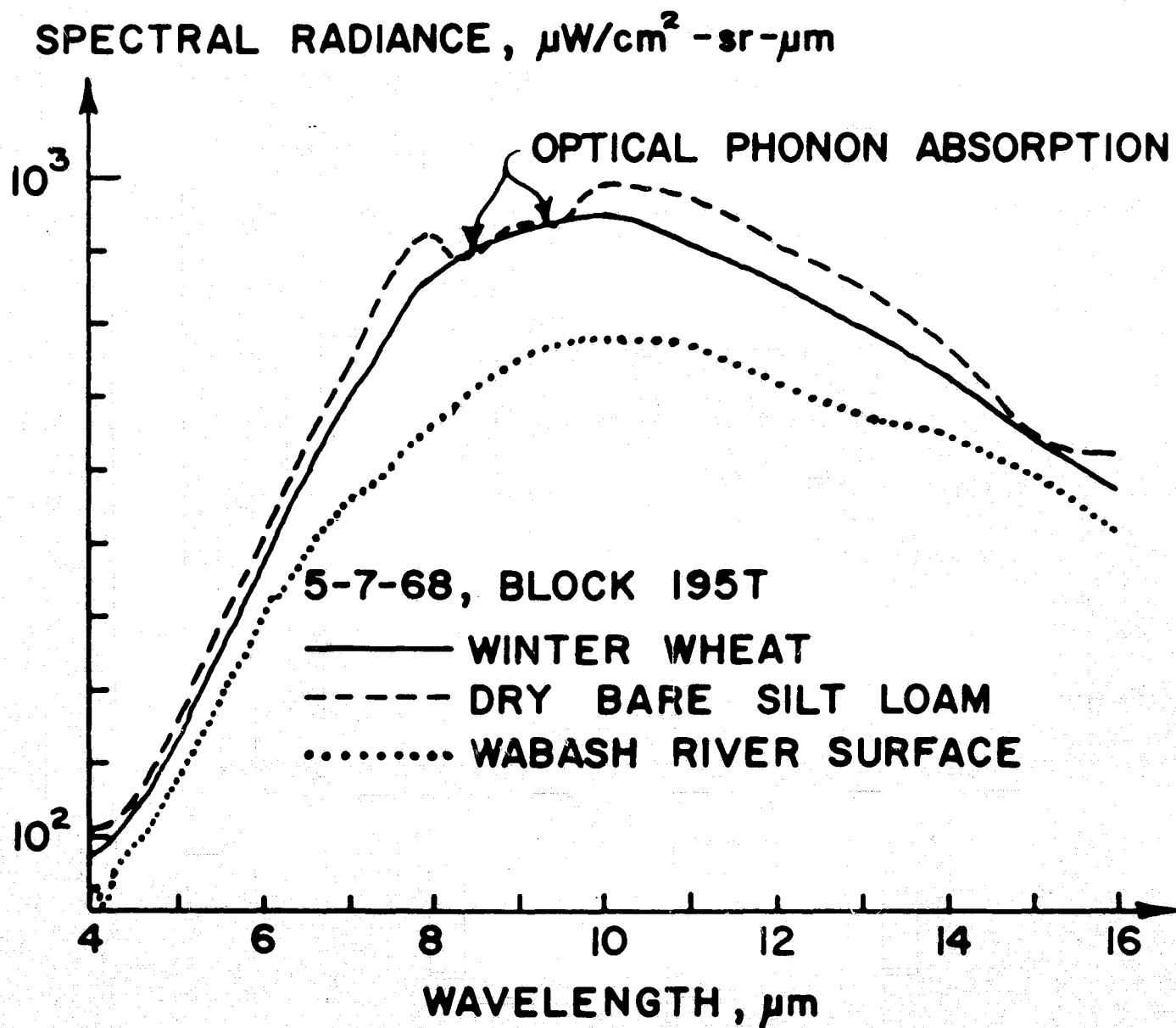


Figure 33-13.- Typical field radiance spectra in the 4- to 16- μm wavelength region.

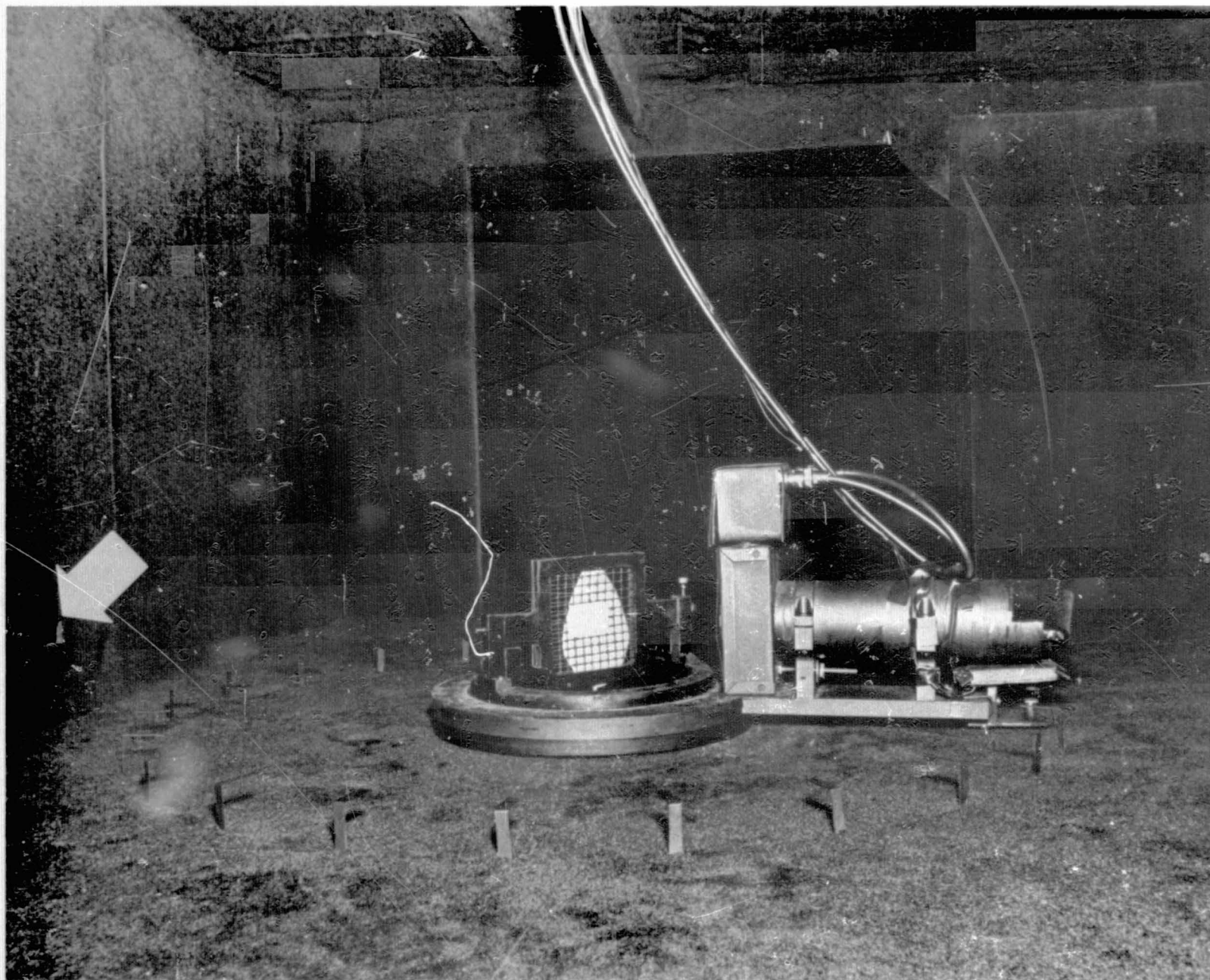


Figure 33-14.- Interior view of the LARS leaf-scattering apparatus. The monochromatic beam enters at the hole shown by the arrow.

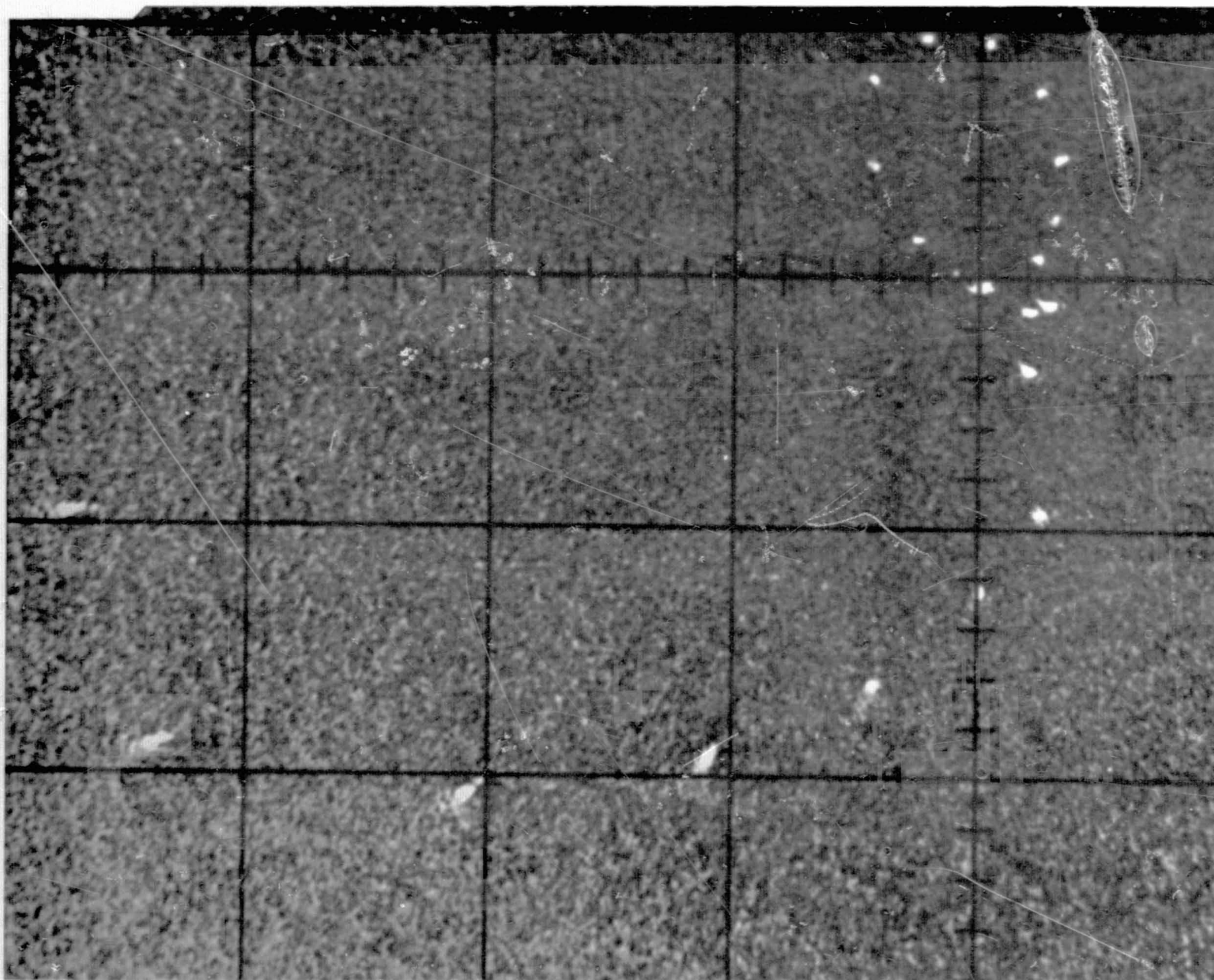


Figure 33-15.- Polar plot of leaf-scattering radiance as presented on the storage oscilloscope.
A point is made every 15° of photomultiplier swing around a circle.

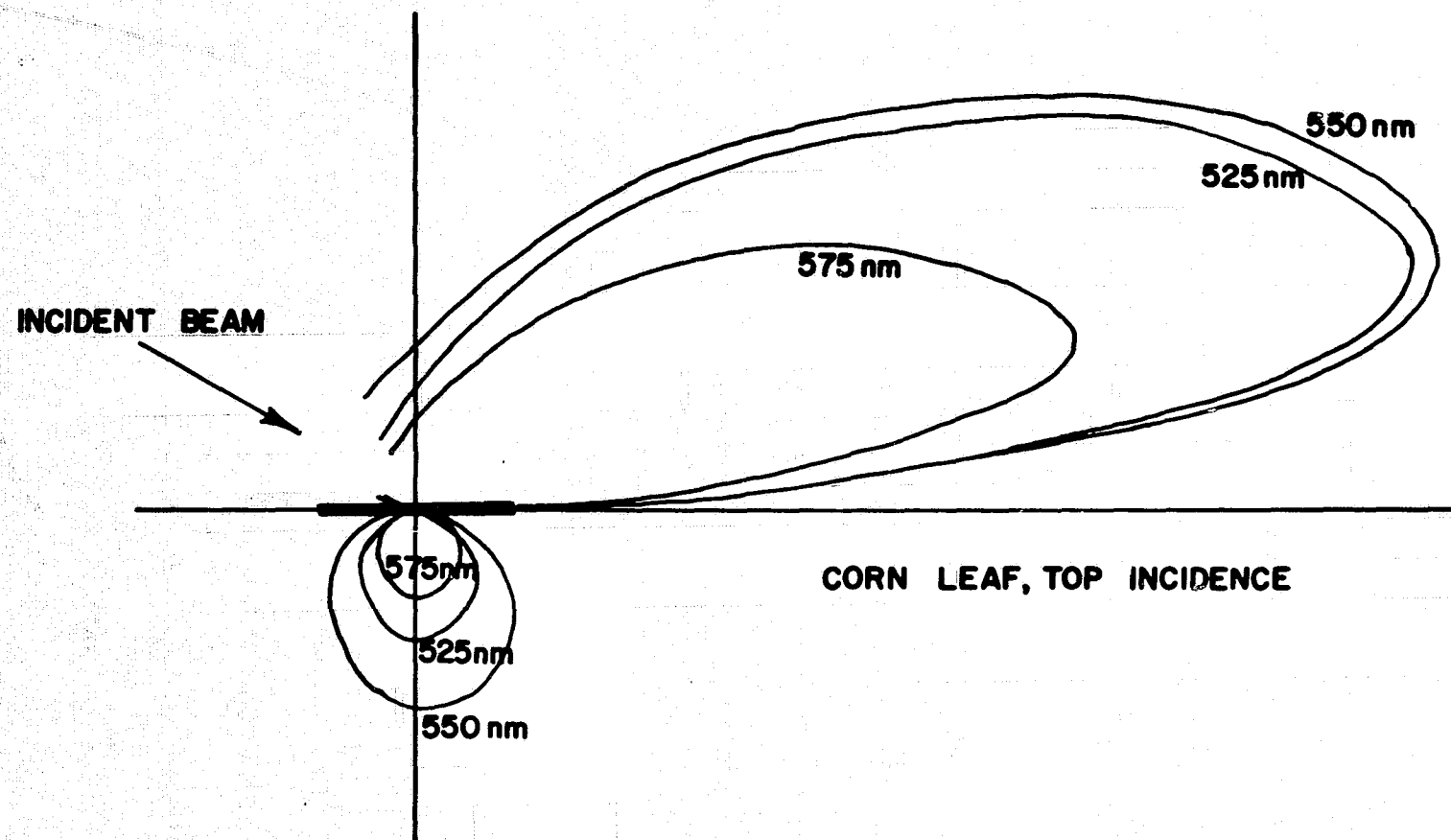


Figure 33-16.- Leaf-scattering data, corn leaf.

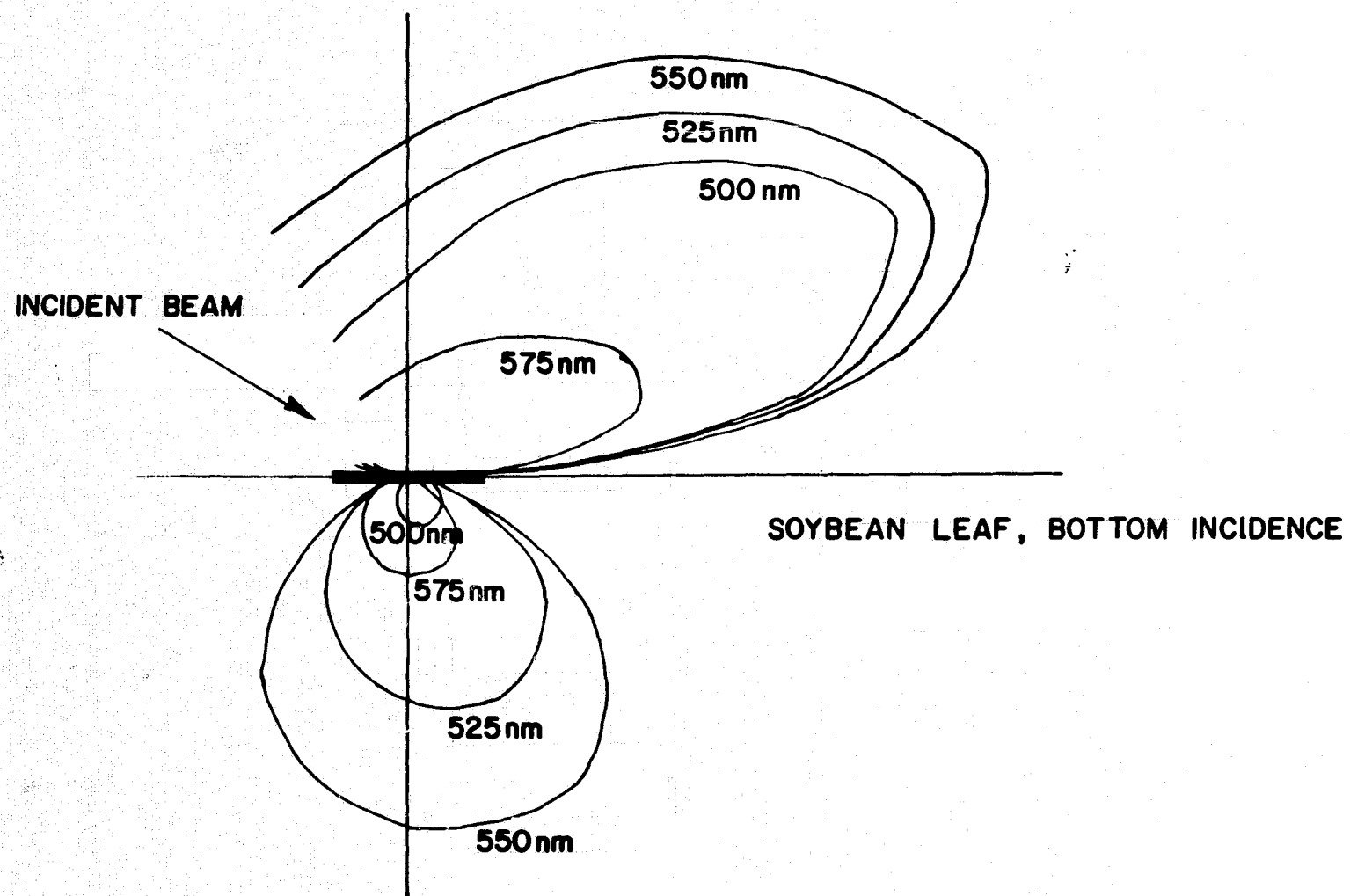


Figure 33-17.- Leaf-scattering data, soybean leaf.

N71-16156

RADAR AS A SENSOR IN AGRICULTURE

By D. S. Simonett
Department of Geography and Center for Research
in Engineering Science
University of Kansas, Lawrence, Kansas 66044

INTRODUCTION

No remote sensor, be it multichannel scanner, camera, or radar, can with accuracy identify farmers' planting intentions, the weather weeks ahead, or the perils yet to be encountered by crops already planted but not at maturity. Consequently, all sensors must be used a number of times during the growing season. Differences in crop phenology may thus be used as a powerful discriminant, such that the need for many channels of information may be substantially reduced, and extrapolation may be based (when feasible) on calibration with small samples. It may well be that one of these fewer channels which will be needed for an effective remote-sensing system may prove to be radar because of the constraints of obtaining timely data under various weather conditions.

STUDIES ON CROPS IN WESTERN KANSAS

The only radar frequency for which acceptable data have been obtained to date in the NASA Earth Resources Program is K-band. Using these data, the effect of crop type, cover, moisture, and other parameters on radar return of the Garden City, Kansas, Test Site has been evaluated.

1. Statistical analysis (covariance and multiple correlation) indicates that the type of crop is the most important variable influencing radar return. Thus, there appears to be a potential for crop discrimination capability in K-band radar sufficient to warrant further testing.
2. Allowing for differences in crop type, other major influences on radar return are crop height, percent of the ground covered by vegetation, and row direction (bare ground and low cover).
3. Crop moisture, which shows a weak relationship to radar return, requires further study as a variable in the radar return.

4. Soil moisture, even for bare ground, shows small influence on radar return during a single month, but studies with scatterometry now being undertaken at the University of Kansas with a 13.3-gigahertz aircraft-mounted scatterometer may define this variable in the radar parameters. Considered over a span of months, crop moisture may make a more significant contribution to radar return. Unpublished theoretical studies at the Center for Research in Engineering Science, University of Kansas (CRES), indicate that soil moisture will be swamped as a contributor to the radar return at short wavelengths by surface-roughness effects, but that at longer wavelengths, the contribution of soil moisture will be more significant.

5. Some crops depolarize an incident-polarized beam to a different degree than others. For example, sugar beets, corn, and unheaded sorghum apparently have a relatively small depolarizing effect, while headed sorghum and alfalfa exhibit a relatively strong depolarizing effect.

6. A study on the delineation of field boundaries and crop types has documented the problems associated with imagery obtained at any one time. At a single time, with a single radar frequency and one polarization, discrimination of field boundaries may not be much better than 60 percent, but with additional frequencies and polarizations and/or different types of imaging at different times, this figure should be raised into the 90-percent level or higher. It is reasonable to assume that similar improvements could be achieved in delineation of crop types with multiple frequencies and polarizations or more particularly with swept-frequency (broadband) systems obtained at different times.

7. Preliminary results indicate that electronic color combining of multiple-polarization imagery will aid in crop discrimination. Further refinement and expansion of this technique is underway with the image discrimination enhancement and combination system (IDECS), including the development of training sets and extrapolation to adjacent areas using Bayesian decision rules.

8. Numerical taxonomic clustering techniques have been applied to the September 1965 and July 1966 multiple-polarization data to determine natural clusters in the data (ref. 34-1). A similar study employing contingent probability and Bayesian decision theory (ref. 34-2) has also been made to determine natural sets within the data. The study was also made for crop discrimination training and extrapolation to adjacent areas.

STUDIES ON NATURAL VEGETATION

Studies on natural vegetation by S. A. Morain, R. M. Peterson, G. R. Cochrane, and the principal investigator have been made in a number

of environments, but the most detailed studies are those already carried out and those still in progress at Horsefly Mountain, Oregon (refs. 34-3 to 34-6). These and future studies are directed to determining the degree to which image gray-scale values and texture may be used for vegetation mapping. Forested areas normally may be separated from nonforested areas by image texture and film density. Areas of clear-cut logging operations can also be located by differences in image texture and radar shadowing. Gross forest distributions can be mapped at scales as large as 1:62 500 for reconnaissance purposes. Small-scale distribution maps may be produced in continuous strips from the original imagery. Areas of previous forest fires can be detected and delimited by combining inferences from the absence of the coarse image texture usually associated with forests, the position of the area on a slope, and the shape of the area believed to have been burned. Low-lying moist, marshy, or seasonally wet spots can be separated from surrounding vegetation types on the basis of image gray scale. Studies are underway to see the degree to which it may be possible to distinguish within-forest structures by image textural analyses and by electronic color combinations.

Inspection of radar imagery of various wavelengths shows that different returns are derived for natural vegetation groupings as a function of radar wavelength. This material is unpublished, but indicates that a vigorous program of evaluating natural vegetation return of short, medium, and long radar wavelengths is most desirable.

Preliminary studies at CRES have also indicated that a vigorous program of research, employing analyses of probability density functions, spectral density functions, contingent nearest-neighbor probabilities for gray scale and textures, and acutance, are appropriate future directions of research.

STUDIES ON SOIL MOISTURE

Soil moisture studies in relation to radar return were begun at Garden City in the expectation that multifrequency scatterometry would be used over the large test fields in that area. Unfortunately, only K-band imagery radar has been available and used to date; thus, no adequate test of the relation between soil and crop moisture and between radar frequency and polarization has been obtained. Results obtained with the various K-band imagers have produced some ambiguous results in that, over a wide range of moisture contents through time, some slight relation between radar return and crop and soil moisture has been detected. Within single months, because of reduced moisture range and variability, no such relation is clearly present for any crop.

Of the NASA scatterometer systems in existence, or under construction, the 13.3-gigahertz system is affected primarily by the roughness or texture of the illuminated surface, with little or no penetration taking place. The roughness scale to which the instrument is sensitive is roughly between 0.1λ and 10λ . The lack of penetration in the high-frequency range not only prevents measurement of possible layering but, likewise, will probably prevent any significant determination of moisture content from either ground or vegetation. The instrument is, however, extremely sensitive to structure size in the size range encompassed by leaves and stems of many agricultural crops.

The 0.4-gigahertz system will be sensitive to much larger structure size, but even more important, it is expected to give significant penetration of the foliage cover and, to some extent, the ground beneath. The amount of reflection from both the vegetation and ground will be determined primarily by the dielectric constant of the material, which in turn is primarily dependent upon the percent moisture content of either the vegetation or the upper layer of ground. This instrument, then, will add several additional dimensions to the data by providing polypolarization and roughness sensitivity in another size range. Perhaps of greatest importance, however, is the possibility of determining moisture content.

FIGURES

Figure 34-1 illustrates the Garden City Test Site in western Kansas. Approximately 400 fields are monitored in this area, which is flat with only two closely similar soil types. There is a variety of irrigated and unirrigated crops; therefore, an array of moisture states and crop states can be studied at almost any time. Since the area is flat and contains big fields, it is possible to use gross-resolution systems and get acceptable-quality data from the area. Ground truth is collected on soil, crop conditions, cover, et cetera, at the time of each NASA-sponsored flight.

Figure 34-2 shows the information available at Garden City, Kansas, in September 1965 on HH- and HV-polarization K-band radar. Fields of sugar beets, corn, grain sorghum, wheat, alfalfa, and bare ground were examined. The Y-axis is the like-density (HH) polarization; the X-axis is the cross-density (HV) polarization. Notice that the hyperplanes erected lie at about 45° , implying that both polarizations contribute information. Apart from a four-polarization matrix obtained in July 1966 at Garden City, Kansas, this is the only multipolarization information with adequate ground truth over any agricultural region in the United States. Hopefully, additional data will be obtained with the 1969 growing season.

In the upper group bounded by the upper hyperplane, there are 30 sugar beets and one corn, suggesting that if this relationship had held in adjacent areas, it would form a useful basis for extrapolation and discrimination. The next lowest region has 23 cases of corn, one of sugar beets, and one of grain sorghum. If this same relationship also holds in adjoining areas, it looks to be promising for projection. The lowermost group has 120 instances of bare ground; 17 instances of emergent wheat, in which the wheat occupies less than 5 percent of the total area — for all intents and purposes, actually bare ground; 10 instances of wheat stubble and weeds in which the wheat stubble was dry and made little contribution to the return; six instances of alfalfa; and four instances of grain sorghum. It will be seen that, with the exception of the alfalfa and grain sorghum, the lowermost category represents bare ground or is, practically speaking, bare ground. Notice that in the next category above (in fig. 34-2), there is only one example of bare ground. Consequently, the lowermost group also looks reasonably encouraging for projection by extrapolation to adjacent areas. Such extrapolation studies have begun.

The next to lowest category is a grab bag of emergent wheat, wheat stubble and weeds, alfalfa, corn, bare ground, and grain sorghum, though it is predominantly grain sorghum. It is obvious that the two-polarization single-frequency radar achieves inadequate discrimination in this region. However, the uppermost portion of the region is dominated by grain sorghum, and a subset might be discriminated which could be used as a basis for prediction for grain sorghum in the lower portion of the mixture. Radar imagery at a different time, optimized for the detection and discrimination of wheat in April, for example, would aid in improving predictions in this area.

It is necessary to make flights sequentially throughout a number of growing seasons to find the nature of the time dependencies in the data and to see the internal consistency of the data from year to year. In the visible and IR regions, it may be that year-to-year variations will be greater than with radar, which may be less sensitive to changes of modest degree. This is a possibility which should be carefully evaluated in further experiments.

Figure 34-3 shows the crop-type categorization of July radar image densities using complete linkage cluster analysis and Euclidean distance coefficients. The clusters are identified by the major crop combinations occurring in them. The absolute number of occurrences of each crop in each cluster is given. The stippled areas correspond to the percentage distribution of each crop in the range of categories. Thus, it can readily be seen that sugar beets are almost unique to category VI and that category VI is almost completely composed of sugar beets but that corn and unheaded sorghum are represented in every category, although there is a definite node in categories IV and V. The overlapping of the clusters shows realistically the difficulty of using July as a date for

high-level discrimination between crop categories with K-band multipolarization radar in this sample. Probably, July would be the most unsatisfactory month for extrapolation into adjacent regions, as can be seen. It is, however, encouraging that bare, or nearly bare, ground and sugar beets are surprisingly well discriminated at even this unsuitable time of the year.

Figure 34-4 shows a comparison of actual land use with the classes derived from clustering image densities from four K-band polarizations in July 1966. The map patterns used were purposely selected to correspond to the image and to give some similarity to the six categories in the clustering groups. The incomplete-data category was the result of reduction of the data to facilitate computation. This was done by eliminating any point lacking complete field data, for example, no soil moisture determination. Strictly speaking, this was unnecessary because the Euclidean distance coefficients used in the numerical clustering did not incorporate the parametric data on crop height and density, but used only the image gray-scale values on the radar images. This map and preceding illustration (fig. 34-3) indicate that in regions in which ground truth is lacking, it may prove feasible to erect some broad classes of natural clusters which correspond to meaningful crop groups. It is clear, however, that until sequential data through time are available, that this possibility and contingent probability analyses cannot be carried further. Extrapolation through use of training sets and Bayesian decision rules, of course, may be done at any time when a small sample is available embedded within a larger area which may be used as a training set. The two approaches, which by no means are the only approaches feasible, present the two extreme situations of use of training data and rational extrapolation for modest distances in geographically homogeneous regions and the alternative of seeking for natural breaks in the data in regions in which there is no ground truth.

Figure 34-5 shows the relative radar return curves for a series of crops at Garden City, Kansas, based on HH-polarization K-band imagery densities. The solid lines connect computed return means derived from the temporal data available. The image data used cover a 3-year time period and do not represent the average return for a given set of fields. The dashed lines were interpolated using known crop growth cycles, maturity dates, and the average return from bare ground and wheat stubble when applicable. These relative radar return curves are intended to indicate possible curves, rather than to represent the final judgment on the matter. Until time-sequential data are available to fill in the areas in which dashes rather than solid lines are used, and until repetitive data are available for the areas in which solid lines have currently been obtained, these graphs must be regarded as representing estimates involving judgment rather than quantitative information. They are, however, instructive in showing areas in which further information

is needed and in which differences between crops may reasonably be maximized to improve discrimination.

Figure 34-6 shows a color-combined HH-HV radar image of a portion of the Garden City, Kansas, Test Site in September 1965. Selective level slicing of the two film density ranges has reduced the display to the following four categories, each dominated by a single crop:

1. Category 1, red — exclusively sugar beet fields, eight samples
2. Category 2, red with black — seven alfalfa fields, a wheat field with an unusually high crop cover (70 percent), and two fields with a high percentage of crop residue and weeds (80 and 60 percent)
3. Category 3, black with red — seven of the 11 grain sorghum fields in this category; three fields of wheat, all less mature than the wheat fields in category 2; and an alfalfa field under irrigation at the time the imagery was obtained
4. Category 4, green — eleven of 13 fields bare ground, and the two deviating fields essentially bare, one having a few sprouts of wheat and the other being a field of stubble

It will be seen that this analog color display produces basically the same kind of results as the two-dimensional density plot (fig. 34-2). It also is comparable to the clustering obtained for the numerical clusters in the September 1965 data.

DATA COLLECTED BY NASA-FUNDED AIRCRAFT

Wright-Patterson AFB Avionics Laboratory

<u>Flight date</u>	<u>Sensors</u>
October 1, 1964	AN/APQ-55 radar imagery
November 24, 1964	AN/APQ-55 radar imagery AN/ASS-18 Eq. IR
July 7, 1965	T-11 metric camera AN/ASS-18 Eq. IR
August 14, 1965	AN/APQ-55 radar imagery Metric camera

Westinghouse Corporation

<u>Flight date</u>	<u>Sensors</u>
September 15, 1965	AN/APQ-97 radar imagery KA-30 photography
July 27, 1966	AN/APQ-97 radar imagery

SUMMARY OF OBJECTIVES AT TEST SITE 73 IN RELATION TO
THE NASA EARTH RESOURCES AIRCRAFT PROGRAM

Radar Calibration Studies

The Garden City Test Site is the prime calibration test site for radar imagery and scatterometry to evaluate the contribution of such parameters as crop type, height, percent ground cover, contained moisture content of crop, direction of crop rows, moisture content of the soil, soil roughness, et cetera, influencing the radar return. This site was initiated as the prime radar team agricultural test site but has been continued also as part of U.S. Geological Survey contract 14-08-0001-10848 to study the utility of radar and other remote-sensor imagery in thematic land-use mapping for geographic research. Studies on crop probability distributions through time are essential at this test site because here more than 400 fields are monitored at the time of each aircraft over-flight, and a considerable volume of ground-truth data is collected. Under the U.S. Geological Survey contract noted previously, color, false color, and multispectral photography are obtained in addition to radar imagery and scatterometry to evaluate the supporting and complementary roles that they have in regard to each other.

The overall program at the Garden City Test Site is to periodically collect scatterometer and imaging radar data at various wavelengths and polarizations across the agricultural growing season. Radar imagery is analyzed empirically and quantitatively to determine what types of agricultural information are consistently identifiable. Radar scatterometry is used primarily to provide radar amplitude or calibration of radar imagery gray scale, but it will also be evaluated for crop discrimination as a function of look angle. All information is used as background for providing radar instrument recommendations for aircraft and spacecraft radars. The radar data are also examined in light of suggesting new methods of data handling and automation of information extraction.

Summary of Scientific Analyses Performed to Date

Two limitations of the data must be mentioned. All of the radar imagery listed previously is limited to K-band wavelengths, and only one set of marginal-quality scatterometry data has been received (mission 32, September 19, 1966) to date. Thus, we have no potential for evaluating the response for the medium and long radar wavelengths, nor much capability for using scatterometry data to calibrate the radar imagery.

Statistical correlation of the agricultural surface parameters with radar return indicates that differences between crops are generally more significant in affecting the return than parameters such as crops, crop height, cover, moisture, and so forth, during a single sensing period in 1 month. When considered over a span of months, the parametric variables are, as one would expect, more significant. Different crops have differing depolarizing effects on an incident-polarized radar signal, and these differences help to distinguish between crop types.

Crop discrimination capability is variable. Sugar beets and bare ground fields are readily identified on September 1965 radar imagery at a time when they are sharply contrasted with other surfaces. Other crops, notably corn, become more readily distinguishable as they mature. The numerical clustering of multidimensional data, such as multiple-polarization data or data through time, creates categories of crops which may be identified with a high probability. Studies have been completed employing numerical clustering techniques (ref. 34-1), contingent probability, and Bayesian decision theory (ref. 34-2) for determining natural sets within the data, for crop discrimination training, and for extrapolation to adjacent areas.

The ability to discriminate fields and crops is improved with multiple-polarization imagery, but an even better discrimination is made if changes through time are monitored. Since the radar return is not inordinately influenced by minor fluctuations of moisture or local weather conditions, it is possible to monitor changes more securely associated with physical changes of crops associated with plant maturity. Imagery of the early growing season must be obtained to evaluate this fully, and regular flights at least every month throughout the growing season are desirable.

Certain data, especially the color and false color photography obtained during the summer of 1967, were intended to support a study to determine if boundaries noted on the September 1965 AN/APQ-97 radar imagery corresponded with boundaries of areas of saline soils. Unfortunately, much of the soil-sample data was accidentally destroyed before analyses were complete. However, it was determined that the radar

boundaries were not consistently associated with soil salinity differences and that the potential for measuring variations in salinity with K-band is minimal.

The one set of scatterometry data which we have received has posed interpretation problems which are only now being overcome. Only recently have we developed a reasonable technique for correlating the scatterometry data with aerial photography from the same flight. Also, the data are not good enough to reliably evaluate return differences from various agricultural phenomena. Poor quality of the scatterometry data is probably largely the result of the undesirable wind direction at the time of flight, necessitating an extreme "crab" angle for the aircraft. Also, questions of adequacy of sampling rate in the scatterometry data are unresolved.

Summary of Scientific Analysis to be Performed

The proposed research still follows the general lines indicated in the test site objectives outlined previously. We look forward to working with the multiband radar system being developed at NASA. We should also have our own polychromatic truck-mounted radar system, funded through Project THEMIS, operational within the next few months. Data from these systems, combined with the scatterometry data from mission 61, 74, and 77, will facilitate both the calibration studies and the estimation of radar potential for crop identification.

The application of electrical and optical image combination, enhancing, and sampling techniques will be expanded. These techniques have shown potential for crop and field discrimination and identification and for thematic mapping applications. These techniques and their application are described in more detail in another section of this report.

SUMMARY OF OBJECTIVES AT THE GARDEN CITY, KANSAS, TEST SITE 76 IN RELATION TO THE NASA EARTH RESOURCES AIRCRAFT PROGRAM

Multi-Image Color-Combining Studies

Imagery obtained by NASA, or with NASA funds, is being used as input data in an experimental investigation of real time image-processing devices known as the IDECS multi-image correlation system. This system was developed under NASA contract NGR 17-004-003 and under USAETL contract DAAK 02-C-67-0089, and work currently being performed is under the USAETL contract. With adequate ground-truth data collected at the time

of each imaging flight, multispectral photographic and K-band radar imagery have been color combined and have been used to measure the ability of the multi-image correlation system to make a map based on single or multifactor stratifications. Such maps include those showing boundaries of soils, natural vegetation, agricultural land use, and trafficability.

Summary of Scientific Analyses Performed to Date

Multiband photography has been used as input data for the multi-image correlation system to produce color-combination images. Human manipulations on the IDECS color combinations within defined boundaries (established by ground truth) have been part of a preliminary study for developing techniques for using the multi-image correlation system with only qualitative results to date. These techniques have produced color-combined image-like maps of agricultural land use within the Garden City Test Site.

Attempts to combine multiband photography and K-band radar images of the same area to produce a single processed image have not been successful because of gross differences in image scale. Optical enlargements of the radar imagery to a scale compatible with the photographic scale has resulted in a radar image that is so degraded that it is unusable. Similarly, many NASA missions carrying photographic sensors have not produced imagery suitable to the multi-image correlation investigations because the resulting photographic scale is too large to be meaningful in the present phase of experiments. In these cases, the mission generally included 13.3-gigahertz scatterometry requiring low-altitude imaging, and multiband photography was only a supporting system. The photography currently being used was flown at 7000 feet absolute with a photographic scale of 1:14 000.

Summary of Scientific Analysis to be Performed

Further investigations of the abilities of the multispectral correlation system to make thematic maps are twofold:

1. Using developed techniques, single and multifactor stratifications of the natural environment will be mapped for selected areas in the Garden City Test Site from multiband photography and multipolarizations of K-band radar imagery. Mapping will include soils, natural vegetation, and agricultural land use in areas where existing ground truth can be used to accurately set the stratified boundaries. Quantified measurements of the degree of correlation between ground-truth data and the patterns apparent on the processed maps will be made.

2. When the maps described previously are produced and their accuracy quantitatively measured, the operational techniques developed will be employed in similar type areas in the Garden City Test Site to produce agricultural land-use maps, for example, for multiband photography, but without the assistance of known ground truth. The resulting maps will be analyzed, and their accuracy will be quantitatively measured for comparison with the previous set of maps. These investigations are based on the concept that human manipulations of the color-combined images within defined boundaries is one method towards the training set with predictable utilities in remote areas in which it is impossible to collect ground truth.

SUMMARY OF OBJECTIVES AT TEST SITE 159 IN RELATION TO THE NASA EARTH RESOURCES AIRCRAFT PROGRAM

Fundamental Remote-Sensing Problems Studied

Horsefly Mountain is part of a land-use analysis investigation designed to document the extent to which remote-sensing devices and procedures can be used to evaluate features of natural vegetation. Because of its wide variation in vegetation types and ecological conditions, the Horsefly Mountain Test Site has been established to aid assessment of such parameters as natural vegetation type, height, percent ground cover, distributional patterns, and boundary conditions through use of a variety of sensors. Originally (1965), the Horsefly Mountain area constituted part of a radar calibration site in the Pacific Northwest for the Geology Radar Team, but its promise as a vegetation test site deserving more intensive research was recognized early.

At present, studies at Horsefly Mountain are directed specifically at evaluating the limits of radar in vegetation probabilistic studies, pattern recognition, and thematic land-use mapping. Ultimately, the aim of our research at test site 159 is to determine the mutually supportive and complementary roles of radar and other remote sensors.

Summary of Scientific Analyses Performed to Date

1. Westinghouse AN/APQ-97 radar imagery has been interpreted qualitatively for HH and HV content. Much of the original thinking concerning the potential of radar in vegetation studies derives from this early work. In addition, the Westinghouse imagery has been compared with conventional aerial photography, used as a mapping base for vegetation patterns, analyzed in part by IDECS equipment including initial studies with the pulse-height analyzer and flying spot scanners, and compared with data collected by the Earth Resources Aircraft Program mission 59.

2. Mission 59 data (abstracted from 90-day report dated May 1968)

a. AN/AAS-5 ultraviolet (UV) has not yet been evaluated as a potential sensor at Horsefly Mountain, although the quality of the data supplied by NASA is excellent.

b. Using air photomosaics as a basis of orientation and reference, 13.3-gigahertz scatterometry is in progress of evaluation. Initial results appear to contain limited information because of (1) the low resolution, (2) the absence of good reference points on the ground, and (3) a probable too-small sampling rate employed in digitally processing the scatterometry data. The grossness of the data is such that referencing is extremely difficult, especially under conditions of natural vegetation. More refined data are required before further work is undertaken in scatterometry at Horsefly Mountain.

c. ITEK multiband photography has been reviewed, and key locations have been analyzed by IDECS equipment. Integration and density-level slicing to aid differentiation of vegetation types have been usefully employed in this regard. Seventeen locations have been selected for special study at Horsefly Mountain, giving 153 transparencies for study on the IDECS flying scanners. From these transparencies, 85 color-combined images have been generated for analysis of vegetation content.

d. RC-8 color photography has been prepared for qualitative evaluation with multiband and radar imagery. One of the immediate uses of this data has been the preparation of a detailed "vegetation types" map for use as a guide in other comparisons. Transparencies of key locations have also been employed in the IDECS color combiner, in combination with radar and multiband photography.

e. Reconofax IV infrared (IR) has not yet been utilized to its potential at the Horsefly Mountain Test Site. A map of vegetation patterns has been completed, using the dual systems of radar and IR imagery, but further work is required to evaluate the contribution each system makes towards discrimination of type boundaries.

In general, results from the various analyses offer encouragement in the remote determination of some natural vegetation parameters using sensors. It has been suggested in recent publications that the use of radar imagery alone in some of the world's cloud-swathed, unmapped, remote, and inaccessible terrain situations offers scope for reconnaissance-type mapping and terrain evaluation. With the addition of multiband, thermal IR, color, and false color photography obtained in cloud-free patches, the discriminant capabilities of radar may be extended through inference from multispectral and higher resolution data.

Summary of Scientific Analysis to be Performed

To date, the radar imagery has been analyzed empirically and semi-quantitatively in an effort to pinpoint which types of natural vegetation information are identifiable. Future studies will have a similar aim, but will also strive to establish the degree of consistency achievable within and among localities using IDECS equipment.

Qualitative evaluations of the supportive and complementary functions of each sensor will continue. Specifically, the UV and thermal IR imagery must be assessed for their contribution to reconnaissance vegetation mapping and terrain evaluation. The radar-thermal IR vegetation map of Horsefly Mountain needs to be redrawn to specifically show the contribution made by each type of imagery.

Remote sensing of natural vegetation at Horsefly Mountain does not lend itself to quantification as readily as do studies at other test sites. Nevertheless, it is recognized that quantification is essential if results are to be meaningfully extended and duplicated in other areas. Future work on test site 159 will be aimed at improving the quantitative aspects of remote-sensor vegetation analysis.

SUMMARY OF OBJECTIVES AT TEST SITE 35 IN RELATION TO THE NASA EARTH RESOURCES AIRCRAFT PROGRAM

The Wichita radar soil-test site is a calibration test site for evaluating radar response in an environment which has some resemblances to subtropical and tropical savannas. This lengthy strip covers a wide variety of soil types. At selected times of the year, these soil types are variably bared by cultivation. At other times, they are covered with crops and pastures. It is the intention to evaluate fine-, medium-, and gross-resolution radar imagery and scatterometer data to determine the types and classes of soil information extractable. It is the ultimate intention that a variety of radars be flown over this test site, but to date, only the K-band Westinghouse AN/APQ-97 data have been obtained of the test site.

Summary of Data Collected and of Work at the Wichita Radar Soil Strip (Test Site 35), Kansas

Aircraft data for the Wichita radar soil strip have come exclusively from a single non-NASA-funded flight of the Westinghouse AN/APQ-97 radar (Westinghouse flight 31) obtained June 26, 1964. This imagery is classified. Several supporting flights with the NASA 240A and P3A aircraft to continue the evaluation with radar scatterometry and supporting color

photography were abandoned because of poor weather or for other reasons connected with scheduling problems of the aircraft. It was on the basis of the availability of the classified radar information that later the unclassified multiple-polarization Westinghouse AN/APQ-97 radar image flight was flown July 27, 1966, under NASA sponsorship funding. Because of system malfunction during this July 27, 1966, flight, no unclassified radar imagery was obtained; therefore, the work with the classified imagery was slowed down. A small portion of the classified imagery was declassified and formed the basis for a report submitted for publication in the International Soil Science Society, Ninth Congress, August 1968 in Adelaide, Australia (ref. 34-7).

Summary of Scientific Analyses Performed to Date

One publication has been produced on this test site using the K-band Westinghouse system. It is appropriate to quote the concluding remarks in the paper: "To summarize these observations, it is clear that the information obtainable from this radar imagery for soil mapping is distinctly uneven in both distribution and quality, for while it is sometimes possible to make clear distinctions between adjacent soils even at the soil series level and more usually at the soil association level, there are many instances when neither is feasible. Separation of soil groups at the association level is more likely in untilled and subhumid to arid regions than in cultivated or densely forested humid lands. To put these conclusions in another way, where extreme differences occur in adjoining plant structures, in soil or plant moisture content, in soil texture, in topography, and — in areas of scanty vegetation — in small-scale surface roughness, then discrimination on the radar image of soil units closely tied to these differences will usually be possible. Lesser differences will not be so easily detected, especially in cultivated areas, and careful timing of aircraft flights to coincide with the greatest seasonal vegetation contrasts will be necessary.

"Additional studies employing multiple wavelengths, polarizations, and radar bandwidths may show that it is possible to better this level of discrimination of soil units. Even if this is not the case, however, the overall perspective provided by radar coverage of large landscape units will be a valuable addition in reconnaissance surveys."

In addition to the small area in northern Oklahoma which was declassified for this publication, maps have been prepared of selected areas along the flight path between north-central Oklahoma and central-eastern Kansas to the south of Lawrence, Kansas. Some six areas have been chosen for detailed study, and maps based upon existing soil surveys and prepared from radar imagery have been produced and will eventually be used for making detailed comparisons to further extend the conclusions obtained in the northern Oklahoma study.

Summary of Scientific Analysis to be Performed

Proposed research at this test site will involve a modest number of flights with radars other than the Westinghouse K-band system. It is appropriate to fly the site with DpD-2 when operational in the P3A and to fly such other imaging radars as NASA may later acquire in its aircraft program. In addition, it is hoped that the Naval Research Laboratory aircraft will, at some time in the future, fly its four-polarization, four-frequency imaging radar system over the strip. When this is done, it will be feasible to prepare a quantitative comparison of the different types of information available as a function of frequency and polarization in reconnaissance soil mapping. It is recognized, of course, that the radar soil strip does not encompass the full range of potential environments needed for a full evaluation of the information as a function of frequency and polarization. However, it is sufficiently diverse that a number of key questions on soil mapping with radar may be answered there.

REFERENCES

- 34-1. Schwarz, D.; and Caspall, F.: The Use of Radar in the Discrimination and Identification of Agricultural Land Use. Presented at the Fifth Symposium on Remote Sensing of Environment, April 16-18, 1968, University of Michigan, Ann Arbor, Michigan. To be published in the Proceedings.
- 34-2. Haralick, R.; Caspall, F.; Moore, R.; and Simonett, D. S.: A Statistical and Conditional Probability Study of Crop Discrimination Using Radar Images. Presented at IEEE International Convention, March 18-21, 1968, New York. To be published in the Convention Record.
- 34-3. Morain, S. A.; and Simonett, D. S.: Vegetation Analysis with Radar Imagery. Proc. Fourth Symposium on Remote Sensing of the Environment, 1966, pp. 605-622.
- 34-4. Morain, S. A.: Field Studies on Vegetation at Horsefly Mountain, Oregon, and Its Relation to Radar Imagery. CRES Technical Report 61-22, 1967.
- 34-5. Morain, S. A.; and Simonett, D. S.: K-Band Radar in Vegetation Mapping. CRES Technical Report 61-23. Also presented at the Annual Convention of the American Society of Photogrammetry, Washington, D.C., March 1967. Published in Photogrammetric Engineering, Vol. 33, no. 7, July 1967, pp. 730-740.
- 34-6. Peterson, R. M.; Cochrane, G. R.; and Simonett, D. S.: A Multi-Sensor Study of Plant Community Densities and Boundaries at Horsefly Mountain, Oregon. (To be submitted for publication.)
- 34-7. Simonett, D. S.: Potentials of Radar Remote Sensors as Tools in Reconnaissance Geomorphic, Vegetation and Soil Mapping. Ninth International Congress of Soil Science, Transactions, Adelaide, Australia, Vol. IV, 1968, pp. 271-280.

BIBLIOGRAPHY

Dalke, G. W., et al.: Multi-Image Correlations Systems Study for MGI, Phase II Technical Report (U), June 1968.

Moore, R. K.; and Simonett, D. S.: Contribution to several chapters in the National Academy of Science — National Research Council Publication entitled Multi-Spectral Sensing of Agricultural Resources. (To be published.)

Moore, R. K.; and Simonett, D. S.: Potential Research and Earth Resource Studies with Orbiting Radars: Results of Recent Studies. AIAA Fourth Annual Meeting and Technical Display, Paper no. 67-767, 1967. Also published as CRES Technical Report 61-32.

Moore, R. K.; and Simonett, D. S.: Radar Remote Sensing in Biology. Bioscience, Vol. 17, no. 6, June 1967, pp. 384-394.

Simonett, D. S.: Land Evaluation Studies with Remote Sensors in the Infrared and Radar Regions. In Land Evaluations: papers of the CSIRO Symposium, G. A. Stewart, ed., Macmillan of Australia, pp. 349-366.

Simonett, D. S.; Eagleman, J. R.; Erhart, A. B.; Rhodes, D. C; and Schwarz, D. E.: The Potential of Radar as a Remote Sensor in Agriculture: 1. A Study with K-Band Imagery in Western Kansas. CRES Report 61-21, 1967.

TABLE 34-I.- REPORT ON STUDIES AT GARDEN CITY, KANSAS, TEST SITE 76

[Principal Investigator, D. S. Simonett]

Mission	Date flown	Data	Date received	Quality	Results
32	September 19, 1966	Scatterometer Reconofax IV AAS-5 Multiband RC-8 (color and false color)		Poor Good Poor Good Good	Malfunctioning scatterometer provided poor data which are not readily correlated with the aerial photography. Reliable inferences as to relative return from agricultural phenomena cannot be made. Remaining imagery will be used in studies of crop response as a function of crop type since the intended radar calibration potential is minimized. AAS-5 imagery is poor because of haze; otherwise, the imagery is good.
54	August 8, 1967	Reconofax IV AAS-5 Multiband RC-8 (color and false color)	August 17, 1967 August 17, 1967 August 17, 1967 November 11, 1968	Good Poor Good Fair	Data are good except multiband photography has poor focus of lens 2, RC-8 camera lacked anti-vignetting filter, and the AAS-5 imagery is generally poor. The flight was designed to detect saline-soil boundaries from the photography and accompanying field work for comparison with radar image boundaries. Accidental disposal of soil samples before complete analysis limited this potential, but further evaluation of these images and earlier radar indicate that the saline-soil boundaries are not coincident with the radar boundaries. (90-day mission analysis report submitted to NASA MSC and U.S.G.S. May 8, 1968.)
61	November 14, 1967	Scatterometer Reconofax IV AAS-5 Multiband RC-8 (color and black and white)	N/R December 1, 1967 December 1, 1967 December 1, 1967 December 11, 1967	-- Good Fair Fair Good	Scatterometer data have not been received to date, precluding major analysis of mission 61 data. Other data received are good, except that the AAS-5 imagery is only fair, and the multiband photography has limited value because of improper functioning of the image motion-compensation system. Selected multiband frames have been color combined on the IDECS system for studies of agricultural land use. (Mission analysis report submitted to NASA MSC and U.S.G.S. July 31, 1968.)

TABLE 34-I.- REPORT ON STUDIES AT GARDEN CITY, KANSAS, TEST SITE 76 - Concluded

[Principal Investigator, D. S. Simonett]

34-20

Mission	Date flown	Data	Date received	Quality	Results
74	June 17, 1968	Scatterometer Reconofax IV AAS-5 RC-8 (color and color IR)	N/R July 9, 1968 July 9, 1968 July 3 and 9, 1968	-- Good Fair Fair	Photography is adequate as index for scatterometer data, although light conditions were marginal for both Ektachrome and Ektachrome IR. Scatterometry data have not been received. Color and color IR are being used as input data in IDECS multi-image color combination experiments of agricultural land-use mapping. (90-day mission analysis report being completed.)
77	July 29, 1968	Scatterometer Reconofax IV AAS-5 RC-8 (color and color IR)	N/R August 26, 1968 August 2, 1968	-- Good Fair Fair	Aerial photography is adequate as index photography for scatterometer data. Scatterometry data have not been received. Color and color IR photography are of marginal use for interpretation of agricultural features because of the large amount of cloud shadowing (colors degraded). Reconofax IV imagery is good.

TABLE 34-II.- REPORT ON STUDIES AT HORSEFLY MOUNTAIN, OREGON, TEST SITE 159

USING NASA/MSC AND NASA-FUNDED AIRCRAFT DATA

[Principal Investigator, D. S. Simonett]

Mission	Date flown	Data	Date received	Quality	Results
59	October 18, 1967	Scatterometer	June 6, 1968	Poor	In progress of evaluation with air photo-mosaics; content limited because of preliminary status of data. Preliminary results indicate either 400-foot resolution too gross to derive plant density and boundary information, or sampling rate in scatterometry is too low for discrimination.
		Reconofax IV	November 6, 1967	Good	Used for vegetation mapping in combination with radar imagery. Initial results show promise in studies of plant community boundaries.
		AAS-5	November 6, 1967	Good	No analyses yet initiated.
		RC-8	November 6, 1967	Excellent	Selected sites subjected to IDECS analysis and compared with radar and multiband photography; used also for vegetation mapping for comparison with radar and IR maps.
		Multiband	November 6, 1967	Poor (3-lens strips under-exposed)	Selected sites subjected to IDECS analysis and compared with radar. Results so far suggest that discrimination of vegetation types and densities is best achieved by combining radar, near IR, and either panchromatic or number 5 or 6 from the multiband.
NASA-funded Westinghouse AN/APQ-97	October 1965	K-band, HH and HV	November 1965	Excellent	Used in preparing several preliminary reports on value of multiple polarization in color combining, texture analysis, and probability density functions.

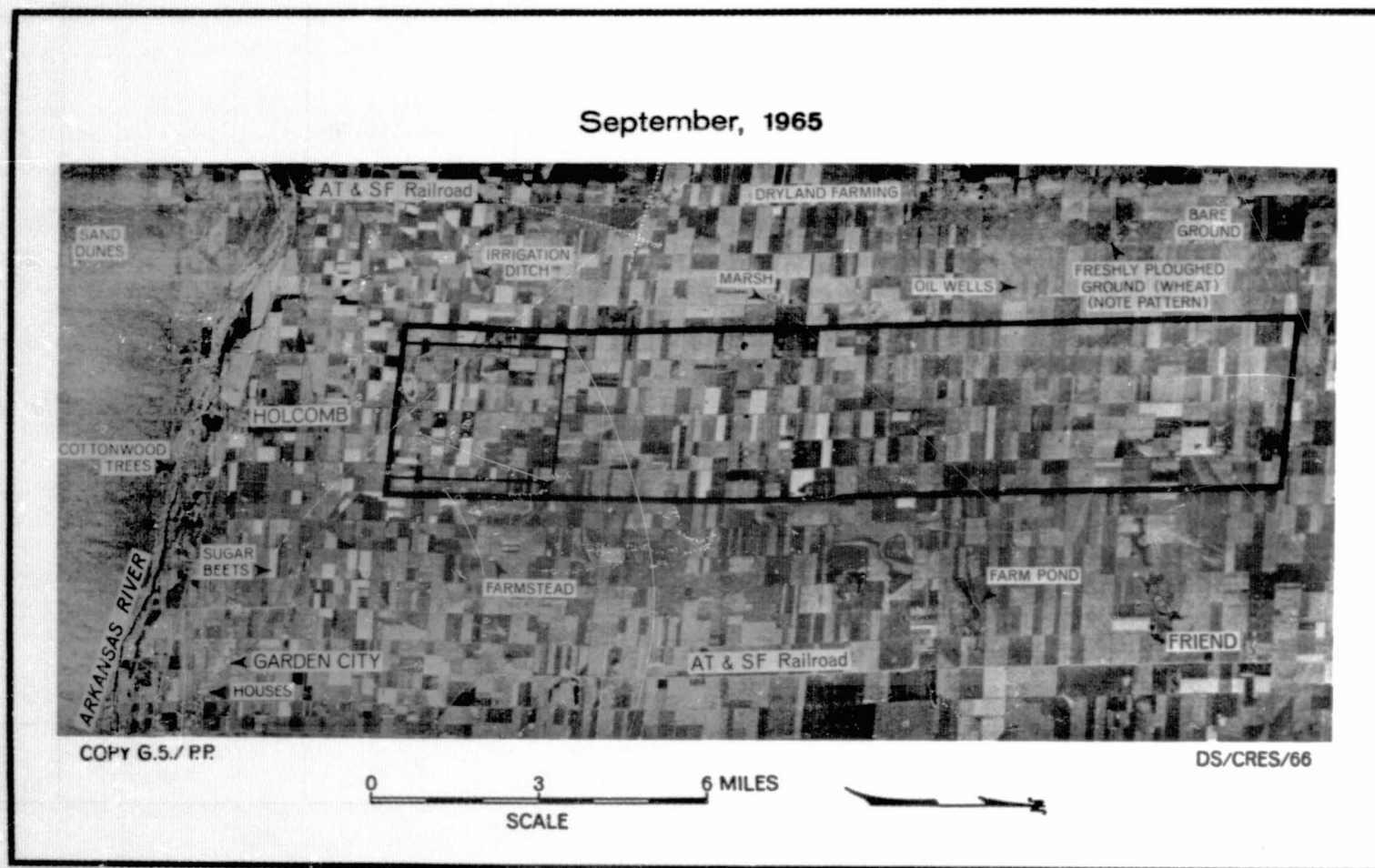


Figure 34-1.- The K-band radar image of Garden City, Kansas, Test Site 76.

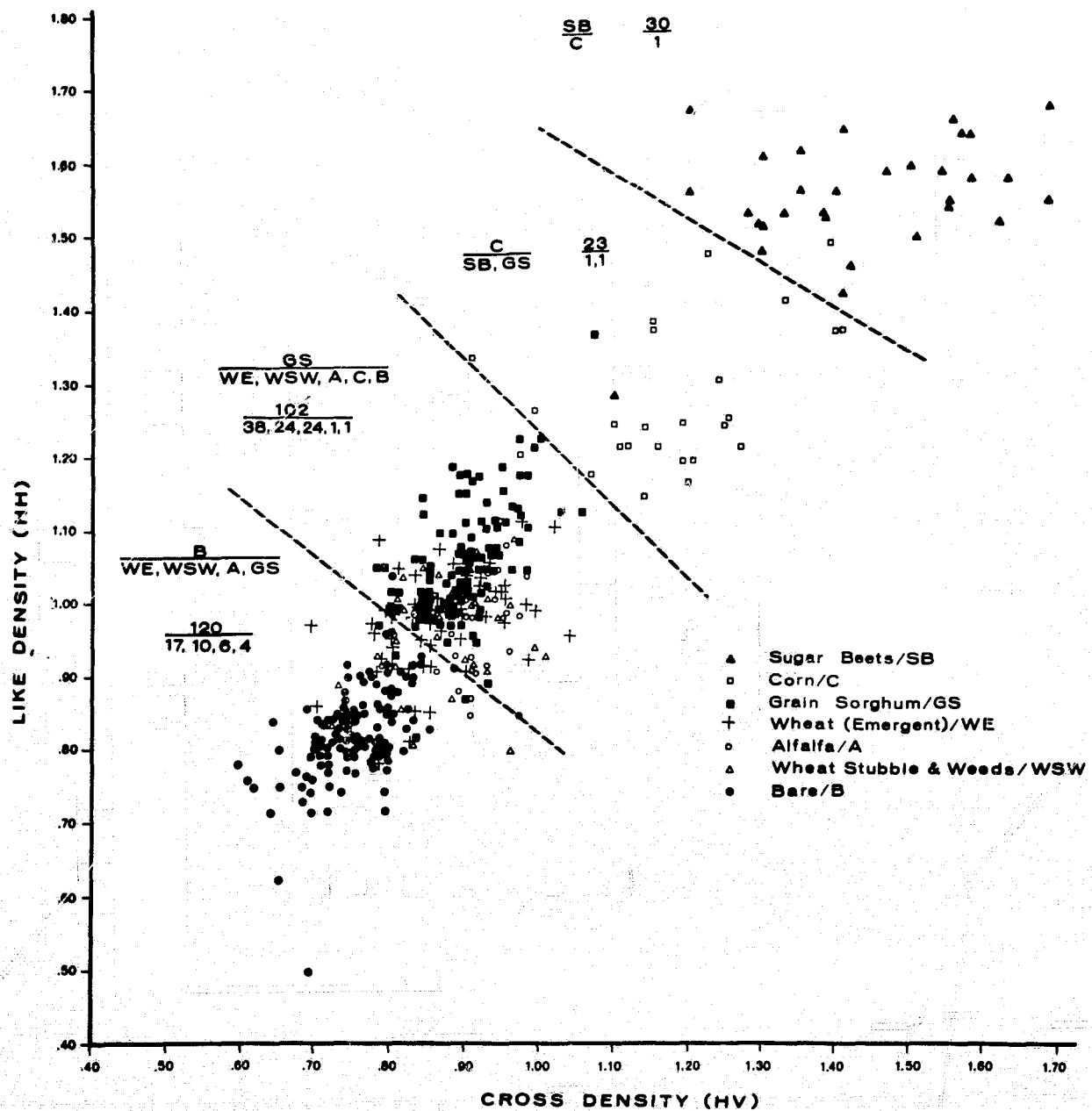


Figure 34-2.- Information available at Garden City, Kansas, in September 1965 on HH- and HV-polarization K-band radar.

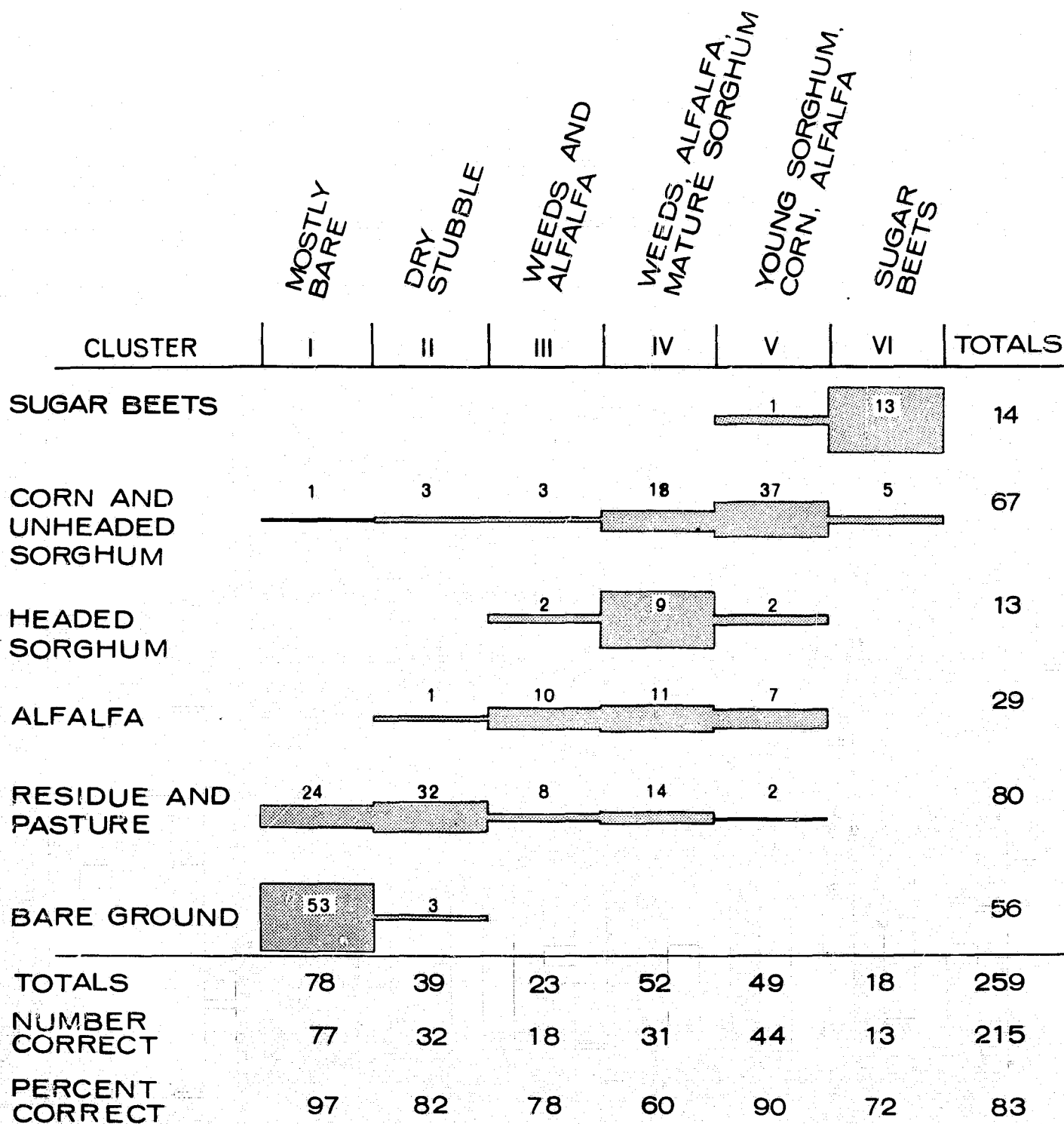
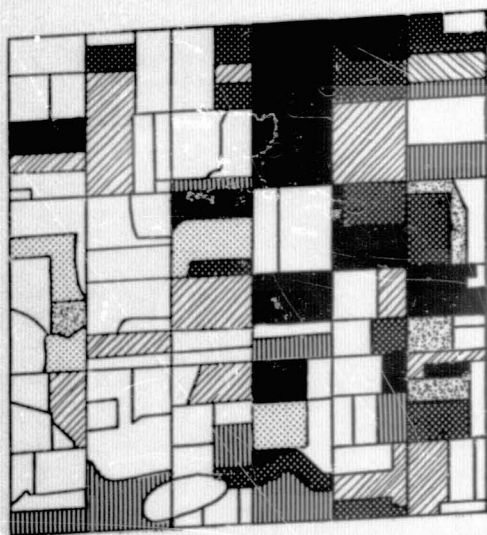









Figure 34-3.- Crop-type categorization of July radar image densities using complete linkage cluster analysis and Euclidean distance coefficients.



LAND USE

Mapped in Field

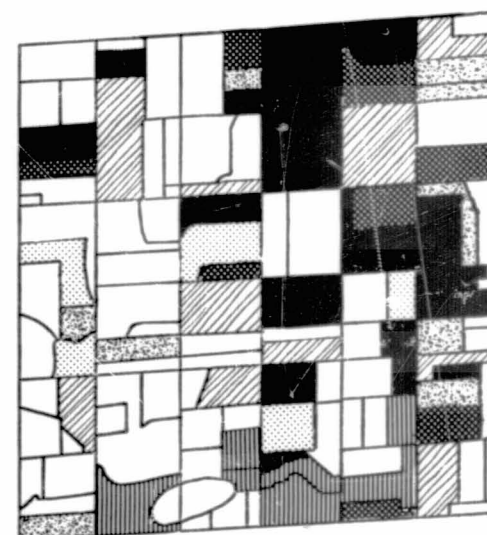
-  Sugar Beets
-  Corn or Unheaded Sorghum
-  Headed Sorghum
-  Alfalfa
-  Weeds, Stubble, or Pasture
-  Bare Ground
-  Incomplete Data



K-BAND RADAR IMAGE

Garden City, Kansas Site

0 1 2
Miles



CLASSES DERIVED FROM CLUSTER ANALYSIS

Four Polarizations








-  I
-  II
-  III
-  IV
-  V
-  VI
-  Incomplete Data

Figure 34-4.- Comparison of actual land use with the classes derived from clustering image densities from four K-band polarizations in July 1966.

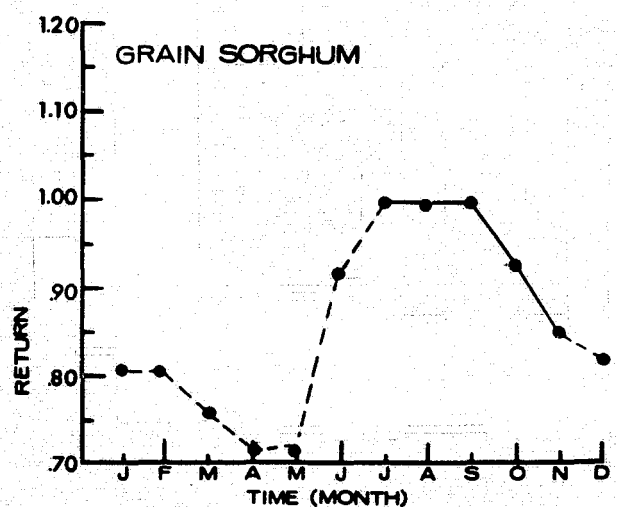
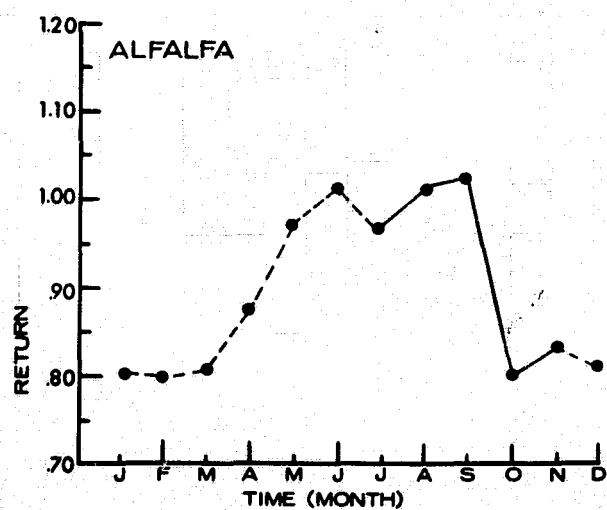
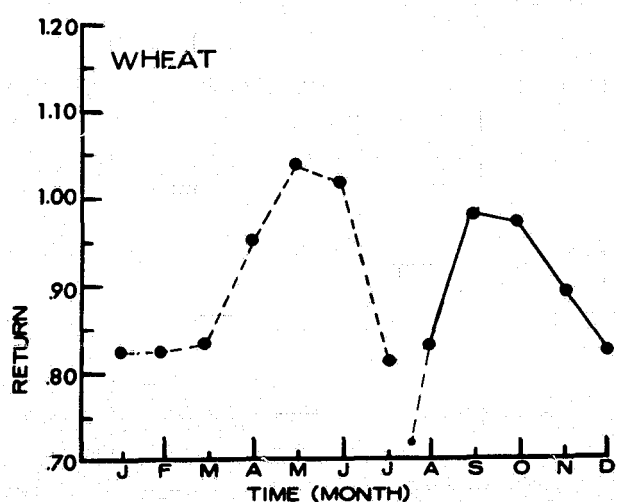
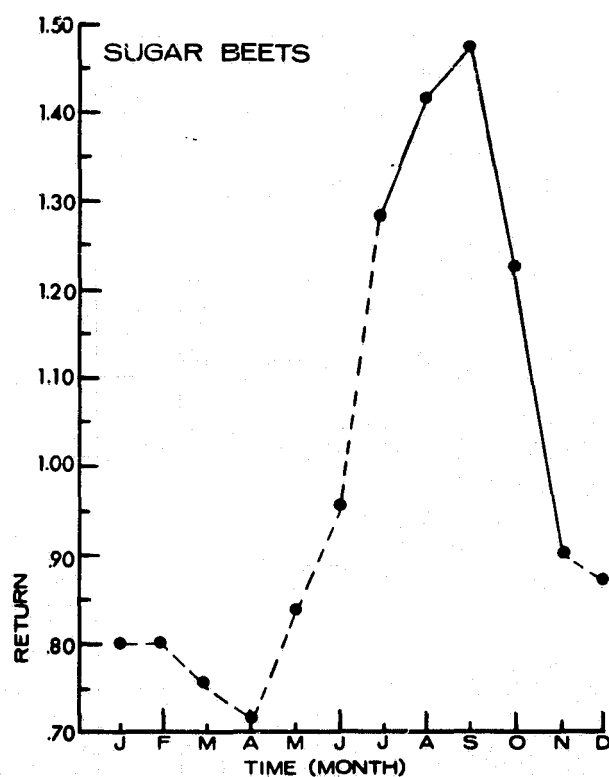
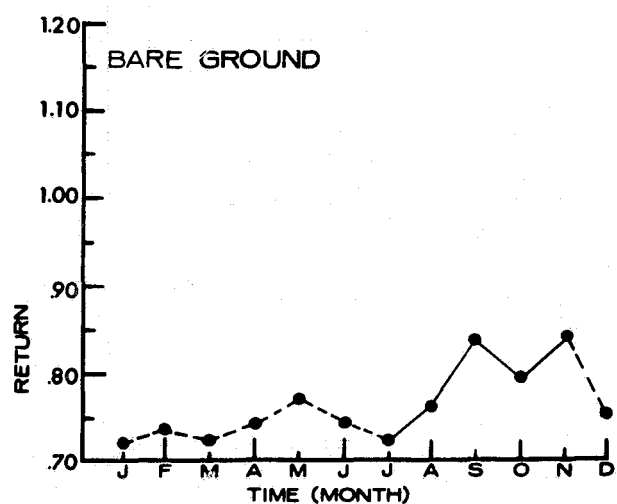


Figure 34-5.- Relative radar return curves for a series of crops at Garden City, Kansas, based on HH-polarization K-band imagery densities.

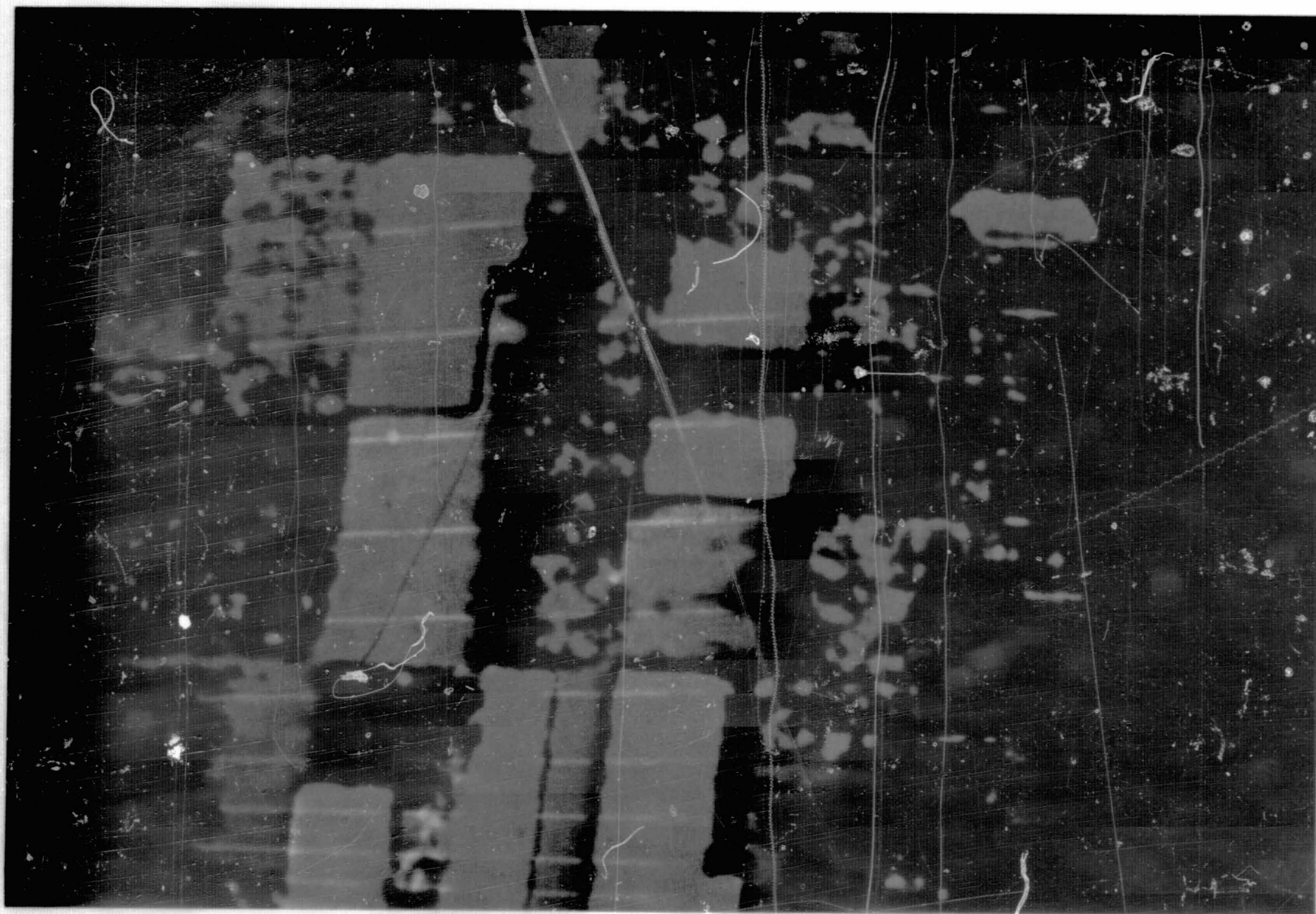


Figure 34-6.- Color-combined HH-HV radar image of a portion of the Garden City, Kansas, Test Site in September 1965.

34-27

REPRODUCIBILITY OF THE ORIGINAL PAGE IS POOR.

N71-16157

WILDLAND RESOURCE INVENTORIES UNDER THE

NASA EARTH RESOURCES SURVEY PROGRAM

By William C. Draeger

School of Forestry and Conservation, University of California

INTRODUCTION

Most of the NASA-sponsored research concerned with wildland resource inventories has been centered in the Bucks Lake Test Site (site 20) in the Sierra Nevada Mountains of California. Emphasis has been placed on the wildland vegetation resources in this primarily forested area. One research objective has been to define the optimum image specifications for inventorying the various vegetation types and other wildland resources on small-scale imagery. From an interpretation of such imagery, the feasibility of identifying representative resource features in the Bucks Lake Test Site has been determined.

RESULTS OBTAINED THROUGH THE USE OF DATA FROM NASA AIRCRAFT

An attempt has been made to obtain imagery of the test site with as wide a variety of sensor types as possible in order to develop a priority listing of sensors for the various applications of interest. Furthermore, examples of particular image types were obtained at various scales and interpreted in order to ascertain resolution requirements for particular resource inventory tasks. Finally, imagery was acquired during various seasonal periods and at different times of day in order to determine the optimum acquisition specification for time-critical interpretation tasks and to evaluate sequential imagery for particular applications. Imagery supplied through the cooperation of the NASA Aircraft Project has been used in all of these determinations.

Figure 35-1 illustrates the evaluation of multispectral black and white photography for the discrimination of various natural terrain features and for the comparison of the interpretability of such multiband images with color infrared photography or color-enhanced images of the same area. Notice that in this example, nearly all the features visible on the multiband photography can be just as easily differentiated

on the color infrared photograph. Figure 35-2 presents a comparison of conventional color film and color infrared film for the interpretation of various wildland features. It is readily apparent that the relative interpretability of the film types is dependent on the particular discrimination to be made.

In terms of the definition of resolution requirements, it has been shown that gross typing can be done on Gemini photography (fig. 35-3). However, such delineations are generally only discriminations and not identifications. Often the low ground resolution is actually an aid in drawing such broad discriminatory boundaries. In terms of actual identification of types and collection of quantitative data, emphasis has been placed primarily on intermediate-scale imagery. This has been done in an attempt to ascertain how such imagery might fit into a double sampling scheme whereby actual quantitative data are retrieved from a limited number of intermediate-scale photographs within the areas delineated on the small-scale images. Such procedures are illustrated in figures 35-4 and 35-5.

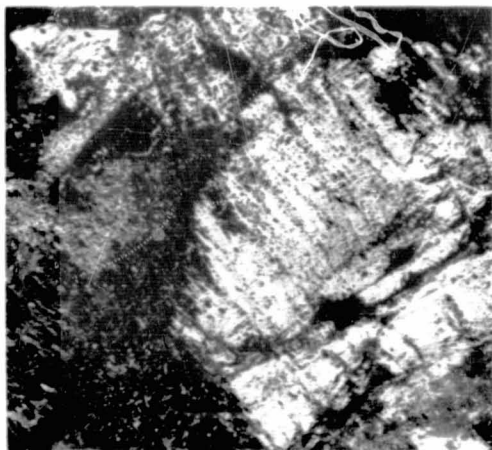
Further studies, an example of which is illustrated in figure 35-6, were undertaken to ascertain the optimum seasonal state in which imagery should be acquired for various applications. Time-critical applications include identification of specific vegetation types on the basis of phenological characteristics of particular species and the evaluation of snow accumulation and retention characteristics of various terrain-vegetation environmental types.

In addition, work has been performed on the investigation of various interpretative methods for the extraction of data from intermediate and small-scale imagery, for which determinations are based primarily on tonal values, and less reliance is placed on image detail. An example of one such technique is illustrated in figures 35-7 and 35-8.

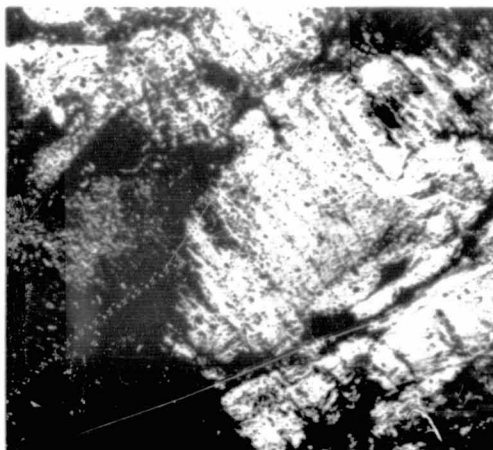
Further examples of the specification determinations discussed previously will be found in the Annual Progress Report for the Earth Resources Program, September 30, 1968.

REPRODUCIBILITY OF THE ORIGINAL PAGE IS POOR.

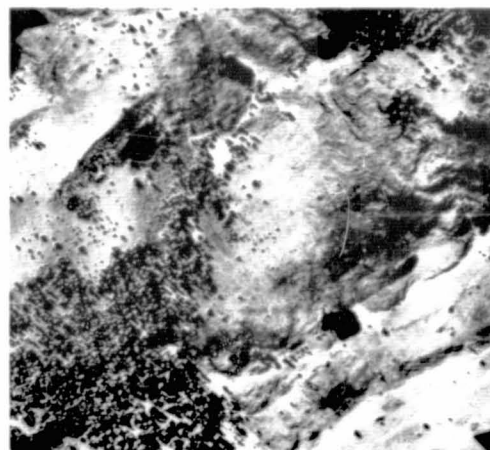
35-3



Panchromatic film,
0.520 μ to 0.580 μ



Panchromatic film,
0.660 μ to 0.720 μ



Infrared film,
0.750 μ to 0.950 μ

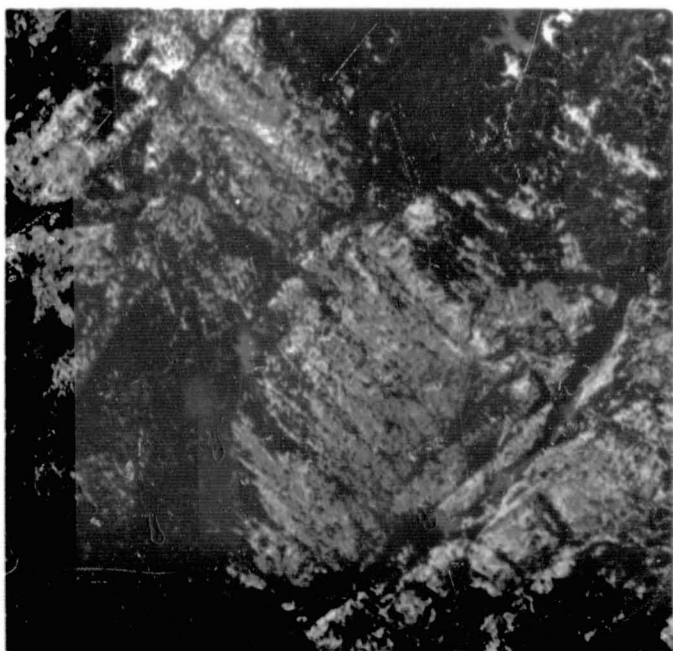
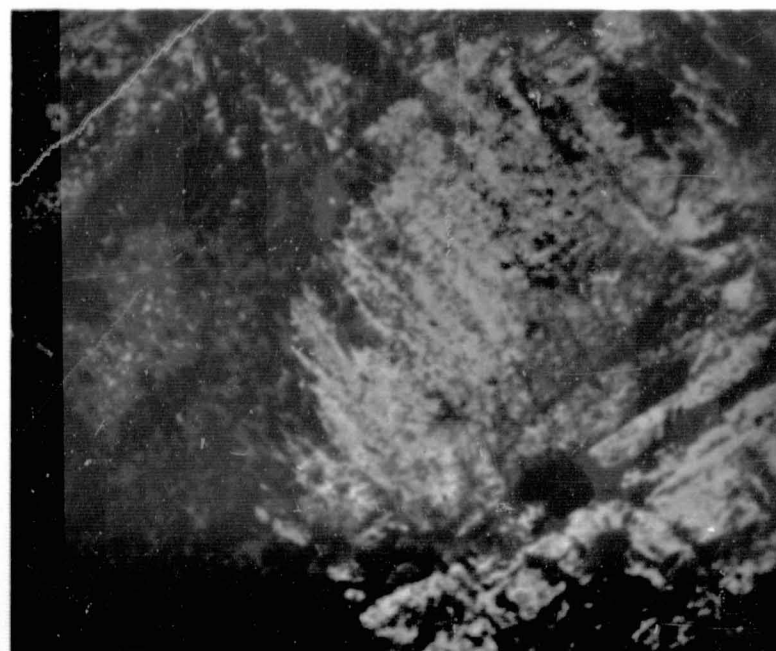


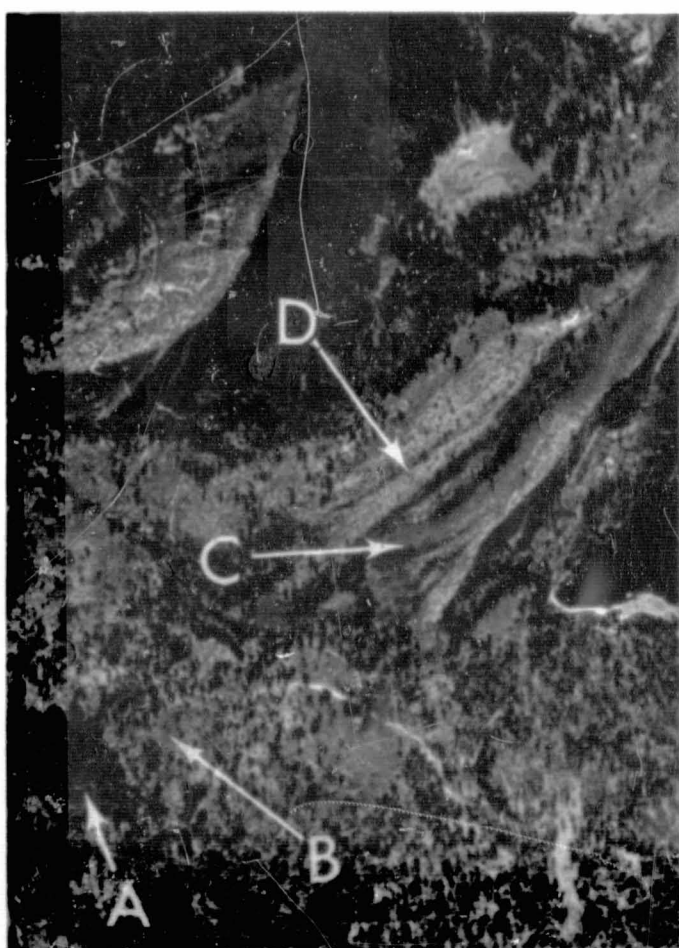
Image obtained directly, using
Ektachrome Aero IR film



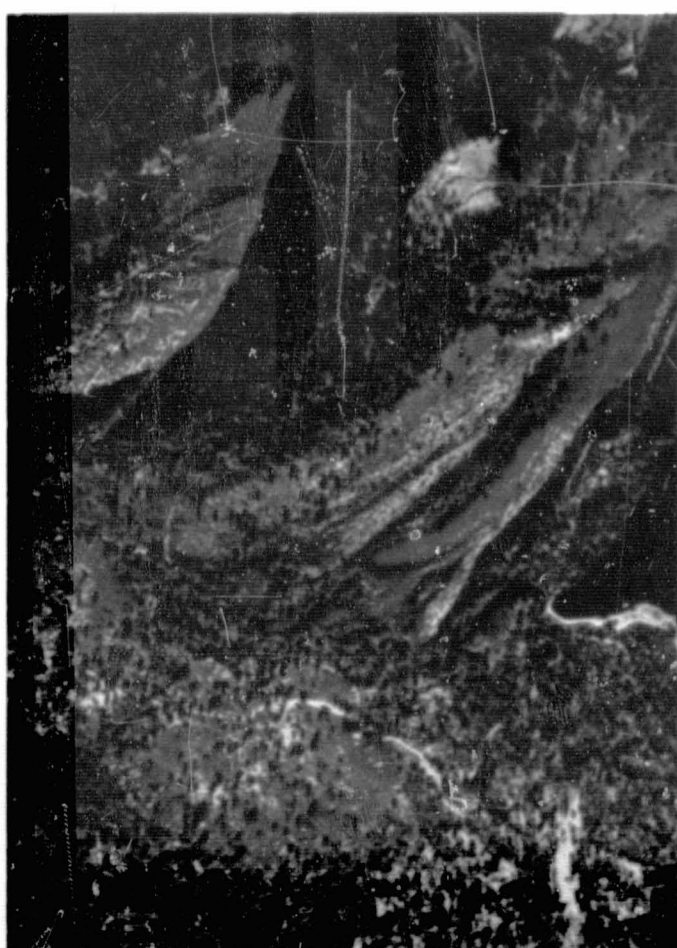
Multispectral color-composite image
obtained by projecting three black
and white images through filters

Figure 35-1.- Multispectral black and white Ektachrome Aero IR and color-enhanced images of an area in the Bucks Lake Test Site. Notice that while no one of the black and white images allowed all of the terrain types present to be discriminated, the three images interpreted in concert make these discriminations possible. Notice also the degree to which it is possible to approximate an Ektachrome Aero IR image closely by means of multicolor enhancement techniques.

35-4



Aerial Ektachrome film



Ektachrome Aero IR film

Figure 35-2.- A comparison of the ease of discrimination of terrain and vegetation features as imaged on conventional color and color IR films. Of particular interest are dense stands of coniferous trees (A), as compared with brush-conifer admixtures (B), and dense brush (C), as compared to granitic outcrops (D).

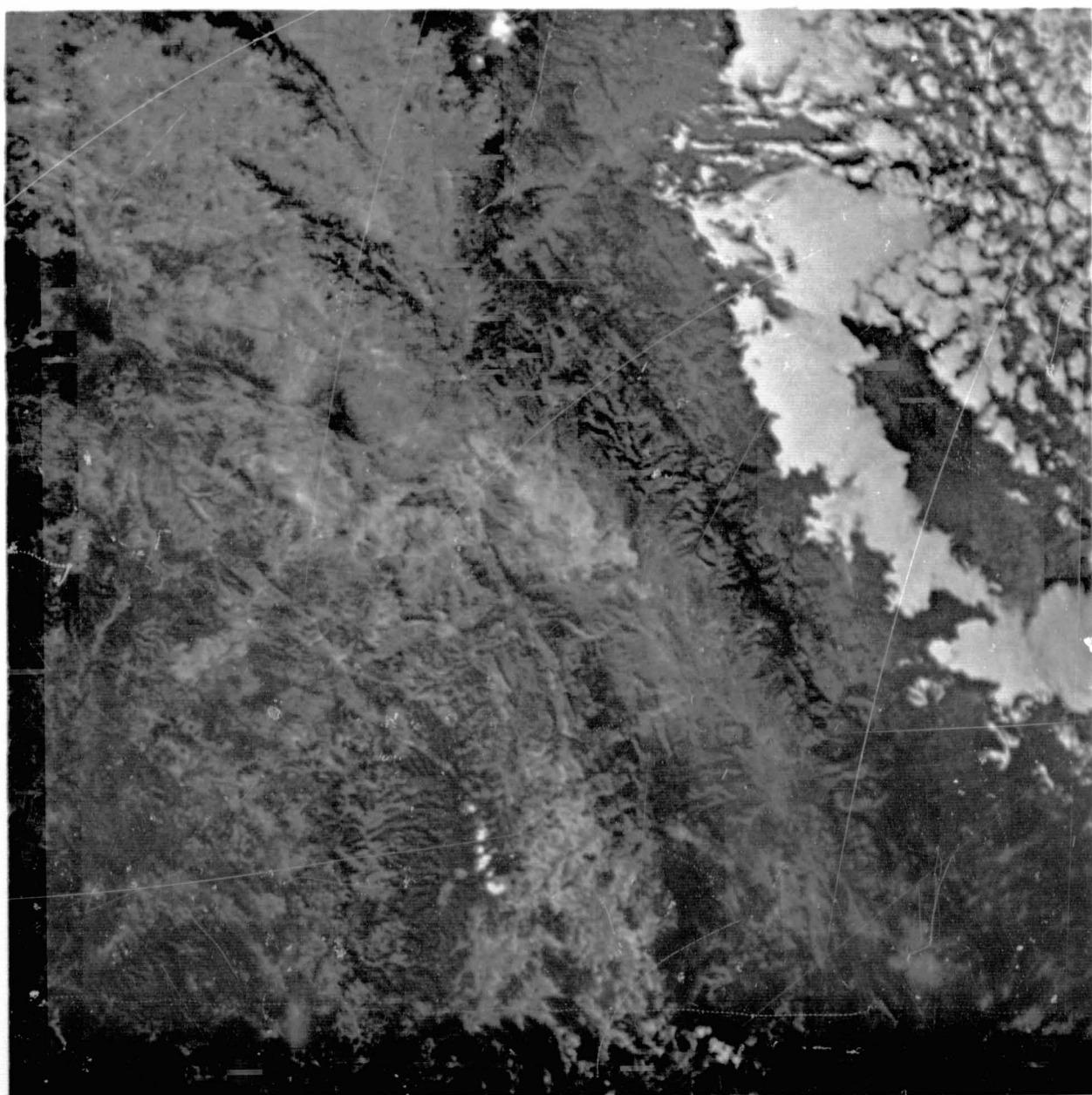


Figure 35-3.- A Gemini photograph of the Orizaba region of Mexico, upon which broad natural vegetation types can easily be distinguished. Positive identification of these types, however, would necessitate at least a limited use of a larger scale photography and/or on-the-ground sampling.



Figure 35-4.- A portion of the Bucks Lake Test Site was delineated on small-scale imagery, and crown closure and average crown diameter were measured in an attempt to determine the degree of relationship between these two parameters and timber volume, which was determined for each stand by means of conventional ground sampling techniques.

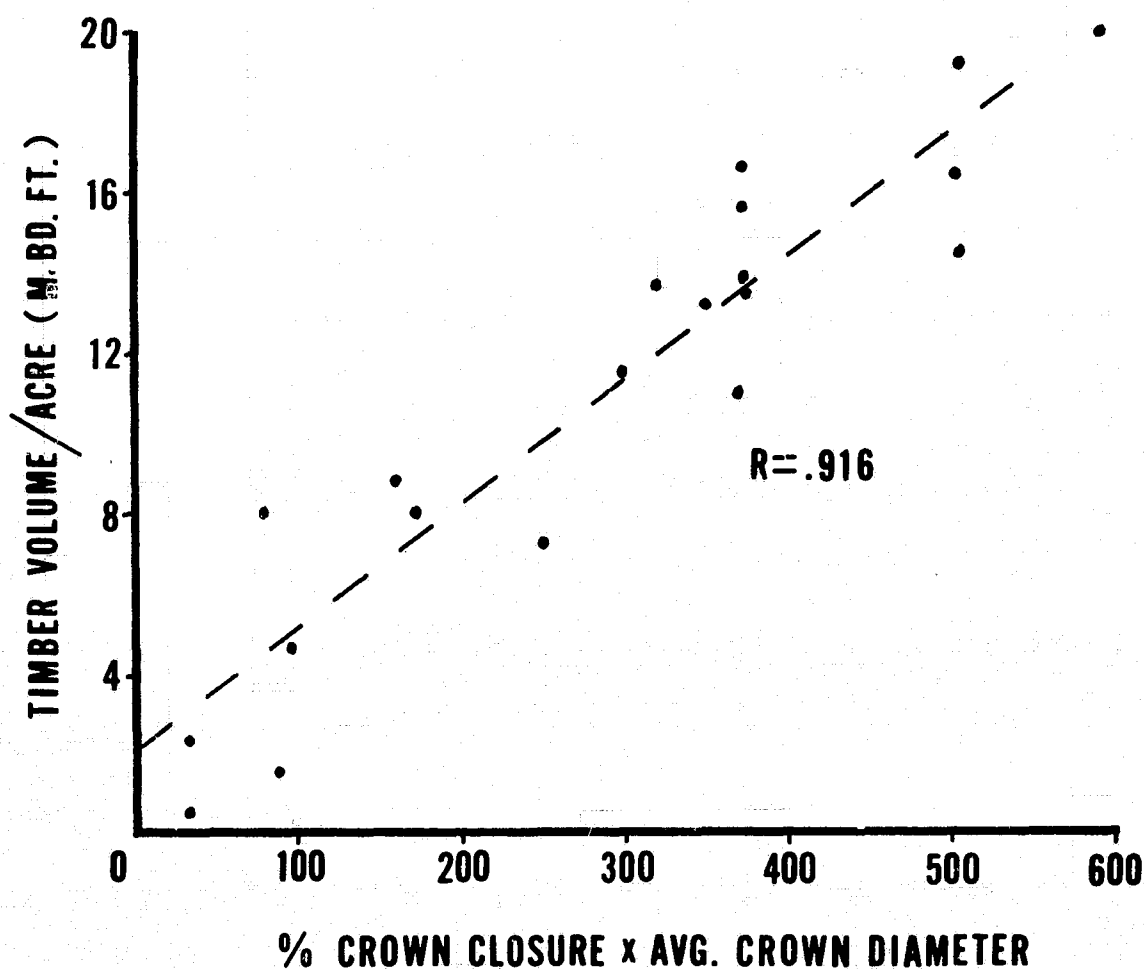
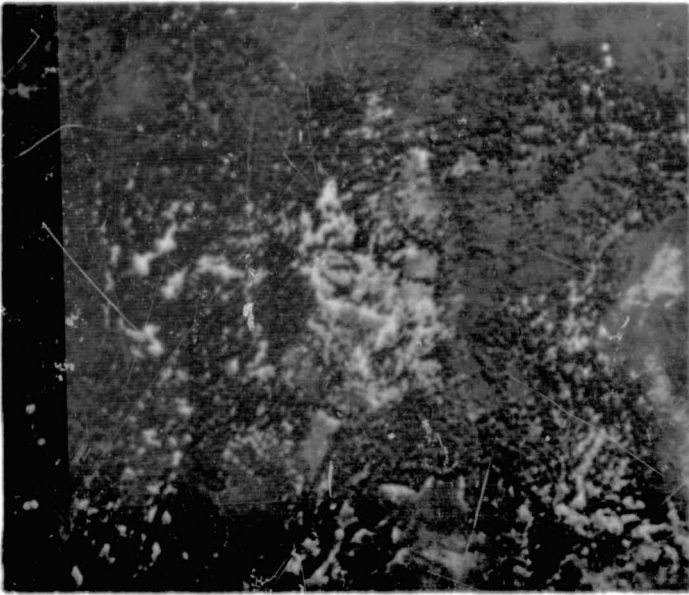
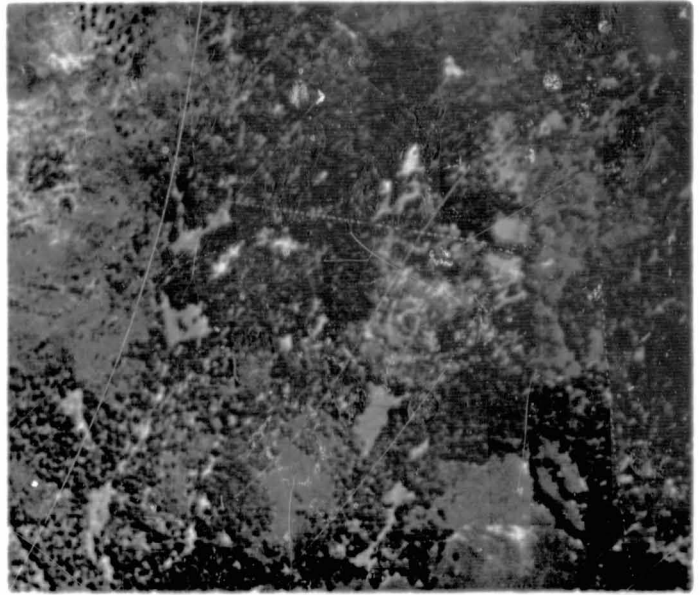


Figure 35-5.- The timber types in figure 35-4 were classified on the photographs in terms of crown closure of merchantable conifers and average crown diameter. The resulting graph indicates that it might well be possible to classify timber stands into gross volume classes on the basis of nonstereo image interpretation, although certainly more precise methods would be necessary if intensive management planning were undertaken.

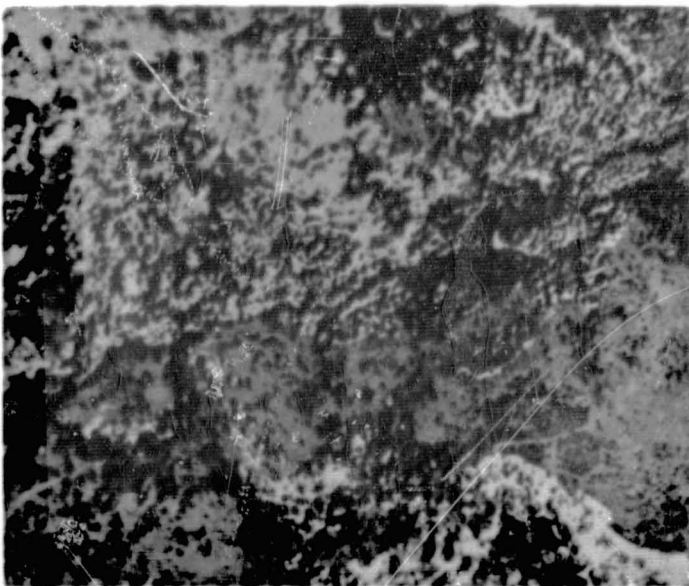
35-8



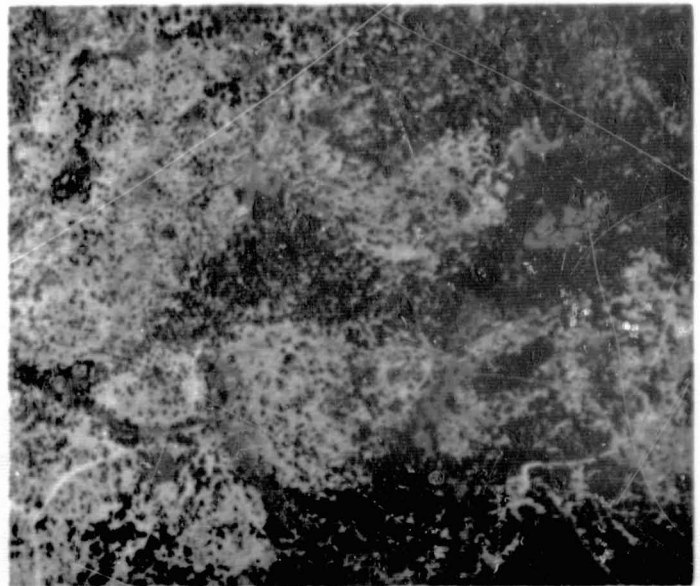
June 9, 1965
Snow clearly seen in open areas



June 11, 1966
Little snow remaining in open areas



June 9, 1965
Area nearly 50-percent snow covered



June 11, 1966
Same area devoid of snow

Figure 35-6.- Sequential small-scale imagery, as illustrated above, can serve as a valuable guide to hydrologists in their determinations of both surface and subsurface runoff that can be expected during a particular period. In addition, such imagery is valuable in the study of topographic and vegetation effects on snow retention and melt patterns, and may be of great help in planning management procedures designed to improve quantity and/or quality of runoff.

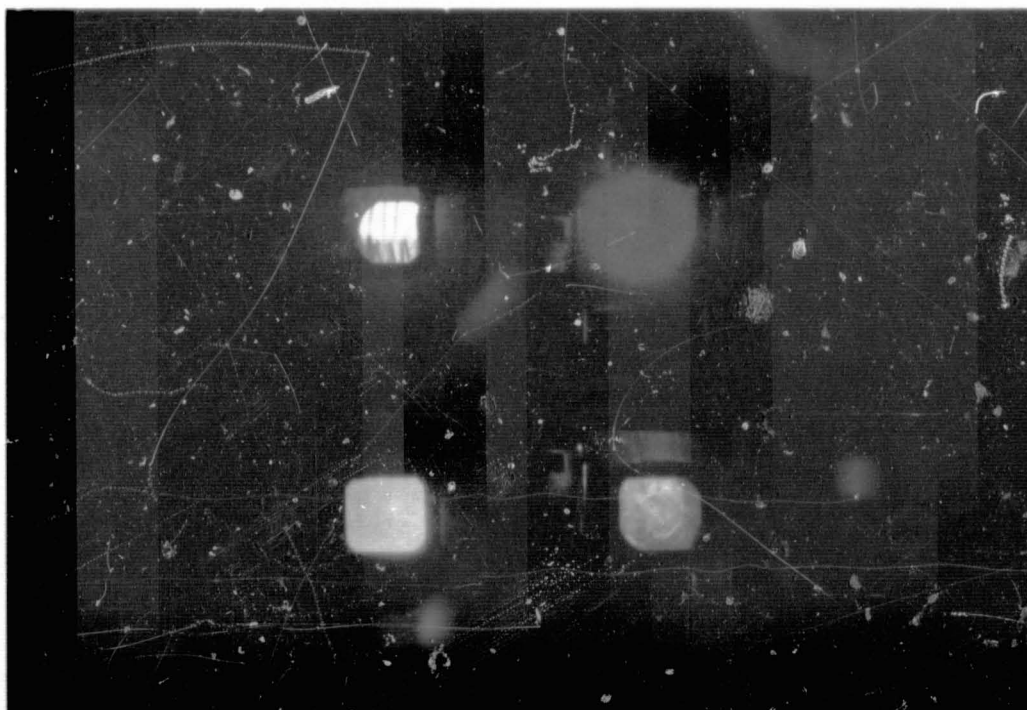
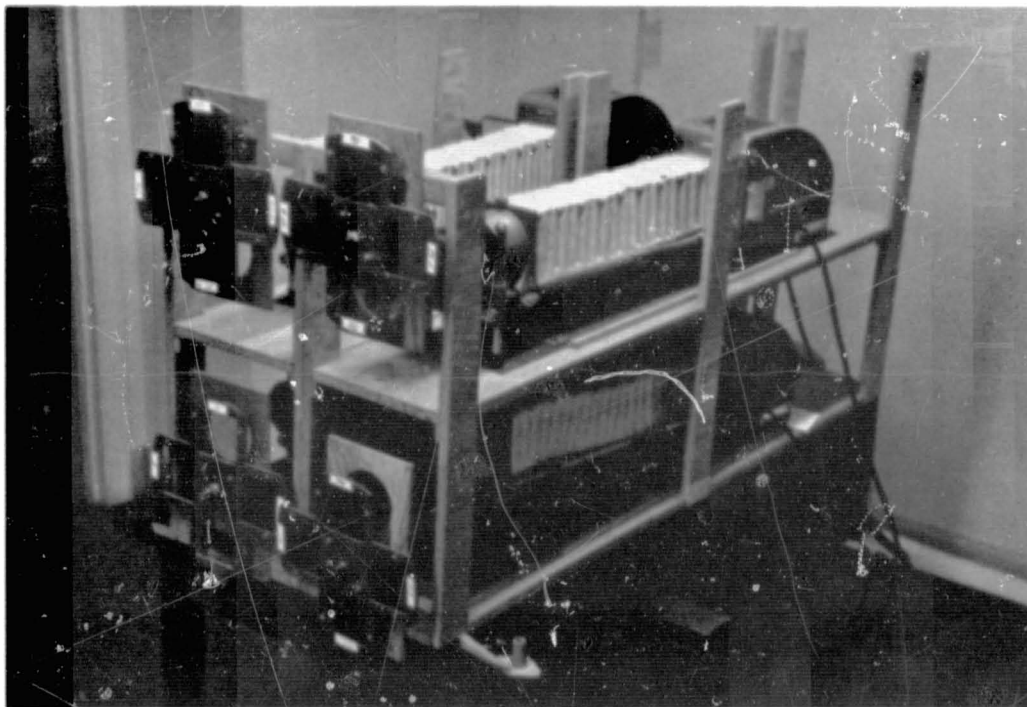


Figure 35-7.- These two photographs show the set of six projectors used to enhance multispectral black and white images. A lantern slide (3-1/4 by 4 inches) is made of each black and white negative, as taken in each particular spectral band. The projectors are then oriented to focus all images in common register on the translucent viewing screen. The composite color image thus formed is then photographed in color from behind the screen and reproduced in color print form as shown in figure 35-8.

35-10

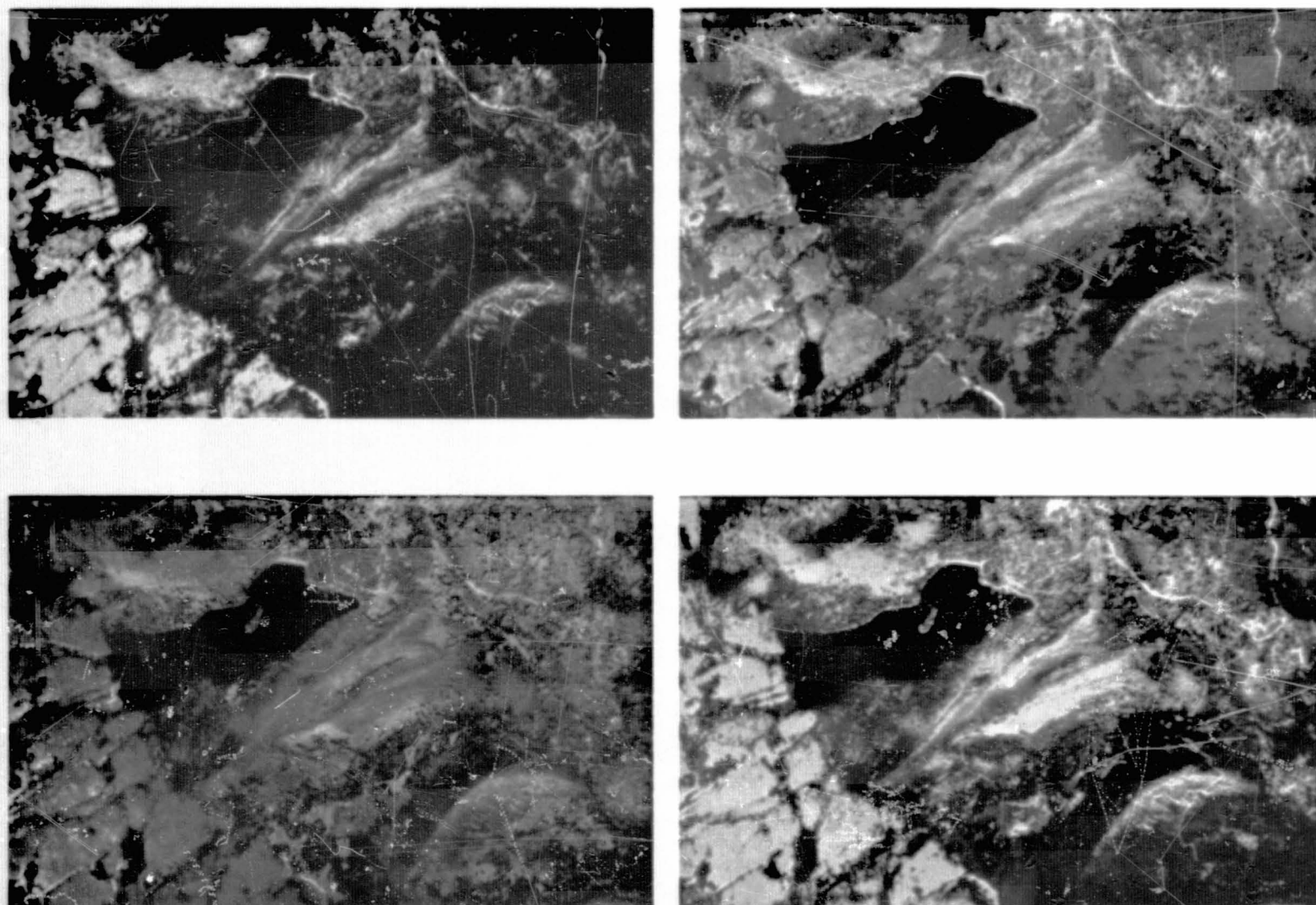


Figure 35-8.- Four color-enhanced multiband images as obtained using the equipment pictured in figure 35-7. Studies are underway to ascertain optimum spectral bands and color combinations for the discrimination of wild-land terrain features using such techniques.

N71-16158

36-1

DEVELOPING SPECTROSIGNATURE INDICATORS OF ROOT

DISEASE ON LARGE FOREST AREAS

By John F. Wear

Remote Sensing Project, Pacific Southwest Forest
and Range Experiment Station

INTRODUCTION

From an orbiting platform, earth resource analysts may be provided with valuable data on the incidence of diseases that seriously affect our valuable forest resources. The remote-sensing techniques that we are now testing, designing, and perfecting at nonorbital altitudes may be a part of the Earth Resources Survey Satellite Program in the not-too-distant future.

The remote-sensing research reported herein is concerned with inventorying and protecting the valuable resources of our forested lands. Forests are important to each of us for wood and timber products, for domestic and industrial water supplies, for wildlife habitat, for game and livestock forage, and for recreation. These values obviously should be protected from the depredations of fire, insects, and diseases.

Forest diseases create a greater destructive impact on our forest resources than either fire or insects. Forty-five percent of the growth loss in forested areas of the United States is attributable to diseases. Root-rot diseases account for an average annual loss of 300 million board feet of sawtimber. Of this total, approximately 170 million board feet of Douglas-fir timber in Oregon and Washington are destroyed or degraded each year by the continuing attacks and spread of Poria weirii root-rot disease. Figure 36-1 represents an infection center with mortality continuing to expand. Openings of this size range upwardly from 100 feet. Once the survey detection remote-sensing technique can be developed, I believe that orbital instruments can provide adequate imagery to assist the forest manager. Douglas fir represents 57 percent of the total sawtimber volume in the Pacific Northwest.

RESULTS ACQUIRED THROUGH THE USE OF DATA
FROM NASA AIRCRAFT

In an attempt to develop spectrosignature indicators of root disease on large forest areas, NASA aircraft are providing overflights of specific target areas for which ground-truth data have been collected. From a study of the photography thus obtained, efforts are being made to determine photographic image characteristics that are specific for forest areas in which the trees are becoming diseased.

Several remote-sensing flights have been made to the Pacific Northwest by NASA aircraft in an effort to secure imagery at nonorbiting elevations on several different test sites in various spectral zones of the electromagnetic spectrum. Problems of many types have been experienced which have precluded the satisfactory completion of a single overflight on test site 156. The first NASA flyby on August 15, 1967, was largely unsatisfactory because of mechanical problems with the equipment, improper film exposure, and inadequate photographic coverage. The second attempt on October 19, 1967, was fraught with adverse weather factors and inadequate coverage of the multispectral photography. Scheduling constraints were so precise as to miss good weather the day before and the day after the scheduled operating day for the NASA aircraft. The makeup flight in October on test site 156 provided good photographic imagery in the Ektachrome infrared (IR) band, but not in the 0.4μ to 0.9μ band with the nine-lens Itek camera system.

The thermal IR imagery from the Reconofax IV sensor does not appear to provide the thermal detail needed to differentiate between healthy and diseased trees. General information about geographical features, drainage patterns, and topographic characteristics are readily discernible on the thermal IR imagery, however.

NASA mission 78 with the NASA Electra P3A was flown during the last week in August 1968. Test site 156, pertaining to the Poria weirii root-rot problem in the Pacific Northwest, had ideal clear weather for all remote-sensing strips at the morning and noon sampling periods. The multispectral capabilities of the NASA Electra P3A that were utilized included two RC-8 aerial cameras (Ektachrome IR films), a four camera 70-millimeter Hasselblad pod (one IR and three panchromatic films), an RS-7 IR imager (8μ to 14μ band), and an IR radiometer (10μ to 12μ band). Imagery from this flight is still being processed, and no interpretation or analysis has been possible.

IMPROVED METHODS FOR THE ACQUISITION OF GROUND TRUTH

Ground survey methods to locate and appraise infection centers of Poria weirii root rot are inefficient. Forty days of effort by a two-man crew is required to obtain ground truth on a single section (640 acres) of timbered land. Present research seeks to develop more efficient survey methods for locating and evaluating the incidence of root-rot disease centers in forested areas by exploiting new remote-sensing techniques.

Before an orbiting satellite survey program for assessing root-rot infection centers in forest areas can be implemented, considerable basic research in applying remote-sensing techniques at lower flight altitudes is required. Judging from remote-sensing research conducted to date, trees infected with root rot do not show previsual symptoms that would normally discriminate them from healthy trees. Only in the most advanced stage of decline do infected trees exhibit slight changes in crown structure and foliage complement and color. Therefore, successful remote estimations of Douglas-fir characteristics will require testing of various sensors at several wavelengths. The physiological parameters of healthy and diseased trees (foliar temperature, soil-moisture tension and availability, solar energy input and output, transpiration rate, leaf moisture tension, spectral reflectance, and others) need to be evaluated for a comprehensive understanding of the problem. Remote-sensing research on this forestry problem indicates greatest success probability in three spectral zones of the electromagnetic spectrum: visible, reflectance IR, and thermal IR.

A spectrometric analysis of Douglas-fir foliage from the tops of healthy and infected trees was considered essential to ascertain the best film-filter combination for an aerial photographic survey of root disease impact over large forest areas. To collect many treetop foliage samples in a very short time for the spectrometric analysis, a special pole pruner was designed, and an efficient helicopter sampling procedure (fig. 36-2) was developed by the principal investigator. Foliage collections were made at three different periods corresponding to three different tree moisture conditions (i.e., those prevailing during overwintering, full new growth, and late summer hardening) to determine any significance in season of the year for discriminating healthy from diseased trees.

Six study plots of 15 trees each were selected for ground truth. Five trees in each plot were chosen in order to represent three different condition classes (healthy trees, diseased trees without visible symptoms, and diseased trees with symptoms). Each plot represented a different age class (young-growth, second-growth, and old-growth

Douglas fir). The universality of various survey techniques was investigated by location of the plots on two different growth site conditions.

Spectral reflectance curves from treetop foliage samples were derived from the General Electric (GE) spectrophotometer and programmed with four black and white photographic films and 23 Eastman filter curves for the SANTAD, IBM 7094 Fortran IV computer program. This program utilizes the relationships between the spectral characteristics of black and white films, filters, and targets to predict what film-filter combinations are likely to produce unique tone values for each target feature that is to be identified. The SANTAD program was specific for the panchromatic (0.4μ to 0.7μ) band and the black and white IR (0.7μ to 0.9μ) band. Results of this analysis showed that no film-filter combination is consistently applicable to all three moisture periods of the year. Analyses of the Ektachrome and Ektachrome IR films are yet to be completed on the SANTAD program. A NASA flyby on August 30, 1968, included some of the black and white film-filter combinations picked by the SANTAD program with good probabilities for separating healthy from diseased trees.

RELATED STUDIES

Tree vigor and availability of moisture in the tree crown for transpiration are two important factors governing the temperature of a tree. A tree of declining vigor caused by drought, partial destruction of root systems, or inability to absorb and transport moisture through roots and stem to the tree crown frequently shows changes in physiological characteristics. Trees under severe moisture stress may not be able to transpire as readily and stay as cool as healthy trees. Tree physiological research is needed for forest types in the Pacific Northwest. A preliminary physiological study of Douglas fir is now underway in the Poria weirii study to ascertain the reasons for differences in tree temperatures between healthy and diseased trees and between different age classes.

Energy emitted from tree crowns in the thermal IR part of the spectrum can be collected through either imaging or nonimaging IR radiometers. The airborne radiometers can be calibrated for a specific portion of the spectrum (2μ to 5μ band, 8μ to 14μ band, etc.). Data derived from the Barnes Engineering PRT-4 and PRT-5 nonimaging radiometers have indicated significant temperature differences between healthy and diseased trees at certain times of the day.

Radiometer readings were taken from a semihovering helicopter orbiting around individual trees at about 150 feet above the forest canopy. Sightings are concentrated within the upper 30 percent of the

tree crown but more than 10 feet down from the tree top (fig. 36-3). This technique minimizes the chance of including spurious temperature readings from other trees or openings. Output readings of the PRT-5 are in terms of irradiance or equivalent black-body temperatures. To improve the ease of recording data, a Cole-Parmer chart recorder was collated with the PRT-5. The self-contained power sources for each unit and relatively light weight provide good portability and operational flexibility for use on the ground or in the air. PRT-5 sampling is an active aerial tool for collecting ground truth yet is a bridge between ground truth and potential satellite capabilities.

Prior to the NASA flyby, an 8- by 36-foot resolution target was constructed and installed on the line 1, Wind River Test Site to determine the spatial resolution of the various sensors assigned to the test site 156 program. Evaluation of the imagery at the resolution target would help to clarify the need for particular sensors and for modifying subsequent technical procedures for NASA flights (film, filters, scales, etc.) to procure the desired measurements.

Ground-truth data were collected during the overflight period with measurements of some physiological parameters between healthy and diseased trees (leaf moisture tension, xylem moisture flow, and various temperature readings). During the same period, a new remote-sensing technique designed by the principal investigator was tried for the first time. The Barnes Engineering PRT-5 IR radiometer was collated with an instant-replay video-scan tape-recording system for remote-sensing operations from a helicopter or fixed-wing aircraft (fig. 36-4). This new system provides an accurate vertical picture of the natural vegetation and geographical features as recorded by a standard closed-circuit television camera. Superimposed on the center of the picture is a circle that covers the 2° scan area of the PRT-5 radiometer. Also superimposed on the video scan is the continuous projection of electronic response from the PRT-5. (A second video camera transfers the digital voltmeter read-out from the PRT-5 through a multichannel mixer to the tape recorder. This read-out appears on the right side of the video picture). A good-quality television monitor and a tape recorder that has stop action are needed to study individual frames in depth. Details needed for field checking and ground-truth elevations may be transferred from the television monitor to good-quality aerial photography without difficulty (fig. 36-5). I believe that this remote-sensing technique will have unique advantages over magnetic or chart tape-recording systems whenever high-quality thermal ground-truth data are needed.

SUMMARY AND CONCLUSIONS

Losses to forest diseases are more serious threats to the forest natural resource than either fire or insects. It is, therefore, of continuing importance to develop remote-sensing techniques that will collect data rapidly on pest problems from aircraft and orbiting platforms. Expanded research on the spectral emission and the spectral reflectance properties of specific forest types and on the physiological parameters of healthy and root-rot-infected trees are of great potential value in analyzing this serious forestry problem. I believe that our space-science technology will keep pace with our needs for higher quality resolution to detect incipient stages of disease activity. Considerable progress has been made in the development of remote-sensing techniques for efficient disease-detection surveys that may eventually become an integral part of resource surveys from orbital altitudes.

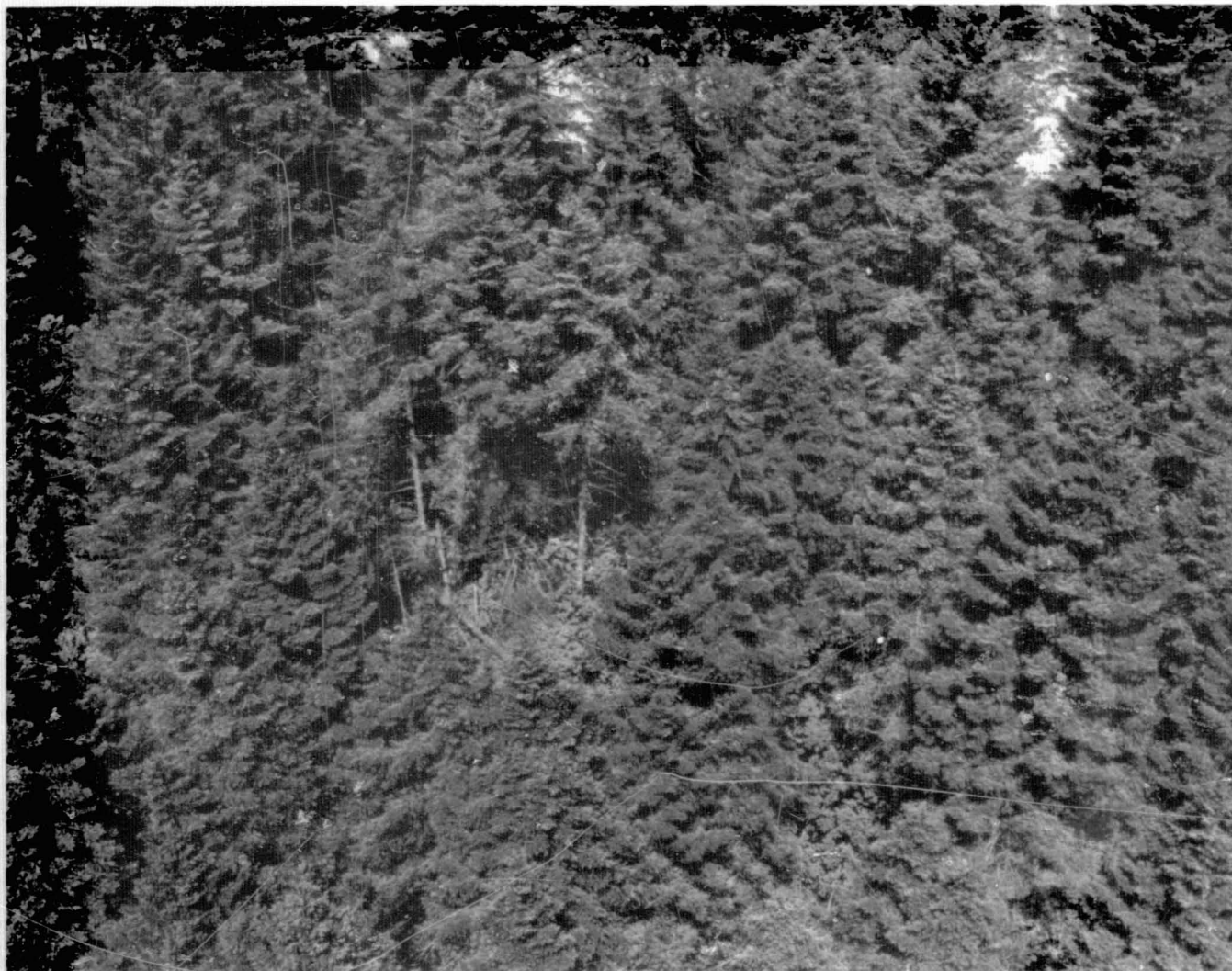


Figure 36-1.- Dense stand of Douglas fir in the center of which an area infested with the fungus Poria weirii can be discerned. Present NASA-financed studies seek to determine optimum image specifications for the early detection of such infection centers so that control measures can be effected promptly.



36-8

Figure 36-2.- A special pole pruner, when operated from a hovering helicopter as shown here, permits the efficient collection of treetop foliage samples from which to make spectrometric analysis as described in the text.



Figure 36-3.- Operation of a PRT-5 radiometer from a hovering helicopter, as shown here, permits the investigator to determine how much energy is being emitted from the upper 30 percent of a tree crown. By comparing such energy returns from healthy and diseased trees, possibilities for differentiating them on thermal IR imagery are being investigated. Streamers flung into the tree crowns facilitate identification of selected trees on aerial photography flown of the test site by NASA aircraft.

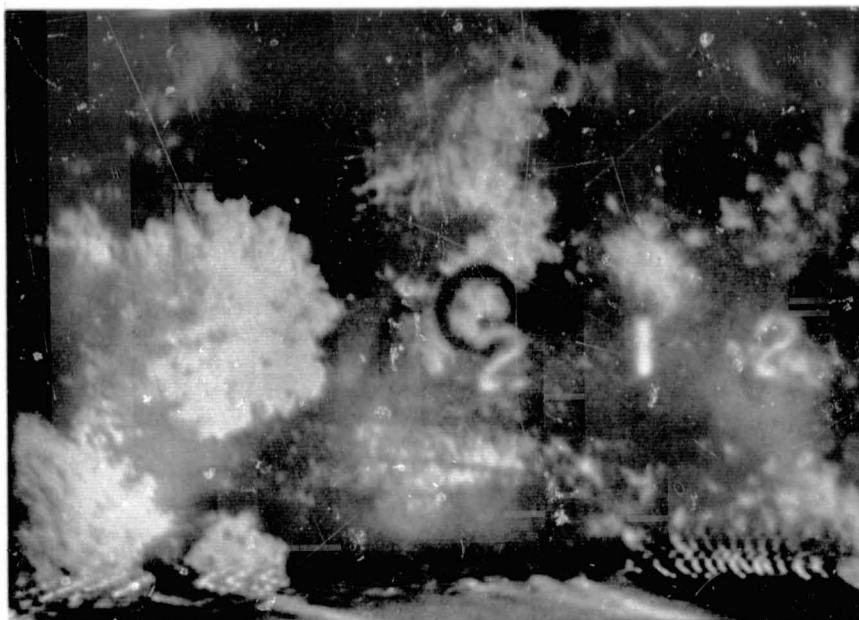


Figure 36-4.- Photograph of a single frame of the tape recording from the Ampex 7500. Black circle represents area covered by the 2° scan of the PRT-5. Digital read-out is the electronic output of the PRT-5, transferred through the number 2 vidicon camera to the tape recorder. Tree temperature is indicated electronically and is converted to degrees Celsius or Fahrenheit.



Figure 36-5.- This new remote-sensing technique incorporates a nonimaging IR radiometer with an instant-replay video-scan tape-recording system that can be used either in a helicopter or fixed-wing aircraft. (a) Number 1 vidicon camera and PRT-5 radiometer boresighted for vertical coverage. (b) Polyurethane block cushions number 1 vidicon camera and PRT-5 from helicopter vibration. (c) Enclosed box has number 2 vidicon camera that takes a video picture of Hickok voltmeter. Picture is transferred electronically to video tape. (d) Concord electronic integrating mixer that cross references input from the two vidicon cameras to the Ampex 7500 recorder. (e) Barnes Engineering PRT-5 nonimaging radiometer in the 8μ to 14μ band. (f) Ampex 7500 tape-recorder uses 110 volts from a Topaz converter (not visible in this picture) to give 60 minutes of tape scan. (g) Nine-inch TV monitor for pilot and observer orientation.

N71-16159

DETECTION OF FOREST INSECT OUTBREAKS BY REMOTE SENSING

By R. C. Heller
Forest Service, U.S. Department of Agriculture
Berkeley, California

ABSTRACT

Studies are underway in the Black Hills of South Dakota to determine the ground instrumentation, aerial sensing equipment, and techniques required to detect vigor loss and previsual signs of tree mortality caused by bark beetles in coniferous timber stands.

Ground data have been collected on spectral reflectance, Munsell color notations, emitted and absolute temperature, transpiration, and needle moisture tension of ponderosa pine trees and foliage.

Aerial photography (color and infrared color) was taken over six ground-instrumented test sites at seven periods (October 1966; May, June, July, and August 1967; and May and August 1968) to capture changes in foliage coloration. Optical-mechanical scanning imagery was obtained in three wavebands (2.0 μ to 2.6 μ , 4.5 μ to 5.5 μ , and 8.0 μ to 14.0 μ) in October 1966, June 1967, and May 1968.

To date, no aerial sensor has been successful in detecting stressed conifers before the foliage discolors. No differences in photointerpretation accuracies have been found between color and false-color films. However, in May, interpreters viewing color transparencies were able to pick out three times as many dying trees as ground observers. Interpreters were 70 percent successful in detecting insect infestation on color films at scales as small as 1:116 000 when the infestation was over 100 feet in size.

By mid-June, foliage temperatures of known dying trees were 6° to 8° C higher than healthy trees at 10:00 hours; the difference was slightly less at 14:00 hours (4° to 6° C). Tree crowns within the forest canopy, whether healthy or dying, were difficult to resolve on thermal imagery. Individual trees growing in the open and casting strong shadows were distinguishable. Scanners with better optical qualities exhibiting improved spatial and thermal resolution are needed before thermal techniques can be used with any degree of confidence.

A General Aniline and Film Corporation microdensitometer was used to analyze field-resolution targets and known dying trees on the thermal imagery. A beginning was made to relate film density to object temperature.

INTRODUCTION

Forests around the world have provided mankind with a wealth of wood products needed in modern civilization. This need is expected to increase, and a shortage of raw materials is expected to develop because of future rapid increases in world population. United Nations demographers estimate that the world population will double every 35 years from 1960. While trees are a renewable natural resource, we shall have to grow them faster, manage what we have more judiciously, and prevent the tremendous losses from epizootics to supply the expected need.

Insects and diseases, in the United States alone, account for a timber loss equal to our annual growth and exceeding the losses from fire by seven times (ref. 37-1). From 1963 to 1965, 40 percent of the pine resource in Honduras, Central America, was lost to an epidemic of southern pine beetle. Similar catastrophes can occur in other developing countries and have occurred even in the more technically advanced ones.

Some rapid method of detecting tree stress or loss of vigor, before visible symptoms occur, is badly needed so that abnormalities in the forest can be pinpointed at an early stage. Thus, forest managers can direct their control action to those locations requiring sanitation cutting, presalvage cutting, or other treatment and thereby reduce the timber loss. Ground survey detection techniques are too slow and costly — and often discover the abnormality after it has grown to an uncontrollable epidemic. Some combination of aerial and ground detection methods must be worked out, and this has a high priority on the forest manager's list of needs. If an airborne technique proves feasible, the next step upward — a space-vehicle platform — may provide the extensive and repetitive coverage needed for the detection of dynamic biological populations, provided that suitable image-resolution capabilities can be attained by spacecraft.

The specific research objective is to learn which portions of the electromagnetic spectrum will differentiate dying from healthy pine trees. Problems to be solved are optimum altitudes for sensing, detectability of stressed trees with various film-filter combinations and electronic scanners, and development of sensitive ground instrumentation.

In August 1968, we tested very small-scale aerial photography (1:116 000) to learn the smallest scale that might be tolerated for use

in making forest management decisions during forest insect epidemics. The implications for space resource photography are quite apparent after viewing the color photographs.

LOCATION OF STUDY AREA

A serious epidemic of the Black Hills beetle (Dendroctonus ponderosae, Hopk.) occurred in the Black Hills National Forest from 1960 to 1965. In areas where no control efforts were exerted, remnant beetle populations from the outbreak were continuing to kill trees in large numbers. The Lead-Deadwood exemption area near Rapid City, South Dakota (fig. 37-1), was an ideal study area. Here, groups of several hundred trees were infested annually, whole hillsides of timber were destroyed, and the total infestation ran to many thousands of trees killed each year (fig. 37-2).

The Black Hills are located in western South Dakota and eastern Wyoming. The hills rise to 7250 feet from the surrounding flat to rolling plains which have an elevation of about 3500 feet. Ponderosa pine is the principal commercial tree, and it occurs primarily above 4000 feet. The total sawtimber volume in the Black Hills is estimated to be 2.3 billion board feet.

METHODS

Biological observations which involve ecological, physiological, and meteorological interactions must be made over a time continuum. Since our objective is to detect loss of tree vigor before visual symptoms occur, we are interested in the rate at which changes take place. To capture these changes, measurements were taken of beetle populations, infested trees, foliage color, foliage internal temperatures, needle moisture tensions, transpiration, solar radiation, soil moisture, air temperature, humidity, and wind velocity.

Most of these data are needed to compute the total energy budget which affects tree growth. For example, the data permit one to explain why trees under moisture stress may produce higher temperatures under similar sunlight conditions than when the same trees are under no moisture stress earlier in the day. Similarly, one can then hypothesize why thermal imagery may differentiate less vigorous trees from healthy ones in one time period and not in another.

These kinds of data were taken over a 3-year period beginning in August 1965 and continuing through October 1968. Much of the ground

2

information was obtained continuously during the tree growing season. The aerial imagery was collected intermittently, primarily during the spring and summer months.

GROUND PROCEDURES

Establishment of Attractant Test Sites

From previous work, McCambridge found that by placing laboratory-reared beetles in screen cages on host trees (fig. 37-3) during the period of active beetle emergence in the summer, he could induce wild beetle populations to attack the tree with the caged beetles, as well as many surrounding trees. In August of each year, attractant test sites were established in this manner within the study area to allow for possible failures and to provide for replication in the experiment.

Establishment of Pilot Study Area

In mid-August 1968, a beetle-infested area about 1 by 3 square miles was chosen to represent rising epidemic conditions over a large area. It included infestation centers (or spots) ranging in size from one to 249 dying pine trees. We want to know at what scale photointerpreters can determine when endemic conditions become epidemic. Entomologists consider that an epidemic is underway when pine trees begin to die in infestation centers of one to five trees. We can also learn what minimum size area can be detected at each scale and extrapolate what size infestation might be detected from space photographs.

We used existing 9- by 9-inch aerial photographs on which infestations had been plotted the previous day by aerial observers to help us find the infestations on the ground. By using stereographic coverage to facilitate ground navigation, we were able to reduce the ground work considerably over a conventional ground cruise. About 100 spots were checked on the ground by six men to determine the number of killed and discolored trees in each infestation center. Thus, we collected the ground truth to compare later with the results of the photointerpretation.

At each infestation, we counted the number of discolored trees, estimated their bole diameter, and measured the area that their projected crowns occupied. We also verified the location of the infestation on the existing aerial photograph. Infestations (mostly single trees) not plotted by the aerial observers were occasionally found on the ground in the course of walking to one of the aerial-plotted spots. These trees were also counted and plotted on the photographs.

Visual Determination of Tree Decline

Once a tree is attacked by beetles, the success or failure of the attack may be in doubt to the observer — even when close ground examination is continued. One manifestation of heavy attack is the presence of pitch tubes on the outer bark. Another is boring dust — like fine sawdust — caused by the attacking beetles when boring in the cambial zone. This dust lodges in bark crevices near the ground and must be searched for very carefully. The surest method of determining whether the attack is successful and the tree will succumb is the observation of the presence of blue stain fungus (Ceratostomella spp.) in the xylem. This fungus is carried into the cambial galleries on the legs and body of the beetle and is an accelerating agent in the death of the tree. On the ground, the presence of blue stain is discovered by making small hacks into the wood with an axe. The amount of time required to kill a tree and the likelihood that a given attacked tree will succumb are both uncertain; therefore, intensive ground examinations are required for accurate appraisal. The detection of small changes in tree vigor, even on the ground, is most difficult.

In October, the locations of all infested trees surrounding each attractant tree were accurately plotted by plane table (fig. 37-4). Each tree was numbered with plastic tape for later identification.

The rate of foliage discoloration was followed in two ways: (1) by taking 35-millimeter ground color photographs of 10 selected dying trees at weekly intervals from May 1 to August 30 and (2) by having one person who had full color perception take Munsell notations of all 209 infested and 47 healthy trees on four occasions — May, June, July, and August. Tree colors were identified by the Munsell color notation system as described by Nickerson (ref. 37-2). In the field, one experienced observer compared the color of foliage of the upper tree crown in full sunlight with a series of Munsell color cards also held in sunlight. The color chips were mounted hue cards with holes punched between the chips to facilitate comparison. The foliage is viewed through the punched holes; thus, the foliage and color chip are adjacent, and the eye can readily compare them. Similar vegetation studies using Munsell notations have been conducted by Nickerson (ref. 37-3) to discriminate between grades of cotton and by Heller, et al. (ref. 37-4), to identify northern tree species. By relying on one observer, we reduced some of the subjective bias and permitted quantification of the color attributes. Furthermore, we hoped to compare the ground observer's Munsell notations with the 10 trees photographed on the ground and with the same trees photographed from the air.

Intensive Study of Healthy and Infested Trees

Spectrophotometric measurements.- The Metrology Division of the National Bureau of Standards, U.S. Department of Commerce, Washington, D.C., very kindly processed replicated samples of ponderosa pine foliage through their reflectance spectrophotometers (fig. 37-5). These included the General Electric (0.40μ to 1.08μ), the Cary Model 14 (0.60μ to 2.50μ), and the Cary White Model 90 (2.5μ to 22.22μ). Additional foliage samples have been taken each year for corroborating evidence and processed through a Beckman DK-2 recording spectrophotometer (0.35μ to 2.70μ).

Needle temperature measurements.- From the beginning of this study, we believed that one of the important factors in the detection of a dying tree would be the identification and measurement of changing patterns of heat transfer. We needed to know how these heat patterns differed between healthy and attacked trees and also how they differed by time of day and by solar conditions.

The needle temperatures were obtained by inserting copper-constantan thermocouples, approximately 2.5 millimeters long and sharpened to a point, into living cell tissue of individual needles. These thermocouples were placed inside needles at three random locations within the upper crown of 18 healthy and 18 insect-infested trees. Wires joined the thermocouples to a recording station on the ground, and temperatures from the remote thermistors were recorded on a Brown Electronic Model 153 by 60 P16 multipoint recorder (fig. 37-6a). Power to run the recorder was supplied from a 1500-watt portable generator wired to a remote starting mechanism actuated by a preprogrammed timer. This setup permitted continuous recording of needle temperatures at preset intervals during the day and night.

Apparent temperature measurements.- Apparent or emitted temperatures were measured with a Stoll-Hardy infrared (IR) radiometer of the type reported by Stoll (ref. 37-5), manufactured by the Williamson Development Company. The radiometer was fitted with an IR filter which cut out all shortwave radiation below 3.5μ . This effectively eliminated most of the energy of reflected sunlight from the surface of the sample needles. A Barnes PRT-5 and PRT-10 were also used for apparent temperature measurement (fig. 37-7a).

Field use of the radiometer was adapted from suggestions made by David M. Gates. The radiometer was carried and used directly in the tree crowns (fig. 37-7b), where it was found that a great many observations could be made in a short period of time. Radiant temperature measurements were made several times each day on each of the 36 study trees (18 healthy and 18 stressed). The radiometer readings were intended to provide a basis for the interpretation of the airborne thermal imagery of the same study site. These data might also help to explain the ability

or inability to detect changes in the thermal patterns of a dying tree from the airborne thermal detector.

Relative transpiration measurements.- To help explain thermal differences that may exist in pine foliage, it is necessary to consider all factors (and their interactions) which could contribute to temperature differences between the foliage of healthy and dying trees. These factors include absolute leaf temperature, emitted leaf temperature, ambient air temperature, wind velocity, and finally relative transpiration rates.

We decided on the basis of Weber's study in Michigan (ref. 37-6) that sap movement could be measured with a specially constructed sap flow detector. This instrument is designed to measure the rate of sap flow by timing the rate of movement of a heat pulse from one point to another in a tree. Basically, the instrument consists of two miniature heat-sensing thermistors which are inserted vertically into the xylem 1.5 centimeters apart, a 6-volt resistance-type heat probe which is inserted into the xylem 0.5 centimeter below the upper thermistor probe, an indicating meter, and a stop watch.

The rate of heat dissipation is a measure of velocity of sap flow and must be calculated from formulas derived by Marshall (ref. 37-7). Heat-pulse velocity is in turn used to calculate sap flux, which finally permits us to compare transpiration rates between trees. Increment cores were removed from the healthy and from the stressed trees so that oven-dry weight, green volume, and water content could be determined and used in the previous formulas.

A portable microvoltmeter, Medistor Model A 60-C (fig. 37-6b), was incorporated into the system. Its sensitivity permitted sap-flow readings near the ground instead of within the top 10 feet of the crown as was done in Michigan.

Wind velocity measurements.- Some quantitative measure of wind velocity is necessary so that a relationship can be established between needle temperature and heat flow into and out of the tree. Wind movement above 15 miles per hour causes stomata along the needles to close but permits the individual needles to act as fins on a radiator, thus speeding heat dissipation. Although the regulation of leaf temperatures is somewhat complex, thermal emission in direct sunlight is always affected by changes in the wind velocity. Therefore, recordings of wind velocity are useful in explaining the ability or inability of an airborne sensor to discriminate between temperature differences in stressed and healthy trees. An instrument tower was erected on the test site (fig. 37-8a), and the velocity transmitter inputs were wired to a 20-pen Esterline-Angus strip-chart event recorder (fig. 37-6a).

Soil-moisture and temperature measurements.- Soil-moisture data are needed to determine availability of water to the roots throughout the growing season to correlate with transpiration and sap movement.

At the beginning of the growing season in April 1967 and immediately following snowmelt, two soil pits were dug near the sample trees. The soil horizons were mapped, and soil moisture and temperature probes were inserted at each horizon and the leads brought to a terminal box at the surface. Soil samples were collected and their field weights carefully determined. The soil pit was then refilled. Thereafter, measurements of soil moisture and temperature were taken each day with a Colman Soil Moisture Meter (fig. 37-8b). Physical and organic characteristics of the soil samples will be determined in the soils laboratory.

Solar radiation measurements.- A recording pyrliograph, which measures solar radiation (fig. 37-9a), was installed on the top of the instrument tower described previously. Data from the pyrliometer can be tied in directly with the timing of the thermal scanner flights to show the total solar radiation to which the sample trees were exposed prior to and during the flights.

Needle moisture tension.- Needle moisture tension is one additional parameter measured in 1967 that may help to determine early vigor loss. The technique was first reported by Dixon (ref. 37-8), and the apparatus was improved and described by Scholander (ref. 37-9). Very briefly, the method is as follows: the twig end of a freshly cut foliage sample (about 4 inches long) is inserted through a rubber O-ring which is fitted into the top side of a pressurized container (fig. 37-9b). The proximal end of the twig is exposed to atmospheric pressure. The needle portion of the sample is then placed inside the bottom part of the container, and the two parts are screwed together. Nitrogen gas is introduced slowly to the container until free water begins to bubble from the tracheid cells in the cut end of the twig (observed with a hand lens). Normal foliage required less pressure to force out the water than foliage from stressed trees. The absolute pressure values — but not comparative values — are affected by time of day, season, soil moisture availability, and sunlight conditions.

Moisture stress apparently causes anatomical changes in conifer foliage that influence the reflection of solar radiation from the tree canopy. We tried to study what cellular changes occur in the needles as a tree begins to die. After dehydration and paraffin embedding, longitudinal and cross sections of healthy and stressed (1966 attacked trees) needles were sectioned with a rotary microtome. A series of color slides was made from 15 μ -thick sections which were stained with complementary dyes — safranin to highlight primary tissues and fast green for secondary tissues. Examples of cellular differences are shown in figure 37-10.

Estimation of Beetle Population

Do the development and number of insects under the bark of the infested tree affect the rate of tree foliage discoloration? Two 6- by 6-inch bark samples were collected in both May and July from each of 30 infested trees (15 discolored and 15 green — from the north and south sides of each tree) to test the hypothesis that no difference existed in insect activity between trees fading early in the season and those fading late in the season. The 30 trees were chosen at random from three of the six attractant test sites — 10 trees at each test site. Each 6- by 6-inch bark sample was examined for the original number of attacking beetles, the length in inches of galleries mined out by them in the cambium layer, and the number of surviving insects.

Preparation of Ground Resolution Target

A ground resolution target measuring 8 by 68 feet was constructed in October 1966 to determine spatial and thermal resolution capabilities of the HRB Singer Reconofax XI and Texas Instruments RS-7 optical-mechanical scanners. Twenty-seven fiberboard panels, each 4 by 8 feet, were covered with 2-mil aluminum foil; the foil was pasted to the smooth side of the panels with wallpaper paste. Half of the panels in widths of 2, 4, and 8 feet were painted with 3M black velvet paint; the remaining panels were left aluminum. They were then laid out in alternating black and aluminum array (fig. 37-11).

This target array was designed to test whether the airborne scanners had a 1-, 2-, or 3-milliradian resolution capability. For example, if the 2- by 8-foot panels were distinguishable on the imagery when the aircraft altitude was 2000 feet above ground, resolution would be 1 milliradian.

The temperatures of the black and aluminum surfaces, plus the temperatures of the grass and bare soil around the target, were recorded with a Barnes PRT-5 and PRT-10 radiometer during all thermal flight runs. Aluminum surfaces actually reflect the cold daylight sky temperatures.

AERIAL PROCEDURE

Aerial Photography

Most aerial photographic studies conducted in the past were directed toward learning what film-filter-scale combination would be optimum for locating and accurately mapping discolored coniferous trees. Color

films (both natural and false color) have been generally more useful than panchromatic or IR emulsions. Medium scales from 1:5000 to 1:8000 have provided acceptable photographic interpretation accuracies when applied over large areas and when used with appropriate correction (regression) factors. However, certain limitations have been recognized in using these scales; namely, individual fading trees are difficult to detect, and with the film emulsions currently available no early indications of mortality have been discernible.

In this study we wanted to explore the largest possible scales of photography so that we could learn the earliest time at which loss of vigor could be detected from the air for individual trees. Also, we were interested to learn what minimum scale would detect small groups (three trees or less) of discolored pine trees.

Two film types were used: Anscochrome D/200 and Kodak Aero Ektachrome IR. All attractant test sites were photographed with the color films (natural and false color) in October 1966, and in May, June, July, and August 1967 at a scale of 1:1584.

Attempts to simulate near-space photography by using a short focal-length lens (1-1/2 inches) at medium altitudes — 22 000 feet above sea level — were made in October 1966, in May, June, and July 1967, and in August 1968. A total of five scales were taken, ranging from 1:116 000 to 1:7920.

Since the sizes of the targets (attractant test sites) were generally less than 1 acre in size, small format, high-speed-shutter cameras were used. All aerial photography was taken with two 70-millimeter Maurer KB-8A cameras equipped with 150-millimeter Schneider Xenotar or 38-millimeter Biogon lenses. The two cameras, impulsed simultaneously by an Abrams CP-3 intervalometer, gave identical photographic coverage on the two film types. This eliminated photographic variables associated with time of day (shadow length, shadow direction, and crown illumination) on the two films and allowed a more valid comparison to be made. Photography was performed from a Forest Service-owned Aero Commander 500B airplane flying at 100 miles per hour to obtain 60 percent overlap for stereoscopic coverage. Shutter speeds were 1/1000 of a second or faster to reduce image motion.

All films were processed in a darkroom made available by the Black Hills National Forest in Spearfish, South Dakota. All aerial photography was 70 millimeters in size and was processed in Nikor equipment. This procedure permitted us to examine the films within a few hours after exposing them and to make reflights while we were in the area, if coverage or exposure was inadequate.

Optical-Mechanical Scanning Imagery

Sensing beyond the visible spectrum (0.7μ) and beyond the capabilities of IR films (0.9μ) was done at three time periods and with three different scanners.

Date	Aircraft type	Scanner	Number of flight runs by wavelength			
			Unfiltered, 0.6μ to 7.0μ	2.0μ to 2.6μ	4.5μ to 5.5μ	8.0μ to 14.0μ
10/3/66	Convair (T-29)	Texas Instr. RS-7	--	4	4	4
6/16/67	Aero Comm. 500B	HRB Sing- er Re- conofax XI	7	6	5	--
6/16/67	Convair (T-29)	Texas Instr. RS-7	--	4	--	13
6/17/67	Aero Comm. 500B	HRB Sing- er Re- conofax XI	11	19	9	--
6/17/67	Convair (T-29)	Texas Instr. RS-7	2	2	--	6
6/18/67	Aero Comm. 500B	HRB Sing- er Re- conofax XI	2	11	9	--
5/29/68	C-47	17-channel multispec- tral	--	19	--	--
5/30/68	C-47	17-channel multispec- tral	--	7	--	--

The Convair (T-29) airplane, equipment, and research personnel were made available by the Northern Forest Fire Laboratory of the Intermountain Forest and Range Experiment Station. The Aero Commander, scanner, and personnel were detailed to the study area by the Fire Mapping Unit of the Division of Fire Control, Region 4, U.S. Forest Service. The C-47 aircraft, operated by the Infrared and Optical Sensor Laboratory, University of Michigan, was contracted for in the absence of NASA available aircraft. A view of the 17-channel scanner is shown in figure 37-12.

The Texas Instruments RS-7 scanner produces imagery on 5-inch-wide Hyscan film which is developed in flight. This film was given a final hypo rinse at a darkroom at Ellsworth Air Force Base, Rapid City, South Dakota.

The Reconofax XI scanner produces 3- by 4-inch Polaroid prints which are immediately available for inspection. It also produces images on 70-millimeter film, prints of which are shown in figure 37-13.

All data from the Michigan scanner were recorded on magnetic tape and are being processed, but the data are not available at the time of this paper.

INTERPRETATION OF AERIAL IMAGERY

Aerial Photography

Interpretations of large-scale photography were made of all attractant test sites for all periods of photography. Beginning with the May 1967 coverage, three kinds of templates were made for each attractant test site. The first template enclosed the boundaries of each test site and included as many infested trees as healthy trees. The second was produced by a photointerpreter who circled each tree image which appeared offcolor in any way. The third was made from the ground truth and is a miniature of the plane-table drawing. Infested trees were depicted in two ways on this template. If the trees appeared faded (discolored) on the ground, they were shown as triangles; if not faded at this examination, they were shown as circles. This third template was used to determine interpreter errors, but only after all interpretations were made. Thus, templates were made for each interpreter, film type, flight date, and attractant test site.

On the pilot study area, roughly 1 by 3 miles in size, three photointerpreters examined five scales (1:116 000, 1:63 360, 1:31 680, 1:15 840, and 1:7920) on the two color films. The order of interpretation was from the smallest scale (1:116 000) to the largest scale (1:7920). Interpreters were instructed to circle and number each

infestation of newly killed trees on transparent templates; they also counted trees whenever possible within each infestation.

Optical-Mechanical Scanner Imagery

All thermal imagery was reviewed on an illuminated table with a 10-power hand lens to select those examples that best resolved the resolution target. The selection was also based on the ability to resolve tree crowns from the background. Twenty-three flight runs were picked from the Reconofax XI imagery — no filter (0.7μ to 7.0μ), 2.0μ to 2.6μ , and 4.5μ to 5.5μ wavelengths — and four flight runs from the RS-7 imagery in the 8.0μ to 14.0μ region.

Four identical points which surrounded the ground-instrumented test site and which could be recognized on aerial photographs were marked on this selected imagery. Several examples of the optical-mechanical scanner imagery are shown in figure 37-13.

In addition to monocular viewing, examples from all wavelengths of the line-scan imagery were examined with a General Aniline and Film (G.A.F.) model 650 microdensitometer (fig. 37-14). This was done to quantify which wavelengths were resolved best over the resolution target. Also, we were interested to learn: (1) whether the microdensitometer could separate tree crowns from openings in the forest and (2) whether subtle differences, not discernible by eye, could be detected among the infested and healthy tree crowns. Thus, on the thermal imagery, warmer crowns should have higher film densities and indicate dying trees, whereas cooler crowns should represent lower densities on the imagery and might indicate healthier trees.

The extreme versatility of the microdensitometer meant that several tests had to be conducted to learn which combination of aperture and scanning speed would produce the most meaningful data. For example, there are 10 scanning speeds, four chart read-out speeds, six aperture sizes, five magnifications, and four color filters to choose from. Most of the tests were finally run at the following settings:

1. Drive scanning rate: 5mm/min
2. Chart read-out speed: 4 in/min
3. Circular aperture: 1.62 millimeters in diameter, effective aperture $200\mu^2$
4. Magnification: 100 times
5. Filter: none

Representative examples of the microdensitometer charts are shown from the panchromatic aerial photography and from imagery obtained in several optical-mechanical scanner wavebands (figs. 37-15, 37-16, and 37-17).

Results

This study is now in its third year. Although we still cannot predict the location of low-vigor trees by previsual symptoms from airborne imagery, some ground and airborne techniques appear more promising than others. In general, we have learned more about the biological and physical changes which occur in the pine trees as they begin to die. We obtained good records on visual and photographic color changes, both on the ground and on aerial transparencies, and we were able to get representative very large-scale and very small-scale color and false-color photography. Optical-mechanical scanner imagery is of better quality than that obtained 1 year earlier. A start has been made on microdensitometer analysis of scanner imagery.

GROUND MEASUREMENTS

Effect of Beetle Population Size on Rate of Foliage Discoloration

After examining 60 bark samples, we must accept the null hypothesis that infested pine trees which discolor early have no different beetle populations, length of galleries, or size of the new generation of insects than infested trees which retain their green foliage color. A comparison of the mean values indicates that no difference exists in insect activity between infested, faded, and nonfaded trees. No consistent difference could be found in measurements, whether they were made on the north side or south side of the trees. Inches of gallery length showed the greatest difference with the faded trees having more damage to the inner bark. The students' "T" test, comparing these differences, was not significant.

Spectrophotometric Results

The spectrophotometric recordings (fig. 37-5) made by the National Bureau of Standards of healthy, newly infested, and old infested (discolored) foliage show comparative reflectance of the samples from 0.4 μ to 22.0 μ . The curves represent the mean of three samples. Each graph presents data taken from a different portion of the electromagnetic spectrum by a different spectrophotometer, the top graph by the General Electric

in the range 0.4μ to 1.08μ , the middle by the Cary-White 14 from 0.4μ to 2.2μ , and the bottom by the Cary 90 from 2.5μ to 22.0μ . Note that the ordinate axes on all graphs are plotted at different percentages of reflectance scales.

The greatest deviation between the curves occurs between the old-infested foliage and the healthy foliage, and these differences can be seen in many parts of the spectrum. This same distinction, however, can be made on film — either color or IR sensitive. There is very little difference that occurs between the foliage from newly infested trees and healthy trees at this early date (approximately 45 days after beetle attack). The newly infested foliage shows a slight increase in reflectance at 0.68μ (the chlorophyll absorption wavelength) and a decrease in reflectance of 5 to 10 percent at 0.75μ to 1.2μ . It is unlikely that these small differences are detectable when the inherent reflectance variations within a species are taken into account.

Visual Determination of Tree Decline

The visual comparisons of foliage color with the prepunched Munsell hue charts are shown in figure 37-18. At a glance one can see the shift in hue of the 209 dying trees as the season progressed from May through August. For example, in May about 75 percent of the infested trees were green-yellow (GY), whereas in August the same percentage of trees were yellow-red (YR). The greatest shift from the normally healthy green-yellow (5 GY and 2.5 GY) foliage to off-green foliage (2.5 GY and 10 Y) seems to take place from the fall following attack until the next May.

About 10 to 15 percent of the healthy trees in May, June, and August have a slightly yellow hue (2.5 GY) which is similar to early fading of infested trees. In July, the healthy trees appeared greener; this is probably a result of new needle growth and dropping of old (dead) needles.

When foliage is healthy, it is fairly dark — the average Munsell value (lightness or darkness) is five and the chroma (color strength) four to six. When the tree loses vigor, it becomes lighter (the Munsell value going up to six and seven). The ground observer also noted during May and June that infested trees appeared lighter and more silvery than healthy trees while both still had the same hue. As infested foliage changes to yellow, the trees become still lighter, and the Munsell value becomes seven to eight, with little change in chroma. The chromas increase appreciably as the foliage becomes drier later in the summer and tends toward the orange or yellow-reds (7.5 YR and 5 YR). It is at this stage in late July, August, and September that the infested trees have their highest reflectivity in the visible spectrum. Note that, even in August, about 12 percent of the infested trees have the same hues as healthy trees. These trees may either not die and consequently not change

color, or they may succumb and discolor in September and October. The ground inspection in October revealed that 17 percent of the infested trees did not die or change color.

Munsell readings made from the ground of 10 sample infested trees are compared with Munsell readings made from ground color photographs and with aerial color photographs in the discussion of photointerpretation results.

Anatomical Changes in Needles

In an effort to explain why conifers do not exhibit early symptoms of vigor loss in the reflective portion of the near IR, we studied examples of needle cross sections taken in October, May, June, and July of healthy and infested trees.

In October 1966, 2 months following insect attack, no real differences at the cellular level could be found between the healthy and infested trees. Differences may be present, but the nature of slide material preparation tends to hide small growth differences that might actually be present in the early attack stage.

In May 1967, real anatomical differences showed up (fig. 37-10) and are noted in the following comparison:

<u>Structure affected</u>	<u>Normal needle</u>	<u>Needle from infested pine</u>
Resin canals	Open	Collapsed or broken
Vascular bundles	Most cells filled with cytoplasm	Cytoplasm absent
Stoma	Intact	Broken, shrunken, degenerate, closed
Cytoplasm	Fills out to cell walls	Shrunken from cell walls, frequently absent
Cell walls	Normally thin	Thicker by comparison

The various changes that occur within the needles probably affect the reflectance mechanism differently. One would expect that with water loss in the needles, IR reflectance would decrease; however, this seems to be offset by the internal anatomical changes shown previously and by possible chemical changes associated with water loss. The net effect is no early change in IR reflectance.

Note also that there is no significant breakdown in mesophyll cells of stressed pine needles as there is in stressed hardwood leaves. In the latter case, the mesophyll breakdown theoretically prevents internal scattering of IR light and reduces reflectance back to the camera. Thus, hardwood images on IR color film or prints appear darker when under stress than when healthy. With needles under stress, the mesophyll walls appear to remain rigid while the cytoplasm shrinks and withdraws from the cell walls. This could be achieved with a very minute transfer of solute. The minute movement of liquid from the cytoplasm results in increasing the concentration of solutes and subcellular particles in the mesophyll; in turn, this decreases the water in mesophyll cells and may contribute to an increased internal scattering or reflectance. Finally, the rigid structure of the pine needle and absence of large parenchyma cells and air spaces in the mesophyll may help explain the difference in reflectance behavior.

Needle Moisture Tension

This pressure measurement, made with the Scholander bomb by means of a pressure gage and described earlier, may be one of the most sensitive ways to determine vigor loss in trees. The number of pounds of gas pressure required to force out sap from a freshly cut twig is fairly simple to obtain — even in the woods — and affords a high level of discrimination between stressed and normal trees. Readings made of healthy foliage in the afternoon (14:00 hours) were always two to four times less than those made from infested foliage. This suggests making only afternoon measurements when transpiration is probably at a low level.

Foliage Emission Temperature

Foliage emission temperature measurements are in situ foliage measurements made with either a Stoll-Hardy or Barnes PRT-5 or PRT-10 radiometer from an instrument tower or from a neighboring tree. To explain differences in emission temperature, one must consider each sampling period separately to determine the effect that weather conditions have on the physiological functions of the tree. For example, at 14:00 hours on June 16 (time of overflight), one might have expected a greater thermal imbalance between healthy and infested trees because of the breakdown in water-conducting tissue in the latter. On this date, significant differences did show up in leaf tensions and sap flow. However, although wind velocity was not excessive, incoming solar radiation apparently was. Absence of full sunlight, in this case, was a limiting factor in creating a sufficient temperature difference in long-wave emission. Similar trade-off logic must be used to explain existing thermal differences at any point in time.

The emittance temperatures of the black and aluminum surfaces of the resolution target and the grass on one side of the target are summarized in table 37-I. Note that the aluminum targets, which reflect sky temperatures, were 51° to 86° colder than the black targets and 30° to 50° colder than the surrounding grass.

Table 37-II summarizes the emitted temperatures of the infested and healthy trees at the same time periods that thermal imagery was obtained by the airborne scanners. The greatest temperature difference between the infested and healthy trees was recorded at 10:00 hours on both days — a 6° C difference on June 16 and an 8° C difference on June 17. On both days, the temperature difference dropped off as the day progressed; transpiration may have been effective in cooling the pine needles in the morning but dropped off if available soil moisture became critical. A reduced cooling rate and continued full sunlight would cause a rise in emitted temperature. Because of the great volume of weather, physiological, and physical data available (over two growing seasons), a computer program is being written to determine which combination of these variables is limiting, significant, and nonconsequential. The job is almost impossible to undertake by desk computer, but it is within the limits of an electronic data processor.

EVALUATION OF AERIAL IMAGERY

Photointerpretation On Attractant Sites

Interpretations from aerial color films still provide the most reliable information on the accurate location and detection of dying coniferous trees. However, we found that May was the earliest that any reliable interpretations could be made on color films; still earlier detection of infested trees is needed for control programs to be more effective. Color films exposed over beetle infestations in October, 3 months after beetle attack, did not discriminate infested from healthy trees. According to entomologists, dry periods in August and September following beetle attack occasionally cause early tree discoloration, but these weather conditions have not occurred since this study began in 1965.

Bias in interpreting films was minimized (1) by including within the boundaries of each attractant test site as many green uninfested trees as attacked trees and (2) by randomizing the order of photointerpretation of each test site, film, and photograph date. Thus, each interpreter examined 209 infested trees on each film (two) and photograph date (four) — a total of 1672 infested trees plus an equal number of healthy trees. This is about 3400 image determinations that each photointerpreter had to make.

What success did the photointerpreters have in identifying the total number of infested trees at each season? As the percentage of discolored trees increased from 10 in May to 81 in August, as rated by the ground observer, a similar progression showed up on the photointerpretation results. Figure 37-19 graphically represents the percentage of correct interpretation calls for all variables. The interpreters agreed very well for the 3 months of June, July, and August and also found that they did as well in color film as in false-color film. These findings substantiate the results from the first year. In May, all interpreters were able to find three times as many infested trees on the average as the ground observer. Apparently, the aerial view affords the photointerpreter with more color discrimination than can be detected on the ground. Two interpreters picked out more infested trees on the May date than the third interpreter; they did this on all sites and on both films.

A factorial design using season (four), attractant test site (four), film type (two), and interpreter (three) as the variables was analyzed by analysis of variance. The percentage of correct interpretations was transformed first to angles where $\arcsin \sqrt{\text{percentage}} = \text{angle}$; this is a procedure developed by C. T. Bliss to permit the mean and variance to be independent for making tests of significance and is described in Snedecor (ref. 37-10). We found that both the photointerpreters and films did not test significantly different from each other despite the May disparity in correct calls between interpreters. This means that under the test conditions the null hypothesis must be accepted that no interpretation differences could be ascribed to the photointerpreter or film used. However, the differences between attractant test sites and season of photography did show highly significant F-values. True interpretation differences did exist between site and season and served to improve the sensitivity of the factorial design.

How did the photointerpreters compare with the ground observer at each period in saying trees were fading? Since the photointerpreters showed sufficiently close agreement in the analysis described previously, their results were pooled (fig. 37-20). The solid line in this figure indicates perfect correlation (1.0); the plotted points show that, except for May, there is excellent agreement between the interpretations made from aerial transparencies and the ground observations. As mentioned previously, the photointerpreters picked up about three times as many discolored trees in May as the ground observers.

Although the photointerpretations in August 1967 detected only 80 percent of the total 1966 infested population of 209 trees, the total number of discolored trees agrees well with the ground observer. Furthermore, a ground examination conducted in October 1967 revealed that the photointerpretations made from August photography agreed within 5 percent of the actual number of trees that discolored and finally died.

In 1966, exactly 20 percent of 243 infested trees did not die; in 1967, 17 percent of 209 infested trees did not die. Thus, 15 to 20 percent of heavily infested pine trees were able to withstand the twin onslaught of cambial damage and fungus growth.

The commission errors, those instances where the interpreters falsely called healthy trees suspected faders, were only 1 percent of the total number of possible calls (includes healthy and infested trees for all test sites). On color film there were 34 commission errors out of a possible 3200 tree images; on false-color film there were 26 out of 3200. This low rate of error lends confidence in the use of color films for detecting discolored trees.

How do Munsell notations vary by the three methods in which they were used, namely: (1) by ground comparison of the Munsell charts with the 10 sample trees in the field, (2) by comparison of the aerial photographic images with Munsell transparencies, and (3) by comparison of the 35-millimeter color photographs taken of the 10 trees on the ground with Munsell transparencies? The hue comparisons made from the 10 representative trees are shown graphically in figure 37-21. There is striking agreement between the ground observations and those made of the identical aerial photographic images; they are not over one hue apart at any time period. The changeover from the GY (green-yellow) hues to the Y (yellow) hues occurred in June for the aerial photographs and in July on the ground. An example of the color shift of tree foliage as the tree begins to die is shown in the series of ground photographs in figure 37-22.

Photointerpretation On Pilot Study Area

Entomologists have found that when Black Hills beetle infestations begin to appear in small groups, a change from endemic to epidemic conditions is imminent. Thus, to detect a potential insect buildup of epidemic proportions, aerial sensors flown at conventional altitudes or from space orbit must resolve these small infestation centers.

Within our study area, we found 48 centers of one to three trees in size — almost one-half of the 97 active bark beetle infestations (fig. 37-23). The distribution of infestations by size classes is shown in the following tabulation. The average dimension of the infestations in each class is also shown.

<u>Size class (number of trees)</u>	<u>Number of infestations</u>	<u>Average of largest dimension, ft</u>
1 to 3	48	16.7
4 to 10	18	41.6
11 to 20	12	79.6
21 to 50	12	182.2
51 to 100	4	171.2
100+	3	445.0

Single trees and infestations up to three trees in size are detected with the greatest success on IR color at the three largest scales. As expected, the larger the scale, the greater the success. Maximum accuracy for the one- to three-tree class is 79 percent on 1:7920-scale IR color. On the 1:31 680-scale IR color, detection success is only 50 percent. The number of successes is reduced rapidly when scale is smaller than 1:31 680. For example, at 1:63 360 the best detection is 7 percent on color film.

If we can afford to wait until infestations become four to 10 trees in size, detection will improve considerably. Almost 95 percent of the infestations are detected on 1:7920 and 1:15 840 scales. There appears to be no difference between IR color and color film at these scales. However, as the scale becomes smaller, color film improves detection. For instance, on 1:63 360-scale color, 37 percent of the infestations are detected. Only 20 percent are detected on IR color of the same scale. On 1:116 000-scale photographs, which we have used in this test to simulate space photography, only 9 and 7 percent of the small infestations (one to 10 trees) can be detected on color and IR color film, respectively.

It is quite common to refer to the capabilities of remote sensors in earth orbit in terms of the smallest objects that can be resolved. Because of this, the largest dimension of each of the infestations was measured on the ground to compare detection success with infestation size. Through this comparison, we should find the resolution requirements for detecting bark beetle infestations.

The following tabulation shows the distribution of the 97 infestations by four size classes. Also of interest is the average number of trees found in each of the classes on the ground.

<u>Size class, ft</u>	<u>Number of infestations</u>	<u>Average number of trees</u>
0 to 20	40	1.6
21 to 50	23	5.3
51 to 100	13	13.9
101+	21	62.2

From this, we can see that, to detect infestations of three trees with any success, sensors must be able to resolve objects or spots (groups of like objects) 20 feet in the largest dimension. The reported capabilities of remote sensors at orbital altitudes are no better than 100 feet. With 100-foot resolution, we could expect to detect only infestations averaging 62 trees in size or larger. An example of Kodak Aero Ektachrome IR film of the largest scale (1:7920) and smallest scale (1:116 000) is shown in figure 37-24. More than 250 times as much area is represented on the small-scale stereographic print — an obvious advantage for wide-area coverage.

The three interpreters used in this study were able to detect 68 percent of all infestations over 100 feet in dimension on 1:116 000-scale IR color film (fig. 37-25). On color film, detection was only 57 percent. No infestation less than 20 feet in dimension was detected on either film at this scale.

Detection success on other photographic scales followed the same pattern as presented in the previous discussion on tree number size classes. The larger the scale, the better the detection. Infrared color resulted in better overall detection on the three largest scales. Color film gave slightly better discrimination between infestations and their surroundings on the smaller scales and resulted in higher detection success.

Optical-Mechanical Scanning Imagery

Visual interpretation.— Both the Reconofax XI and RS-7 scanners have an effective focal length of approximately 0.9 inch. This was determined by relating distance measured on IR imagery to distance on 1:3450-scale panchromatic photographs to find the effective scale (representative fraction). This scale was then related to flying height to determine the unknown focal length.

$$\begin{array}{rcl}
 \frac{\text{Focal length (feet)}}{\text{Height (feet)}} & = & \text{RF} \\
 \frac{\text{FL}}{2000 \text{ feet}} & = & \frac{1}{25 \ 345} \\
 \text{FL} & = & 0.079 \text{ foot or } 0.95 \text{ inch}
 \end{array}
 \quad \left. \vphantom{\begin{array}{rcl} \frac{\text{Focal length (feet)}}{\text{Height (feet)}} & = & \text{RF} \\ \frac{\text{FL}}{2000 \text{ feet}} & = & \frac{1}{25 \ 345} \end{array}} \right\} (37-1)$$

Reconofax XI.- This thermal IR line scanner resolved the resolution target best in the 4.5 μ to 5.5 μ band. Table 37-III shows that 60 percent of all flights made in the 4.5 μ to 5.5 μ band resulted in ground resolution of better than 4 feet. Comparable imagery with no filter and with a 2.0 μ - to 2.6 μ -band filter showed 4-foot ground resolution of only 22 and 17 percent, respectively. Good or better target contrast on 63 percent of the 4.5 μ to 5.5 μ imagery also indicates the superiority of this bandwidth.

The afternoon time period resulted in better thermal imagery than noon or morning time periods. For instance, 40 percent of the imagery in the afternoon period had better than 4-foot ground resolution in all bands. Imagery taken during the morning (08:00 to 11:00 hours) and noon (11:00 to 13:20 hours) periods resulted in 33 and 21 percent, respectively. It should be noted, however, that the 2.0 μ - to 2.6 μ -band imagery during the noon period was better than during other time periods.

Two statements can be made regarding Reconofax XI imagery: (1) the 4.5 μ to 5.5 μ bandwidth resolves 4-foot thermal resolution targets better than imagery in the 2.0 μ to 2.6 μ band or when no filter is used, and (2) in general, afternoon thermal imagery has better resolution and target contrast than morning imagery.

Texas Instruments RS-7.- There were only 23 effective flights (table 37-IV). No flights were made during the period 11:00 to 13:00 hours for comparison with Reconofax XI imagery for that period. When imagery from the morning and afternoon periods are compared with Reconofax XI imagery, we arrive at two general evaluations: (1) afternoon imagery in the 8.0 μ to 14.0 μ band is better than morning imagery in terms of thermal target resolution and target contrast and (2) imagery in the 4.5 μ to 5.5 μ bandwidth has better target resolution and contrast than the 8.0 μ to 14.0 μ imagery for the afternoon period.

From the IR line-scanner flight tests made on June 16 to 18, 1967, we can make the following evaluation:

Infrared scanner	Filtered bandwidth	Best resolution target contrast			Order of image quality
		08:00 to 11:00	11:00 to 13:30	13:30 to 16:30	
Reconofax XI	No filter	--	--	X	4
	2.0 μ to 2.6 μ	--	X	--	3
	4.5 μ to 5.5 μ	--	--	X	1
RS-7	8.0 μ to 14.0 μ	--	--	X	2

These results are not conclusive. As more data are collected under more stringent flight and instrument-controlled conditions, we will re-examine and adjust these results if found necessary. Four examples of the imagery taken in the above wavebands over the Black Hills test site are shown in figure 37-13.

Microdensitometer Interpretation

The G.A.F. Model 650 microdensitometer was used to check line-scanner imagery for image densities caused by differences in emitted energy. An example of the best imagery for each of the IR bands during both morning and afternoon flights was used for the evaluation. Three tests were made: (1) a diagonal trace across the imagery (fig. 37-15a) through a reference point near the edge of attractant test site 4, (2) a trace along a single thermal scan (fig. 37-15b), and (3) traces across the image of the thermal resolution target (fig. 37-16).

Evaluation of the recorder chart for the diagonal trace (fig. 37-15a) is very difficult. Gaps between scans on Reconofax XI imagery cause regularly spaced low-density values in the trace. These low-density values tend to mask out thermal differences on the low-density end of the scale. This means that areas of lowest thermal energy (cool) will not show up, and the scale of density values is extended beyond the normal range of expected values.

To overcome this, the microdensitometer was set to trace a single thermal line scan passing through attractant test site 4. The resultant trace for the 4.5μ to 5.5μ band is shown in figure 37-15b. We found that the densities shown in this figure match with the actual images of the forest openings and forest crowns on the photograph.

Evaluating densities on the microdensitometer trace is a special art that requires new interpretation techniques. One must determine a scale of density values that represents the various ground objects; that is, healthy trees, dying trees, stand openings, rock outcrops, exposed soil, grass, and many others. Until further research provides this scale of values, evaluation must be restricted to generalities.

At our present state of the art, three broad interpretations are possible. For example, on the 4.5μ to 5.5μ image (fig. 37-15b), (1) high densities, 2.2 to 2.8, are openings in the forest stand and are warmer than the surrounding forest canopy, (2) low densities, 1.2 to 2.0, are the forest canopy, and (3) densities between 2.0 and 2.2, which are in the vicinity of dying trees on the ground, may be warmer crowns caused by loss of tree vigor.

Figure 37-16 shows microdensitometer traces across the thermal resolution target for each of the thermal IR bands. The highest density (3.5) is recorded for black panels and the lowest density (1.1) for aluminum panels. The temperature difference between panels on the ground, measured with a Barnes PRT-5 radiometer, was 53°C ; the black is much warmer than the aluminum, which acts as a mirror and reflects the temperature of the cold sky. At the same time, grass along the side and at the end of the largest black panels was 27°C cooler. The temperatures of various objects in relation to black and aluminum panels are shown in the diagram in figure 37-26.

The density scale in the right of the diagram shows how the resolution target sets the upper and lower limits in thermal emittance by establishing the density limits for interpreting the traces. The example shown was for 4.5μ to 5.5μ imagery for June 16 at 14:00 hours (fig. 37-16). Thus, sunny openings in the stand could be expected to register 2.92 on the density scale, infested pines at 2.62, healthy pines at 2.45, grass at 2.24, and shaded openings at 2.01. Unfortunately, these expected values do not coincide with the actual values in figure 37-15b. Other factors, including the gain control on the scanner electronics, scan angle, direction of scan, scattering of emitted energy, and atmospheric conditions will affect the image density.

The microdensitometer trace does set limits of resolution for the IR scanners. In the illustration (fig. 37-17), the best resolution for the Reconofax XI with no filter was 2 feet. The Reconofax at 2.0μ to 2.6μ and the RS-7 at 8.0μ to 14.0μ resolved only 8 feet. Reconofax XI at the

4.5 μ to 5.5 μ band resolves 4-foot panels. Differences in amplitude must be attributed to the direction of the trace and contrast.

How does the resolution for thermal IR line scanners compare with regular panchromatic photography? Figure 37-17 shows a microdensitometer trace across the thermal resolution target on Plus-X Aerographic film taken simultaneously with the thermal imagery. Because this is negative material, the black panels register as low density and the aluminum panels as high density. The original scale of the photograph illustrated was 1:4400. It is obvious that line scanners will need much improvement before they will approach the resolution of ordinary panchromatic photography.

Microdensitometer traces show that subtle differences in thermal emission recorded on film for dying trees are not detectable at the present time. Gaps in the image between scan lines distort the density scale on traces made across scan lines and make interpretation impossible. Traces made along scan lines remove this distortion, and densities are recorded in their normal range. Warmer openings in the stand and general tree canopy are interpretable from the traces. Traces across the thermal resolution charts help to assess resolution capabilities of the IR scanners. The high and low densities of black and aluminum panels in the chart assign a range in thermal density for the images within the trace. As the resolution panel size decreases, resolution becomes less distinct, and the amplitude in density for the change from black to aluminum becomes drastically reduced. This is contrast reduction, and though the apparent temperature difference between panels (53° C) is detectable, smaller temperature differences would not be.

ACKNOWLEDGMENTS

This experiment is being performed under the Earth Resources Program in Agriculture/Forestry under the sponsorship and financial assistance of the National Aeronautics and Space Administration, Contract No. R-09-038-002. This paper reports on a cooperative study by the Forest Service, U.S. Department of Agriculture, and involves three Forest and Range Experiment Stations and one Region: the Pacific Southwest at Berkeley, California; the Rocky Mountain at Fort Collins, Colorado; the Intermountain at Ogden, Utah; and the Western Zone Air Unit, Region 4, Boise, Idaho.

Special thanks are due the Homestake Mining Company, Anaconda Copper and Mining Corporation, and the Bureau of Land Management, U.S. Department of Interior, for the use of their land and timber to conduct the study.

The Spearfish, Rochford, and Nemo Ranger Districts of the Black Hills National Forest have been particularly helpful in providing dark-room facilities, vehicles, and equipment.

REFERENCES

- 37-1. Anon.: Timber Trends in the United States. Forest Service, U.S. Dept. of Agr., Forest Resources Rept. 17, 1965.
- 37-2. Nickerson, D.: History of the Munsell Color System and Its Scientific Application. Opt. Soc. Amer. J., vol. 30, 1940, pp. 575-586.
- 37-3. Nickerson, D.: Color Measurement and Its Application to the Grading of Agricultural Products. U.S. Dept. of Agr., Misc. Pub. 580, 1958.
- 37-4. Heller, R. C.; Dovespike, G. E.; and Aldrich, R. C.: Identification of Tree Species on Large-Scale Panchromatic and Color Aerial Photographs. U.S. Dept. of Agr. Handbook 261, 1964.
- 37-5. Stoll, A. M.; and Hardy, J. D.: A Method for Measuring Radiant Temperatures of the Environment. J. Appl. Physiol., vol. 5, 1952, pp. 117-124.
- 37-6. Weber, F. P.: Exploration of Changes in Reflected and Emitted Radiation Properties for Early Remote Detection of Tree Vigor Decline. Master's thesis. Sch. of Nat. Res., Univ. of Mich., 1965.
- 37-7. Marshall, D. C.: Measurement of Sap Flow in Conifers by Heat Transport. Plant Physiol., vol. 33, 1958, pp. 385-396.
- 37-8. Dixon, H. H.: Transpiration and Ascent of Sap in Plants. Macmillan, London, 1914.
- 37-9. Scholander, P. F.; Hammel, H. T.; Bradstreet, D.; and Hemmingsen, E. A.: Sap Pressure in Vascular Plants. Science (AAAS), N.Y., vol. 148, 1965, pp. 339-346.
- 37-10. Snedecor, G. W.: Statistical Methods. Iowa State College Press, Ames, Iowa, 1950.

TABLE 37-I.- EMITTANCE TEMPERATURES (IN DEGREES KELVIN) OF GRASS
AND A RESOLUTION TARGET MEASURED WITH A BARNES PRT-5

RADIOMETER — 8.0 μ TO 14.0 μ

Date	Time	Temperature, °K			Sky conditions	Solar radiation, cal/cm ² /sec
		Resolution target		Grass		
		Black	Aluminum			
6/16/67	10:00	307	233	288	Full sun	1.12
	12:00	338	253	294	Full sun	1.35
	14:00	320	267	293	Haze	.95
6/17/67	10:00	327	253	293	Full sun	1.14
	12:00	339	253	303	Full sun	1.40
	14:00	331	260	300	Broken clouds	.50
	16:00	320	269	299	Broken clouds	.30

TABLE 37-II.- EMITTANCE TEMPERATURES (IN DEGREES KELVIN) OF
 TREE FOLIAGE AND FOREST FLOOR IN SUN AND SHADE AS MEASURED
 WITH A STOLL-HARDY HL-4 — SPECTRAL BANDPASS $> 3.5\mu$

Date	Time	Foliage in situ (a)		Δ , I-H	Forest floor (b)	
		Healthy	Infested		Shade	Sun
6/16/67	10:00	292	298	6	284	303
	12:00	292	297	5	293	312
	14:00	298	302	4	288	309
6/17/67	10:00	291	299	8	285	305
	12:00	304	311	7	297	315
	14:00	296	301	5	289	312

^aFour samples of each.

^bOne sample of each.

TABLE 37-III.- GROUND RESOLUTION FOR THE HRB SINGER RECONOFAX XI AT
1500 TO 2000 FEET ABOVE THE TERRAIN DURING THREE DAYLIGHT TIME
PERIODS — JUNE 16 TO 18, 1967

Time periods, hr	Filtered bandwidth, μ	Total flights	Resolution, percent		Target contrast, percent	
			8 feet or greater	4 feet or less	Good	Poor
08:00 to 11:00	No filter	6	50	50	0	100
11:00 to 13:20	No filter	10	100	0	0	100
13:30 to 16:35	No filter	6	67	33	0	100
All periods	--	22	78	<u>22</u>	0	100
08:00 to 11:00	2.0 to 2.6	21	85	15	15	85
11:00 to 13:20	--	13	70	30	15	85
13:30 to 16:35	--	7	100	0	15	85
All periods	--	41	83	<u>17</u>	15	85
08:00 to 11:00	4.5 to 5.5	9	33	67	67	33
11:00 to 13:20	--	10	70	30	40	60
13:30 to 16:35	--	5	0	100	100	0
All periods	--	24	40	<u>60</u>	<u>63</u>	37
Average All periods	All bands	87	70	30	25	75

TABLE 37-IV.- GROUND RESOLUTION FOR THE TEXAS INSTRUMENTS RS-7 AT
 2000 FEET ABOVE THE TERRAIN DURING TWO DAYLIGHT TIME
 PERIODS — JUNE 16 AND 17, 1967

Time periods, hr	Filtered bandwidth, μ	Total flights	Resolution, percent		Target contrast, percent	
			8 feet or greater	4 feet or less	Good	Poor
08:00 to 11:00	8.0 to 14.0	14	85	15	36	64
13:00 to 15:00	8.0 to 14.0	9	67	33	67	33
All periods	8.0 to 14.0	23	78	22	48	52

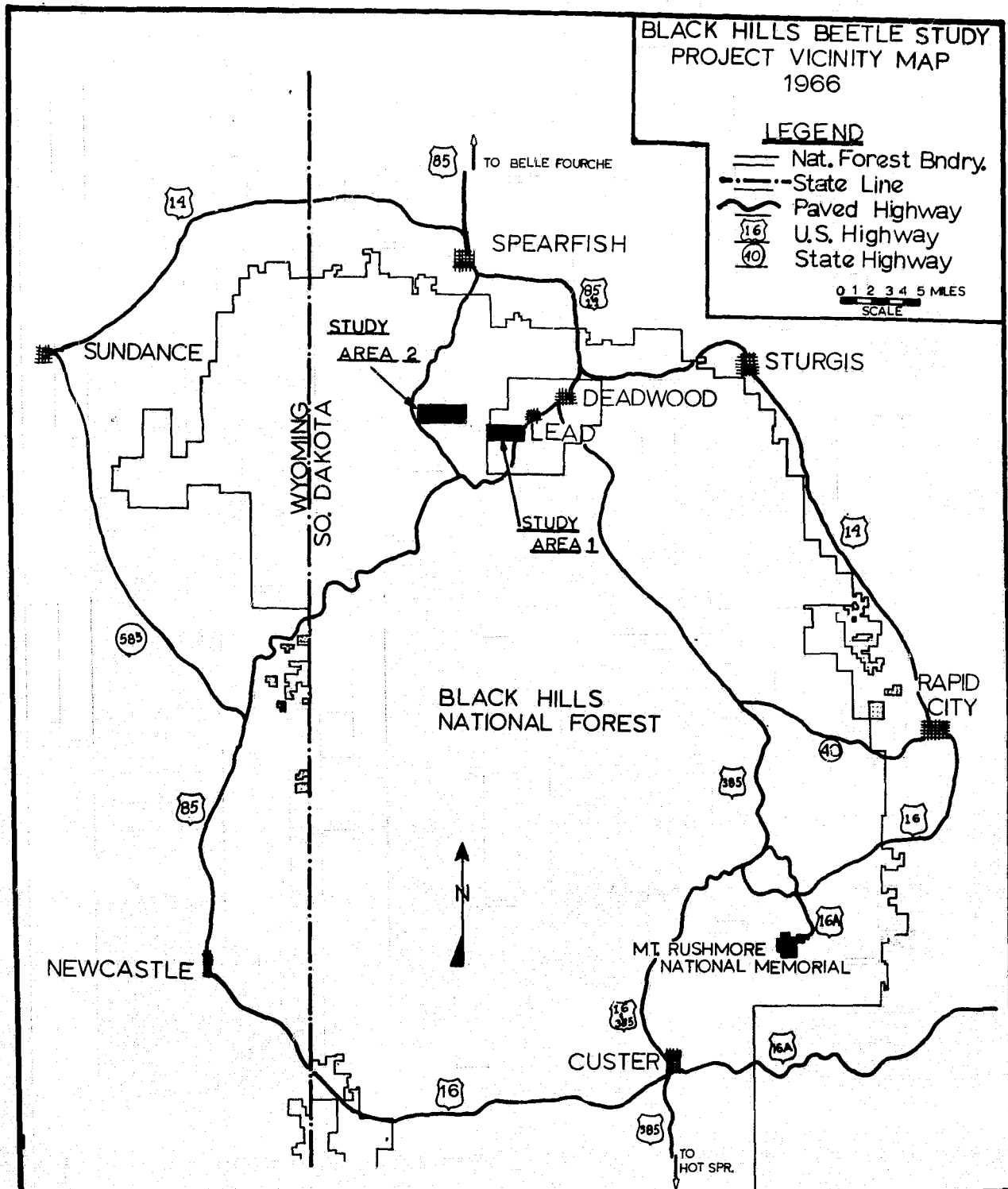


Figure 37-1.- Study areas I and II near Lead, South Dakota. Study area I is near site of previous tree biological and thermal sensing studies. Pilot study area II represents an area where beetle epidemic conditions exist and where tests were conducted to determine the likelihood of using space photography to detect the damage.

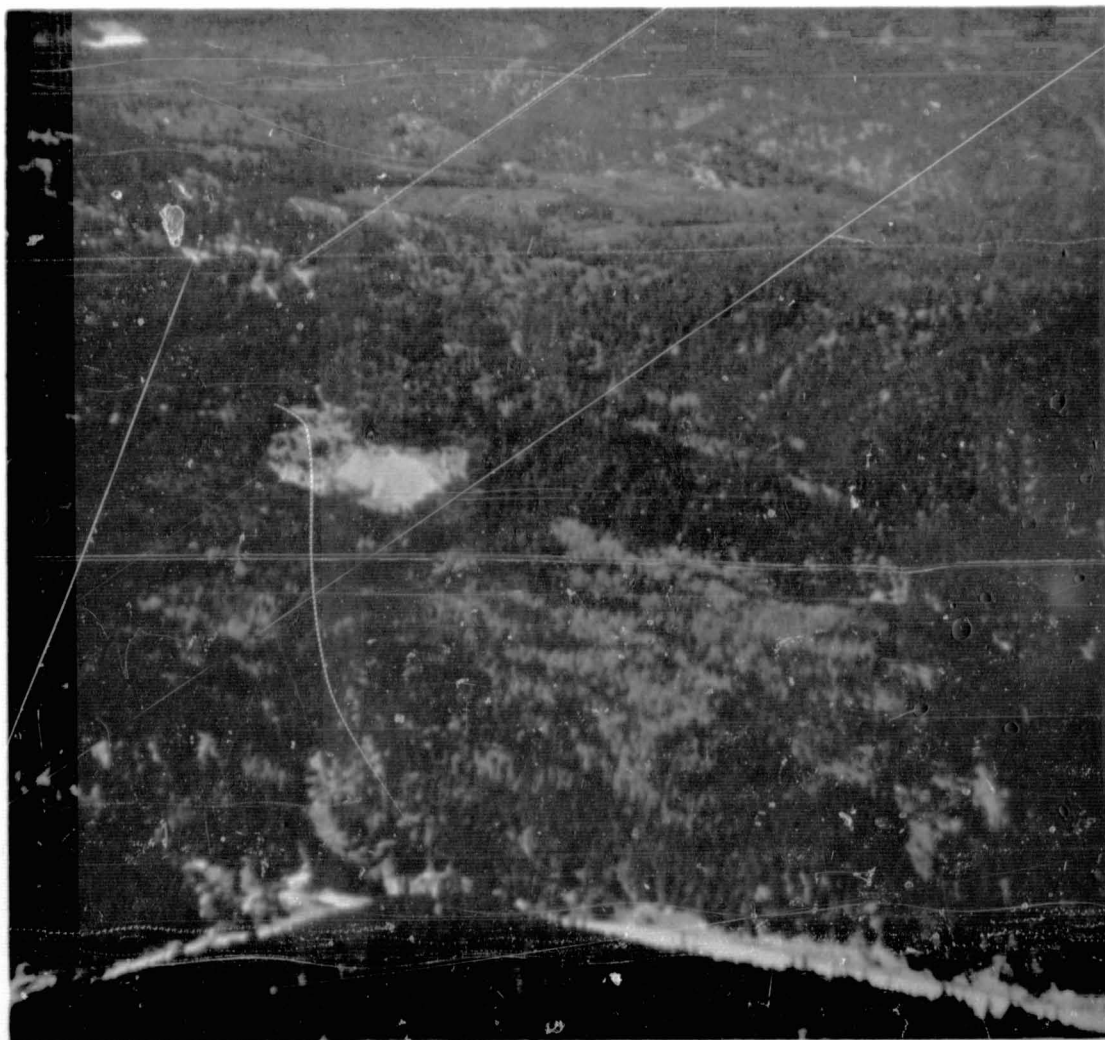


Figure 37-2.- Oblique photograph of bark beetle-induced tree mortality of ponderosa pine, Lead, South Dakota. Color photography detects trees with discolored foliage only; dying green trees are not detectable. Random pattern of group killing makes aerial sensing methods more effective than ground surveys.



Figure 37-3.- Screen cage on attractant pine tree.
Screen wire cage stapled to ponderosa pine trunk.
The cage is charged with live beetles to induce
attack by indigenous beetles on a normally healthy
tree.

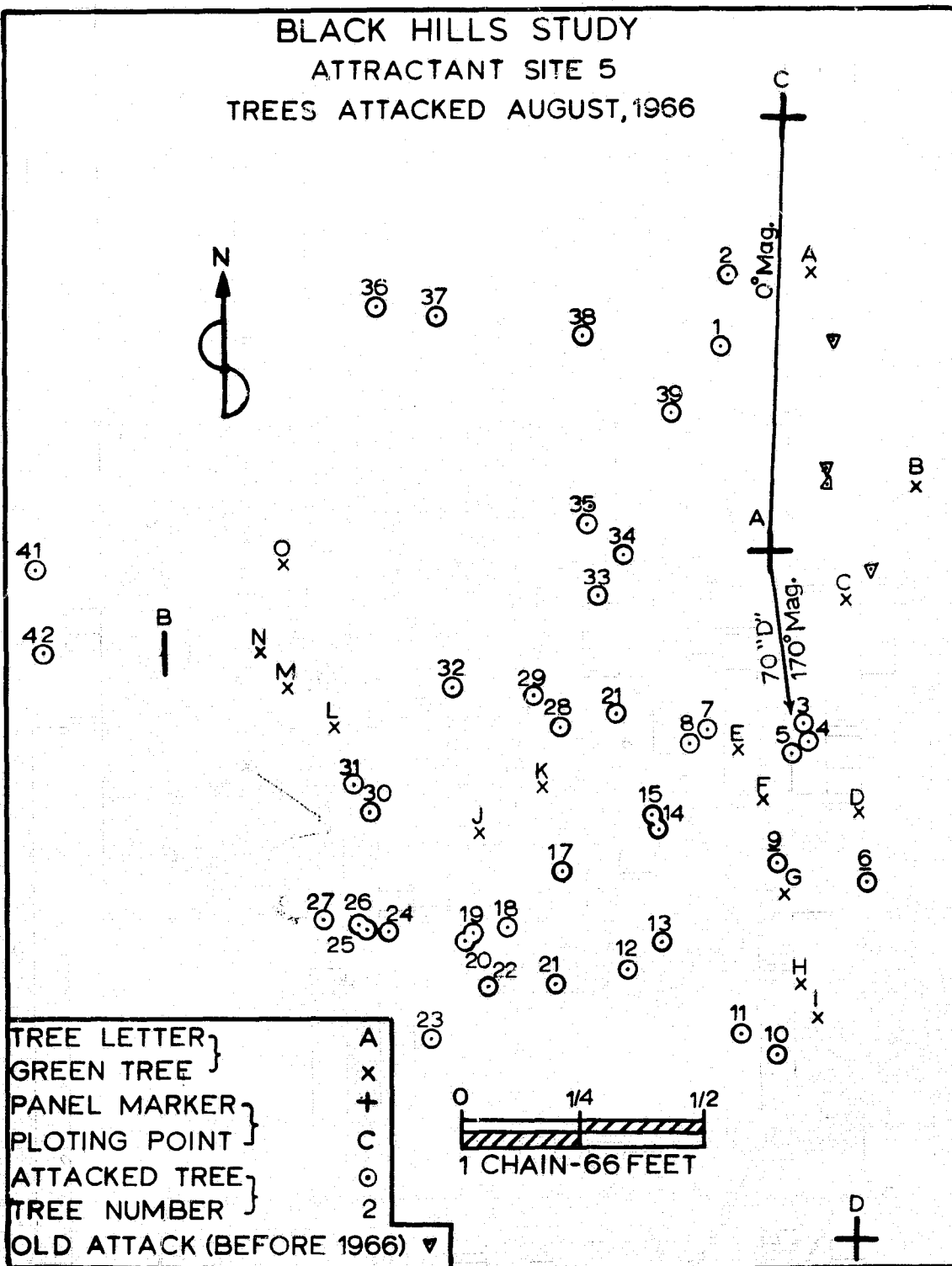
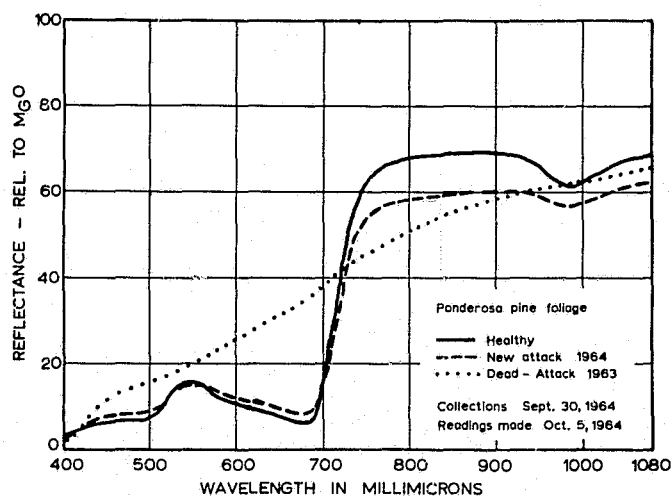
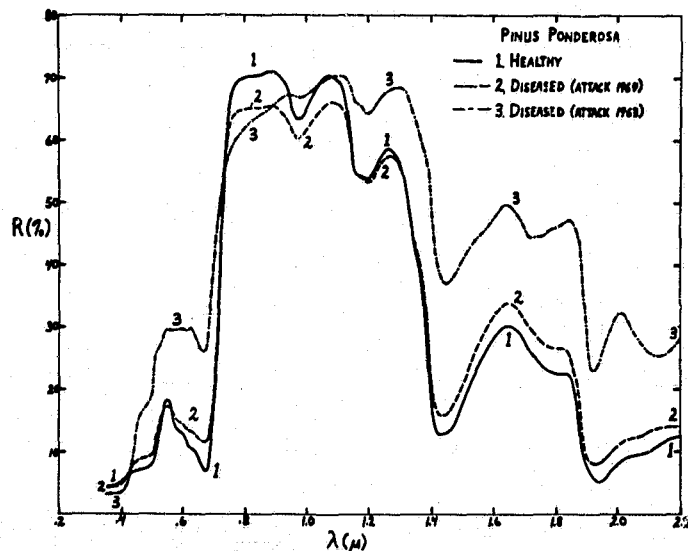


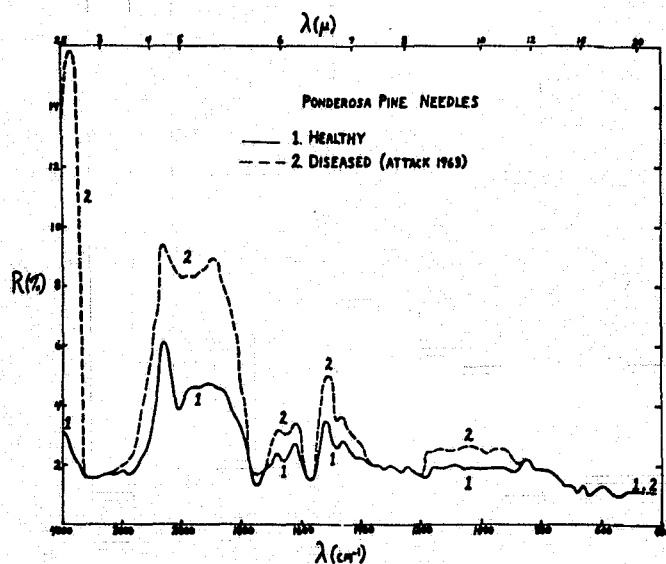
Figure 37-4.- Ground plot of infested trees. Plane table map constructed at one of six attractant test sites. Panel markers for aerial photography, infested trees, and several noninfested green trees are shown by symbols.



a. Foliage reflectance from 0.4μ to 1.08μ .

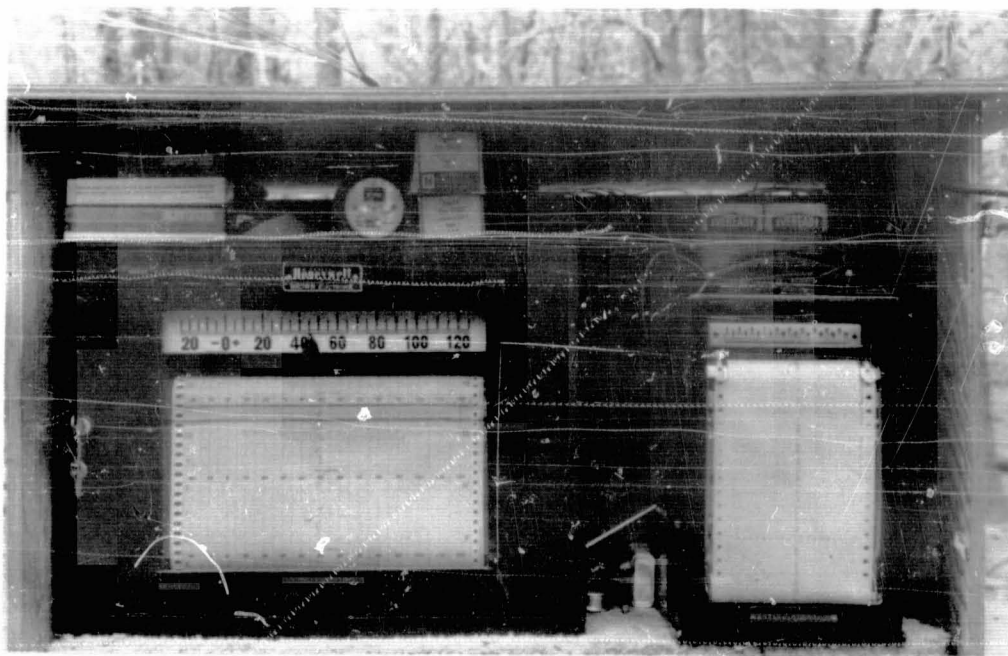


b. Foliage reflectance from 0.4μ to 2.2μ .



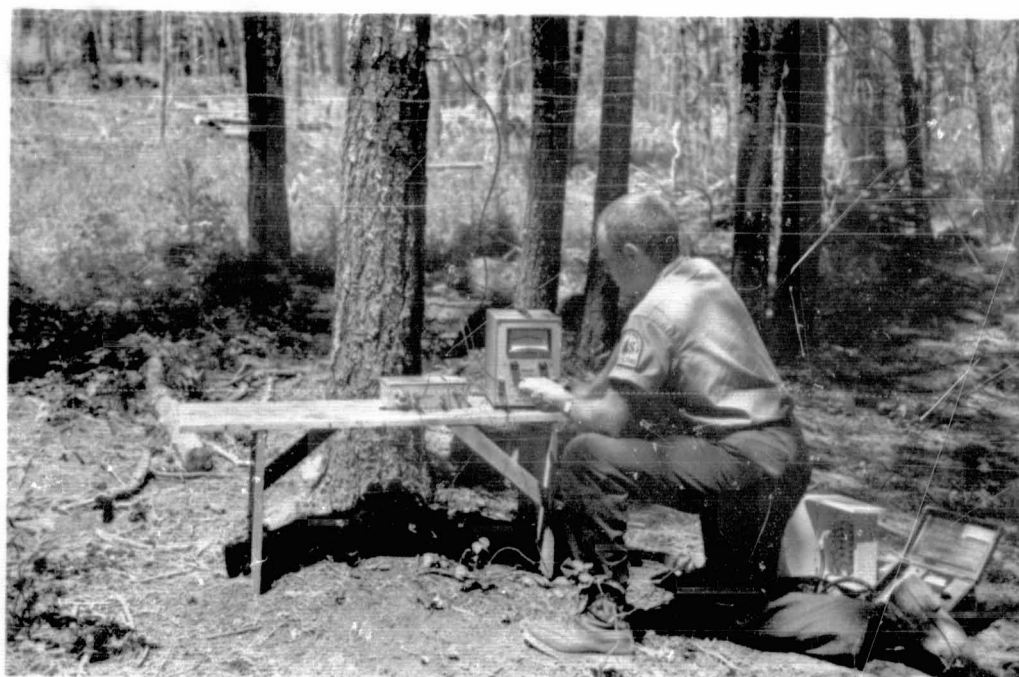
c. Foliage reflectance from 2.5μ to 22.0μ .

Figure 37-5.- Spectral reflectance from pine foliage (0.4μ to 22.0μ). Spectral reflectance curves from foliage taken from healthy, newly infested, and old infested pine trees (courtesy of the National Bureau of Standards).



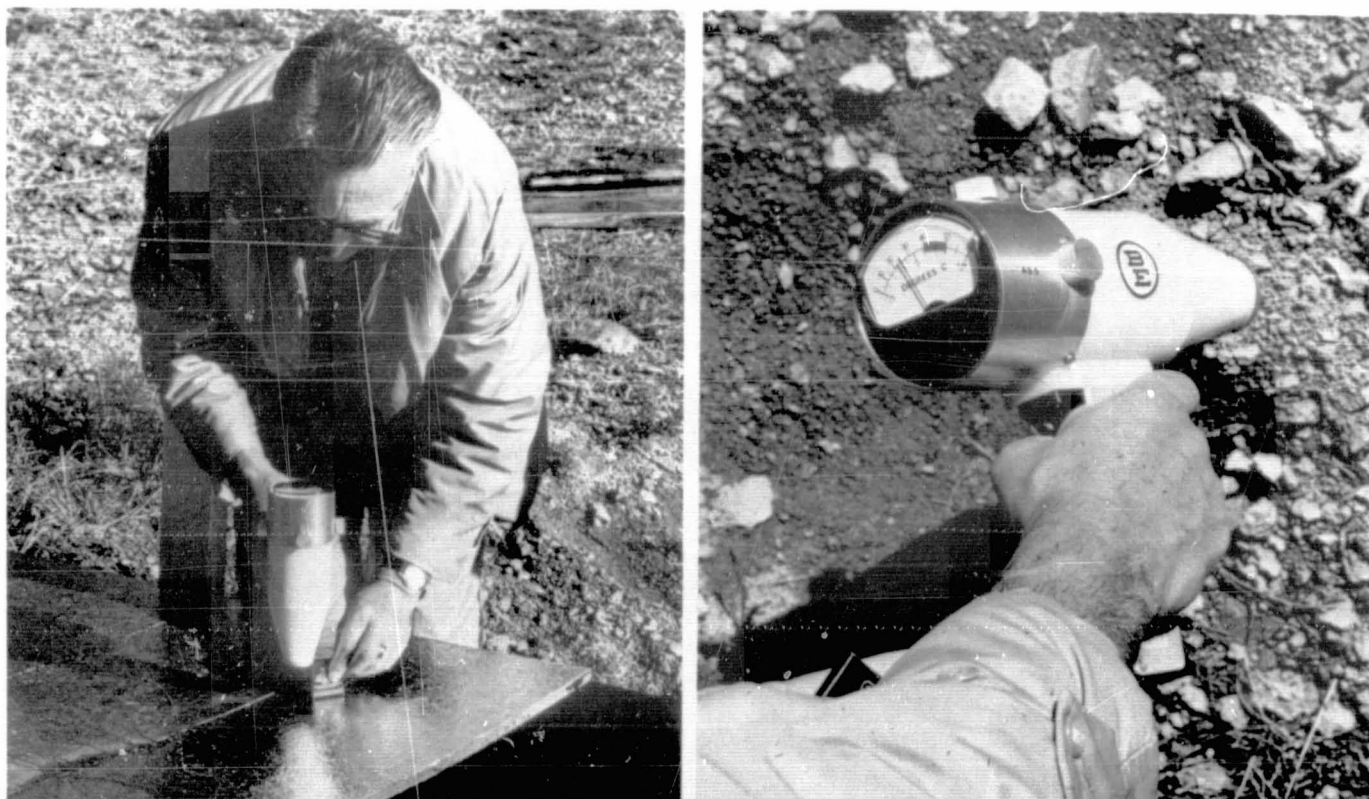
- a. Brown Electronic Model 152 by 60 P16 multipoint temperature recorder on left and Esterline-Angus 20-channel event recorder on right. Internal needle temperatures were recorded from crowns of infested and healthy trees; note wires leaving rear of instrument to attach to needles. The event recorder was used to measure wind direction and velocity.

Figure 37-6.- Needle temperature and wind velocity recorders and sap flow instrument.



- b. Portable microvoltmeter, Medistor Model A-60-C, is used with two heat detectors and a heat source to measure relative transpiration rates between healthy and dying ponderosa pine.

Figure 37-6.- Concluded.



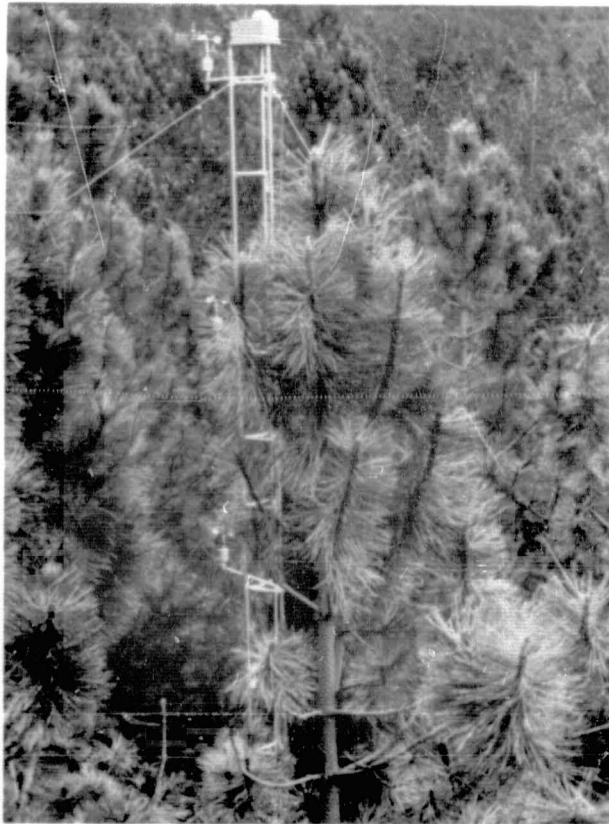
- a. A Barnes PRT-10 portable radiation thermometer was used at the resolution target to record apparent emitted temperatures. The photograph at left indicates manner in which temperature readings were taken a fixed distance above aluminum and black surfaces of resolution target. The photograph at right shows temperature indicator in degrees Celsius with instrument pointed at bare soil. Knob on right side of instrument is used for calibration.

Figure 37-7.- Barnes PRT-10 radiation thermometer and Stoll-Hardy IR radiometer.



- b. Stoll-Hardy IR radiometer being used to measure apparent needle temperature in the upper crown of a ponderosa pine tree. The radiometer head is fitted with a 3.5μ cut-on filter. A Barnes PRT-5 was also used to measure apparent emitted temperature.

Figure 37-7.- Concluded.



- a. Stationary 60-foot tower erected to record wind velocity at four levels in the tree crown, to record solar radiation, and to provide a platform for making emitted foliage temperature measurements in the tree tops.

Figure 37-8.- Instrument tower and soil moisture instrument.



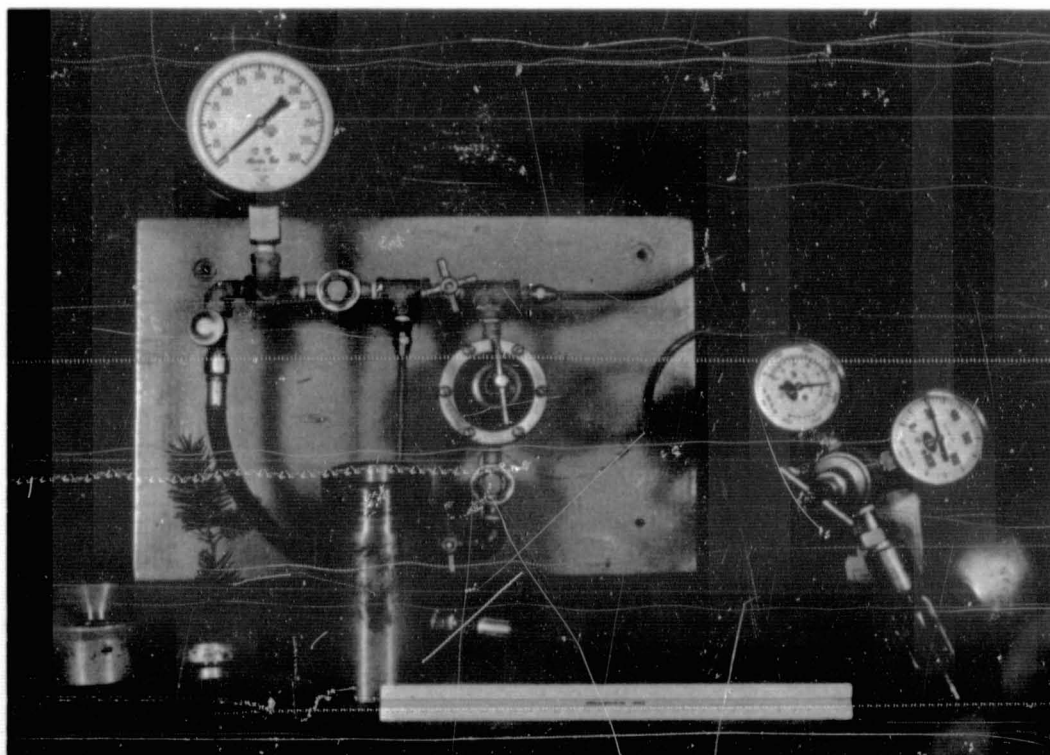
- b. Colman Soil Moisture Meter being used to measure soil moisture and temperature from probes buried in the soil profile.

Figure 37-8.- Concluded.



- a. Weather cabinet housing hygrothermograph in opening near healthy and infested trees. Recording pyrliograph (resting on roof of weather cabinet) measures total solar radiation.

Figure 37-9.- Pyrliograph and needle tension instrument.



- b. Scholander bomb for measuring needle moisture tension. Foliage is inserted into top part of bomb, which screws onto cylinder. Pressure gage reads pounds per square inch required to force water from twig end of foliage extruding from top part of bomb.

Figure 37-9.- Concluded.

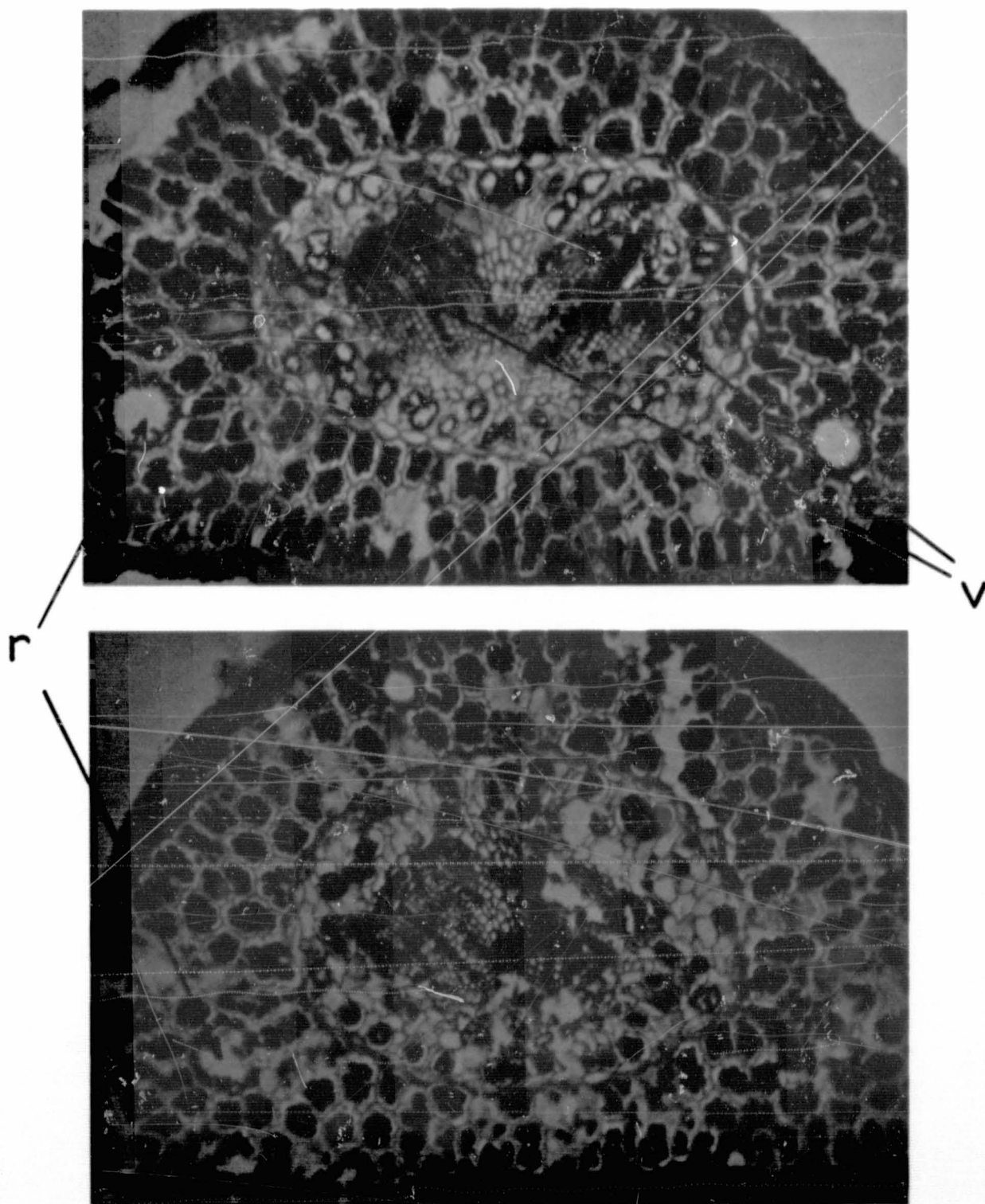


Figure 37-10.- Microscopic cross sections of ponderosa pine needle tissue. Upper photograph is from healthy needle; most cell walls are intact and filled with cytoplasm. Lower photograph is needle cross section from infested tree; many cell walls are broken. Vascular bundles (v), resin canals (r), and stoma are collapsed.

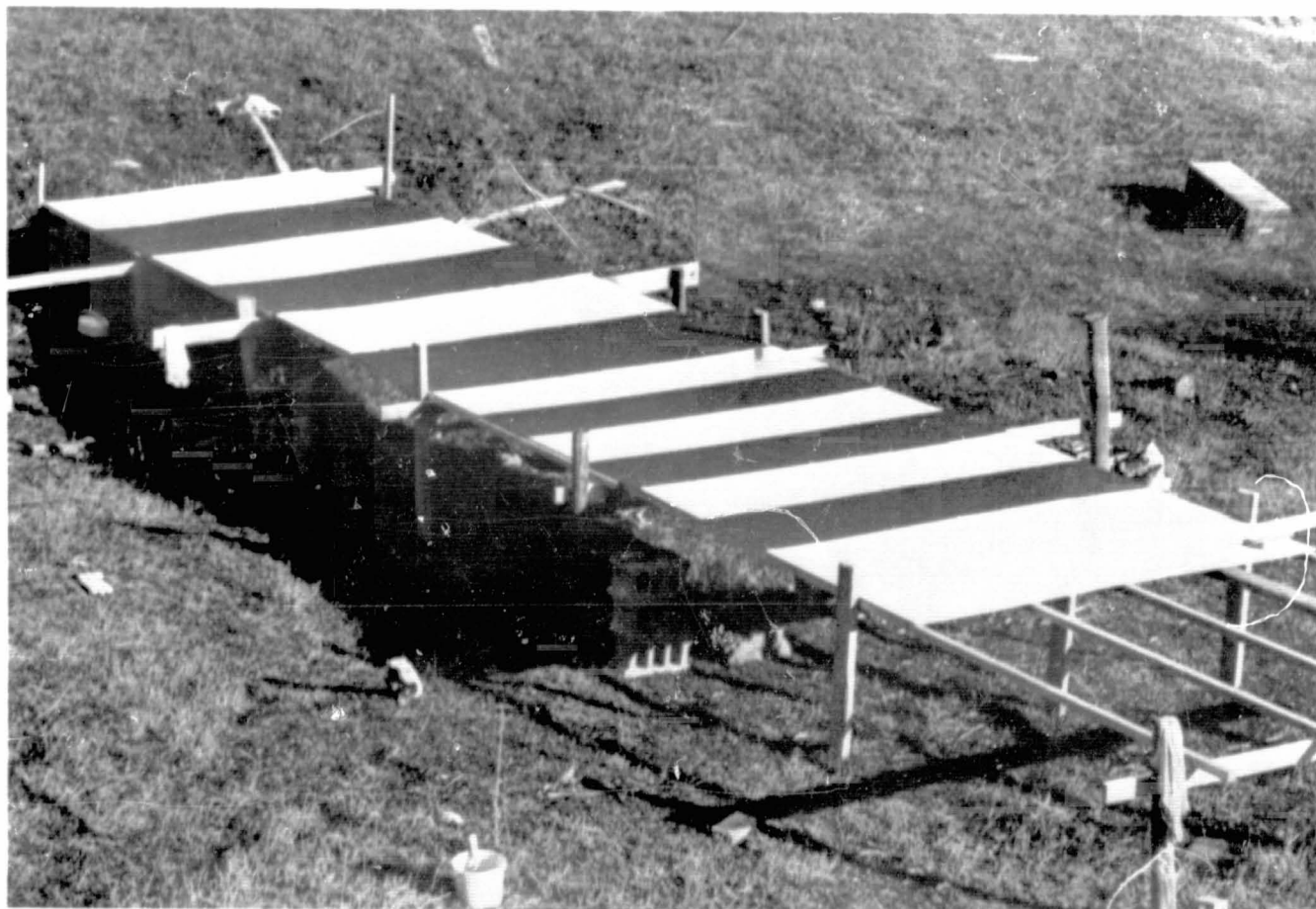


Figure 37-11.- Field thermal resolution target. Resolution target under construction at Black Hills Test Site. Panels were 8 feet long and in one of three widths: 2, 4, and 8 feet. They alternated between aluminum painted with black velvet paint and aluminum. Stereographic pair shown in lower photograph is from Anscochrome D/200 transparency, scale 1:1584.

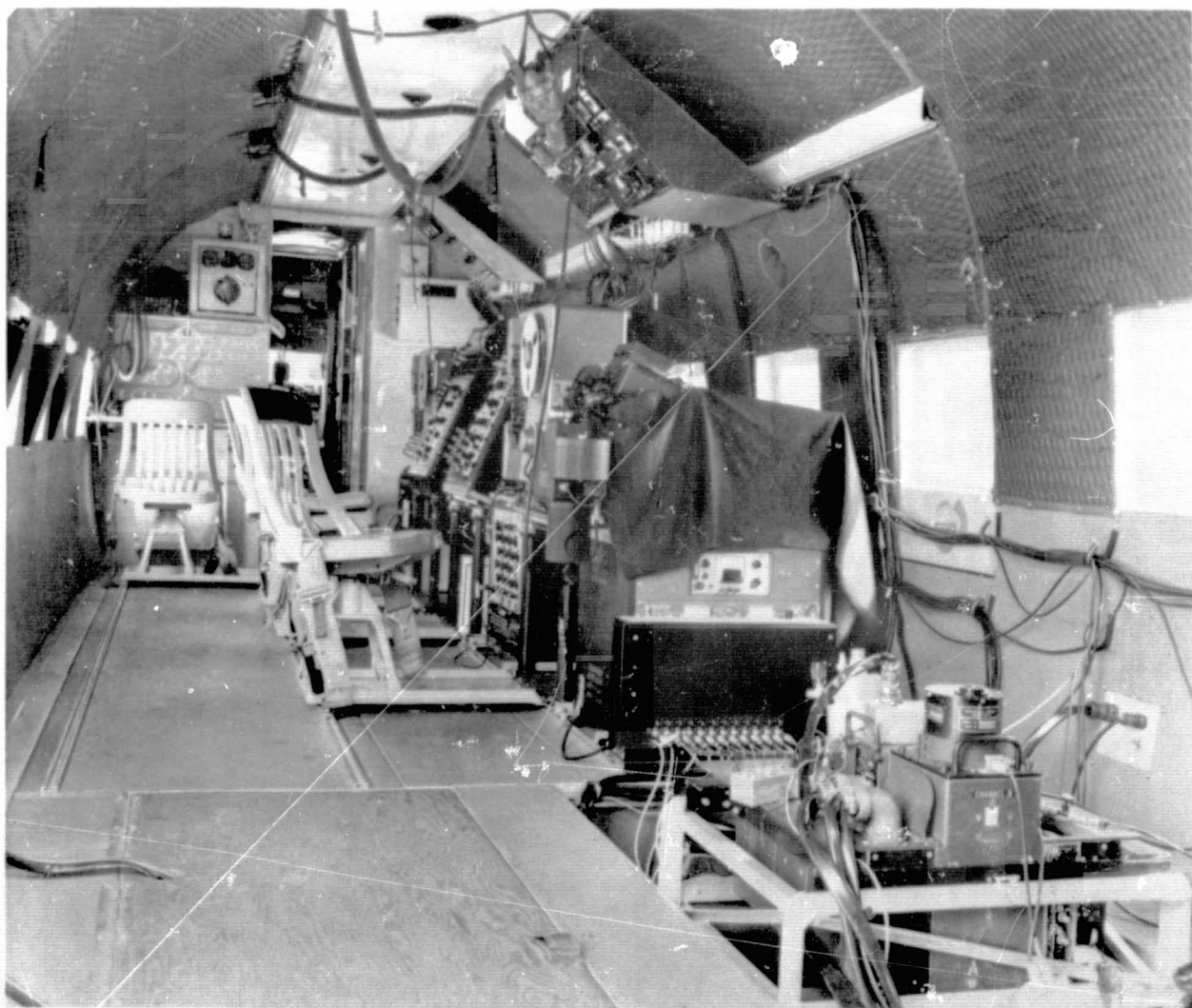
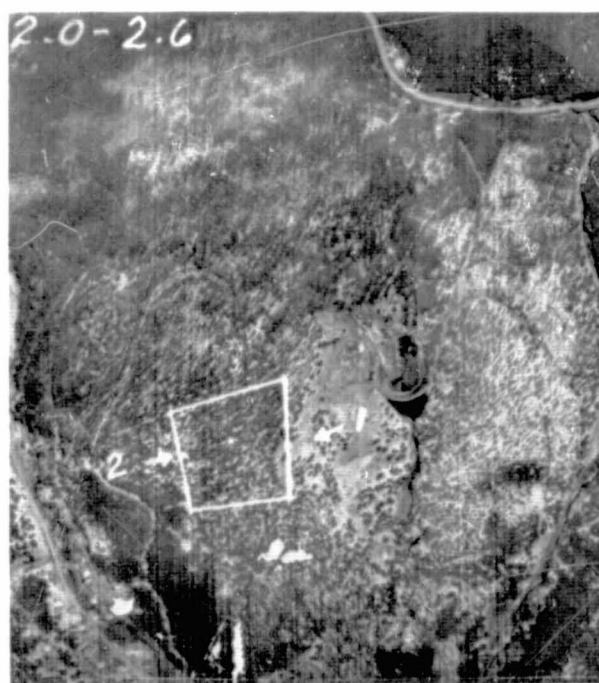


Figure 37-12.- Interior view of multispectral electronic equipment used by the Willow Run Laboratories, University of Michigan, and mounted in a C-47 type aircraft. Both optical-mechanical scanners are mounted in the floor opening — lower right of picture. All scanner voltage signals are fed to the two magnetic tape recorders shown in the right forward section of the cabin.



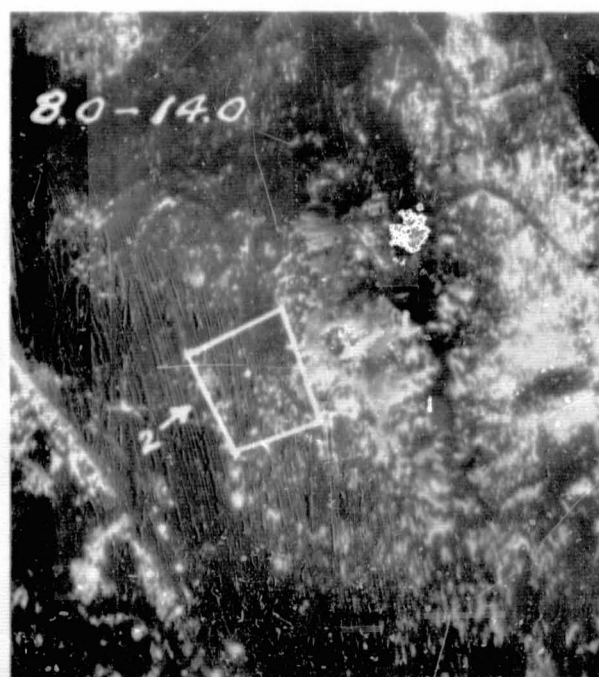
a. Reconofax XI — no filter, mostly reflected energy.



b. Reconofax XI — 2.0μ to 2.6μ , some reflected, some thermal energy.



c. Reconofax XI — thermal energy, 4.5μ to 5.5μ .



d. RS-7 — thermal energy, 8.0μ to 14.0μ .

Figure 37-13.— Four wavebands of line-scan imagery. Sample imagery from optical-mechanical scanners. Warm objects on this imagery appear light in tone; cold objects such as water or the aluminum target appear dark in tone.

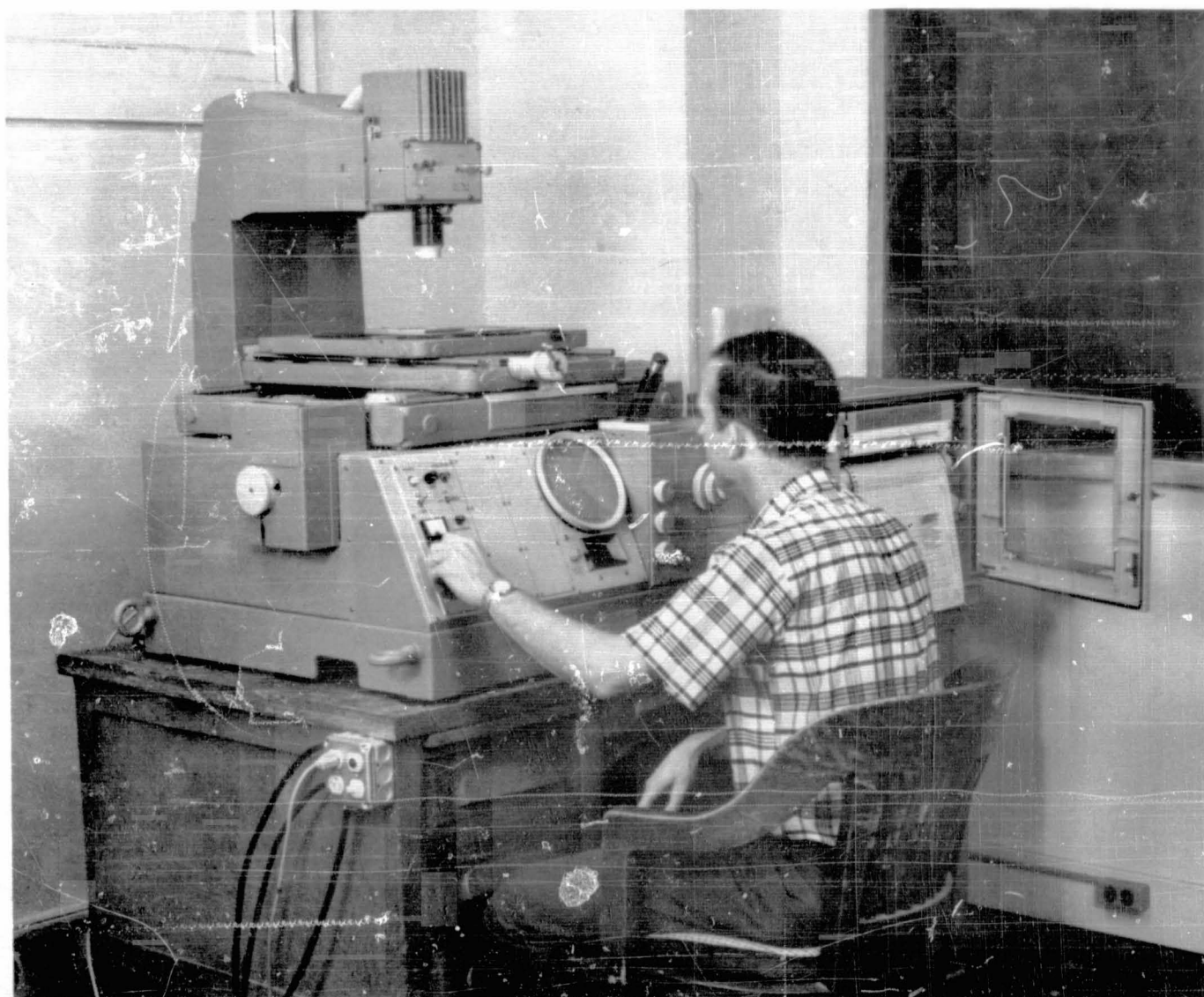
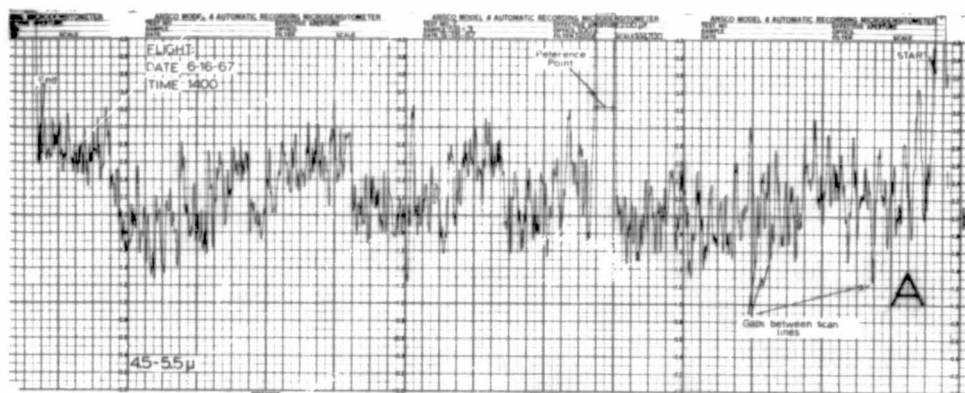
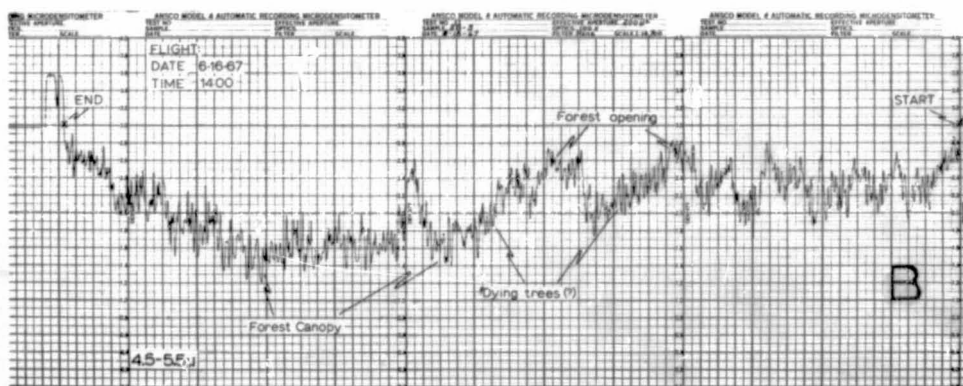


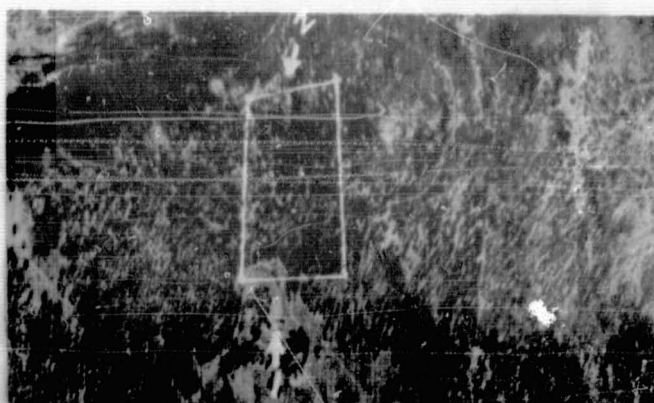
Figure 37-14.- G.A.F. Model 650 microdensitometer permits microanalysis of black and white and color film densities. Density is recorded on chart at right in analog form from density values of 0.0 to 4.0.



- a. Traces diagonally across scan lines. Note regularly spaced low-density readings caused by gaps between scan lines.



- b. Trace along scan line. Note the reduced amplitude between the coolest (forest canopy) and warmest (forest opening) objects.



- c. Also, note distortion in outlined figure surrounding dying trees; it was roughly square but, because of changes in V/H with respect to scanning speed, is distorted on the thermal imagery.

Figure 37-15.- Microdensitometer traces across and along scan lines. Microdensitometer traces across Reconofax XI thermal IR imagery in the 4.5μ to 5.5μ band shown below. Flight made at approximately 14:00 hours, June 16, 1967.

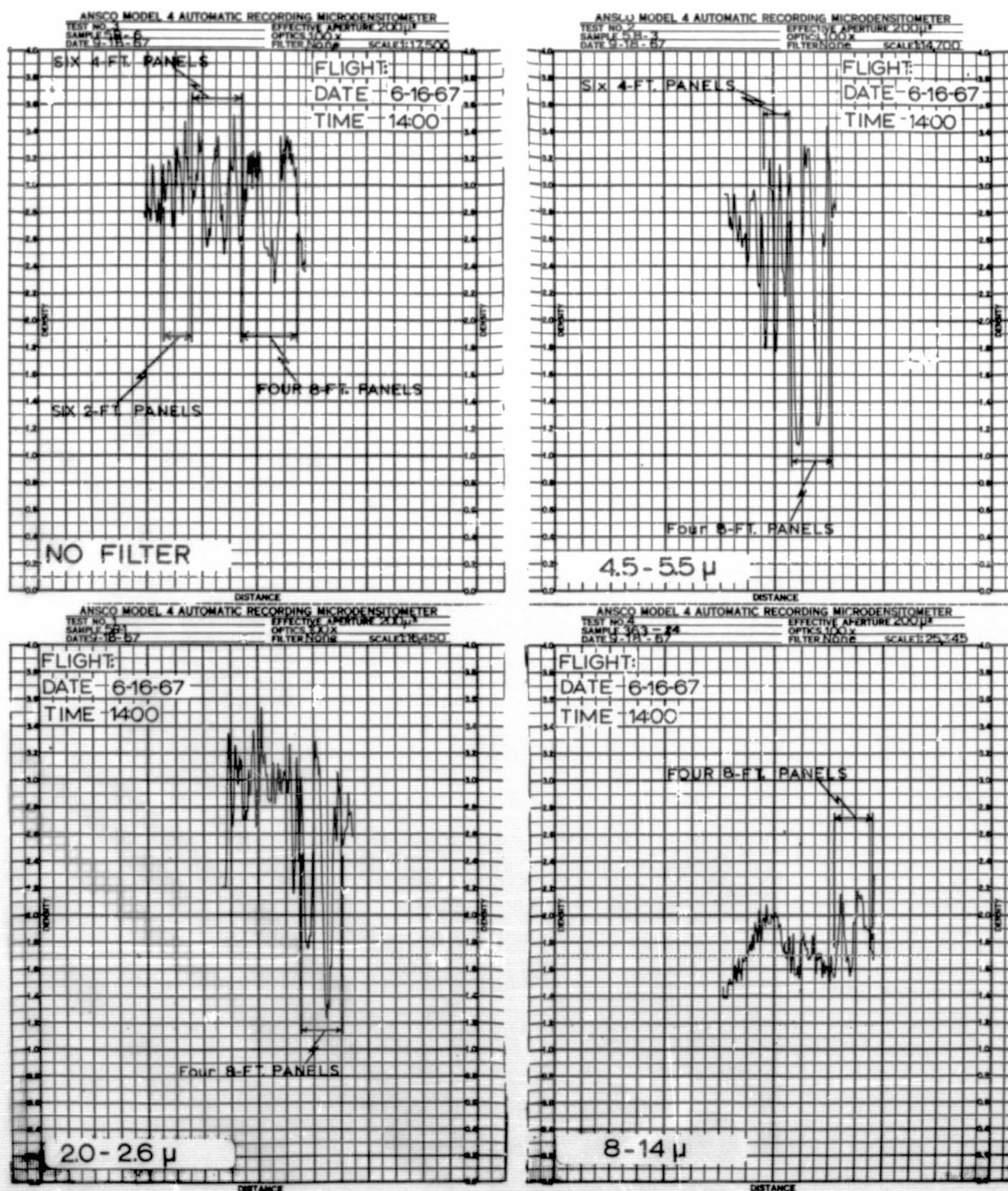


Figure 37-16.- Microdensitometer traces of four wavebands across resolution target. G.A.F. microdensitometer traces across the thermal resolution target on four wavebands of thermal IR imagery taken at approximately 14:00 hours, June 16, 1967.

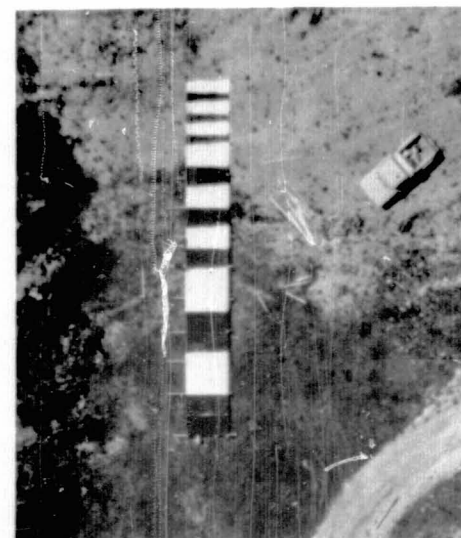
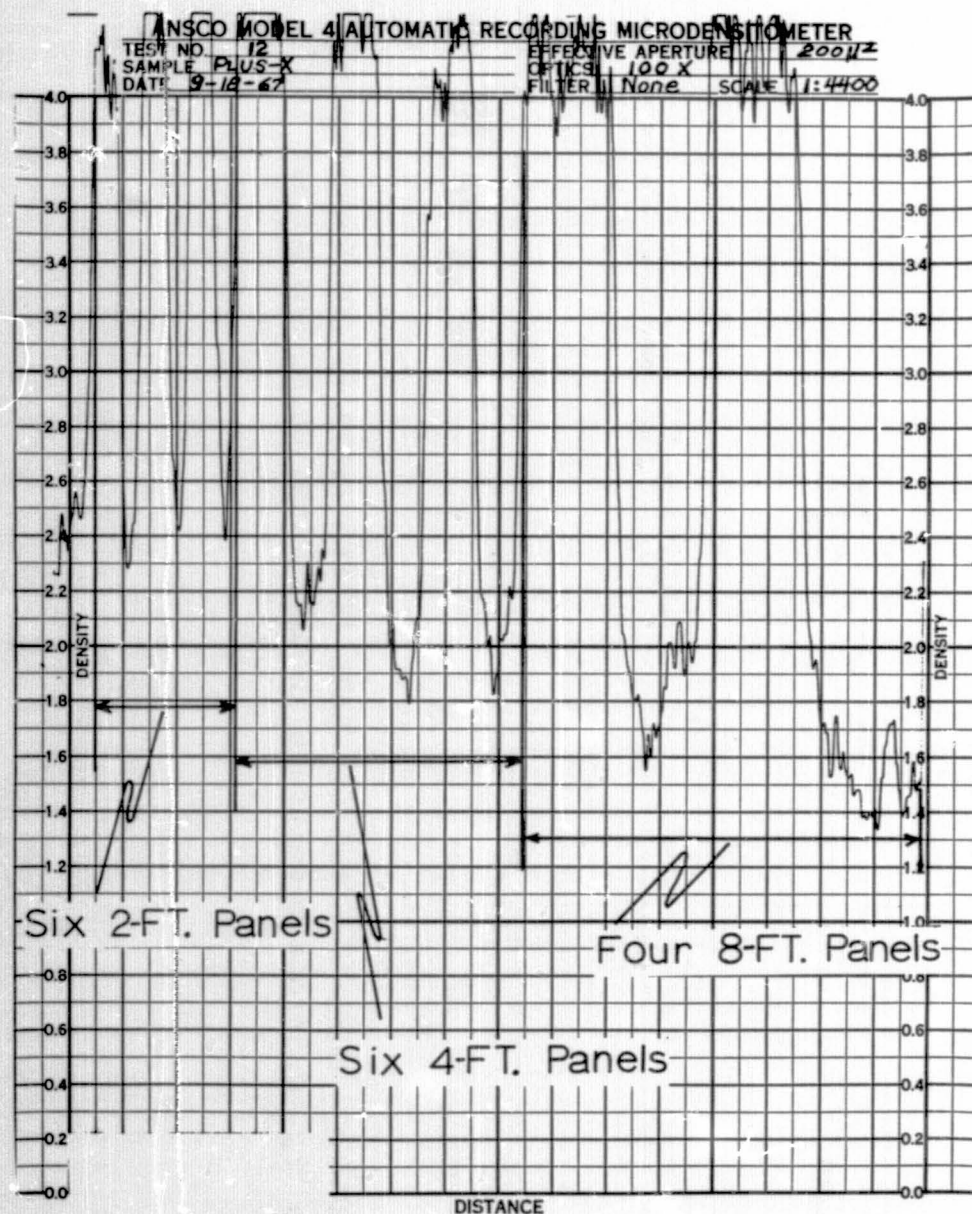


Figure 37-17.- Microdensitometer trace of target on pan film. A microdensitometer trace across the resolution target photographed on Plus-X Aerographic film. The photograph shows the target image at four times the original 1:4400 scale.

PERCENT SHIFT IN HUE OF FOLIAGE COLOR FOR HEALTHY AND INSECT INFESTED TREES

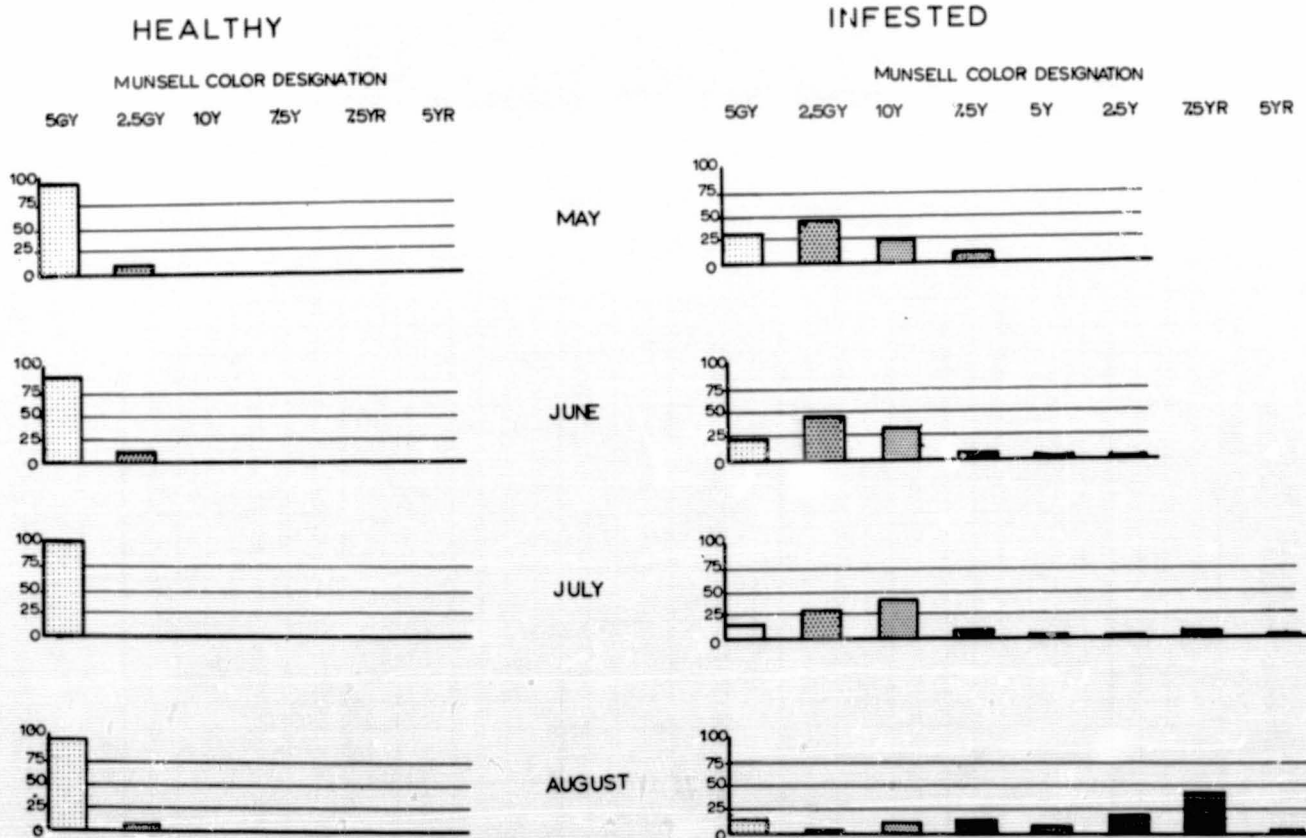


Figure 37-18.-- Munsell notations made in the field of 209 infested and 47 healthy ponderosa pine trees in May, June, July, and August 1967.

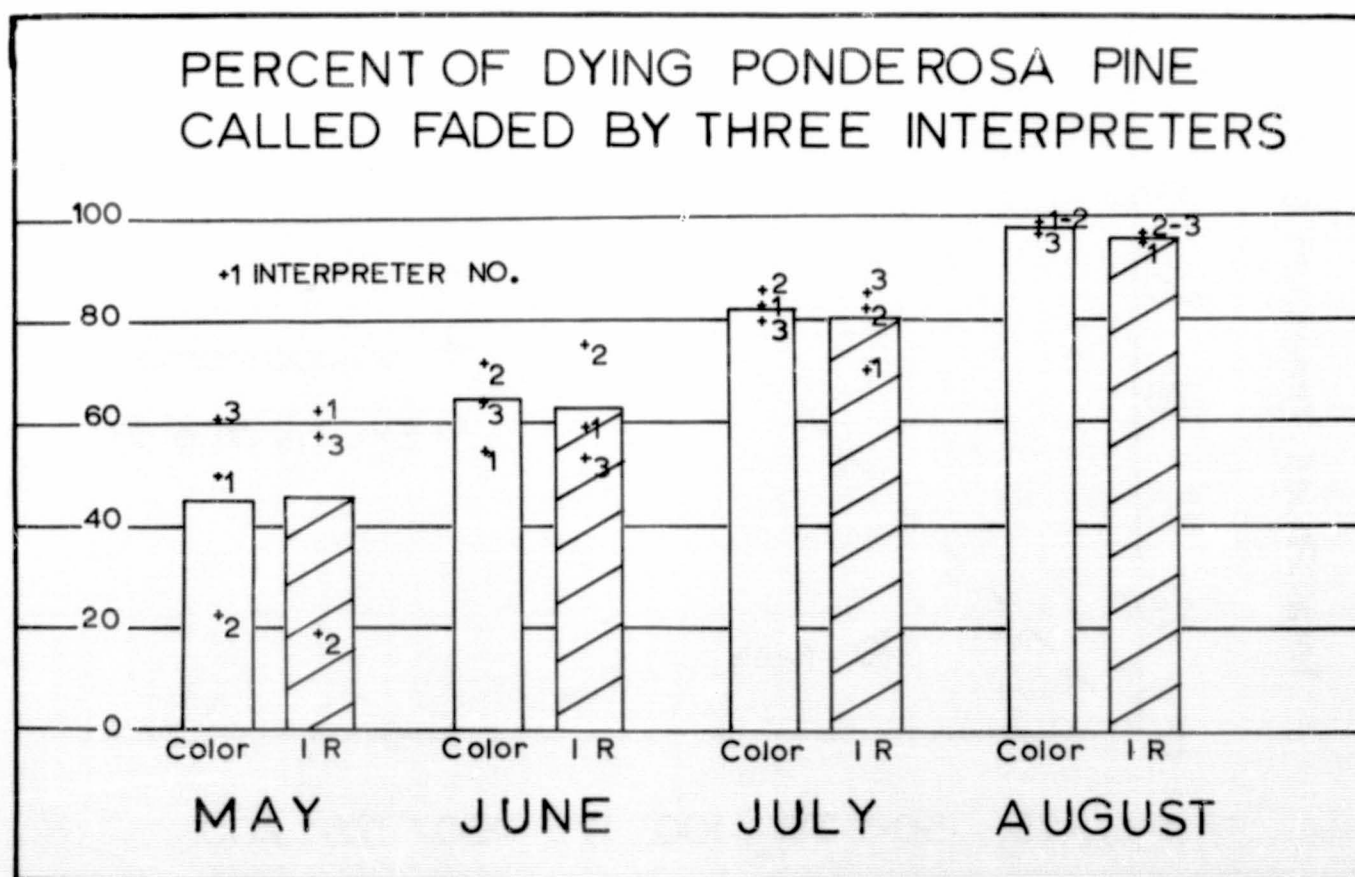


Figure 37-19.- Photointerpretation results. Comparison of photointerpretation results from three experienced photointerpreters using Anscochrome D/200 and Aero Ektachrome IR films at 1:1584 scale with total number of ground infested trees. Note the increased ability to detect infested trees as the season progresses and also the greater consistency of results obtained by the three interpreters in July and August.

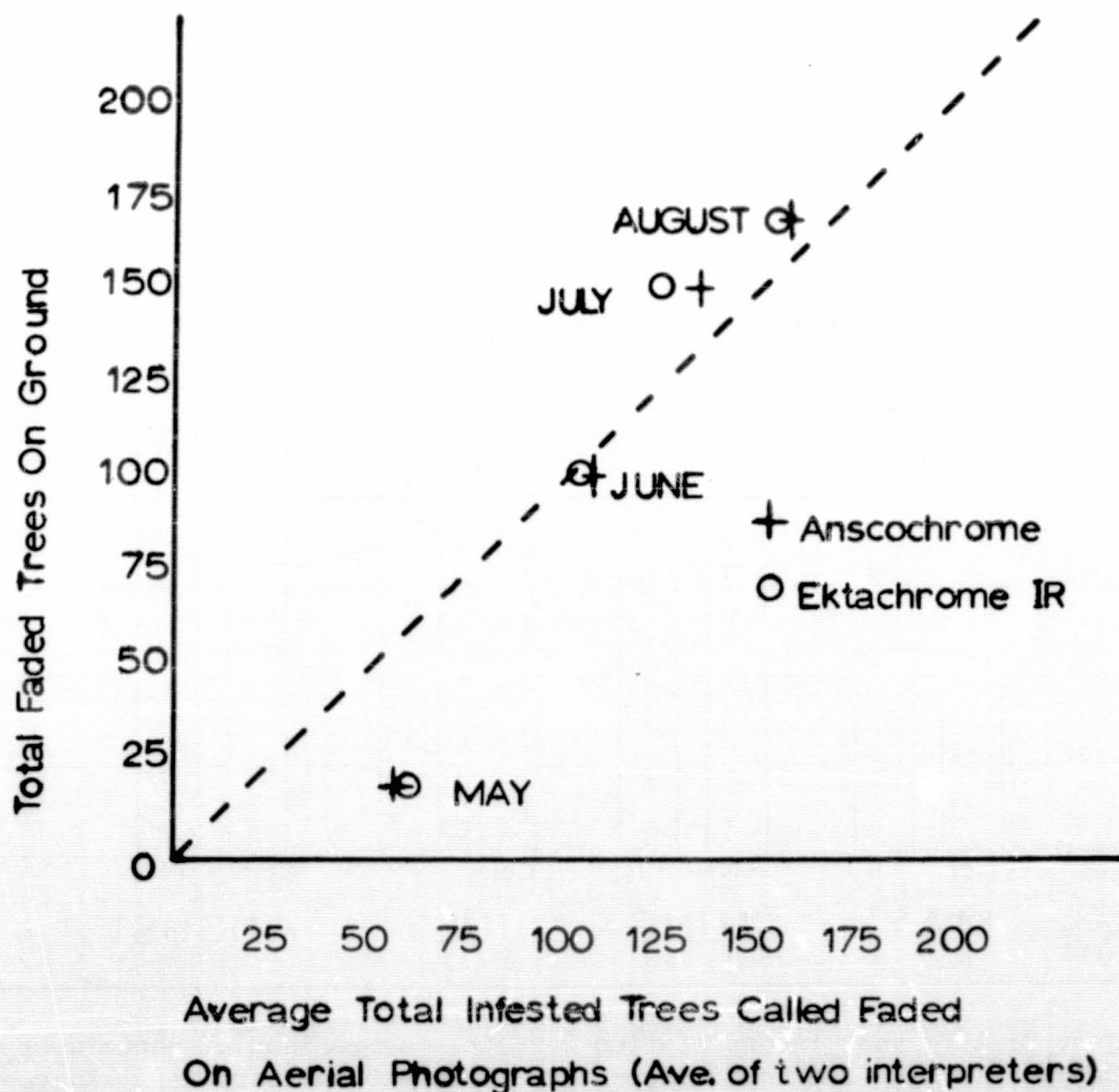


Figure 37-20.- Ground estimate of dying pines versus photointerpreter. Comparison of number of discolored infested trees seen on the ground with aerial photointerpretations of same trees. A total of 209 trees were examined by three interpreters on two films — Anscochrome D/200 and Aero Ektachrome IR — at each time period. The closer the plotted points to the dashed line, the closer the correlation. Note that photointerpreters discovered more trees in May than the ground observer.

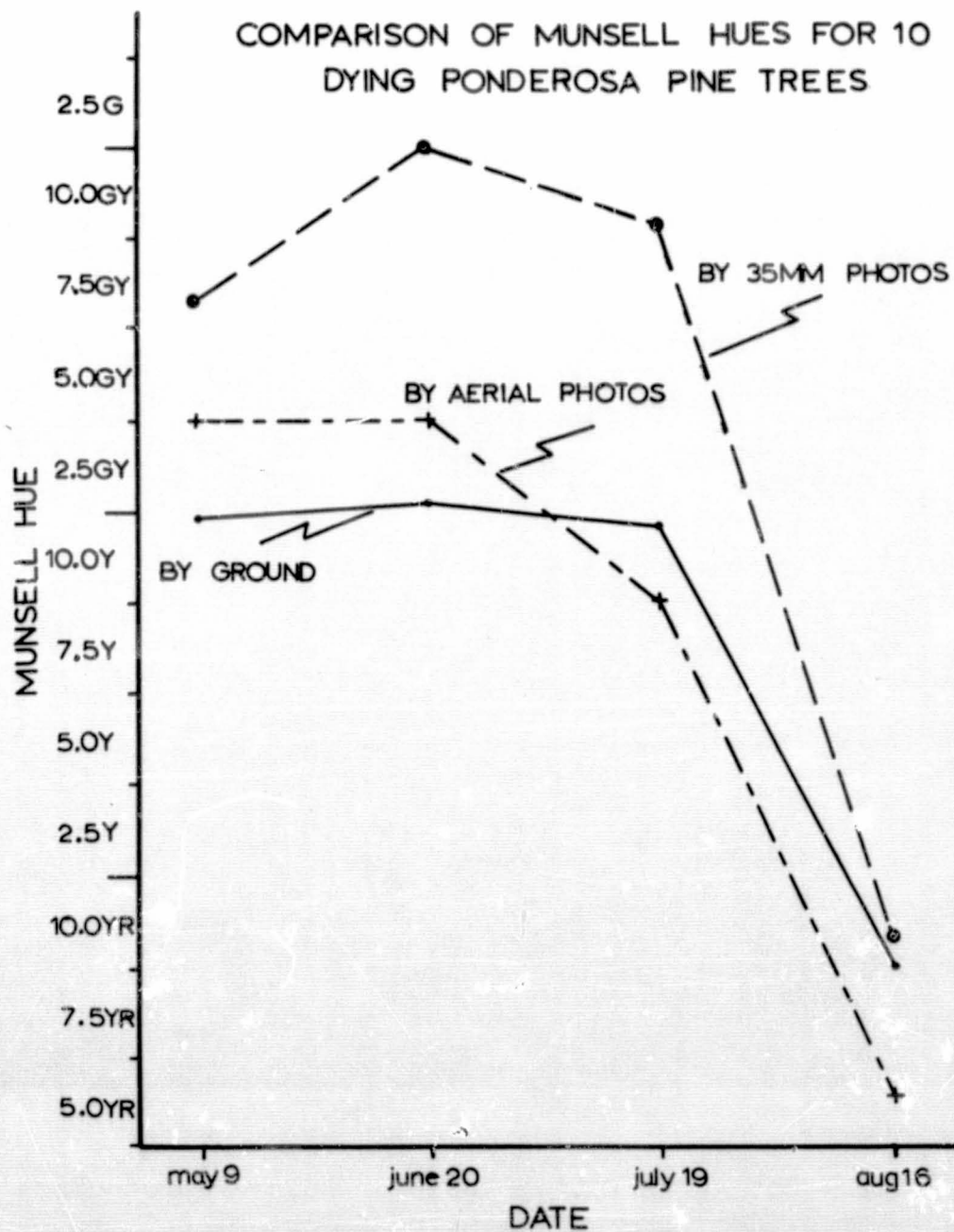


Figure 37-21.- Munsell hue notations by three methods. Comparison of Munsell hues of 10 sample trees taken by three methods (ground observation, 35-millimeter ground photographs, and aerial photographs) at four time periods.

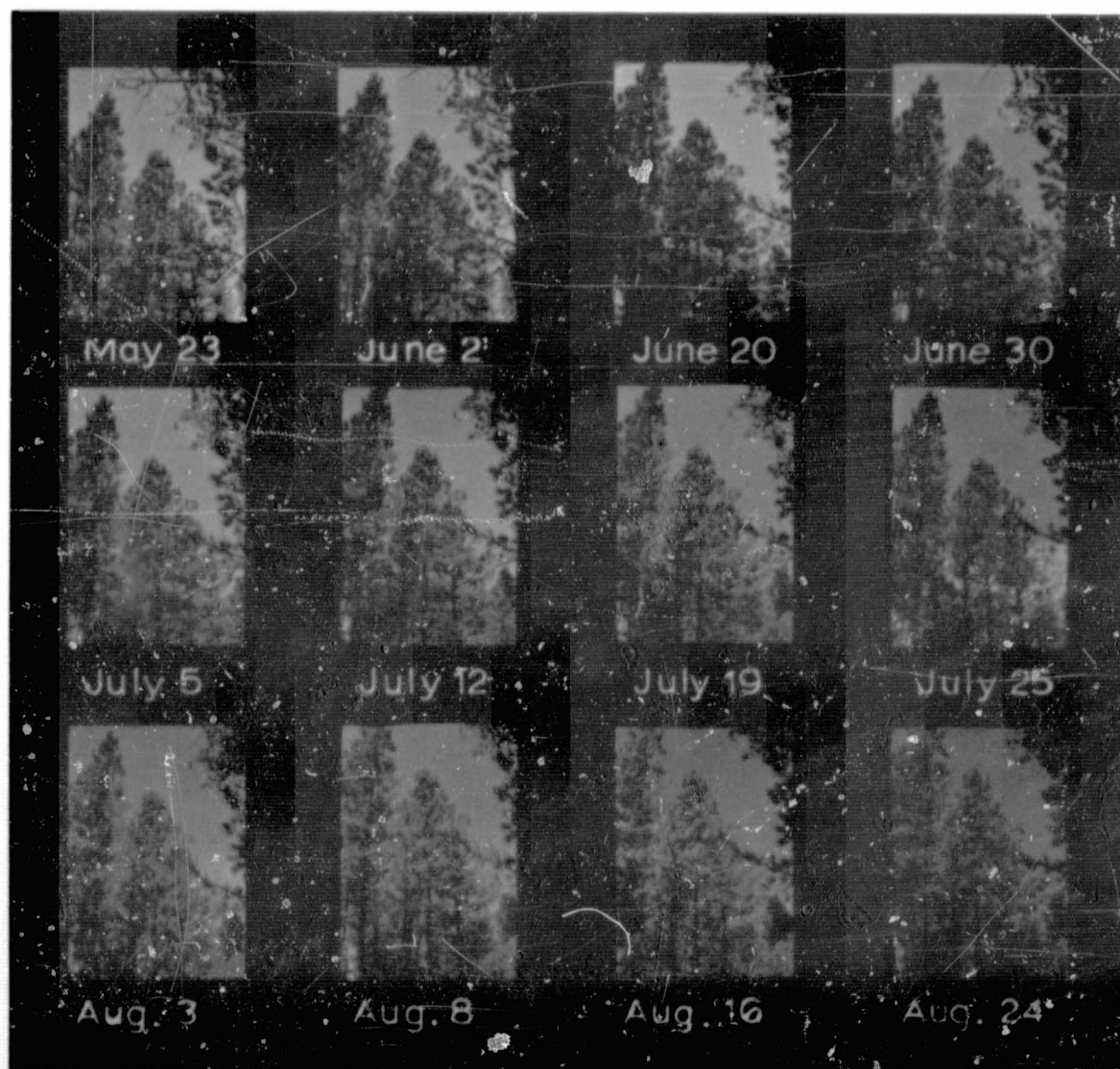


Figure 37-22.- Change in foliage color. Color reproduction of 35-mm color slides taken of dying ponderosa pine trees over a 12-week period from May to August 1967.

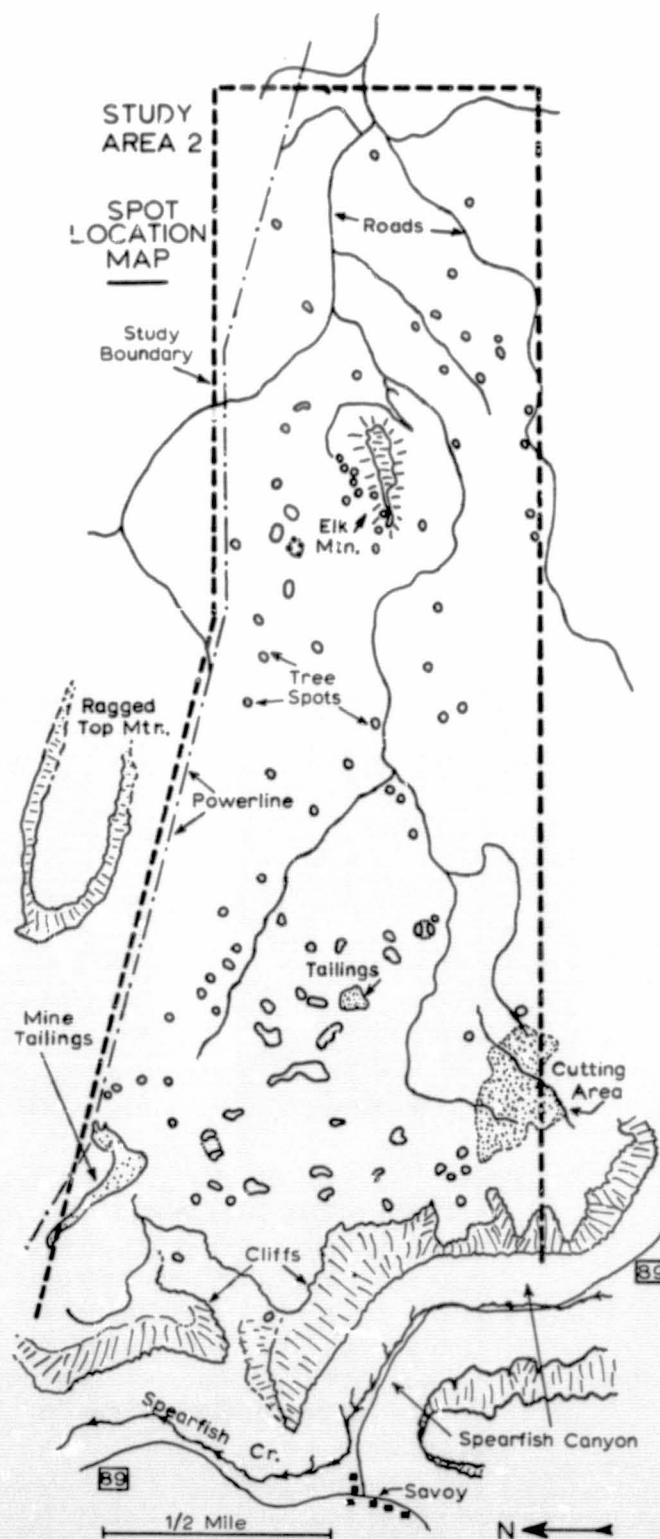
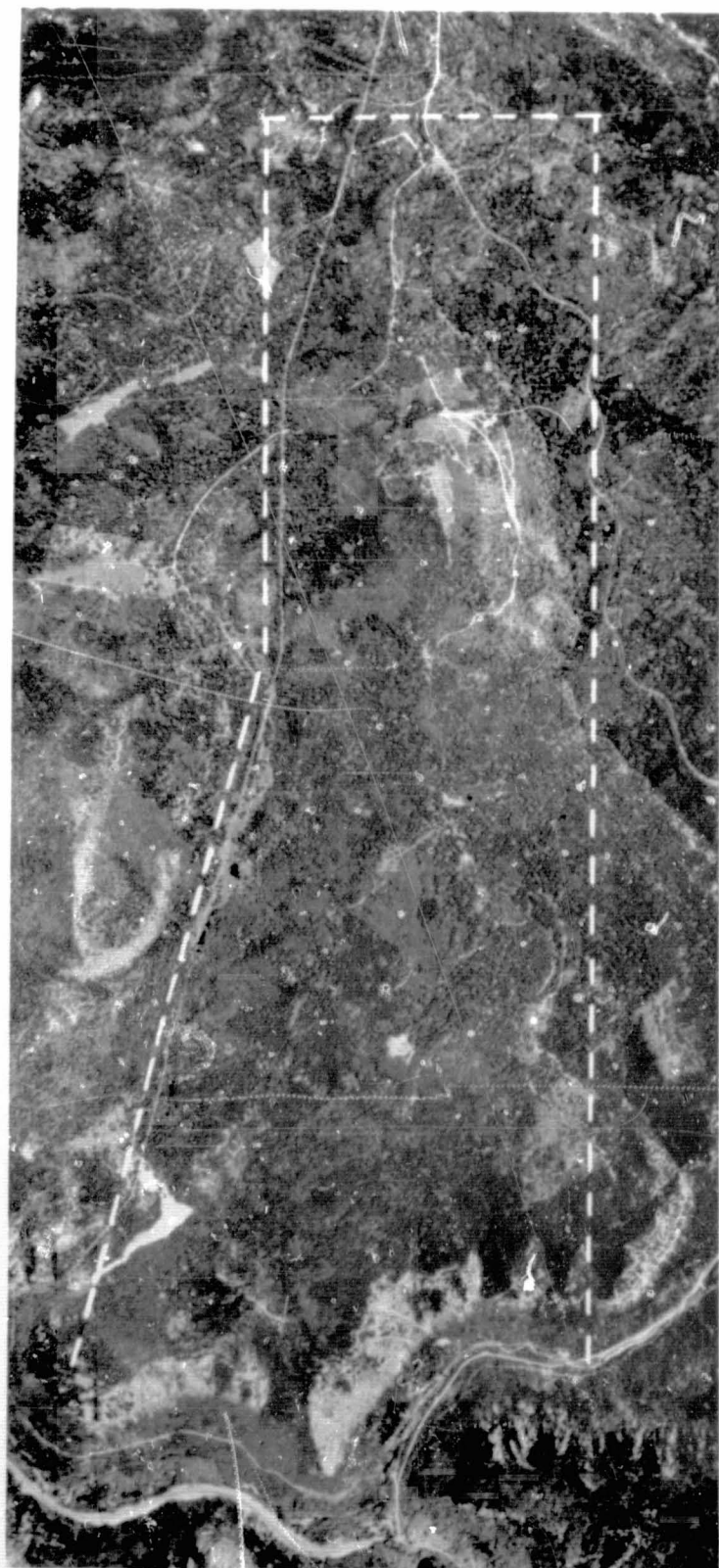


Figure 37-23.- Pilot study area enlarged from 1:116 000 scale Kodak Aero Ektachrome IR transparency. Adjoining base map shows infestation locations as plotted on ground.

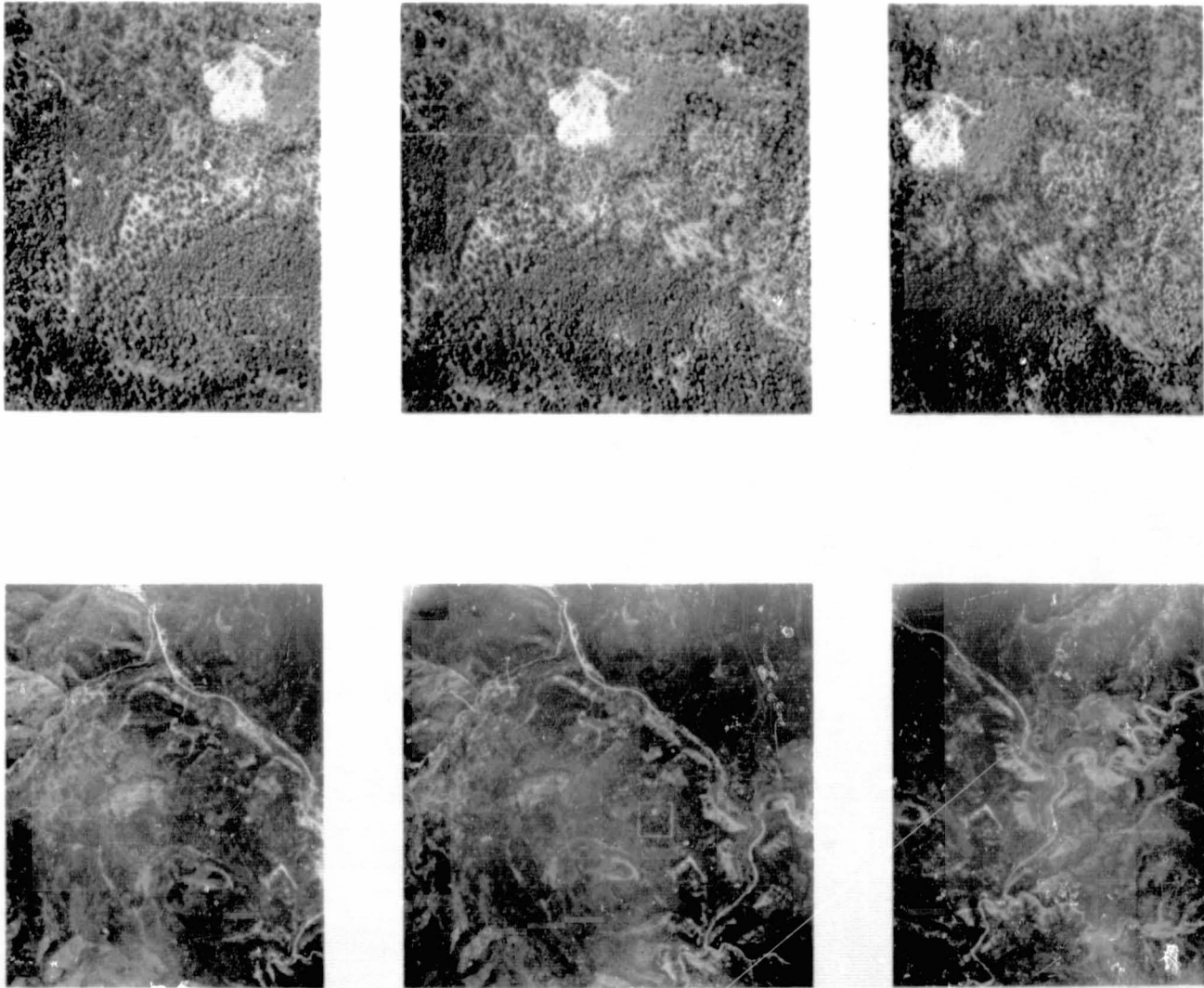


Figure 37-24.- Stereographic example of prints made from very small-scale (1:116 000) and normal-scale (1:7920) transparencies (Kodak Aero Ektachrome IR) of Black Hills beetle infestations near Lead, South Dakota. Newly dying foliage of ponderosa pine trees attacked 1 year prior to photography appears pink to white and yellow; foliage of trees attacked 2 years prior to photography appears yellow-red to green on the 1:7920 prints. The coverage of the 1:7920 scale can be related to the white etched line on the center photograph of the small-scale print.

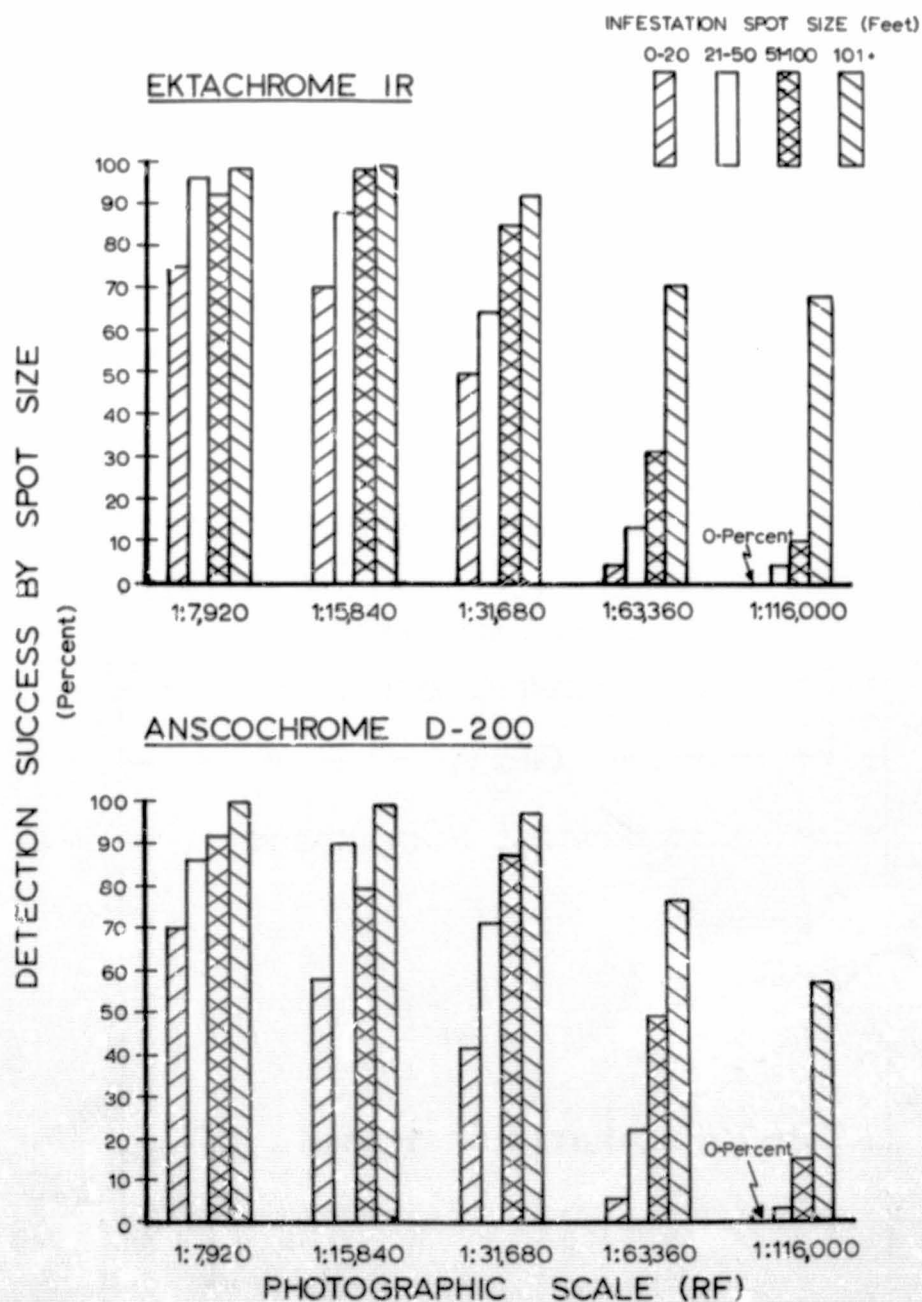


Figure 37-25.- Detection success (mean of three interpreters) expressed as a percent for four infestation size classes (in feet), five photograph scales, and two films. The upper chart shows percent correct on IR color film, the lower chart on color film. Notice that detection is better on IR color at the larger scales (1:7920, 1:15 840, and 1:31 680). On the smaller scales used to simulate space photography, detection is greater for all infestation sizes using color film.

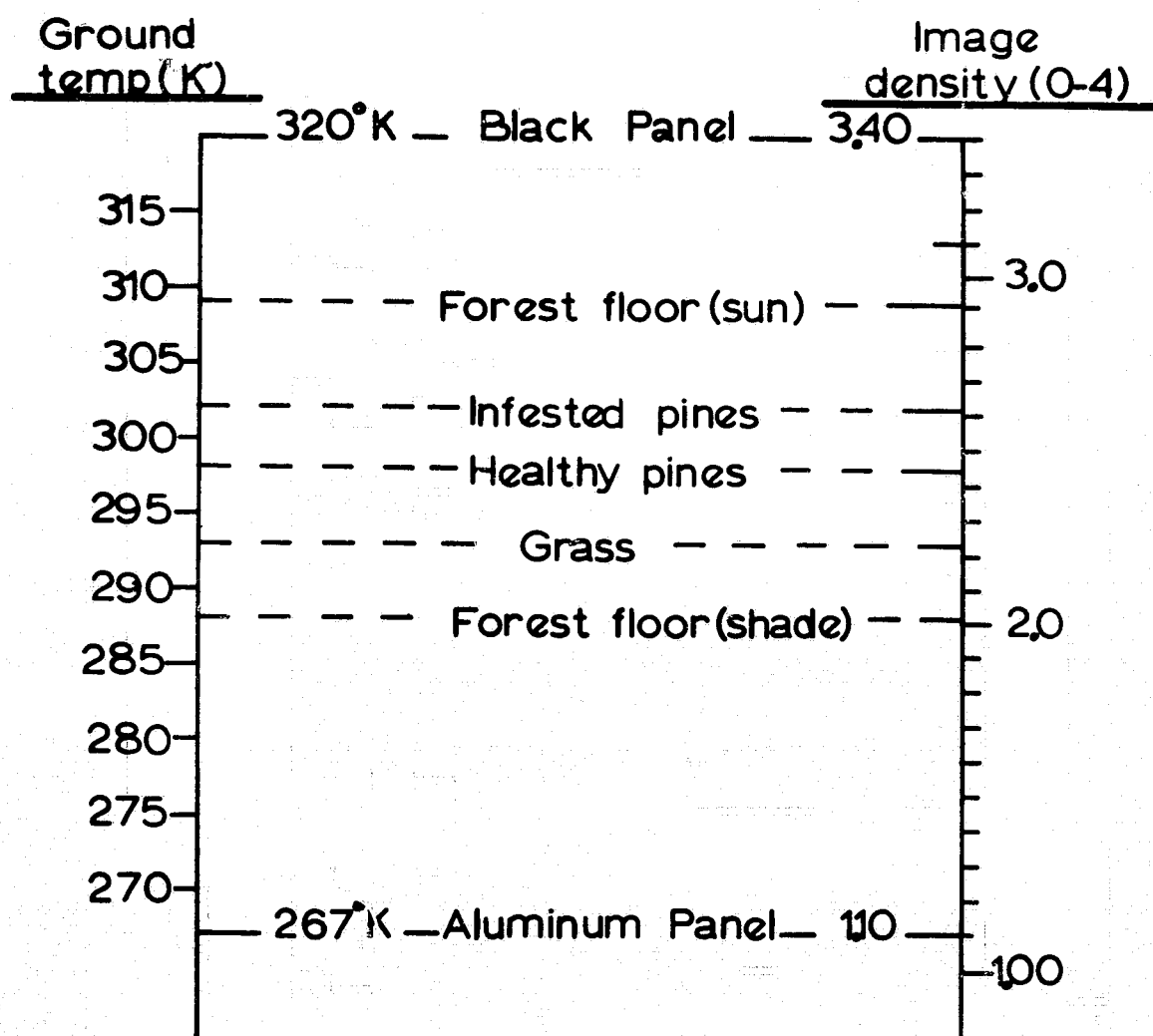


Figure 37-26.- Comparison of ground temperatures obtained with a Barnes PRT-5 instrument related to thermal image density on film determined by G.A.F. microdensitometer.

N71-16160

THE IDENTIFICATION OF WESTERN FOREST SPECIES

BY MEANS OF REMOTE SENSING

By Donald T. Lauer
School of Forestry and Conservation,
University of California

INTRODUCTION

The primary objective of the research reported herein has been to analyze systematically each of several factors governing the interpretability of tree species on high-altitude, small-scale imagery obtained by remote sensing. This research has sought, in particular, to determine which image characteristics are most useful for identifying the major tree species and timber types that occur in the western United States.

Data acquired from the NASA aircraft are discussed and illustrated in the form of certain advanced techniques such as (1) acquisition of sequential imagery, (2) acquisition of spectrozonal imagery, and (3) false color image enhancement of multiband imagery. In addition, a comparison has been made to determine the ease with which tree species composition, timber-type boundaries, and cultural patterns can be interpreted on Gemini photography and on a 10- by 15-foot aerial photographic mosaic comprised of 3200 conventional aerial photographs suitably reduced in scale.

RESULTS ACQUIRED THROUGH THE USE OF DATA
FROM NASA AIRCRAFT

NASA test site, 48 (San Pablo Reservoir) occurs in the California Coast Range, chaparral-hardwood forest type. Predominant pure-stand types are (1) Pinus radiata (Monterey pine), (2) Eucalyptus globulus (blue gum eucalyptus), (3) Quercus agrifolia (coast live oak), (4) Umbellularia californica (California bay), (5) Salix sp. (willow), (6) Aesculus californica (buckeye), and (7) mixed hardwood (bigleaf maple, madrone, buckeye, coast live oak, and California bay).

On June 6 and 7, 1965, and on September 28 and 29, 1965, the Houston-based NASA remote-sensing Convair airplane flew at high and low

altitudes over the test site with the following film-filter combinations: (1) Aerial Ektachrome (E-3) film with no filter, (2) Ekta Aero infrared (IR) film with a Wratten 12 + EF 2200 filter, (3) Panchromatic Plus-X Aerographic film with a Wratten 12 filter, and (4) IR Aerographic film with a Wratten 89B filter. Subsequent office and field work involved a detailed interpretation of all available photography. Hypotheses were formulated and tested in an effort to determine the optimum film-filter combination, photographic scale, and season of year for the identification of forest species found to occur in this region. From this analysis, a dichotomous aerial photointerpretation key for the timber species examined in this area was made and was illustrated in the 1966 Annual Progress Report.

In 1967, a 100-percent ground-truth survey of the timber resources (providing information of timber-type boundaries, stand composition, and stand density) was made with the aid of large-scale NASA photography for a continuous strip one-half mile wide and 5 miles long. The data obtained by photointerpretation were compiled in the form of planimetric maps illustrated in color. Each annotated map represents a summation of the information derived from photointerpretation of each of the four film-filter combinations used in this test. With a dot-grid overlay system, each map was compared with the ground-truth map for the same area, thereby enabling a quantitative analysis to be made. Among the factors quantified were the usefulness of photointerpretation keys, and the relative accuracy of timber stratifications and individual tree species identifications on each film-filter combination.

On August 15, 1967, and on May 27, 1968, the Houston-based NASA remote-sensing Convair airplane flew the test site at altitudes of 2000 and 20 000 feet with the following sensors and films: (1) Reconofax IV thermal IR imagery, (2) AAS-5 ultraviolet (UV) imagery, (3) black and white multiband photography, and (4) Ekta Aero IR photography. Concurrent with the aerial mission, a ground crew recorded ground truth by taking 35-millimeter stereo pair terrestrial photographs of each of the vegetation types found to occur in the area. In addition, surface-temperature measurements were made of representative terrain features and were subsequently correlated with the thermal imagery.

A detailed study of the previously discussed photography has been made. The following general conclusions apply to the major factors governing the interpretability of small-scale remote-sensing imagery for identifying the major tree species and timber types in selected parts of the world. Figures 38-1 to 38-9 illustrate with the aid of data obtained by the NASA aircraft (1) how correlations can be made between spectrometric analyses and photographic tones as imaged on various multiband images and (2) the value of interpretation results obtained from sequential imagery, spectrozonal imagery, and Gemini photography.

Photographic Tone or Color

It is quite generally recognized that the photographic tone or color registered by an object is a function of (1) spectral reflectance characteristics of the objects; (2) the film-filter combination employed (since this governs the spectral zone in which a photographic exposure is made); (3) the spectral nature of the energy source which illuminates the object; and (4) certain atmospheric haze effects which modify both the spectral composition of the energy that illuminates the object and the spectral composition of the energy reflected from the target as it travels toward the camera or other sensing device. It was not considered appropriate in the present study to make an exhaustive study of each of these many factors. However, a few pertinent conclusions were drawn from this study:

1. Film-filter combination. Photography taken in a combination of bands of the spectrum offers advantages over single-band types. Multiband photography utilizing the green, red, and near-IR zones of the electromagnetic spectrum (500 to 900 m μ) appears to be the most useful form of spectrozonal imagery when attempting to inventory forest species composition from earth-orbital altitudes.

2. Reflectance characteristics of the object. It appears highly feasible to evaluate, from earth-orbiting reconnaissance satellites, certain life-cycle, seasonal, and possibly daily variations in the reflectance characteristics of different vegetation types. Because no generalizations can be made regarding physiologically induced reflectance characteristics for all forest types, a final determination of the optimum timing of image acquisition for a particular region is ultimately made through periodic field observations.

3. Spectral composition of the energy source. In order to avoid troublesome "hot spots," unfavorable shadow characteristics, and failures in film reciprocity, photography procured from space should be taken during midmorning or midafternoon hours. (A midmorning timing may be preferable in order to avoid atmospheric disturbances that accumulate during daylight hours.)

4. Atmospheric haze effects. Haze interference is a potential problem when photographing the surface of the earth from space. Because shorter wavelengths are scattered the most, properly selected spectrozonal photography which eliminates these wavelengths reduces haze interference problems.

Photographic Detail

1. Photographic scale. Long-focal-length, high-resolution systems planned for satellite reconnaissance could theoretically resolve detail small enough to reveal many morphological features of individual tree crowns and thus facilitate tree species identification.

2. Resolution characteristics of the lens and film. Optically precise lenses and fine-grained, medium-contrast, and high-resolution films should be used in order to assure maximum photographic detail.

3. Image motion. Image blur, a potentially serious problem in space photography, can be remedied by using the principle of forward-motion compensation.

Stereoscopic Parallax

Stereoscopic parallax is unlikely to be a useful photographic-image characteristic when attempting to identify individual tree species and stand types in space photography. Because of the adverse ratio of flying height to tree height, stereoscopic parallax (and consequently depth perception) is negligible on satellite photographs. However, an ability to fuse conjugate images may give a desirable binocular reinforcement that significantly improves the signal-to-noise ratio when overlapping satellite photographs are being studied.

Perception and Interpretation of Imagery

1. Visual and mental acuity of the image analyst. Personnel should be selected on a basis of proper motivation; patience; good judgment; a capability for deductive reasoning; and high acuity for the perception of tone and color, image sharpness, and the binocular fusion of conjugate images.

2. Interpretation equipment and techniques. Image enhancement by means of projection techniques (as described in the 1967 report) can greatly facilitate the interpreting of forest species on multiband photography. Not only are several images viewed simultaneously by this means, but minute tone differences between objects of interest are enhanced and converted to more readily discerned color differences.

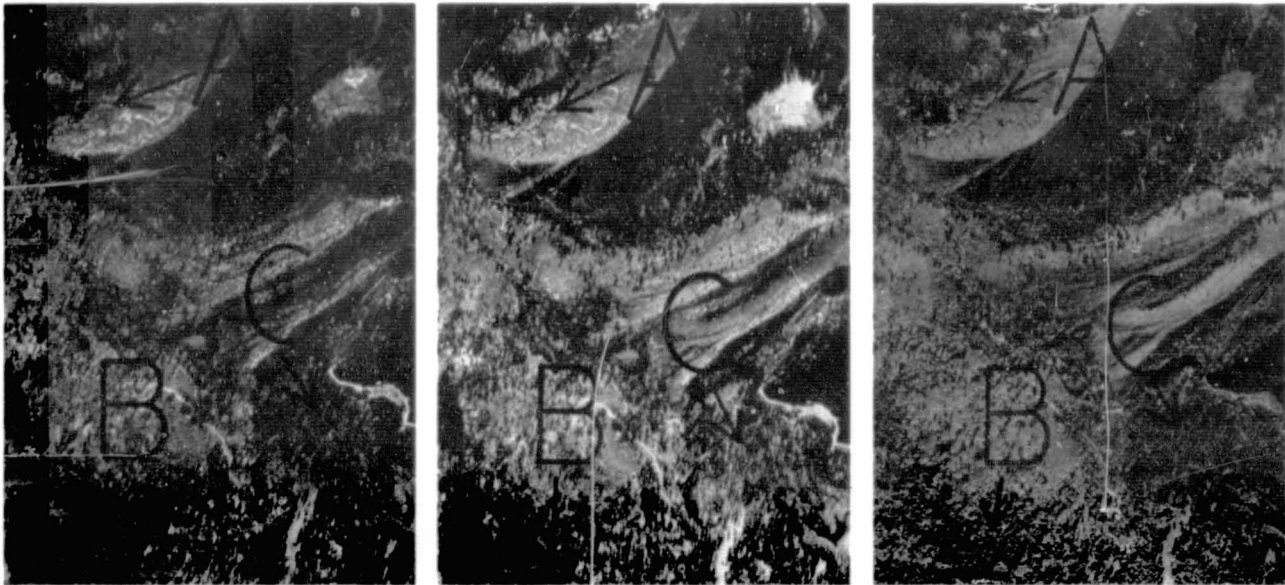
3. Film exposure and processing. Accurate light-meter readings and corrections to exposure time according to filter factors should be made because variations from optimum exposure are likely to result in reduced accuracy when interpreting image tone or color.

4. Training aids. An image analyst can often identify tree species or other features of interest within an unfamiliar area if some type of reference material or guide is available, depicting such features as imaged either in the area to be studied or in a similar area. Probably the most useful training aid yet developed for this purpose is the photo-interpretation key.



Figure 38-1.- Brazilian and Mexican representatives were cordially invited to observe and participate in forest remote-sensing activities for a combined period of 1 month (May 12 through June 8). Aerial photography, flown May 26 and 27 by the Houston-based Convair aircraft, was quickly processed at the MSC photography lab and immediately returned to the principal investigator in the field. Six days after the photography mission, the principal investigator and foreign visitors were on site evaluating the usefulness of aerial photography for forestry purposes.

Meadow Valley-Bucks Lake Test Site, California



Film: Panchromatic
Filter: Wratten 47B
Sensitivity: 340 to 500 m μ

Film: Panchromatic
Filter: Wratten 25A
Sensitivity: 590 to 710 m μ

Film: Infrared
Filter: Wratten 89B
Sensitivity: 700 to 950 m μ

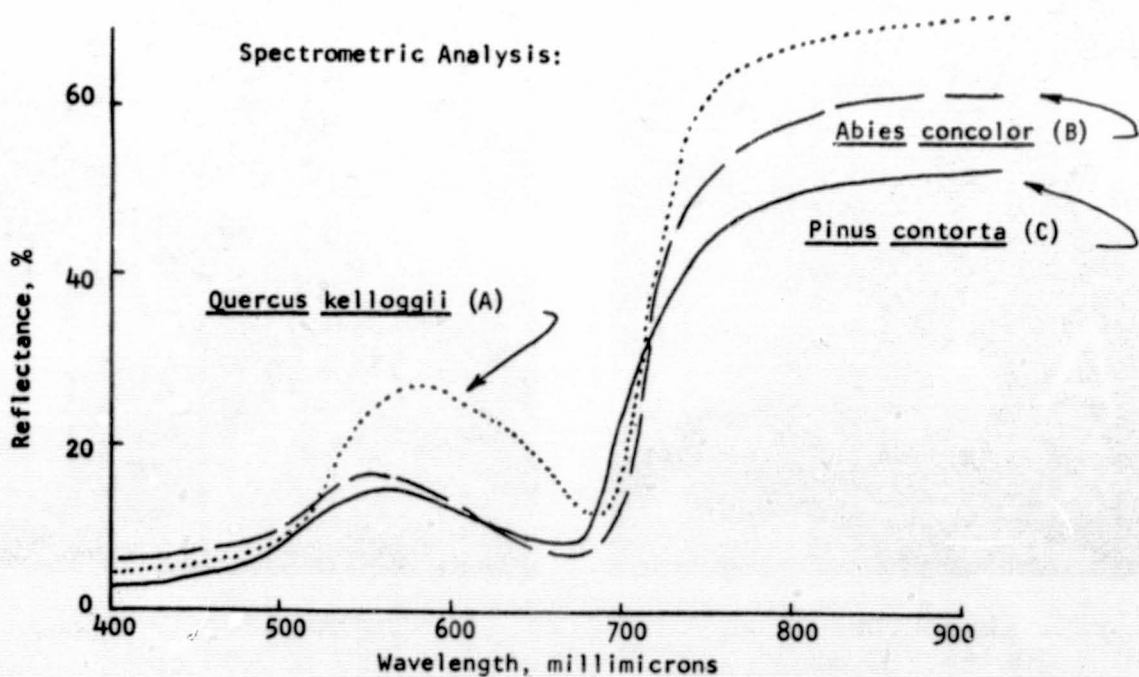
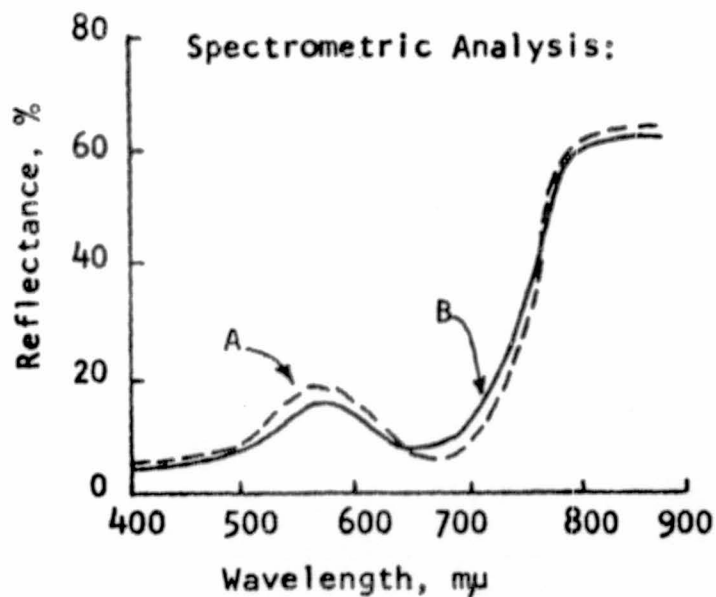
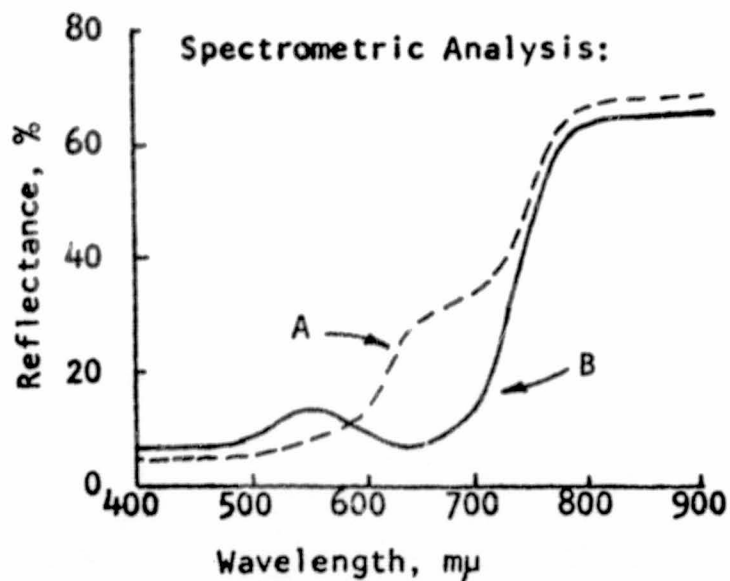


Figure 38-2.- Photography taken in a combination of bands of the spectrum offers advantages over single-band photography for the mapping of vegetation types. In the example shown here, correlations can easily be made between light reflectance curves of three Sierra Nevada vegetation types and the tones of these types as imaged on the various film-filter combinations.

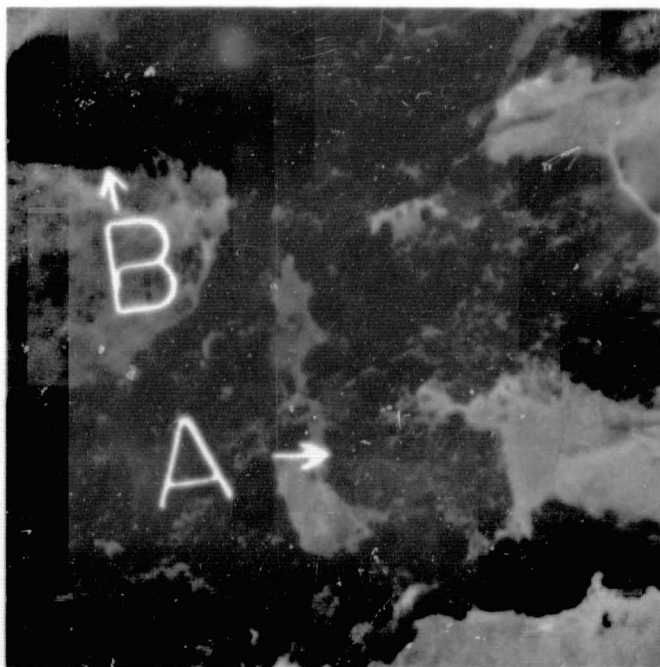
SUMMER SEASONAL STATE



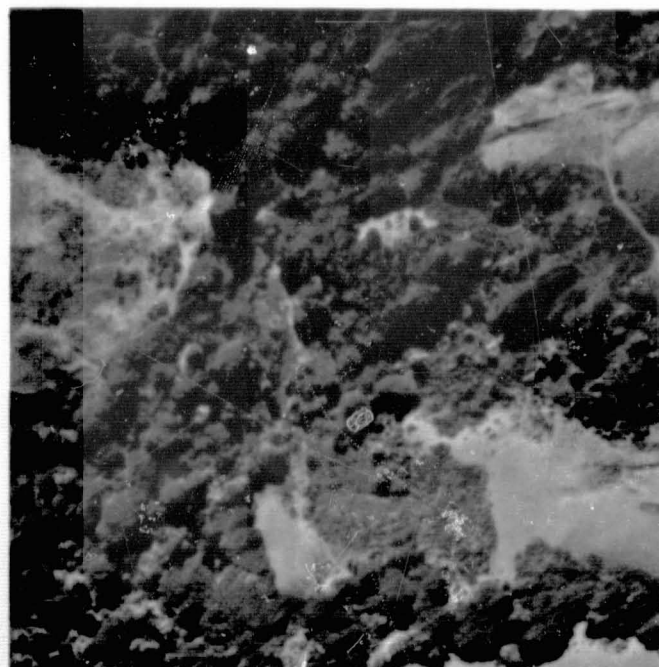
FALL SEASONAL STATE



Fall Seasonal State



Aerial Ektachrome film,
300 to 730 $m\mu$



Ektachrome Aero IR film,
510 to 900 $m\mu$

Figure 38-3.- Increased accuracy can be obtained when distinguishing deciduous from evergreen species if care is taken in selecting the optimum season of photography. Rhus diversiloba (poison oak) at A, when exhibiting a brilliant fall coloration, is easily separated from Baccharis pilularis (coyote brush) at B. At most other seasons of the year, these species are difficult to differentiate. (San Pablo Reservoir Test Site, California).



Photograph 1
Film: Ektachrome Aero IR
Filter: Wratten 15
Date: September 1965

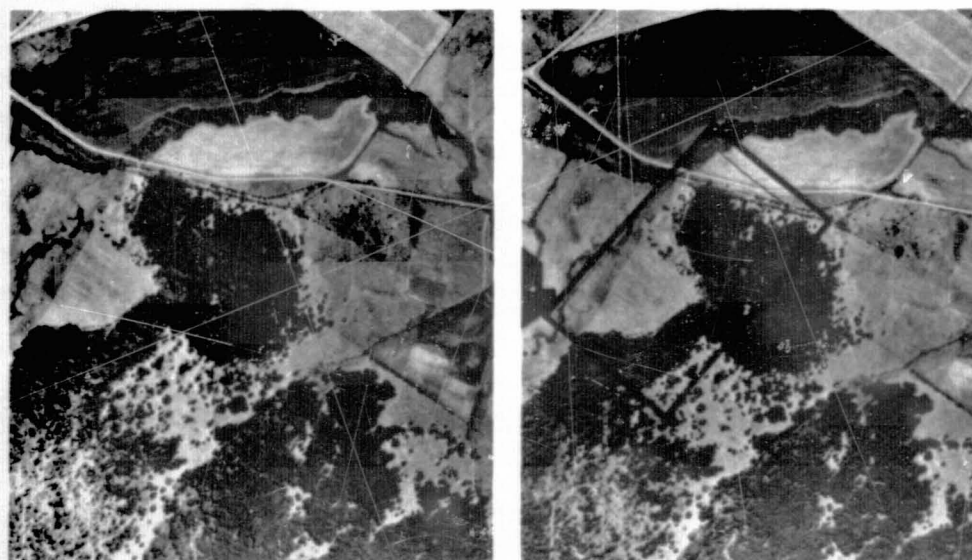


Photograph 2
Film: Ektachrome Aero IR
Filter: Wratten 15
Date: October 1967



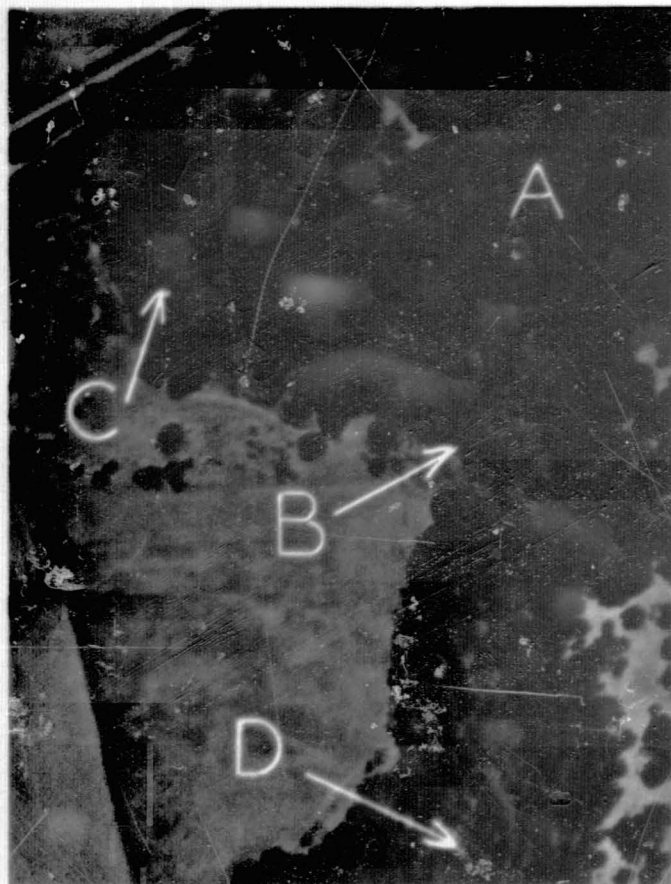
Photograph 3
Film: Ektachrome Aero IR
Filter: Wratten 15
Date: May 1968

Figure 38-4.- Seasonal variations in the reflectance characteristics of different terrain features and conditions can be observed on high-quality sequential imagery. In this example, note the ease with which fluctuations in water level can be observed over a period of time. On photograph 1, Rhus diversiloba (poison oak) at A and B is easily identified because of its unique fall coloration. Fresh water seepage at C, an important resource for the maintenance of range and wildlife animals, is most easily observed on photograph 2. (At this time of year, the high IR reflectance from lush grasses and forbs contrasts greatly with adjacent dry areas exhibiting low IR reflectance). Stands of Baccharis pilularis (coyote brush), an undesirable brush species, were sprayed from a helicopter with a mixture of 2-4-D and 2-4-5-T, a "brush killer," in the spring of 1967. The effectiveness of this brush removal technique is best evaluated on photography flown during the following growing season (photograph 3). Note on photograph 3 areas of complete kill at D, hardwood vegetation unaffected by the spray at E, and an area at F where the spraying technique was only partially successful. (Surviving leaf material exhibits high IR reflectance, resulting in a reddish tone on the Ektachrome Aero IR photograph). (San Pablo Reservoir Test Site, California).

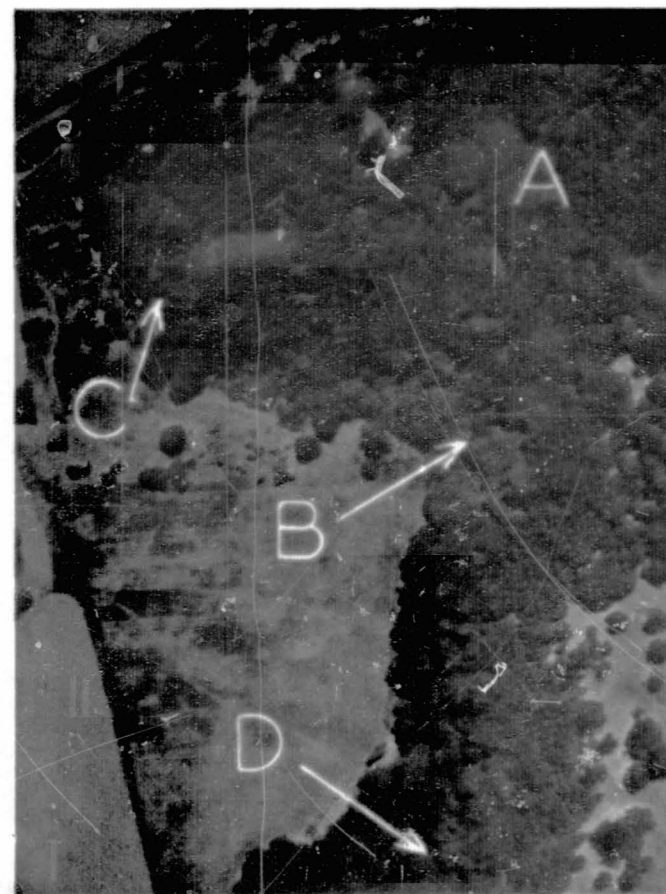


a. Film: Panchromatic
Filter: Wratten 15
Scale: 1:20 000

Figure 38-5.- Species composition: Quercus garryana (Oregon oak) at A, Acre macrophyllum (bigleaf maple) at B, and Pseudotsuga menziesii (Douglas fir) — a young stand at C and a mature stand at D. Note the lack of color contrast between young Douglas fir (a merchantable species) at C and the surrounding hardwood stand (unmerchantable species) on the Ektachrome Aero IR photography. However, sufficient color contrast on Aerial Ektachrome facilitates the detection of this valuable species. Nevertheless, the color of areas B and C is so similar on the Ektachrome photograph that only when it is used in conjunction with the Ektachrome Aero IR photography can anyone be sure which trees are young Douglas fir and which are bigleaf maple. (Sheridan study area, Oregon.)

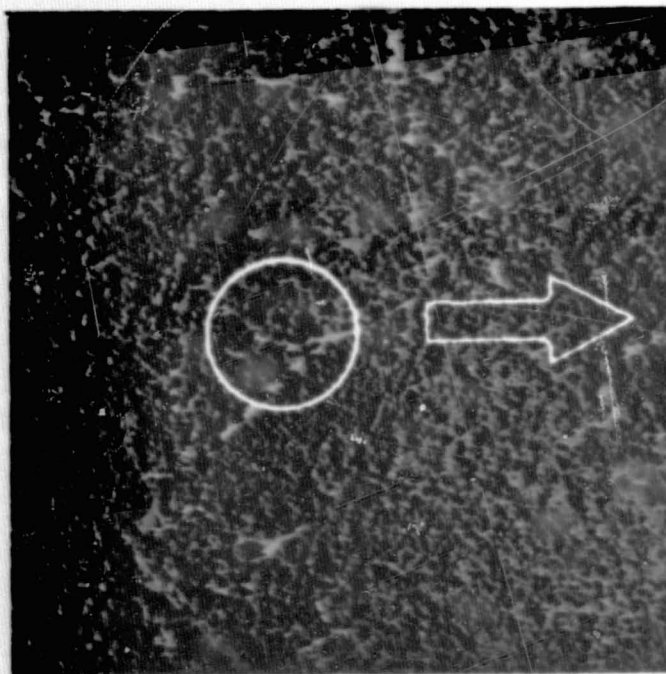


b. Film: Aerial Ektachrome
Filter: None
Scale: 1:3500

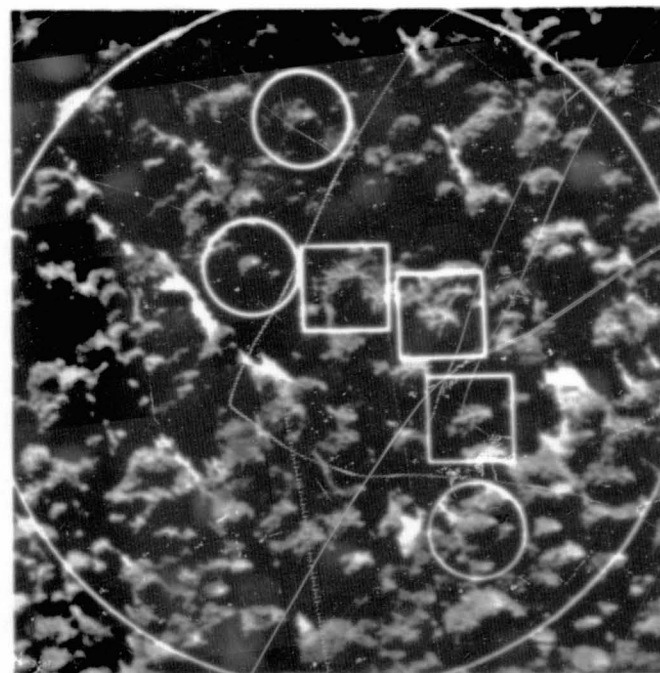


c. Film: Ektachrome Aero IR
Filter: Wratten 12 plus EF 2200
Scale: 1:3500

Figure 38-5.- Concluded.



a. Film: Aerial Ektachrome
Scale: 1:10 000



b. Film: Aerial Ektachrome
Scale: 1:2500

Figure 38-6.- Pinus lambertiana (sugar pine), squared, and Abies concolor (white fir), circled, can easily be identified on the larger scale aerial photograph shown above by virtue of such crown characteristics as branching habit and shape of crown apex. On the smaller scale photograph, these tree species are much more difficult to identify because there is insufficient detail discernible. However, long-focal-length, high-resolution systems planned for satellite reconnaissance could theoretically resolve detail small enough to reveal many morphological features of tree crowns and thus facilitate tree species identification. (Blodgett Forest study area, California)

Pinus lambertiana (sugar pine)

Crown Apex:



Truncate

Crown Margin:



Parted

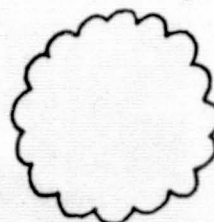
Abies concolor (white fir)

Crown Apex:



Acute

Crown Margin:



Crenate

c. Comparison of Pinus lambertiana and
Abies concolor

Figure 38-6.- Concluded.

Meadow Valley-Bucks Lake Test Site, California

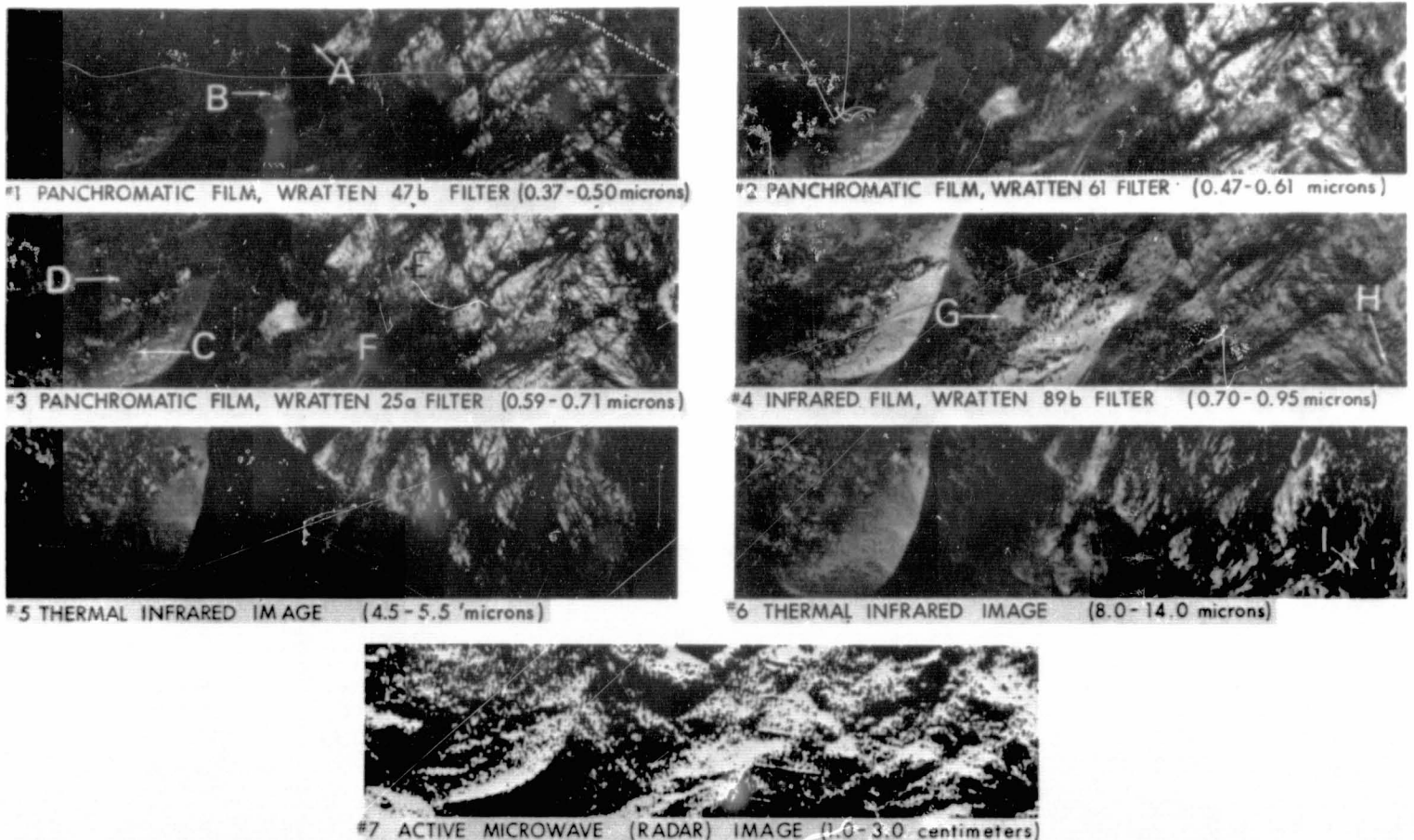


Figure 38-7.- Spectrozonal imagery offers unique advantages in determining forest species composition and mapping vegetation types. For example, note the degree of shadow penetration at A on image 1. Also, two different plant communities are easily mapped in a meadow at B. Only on image 3 can Quercus kelloggii (black oak) at C be discriminated from Pinus ponderosa (ponderosa pine) at D. In addition, note how unproductive granite outcroppings at E can be differentiated from potentially productive brushlands at F. Deteriorating stands of Pinus contorta (lodgepole pine) at G are most easily separated from healthy Abies magnifica (red fir) at H on image 4. Bare ground at I can be distinguished from most other terrain types on image 6.

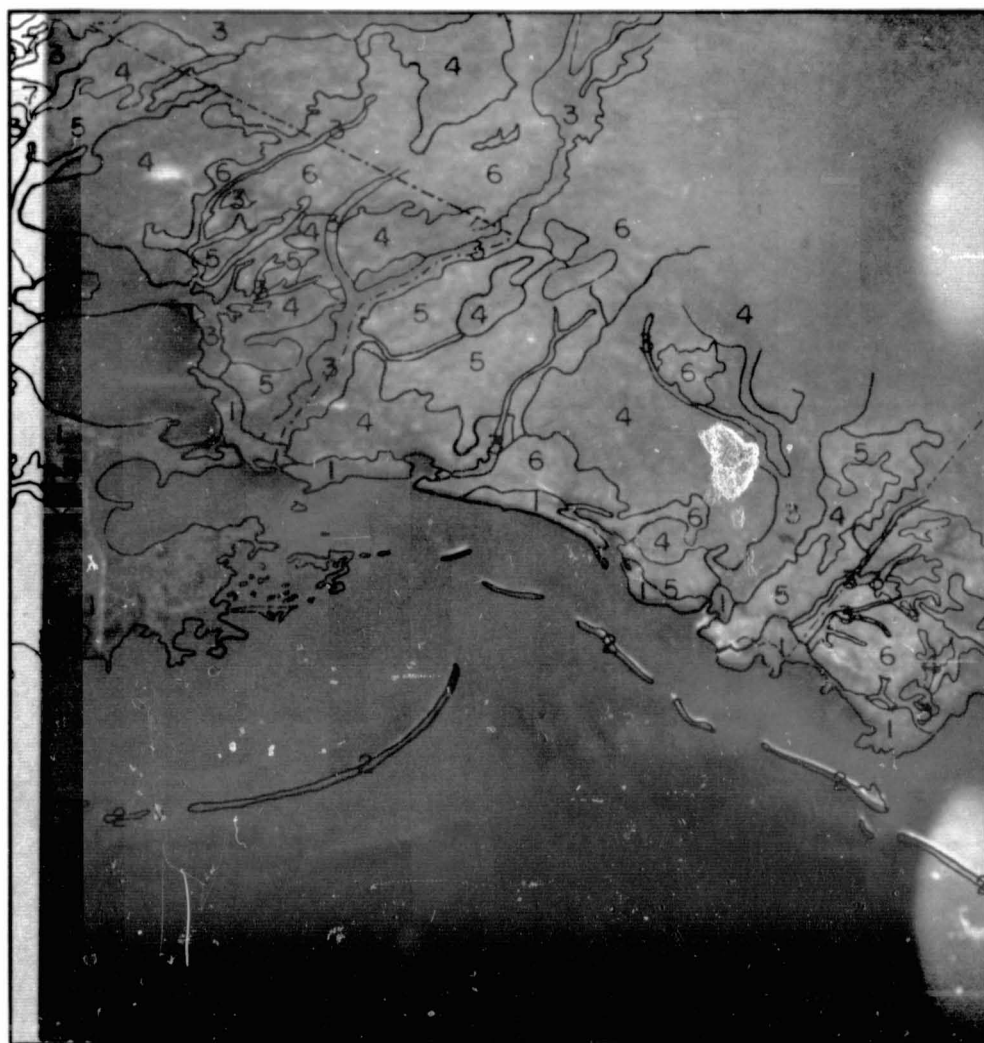


Figure 38-8.- A three-diameter enlargement of an Ekta Aero IR duplicate transparency taken from Gemini VII on December 7, 1965, over the southeastern United States. By comparing the interpretation data here with those of figure 38-9, note the accuracy with which certain vegetation types and culturally induced vegetation patterns were mapped on the Gemini photograph. The annotated types are as follows: (1) coastal tidal marshes or prairies, (2) coastal beaches or sand dunes, (3) bottomland hardwoods, (4) conifer forests with varying concentrations of hardwoods, (5) grassland areas, (6) areas of general farming, and (7) sugarcane fields. Photographic tone and color are the primary criteria used for image analysis. Because of the poor resolution capability at the great altitude of the sensing system used, photographic detail provides little information. Note how such factors as film-filter combination (IR sensitivity), reflectance characteristics of the terrain features (deciduous hardwoods in a leafless state, dead grass, and evergreen conifers), and atmospheric effects (concentration of CO_2 and water vapor) affect the interpretability of photographic tone and color.

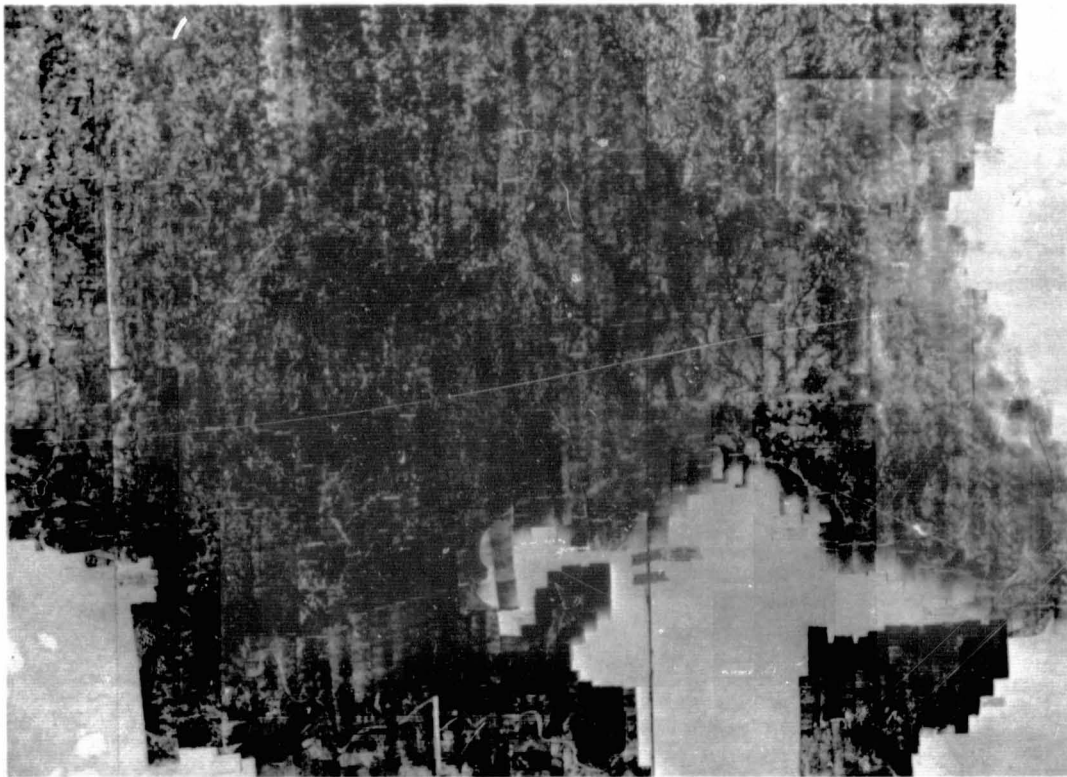


Figure 38-9.- For purpose of comparison, the 3200 conventional aerial photographs that were required to cover a portion of the area shown on the Gemini photograph were examined in mosaic form. The mosaic is somewhat easier to interpret than the Gemini photograph because of an increase in photographic detail, which primarily is a result of increased photograph scale. Yet certain advantages of mosaic coverage often are offset by limitations. Among the advantages of a spaceborne image over a conventional photomosaic are (1) synoptic view, (2) opportunity for sequential coverage, (3) rapidity of obtaining data, (4) uniformity of the image, and (5) economy.

N71-16161

REMOTE-SENSING APPLICATIONS FOR THE INVENTORY
OF RANGE RESOURCES

By David M. Carneggie
School of Forestry and Conservation
University of California, Berkeley, California

INTRODUCTION

This report summarizes the U.S. Department of Agriculture-NASA-sponsored research which investigates the feasibility of applying remote sensing, either from aircraft or spacecraft, as a tool for the inventory and management of range resources. Primary concern is focused upon (1) the results from our analyses of remote-sensing data procured by NASA-Houston aircraft, (2) applications and possible benefits to accrue from remote sensing, and (3) relationships between aircraft-program and space-obtained remote-sensing data.

It is important to define "range" and "range resources" at the outset in order that the reader has a clear idea of the environment and resource under investigation. Range is nonarable land capable of producing native forage or browse for consumption by domestic or wild grazing animals. It encompasses a variety of diverse wild-land environments which include tundra, semiarid regions, mountain meadows, open-forested areas, and savannas. Of the approximately 2.5 billion acres of land comprising the United States, there are nearly 1 billion acres of grazing land. Of this grazing land, over 50 percent is considered rangeland. It is estimated that 50 to 60 percent of the total number of grazing animals in this country spend all or part of their lives on rangeland. On a global basis, nearly one-half of the landmass is suitable for grazing use, and more than 60 percent of the grazing animals of the world use these ranges.

The term range resources applies to goods, services, products, and physical and biological features found on or derived from rangeland. It includes: vegetation (forage and browse), animal products, wildlife, water, timber, minerals, soil, and fish. Vegetation is the resource with which rangemen generally are most concerned because it is the annual forage and browse crop which is converted by grazing animals, both domestic and wild, into useful animal products (i.e., meat, milk, hides, wool,

etc.). The forage crop, like an agricultural crop, should be harvested annually if it is to be utilized and provide benefit, but unlike an agricultural crop, forage production may be highly variable in amount from one season to the next because of variation in the amount and distribution of rainfall and in temperature regimes and because of previous management practices.

On many ranges, grazing may be the most apparent and immediate, or the only use of the land, and economic return from this use may be quite low. On such ranges in particular, but on others as well, the water, recreation, timber, urban development, and wildlife values may likewise be very important for justifying an inventory of the range (e.g., through remote-sensing techniques) that will lead to better management of it.

RESULTS ACQUIRED FROM THE USE OF DATA FROM NASA AIRCRAFT

This section summarizes the results of 2-1/2 years of interpreting imagery (both photographs and thermal infrared (IR) images) of the Harvey Valley Range Test Site and the San Pablo Test Site, both located in California. Much of the data interpreted were supplied by NASA-Houston aircraft, which flew missions over San Pablo Test Site in June and September 1965, August 1967, and May 1968, and over Harvey Valley in September 1966, and October 1967. Additional photography and other imagery were obtained to supplement NASA aircraft imagery when it was necessary to investigate changes within a range environment occurring with time on sequentially obtained imagery.

It was possible to prepare table 39-I after various film-filter combinations were investigated and compared with each other and the thermal IR imagery and after imagery, including Gemini photography, was examined at various scales ranging from 1:600 to 1:84 000. Table 39-I indicates the feasibility of making significant interpretations of range features or conditions at varying levels of ground resolution. In such a table, it can readily be seen which film-filter combinations are more interpretable and at what level of ground resolution pertinent information which may be required for preparing improved range resource inventories begins to be lost. It should be recognized that interpretations of certain significant features is partially a function of the date of imagery and of the size or areal extent of the feature.

Research objectives, description of test sites and ground information collected, and discussion of research results and their applications appear in detail in later sections of this paper.

RESEARCH OBJECTIVES

The primary research objectives for using remote sensing to analyze range resources are as follows: (1) to investigate sensor capabilities, (2) to identify feasible range and wildlife applications and benefits, and (3) to develop specifications for data-collection systems. As is evident, it is desirable to investigate various remote-sensing devices in order to determine the capabilities of the sensors for satisfying inventory needs. Under normal operational situations, it is desirable to first define specific resource problems and employ suitable sensing devices for collecting information that can be used in determining a solution to the problem. However, for our research efforts, we are obliged to identify specific problems or applications of remote sensing, given certain resolution constraints as may be expected from initial operational space systems. Consequently, it must be kept in mind that although some remote-sensing applications seem feasible when using devices flown in conventional aircraft, these applications may not be feasible from earth-orbital altitudes.

To fulfill the research objectives, specific attention is directed to (1) various remote-sensing devices, (2) data collected at various scales, (3) data collected at different seasonal stages, (4) other factors besides those listed which affect image quality and interpretability, and (5) a comparative analysis of the ground information collected at the time of the overflights with the remote-sensing data.

The various types of remote-sensing equipment flown over the range study areas are presented in table 39-II. Attention is called to those sensors indicated as being operated from NASA-Houston aircraft. It should be recognized that, with the exception of the Hasselblad camera, all the other sensors were operated from aircraft flying at various altitudes, and that it is from these data that educated assessment is made of the kinds of applications which may be possible from lower resolution imagery of the kind to be obtained from earth orbit.

TEST SITES — GROUND INFORMATION

The research investigations were conducted principally on two recognized NASA test sites: (1) The San Pablo Test Site 48, located just east of Berkeley, California, contains rolling foothill topography covered mainly by annual grassland vegetation, on which the principal land use is grazing. (2) The Harvey Valley Test Site 135, located in the Lassen National Forest in northeastern California (fig. 39-1), is characterized by perennial bunch grass and sagebrush. However, many

other important range types are also found in test sites 48 and 135 which have counterparts in other range environments of much larger regional extent.

In addition to photographs which will document the appearance of range conditions and reflectance data as obtained with a spectroradiometer, other kinds of ground information are needed in order to analyze the remote-sensing data. Much of this additional ground information which is obtained at the NASA range test sites is listed in table 39-III.

RESULTS

In order to put into perspective the results of the analysis of remote-sensing data, it is helpful to have some idea of the kind of information that the range and wildlife manager needs from a survey of the resources which he manages. Basically, this information can be divided into three categories: (1) quantitative data on the amount, kind, condition, and distribution of range vegetation, (2) dependable maps showing location and extent of forage types and subtypes and physical and cultural features of the area, and (3) detailed descriptions of management problems (e.g., undesirable or noxious plants, insect infestations, rodents, erosion, competition for use of rangeland).

One aspect of our research is to compare different film-filter combinations in order to determine which is most useful for delineating vegetation-soil boundaries and for identifying various vegetation, soil, and moisture conditions. Figures 39-2 and 39-3 show the four film types which were analyzed and several ground photographs of specific range test sites where ground information was collected. The ground photographs, together with a brief description of the characteristics of the test site, provide a kind of reference material for training interpreters to recognize important range conditions. The various conditions seen in the aerial photographs in figure 39-2 were mapped by experienced photo-interpreters. By comparing these maps with ground truth, it was possible to rank the films in order of increasing usefulness. Black and white near IR photographs were least useful for general vegetation-soil mapping. However, this photography is particularly useful for detection of lush meadow vegetation. Black and white panchromatic photographs provided an adequate map base, but did not reveal as much information as the color photographs. Ektachrome Aero photography was particularly good for mapping the various soil types in the area, but Ektachrome Aero IR photography was judged to be the best for evaluating most of the vegetation, soil, and moisture conditions. It is important to recognize that these results apply to the specific date of photography and the particular area seen in figure 39-2.

Figure 39-4 shows the same range area at smaller scale in color and color IR photographs. Notice that here the Ektachrome Aero photograph is good for delineation purposes, but that species composition and density of forage are best determined by interpretation of the color IR photographs. This is partly the result of the color renditions produced by the three-layer film that is sensitive to visible as well as near IR wavelengths of light and of the distinctive contrast between the vegetation and the soil. Here again, the range imaged in figure 39-4 is the type for which color-IR photographs can be employed to good advantage for evaluating the range resources. As it is visualized how this same range might look on small-scale photography in which the ground resolution may be no better than 100 feet, it is probable that the photointerpreter could still easily differentiate timber from grazing land. Within the grazing land, the photointerpreter should be able to distinguish the meadow areas having the highest forage production and the very low producing sites, indicated as areas having very light-colored soil.

Before finally concluding that color IR photographs are best for evaluating range areas, figure 39-5 should be studied quite carefully. Here is an area in which timber can be readily differentiated from brush and open grassland, but this could have been done on panchromatic film as well. There seems to be little advantage to interpreting color IR photographs instead of panchromatic photographs for such range types.

Suppose now that more information was desired concerning plant composition and structure and soil surface phenomena. It is this kind of information which will be more useful to the rangeman than just a broad vegetation-type map of the range area. One way of collecting more detailed information is by employing a low-flying aircraft (e.g., aircraft flown at 300 feet with a Mauer KB-8 70-millimeter camera) to procure very large-scale (1:600) photographs as part of a double sampling procedure. Photographs such as those seen in figure 39-6 could be obtained. Notice that these photographs were taken at three dates during the grazing season: June 10, July 25, and October 25, 1967. Preliminary interpretation indicates that phenological changes in the vegetation are important for differentiating and identifying dominant range species. At such large scale, many surface features, in addition to the range plants (e.g., soil disturbance, rodent activity, rockiness, dead plant material, cattle droppings, etc.), can be positively identified. Furthermore, measurements of vegetation parameters such as plant density and shrub size, can be made quite easily, and estimates can be made of foliage cover and degree of animal use. Finally, the detailed information seen on large-scale photographs aids in analyzing lower resolution imagery. For example, the large-scale photographs taken in October were extremely useful in understanding certain features seen in thermal IR imagery and color IR photography taken by NASA-Houston aircraft at nearly the same time.

An example of color IR photography taken by NASA-Houston aircraft in October 1967 is illustrated in figure 39-7. Comparative analysis of this photograph with the color IR photograph in figure 39-2 will reveal that striking changes do occur between the early growth stage (in June) and the postmaturity stage (in October, when soil and vegetation are dry). Results from simultaneous interpretation of the two photographs mentioned previously indicate that even at 100-foot ground resolution, the following may be possible: (1) It should be feasible to monitor changes in the moisture regime (e.g., springs, intermittent streams, and standing water). These moisture conditions are particularly important on many ranges when adequate water is a limiting factor in achieving optimum utilization of the forage produced. (2) Sequentially obtained photographs at short intervals would allow monitoring of the rate of growth or of the drying of the vegetation. Observation of the time when soil is dry enough to withstand heavy grazing pressure is also important. Grazing too early in the season can cause damage to the range plants and effect an overall deterioration of range condition. (3) It may also be possible to identify unique changes in reflectance phenomena associated with moderately to heavily grazed areas and thereby assess the extent of animal use.

Seasonal variations in the annual grassland type of California have been studied on aerial photographs procured by NASA-Houston aircraft on frequent passes over the San Pablo Test Site. Only the optimum spring seasonal stage and the dry summer stage are shown in figure 39-8. On this annual grass range, color IR photographs taken at the spring seasonal stage appear to be superior to other photographs for showing important details needed to analyze the forage resource. Notice in particular, however, that at the dry seasonal stage, when the annual grasses and forbs are dry, the color IR photograph reveals little about the forage except that it is very dry. Under these dry conditions, other films are equally useful for this kind of determination.

At the optimum seasonal stage imaged on color IR film (fig. 39-8), it is possible to discriminate between those sites where the forage has dried because of early moisture depletion and those sites where the forage is still healthy and abundant. Subtle changes in the intensity of red coloration can be correlated with the degree of animal use. Observe that the area covered by brush is clearly discernible; hence, conversion practices could result in increased forage yields. Recognition of sites having a dense forage crop may aid in determining the fire hazard of the area when the vegetation has dried. Sequentially obtained photographs of the annual grassland range may allow predictions to be made concerning the time remaining in the green feed period. This in turn allows the rancher to determine how much hay will be needed in the barn or how soon he should move his animals to greener pastures or to the market in order to get the best price.

Figure 39-9 permits comparison of a thermal IR image (8μ to 14μ , NASA Reconofax IV recorder) with a color IR photograph taken simultaneously in October 1967. On the thermal IR image, taken at about 10:00 a.m., the springs (at area A) which flow out over the range can be detected. (Also compare with fig. 39-7.) Standing water from one of the springs is marked at area B, and water which has been ponded during the summer in watering holes or between small check dams is indicated at area C. This water is warmer than the spring water, as indicated by the lighter tone. With the possible exception that water-temperature differences can be detected on the thermal IR imagery, the previously mentioned features are seen as readily on the color IR photography. In fact, there is considerably more detail seen on the photograph than on the thermal IR image, which may prompt the question of what value a thermal IR sensor would be for evaluation of rangeland. Perhaps the most important application of the thermal IR sensor is in monitoring the moisture regime from very early spring, when the range is very moist, to late fall, when the range is very dry. Determination of range readiness (i.e., the time animals can use the range without causing damage) and the availability of stock water are essential for the efficient management of rangeland.

Through use of an optical-mechanical scanner, 18-channel line-scan imagery has been procured for the Harvey Valley Test Site. Tone signature analysis of the photographic read-out from this instrument reveals that the total number of useful bands for making range evaluations can be reduced to five or six. Figure 39-10 shows the six bands which appear to be most useful. Results from densitometric analysis of these bands reveals that moist sites are most readily differentiated from the dry sites on the ultraviolet and thermal IR bands. Dense meadow vegetation is most conspicuous on the near IR band (0.8μ to 1.0μ), and the greatest number of actual vegetation-soil delineations can be made on the bands in the visible portion of the spectrum, even though the variation of gray tones is not as great as in photographs of other bands. These results may be of considerable importance because they show that the detection and identification of significant features on rangeland can be made on the basis of tone signature from very low-resolution imagery.

CONCLUSIONS

Rangeland covers a vast amount of the land area of the earth, and for much of the rangeland, little or no inventory information exists. Hence, the preparation of the broadest vegetation-soil maps such as can presently be prepared using existing Gemini photographs will provide information of great value to the land manager and will serve as a base for collecting more detailed information.

Since resolution constraints may be placed upon the data initially collected from earth orbit, less emphasis may be placed upon employment of high-resolution systems. Preferably, a double sampling scheme should be considered. For example, a relatively low-resolution system (e.g., optical-mechanical scanner, television vidiocons, camera systems, etc., capable of procuring data that can be rapidly analyzed to give broad categories of information) could be operated from earth orbit to give a synoptic view of range areas. At the same time, conventional aircraft (with high-resolution cameras) could be employed to secure very detailed data from a small number of representative sample areas.

From our studies of various remote-sensing devices, it is apparent that the devices which are capable of obtaining high-resolution data are best suited for collecting useful information regarding range resources. In particular, high-resolution cameras using Ektachrome Aero IR film promise to be an extremely practical tool for improving range analysis when used in an appropriate range environment at the proper season of the year. The utility of this film is based upon its sensitivity to energy in the visible and the near IR portion of the spectrum. Because color IR is subject to a narrow range of exposure, getting an interpretable image may be more feasible by the use of a high-resolution multilens or multicamera system which can obtain separate black and white images in the three distinct bands for which color IR film is sensitive, namely, green, red, and near IR. (Black and white films have a wider exposure range; hence, tone contrast can be more readily manipulated in development and processing to get a usable image.) The practicality of such a system is dependent upon procurement of geometrically matched images which can be either (1) readily combined to form color composite images for easy interpretation, or (2) stored on such a format that can be processed through automated signature analysis systems for rapid extraction of information.

In addition to the synoptic view afforded from orbital altitudes, another desirable advantage of an orbiting data-collection system is the capability of the system to obtain sequential imagery. From the studies of range resources, there is convincing evidence that sequential imagery is essential for monitoring changes in the vegetation and moisture regimes. This information is of extreme importance in managing range environments. If, however, an optimum time or season had to be prescribed, it would coincide with that time period when the range foliage has reached near-maximum development. Figure 39-11 shows the time period when interpretable data could be collected for various range areas in the United States. For such a large regional area, the optimum time for collecting interpretable imagery is spread out over a period of several months. For any one specific area, however, there is usually a period of about 1-month duration in which interpretable imagery could be obtained. Fortunately, most range areas, particularly semiarid regions, have a much higher probability of cloud-free days, compared to other

areas (e.g., agricultural areas). This fact, combined with the repetitive coverage afforded by orbiting vehicles, insures a high probability of securing useful data for preparing range inventories. Hence, an earth-orbiting vehicle (including unmanned space vehicles which are equipped so that ON-OFF command signals can be given to the sensors from the ground) equipped with data-collecting devices would undoubtedly be the most efficient means for procuring information to aid the man on the ground to improve the management of range resources.

TABLE 39-I.- FEASIBILITY OF INTERPRETING SIGNIFICANT RANGE FEATURES AND CONDITIONS

Range feature or condition	Ground resolution, ft																			
	0.1 to 0.3					1 to 3					10 to 30					100 to 300				
	Film-filter combination or sensor																			
	Pan- chro- matic 12	IR (89B)	Color	Color IR (15)	Thermal IR (8μ to 14μ)	Pan- chro- matic 12	IR (89B)	Color	Color IR (15)	Thermal IR (8μ to 14μ)	Pan- chro- matic 12	IR (89B)	Color	Color IR (15)	Thermal IR (8μ to 14μ)	Pan- chro- matic 12	IR (89B)	Color	Color IR (15)	Thermal IR (8μ to 14μ)
Vegetation features or conditions																				
Grazing versus non- grazing land	++	++	++	++	+	++	++	++	++	+	+	+	++	++	+	+	-	+	++	-
Gross vegetation types	++	++	++	++	++	++	++	++	++	++	++	++	++	++	+	+	+	+	++	+
Meadow	++	++	++	++	++	++	++	++	++	+	+	+	+	++	+	-	+	+	++	+
Open grassland	++	++	++	++	+	++	++	++	++	+	+	+	++	++	+	-	-	+	+	-
Brushland	++	++	++	++	++	++	++	++	++	+	+	-	+	++	+	-	-	+	+	-
Open timber	++	++	++	++	++	++	++	++	++	++	++	++	++	++	+	+	-	+	++	+
Nonproductive sites	++	+	++	++	+	+	+	++	++	+	-	-	+	++	-	-	-	+	+	-
Range grass and forb species	+	+	++	++	-	-	-	-	-	-	-	-	-	-	-	-	-	-	-	-
Range shrub species	++	++	++	++	-	-	-	+	+	-	-	-	-	(+)-	-	-	-	-	-	-
Gross-forage- density cover classes	++	++	++	++	+	-	-	+	++	-	-	-	-	+	-	-	-	-	+	-
Plant health (greenness, dry- ness)	+	+	++	++	+	+	+	++	++	-	-	-	+	++	-	-	-	+	++	-
Gross assessment of forage utili- zation	+	++	++	++	-	-	-	+	+	-	-	-	-	+	-	-	-	-	-	-
Surface features or conditions																				
Soil texture	++	+	++	++	-	-	-	+	+	-	-	-	-	-	-	-	-	-	-	-
Rockiness	++	++	++	++	+	+	-	+	+	-	-	-	-	-	-	-	-	-	-	-
Soil disturbance caused by																				
Rodents	++	++	++	++	-	-	-	-	-	-	-	-	-	-	-	-	-	-	-	-
Livestock use	++	++	++	++	-	+	+	+	+	-	-	-	-	-	-	-	-	-	-	-
Erosion	+	+	++	++	-	+	+	++	++	-	+	+	++	++	-	-	-	+	+	-
Burned rangeland	++	++	++	++	+	++	++	++	++	+	+	+	++	++	+	-	-	+	++	-
Numbers of animals	++	++	++	++	+	++	+	++	++	+	-	-	-	-	-	-	-	-	-	-
Moisture regimes																				
Standing water	++	++	++	++	++	+	++	+	++	++	+	+	+	++	+	-	-	-	-	+
Springs	+	++	++	++	++	+	+	+	++	+	-	-	-	+	-	-	-	-	-	-
Permanency of streams	+	++	++	++	++	+	++	+	++	++	-	-	-	-	-	-	-	-	-	-

LEGEND: ++ The feature is readily and consistently interpretable (i.e., detected, identified, estimated or measured, depending upon feature or condition), even by people with limited photointerpretation training and experience.
 + The feature usually is interpretable, but only through careful study by photointerpreters who, by virtue of training, experience, and motivation, are expert in identifying such features.
 - The feature is not consistently interpretable, even though expert photointerpreters are able to identify such features occasionally on photography of the film-filter-scale combination indicated.
 -- Although the feature is an important one from the earth resources standpoint, it is almost never interpretable even by expert photointerpreters.

TABLE 39-II.- REMOTE SENSORS OPERATED OVER RANGELAND

Camera systems		Scanners
Single lens	Multilens	
Wild RC-8 (6 in.) ^a	Itek 9 lens ^a	Reconofax IV IR imager ^a
Wild RC-9 (3-1/4 in.)	Univ. of Michigan 16 lens	Univ. of Michigan 18-channel optical-mechanical scanner (0.32 μ to 14 μ)
Zeiss RMK-A-15/23 (6 in.)	Long Island Univ. 4 lens	K-band AN/APQ-56 radar system
Mauer KB-8 (150 mm)	Cartwright 4 lens Spectraband	Bendix thermal IR scanner
T-11 (6 in.) ^a		
K-17 (8-1/4 in.)		
HyAc panoramic (12 in.)		
Hasselblad 500 (80 mm)		

^aSensors operated from NASA-Houston aircraft.

TABLE 39-III.- GROUND INFORMATION COLLECTED TO ANALYZE
REMOTE-SENSING DATA

Vegetation	Surface features
Species composition	Soil type, depth, texture, color
Phenological characteristics	Soil radiance
Stage of plant development	Rockiness
Plant color	
Leaf-stem ratio	Disturbance factors
Greenness-dryness ratio	Erosion
Health (vigor)	Trampling
Plant density, distribution, spacing	Rodent Activity
Foliage cover	Slope aspect
Plant height	Amount of litter, residual dead plant material
Degree of animal utilization	Moisture regimes
Radiance	Soil moisture
	Standing water
	Proximity to available water
	Cultural features and management practices

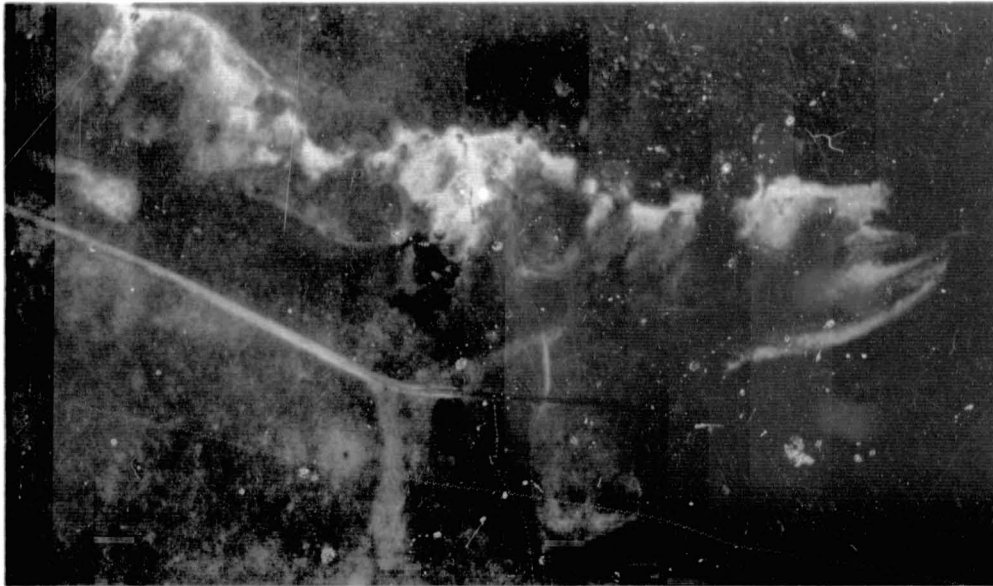


Figure 39-1.- NASA Harvey Valley Range Test Site 135.

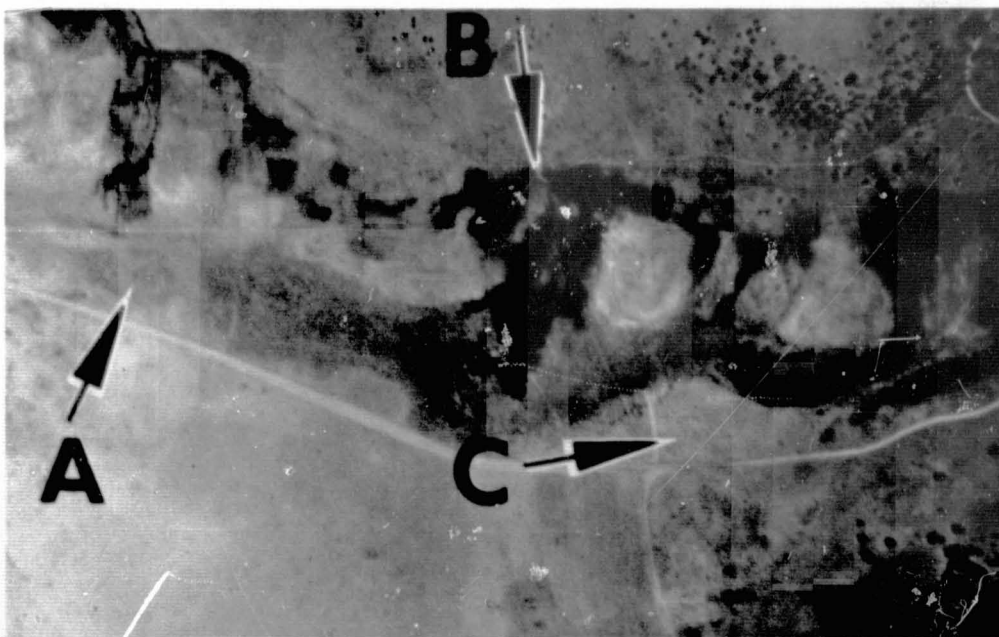


a. Panchromatic (Plus X Aerographic).

Figure 39-2.- These aerial photographs (scale 1:8500) of Harvey Valley Range illustrate a variety of vegetation types associated with changes in soil type and moisture regime. The reader is encouraged to compare the appearance of each of the five vegetation types (fig. 39-3) on all four films. For example, a nearly pure stand of blue grass (Poa nevadensis) at A may have been overlooked on panchromatic and Ektachrome photographs, but is readily detected on the two IR-sensitive photographs. Note the contrast of tones for the meadow vegetation seen at B on panchromatic and Ektachrome Aero IR photographs. Also, notice how distinctly wet meadow vegetation can be detected by its characteristic red color on Ektachrome Aero IR photography. Standing spring water on the meadow vegetation appears brownish on color IR photography. Low sagebrush dominates the site at C. The very light colored soil is a useful indicator for this site. Subtle differences in soil color are best seen on Ektachrome Aero photographs. A sharp vegetation boundary between wet meadow and big sagebrush vegetation is seen at D, and a big sagebrush community is seen at E. Compare the ease of differentiating soil colors at sites C and E for all four aerial films.



b. Aerographic IR.



c. Ektachrome Aero.

Figure 39-2.- Continued.



d. Ektachrome Aero IR.

Figure 39-2.- Concluded.



- a. Blue grass (Poa nevadensis)-silver sagebrush (Artemisia cana) community. The blue grass (arrow) on this site is so dense that the underlying soil is nearly obscured. Hence, the vegetation boundary is readily seen on the IR-sensitive photography. It is more difficult to distinguish this type on the Panchromatic and Ektachrome Aero photographs because the blue grass vegetation is nearly the same tone and color as adjacent types.



- b. Wet meadow site at Cone Spring. The dominant species in this type are sedges (Carex sp.) and forbs. Rushes (Juncus sp.) and water-loving grasses are also present. Foliage cover is approximately 100 percent. Both changes in species composition and in the presence of standing water can cause variations in the tone or color which is most easily interpreted on Ektachrome Aero IR photography. The highest forage yields come from these types of sites.

Figure 39-3.- Vegetation types.



- c. Low sagebrush community. The sparse cover of low sagebrush (Artemisia abruscula) with associated bunch grass and sandberg blue grass, coupled with light colored soil and numerous rocks, characterize this near-nonproductive site. The type boundary for this site is most easily discerned on Ektachrome Aero photography.



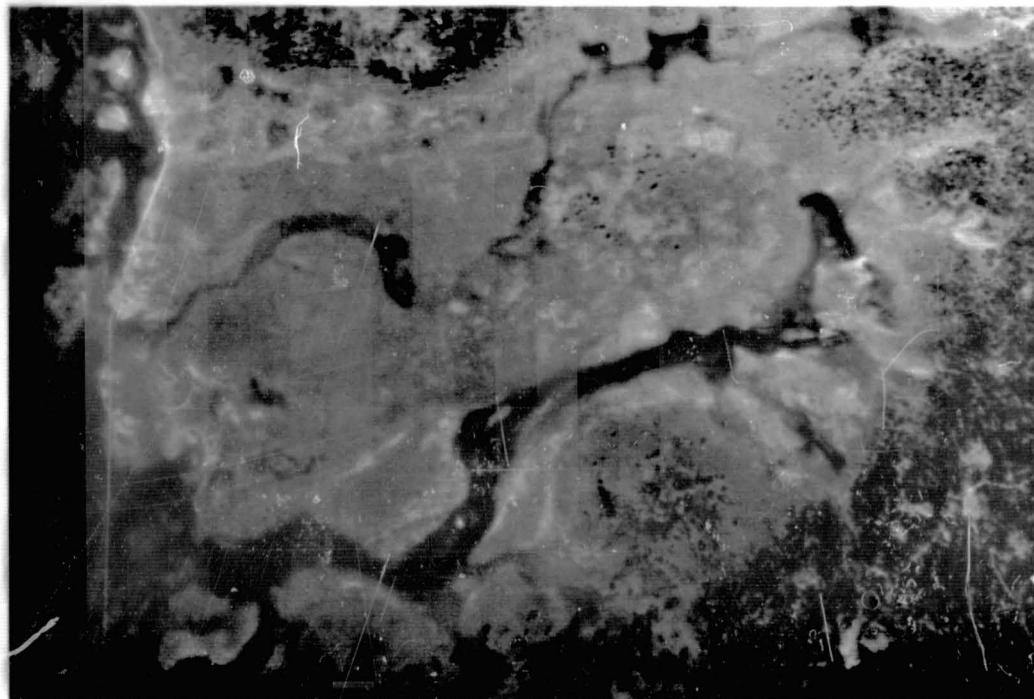
- d. Sharp vegetation boundary between wet meadow site and big sagebrush site, caused by an abrupt change in soil type, topography, and moisture regime.

Figure 39-3.- Continued.

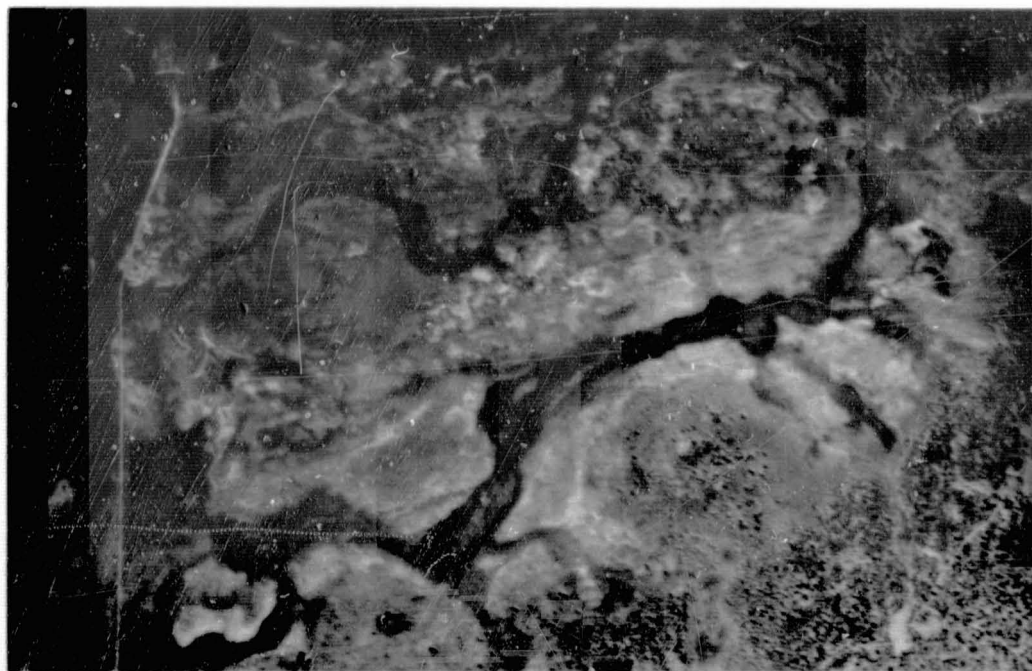


- e. Big sagebrush (Artemisia tridentata) community. Associated forage species include Western needle grass, Idaho fescue, Squirreltail, and sedge (Carex sp.). The large shrubs and associated reddish brown soil characterize this site, best seen on Ektachrome Aero photography.

Figure 39-3.- Concluded.



a. Ektachrome Aero.



b. Ektachrome Aero IR.

Figure 39-4.- Portion of the Harvey Valley Test Site, taken June 11, 1966. Scale approximately 1:30 000.

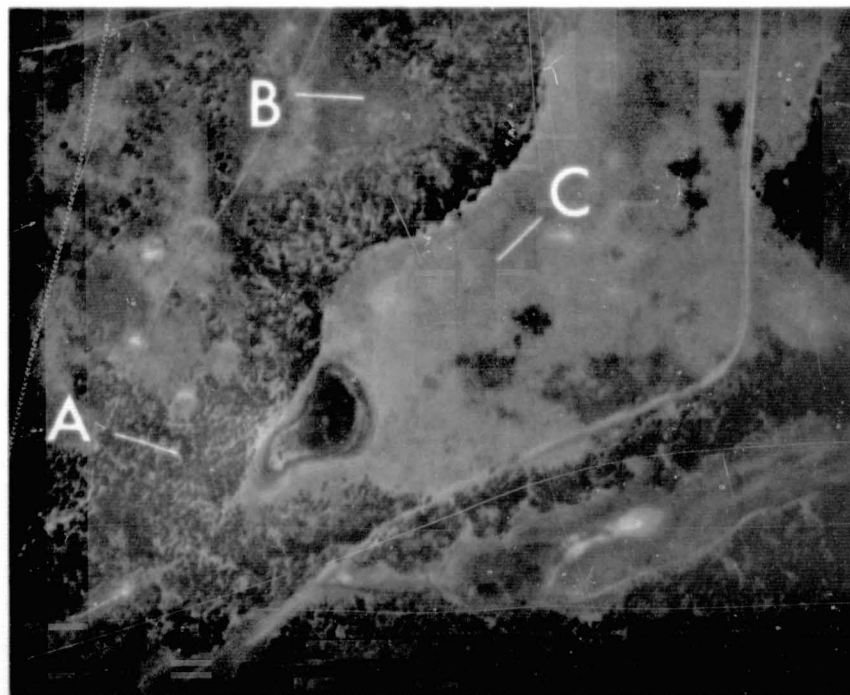
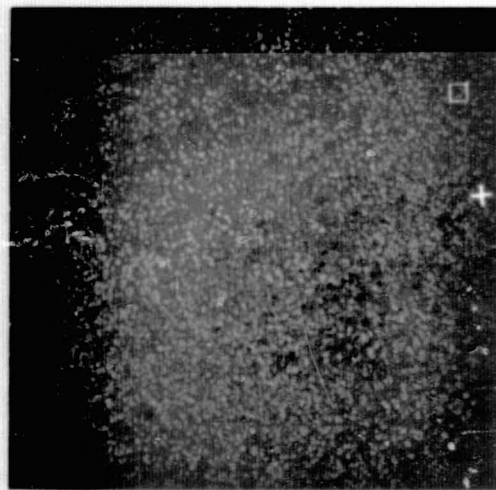
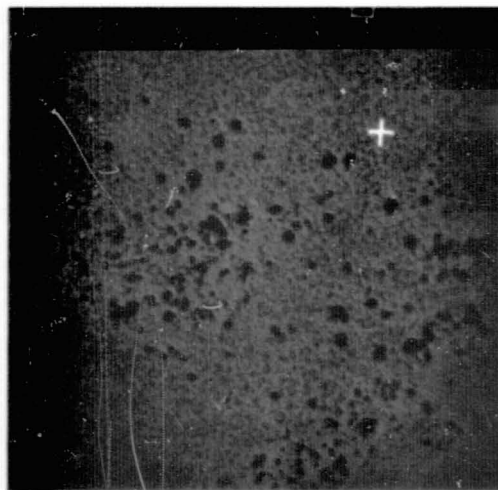


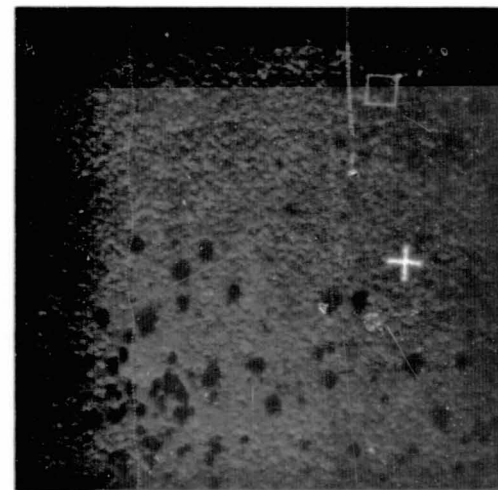
Figure 39-5.- Ektachrome Aero IR photograph.
Scale 1:30 000. Coniferous timber at A, mixed
shrub species at B, and open grassland vegeta-
tion at C.



June 10, 1967



July 25, 1967



October 25, 1967

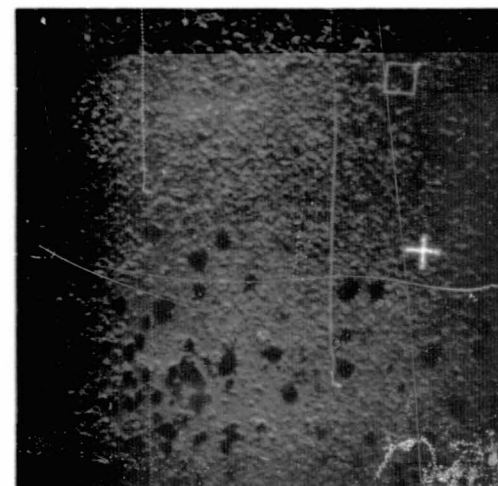
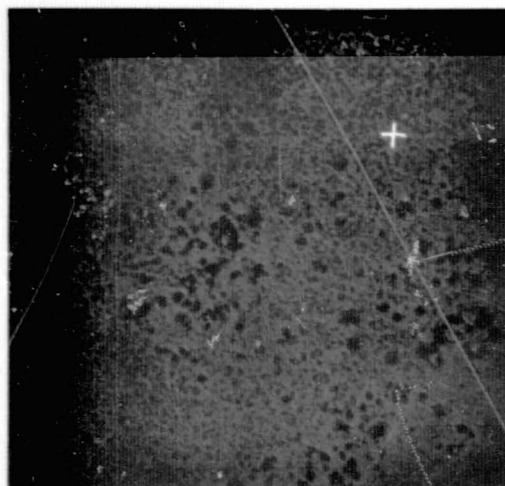
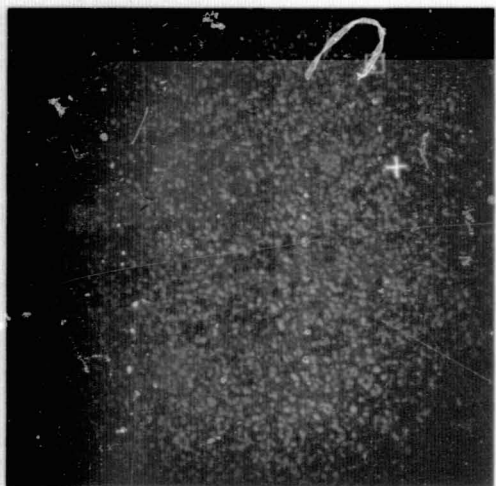


Figure 39-6.- Large-scale 70-mm color (Anscochrome D-200, top) and color IR (Ektachrome Aero IR, bottom) photographs. Scale ranges from 1:900 to 1:640.

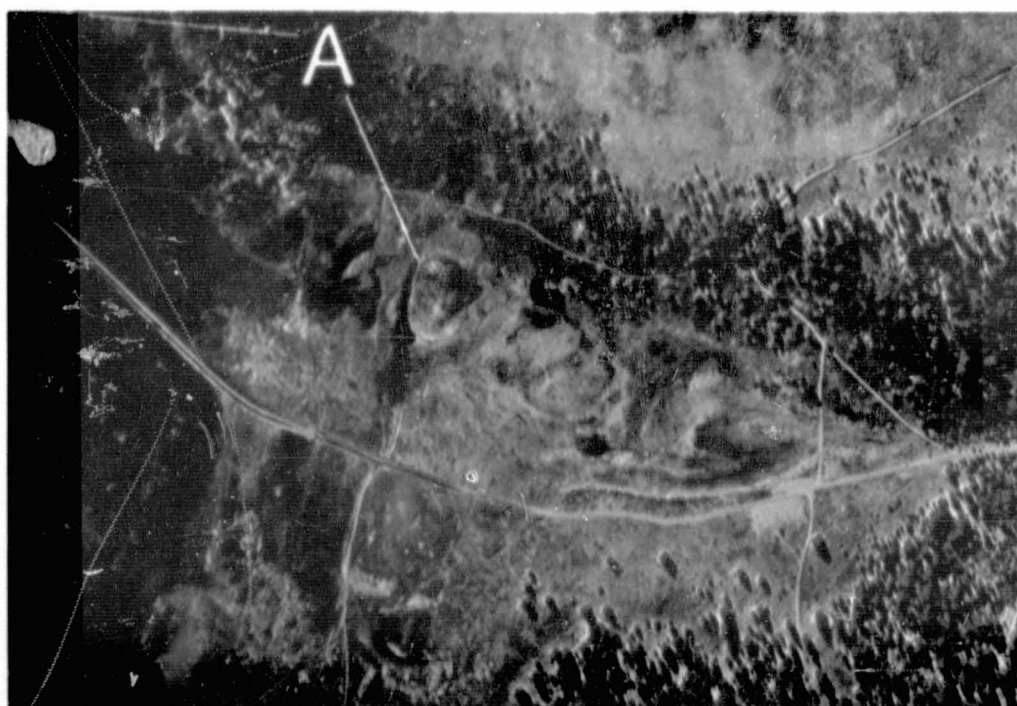
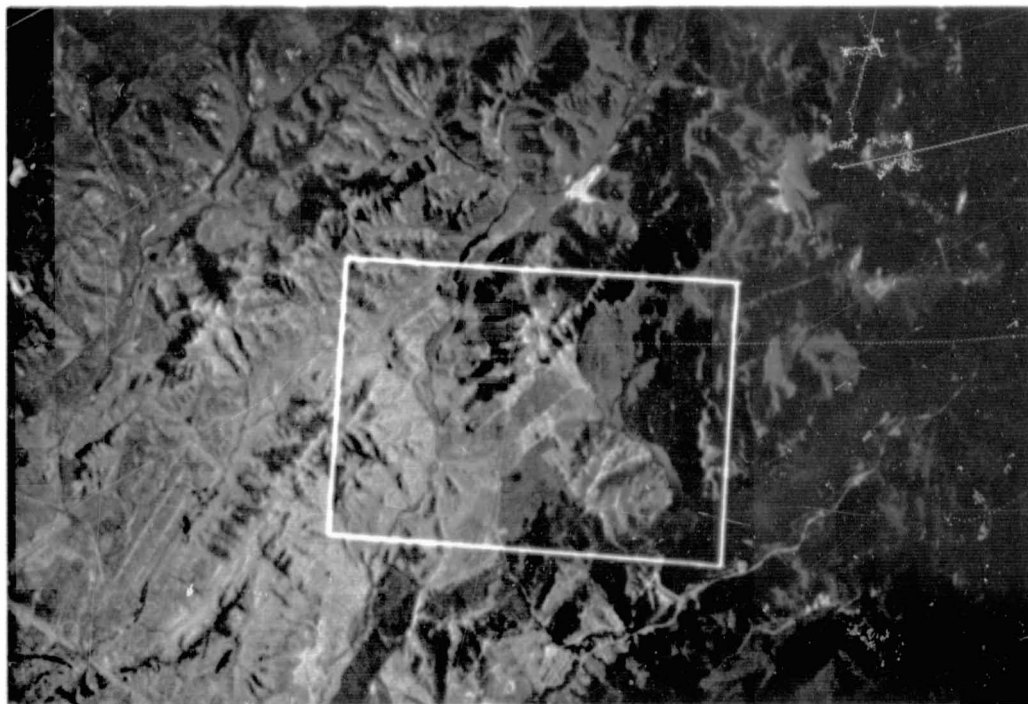
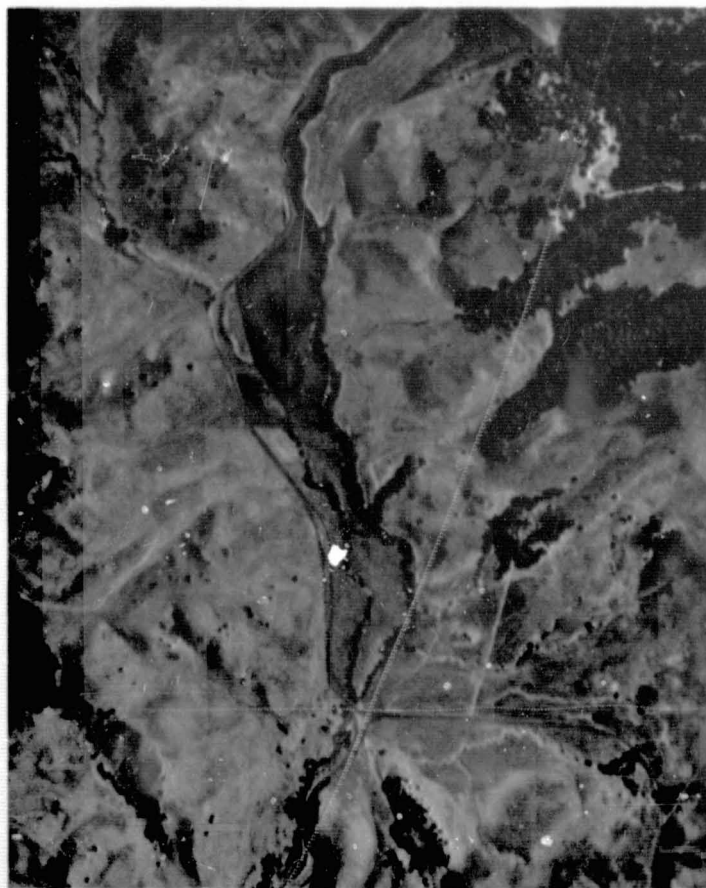


Figure 39-7.- Ektachrome Aero IR photograph, taken October 18, 1967, by NASA-Houston aircraft. Point A denotes location of two springs which are still active, despite the otherwise dry condition of the range.

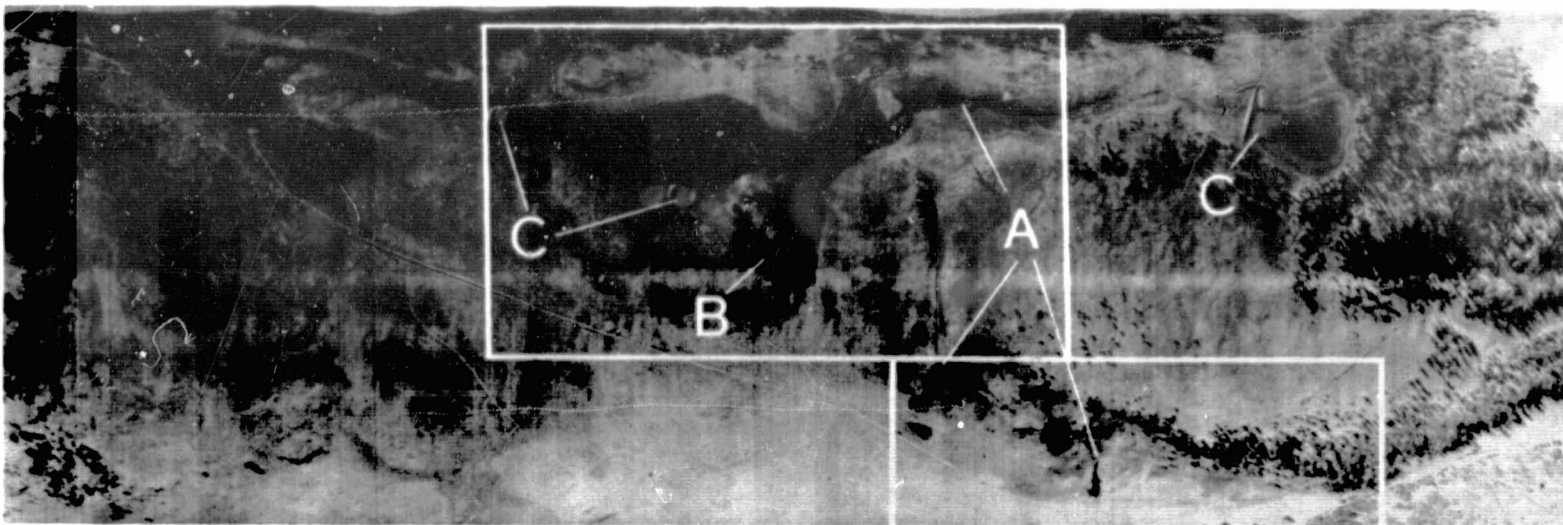


a. Taken in early May.

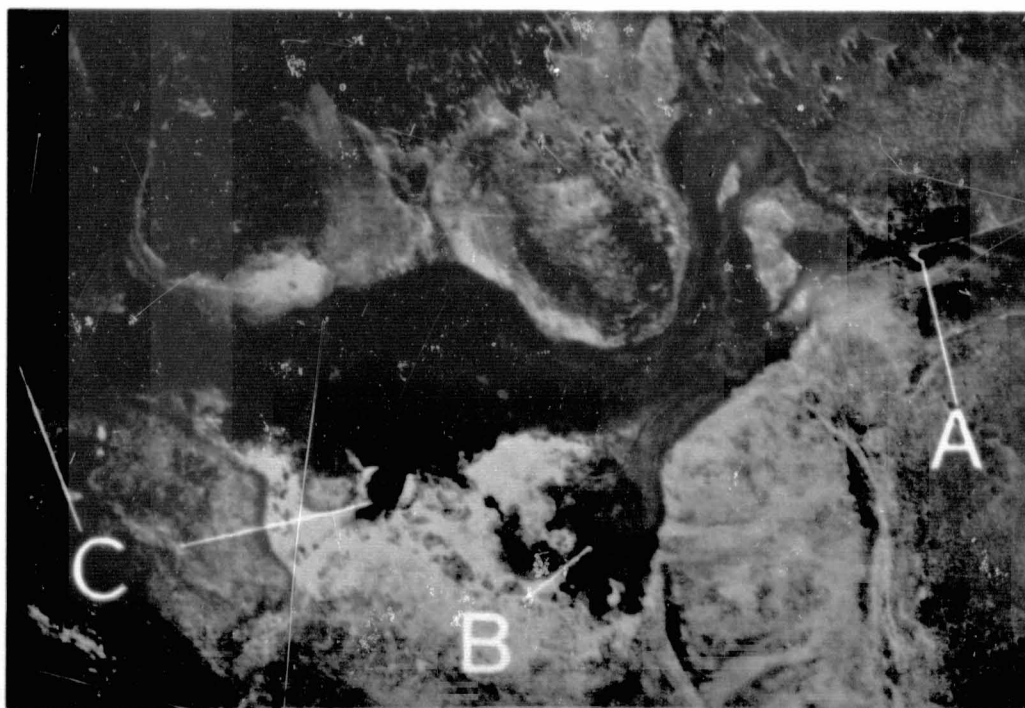


b. Taken in late August.

Figure 39-8.- Ektachrome Aero IR photographs.

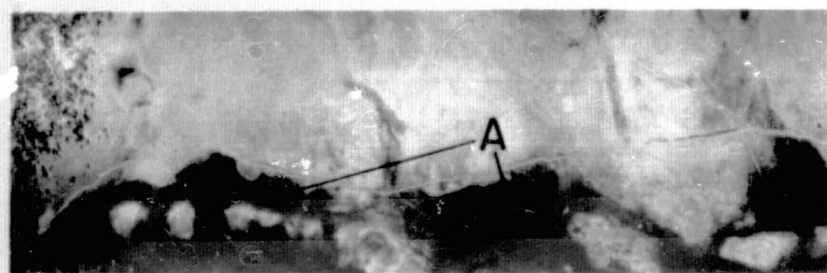


a. Thermal IR imagery (8μ to 14μ), Reconofax IV.



b. Ektachrome Aero IR photograph.

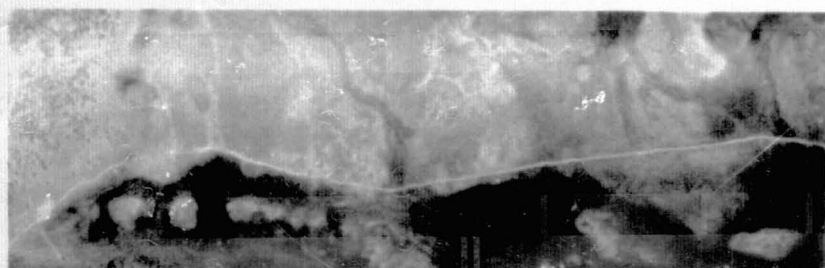
Figure 39-9.- The two images were taken simultaneously on October 18, 1967. Compare the origin of a spring at A, standing spring water at B, and ponded drinking water for stock at C.



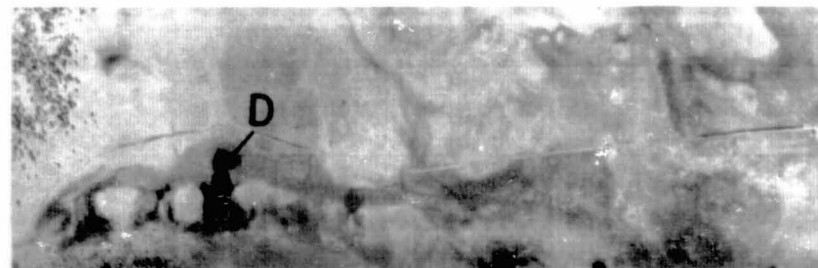
.32-.38 u ultraviolet



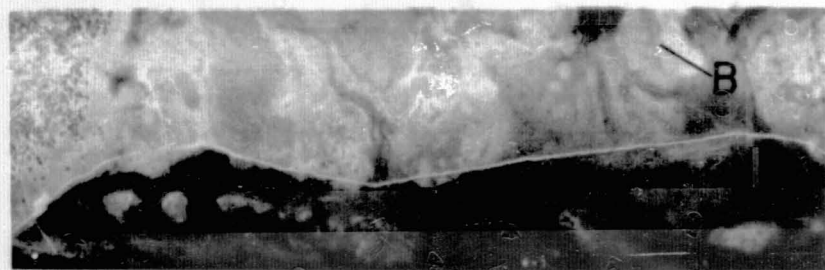
.80-1.0 u near infrared



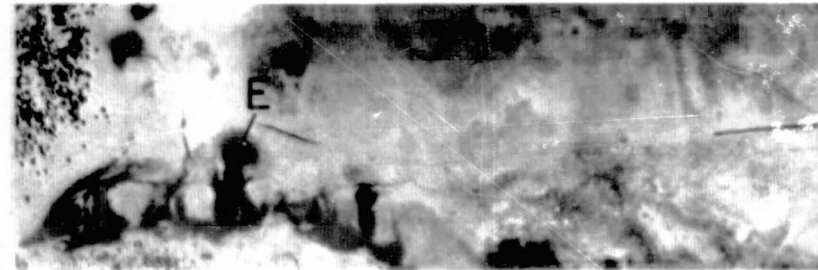
.55-.58 u



1.5-1.8 u



.62-.68 u visible-red



8.0-14.0 u thermal infrared

A. moist sites

C. dense forage

E. soil moisture

B. vegetation type

D. ponded spring water

Figure 39-10.- Multiband line-scan imagery obtained by an optical-mechanical scanner (May 18, 1966) showing range resources.

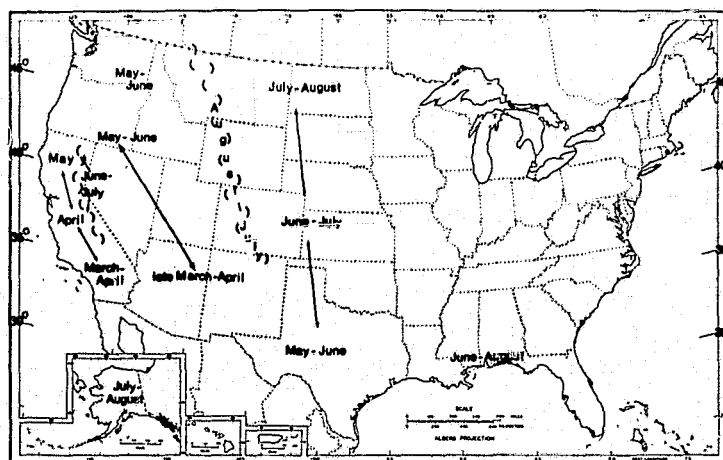


Figure 39-11.- Seasonal stage when range foliage is near maximum development.

N71-16162

THE FEASIBILITY OF INVENTORING NATIVE VEGETATION
AND RELATED RESOURCES FROM SPACE PHOTOGRAPHY

By Charles E. Poulton
Professor of Range Ecology, Oregon State University
Corvallis, Oregon 97331

INTRODUCTION

The development of practical uses for earth resources photography taken from space platforms is of vital interest to the National Aeronautics and Space Administration. The effectively coordinated use of NASA and other aircraft data is essential on a subsampling design to solve interpretation problems associated with the use of space imagery over rangeland and forested vegetation areas. With the amount of photographic imagery now available and projected for the relatively near future, it is critically important that the use of available imagery be tested for all earth resources applications. Rangeland resource areas need increased attention in the Earth Resources Program because of their economic importance in world food production and their extensive coverage of the national and world land mass (ref. 40-1). Inclusion of these vegetation resources in the research program on space photography applications will make it possible to plan new tests with systems optimized on the basis of relevant experience in all of the major earth resources areas. One of the most important potential uses of space imagery is in the broad-scale analysis and synoptic treatment of ecosystems comprising the native vegetation resources (rangeland and forests) of our nation and the earth. According to a National Research Council Survey (ref. 40-2), only 30 percent of the world has been adequately mapped in terms of even small-scale resource maps.

Activities of numerous natural-resource-oriented groups in the United States have recently emphasized needs in areas where space photography in conjunction with small-scale aerial color and/or color infrared (IR) photography could play an important role. The American Society of Range Management is establishing an ad hoc committee to foster "a comprehensive appraisal of the nation's grazing resources." Similarly, the National Forestry Research Advisory Committee to the Secretary of Agriculture has repeatedly discussed and recommended a nationwide survey and analysis of rangeland resources. The president of the National Association of Soil and Water Conservation Districts

has just gone on record in support of complete natural resource surveys, saying that "... Districts and counties can't make intelligent resource plans without such an inventory." In addition, county and state planning commissions, in recognition of this same need, are actually now putting together the best comprehensive resource maps they can without the benefit of synoptic photographic coverage that the Earth Resources Program could provide.

Recognizing these potentialities and needs, Oregon State University became involved with the Forestry Remote Sensing Laboratory (NASA-U.S. Department of Agriculture) in a study of the feasibility of inventorying native vegetation and related resources from space photography. Initial exploratory work was done in 1966 (ref. 40-1), and the work was substantially expanded with modest funding from NASA in May 1968.

The substantial contributions of graduate research assistants Barry J. Schrupf and Edmundo Garcia-Moya to research accomplishment and to this report are gratefully acknowledged.

RESULTS ACQUIRED FROM THE USE OF DATA FROM NASA AIRCRAFT

The Objectives of the Investigation

Our study has the following objectives:

1. Determine the potentialities and limitations of mapping and interpreting characteristics of native vegetation areas from space photography.
2. Compare vegetation maps prepared from this photography with other available vegetation-resource maps.
3. Identify problems and limitations in the practical use of space photography in earth resources applications.

Our work to date has contributed to all three of these objectives, with effort focused primarily on objective 1. In addition to the author, the project is staffed with two particularly capable research assistants and a small group of volunteer photointerpreters who participate in testing phases of the research.

In the work to date, NASA aircraft data for the study area in southeastern Arizona have not been available. We have, however, examined as much of this material as is available at the NASA Manned Spacecraft Center and have determined which portions may be useful to us as supporting data in the interpretation of space photography. The available

radar data can be located in respect to the space photography and do cover an area where interpretation problems exist. The available aerial photography is of good quality and should be useful to us if it can be located on the space photography and if it does cover areas in which interpretation problems actually exist. These determinations are yet to be made. With the use of both relatively large-scale (1:16 000) aerial photography taken for us in designated problem areas by the Forestry Remote Sensing Laboratory and small-scale (1:200 000) aerial photography made available to us by the U.S. Geological Survey, we have demonstrated both the need and usefulness of supporting aircraft data taken on a subsampling basis to aid in the interpretation of space photography.

Plans for the coming fiscal year will result in more thorough evaluation of existing NASA aircraft data if we find that it does cover problem areas.

A request has also been placed through channels to have supporting aircraft data flown in intermediate and small scales in conjunction with forthcoming Apollo missions. This request identifies specific problem areas in which subsampling data are needed and identifies other minimum guidelines for a successful mission.

Methodology

Our 1967 Progress Report (ref. 40-1) recognized that useful ecological interpretation of vegetation from space photography cannot be made without research to acquire and analyze both vegetational and soil-surface ground truth in relation to photographic-image characteristics. This is the problem on which 1968 activity has been concentrated.

Minimum ground-truth information for accomplishment of our objectives requires data on native vegetation, soil-surface conditions and characteristics, and the landforms represented in each homogeneous photographic-image area. These vegetation-soil-landform complexes then need to be analyzed and interpreted in a meaningful hierarchical classification that is compatible with the amount of detail observable and/or interpretable in the imagery obtained from space.

The procedures used in this project have been adapted from parallel work by the study leader and his graduate students in the Department of Range Management at Oregon State University. Our research programs have been developing vegetation classifications in both rangeland and forested environments. Within this framework, we have been concerned about vegetation-environment relationships, about the characterization and description of these ecosystems, and about the use of this information

in practical resource analysis programs. These programs have made heavy use of aerial photointerpretation as a means of (1) increasing efficiency and cutting costs of resource analysis and (2) minimizing, but not replacing, groundwork in the survey procedure. This experience has resulted in the identification of applicable principles and concepts and the development of procedures that are directly useful in the analysis of vegetation resources from space photography.

From among numerous ecological principles and concepts, the following is the dominant premise upon which our procedures are based:

"In native vegetation areas, the homogeneous communities of plants that occupy the landscape are the best indicators of the biological similarity of the areas so occupied. These plant communities integrate and thus index the inherent productive capacity, or natural site capability, of the collective and usually discontinuous areas that these similar vegetations occupy."

Vegetation-resource examination is, therefore, fundamentally phytosociological. The understanding of vegetation-soil-climatic interrelationships developed from phytosociological studies provides the basis for the extraction of information about vegetation resources from remote-sensing data.

The mapping legends based on the previous concept must clearly differentiate taxonomic units from mapping units. The taxonomic unit is the smallest hierarchical grouping of vegetation and soil-surface features that can be identified in the remote-sensing data and that has relevance to the objectives of the resource analysis. The mapping unit, however, is derived from a knowledge of the taxonomic units and an analysis of the imagery. Where cartographically feasible, mapping units may represent individual taxonomic units. These may be referred to as pure or simple mapping units. Where intricate patterns of vegetation and other ground features dictate, mapping units may include two or more kinds of taxonomic units. These are appropriately referred to as complex mapping units or complexes of taxonomic units. To effectively convey information about the mapped delineations, it is important that each component of a complex mapping unit be individually identified in the legend and not "averaged" into a description of something that does not exist on the ground. In developing mapping procedures, it is also important to recognize that any mapping unit or delineation may circumscribe inclusions which are ignored for practical reasons because of their small physical size in relation to the delineation.

When working at larger scales, one may be able actually to map individual plant communities. The phytosociological classes, or

taxonomic units, used in mapping from space imagery with present resolution and scale limitations, will, however, usually represent a higher level of generalization than the specific plant communities discernible on the ground. These broader taxonomic units must, however, (1) have biologically valid common denominators that support or justify their hierarchical class, (2) be relevant to the purposes and objectives for which the resource analysis is being prepared, and (3) be compatible with the resource discriminations that may be delineated and reliably identified on the imagery at hand.

The development of procedures for the practical use of space photography must, in addition, be done from an awareness of the major activities for which information is needed by the earth resources decision maker. In the past, much thinking has been done about space applications to earth resource problems without clearly identifying these needs in relation to the capability of imagery obtained from space platforms. These needs may be grouped into the following four classes:

1. Broad policy and planning
2. Land-use decisions
3. Resource management decisions
4. Monitoring effects of decisions

With present resolution limitations on space photography, classes 1 and 2 are the ones most likely to benefit from earth resources interpretations made from space photography. In some instances, benefits may accrue to class 3 (resource management decisions), but the likelihood of monitoring the effects of decisions in native vegetation areas in a manner directly useful to the resource manager will likely be minimum. We have, therefore, developed procedures which we feel are particularly compatible with the acquisition of information needed in classes 1 and 2 (broad policy and planning and land-use decisions).

We have selected the area covered by Gemini IV photograph S-65-34681 (magazine 8, frame 11) as our area of concentrated attention. We will also be using Apollo coverage for this same area roughly bounded by a line connecting Tucson, Wilcox Lake, Bisbee, and Nogales, Arizona.

Workflow Chart

A practical resource analysis of rangeland areas involves a workflow that can be organized into the following five steps:

1. Assembly and preparation of working materials
2. Preparation of legends and photointerpretation aids
3. Project survey or resource analysis
4. Compilation and reporting
5. Interpretation and practical use of information obtained

Actually, significant practical use begins with step 3. Research and development under steps 1 and 2 provide the basis for an action program, but some practical benefits may be realized from this activity. A somewhat detailed workflow chart has been prepared as a procedural guideline covering major steps 1 and 2. A greatly simplified version is presented in figure 40-1. In considering a workflow chart, it is important to realize (1) that all blocks are not mutually exclusive, (2) that they are often intricately related by a complex series of activities that merge into one another, and (3) that the workflow is not always progressively down the chart. Work is currently being concentrated in block 4 (Vegetation-Image Relationships), but this does not imply that all activity in blocks 1, 2, and 3 is completed, nor that no contributions have been made to the lower blocks.

Ground-Truth Methods

The ground-truth record card was also adapted from our other research experience to meet the requirements for documenting vegetation, soil-surface, and physiographic factors that may influence the visible spectrum images in space photography. Marginal, hand-sorted punched cards were used to facilitate data summarization as the number of records increases. The ground-truth record provides notes on the major plant species in each stand examined. Individual dominance scores, ground-cover percentages, and a rating of sociability, or tendency to cluster, is assigned to each species. Soil-surface color is recorded according to standard Munsell color charts. The percentage of the ground surface covered by gravel, stones, and litter is estimated, as well as is the amount of bare, mineral soil surface evident when viewed from above the vegetation.

These records are documented by ground photography with both color negative and Ektachrome Aero IR film.

The location of ground-truth stations is decided from a careful study of 8- by 8-inch transparency enlargements or color prints of the space photography. Examination in stereo is frequently helpful. Images are tentatively classified or grouped on the basis of color, texture, and pattern, and representative examples are selected. These are located and visited on the ground, and the appropriate records are made. A second documentation procedure involved logging changes in vegetation and/or soil-surface conditions as these were observed along routes of travel. These road-log points were carefully located and then related to their position on the space photography. The success of this latter approach depended very largely on accuracy of location. We found it necessary to prepare a rectified enlargement of the Gemini IV frame on which our work was concentrated. Without this, it was impossible to locate all ground-truth stations. Preliminary viewing of Apollo photography indicates that rectification of these photographs will not be necessary because of the small tilt angle and because a very large percentage of the major roads are visible.

These ground-truth records were further supplemented by color negative and color IR photographs taken from a small aircraft flying at an elevation of 1500 to 3500 feet over those portions of the study area where we had the best distribution of ground-truth stations.

To aid with some particularly critical interpretation problems, Robert C. Heller of the Forestry Remote Sensing Laboratory, Pacific Southwest Forest and Range Experiment Station, also took some useful color and color IR aerial photography over designated areas in 70-millimeter format at a scale of approximately 1:16 000.

In addition, we were fortunate to obtain access to some color IR aerial photography taken by the U.S. Geological Survey in the study area. This photography was taken with a high-resolution lens on a 5-inch format at a scale of approximately 1:200 000. We were able to select some areas from this photography which provided useful subsamples in problem areas.

Data Analysis and Legend Development

The ground-truth data are being analyzed by standard phytosociological methods used in the classification of vegetation (ref. 40-3). These procedures result in the assembly of the data records which represent concrete stands of vegetation into similar groups and the assembly of these in turn into a hierarchical classification. The groupings are on the basis of similarities in the plant species that comprise the

societies at each ground-truth station. These groups are then described on the basis of the data contained in the ground-truth record for the group. This phytosociologically interpreted information then becomes the basis for developing the legend to use in interpreting photographic images.

The ecological groupings are correlated with the photographic images so that it becomes possible to state which are represented either singly and uniquely or in combination by the various photographic images. The descriptive legend for these image-related groups will consist of the written description, data summaries, and supporting ground photographs that represent each group. The descriptive legend is abbreviated for practical use by a symbolic legend. This may be either a connotative or nonconnotative symbol system that permits one to label concisely each mapped delineation in terms of the descriptive legend units. It is from this legend information that photointerpretation keys and aids will be developed for practical use. It is through this comparison of legend units and classes of photographic images that the signature relationships are worked out.

Interpretability Tests

The proof of the apparent signature relationships rests not on those worked out as a direct result of research, but rather in the answer to the question: Can practically oriented users consistently apply the knowledge of signature relationships in the extraction of valid data from space photography?

For each interpretable feature, we need some measure of the reliability of statements that may be made by image analysts. It should be recognized from the outset that completely accurate interpretation cannot be made without ground-truth information, and, in some instances, the validation of these statements will be possible only through ground examination. One of the purposes of our study is, however, to determine how far people with varying levels of experience and with access to varying levels of ground-truth data can go in making true and useful statements about native vegetation and related resources from the critical examination of space photography.

With these thoughts in mind, we have begun a testing program with volunteer interpreters. Their experience, background, and familiarity with the subject area varies. Each volunteer interpreter is given a good-quality, 8- by 8-inch color print of space photography for the subject area. He is instructed to examine the photograph carefully, delineate the similar image areas, indicate their similarity by a numerical code, then turn his imagination loose and make as many potentially

valid statements as he can about each delineation. He is to focus attention on statements of potential value in the decision process relating to the use, development, and management of rangeland and forest resources in the subject area. The procedure calls for repeating this process at three levels of background information:

1. Initially, the interpreter will draw only on the experience and knowledge he already has about vegetation and related resources in the subject area — his prior experience, memory, and skill.

2. At the second stage, he will be asked to repeat the job, and selected items from vegetation resources literature in the subject area will be made available to him.

3. At the third stage, each interpreter will, in addition, be provided our complete ground-truth record and be allowed to consult this, as well as the available literature in making his interpretation statements.

At each step, the accuracy of statements will be scored in one of the following categories:

1. Completely correct
2. Partially correct
3. Completely erroneous
4. Indeterminant

This three-phase test should provide a good indication of the validity of statements and the kinds of information that might be obtained if a space-photography program oriented to vegetation-resource analysis were to go operational in the near future. While these experiments will not index ultimate capability, they will certainly give a reasonable indication of some of the immediate practical benefits and limitations in these kinds of uses of space photography.

PROJECT JUSTIFICATION

Highly productive rangelands comprise fully 46 percent of the land mass of the earth according to the best available estimates (ref. 40-4). If one adds to this figure the useful desert-vegetation types and grazable open forests the figure goes much higher. On the domestic scene, rangeland comprises 49 percent of the area of the United States (ref. 40-5). This figure includes Hawaii, but excludes Alaska and the

tremendous areas of tundra, meadow, and forage- and browse-producing forest openings that might be added to this grazing-resource acreage in our own nation. The total would greatly exceed half of our land area. Unfortunately, this vast resource has not been particularly well recognized, and many people tend to look upon range-resource areas as mere wasteland and an economic desert.

The terms range and rangeland are unique to North America. In other languages and nations, these terms convey the concept of native pastures, but they do not pass out of the range or rangeland classification just because they may have been culturally improved, if the management objective is to manage and perpetuate the resource as though it were naturally vegetated.

These naturally vegetated areas are grazed by both domestic animals and wild game, and it has been estimated (ref. 40-6) that these rangeland resources provide 6 months of the annual feed needs for one-half of the beef cattle, three-fourths of the sheep, and nearly all of the game animals produced in the United States (fig. 40-2).

These estimates notwithstanding, good figures do not exist on the contribution that this resource makes to our gross national product. In desperation, this author once attempted to estimate this contribution from the deplorable statistical working base. From available statistics and a few reasonable biological assumptions, I guesstimated that our rangelands produce domestic livestock gains worth somewhere between \$500 million and \$700 million per annum. This figure, right or wrong, makes no allowance for the tremendous value of game animals harvested annually from this same resource. No one knows an accurate total, but it is very high in nine figures and may even reach a billion dollars or more per annum.

Slightly more accurate figures can be calculated by individual states. In Oregon, for example, our rangeland resource comprises close to 50 percent of our land area and accounts for 28 percent of the agricultural income to our state in the form of a native forage resource that is converted to usable animal products by domestic livestock alone. Many states in the West and in the southern Coastal Plain can equal or better this level in the importance of their range resources to the local economy.

Looking at our national forests, where statistical information may, on the average, be considerably better, one can derive figures indicating very clearly that rangelands and range forage production within the national forests are making an increasing contribution to our national economy from domestic livestock products alone and that the domestic animal product of national forest ranges is still over one-third of the timber stumpage sales from these lands (table 40-I).

The figures in table 40-I exclude all credit for the wildlife yield of our national forests — a yield directly and critically dependent upon the forage and browse production of these lands — and gives no credit to range vegetation for its indirect contribution to watershed and recreational values.

Thus, it should be obvious to all that we are dealing with a sufficiently important resource that cannot be overlooked in the conduct of the Earth Resources Program and that we do have some information needs that may be appropriately met with space photography playing a potentially important role.

RESULTS AND DISCUSSION

Preliminary analyses of ground-truth records, initial attempts at a phytosociological classification of these data, and progress to date in relating photographic images to ground truth indicates that our procedures are working satisfactorily.

While we were not fully aware of the vegetation diversity at the outset, we have found that the area selected for concentrated study spans examples of the following four major vegetation-resource areas on single frames of Gemini and Apollo photography:

1. The Sonoran Desert
2. The Chihuahuan Desert
3. The "Desert Grassland" or Southwestern Shrub Steppe
4. The Chaparral and forested vegetation zones in the higher hill and mountain ranges

This complexity represents both advantage and disadvantage to the project. The disadvantage lies only in the complexity of the vegetation-image relationships that result from this diversity. It would be much simpler to work entirely within one of these provinces, but such a concept is not compatible with the potentialities of synoptic coverage from a space platform. Each of these major vegetation types represents millions of acres of land in southwestern United States and Mexico. From the standpoint of developing and testing capability in the interpretation of vegetation resources from synoptic space photography, we believe we made a wise selection. The information we shall develop from this one frame can be tested in similar areas on a number of adjacent frames to the east and west. This will provide a better test of capability

and a clearer definition of problems than would result from more intensive study in a narrowly restricted area. The procedures need to be tuned to the synoptic coverage and levels of generalization to which space photography is suited and where it truly holds advantages over aircraft photography.

Correlation of Ground Truth with Photographic Images

The Gemini IV photography with which we have worked to date presented some unique problems in relating ground-truth records to specific photographic-image components. This resulted from the low resolution which failed consistently to show major routes of travel and from spatial distortion in the slightly oblique view. Preliminary perusal of Apollo photography indicates that its slight tilt angle and higher resolution may have eliminated most of these problems. In using the Gemini IV photography, we found it necessary to rectify our study photograph to the 1:250 000-scale Army Map Service (AMS) topographic sheet (fig. 40-3). After performing this rectification and making a tracing of major travel routes from the AMS topographic sheet to overlay the rectified enlargement, we were able to locate nearly all ground-truth stations with reasonable accuracy and to relate each to a specific image area.

While stereoscopic viewing of duplicate 70-millimeter transparencies in the field has some advantages, the most desirable enlargement for study is in the range of 8 by 8 to 10 by 10 inches. Color transparencies (accurately controlled for color balance and saturation from frame to frame) are the desired working document. Color prints of the same size were found satisfactory. They have some advantages as semi-expendable working documents when color balance is adequately controlled (a requirement rarely met by commercial suppliers and subcontractors). In all cases, it is extremely important to work with first generation duplicates or copies made from a first generation internegative. Until consistent color balance is achieved or purposefully manipulated to refine interpretations, earth resources surveys of native vegetation and soil areas from color photography will very likely not be able to go operational.

Classifying Vegetation Data — Preliminary Legend

This phase of the work has just barely gotten underway. All of the ground-truth stations have been provisionally classified into six major classes of groups and six lesser or miscellaneous groups. At the present time, we feel that these major classes and some of the minor classes are compatible with Gemini IV image characteristics — that is, may be

interpretable from image characteristics — but this hypothesis has not been tested. We are quite sure that these classes will be equally compatible with other photographic-imaging systems and that the legends we are developing will also serve as vegetational ground truth for analyzing the capability of other imaging systems, particularly Apollo photography.

Signature Relationships

Work to date strongly suggests that the individual plant communities can only rarely be interpreted from imagery of Gemini IV quality, yet meaningful vegetation interpretation can certainly be made from this imagery. Interpretation of the imagery will require capable people with considerable knowledge and insight about vegetation-resource ecology and about the information needs of those who will make decisions about these resources. In addition, accurate interpretation will require the logical, biologically accurate, and managerially meaningful grouping of plant communities into larger hierarchical classes that are consistent with the interpretable image characteristics. The interpreter of space photography for vegetation-resource application will continually be faced with the problem of generalizing from the high amount of detail evident to him on the ground to a point that matches the grossly integrated images obtained with space photography of low resolution. This problem does seem to have a practical and not too difficult solution for those who are willing to seek the common denominators that tie similar vegetations together above the specific plant communities or association level.

We are striving to develop workable mapping legends that will permit interpreters to extract all possible information from space photography available to us. We are not content to develop a broad, highly generalized legend which merely permits one to make pretty pictures of extremely broad generalizations. We should work instead to prepare legends that are related to image characteristics, but which may permit exceeding the limits of reliability in interpretation. Subsequent experiments to test interpretability should identify the highest feasible limits on interpretability and insure maximum usefulness of the imagery.

Starting to move in this direction, we have been able to group a few photographic images into three classes: (1) those highly and consistently interpretable, (2) those moderately interpretable with reasonable consistency, and (3) those with low interpretability. Examples of highly interpretable images are seen in figure 40-4, delineations number 1, 5, 8, and 9. Delineations 4, 6, 7, and 10 represent moderately interpretable images. The area represented by delineation 3 contains images having low interpretability. It may be possible to move images

presently classed in the low group to a higher level of interpretability by (1) better image quality control, (2) quantitative study and characterization of image features, and (3) more thorough analysis of subsampling by aerial photography in these problem areas.

If questionable delineations can be ground checked in areas where phytosociological research is adequate and where legends consistent with image characteristics have been developed, the uncertain or questionable interpretations can obviously be corrected and near 100-percent accuracy achieved. Particularly where small-scale synoptic coverage is involved, it is not feasible to ground check all mapping and every interpretation. The research and development objectives should, therefore, be to refine and clarify the vegetation-image relationships so that the amount of ground checking required to meet resource analysis objectives can be held at an economically feasible minimum. Subsampling problem areas with appropriate aerial photography seems to be one of the best ways to solve these kinds of problems and hold groundwork to a minimum on an operational survey program.

Notwithstanding the photointerpretation problems that result when one attempts to interpret space photography without complete ground checking, the increased accuracy of delineation that is evident in figure 40-4, as compared to available small-scale vegetation-resource maps for this area (refs. 40-7, 40-8, and 40-9), casts a strong vote in favor of using space photography for the development of small-scale vegetation-resource maps.

Soil-Vegetation Interaction

Soil and vegetation interact strongly to determine photographic-image characteristics in arid areas. In some cases, this interaction enhances interpretability, and in other cases it creates definite problems and is the result of potential interpretation error.

Where the primary interest is in soils characteristics, the vegetation may so strongly obscure the soil as to deny it the opportunity to show through and directly influence photographic-image characteristics. Dense forests are an example. In these cases, soil characteristics can be interpreted only from prior knowledge of the vegetation-soil relationship. The accuracy of soils interpretation is dependent almost entirely on the adequacy of background research and on accuracy with which the vegetation component can be identified from the image.

However, the vegetation in arid environments may be so sparse that the bare soil surface is the dominant feature controlling image characteristics. In these instances, vegetation variation may not create observable differences. This is particularly true in extremely small-scale

images for which ground resolution is low. In these instances, vegetation interpretations are almost entirely dependent upon the level of understanding of landform-soil-vegetation relationships and upon the degree to which imageable soils differences are correlated with significant vegetation features.

These observations serve to emphasize that no one imaging system is likely to provide all the informational needs of earth resources workers who are concerned with naturally vegetated areas. These seeming disadvantages and limitations resulting from the soil-vegetation interaction are, in our present opinion, less serious in rangeland than in forestry applications. Our needs are to see and analyze the whole ecosystem — with emphasis on the plant community and the vegetation-soil unit, rather than the individual species or tree. Thus, rangeland resources would seem to be ideally suited to inventory with high-quality satellite photography because the imaging system, in fact, sees the whole ecosystem. Important portions of the ecosystem (e.g., soil surface and undergrowth vegetation) are not often completely obscured by a dense canopy, as is frequently the case in forested environments.

Practical Use of Supporting Aerial Photography

It would be extremely misleading to imply that the interpretation of space photography is free of some difficult problems. One of the most critical is the dearth of ground truth (phytosociological studies and research results on vegetation-environment relationships) in areas that may be potentially served by space photography of other imaging systems. Small-scale, high-resolution aerial coverage at scales of 1:150 000 and smaller can play a real part in filling the voids in ground-truth information. Ground-truth studies must be reasonably related to what can be seen and to the manner in which subjects are imaged by an anticipated system. Having had experience with aerial photography taken at scales from 1:600 to 1:200 000, it seems that ground truth developed by the use of the smallest available scale is not only desirable but highly advantageous when the intended purpose is application to the interpretation of space photography. In spite of the higher resolution, such small-scale aerial photography does effectively simulate space photography in a usable way.

High-resolution, small-scale aircraft photography provides effective support for the interpretation of space imagery. Multistage subsampling of these areas is sometimes necessary. In some cases, images which cannot initially be discerned on space photography can be both detected and identified after they have been studied on the aircraft photographs. In other instances, cues to recognition are oftentimes first identified from the study of larger scale and particularly high-resolution images.

In putting delineations on space photography, the location of mapping unit boundaries sometimes becomes indistinct because of gradual changes in the vegetation (broad ecotones) or because of the integrative effects of the space imagery and/or anomalies in photographic reproduction. These boundaries can sometimes be more clearly discerned and more accurately mapped on the space photography after they have been studied on the larger scale photographs.

Before an earth resources satellite, tuned to the needs of native vegetation-resource inventory, can go operational, many problems relating to optimum spectral bands, season of photography, optimum sun angle, and optimum resolution will have to be worked out — at least to the point that a satisfactory compromise can be achieved with other uses and application of the earth resources imaging system. Most of these answers can be achieved more economically by the use of aircraft systems in experiments especially designed to consider remote-sensing problems in rangeland resource areas. Thus, effective aircraft systems must be an integral part of investigations seeking application of space photography to native vegetation and related resource analysis objectives. Some of the potentials of using aircraft photography in conjunction with interpretation and mapping from space photography can be illustrated by a comparison of figures 40-4 and 40-5.

SUMMARY

We are approaching our research on the feasibility of using space photography for vegetation and related resource inventory of rangeland areas from one dominant philosophy — namely, that we should strive to determine the limits of interpretability and practical use of available spacecraft imagery. We are particularly concerned about information that will contribute to the solution of problems in resource policy, broad planning, and use decisions to the extent that the imaging systems permit. We believe that we should also strive to obtain information useful at management decision levels, but spacecraft imagery does not seem to be well suited to this latter need.

Depending on the nature of information required, the relatively low resolution presently obtainable from space platforms can, to a point, be an advantage because of the integrative effect of distance, small scale, and low resolution on the images registered by the system. Where major differences and broad groupings are the objective, more accurate pictures of resource characteristics can often be obtained from very small-scale than from large-scale imagery.

Where ground-truth research has provided an understanding of the phytosociology and vegetation-soil relationships, where emphasis is on

the interpretation of the plant community rather than on the single species, where the information needs and resource analysis objectives are clearly stated and a large amount of detail is not a requirement, and where small-scale synoptic coverage can be supplemented as necessary by intermediate-scale and higher resolution aerial-photography subsampling, space photography would seem to have a real place in vegetation-resource analysis.

In rangeland environments, the whole ecosystem tends to be registered in an effective and usefully integrated image. Rangeland environments, therefore, seem ideally suited to analysis with small-scale synoptic photography.

In developing this capability, high-quality aerial systems must play a substantial part. Aircraft missions timed effectively to support imagery obtained from space platforms can help by providing information useful in the following ways:

1. To determine optimum season or sequencing of imagery for specific objectives
2. To help unravel the especially difficult interpretation problems
3. To provide a working base for the development of vegetation-soil legends for use in interpretation and mapping from spacecraft imagery
4. To provide a broader spectrum of sample imagery to be used in the training of interpreters and to give them experience ahead of the availability of space photography in northern latitudes or prior to going operational on a space system for earth resources analysis

We feel confident that continuing work on our project will determine many of the feasibility limits to the use of spacecraft photography for inventorying vegetation and related resources in rangeland areas. Our research will more clearly identify many of the problems and needs which must be given attention before a space system goes operational. We are presently encouraged by the indications of feasibility and believe our methods and procedures are working satisfactorily. We hope that research in the forthcoming year will be able to make greater use of supporting aircraft data.

REFERENCES

- 40-1. Carneggie, David M.; Poulton, C. E.; and Roberts, E. H.: Remote Sensing Applications in Forestry: The Evaluation of Rangeland Resources by Means of Multispectral Imagery. Forestry Remote Sensing Laboratory, Berkeley, California, Annual Progress Report, September 1967.
- 40-2. Lauer, Donald T.: The Feasibility of Identifying Forest Species and Delineating Major Timber Types by Means of High Altitude Multispectral Imagery. Forestry Remote Sensing Laboratory, Berkeley, California, Annual Progress Report, September 1967.
- 40-3. Ellenberg, H.: Grundlagen Der Vegetationsgliederung. Part 1 of Aufgaben und Methoden der Vegetationskunde as vol. 4 of H. Walter, Einfuhrung in Die Phytologie, 1956.
- 40-4. Shantz, H. L.: The Place of Grasslands in the Earth's Cover of Vegetation. Ecology 35 (2):143-145, 1954.
- 40-5. Williams, Robert: Personal communication with data compilation. Soil Conservation Service, Washington, D.C., Files, Range Management, Oregon State University, 1968.
- 40-6. United States Department of Agriculture: A National Program of Research for Forestry. U.S. Gov't Printing Office, Washington, D.C., 1967.
- 40-7. Shantz, H. L.; and Zon, R.: Natural Vegetation; Grassland and Desert Shrub. U.S.D.A. Government Printing Office, Washington, D.C., 1924.
- 40-8. Humphrey, R. R.: Arizona Natural Vegetation. University of Arizona Bulletin A-45 (map) Ag. Expt. Sta. & Coop. Ext. Ser., Tucson, Arizona, 1963.
- 40-9. Kuchler, A. W.: Potential Natural Vegetation of the Conterminous United States. American Geographical Society. Spec. Pub. No. 36, 1964.

TABLE 40-I.- COMPARATIVE VALUE OF LIVESTOCK PRODUCTS
FROM THE NATIONAL FORESTS

Year	Timber sales, dollars	Value of livestock gain, dollars	Livestock gain, percent of timber sales
1955	73 187 364	51 918 477	71.0
1960	139 900 000	68 090 472	48.7
1967	208 603 585	71 963 478	34.5

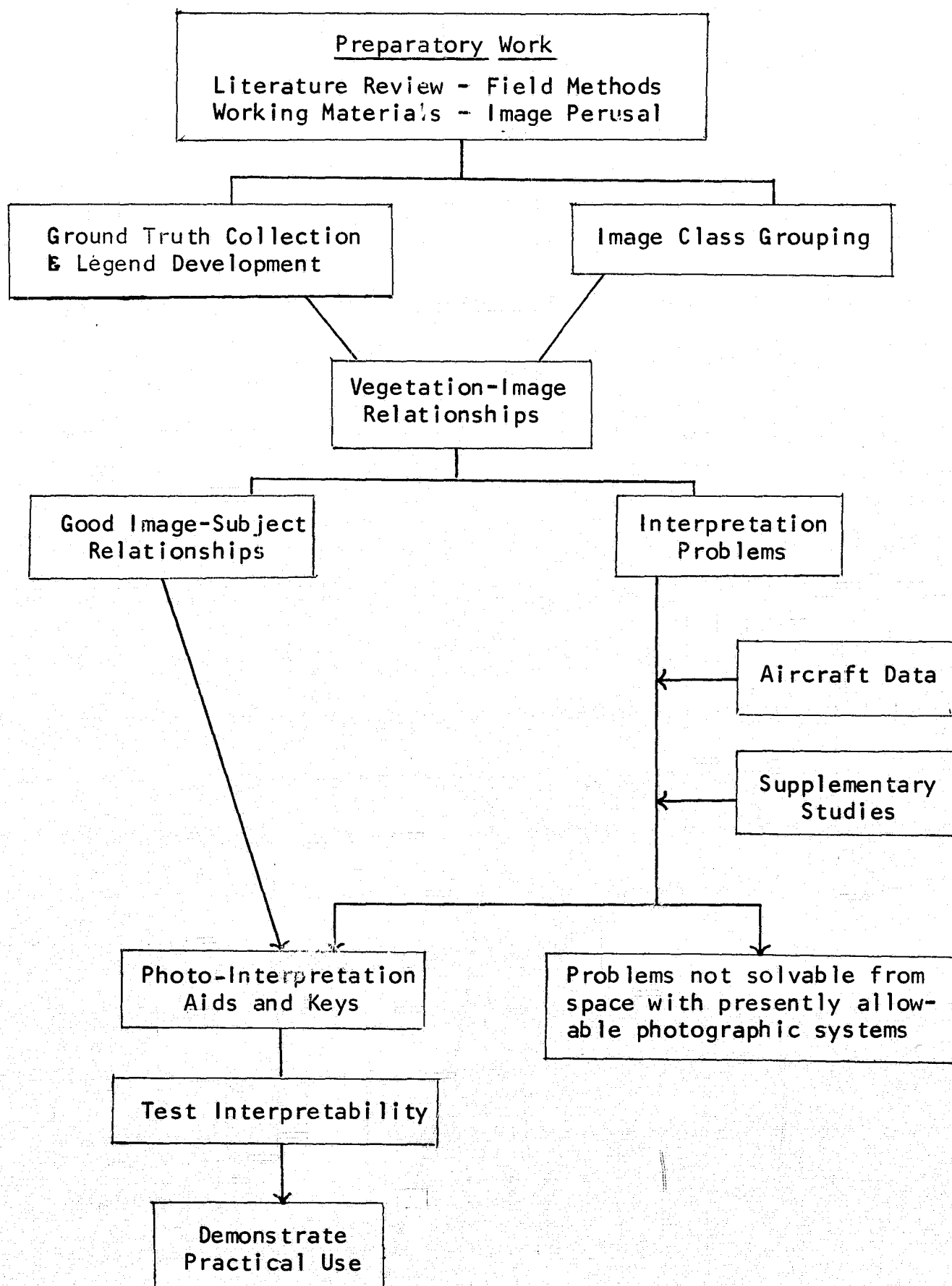
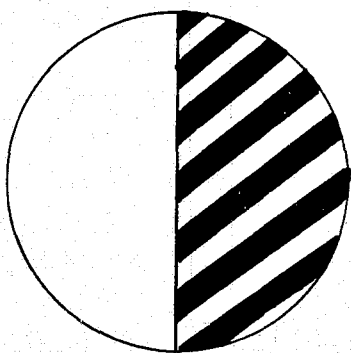


Figure 40-1.- Chart of work flow for the use of space photography in the inventory and analysis of rangeland vegetation and related resources.

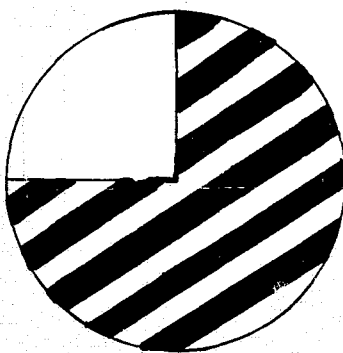
RANGELAND FEED, WATER AND COVER
(Steppe, Desert, Forest)

Provide Six Months of the
Annual Feed Needs
for

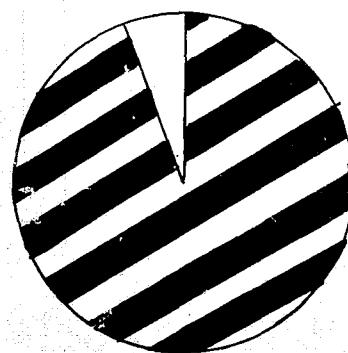


BEEF

And Nearly All
of the Feed
for



SHEEP



GAME

Figure 40-2.- Range vegetation provides a critical part of the feed base for the domestic livestock industry and supplies nearly all the feed and cover for big-game population.

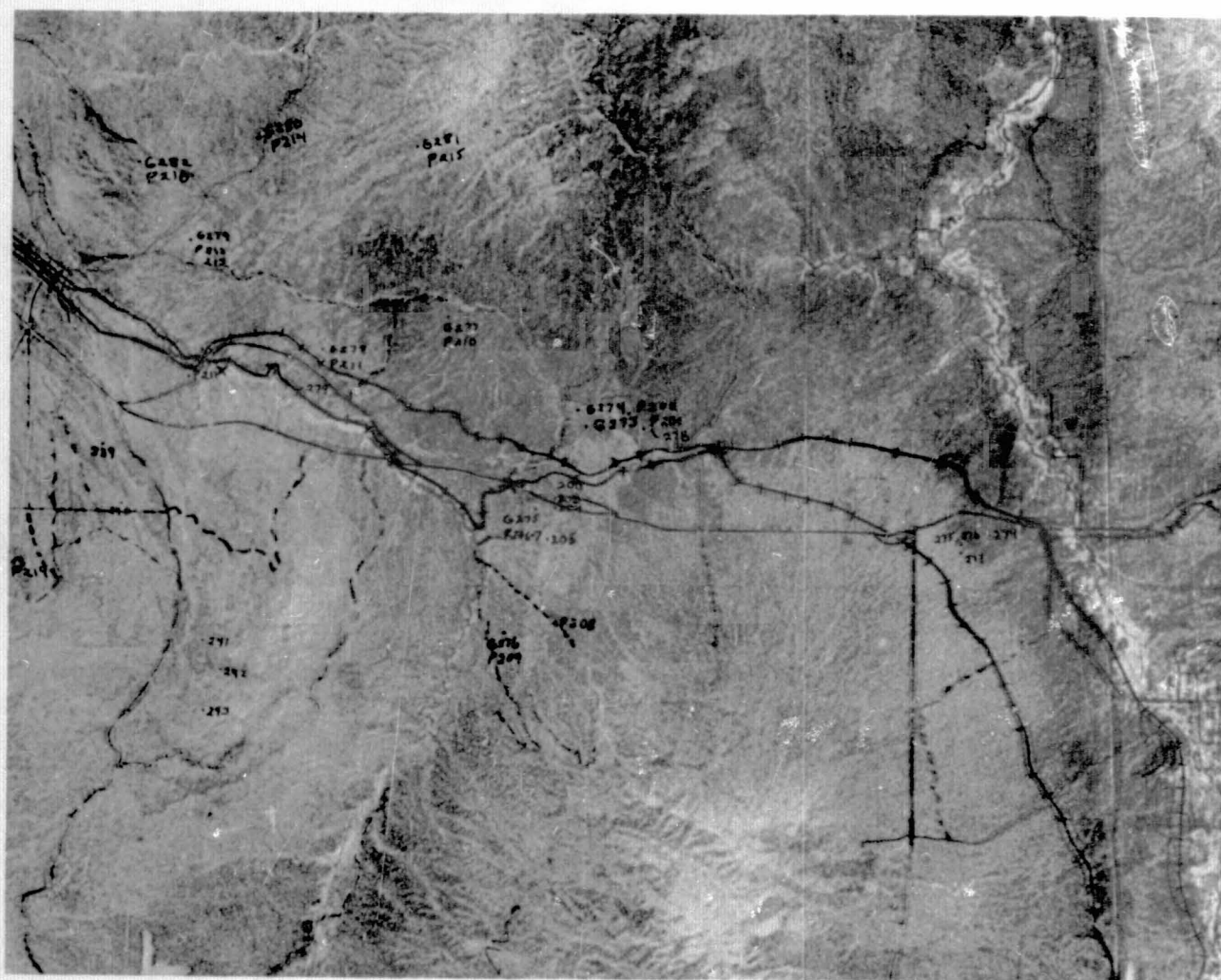


Figure 40-3.- Part of a Gemini photograph enlarged and rectified to a topographic map (1:300 000 scale). The black lines are travel routes traced from the topographic sheet and superimposed over the rectified enlargement. This combination enabled researchers to relate ground-truth data to specific image components.



Figure 40-4.- A preliminary vegetation resource map prepared on Gemini IV color photography. These photography images have been identified according to the major plant communities and soil surface conditions that each image represents. Some photography images are highly interpretable, and others are difficult to identify. Some images represent highly specific kinds of vegetation, and others merely indicate areas with certain general features in common.

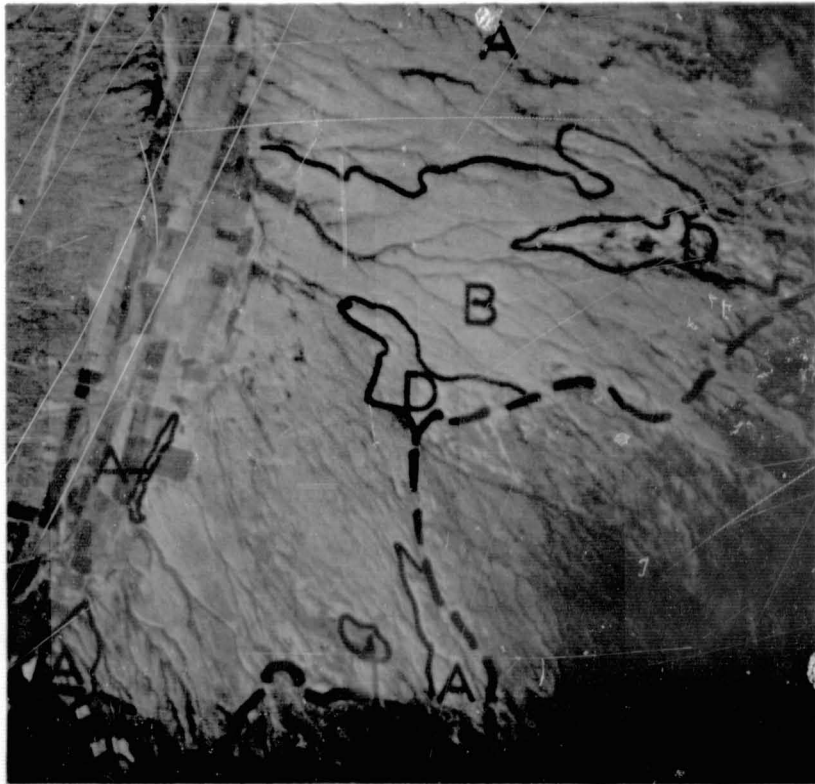


Figure 40-5.- A comparative example of vegetation mapping with the same information as in figure 40-4 on high-resolution aerial photography. Judicious subsampling of problem areas with aerial photography is essential in detecting important image features in space photography, in working out ground-truth image relationships, and in improving mapping delineations where meaningful image differences are subtle. (Original scale approximately 1:200 000; color IR photographs courtesy of U.S. Geological Survey.)

N71-16163**RESULTS OF EARTH RESOURCE INVESTIGATIONS**

By Marvin R. Holter

University of Michigan Research for the NASA/U.S. Department
of Agriculture Earth Resources Program

Research at the University of Michigan under the Earth Resources Program is focused on the problems of data processing/interpretation/utilization for agricultural purposes. The results presented here are representative of those being obtained. All the results obtained under this program cannot be presented in this paper because of time and space limitations.

Imagery and discrimination results for data obtained at an agricultural test site are presented and discussed. The aerial photography and scanner data were obtained by scientists at the University of Michigan, and the discrimination results were produced by the same University of Michigan group. Ground data and measurements were provided by scientists of the University of California, Berkeley.

The basic data were obtained with the University of Michigan multi-spectral sensor carried in the University of Michigan C-47 aircraft. Since NASA provides the funding for the use of this facility in the Earth Resources Program, it seems legitimate to regard it as a part of the data-gathering facilities provided to the scientific users by NASA MSC.

The results presented demonstrate great progress in discrimination over current operational aerial survey techniques. Lest these results be misinterpreted, however, it is well here to point out equally the limitations in what they demonstrate. All the discrimination results shown have been achieved by employing the data from a single flight over the test site to derive signatures and by then applying those signatures to data (from the same flight) used to generate the signatures. Therefore, what is demonstrated is that signatures can be generated and a high order of discrimination achieved by applying the signatures in pattern-recognition processes to data taken on the same date, at approximately the same time, with the same weather and sun angles, and at geographical areas in the immediate vicinity of the areas used in deriving the signatures. The extent to which those signatures and those decision processes can be employed to effect satisfactory levels of discrimination at different times of day, at other parts of the year,

under different weather conditions, at geographically distant locations, and so forth, remains yet to be determined. That research work remains to be carried out. However, the level of performance achieved under the restricted conditions outlined previously does provide a high degree of encouragement and motivation for continuing the research to investigate the extension of the methods in time, space, and variety of environmental conditions. Based on the results accomplished to date, the prognosis for achieving marked improvements under the wider variety of conditions appears very favorable.

The area for which data are presented is an agricultural area in the vicinity of Davis, California. The area is approximately one-half mile wide and 7 miles long, containing about 1600 acres. The airborne data were obtained in a 3-minute flight time. A number of display and recognition results are shown. Figure 41-1(a) is a photomosaic of the area produced from panchromatic film exposed with a K-17 aerial camera and a K-2 Star filter used under conditions described on the figure. As indicated on the figure, only four types of surface material are present in significant amounts: mature green rice, immature rice, safflower, and bare earth. Figure 41-1(b) shows the same mosaic without annotations. Figure 41-2 shows 18 images of the same area, each in a different narrow wavelength band, produced by a nonphotographic optical-mechanical-multispectral scanning sensor. Two things are immediately apparent: (1) by the simple expedient of making the observations in narrow spectral intervals, greater contrasts among the materials present are frequently achieved and (2) the relative contrasts tend to be different in the different bands. The latter provides a clue that spectral discrimination may be profitable.

Before proceeding to the automatic discrimination results, it is worth pointing out several other features and uses of such data. Having data available in many narrow spectral bands makes it unnecessary, except for purposes of proving the point, to employ photographic sensors. Results identical to those obtainable with photography (except for the very high geometrical resolution and fidelity of photography) can be had by combining and printing data from the subset of the total scanner channels which cover the same spectral regions as the photography. Figure 41-3 is an image reconstituted from scanner imagery to appear in the same manner as panchromatic photography. In fact, in one respect the reconstituted image is improved over the photomosaic (i.e., has greater fidelity with respect to the real situation). In the panchromatic photomosaic, it will be noted that the four large fields at the right of the image (three identified as mature green rice and one as immature rice) are lighter in tone than the adjacent fields to the left, while in the reconstituted panchromatic image, the fields are not lighter in tone. Examination of the original photomosaic, in which the individual frames overlap along the irrigation ditch that bounds the two groups of fields

reveals that the lighter fields are an artifact, the exposure of the lighter toned prints being different than the darker toned ones. In this respect, the reconstituted image is a more faithful reproduction of nature than the camera-produced photomosaic. Figure 41-4 shows a reconstituted image representing the way an infrared (IR) Aerographic film would appear.

Figure 41-5(a) shows a reconstruction of the way in which normal color film would appear. In one respect, this reconstruction differs from color film in being more faithful in reproducing the surface colors. All color films exposed at altitude have more or less of a bluish cast to the images, resulting from differential scattering of the visible wavelengths. This blue "haze" is absent from the reconstructed color image because it is possible to remove most of it from the electronic data before the image is printed. Such removal is not possible in any simple manner with the photographic sensor. Figure 41-5(b) shows a reconstructed IR Ektachrome (or as it is sometimes called — IR camouflage film) image.

In the imagery presented here, there will be three distinctly different uses of color presented. Ordinary color and IR Ektachrome film and reconstituted images are one use of color; the coding of wavelength in color is another. Ordinary color film is not usually regarded as a coding of wavelength by color because the coding is very much as the human eye sees the colors, but it is no less a color coding than any false color film such as IR Ektachrome. There is no technical reason why any wavelength, visible or invisible, cannot be coded in visible colors, especially when the data are available in many narrow bands, as represented in figure 41-2. A few of the very many possible color-coded wavelength presentations are given here. Figure 41-5(c) is, in a sense, the symmetric twin of IR Ektachrome film in that one ultraviolet (UV) and two visible bands are coded in color, as indicated in the figure. There are tonal distinctions, although of a somewhat subtle character, present in this image which are not apparent in the previously discussed images. Therefore, presumably, additional information can be obtained from the image. Specifically, notice that the two safflower fields have noticeably different tones. The difference is caused solely by differences in the appearance of the fields in the UV channel. The two fields appear in identical tones in all the other channels, as can be verified by reference to figure 41-2. This example demonstrates that additional unique information can sometimes be obtained by use of the UV region, a fact concerning which there has been much skepticism expressed. Exactly what many of these distinctions represent and to what use they may be put are not known yet because the information regarding the details of the ground situation are not available, and little is known regarding the spectral signatures of these crops and soils. The yellow band along the bottom of this image is a correctable defect of the existing sensor

system. One channel has a slightly different ground field of view than the others, and the yellow band represents the region out of the field of view of that channel. It was deemed preferable to present this image to include the same ground region as the other imagery, rather than to remove the defect by cropping this image.

Figure 41-5(d) is a color coding of three IR bands, as indicated in the figure. This is how the area might appear to IR sensitive eyes. There are some tonal distinctions which can be made here that are not apparent on any of the previous images. The strongest of these is the pair indicated by the arrows on the figure. The reason for this tonal difference between two fields containing the same crop — immature rice — will be clarified later. Figure 41-5(e) is another color coding of wavelength, being one UV band, one visible band, and one IR band coded as indicated on the figure. Again, there are differences not noticeable in the reconstructed photographic imagery of the several types, and the strongest of the differences is in the pair of fields containing the same crops noted on the figure 41-5(d).

Figure 41-5 represents only a few of the many possible codings of wavelength by color. The value and utility remain yet to be established by further research, but these codings represent the simplest of all discrimination techniques. They accomplish the translation of invisible wavelengths to the visible and then rely on the human interpreter for the use of the new tonal distinctions to draw conclusions regarding crop type, condition, and so forth. Such presentations may provide a useful bridge between conventional imagery and highly processed imagery for the traditional photointerpreter. These presentations have obvious resemblances to conventional imagery but represent a step in the direction of using nonvisible wavelengths and refined processing. However, the codings also provide further experimental evidence that simple additive techniques are far less powerful than the more refined processing techniques illustrated in the following.

With information in 18 channels and three primary colors available for coding, there are more than 4000 simple color codings of wavelength. By adding channels before color coding, many additional simple additive combinations are possible. This not only makes it possible to portray visually the wavelengths outside the visible range, but also makes possible the investigation of an extremely large number of possible film-filter combinations without the need for large expenditures to generate the data photographically. This generation would require a prohibitive number of cameras or a prohibitive number of flights, changing the filter between each.

Figure 41-6 portrays three different ways of coding the amplitude of the signal within a single band. The 8 μ - to 14 μ -wavelength band has been shown, since it represents apparent temperature. The radiant power

in this band is, for all practical purposes, entirely due to self-emission, both during the darkness hours and during daylight. The temperature has been termed apparent because the true emissivities of the surface materials and the effects of the atmospheric transmission have not been taken into account.

Figure 41-6(a) shows a signal that has been quantized into eight levels, and only the boundaries at which the signal changes from one level to another are printed. Thus, the image consists of contours between regions with temperatures that are uniform within the ranges of the quantizing levels. Figure 41-6(b) is the same information presented in a different fashion. Rather than the contours being printed, each quantized level has been assigned a density level, and the entire region within the limits of that quantized level is presented at the same density. The colored image of the figure (fig. 41-6(c)) shows each quantized range coded in a different color. Note that this is a distinctly different use of color than the wavelength coding discussed previously. Any one of these presentations of apparent temperature may be useful in providing information leading to understanding of microclimate as one of the several uses of the three coding methods.

Reference to the images of apparent temperature in figure 41-6 now make it possible to understand why, as previously mentioned, two fields of immature rice appear quite different on two of the wavelength-color-coded presentations, but appear essentially identical on the other presentations. Reference to any of the apparent temperature presentations shows the lower triangular field to be at a significantly higher temperature than the adjacent field of the same crop. Agreeing with this is the fact that, among the images with wavelength coded in color, these fields are differentiated only in those images containing data from either the 8μ to 14μ or the 4.5μ to 5.5μ band, which are the only two bands dominated by emitted radiation. Furthermore, of the two wavelength-color-coded images, the contrast between the two adjacent fields is strongest in the image containing a contribution from the 8μ to 14μ band. This is in agreement with the fact that there is a greater amount of emitted radiant power in the 8μ to 14μ band than in the 4.5μ to 5.5μ band. In the color-coded apparent-temperature image, it will be noticed that the triangular field is blue, indicating an apparent temperature next to the highest in the area. The highest apparent temperature, colored violet, occurs in the fields identified as bare earth. This provides a clue as to the likely reason for the differing appearance of the two fields containing young rice. The young rice plants do not completely cover the ground; therefore, significant amounts of soil will be visible between the plant leaves. If the triangular field had been drained of water while the other field was still partially flooded, with plant leaves growing above the water surface, the results observed would be expected. The dryer soil of the better

drained field should reach a higher temperature at that time of day. The ground information is not sufficiently complete to verify this conjecture, but it fits the phenomena observed in the imagery. A rational physical explanation is also available.

A word of caution regarding the application of this quantizing and contouring technique to IR scanners is in order. For the levels or contours to be meaningful on a relative basis, the scanner electronic passband must extend down to very low frequencies, essentially to dc. Otherwise, there will be level shifts in the signals because of the characteristics of the electronics and not because of true temperatures on the ground. Under these circumstances, the meaning of the contours or levels is questionable. To the knowledge of the author, the only scanning equipment meeting these requirements is the instrument at the University of Michigan which produced the data shown. If, in addition to attaching significance to the relative levels or intervals, it is desired to associate quantitative meaning to the quantized intervals, the scanner must meet additional requirements; it must carry internal calibration sources on the ground adjacent to the area of interest. It is desirable that the scanner output be linearly related to radiation input to simplify interpolation between calibration levels. Again, the only scanner meeting those conditions known to the author is the one at the University of Michigan.

Shown in figure 41-7 are four images, each image containing only one type of surface material. Hence, these materials have been "recognized" and "identified" by a spectral pattern-recognition technique. Each recognition was effected using only two wavelength bands. The bands employed are indicated under each image. The recognition image for immature rice shows the fields not filled in solidly. This may indicate failure to classify correctly some of the rice present. It appears more likely, however, that the classification is correct and that the fields represent regions in which the rice plants are less fully developed, allowing more of the soil to show through and thus altering the wavelength distribution of radiation from the fields. Similarly, the left ends of the two mature green rice fields not classified as rice may not be errors but regions of the fields in which the crop is stunted in its growth because of poor drainage or some other reason. This illustrates a difficulty of interpreting the importance of errors in these pattern-recognition techniques. A common method of estimating the probability of correct classification is to add the areas or numbers of resolution elements that are correctly and incorrectly classified. The probabilities of correct classification thus obtained are frequently quite high, being in the 80- to 90-percent range. The operationally significant probabilities may, however, be still higher when the distribution of supposed errors is taken into account. If the supposed errors are randomly distributed like pepper specks over the image, it is

fair to assume that they are true errors and are caused by some deficiency in the pattern-recognition process. If, however, as appears in one corner of one of the mature green rice fields, the supposed errors are all grouped together, it is reasonable to assume they are not, in fact, errors but represent a corner of the field in which, because of poor drainage or some other such factor, the crop is not healthy and is not likely to produce a good yield. Under those circumstances, the operational probability of correct classification when making use of such additional considerations will be higher than the probability simply calculated on the respective classified areas that are not classified as crop. It is too frequently forgotten in remote-sensing research that operational systems will employ additional sources of information, knowledge of past history, a priori knowledge of common practices, and so forth, to check and refine the immediate sensor outputs.

A question frequently asked by potential users of these techniques is, "What is the minimum number of wavelength bands needed to identify a crop or soil?" This set of recognition images provides a type of answer and may indicate that it is not a very illuminating question to ask. It will be noted that, although only two bands were employed in each recognition, it was a different pair of bands which worked best for each crop. This indicates that while discrimination of a single material from a very limited set of background materials may be satisfactorily accomplished by using only two bands, the requirement to identify more than one material and one or more materials in the presence of a greater diversity of backgrounds will almost certainly require more than two bands. As the number of materials to be identified and the diversity of backgrounds present increase, the number of bands required for satisfactory performance almost certainly increases. Therefore, a more useful phrasing of the question might be something similar to, "For a desired probability of correct classification of a specified number of materials embedded in a specified number of backgrounds, what is the minimum number of bands for specified discrimination methodologies?"

As mentioned previously, it is not necessary to devote a separate image to each material recognized. There are several ways of combining the individual classifications. One way is shown in figure 41-8, in which each surface material is coded in a different color. Note that this is a third use of color, distinct from each of the two uses previously discussed. In this instance, decisions and classifications are made by some pattern-recognition methodology implemented in some device, and the results of the decisions are then assigned colors for display purposes.

This type of display is intriguing in that it furnishes a mechanization of what are now standard practices carried out manually. Quite

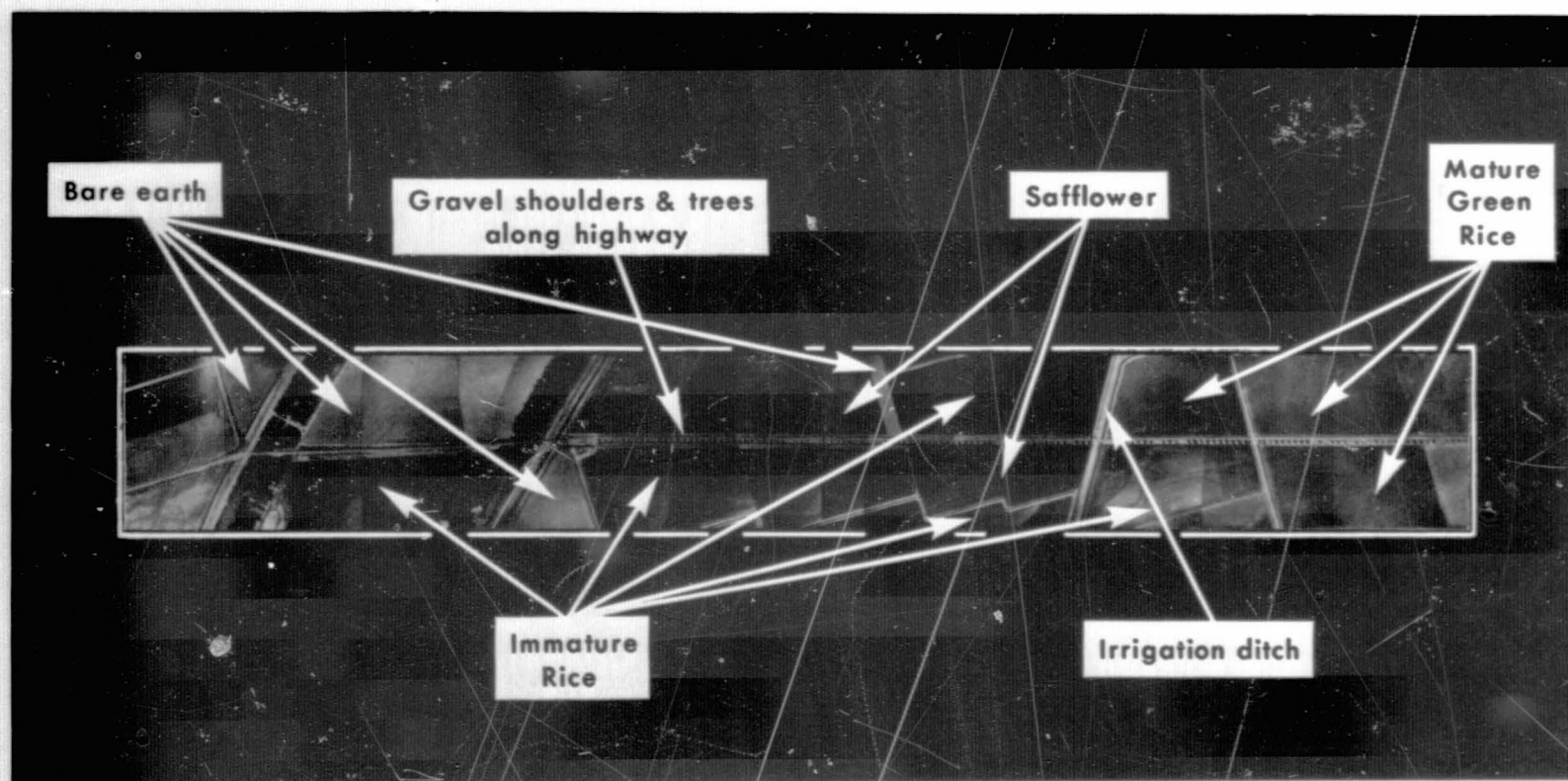
frequently, agriculturalists, foresters, and a host of others working with data from geographically distributed materials and conditions will laboriously gather great quantities of data on foot, and with tremendous labor on the part of draftsmen and others, transform it to maps which are color coded, cross hatched, or labeled with symbols or contours. Much past experience appears to indicate that such a presentation of the data is most comprehensible by the human user. What the image of figure 41-8 appears to indicate is that methods are being developed to gather and present that type of data in such presentations without requiring the large amounts of manual labor. (That is, it is becoming possible to go automatically from the data gathering to the final presentation in a single step.) As will be indicated shortly, it appears possible to carry the process at least one step further to the production of summary tabular results which may be more useful than coded maps for some purposes.

It was remarked previously that the decision processes can be carried out with any of the available computation methods. Figure 41-9 shows recognitions of the several materials, carried out by a digital computer. The prominent vertical lines of obvious misclassifications are not deficiencies of the process but intermittent computer electronic malfunction. The digital pattern-recognition techniques used by the University of Michigan to produce this result will not be described here. They are the same methods employed by other workers in remote sensing and other fields.

Having classified the surface materials according to type, there is no reason the computer cannot carry the process one step further and sum the areas of each. The result of doing this on the same data is shown in figure 41-10. For some of the operations of the U.S. Department of Agriculture Statistical Reporting Service, for instance, the summary data will be the preferred output. In fact, it does not appear likely that any users will find it very convenient to employ typewriter-produced pictorial presentations.

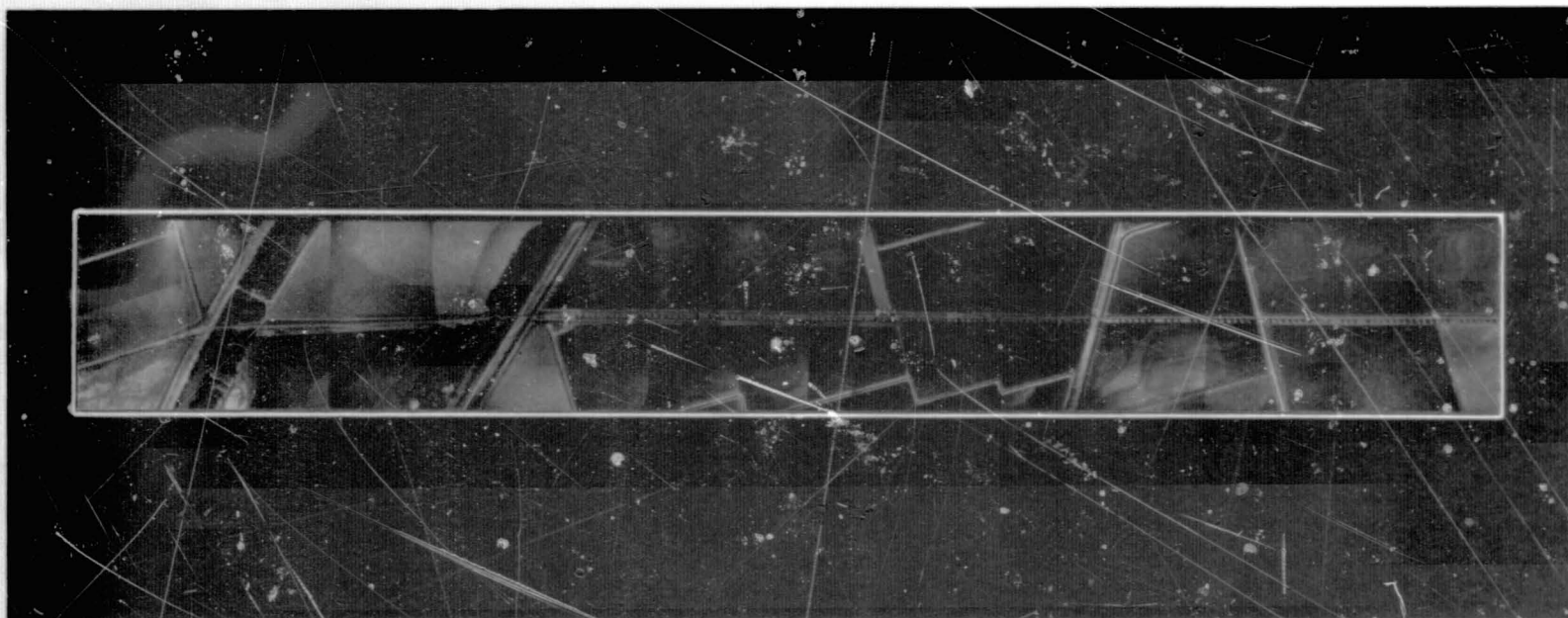
This last tabular presentation illustrates an aspect of remote-sensing research not yet receiving the attention it deserves. The ultimate results of remote sensing are operating decisions concerning acreage allotments, irrigation, fertilization, and so forth. There are many steps between recognizing a crop or a condition and arriving at the operating decisions. To date, most of the work has dealt with the recognition steps, and very little work has been done on the successive steps which make the recognitions useful. The same pattern-recognition and classification techniques being used to identify crop types and conditions will be useful in automating some of the succeeding steps because the pattern recognition methods are fundamentally statistical decisionmaking techniques. The automatic reduction of the pictorial presentation to tabulated areas is a first step in this direction.

It is not at all inconceivable that, for instance, the factors leading to a decision to irrigate can be so specified that the decision can be made automatically. For some time to come, of course, it will be well to have human beings check such automatic decisions, but such automation can, nevertheless, greatly reduce the manpower and labor in reaching the final decisions. It may be that the larger economies could result from automating or partially automating the more routine steps subsequent to crop and condition recognition than could result from automating or partially automating the recognitions.



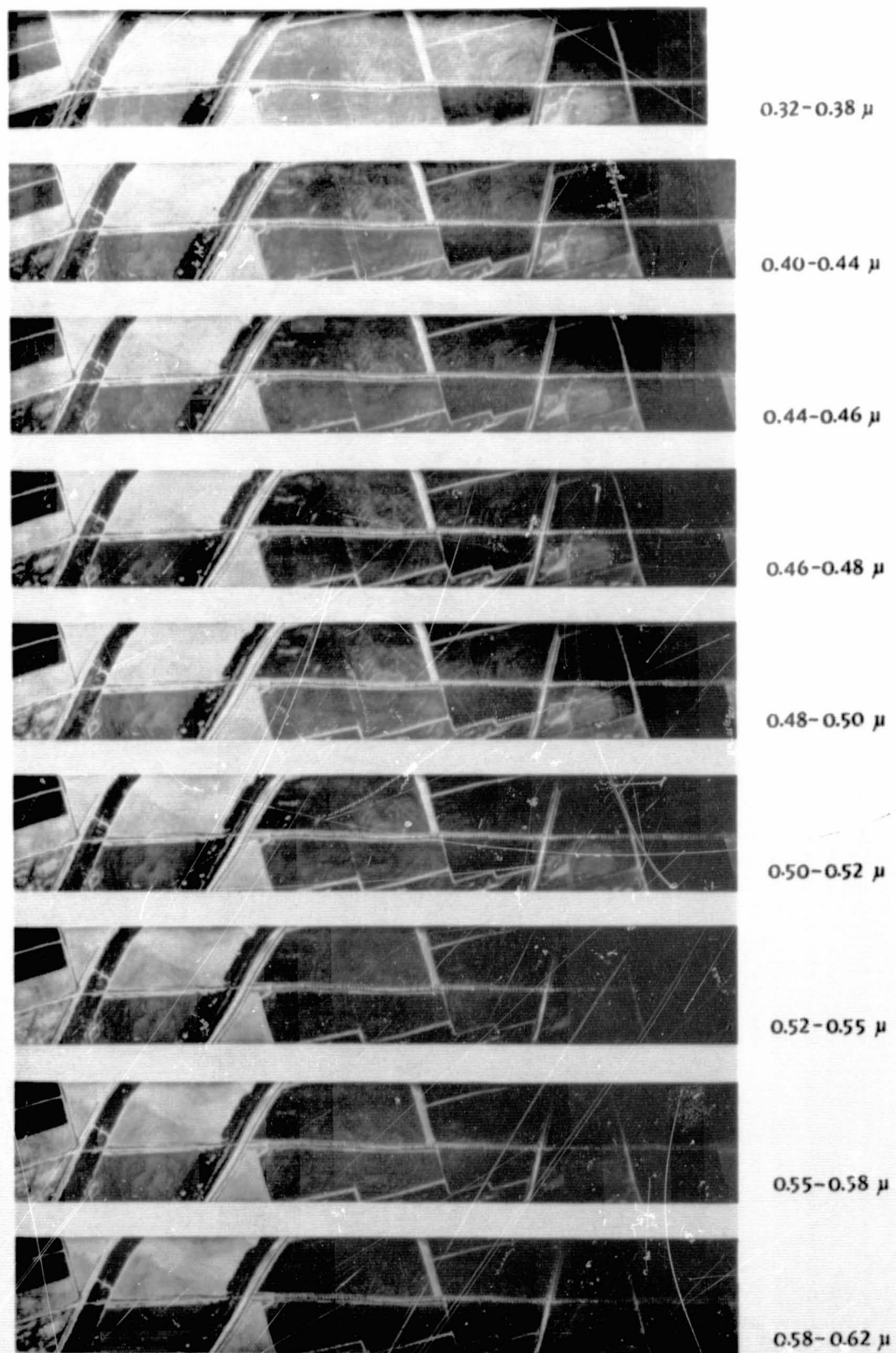
a. Photomosaic with annotations.

Figure 41-1.- Panchromatic photomosaics of Davis, California, agriculture area taken 16:00 hours, May 26, 1966, at 2000-foot altitude; sky condition clear and bright; 10-percent cloud cover at 30 000 feet; surface temperature, 27° C.



b. Photomosaic without annotations.

Figure 41-1.- Concluded.



a. Imagery from 0.32 μ to 0.62 μ .

Figure 41-2.- Eighteen multispectral images of Davis, California, agricultural area taken at same conditions and altitude as figure 41-1.



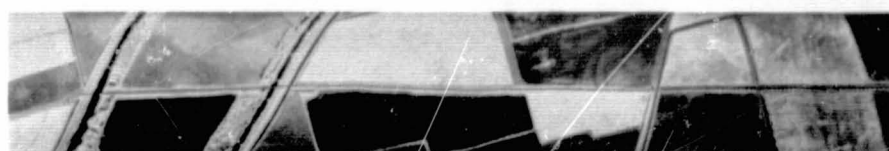
0.62-0.66 μ



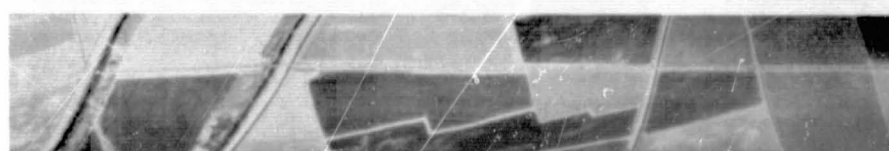
0.66-0.72 μ



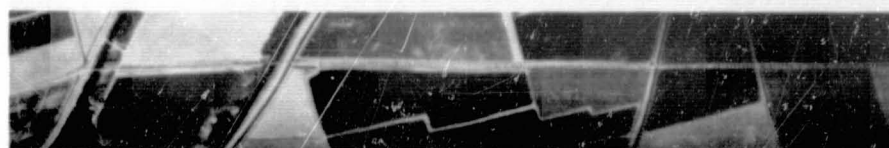
0.72-0.80 μ



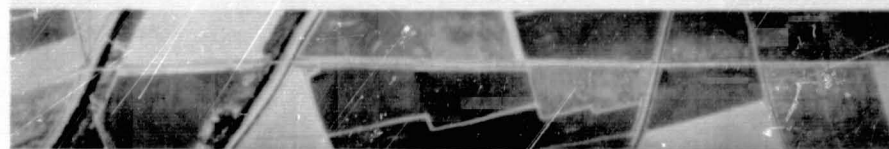
0.80-1.0 μ



1.5 - 1.8 μ



2.0 - 2.6 μ



3.0 - 4.1 μ



4.5 - 5.5 μ



8.0-13.5 μ

b. Imagery from 0.62 μ to 13.5 μ .

Figure 41-2.- Concluded.

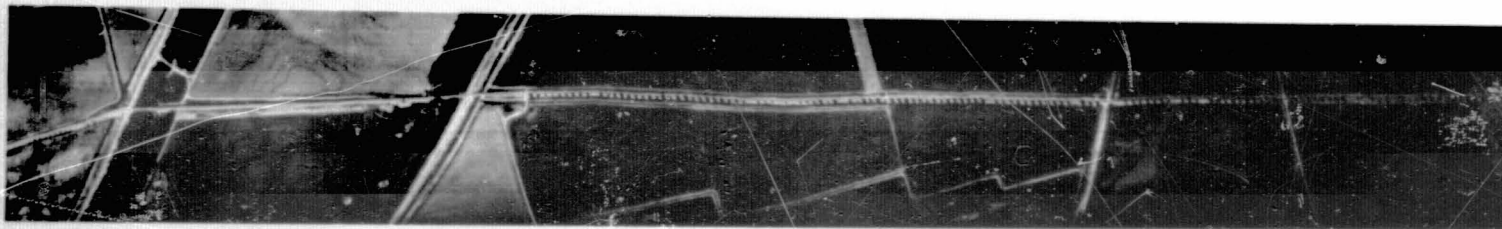


Figure 41-3.- Simulated panchromatic film imagery (with yellow K-2 Star filter) of Davis, California, agricultural area (three spectral regions: 0.52μ to 0.55μ , 0.55μ to 0.58μ , and 0.58μ to 0.62μ).

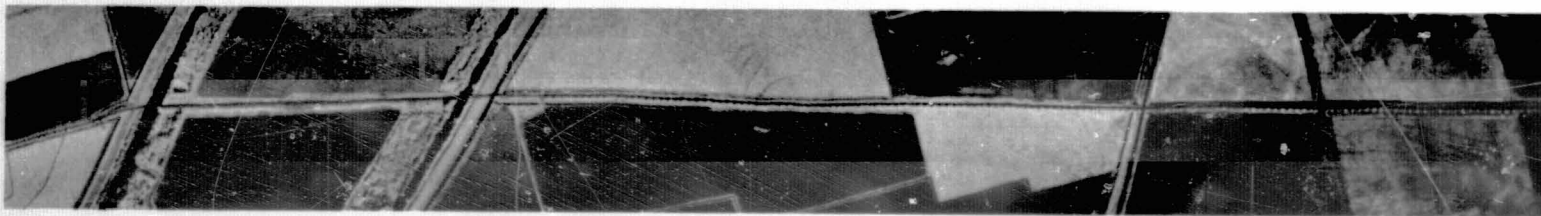
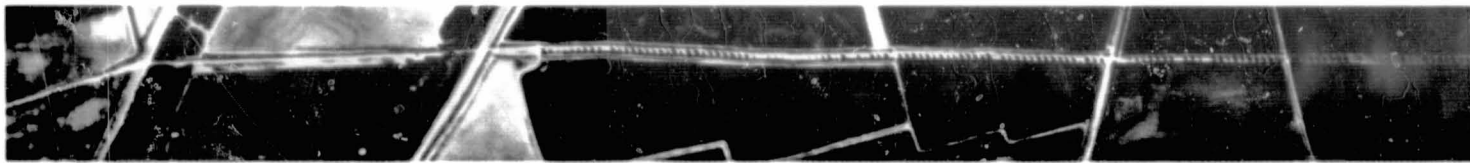


Figure 41-4.- Simulated IR Aerographic imagery of Davis, California, agricultural area
(positive transparency, 0.8μ to 1.0μ).

REPRODUCIBILITY OF THE ORIGINAL PAGE IS POOR.

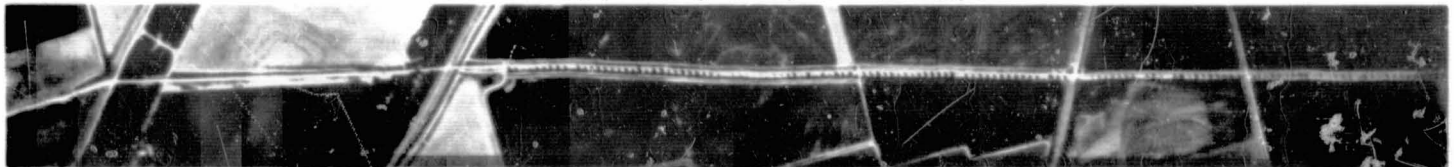
41-16



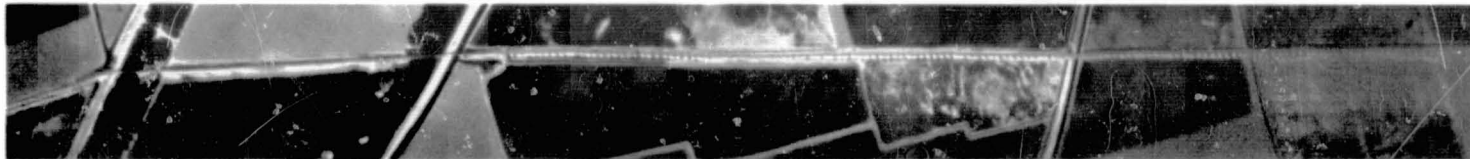
- a. Simulated color (blue, 0.44μ to 0.46μ ; green, 0.52μ to 0.55μ ; red, 0.62μ to 0.66μ).



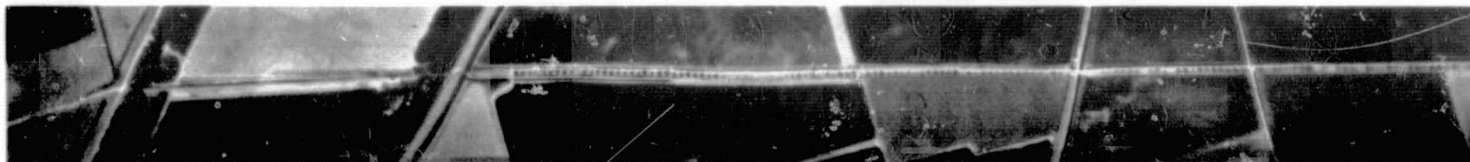
- b. Simulated IR Ektachrome (blue, 0.52μ to 0.55μ ; green, 0.62μ to 0.66μ ; red, 0.8μ to 1.0μ).



- c. Color-wavelength translation, UV, visible (blue, 0.32μ to 0.38μ ; green, 0.40μ to 0.44μ ; red, 0.52μ to 0.55μ).

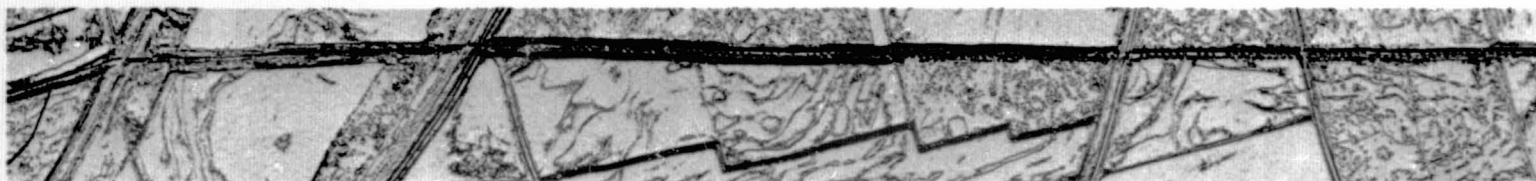


- d. Color-wavelength translation, IR (blue, 0.72μ to 0.80μ ; green, 2.0μ to 2.6μ ; red, 8.0μ to 14.0μ).

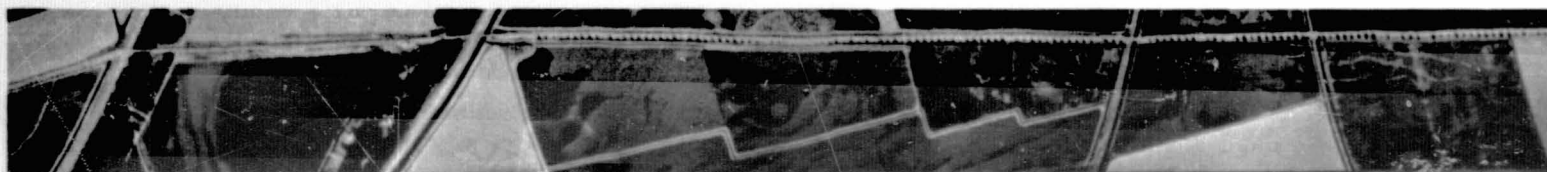


- e. Color-wavelength translation, UV, visible, IR (blue, 0.32μ to 0.38μ ; green, 0.66μ to 0.72μ ; red, 4.5μ to 5.5μ).

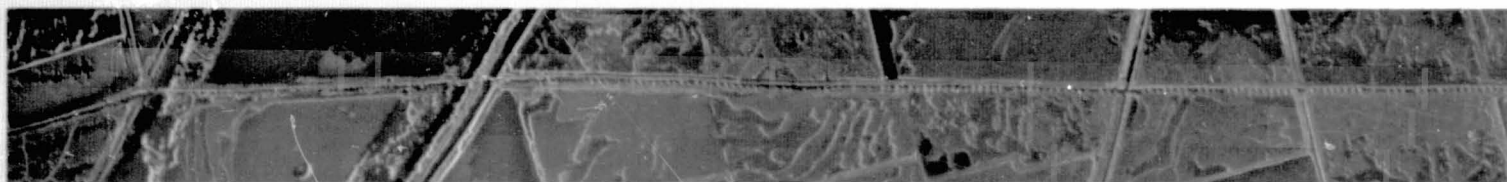
Figure 41-5.- Color imagery of Davis, California, agricultural area.



a. Thermal contours.



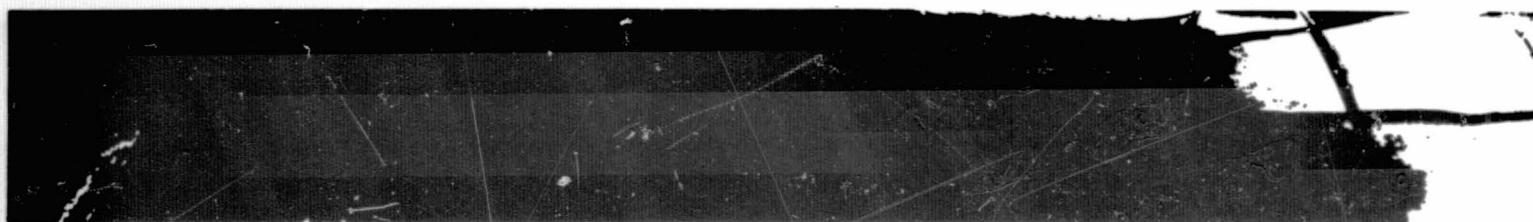
b. Quantized levels assigned density levels, with entire region within a quantized level presented at same density.



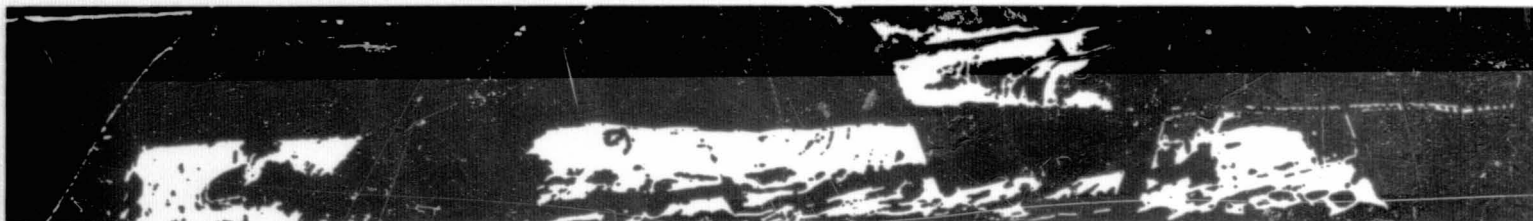
c. Quantized levels color coded. Highest temperature, violet, decreasing through sequence violet, blue, green, yellow, orange, red, brown, black (lowest temperature).

Figure 41-6.- The ways to code the amplitude of the signal within a single band (8μ to 14μ).

41-17



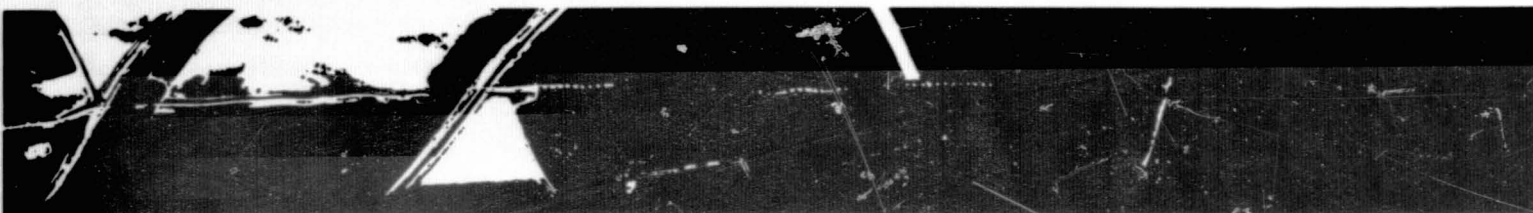
MATURE GREEN RICE, Channels .46 to .48 μ & .58 to .62 μ



IMMATURE RICE, Channels .48 to .50 μ & .62 to .66 μ



SAFFLOWER, Channels .72 to .80 μ & .80 to 1.0 μ



BARE SOIL, Channels .46 to .48 μ & .62 to .66 μ

Figure 41.-7.- Recognition pictures, Davis, California, agricultural area.

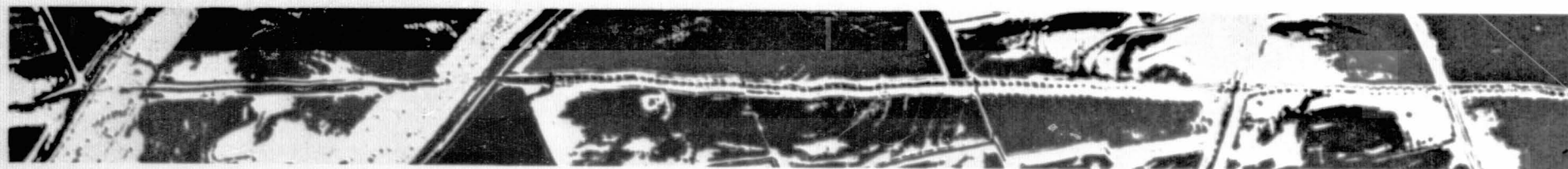


Figure 41-8.- Color recognition picture, Davis California, agricultural area (red, relatively mature green rice; blue, immature rice; green, safflower; black, bare earth).

Symbol

•
(
/
X

Crop

Bare Soil
Safflower
Immature Rice
Mature Rice

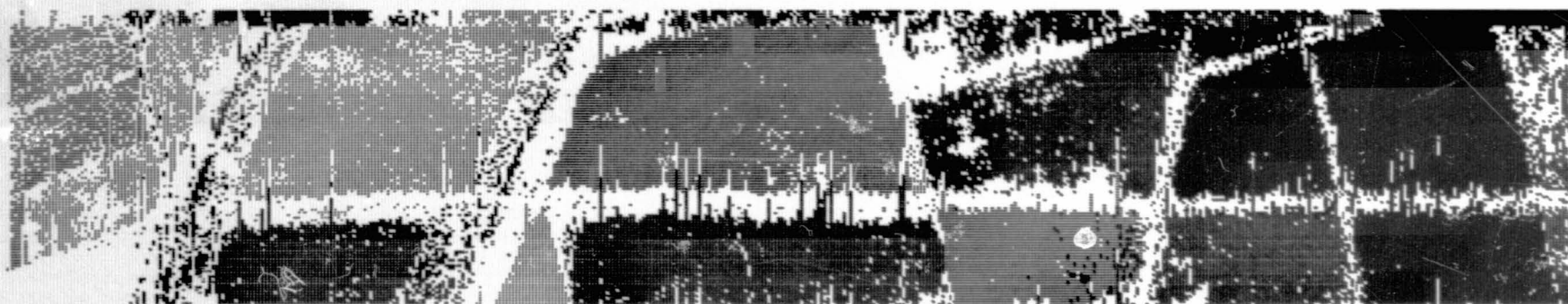


Figure 41-9.- Digital recognition map, Davis, California, agricultural area.

<u>Crop</u>	<u>Symbol</u>	<u>Acres</u>
Bare Soil	.	190
Safflower	(290
Immature Rice	/	410
Mature Rice	X	270
Other		440

Figure 41-10.- Crop acreage (obtained by digital processing) of Davis, California, agricultural area.

N71-16164

RADAR PROGRESS IN THE NASA EARTH RESOURCES

AIRCRAFT PROGRAM

By R. K. Moore
Center for Research in Engineering Science
University of Kansas

INTRODUCTION

Much progress has been made in the application of radar to the earth sciences in the 4 years since what is now the NASA Earth Resources Aircraft Program began. In 1964, the word scatterometer had not been invented. Although the scatterometer had been proposed for sea-state measurement, the available data were much poorer than those obtained to date in the NASA Program. Use of a scatterometer to measure parameters of the land had never been attempted. Today, enough measurements have been made to show that scatterometry can be a useful tool for land geoscience, at least from aircraft. In 1964, very few studies had been conducted (nearly all by the U.S. Army) on the use of imaging radar for earth-resources-type applications. In 1968, some geologic uses of radar have been proved and many others are indicated. Preliminary evidence is at hand that radar will be useful in discriminating both cultivated and natural vegetation. Land-use studies have been conducted by using radar on at least a preliminary experimental basis. At least one hydrologic application of radar, determining drainage basin parameters, has been shown to be promising. In 1964, multipolarization radar imagery had never been tested for earth resources application and seldom for any other purpose. In 1968, the value of multiple-polarization images has been clearly indicated by numerous experiments. In 1964, polychromatic radar had been postulated, but no polychromatic image studies had been made. In 1968, a beginning test at Pisgah Crater has been completed, and the potentially great value of multiple frequencies has been indicated, at least for that environment.

The NASA Earth Resources Aircraft Program and its predecessors have contributed, we believe, more to the peaceful uses of radar mapping (imaging) systems than all previous efforts. In 1964, the application of radar to earth resources was speculation. In 1968, although most applications need to be really proved, enough experiments have been conducted to show that radar has a prominent place in earth resources

studies. We believe, in fact, that it may play the primary role when short-time repetitive coverage is required in areas with frequent cloud cover.

This report primarily covers the activities of the past year, but it necessarily depends upon work done in the previous years. No radar system yet flying on a NASA Manned Spacecraft Center aircraft was designed or even procured for this program. Results to date have been based on use of the 13.3-gigahertz scatterometer originally procured to obtain engineering data for the Apollo landing radars. The Westinghouse AN/APQ-97, owned by the U.S. Army but flown under NASA-funded contract; the U.S. Air Force Avionics Laboratory AN/APQ-56, flown under NASA contract; and the Naval Research Laboratory (NRL) four-frequency radar (equipped for imaging by NASA funding through the University of Kansas to the University of Michigan) have provided the images studied so far. We look forward to the new radars that will be installed on the NASA Manned Spacecraft Center aircraft and to improvements in the NRL system, so that the years ahead may be even more productive than those just past.

This report is concerned first with the scatterometer and then with the imaging radar. The scatterometer is a specialized instrument with an output that is difficult for most users to interpret. The radar imager, however, at least superficially, should be much easier for a wide variety of user disciplines to apply.

Details of specific mission results are given in the reports by Dellwig, McCoy, Pierson, Rouse, and Simonett.

RADAR SCATTEROMETER

The radar scatterometer is an instrument permitting measurement of the radar differential scattering coefficient (radar reflectivity). The scatterometers used in the NASA Earth Resources Aircraft Program determine scattering coefficient as a function of angle of incidence. Other scatterometers can be built to vary such parameters as polarization and frequency, as well as angle of incidence.

Aircraft Program Measurements

Sea-state measurement is probably the most promising spacecraft application of radar scatterometry. Details of the sea-state measurements under the program have been reported here by Pierson and will not be repeated. The sea-state measurements may be unique in that they are the first in which the complete curve of scattering coefficient versus angle is provided for each patch of sea. Thus, the measurements in this program should be and, in fact, are more consistent than those

in many other programs. "Sea truth" in this program has been more complete than in nearly every other program of radar sea-return measurements. Sea returns have been measured in this program from seas with stronger winds and higher waves than in other programs.

The scatterometer has shown itself, in a first test, to be able to discriminate different kinds of polar sea ice, at least from aircraft altitudes. Rouse has reported on this elsewhere (ref. 50-1), and the details are not given here. We believe that this is the first time a scatterometer has been flown over sea ice, although radar imagers have been used over the sea ice and have shown great promise in distinguishing kinds of ice (refs. 50-2, 50-3, and 50-4).

The radar scatterometer has been flown over several land test sites. Its resolution on these test sites is of the order of 30 to 150 meters; therefore, extrapolation of the results to space where the resolution will be kilometers is dangerous. Nevertheless, the results have indicated possible values of the scatterometer as an aircraft instrument, and data-processing techniques are being investigated that should apply when scatterometers are flown in spacecraft over the land.

The only land scatterometer data thoroughly investigated to date are from Pisgah Crater, where the ability of the scatterometer to distinguish the different geologic units has been shown (refs. 50-5, 50-6, and 50-7). Data-processing techniques have also been studied in connection with these flights. Figure 50-1 shows an aerial photograph of the Pisgah Crater area with the curves of differential scattering coefficient σ^0 as a function of angle indicated for each of the separate geologic units. Clearly, such an ensemble of curves is difficult to interpret. An attempt to improve the situation was made by plotting the difference between each individual curve and an average curve for the entire flight line, as shown in figure 50-2. Differences between alluvial material and lava are more clearly indicated on this illustration than on figure 50-1. Even so, the results are difficult to interpret.

A principal components analysis of the scatterometer data indicates that three components contain more than 90 percent of the variance of the data. Thus, it seems reasonable to express the results in terms of only three components. The three principal components actually contain information from more than three angles of incidence. However, a simpler experiment was conducted in which the scattering coefficient measurement at each of three angles of incidence was used to set the intensity of a light with one of the primary colors. Superposition of these three colored lights gives a resultant color that is the result of the combination of the three scattering coefficients (fig. 50-3). Although figure 50-3 is not as quantitative a presentation as figure 50-1 or 50-2, figure 50-3 is much easier to interpret when compared with a

photograph. Several other display techniques were tried, but this one was found most acceptable to the geologists involved in analysis of Pisgah Crater radar data. More details are given by Masenthin (ref. 50-6).

The next area subjected to this type of analysis is the Garden City agricultural test site. Because of difficulties in alining the scatterometer data with the photographs, insufficient time has been available to produce the color output such as that in figure 50-3. Figures 50-4 and 50-5, however, show the sort of variation in scattering coefficient curve and deviation of the scattering coefficient from the mean curve indicated for the Pisgah Crater data in figures 50-1 and 50-2. Further analysis of the Garden City data will be forthcoming. These Garden City observations have also been subjected to pattern recognition computations like those reported in another section of this report.

Techniques for alining scatterometer outputs with aerial photographs have been under development for some time. When the auxiliary data annotation set (ADAS) system is operating, the alinement presumably will be easy, but it is far from easy without the ADAS. The technique used now depends on a continuous recording of the scatterometer output at a particular angle of incidence. Correlation of data-panel photographs, aerial photographs of the area, tape-recorder annotations, and the scatterometer trace should make it possible to aline the scatterometer trace with the photographs. To accomplish this, a clearly defined boundary is required. Such clearly defined boundaries were located rather easily with the polar sea ice and somewhat less easily at Pisgah Crater. At Garden City, the boundaries seem to be much harder to find. Part of this appears to be caused by the switch from analog filtering to digital filtering in producing the output traces. Some characteristics of the digital-filtering process used makes the outputs less susceptible to interpretation than the analog process used. An extensive investigation is underway to determine the difference since the two filtering processes should give the same results. A final determination cannot be made until the computer program flow chart and the computer program itself are supplied to the University of Kansas.

Experience over the past year in working with the Garden City scatterometer data emphasizes the need both for better data correlation (which ADAS is expected to do) and for selection of a flight line in which outstanding isolated boundaries are included near the end of the line that should appear in both the photograph and the scatterometer trace.

In 1965, the U.S. NRL four-frequency radar aircraft conducted a series of measurements of radar sea return off Puerto Rico in conjunction with the Applied Physics Laboratory of John Hopkins University. A ship near the area of radar measurements made stereophotographs of the ocean surface. Unfortunately, most of the data were obtained while winds were

less than 16 knots, and only one point above that (at 18 knots) appears in the data (ref. 50-8).

A most significant result of these measurements is the relative independence of frequency for radar sea return. Of course, the applicability of this result to wind speeds of more interest in foul-weather conditions is unknown. The average data are shown for horizontal and vertical polarizations in figures 50-6 and 50-7. No cross-polarized data on frequency dependence were reported. If this result applies at higher wind speeds, the choice of frequency for a spaceborne radar scatterometer for sea-state measurements should be determined almost completely by equipment considerations, since it appears that any frequency will give about the same variation of sea return with winds/waves.

Aircraft Program Equipment

The 400-megahertz scatterometer system was in Houston at the time of the meeting. The antenna was reworked and was scheduled for pattern measurements in October. Should it pass these tests, the system will be ready for installation. A 1.6-gigahertz system has been recommended for purchase, and it is our understanding that negotiations are underway.

A system somewhere between 1.6 and 13.3 gigahertz would be desirable if no plans were made to provide images in that frequency region. If an imaging radar can be obtained in that region, no further scatterometers are required for the low-altitude aircraft.

Flight of a scatterometer in the B57 should give evidence of two differences of spacecraft measurements from the low-altitude aircraft measurements, although the B57 does not actually fly high enough to test either fairly. Over the sea, the high altitude should permit averaging over a sufficiently large area so that local variations in the wind will have less effect on the data than they do at low altitudes. At satellite altitudes, the illuminated area will be so large that a truly excellent average should be obtained. The B57 at least approaches this. Over land, the scatterometer and other poor-resolution instruments should be tested at high altitudes to see what they can do. Many of the low-altitude experiments over land for poor-resolution instruments are relatively meaningless in terms of application to spacecraft because the resolution is so important to the results of the experiment. We believe that the radar scatterometer will have considerable value over land when flown in a spacecraft, but because of the poor angular resolution, it will be difficult to predict such uses without testing them in a platform such as the B57.

Accordingly, we believe that the B57 should be equipped with a scatterometer. Since a new one will have to be designed to work at that altitude, an intermediate frequency such as 3 gigahertz (or perhaps even 6 gigahertz) may well be appropriate.

Related Theory and Experiment

Radar return theory has been the subject of many papers over the years. At the University of Kansas, this work has been supported by the National Science Foundation¹ and, to a limited extent, by the Earth Resources Aircraft Program through the Naval Oceanographic Office.² All theories assume some sort of rough surface that may be statistically described. In order to make the theories analytically tractable, the statistical description is customarily greatly simplified and, in fact, is usually given in terms of an autocorrelation function selected for its integrability rather than for its relation to reality. Comparison between radar returns as modeled with an ultrasonic simulator for a known surface and the theoretical calculations for this known surface have been underway at the University of Kansas for some time, with varying degrees of success (refs. 50-9 and 50-10).

The boundary between the ocean and the air would appear to be a much simpler boundary to describe analytically than most land boundaries. This is true not only because it is simpler than one involving vegetation, but also because the sea is (for radar purposes) a homogeneous half space, with the air being another homogeneous half space. Over land, however, the land itself is far from homogeneous and, in fact, is usually made up in layers which frequently contain inhomogeneities themselves. Thus, the prospect of determining the radar return from the sea using the actual sea statistical description appeared, at first sight, to be easy.

The results for computation of the radar backscatter from the sea, using the spectrum for a fully developed sea to determine the autocorrelation function of the surface, are not very encouraging. Computed scattering shows almost no variation with wind speed (ref. 50-11); whereas, in fact, measurements at all frequencies indicate that the scattering coefficient varies strongly with wind speed (ref. 50-12). Apparently, the spectrum normally valid for most oceanographic uses neglects some factors that are most important for scatter of the short radar wavelengths. Pierson believes that these factors may include

¹Grants GP-2259, GK-875, and GK-1153.

²Contract N62306-67-C-0044.

nonlinear effects, the short-crested nature of actual waves (assuming in the theory that the waves are all going in the direction of the wind), and the effects of foam, spray, and breaking waves. None of these is covered in the gross theory, since the linear theory is intended more to describe the components of the waves that are significant for ship navigation rather than the components that contribute most strongly to the radar signal.

Progress has recently been made both at the University of Kansas and at the NRL in application of a small-perturbation model to describe the small structure on the surface of the ocean. Wright at the NRL has used this small perturbation alone (ref. 50-13), whereas Fung at the University of Kansas has combined it with the description for the full-scale ocean (ref. 50-14). Thus, Fung's approach might be characterized as a two-component description of the sea: large-scale effects and small-scale effects. Unfortunately, it is difficult to know where to draw the line between large- and small-scale effects; therefore, this is only a preliminary attempt at explanation of sea return. Nevertheless, the results obtained for variation of scattering coefficient with angle appear hopeful and seem to describe the experimental results somewhat better than methods using the full-scale wave description alone. It appears that the description of the ocean surface is not as simple as one might hope in developing a radar theory!

With Naval Oceanographic Office sponsorship, ultrasonic simulation of scatter from the ocean is underway at the University of Kansas. The recently observed data are presently being checked; therefore, no curves are presented. The conclusions are clear, however. A combination of relatively long surface waves generated by a plunger and very short surface waves generated by a fan indicates that even when the short waves are much lower than the long waves, they are the major contributors to the off-vertical radar return. This seems to be in accord both with theoretical discussions and with the general feeling of all who are working in radar sea-return research that the small structure (which is wind dependent) is the primary determinant for radar return from the ocean. Of course, this technique does not permit the modeling of breaking waves, foam, or spray.

Use of multifrequency or swept-frequency radar scatterometers and imagers should give the same kind of "signatures" (but different ones) found in the visible and infrared (IR) regions. An acoustic simulation of the frequency variation of radar return over approximately a three-to-one frequency range was recently completed by Rouse (ref. 50-15). His results clearly show, for the targets investigated, that frequency signature is indeed feasible in the radar region.

Rouse's ultrasonic simulation involved two targets. The first was a rough surface of known characteristics used also for comparison

between theory and experiment. Figure 50-8 shows the frequency variation of scattering coefficient observed for this target. The target was relatively smooth. It had no undulations with lengths comparable with the wavelength of the illuminating radiation at any of the wavelengths used. All undulations were much larger. This target was then covered thinly with fine sand particles with diameters near a wavelength at the high-frequency end of the range. The result is shown in figure 50-9. A radar scatterometer operating across this frequency range would obviously be able to distinguish between the target with and without the sand, as indicated by the two figures.

A 4- to 8-gigahertz frequency-swept ground-based radar system is being completed at the University of Kansas under sponsorship of the Advanced Research Projects Agency and the Engineering Topographic Laboratories of the U.S. Army Corps of Engineers (ref. 50-16). Except for a system going into use at the U.S. Army Waterways Experiment Station, this is, we believe, the only octave-bandwidth earth-oriented radar in existence. It will be used to verify the potential of broad-spectrum radar measurements both for determining signatures and checking swept-frequency scatterometry and for improving image gray scale, as discussed later.

Use of the instrument as a ground-truth device in connection with NASA aircraft overflights, particularly when an imaging radar system operating within the band of this system is provided on one of the NASA aircraft, will provide interesting comparisons comparable to those now provided in the IR region. We hope that such comparisons can be made soon.

New Techniques

Radar scatterometers operated in spacecraft, or even in aircraft, may be power limited. Techniques by which the power required can be reduced are, therefore, always of interest. At the University of Kansas recently, a radar receiver concept has been analyzed that uses a receiver for the scatterometer, similar to that for a Dicke radiometer. In the Dicke radiometer, the receiver input is switched alternately to a known temperature source and to the antenna which is observing an unknown temperature. Thus, a continuous calibration is obtained. By integrating the signal from the known source long enough, the effective temperature of the receiver may be determined very accurately. A comparable integration of the unknown source determines the combination of a signal and receiver noise accurately, so that the difference between signal plus noise and noise alone may be ascertained with great precision. In applying this technique to the scatterometer, one need not use a known temperature source. The total noise at the input to the scatterometer is a combination of the receiver noise and the noise

picked up by the antenna (radiation from the target). By integrating long enough, this noise may be accurately determined. Similar integration of the signal plus noise, when the radar transmitter is activated, gives an accurate value for signal plus noise. The difference may thus be determined accurately. With a signal-to-noise ratio of unity, an accuracy of about ± 0.7 decibel can be achieved with the integration time involved in one example system for space (ref. 50-17).

Several authors have indicated the value of using radars and radiometers together (ref. 50-18). The radiometer measures the product of emissivity and temperature, and emissivity is closely related to the radar cross section (ref. 50-19). Thus, making both measurements together may well permit using the radiometer as a temperature-measuring device, even with varying emissivities. Calculations made recently show that the amount of radar power required is very small with a radiometer which must use a very high gain antenna to achieve its spatial resolution. For example, a power of about 50 milliwatts is all that is required for one system operating at nimbus altitudes with about 2.5° beamwidth. Introduction of such a small transmitter on a time-shared basis into the radiometer system should be easy. The only modification in the receiver is a separate narrowband receiver channel for the radar, and this may be added after the low-noise part of the receiver. Because of the narrow pass band, either a stable transmitter and receiver local oscillator is required, or an automatic frequency control must be used for the receiver.

IMAGING RADAR

Most earth scientists make extensive use of spatial relations and texture in analyzing remote-sensor observations. Thus, they prefer either photographs or images that have some of the characteristics of photographs, as obtained by line scanners or side-looking airborne radars. Because of the importance of spatial context in analysis, we believe the imaging radar to be a much more important tool for the land geoscientist than the scatterometer, and research emphasis should be placed accordingly. Multispectral radars (polychromatic systems) are urgently needed in the program, for preliminary indications are that such radars will indeed prove valuable in the earth resources activities, whether they are flown in aircraft or spacecraft. Multispectral systems call for elaborate data processing if the results are to be applied efficiently.

Aircraft Measurements

No new radar images have been produced within the past year under NASA Earth Resources Program sponsorship. This is most unfortunate, but the big backlog of images provided by the AN/APQ-97 in previous years is still being analyzed. The need for additional measurements with careful experiment design is clear, however.

New analyses completed or published within the past year have been reported here by Simonett, Dellwig, McCoy, and several U.S. Geological Survey personnel. Dellwig's report on the first analysis of four-frequency radars at Pisgah Crater is most encouraging and important.

The NRL four-frequency imaging radar³ has been flown experimentally several times within the past year under sponsorship of the NRL and other Department of Defense (DOD) agencies as well as the Coast Guard. A mission was flown north of Point Barrow over the Arctic ice in April 1968 for the Naval Oceanographic Office. Preliminary investigation of the images indicates that resolution appears adequate, but gray scale leaves much to be desired. The NRL has recently installed new amplifiers in the receiver, which should improve the dynamic range. We have not heard the results of this change; although signal films have been obtained, they had not been processed to produce images by the time of writing.

Should the gray scale of the NRL images be significantly improved by addition of this amplifier, we believe that every effort should be made to reincorporate this aircraft in the Earth Resources Aircraft Program, so that polychromatic images can be obtained as soon as possible.

The AN/DPD-2 is, we understand, presently in Houston awaiting installation on the P3A. When it is installed, we hope that a significant set of experiments can be scheduled to test its capabilities.

We believe it to be most urgent that a new multifrequency synthetic-aperture system be procured for the NASA aircraft program. Such a system should have between three and five frequencies in the range between 1 and 10 gigahertz. Although it would be desirable to fly all frequencies at once, a system permitting single frequencies to be flown on each path and changing frequency from one flight path to the next would be acceptable for the early experiments.

³This system was built for DOD missions but equipped for imaging by the University of Michigan through a subcontract from the University of Kansas/NASA contract in 1965 and 1966. Improvements have since been made at DOD expense.

Related Experiments

Most synthetic-aperture radars and many real-aperture radars obtain only one independent look at each target. Since tens to hundreds of looks are required to obtain reasonable average values of the radar scattering cross section, the individual look at each target means that the observed strength of the target echo may vary widely. The result is a speckled image. The same phenomenon can be seen in photographs produced with laser (monochromatic) illumination.

One possible way to overcome this monochromatic illumination problem for radars is use of a panchromatic system, just as in optics. A system might be used, for instance, in which a range of frequencies is used so that frequency averaging removes much of the uncertainty and produces a reasonable average value for each target echo.

A demonstration of the value of the panchromatic radar was recently conducted by Rouse using the ultrasonic simulator (ref. 50-15). Figure 50-10 shows two images, one produced with a monochromatic source and the other with a panchromatic source. The structure shown in the monochromatic image is not relevant to the description of the target, which should appear relatively smooth in an image. Clearly, the panchromatic image accomplishes this purpose.

Figure 50-11 demonstrates this even more strikingly. Here, a set of monochromatic images produced at different single frequencies is compared with two panchromatic images, one with ± 3 -percent frequency variation and the other with ± 6 -percent variation.

The 4- to 8-gigahertz electromagnetic system being assembled now will be used to produce panchromatic images, as well as scatterometer data.

We believe that airborne or spaceborne radar systems in the future will use the polypanchromatic concept shown in figure 50-12. Here, the radar uses a somewhat broad spectrum about each of three isolated center frequencies. Because each center frequency has a "panchromatic" character, good average values for the echoes are obtained. The lowest frequency may be assigned red, the middle frequency green, and the higher frequency blue in an image-combining system, and the result should be a consistent color every time the target is imaged. Without the panchromatic nature, consistency would exist over an area, but at individual points there would be considerable variation in color.

Data Processing

The production of multispectral image data, whether in the microwave range or in some other frequency range, makes some sort of automatic or semiautomatic data processing almost essential. Difficulty of going from one image to another to pick out the differences is indeed great. Work has proceeded at the University of Kansas since 1964 along two parallel lines: (1) semiautomated development involving extensive use of a human operator, but with color presentation of the results so that the human interpreter's eye-brain communication channel can best be used, and (2) the computer recognition of multispectral (and, for the scatterometer, multiangle) information.

We believe that the general-purpose computer, which is relatively slow and expensive, should be used to determine the program settings for a real-time processor, either on an absolute signature basis or by comparison with a learning set of observations over a ground-truth site to determine the signature at the time of imaging.

The image discrimination enhancement and combination system (IDECS), developed at the University of Kansas with NASA funds and recently improved and expanded with DOD funds, permits real-time combination and enhancement of images. Furthermore, through use of its "spectrance selector" (formerly called "signature selector"), signatures are recognized and presented on a color TV display in the form of colored maps of recognized areas. Unfortunately, few adequate signatures are available at present to program the spectrance selector.

Modifications currently underway will permit coupling the IDECS to magnetic tape units so that images may be scanned in the IDECS, digitized and processed on a digital computer, and the results displayed in color, with and without further IDECS processing. Figure 50-13 is a block diagram showing the IDECS and associated equipment. The only equipment missing is the small computer for which funds have never become available. The following is a list of the characteristics of the IDECS:

1. High-speed image processing
2. Acceptance of single- or multiple-input images
3. Variety of outputs, including enhanced images, false-color images, thematic map format, area totals
4. Capability of using a variety of "pattern-recognition techniques" to identify selected features

Numerous improvements have been made in the IDECS within the past year. These are indicated in the following list of IDECS investigations during the year ending August 1968.

1. Application to a variety of image formats and test areas
2. Development of computer programs to determine optimum settings for IDECS controls
3. Breadboard of circuits to give capabilities for area measurement and texture discrimination
4. Design of interface equipment between IDECS and digital tape
5. Completion and initial application of the spectrance selector

Although the IDECS has been used with multiple-polarization radar imagery, the lack of multispectral radar imagery has led to testing with multispectral photographs. The tests described here were performed with multispectral photographs of the Bucks Lake forestry test site obtained by the NASA aircraft (figs. 50-14 to 50-18). This work has been conducted cooperatively with Colwell's group at the University of California. Following is an extract from a report by Estes, Draeger, and Haiman, graduate students of Colwell, who came to Lawrence and applied the IDECS to the multispectral images for their test site (ref. 50-20).

"The false-color image in Figure 14 was used to differentiate the serpentine-derived soils, which on this image appear green in color. The Dubakelle and Cohasset are the two soil types involved, and no attempt was made to further discriminate between them....

"In Figure 15 well-stocked mature timber stands appear black, while areas of medium-stand density appear mottled green. Areas with little or no timber cover appear blue, white, or red.

"In Figure 16 areas of dense timber appear in red. In Figure 17 areas of intermediate timber densities appear in green. By a simultaneous interpretation of these two images, a regional stratification can be made, based on density criteria (sparse, intermediate, and dense)....

"The false-color-enhanced image in Figure 18 effectively discriminates meadow and riparian vegetation from a forest matrix. The result indicates drainage patterns as well as vegetational differentiation. The red areas are higher in soil moisture.

"Preliminary interpretation indicates that many important ground conditions in this area can be analyzed through the use of electronically enhanced imagery. Soil and vegetation types (riparian and meadow versus

other associations in the area) can be differentiated, leading to still further inferences, such as estimates of soil moisture content."

These preliminary tests show this technique to be valid but requiring a great deal of attention from the human operator. Whether adequate signatures permitting use of the spectrance selector can be derived either in the visible or radar region remains to be determined by further experiment. Perhaps, because illumination with radar is better controlled, radar signatures will be more suitable for such quantitative application than visible and IR signatures.

The University of Kansas has also investigated a group of digital data compaction and pattern-recognition techniques for multiple images and multiparameter scatterometer data, using both real and artificial data. The techniques are as follows:

1. Bayes' statistical decision theory
2. Principal components analysis
3. Nonlinear adaptive learning
4. Spatial clustering
5. Measurement space clustering

Bayes' statistical decision theory is a classification technique applicable when a priori knowledge exists of the statistics of the desired categories, as might be obtained by analysis of data from a ground-truth region. Principal components analysis may be used for data compaction. The other three techniques assume no prior knowledge of data statistics for known categories. They may be used to find natural classes in the observations, which may then be identified with desired classifications by a user. Application of such techniques avoids unproductive efforts at use of categories not really distinguishable by the sensor.

Bayes' theory (ref. 50-21) leads to a statistically optimum decision rule on the basis of our prior knowledge of the probability distributions of the categories we consider and on the basis of our economic gains and losses for correct and incorrect identifications. A Bayes' classification was constructed for two sets of Garden City agricultural radar imagery

(ref. 50-22). The first set consisted of three images in time sequence with the following polarization combinations:

1. HH polarization taken in August 1965
2. HH polarization taken in September 1965
3. HV polarization taken in September 1965

The second set consisted of four images taken simultaneously:

1. HH polarization taken in July 1966
2. HV polarization taken in July 1966
3. VH polarization taken in July 1966
4. VV polarization taken in July 1966

Each data set was randomly divided in half. The first half was used to estimate the conditional probability statistics, and the second half was identified on the basis of a Bayes' classification. A unit one was gained for a correct identification, and a zero was gained for an incorrect identification. The identification of the second half of each data set produced the results shown in figures 50-19 and 50-20. Ninety percent of the types of surface cover, grouped as shown, were correctly identified for the "time sequential" set (August plus two-polarization data in September); 78 percent of the types of surface cover, grouped as shown, were correctly identified in the "simultaneous" set (July). September simultaneous two-polarization data would give better results than July four-polarization data (as discussed in the report by Simonett), but September data have been used only with the time-sequential analysis/application of Bayes' theory.

A Bayes' classification was also constructed for Pisgah Crater scatterometry data. The four geologic formation categories were alluvial material, porphyritic olivine basalt flows of the second and final eruptive phases, microporphyritic olivine basalt flows of the first eruptive phase, and playa-lake sediment. The gain function was the same one used with the Garden City data. The data set was randomly divided in half. The first half was used to estimate the conditional probabilities, and the second half was identified on the basis of the Bayes' classification; 82 percent was identified correctly. Figure 50-21 summarizes these results.

Principal components analysis provides a way for reducing the dimensionality of the data while the essential data structure is preserved

(ref. 50-23). The method works particularly well if most of the elements in measurement space which have high probability lie in a linear subspace or flat. Both the Garden City image data sets, as well as the Pisgah Crater scatterometry data set, showed that most of the data do indeed lie in a flat (ref. 50-22). This is an important fact because it means that data of high dimensionality may be collected by radar imagers and scatterometers, and they can be compacted and stored or transmitted with low dimensionality. The compacted form may be expanded by linear transformation, and the original data set may be reproduced with little loss of information.

The technique may also be applied to reduce the dimensionality of the input patterns employed with other pattern-recognition algorithms. This enables the data-processing time and cost to be lessened. The results of principal components analysis for various data sets are as follows. Ninety-eight percent of the variance of the three-dimensional time-sequential Garden City image data is accounted for in a two-dimensional flat. Ninety-five percent of the variance of the four-dimensional simultaneous Garden City image data is accounted for in a two-dimensional flat. Ninety-two percent of the variance of the eight-dimensional Pisgah Crater scatterometer data is accounted for in a three-dimensional flat. Eighty-eight percent of the variance of one set of the nine-dimensional ice scatterometry data was accounted for in a three-dimensional flat. Ninety-two percent of the variance of another set of nine-dimensional ice scatterometry data was accounted for in a three-dimensional flat. Figures 50-22 and 50-23 illustrate the data projected onto the principal two-dimensional flat for the simultaneous Garden City image data.

The adaptive learning algorithm has a structure similar to Rosenblatt's five-layer perception device (ref. 50-24). However, the weights are interpreted as measures of association between the corresponding output patterns δ of the sensor units and the output categories n of the association units. The weight matrix for the fourth layer is the transpose of the weight matrix in the second layer. The predictive reinforcement procedure is based on the following consideration. If the output category is a good one and if g_{ij} is indeed a measure of association between the j th pattern component and the i th category component, then from the output category n , a good prediction should be made of the input pattern δ . If the problem has a solution and if some of the predicted components are wrong, then the corresponding weights are reinforced in such a way that they take on values more nearly consistent with the measure of association the problem is supposed to represent. Within a few hundred reinforcements, the algorithm constructed category groups from the Garden City image data, which it was able to identify almost as well as the Bayes' decision algorithm did (fig. 50-19, ref. 50-25). In a very noisy set of made-up data, the algorithm converged to a perfect answer within a few thousand iterations.

The spatial clustering technique is specifically designed for multi-image data. Data structure is examined from the perspective of spatial closeness, measurement space closeness, and the empirical probability distribution on measurement space. A chaining procedure is defined which constructs the classification by finding center sets and then links the most similar points to each of the respective center sets. By this means, it is not necessary to compute the astronomic number of distances between each pair of points on the multiple image as would be required with the multiple-linkage clustering method employed in numerical taxonomy (ref. 50-26).

With a set of three made-up images, each with dimensions of 80 by 80 (figs. 50-24, 50-25, and 50-26) with normally distributed noise 0.27 variance added, the spatial clustering algorithm identified the 12 categories 99.5 percent correctly (fig. 50-27).

The measurement space clustering method is similar to the spatial clustering method except that spatial closeness is not taken into account, and a more exacting definition is required for measurement space similarity. With the same set of three made-up images, the measurement space clustering identified the 12 categories 98.5 percent correctly (fig. 50-28, ref. 50-26).

EXPERIMENT PHILOSOPHY

Scatterometer

The scatterometer is a poor-resolution instrument by nature. The microwave radiometer is also naturally a poor-resolution instrument. Some IR devices are poor-resolution instruments as well. This poor resolution must always be kept in mind when considering space applications of the scatterometer, for the type of thing that can be done from an aircraft may not be feasible with a spacecraft which is at a much higher altitude and, consequently, has a much larger resolution cell.

We believe, as indicated by Pierson, that the validity of the scatterometer for measuring sea roughness parameters closely related to the surface winds has been demonstrated, although it has certainly not been calibrated. Sea roughness and winds do not require fine resolutions. In fact, coarse resolutions are probably better for the synoptic scale computations required for oceanwide wave/wind mapping.

The scatterometer probably can be used to determine the major ice boundaries in the Arctic and perhaps major features of the Antarctic continent. Certainly, ice types are differentiated at small scale;

whether they will be equally well differentiated at large scale remains to be determined. Gross boundaries, such as those between grasslands and forests, between frozen and unfrozen ground, and between dry land and land that has recently been wet down by rain can possibly be determined by the scatterometer from space. The poor resolution should not stand in the way of the scatterometer for this function, but these applications have not been fully tested with aircraft to determine whether, in fact, the scatterometer return is different on the opposite sides of the boundaries.

A gross-resolution sensor may well have other applications from space. For example, the gross-resolution sensors in Tiros have been used in providing maps of the Sahara (ref. 50-27). The sort of application we will find with a resolution cell that is kilometers or tens of kilometers across will be difficult to establish before the scatterometer is flown in space; however, its generalizing capability may well be of great significance. It is difficult to see how this sort of application can be checked using an aircraft; perhaps use of the B57 at maximum altitude will permit at least a preliminary check in some areas.

The aircraft scatterometer can be used to check the applications of spaceborne scatterometers for which the size of the resolution cell does not matter. Over the ocean, as long as the aircraft is high enough so that major wave structures are illuminated completely, this certainly should be true. The same may be true over the ice, and the aircraft can be used for checking the ability to determine frozen-unfrozen boundaries, wet-dry boundaries, and forest-grassland boundaries. Low-altitude aircraft measurements with 50-foot to a few-hundred-foot resolution probably will not be too helpful in determining other spacecraft uses of scatterometers.

Aircraft scatterometers, however, can be used in the absence of appropriate aircraft imaging radar to learn many useful pieces of information about potential applications of imaging radars in space. Thus, an aircraft mission at low altitudes using the 400-megahertz scatterometer should be able to determine the difference between a signal at this frequency and one at 13.3 gigahertz, or at the 16.5 gigahertz of the DPD-2. In the absence of an imager near 400 megahertz, this will give very useful information about the potential of the polychromatic imager. When a calibrated imager with its ability to provide good spatial context is available, however, the aircraft scatterometer will fade into the background for this application.

Radar scatterometers were originally installed in aircraft to obtain system design information for radars (imagers, altimeters, autonavigators, etc.). Because most of the programs to obtain such information had limited objectives and little or no ground truth, information is still spotty on the values of scattering coefficient to be used in radar system design.

As a consequence, designs are probably more conservative than they need be; hence, a more extensive use of aircraft scatterometers should provide system design data which would permit lower power space radar systems and should provide knowledge of possible penalties to be paid for using the lower power. Furthermore, the aircraft scatterometer can be used to determine the variation of scattering coefficient with incident angle so that an optimum angle of incidence can be picked for a spacecraft or aircraft radar imager. This, we believe, is an important application of the radar scatterometer in aircraft; but data analysis is primarily important for the radar designer. The user scientist is important here only to guarantee that the designer is meeting the user's real needs rather than those imagined by the radar engineer.

Radar Imager

Obtaining multifrequency multipolarization radar imagers for use in the NASA Program is most important. Multifrequency imagers will certainly be important in space.

It is easy for the radar imager to cover large areas. The large-area coverage obtained with the AN/APQ-97 has been used to advantage in both geographic and geologic studies. The use of very small test sites in which extensive ground truth is gathered may be appropriate for some radar applications, but the experiments for the imager should also include large-area "test sites" in which the generalizing capability of the imager can be used to advantage. Furthermore, the simplicity of operation for obtaining wide-area coverage may make it desirable to obtain images for users not in the NASA Earth Resources Aircraft Program while going from one place to another as a part of the program. Thus, a larger group of the scientific community would be drawn into the program, at least superficially, and more users will be ready when images are available from space.

Numerous experiments should be conducted using the radar imager to determine such things as the effect of look angle, angle of incidence, repeatability of the imaging, the effect of the "pebbliness" of synthetic aperture image on interpretation, and similar information. Much work remains to be done along these lines.

CONCLUSION

The NASA Earth Resources Aircraft Program has led to a great expansion in our knowledge of geoscience-resource applications of radar, even though the MSC aircraft are just being equipped with a radar imager and multifrequency/polarization scatterometers. Multifrequency imaging

radar, preferably "polypanchromatic," should give even more important results. The progress in multiimage data processing shows great potential of both semi-real-time and general-purpose computer techniques, but progress here, too, will be even greater when multifrequency radar data are available.

REFERENCES

- 50-1. Rouse, J. W., Jr.: Arctic Ice Type Identification by Radar. Tech. Report 121-1, CRES, Univ. of Kansas, Aug. 1968.
- 50-2. Simonett, D. S.; and Brown, D. A.: Spacecraft Radar as a Means for Studying the Antarctic. Proceedings of the VII Congress International Quaternary Assoc., Boulder, Colo., Sept. 1965. Also published as CRES Tech. Report 61-4.
- 50-3. Anderson, V. H.: Radar Imagery of Arctic Pack Ice, Kane Basin to North Pole. U.S. Army CRREL Special Report 94, 1962.
- 50-4. Anderson, V. H.: High-Altitude, Side-Looking Radar Images of Sea Ice in the Arctic. Proceedings of the Fourth Symposium on Remote Sensing of Environment, Univ. of Michigan, April 1966, pp. 845-857.
- 50-5. Dalke, G. W.: Identification of Remote Objects by Means of Scatterometry Data and Applications to Pisgah Crater. Tech. Report 61-17, CRES, Univ. of Kansas, Feb. 1967.
- 50-6. Masenthin, H. W.: Scatterometer Data Analysis Techniques. Tech. Report 118-3, CRES, Univ. of Kansas, July 1967.
- 50-7. Lundien, J. R.: Analysis of Scatterometry Data from Pisgah Crater. Tech. Report 118-2, CRES, Univ. of Kansas, Aug. 1967.
- 50-8. Daley, J. C.: Sea Clutter Measurements on Four Frequencies. Presented at Fall Meeting, U.S. National Committee, URSI, Northeastern Univ., Sept. 1968.
- 50-9. Parkins, B. E.: The Omnidirectional Scattering of Acoustic Waves from Rough Surfaces with Application to Electromagnetic Scattering. Tech. Report 48-4, CRES, Univ. of Kansas, June 1965.
- 50-10. Fung, A. K.; and Leovaris, A.: Frequency Dependence of Ultrasonic Scatter from Statistically Known Rough Surfaces. 1968 WESCON Technical Papers, Session 22. WESCON, Los Angeles, Aug. 1968.
- 50-11. Chia, R. C.: The Theory of Radar Scatter from the Ocean. Tech. Report 112-1, CRES, Univ. of Kansas, Oct. 1968.
- 50-12. Pierson, W. J.: Radar Sea Return as a Function of Wave Height and Wind Speed for Fully Developed Seas. Earth Resources Aircraft Program Status Review, 1968.

50-22

- 50-13. Wright, J. W.: A New Model for Sea Clutter. IEEE Trans., vol. AP-16, Mar. 1968.
- 50-14. Fung, A. K.: Backscattering of Waves by Composite Rough Surfaces. Presented at Spring Meeting, U.S. National Committee, URSI, National Academy of Science, Washington, D.C., Apr. 1968.
- 50-15. Rouse, J. W., Jr.: Frequency Dependence of Backscatter from Rough Surfaces. Interim Tech. Report 133-4, CRES, Univ. of Kansas, Aug. 1968.
- 50-16. Ellermeier, R. D.: Project THEMIS: A Center for Remote Sensing Semi-Annual Technical Report. CRES, Univ. of Kansas, Apr. 1968.
- 50-17. Pierson, W. J.; and Moore, R. K.: Global Radar for Ocean Waves and Winds (GROW), An Experiment Submitted to NASA for Flight on a NIMBUS E or NIMBUS F Spaceflight. CRES, Univ. of Kansas and NYU School of Engrg. & Science, Feb. 1968.
- 50-18. Janza, F. J.: A Comparison of the Microwave Scatterometer and Radiometer for Sea State Measurements. Presented at the 49th Annual Meeting, AGU, Washington, Apr. 1968.
- 50-19. Peake, W. H.; Riegler, R. L.; and Shultz, C. H.: The Mutual Interpretation of Active and Passive Microwave Sensor Outputs. Proceedings of the Fourth Symposium on Remote Sensing of Environment, Univ. of Michigan, Apr. 1966, pp. 771-777.
- 50-20. Dalke, G. W.: Multi-Image Correlation Systems Study for MGI Phase II Technical Report. CRES, Univ. of Kansas, June 1968.
- 50-21. Raiffa, H.; and Schlaife, R.: Applied Statistical Decision Theory. Harvard Univ. Press, 1961.
- 50-22. Haralick, R. M., et al.: A Statistical and Conditional Probability Study of Crop Discrimination Using Radar Images. Presented at the International IEEE Meeting, New York, Mar. 1968. Also appears as CRES Tech. Memo. 133-5, 1968.
- 50-23. Kendall, M.; and Stuart, A.: The Advanced Theory of Statistics. Hafner, (London), 1966.
- 50-24. Rosenblatt, F.: Principles of Neurodynamics. Spartan Books, 1962.

- 50-25. Haralick, R. M.: Adaptive Pattern Recognition of Agriculture in Western Kansas by Using a Predictive Model in Construction of Similarity Sets. Proceedings of the Fifth Symposium on Remote Sensing of Environment, Univ. of Mich., Apr. 1968.
- 50-26. Haralick, R. M.: Pattern Recognition Using Likelihood Functions. Tech. Report 118-4, CRES, Univ. of Kansas, Aug. 1967.
- 50-27. Pouquet, J.: Remote Detection of Terrain Features from NIMBUS I High Resolution Infrared Radiometer Nighttime Measurements. NASA TN D-4603, 1968.

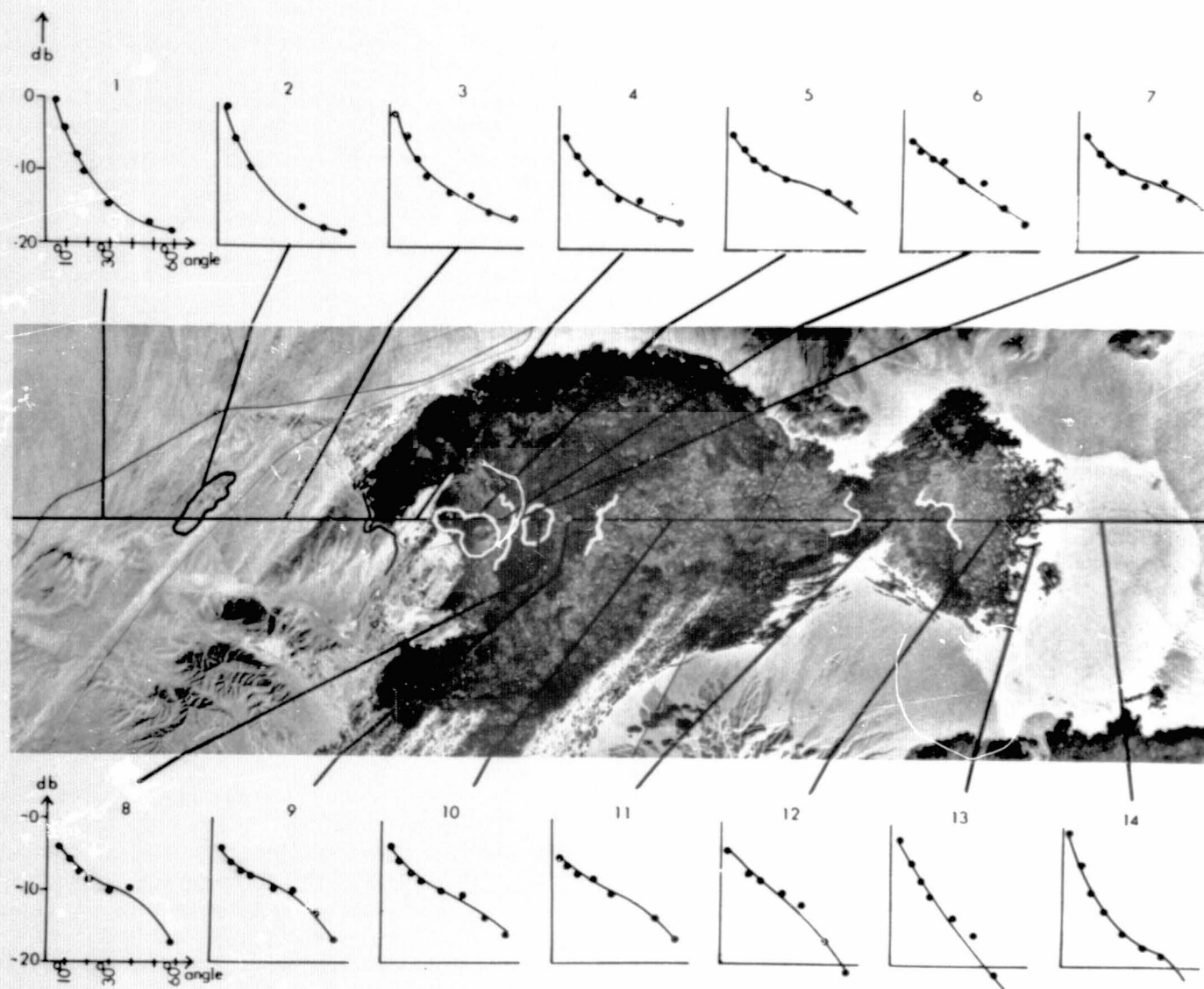


Figure 50-1.- Curves of radar differential scattering coefficient versus angle of incidence compared with photograph showing regions from which the data were obtained using the 13.3-gigahertz scatterometer.

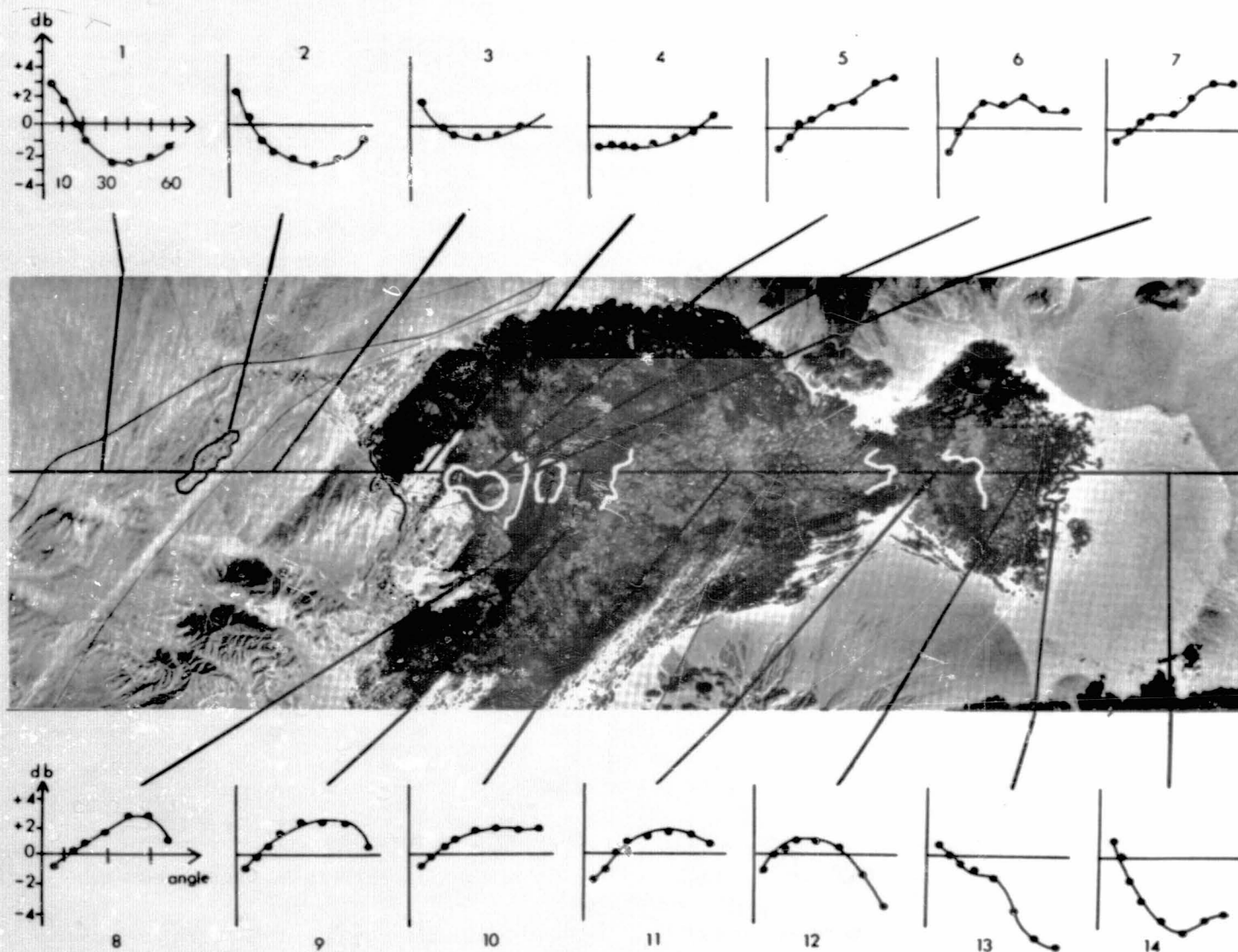


Figure 50-2.- Curves of difference between radar differential scattering coefficient and values for a mean curve compared with photograph of Pisgah Crater area from which the data were obtained by the 13.3-gigahertz scatterometer.

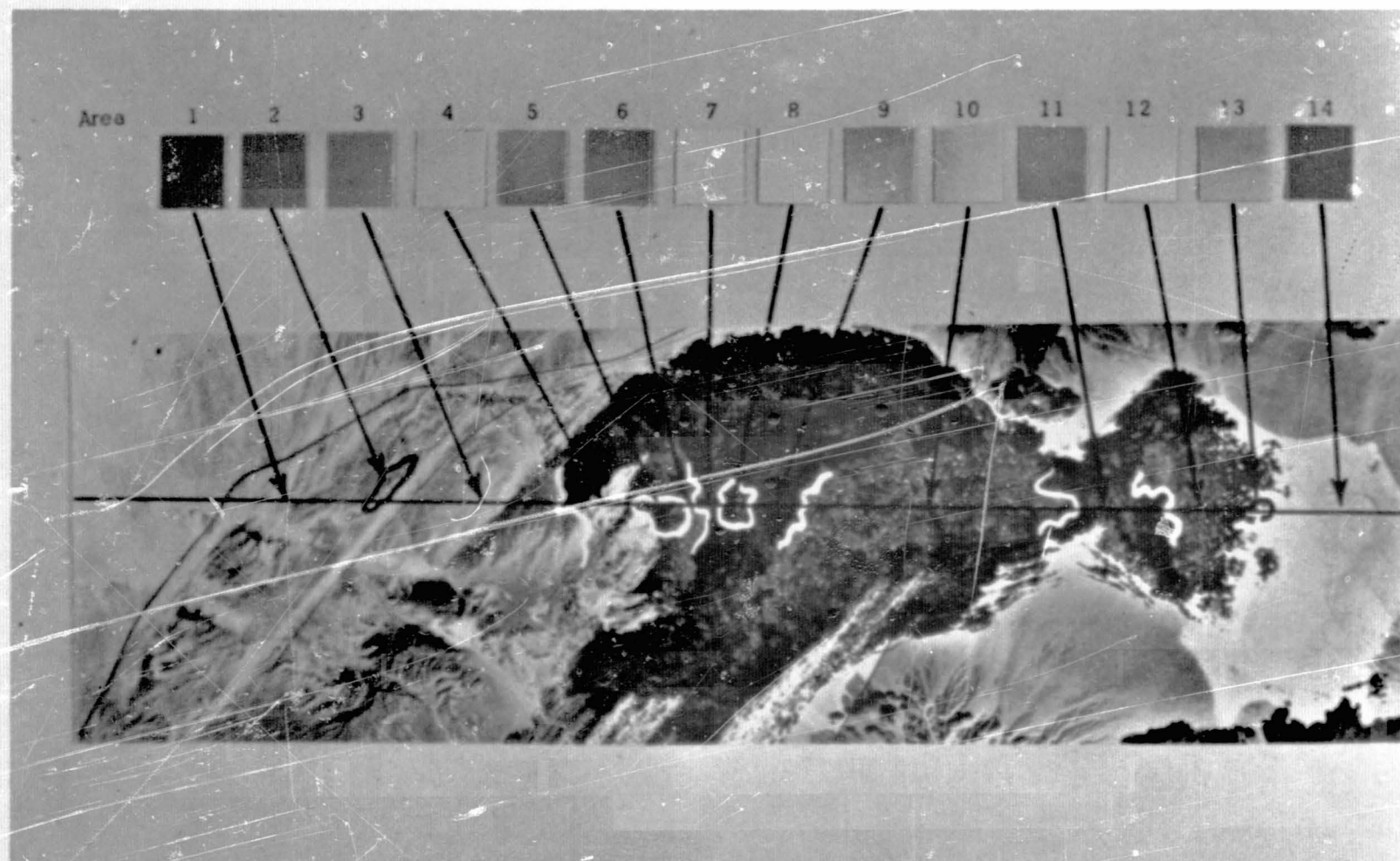


Figure 50-3.- Color codes for the information obtained by scatterometer from the Pisgan Crater area, compared with a photograph of the area.

REPRODUCIBILITY OF THE ORIGINAL PAGE IS POOR.

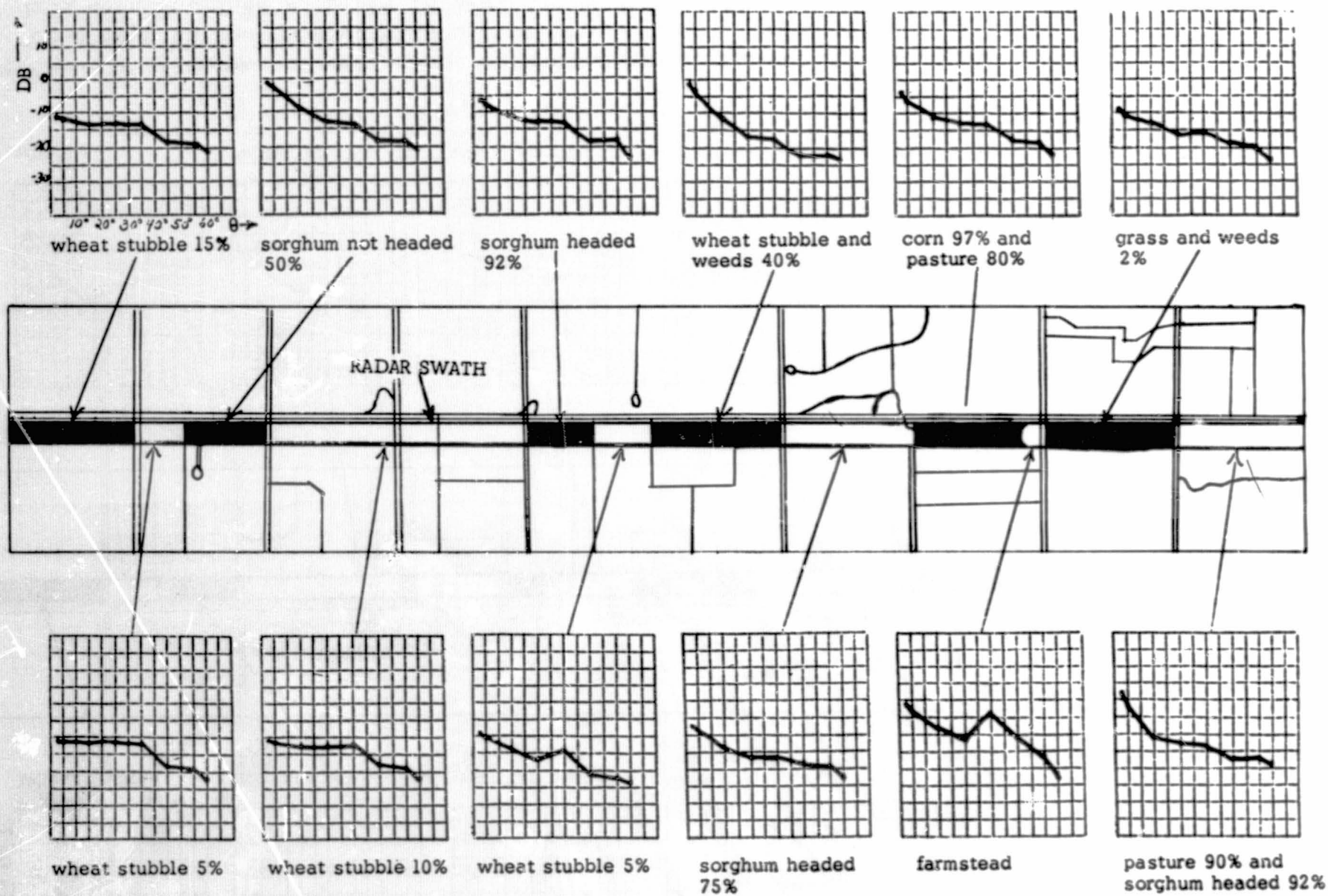


Figure 50-4.- Curves of radar differential scattering coefficient versus angle of incidence compared with a line map of the Garden City Test Site area from which the data were obtained with the 13.3-gigahertz scatterometer.

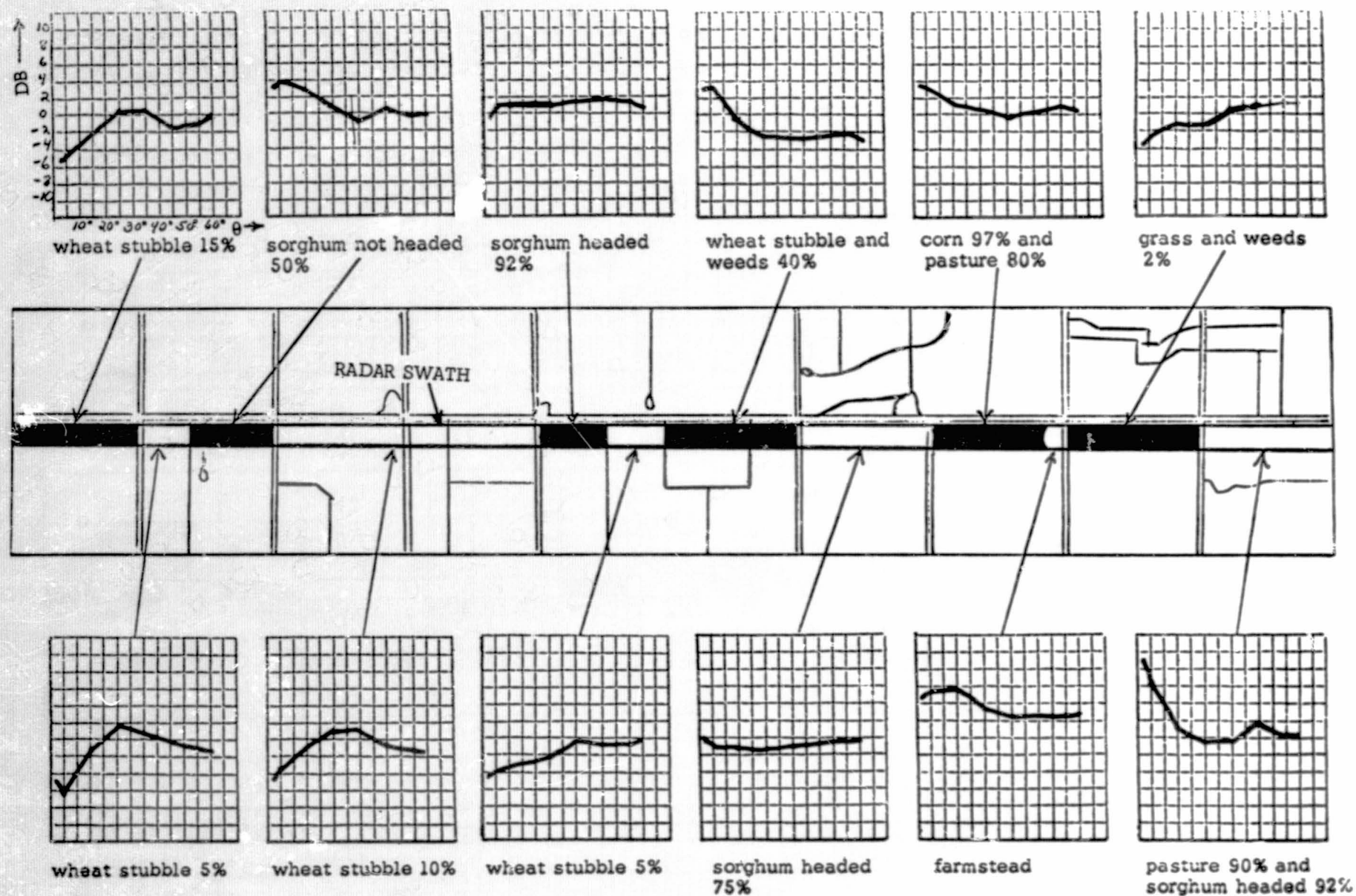


Figure 50-5.- Curves of difference between radar differential scattering coefficient and values for a mean curve compared with a line map of the Garden City Test Site area from which the data were obtained with the 13.3-gigahertz scatterometer.

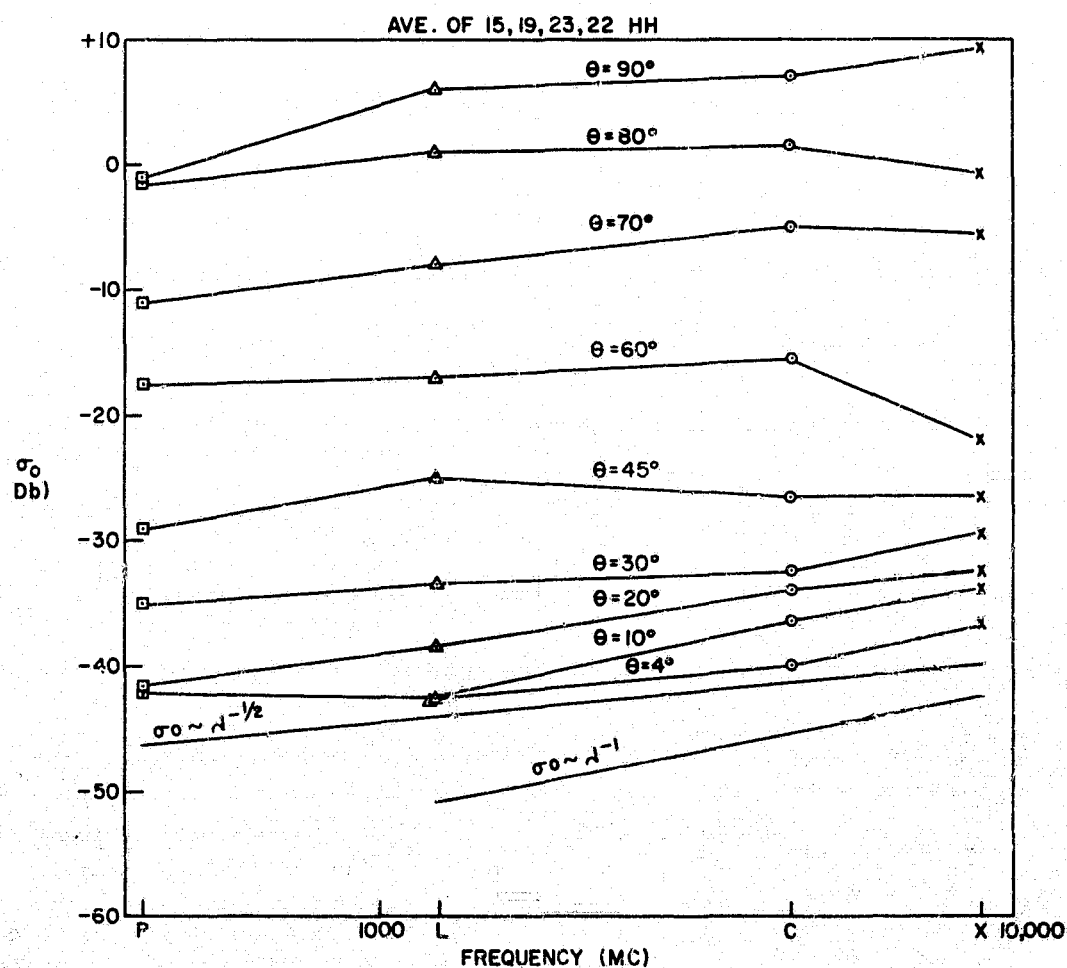


Figure 50-6.- Variation of radar differential scattering cross section with frequency as reported by Daley of NRL (horizontal polarization). The parametric angle is the elevation angle, the complement of the angle of incidence.

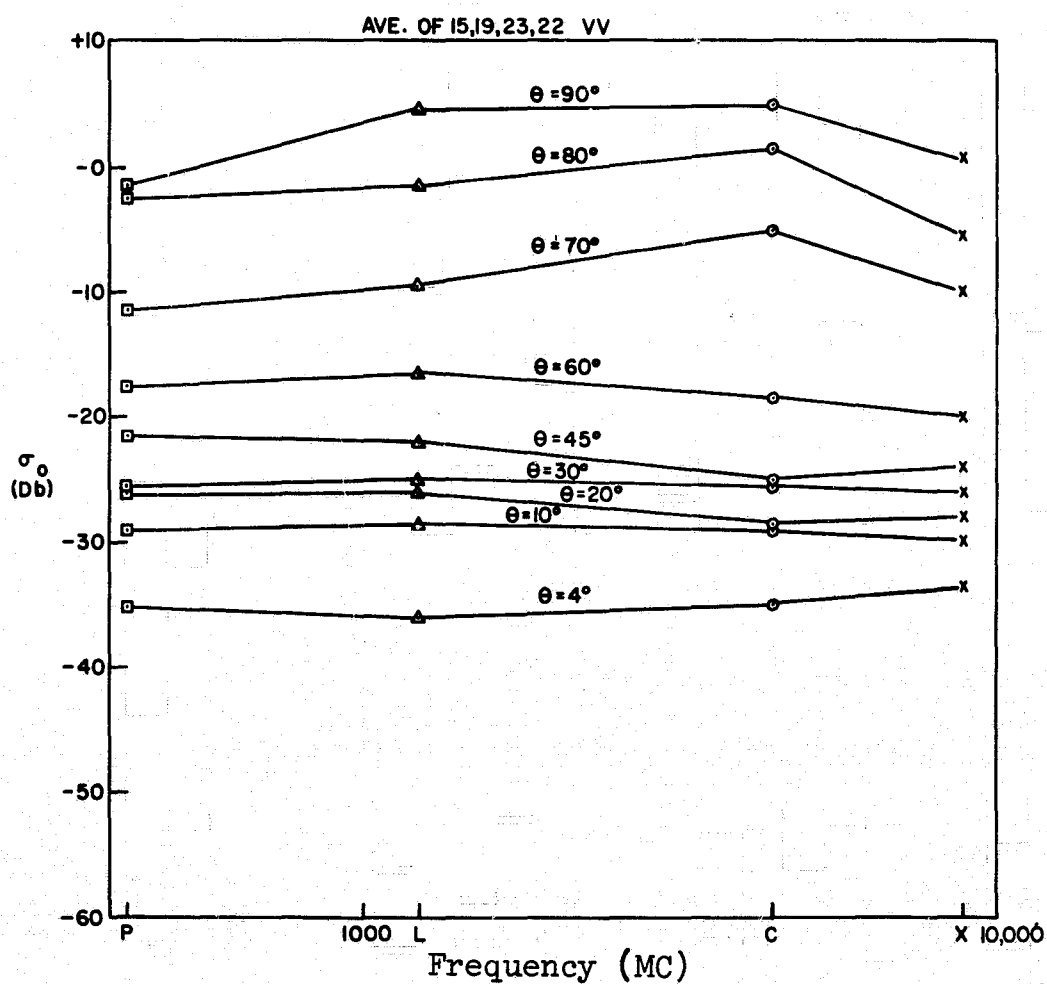


Figure 50-7.- Variation of radar differential scattering cross section with frequency as reported by Daley of NRL (vertical polarization). The parametric angle is the elevation angle, the complement of the angle of incidence.

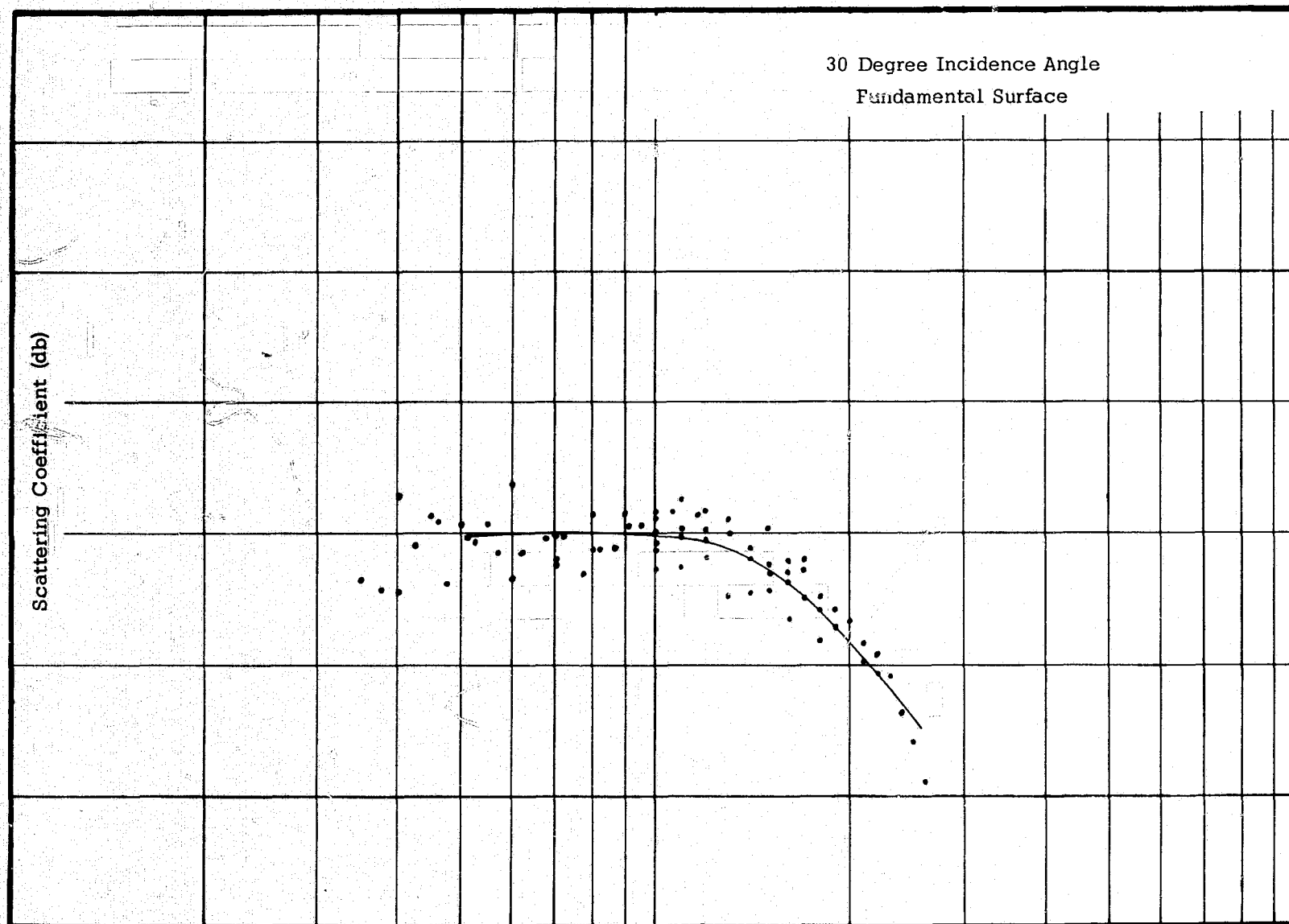


Figure 50-8.- Frequency dependence of scattering coefficient obtained by ultrasonic simulation (undulating surface).

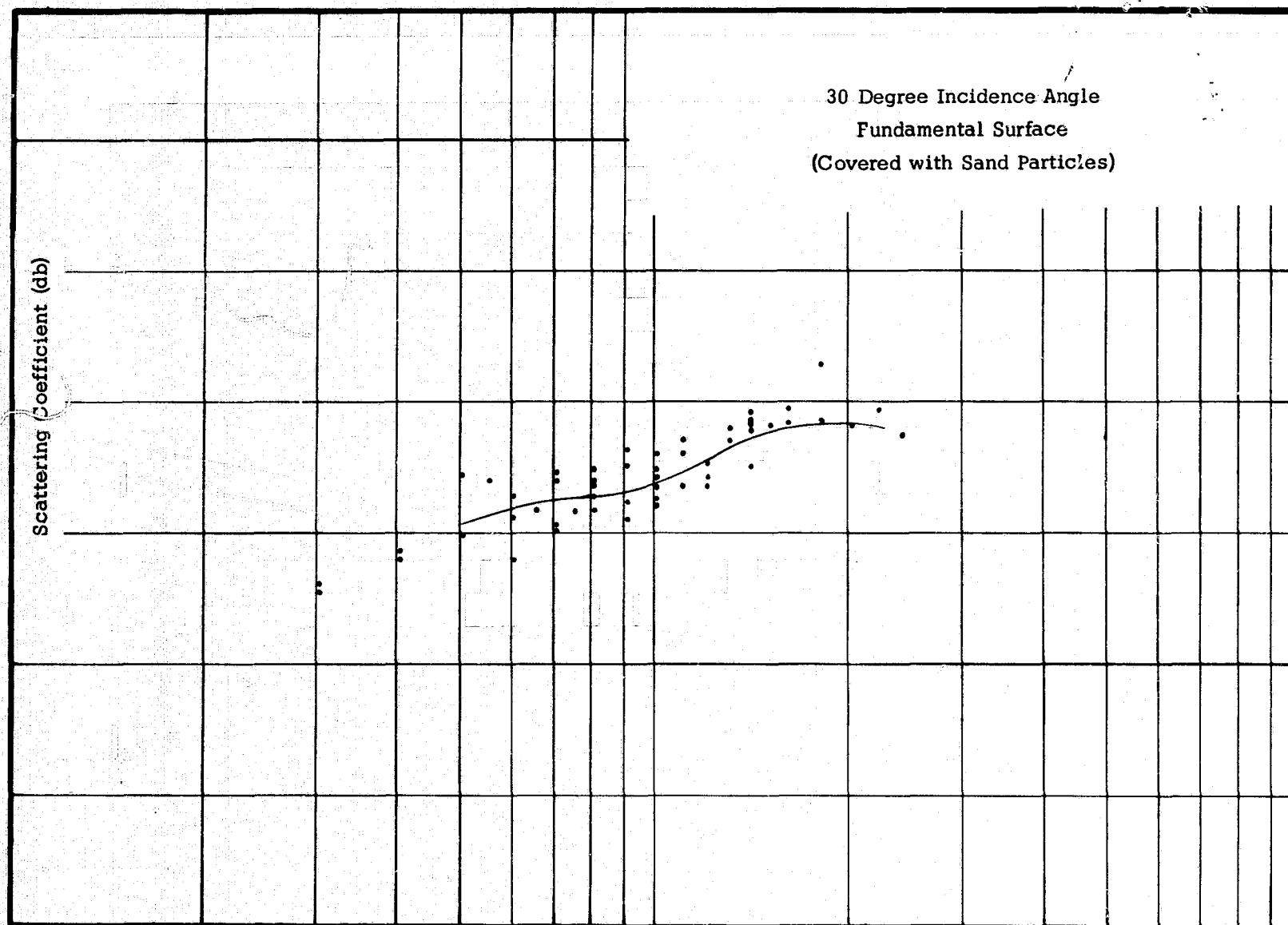
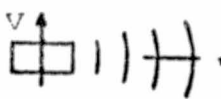
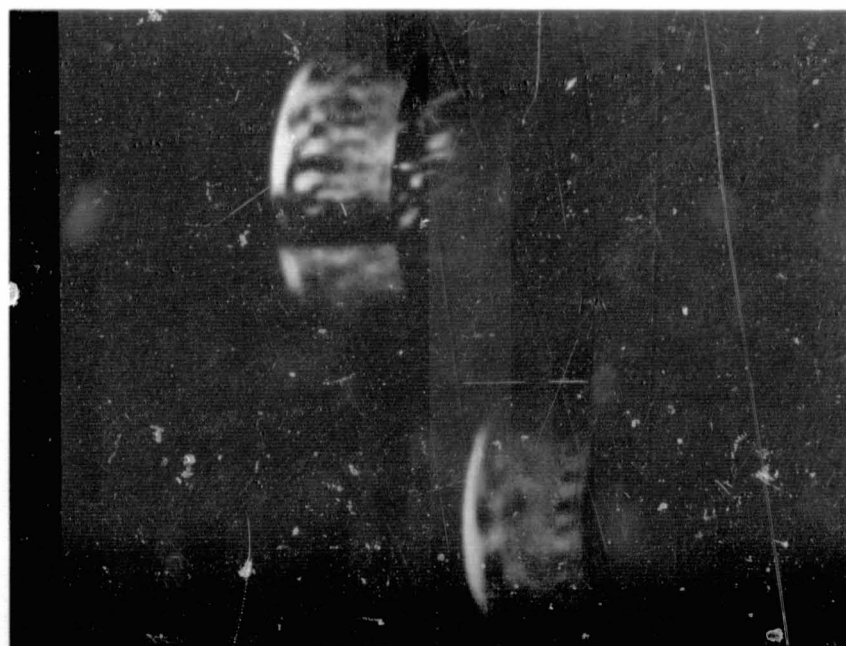
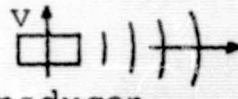


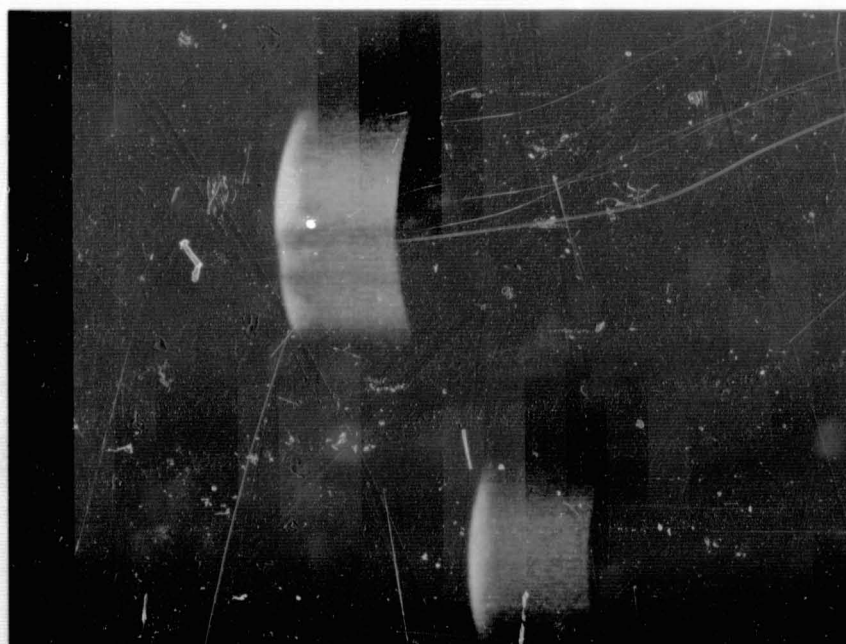
Figure 50-9.- Frequency dependence of scattering coefficient obtained by ultrasonic simulation (undulating surface roughened with sand particles).


 transducer



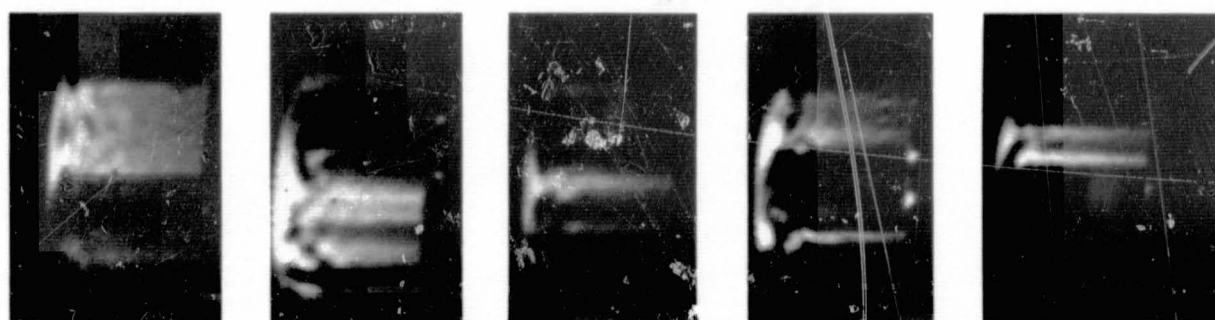
(a) Monochromatic image of two spheres
($f = 1.5 \text{ MHz}$)


 transducer

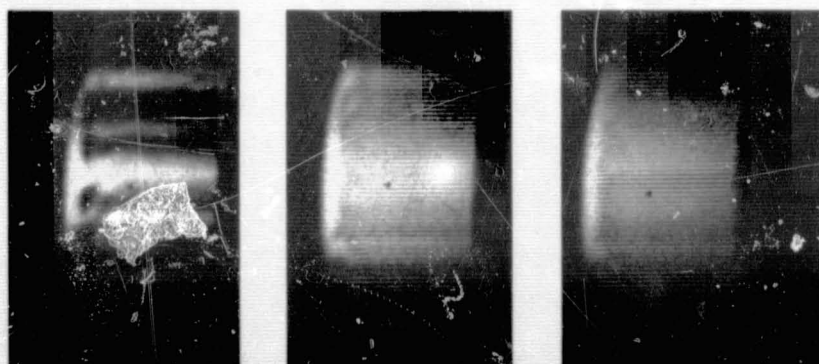


(b) Swept frequency image of two spheres
($f = 1.5 \text{ MHz} \pm 10\%$)

Figure 50-10.- Effect of frequency average on image of sphere targets.



$f = 1.43 \text{ MHz}$ $f = 1.52 \text{ MHz}$ $f = 1.64 \text{ MHz}$ $f = 1.74 \text{ MHz}$ $f = 1.82 \text{ MHz}$



$F = 1.64 \text{ MHz}$ $f = 1.64 \pm 0.05 \text{ MHz}$ $f = 1.64 \pm 0.1 \text{ MHz}$

Figure 50-11.- Monochromatic images of the same target made at nearby frequencies compared with panchromatic images with ± 3 -percent and ± 6 -percent frequency variation. These images were produced in the ultrasonic simulator.

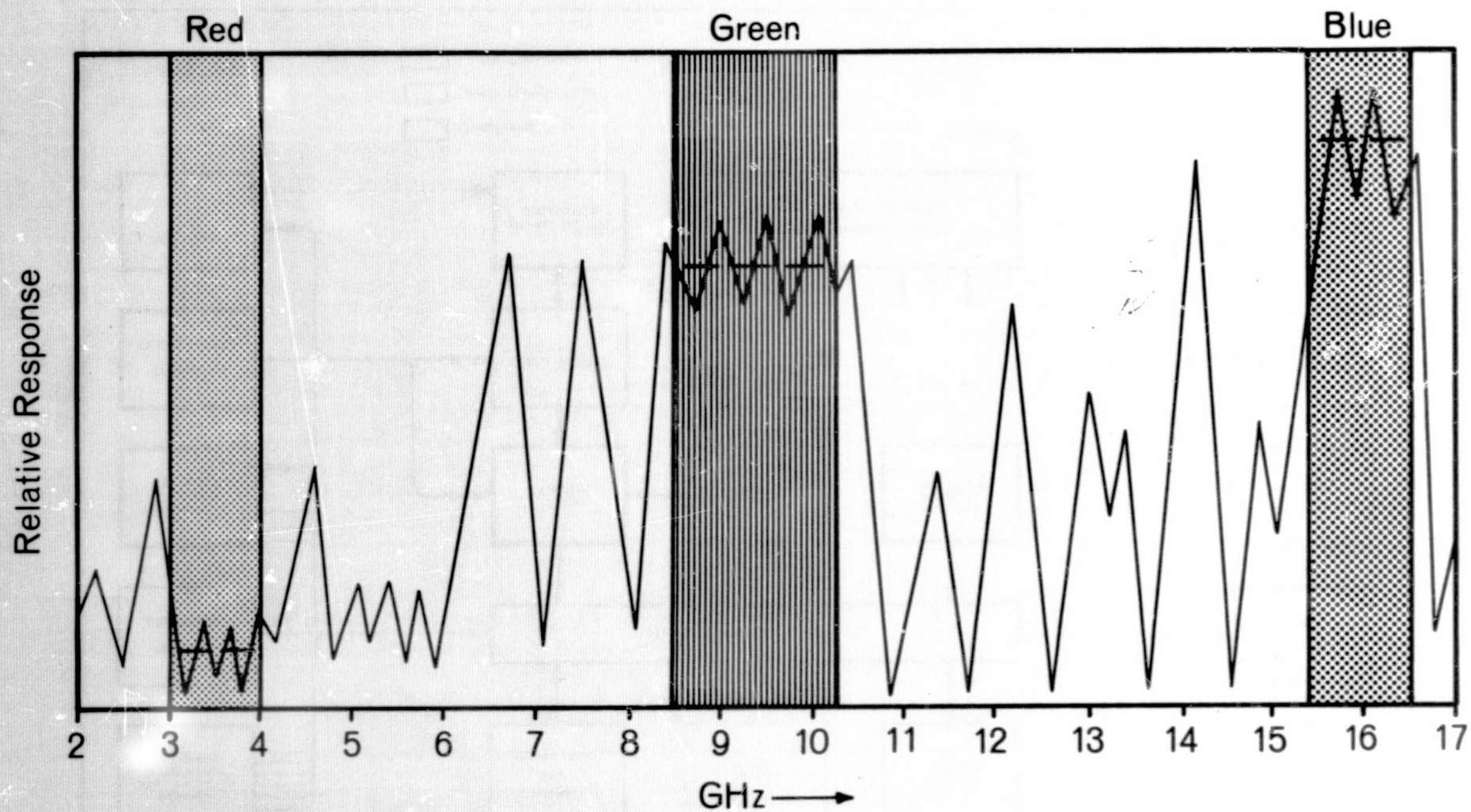


Figure 50-12.- Example of possible spectral-response-separated trichromatic radar.

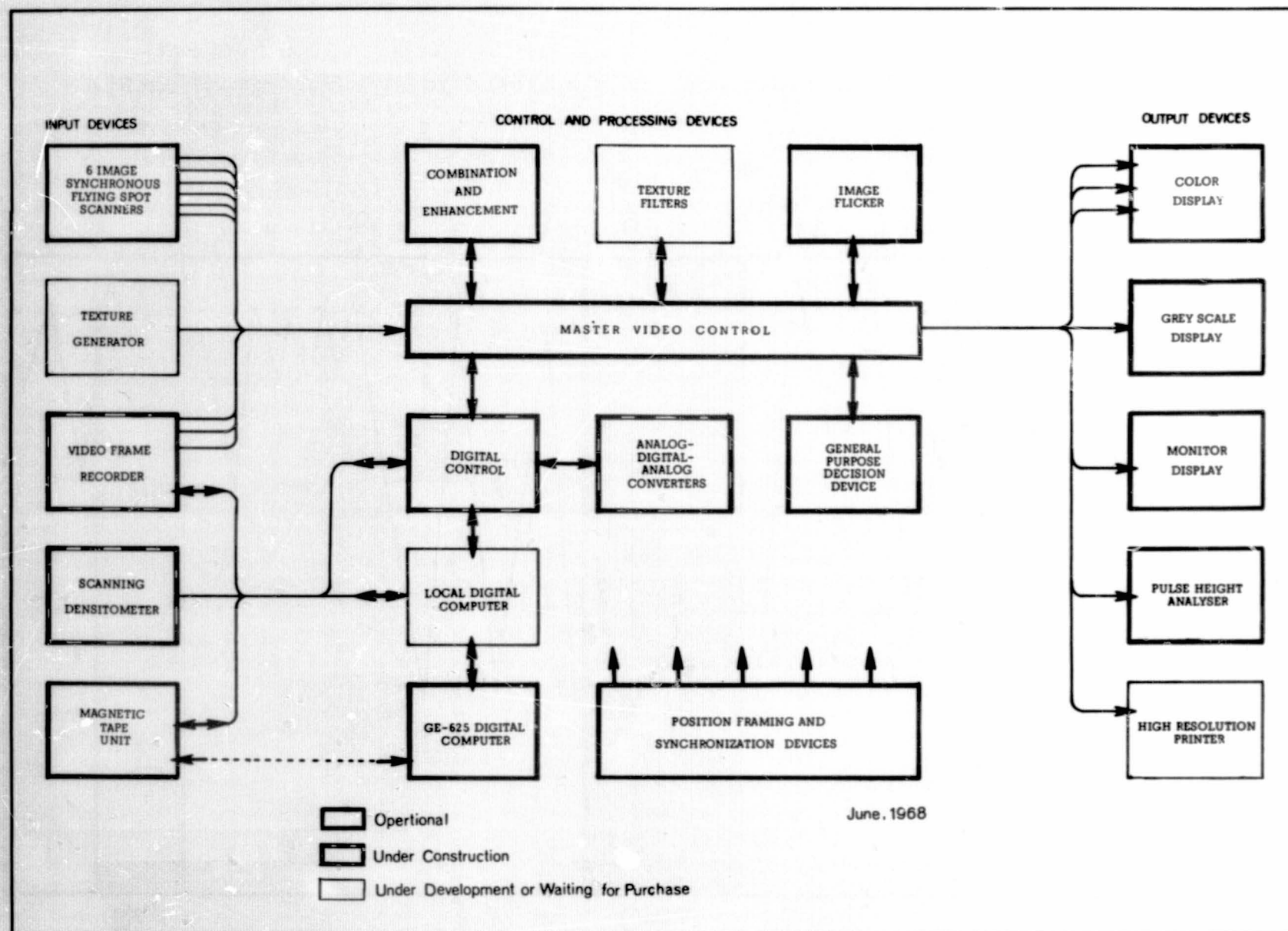


Figure 50-13.- Block diagram of the IDECS and associated equipment.

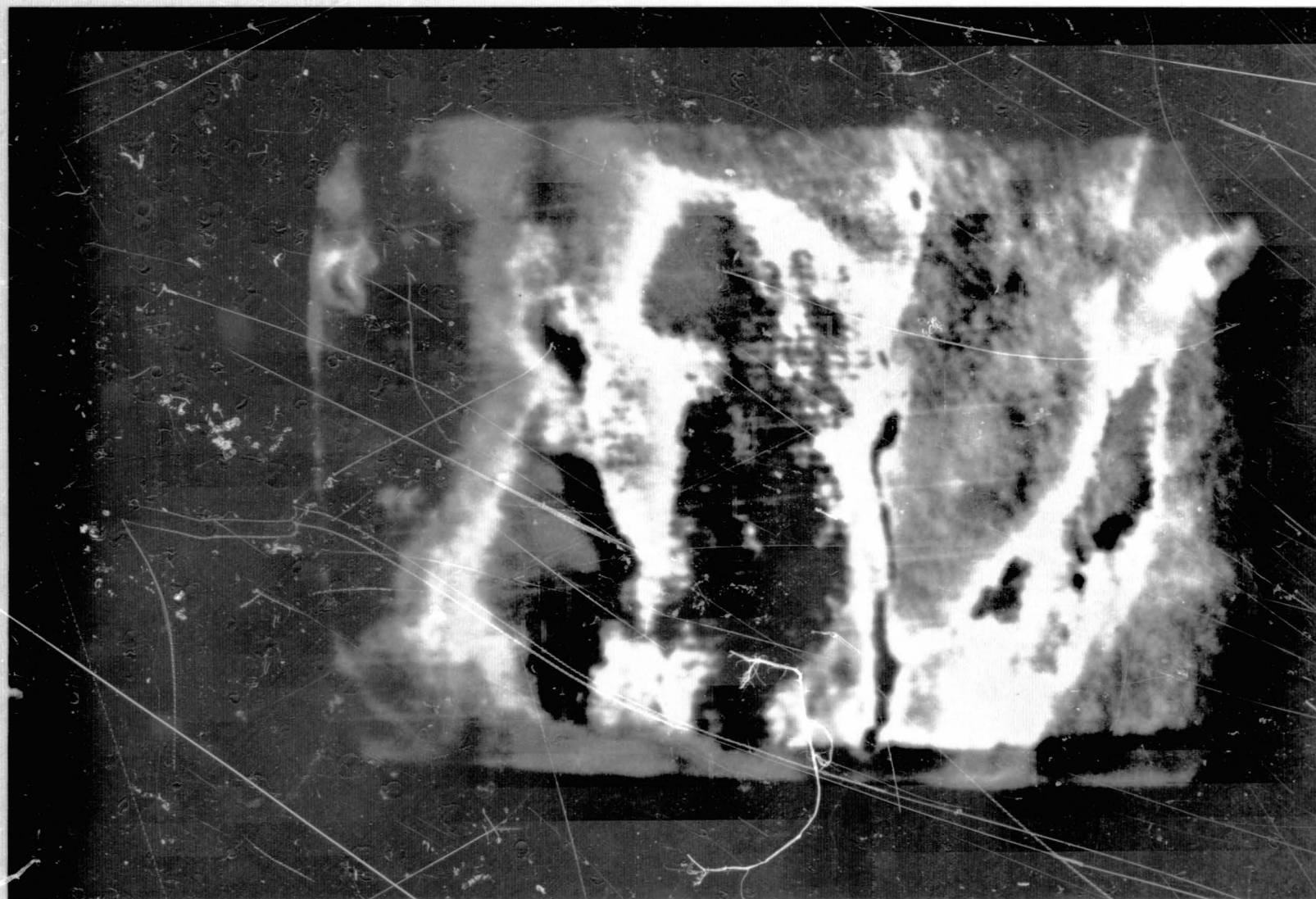


Figure 50-14.- False-color IDECS-enhanced image of Bucks Lake Test Site. Original data multi-spectral photographs from NASA aircraft 926 overflight.

50-37

REPRODUCIBILITY OF THE ORIGINAL PAGE IS POOR.

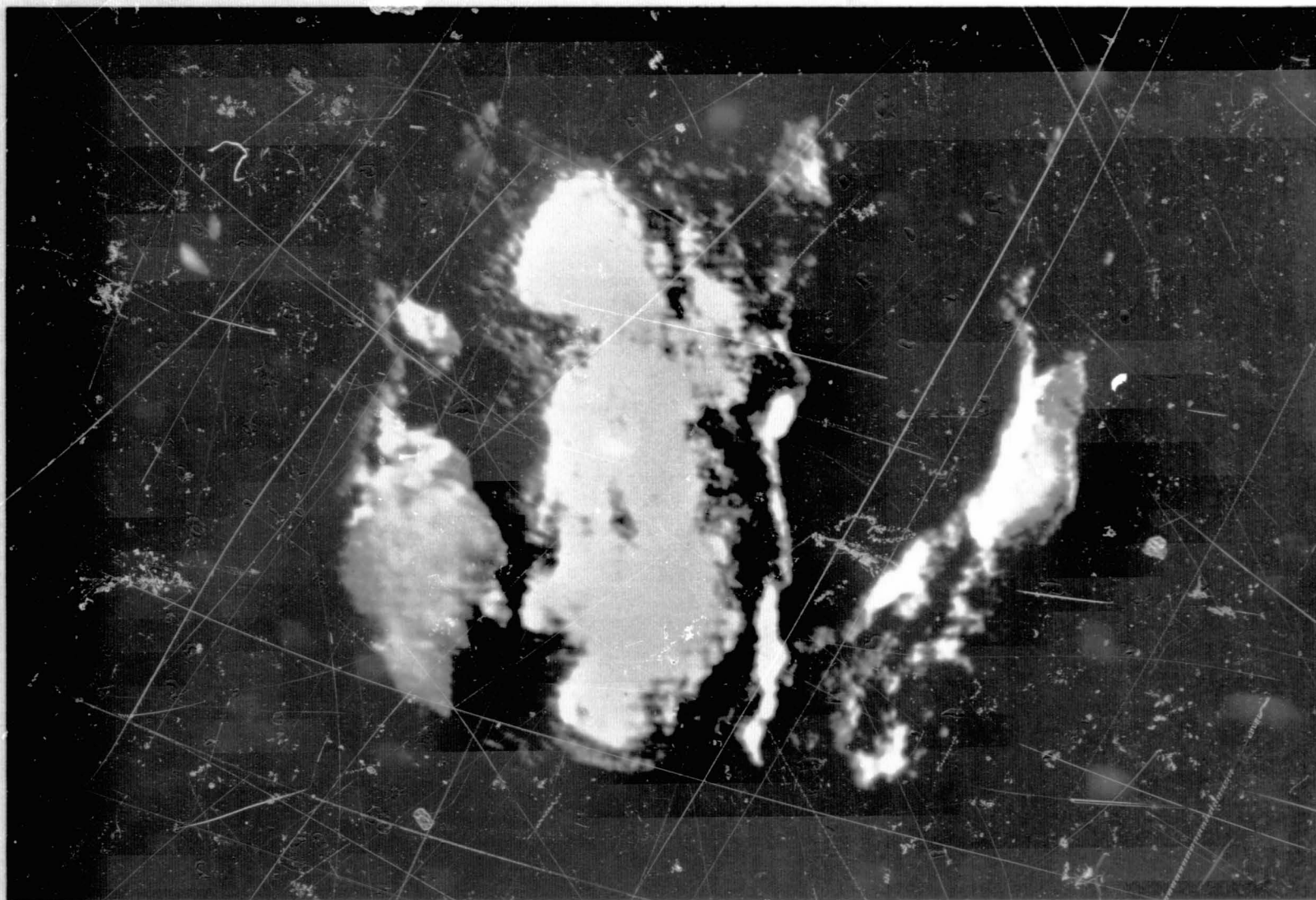


Figure 50-15.- False-color IDECS-enhanced image of Bucks Lake Test Site. Original data multi-spectral photographs from NASA aircraft 926 overflight.

50-38

REPRODUCIBILITY OF THE ORIGINAL PAGE IS POOR.

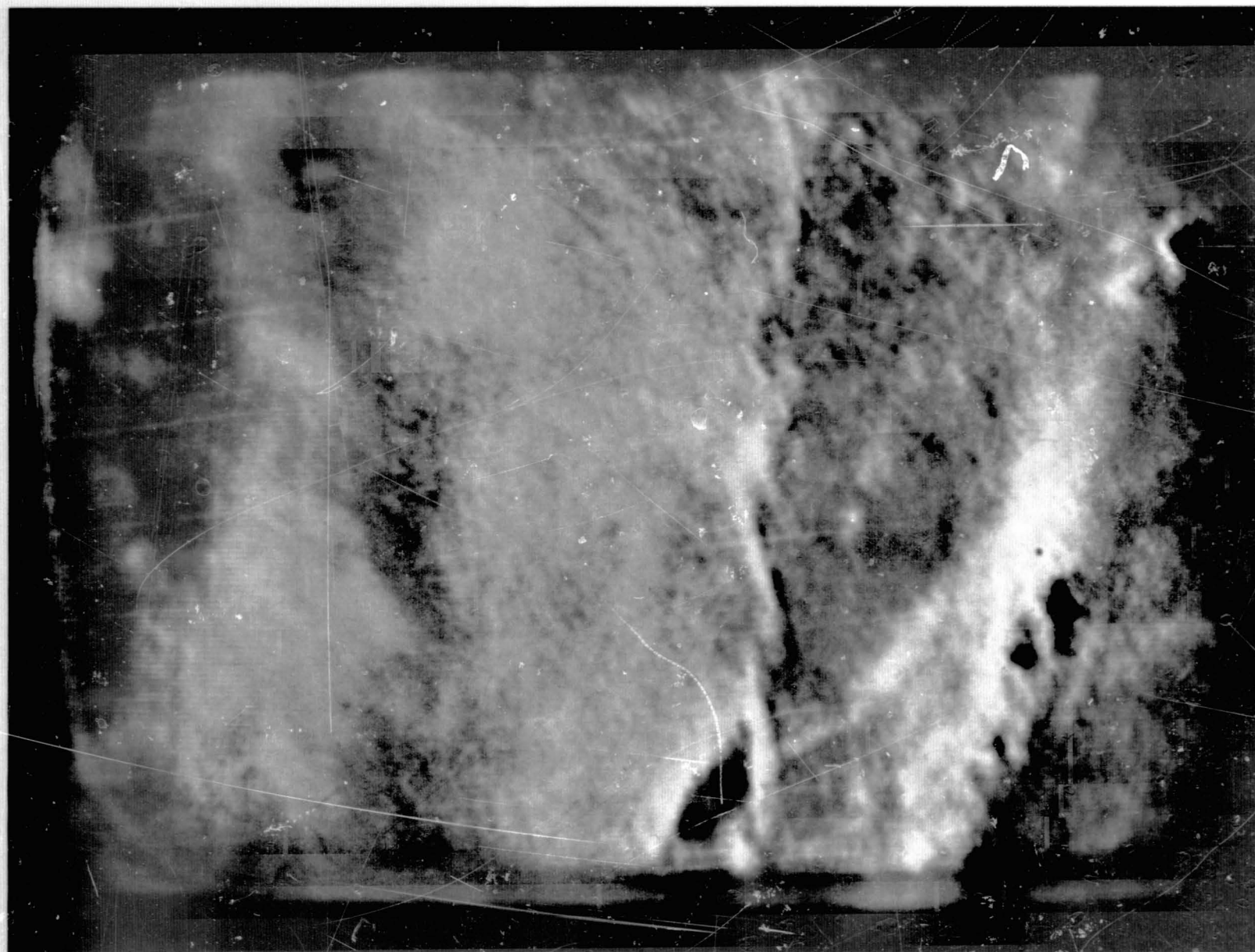


Figure 50-16.- False-color IDECS-enhanced image of Bucks Lake Test Site. Original data multi-spectral photographs from NASA aircraft 926 overflight.

50-39

50-40

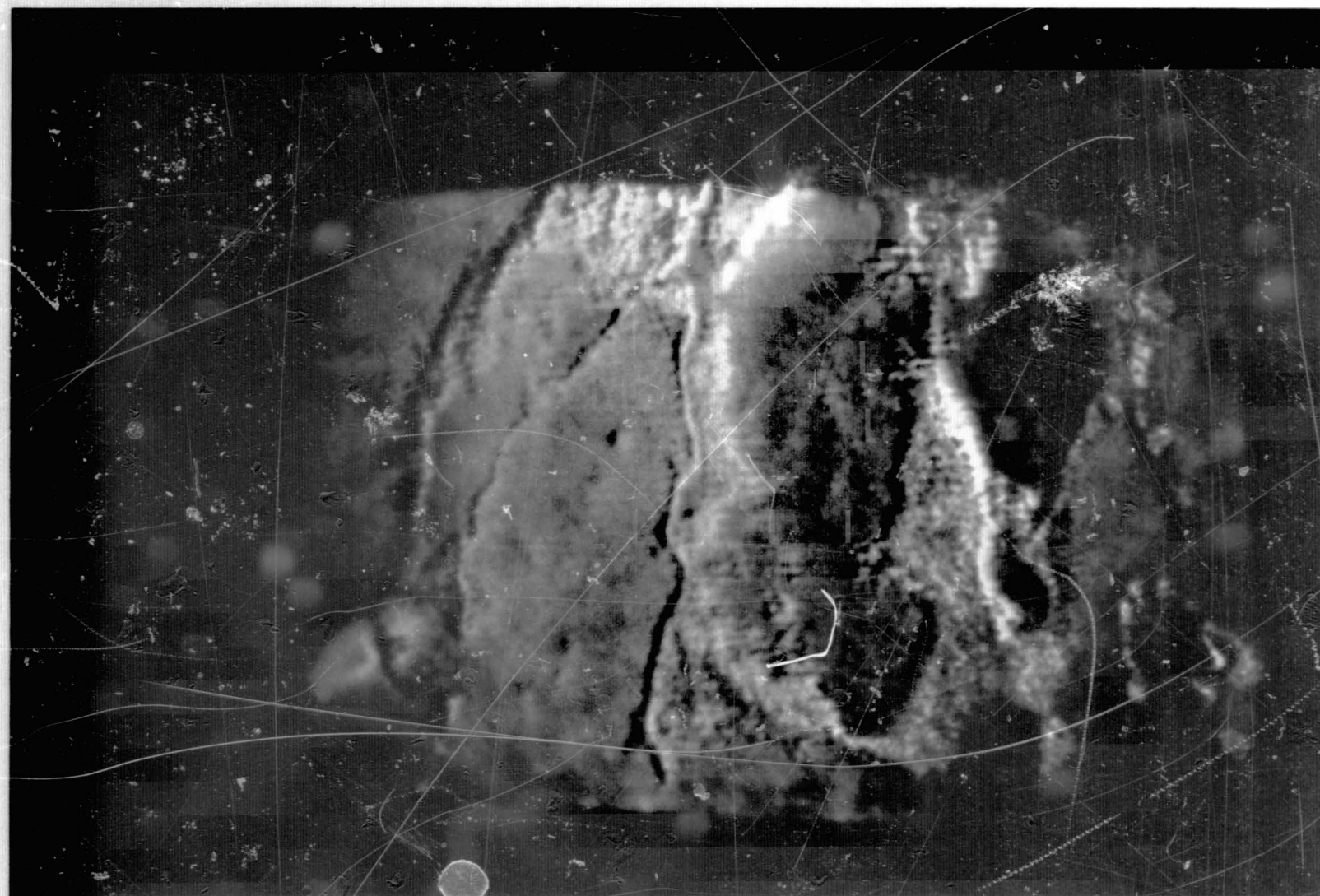


Figure 50-17.- False-color IDECS-enhanced image of Bucks Lake Test Site. Original data multi-spectral photographs from NASA aircraft 926 overflight.

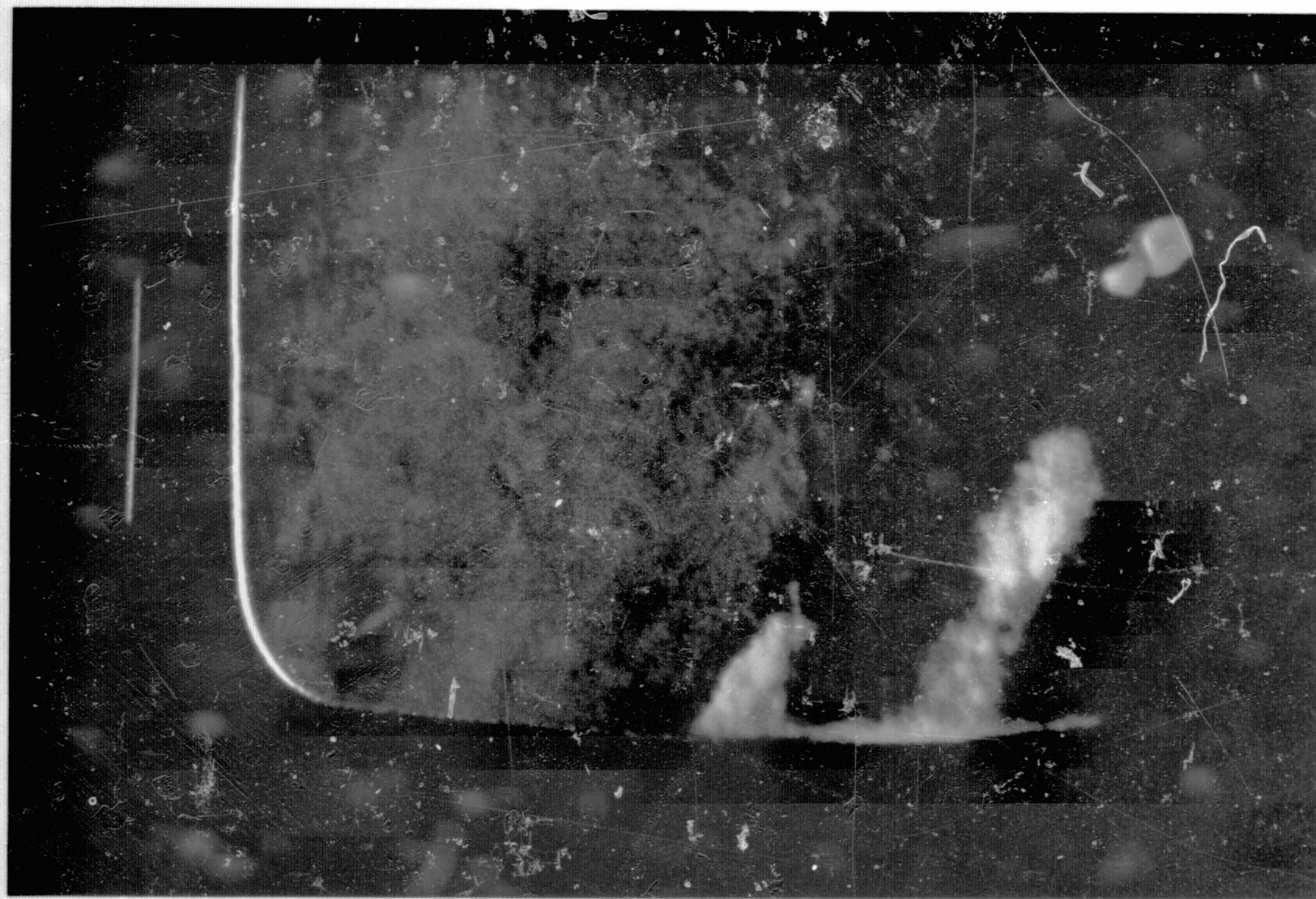


Figure 50-18.- False-color IDECS-enhanced image of Bucks Lake Test Site. Original data multi-spectral photographs from NASA aircraft 926 overflight.

50-41

		Number of Measurements Identified as:			
		(a) bare ground pasture	(b) grain sorghum, bare ground-wht., alfalfa wheat stubble-weeds	(c) corn	(d) sugar beets
Surface Cover Actually Measured:	(a) bare ground pasture	22 (91% cor. id.)	2	0	0
	(b) grain sorghum, wheat stubble- weeds, alfalfa, bare ground- wheat	5	73 (91% cor. id.)	2	0
	(c) corn	0	0	2 (67% cor. id.)	1
	(d) sugar beets	0	0	1	5 (83% cor. id.)

Figure 50-19.- Identification accuracy for August-September 1965 radar imagery. A random sample of 113 measurements of field averages from a total set of 226 were used to train a Bayes' decision classifier, and the other 113 measurements of field averages were classified on the basis of the Bayes' decision rule. Ninety percent of the types of surface cover, grouped as shown, were correctly identified. Each field had the indicated type of surface cover for both the months of August and September, the exception being bare ground/wheat, which was bare ground in August and wheat in September. (The 91-percent-correct identification in groups a and b means that 91 of the measurements in each of these groups were actually identified as being in that group. In general, the individual types of surface cover within each group were completely confused with one another.)

		Number of Measurements Identified as:		
		(a) bare ground	(b) corn, alfalfa, grain sorghum, weeds, pasture, wheat stub.	(c) sugar beets
Surface Cover Actually Measured:	(a) bare ground	14 (52% cor. id.)	13	0
	(b) corn, alfalfa, grain sorghum, weeds, pasture, wheat stubble	11	75 (85% cor. id.)	2
	(c) sugar beets	0	1	6 (86% cor. id.)

Figure 50-20.- Identification accuracy for July 1966 radar imagery. A random sample of 129 measurements of field averages from a total set of 251 were used to train a Bayes decision classifier, and the other 122 measurements of field averages were classified on the basis of the Bayes decision rule. Of the types of surface cover shown, 78 percent were correctly identified in the groupings. (The 85-percent-correct identification means that 85 percent of the measurements in group b were actually identified as being in group b. In general, the individual types of surface cover in group b were completely confused with one another.)

NUMBER OF MEASUREMENTS IDENTIFIED AS:

Surface Cover Actually Measured	Alluvial Material	Porphyritic Olivine Basalt Flows of the Second and Final Eruptive Phases	Microporphysitic Olivine Basalt Flows of the First Eruptive Phase	Playa Lake Sediment
	20	0	0	1
	15	67	3	3
	0	0	7	0
	2	0	0	16

Figure 50-21.- Identification accuracy for Pisgah Crater scatterometer data. A random sample of 134 measurements from a total set of 268 was used to train a Bayes' decision classifier, and the other 134 measurements were classified on the basis of the Bayes' decision rule. Eighty-two percent of the measurements were identified correctly.

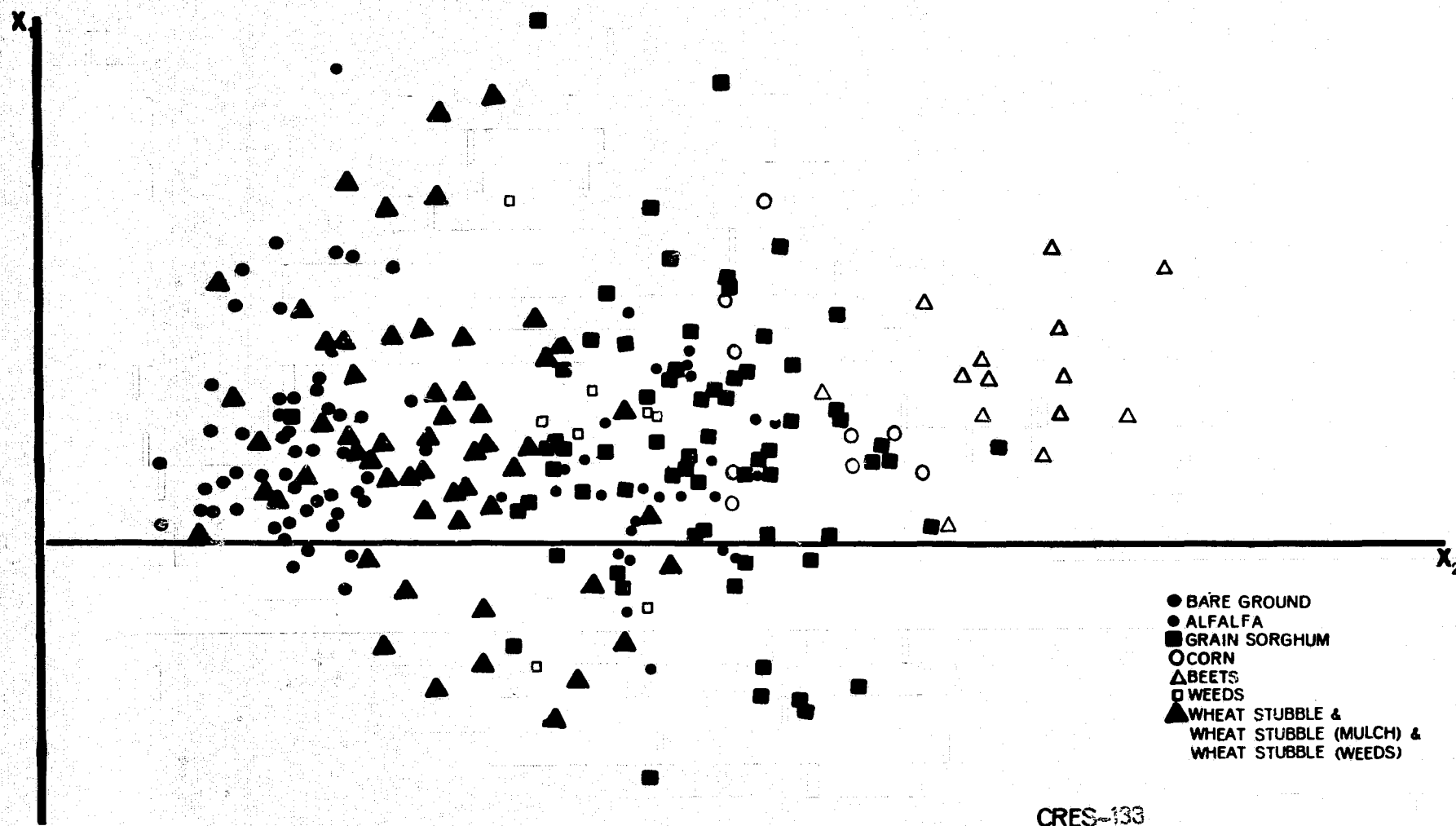


Figure 50-22.- Scattergram of July 1966 Garden City radar image data projected on its first two principal axes.

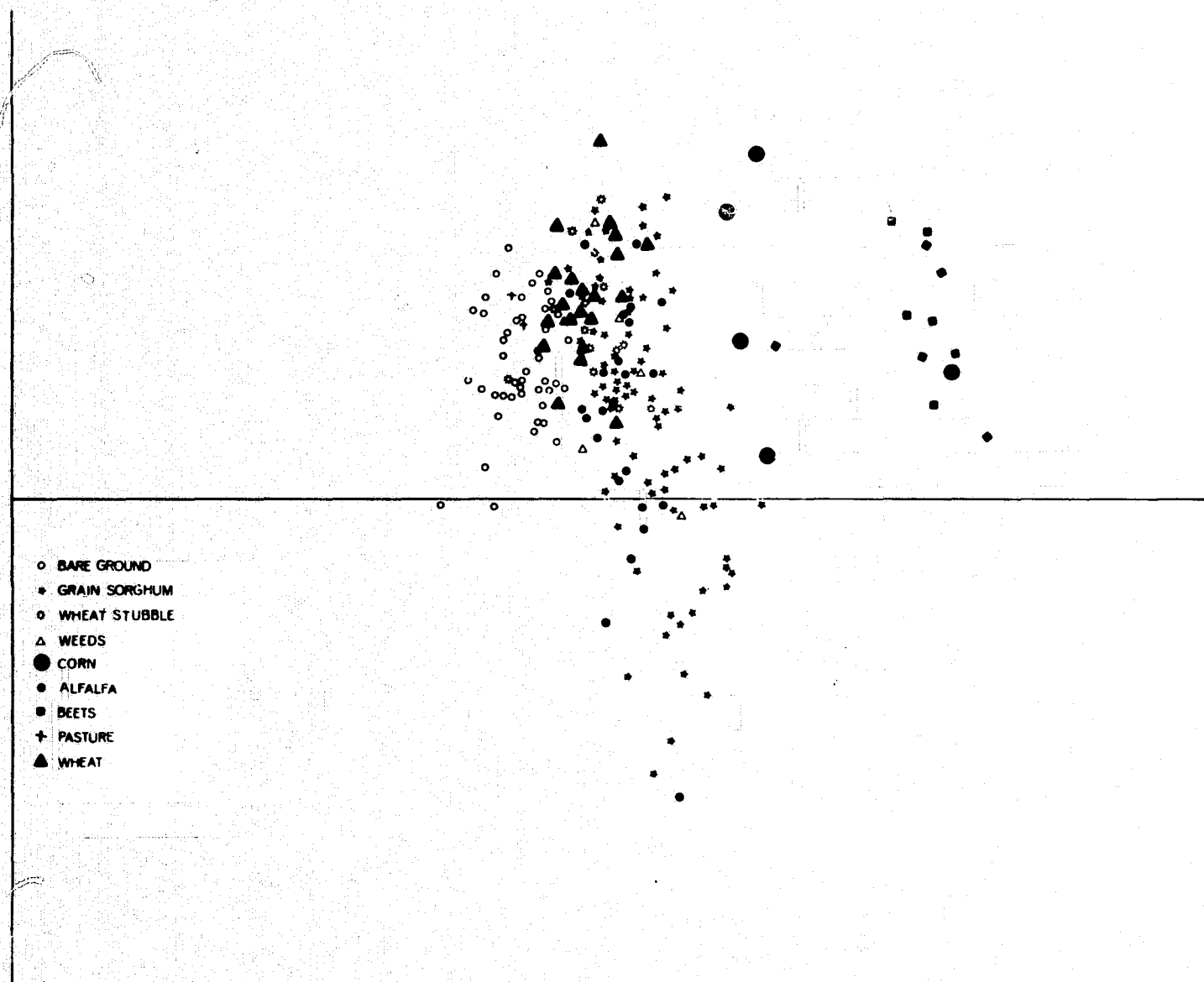


Figure 50-23.- Scattergram of August 1965 to September 1965 Garden City radar image data projected on its first two principal axes.

[illegible]

Figure 50-25.- Image 2 of made-up data.

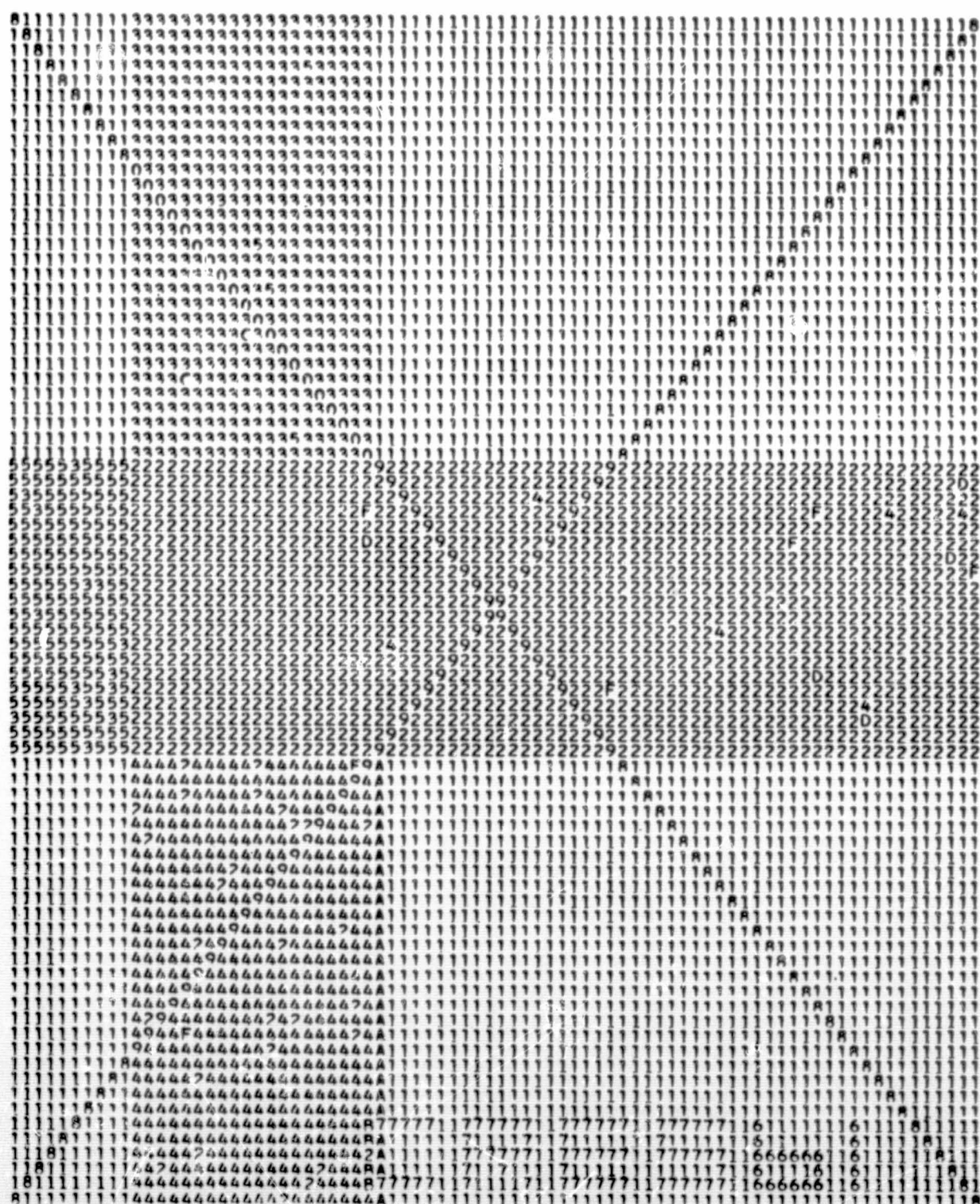


Figure 50-28.- Classified image of made-up data using measurement space clustering.

N71-16165

INFRARED STUDIES

By D. S. Lowe
University of Michigan

The NASA Remote Sensing Aircraft Program uses infrared (IR) scanners for thermal mapping and multispectral sensing. This paper discusses a few aspects of what can or cannot be done with the current scanner instrumentation.

Optical-mechanical scanning is a well-established technique despite the many engineering problems that seem to plague scanners. Some examples of optical-imaging scanners are early television systems, aerial reconnaissance scanners, the Nimbus scanning radiometers, and more recently, the Soumi spin-scan camera in the ATS satellite. Compared with cameras of comparable resolution, the scanner, though simple, is relatively complex. Why then, use scanners? The following are some of the advantages:

1. The scanners can operate in any region of the optical spectrum.
2. The electrical signal can be readily transmitted, recorded, analyzed, or processed as needed or desired.
3. The detectors generally have a very large dynamic range, and the detection process is reversible. (That is, unlike photographic film the detectors are reusable.)
4. The sensor is amenable to calibration and can yield quantitative data.
5. Collection of data simultaneously in many wavelength channels is possible.

To be detected, an object must be contrasted with its background. To identify, one needs additional information which is gleaned from such parameters as shape, tone, texture, environment, and knowledge of the subject matter. We have seen a number of examples of investigators searching for the optimum wavelength of best contrast. About 6 years ago, researchers at Michigan recognized that conventional black and white images are limiting in their ability to contrast an object in a large variety of backgrounds. In large-area search, it is apparent that

some means of object-to-background contrast enhancement would be desirable for quick detection. Since spectral information is lost in systems that record broadband reflectance or emittance, the question was asked whether or not a sensor could be developed which would use the spectral information in a scene so that the resulting image contrast takes advantage of this spectral information. For example, perhaps the tone in the resulting image may represent how well the spectrum of a scene point correlates with one known to exist for the object being sought. If contrast is enhanced to the point that all backgrounds are suppressed, one then has spectral recognition of the object. The multispectral sensor described in the following discussion was designed to investigate the feasibility of developing such a sensor.

In an IR scanner the detector is used as the field stop, and a filter is placed in the radiation path to limit the wavelength of operation. Instead of throwing away this unwanted radiation, the entrance slit of a multichannel spectrometer can be used as the field stop (fig. 51-1). In such a system, each detector of the spectrometer observes the same resolution element of the scene, but in a different wavelength region.

The airborne multispectral instrumentation at Michigan obtains data in 18 bands simultaneously in the wavelength interval of 0.32μ to 13.5μ . Four scanners are used to obtain this coverage. Twelve channels are collected with a multichannel spectrometer so that the signals are registered and can be mixed or processed electrically. Two of the scanners are fitted with filtered three-element arrays of InSb and InAs detectors. The detectors are aligned to scan a scene point sequentially, and the video signal can be brought into registration through time-delay lines. Other spectral bands are obtained with a filtered ultraviolet (UV) photomultiplier and/or filtered single-element InSb and Ge:Hg detectors.

The output signal from each detector element is a video signal corresponding to the scene brightness in the particular wavelength region of operation. The tape-recorded multichannel video signals can be displayed and analyzed in a number of ways to obtain information about the spectral characteristics of signatures necessary for designing an optimum signal processor for an operational spectrum-matching sensor.

Figure 51-2 shows typical A-scope traces from two channels of data. In this format, the detector signal deflects the oscilloscope beam in the y-direction, while the scan position within a line is the x-direction. This format is not too unlike a microdensitometer trace over a photograph. In the two traces of figure 51-2, at the left the detector is looking inside the dark scanner. As the detector moves to the right, it scans the scene below the aircraft and then back inside the scanner and two calibration sources.

Another useful way to examine the data is shown in figure 51-3. This figure shows two examples where the video signals from two channels are used to deflect the beam of an oscilloscope in the x- and y-directions. Since the deflection in the x-direction is determined by the signal from one wavelength channel (color) and the signal in the y-direction from another channel, this x-y plot can be considered to represent a two-dimensional color space. As the tape-recorded data are played back, the position of the oscilloscope beam is determined by the brightness of the resolution element in the two bands used to deflect the beam. Inspection of data played back in this manner allows one to make judgments of the color variations in the scene.

The video signals from the multiple detectors can be sampled to determine the spectral distribution of the radiation from scene elements. Figure 51-4 shows a sampled raw spectrum of a calibration panel as observed by the 12-channel scanner, and figure 51-5 shows the reduced spectrum of the panel. The solid curve is the spectrum as measured in the laboratory. This measurement is what is called hemispherical reflectance. In the field, hemispherical reflectance is not observed, since direct solar illuminance, plus down-welling radiation from the clouds and sky, are available. The circles represent the spectrum value measured by a spectrometer on the ground under natural illumination during the overflight of the aircraft. The x's are the reflectance values observed with the airborne scanner as it flew over, taking approximately 20 000 spectra/sec. These spectra do not have to be reduced manually. Rather, the data can be digitized and analyzed by a digital computer.

To determine the effect of observation and illumination angles on the spectral signature of crops, the aircraft is flown low over large fields so that they subtend a large angle beneath the aircraft. Figure 51-6 shows a computer print-out of the manner in which the radiance of a wheat field varies with scan angle in four wavelength channels. Each scan line represents the mean value of as many as 100 scan lines. It can be noted that there is correlation among channels (i.e., all the signals increasing with angle). The cause of this effect is illustrated in figure 51-7, in which the aircraft heading with respect to the sun is changed. When the scan plane is parallel to the sun, the scanner observes the field under highlighted and backlighted conditions. Under this condition, the signal varies strongly with angle. When the scanner scans perpendicular to the plane of illumination, the signal is relatively constant with scan angle.

While the variation in reflectance with angle at first appears too formidable to correct, it is interesting to see how the spectral information varies with angle. Figure 51-8 plots the signal from a wheat field in color space using the signals from channels 5 and 10 of the multispectral scanner. It is noted that there is a strong correlation

in variation of the signals from these two channels as the angle of observation changes. With the knowledge of the spectral characteristics of objects and their background it is possible to develop optimum decision rules for making the spectral discriminations as shown by Hoffer, Landgrebe, and Holter.

The current multispectral scanner has the serious shortcoming that it operates in a narrow interval of the optical spectrum. In 1966, the University of Michigan performed a design study for NASA and came up with the specifications of an instrument given in table 51-I. This scanner would cover the spectral interval of 0.32μ to 13.5μ in as many as 29 bands with perfect time and space registration.

TABLE 51-I.- SCANNER-SPECTROGRAPH SPECIFICATIONS

Velocity/height (VH), radians/sec ⁻¹	0.1
Angular resolution β , radians	0.003
Collector aperture, cm	15 (6 in.)
Scan mirror rate, rpm	2000
Amplifier bandwidths, kcps	35
Spectral resolving power, $\lambda/\delta\lambda$, at 0.6μ and 10μ	20
Performance, (1) NE $\Delta\rho$, percent for direct solar illumination and $\lambda < 2\mu$	<1

Turning now to IR imagery, I would like to make two comments regarding tonal distortions. Many of the earth resource applications require a scanner to determine surface temperature on a quantitative or semi-quantitative basis. For ease of signal handling and recording, the electronics of scanners developed by the military are ac coupled. As a result, the average signal level at the output of the electronics is zero, and the instantaneous signal is known only as to its value with respect to this average. In such a system, the tone of an object in an image is dependent upon other objects that lie within the scan lines which determine the average signal level. Consider a scanner flying parallel to a land/water interface. Assume that the land is warmer than the water and that two passes are flown, one directly over the shoreline and the other off shore. The resulting video signals from ac-coupled

electronics are hypothesized in figure 51-9, along with the average signal level. As shown in figure 51-9, the signal difference B between land and water is independent of the flight line, while the magnitude of the voltage representing land A is smaller when the scanner is flown over the shoreline than when it is flown over the water. Thus, when the scanner is flown off shore, both the land and the water appear warmer in the imagery than when the scanner is flown directly over the shoreline. The difference in signal between land and water, however, is the same. By similar synthesis of video signals over terrain, it can be shown that the tone of any object in the imagery is affected by the signal from other objects within its environment. Figure 51-10 shows imagery generated with an ac-coupled scanner without dc restoration. It should be noted that thermal patterns are clearly evident, but that some of the tonal variations (vertical striations) are an artifact of the instrument arising from ac coupling.

This problem of nonquantitative tones in ac-coupled imaging systems can be readily corrected by a technique known as dc restoration. This technique requires that the video signal contain a repetitive signal of constant level from a source whose position in the video is known. One such signal may be the inside of the scanner housing, provided it can be made constant throughout the data-collection mission. Since the relative magnitudes of the signals are preserved in an ac-coupled system, if the tone of the source known to be constant is maintained constant, the tones of all other objects are quantitative, provided the amplification gain is constant and the sensor is calibrated. The circuitry for dc restoration is well known and is used in television systems. The circuitry requires electronically sampling the output level of the known and constant signal and adding or subtracting a dc voltage to make the signal constant.

While dc restoration, or clamping, makes the tone of an object independent of its environment, the tone is quantitative if, and only if, the system response (volts out/watts in) is constant and known. If the response is constant, which implies fixed detector response and amplifier gains, then the response can be computed from the observation of two or more sources of known radiance ($\text{watts/cm}^2 \text{ster}$). If the response is linear, two sources will suffice. Because the detector response is temperature dependent, frequent calibration is desirable, which leads to a scanner that carries its own reference and calibration sources. Even with these calibrations, one can only be quantitative with respect to the apparent radiance, the true surface radiance as modified by atmospheric absorption and emission. By observing sources on the ground of known radiance, the atmospheric effects can be determined. Surface temperature is then related to the radiance through emissivity and the Planck radiation law for blackbodies. The NASA MSC is concerned about the lack of dc restoration in its scanners, and plans are underway to

correct this deficiency in scanners aboard their aircraft. The dual-channel scanner under procurement will have calibration sources, as well as dc restoration.

Another source of tonal distortions in IR imagery is from the limited dynamic range of the display and/or recording medium. The output signal from the detector is generally linear with respect to the radiation input over the levels encountered in the thermal mapping of natural features. When one is interested in observing thermal details of a particular feature, the gain setting for photographic recording is usually adjusted to give optimum contrast of the feature being investigated. As an example, figure 51-11 is a stripmap which NASA generated over test site 162. The mission was to map the thermal patterns in Lake Michigan. With the gain setting properly adjusted to observe this feature the thermal features on the land were "washed out." Thus, it is highly important that the investigator inform the operator as to the purpose of his data so that the proper gain setting be made. Had the operator adjusted the gain in figure 51-10 to avoid saturation of the land feature, the fine thermal detail in the water would be lost. Solutions exist for overcoming the limited dynamic range of the recording medium such as parallel recording of the data at different gain levels and automatic gain control. The University of Michigan is currently studying this problem with particular emphasis on space applications for which telemetry and recording bandwidths are a premium. Preferred methods for recording the full dynamic range of the scanner signal will be recommended.

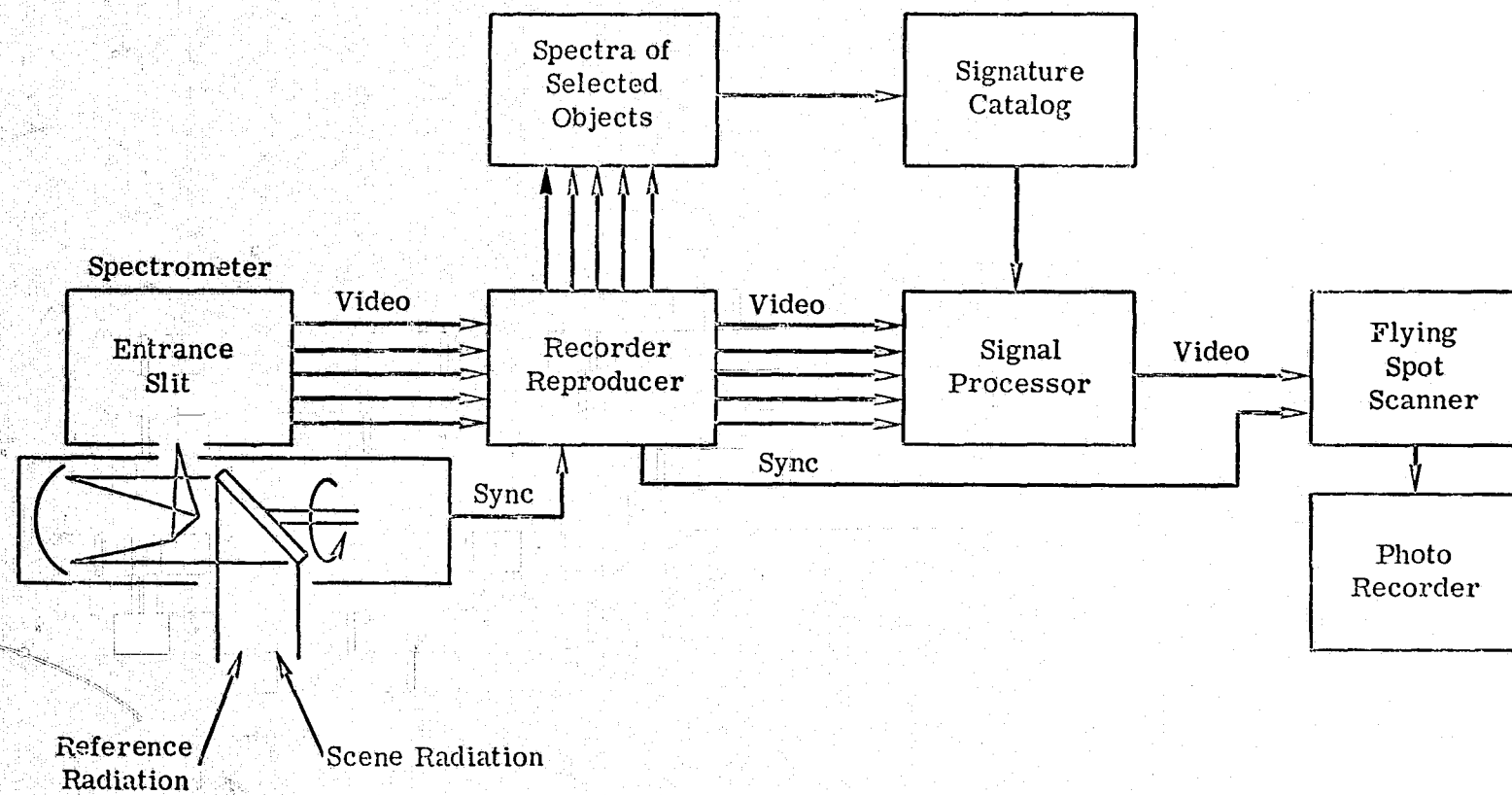


Figure 51-1.- Schematic of multispectral scanner and data processor.

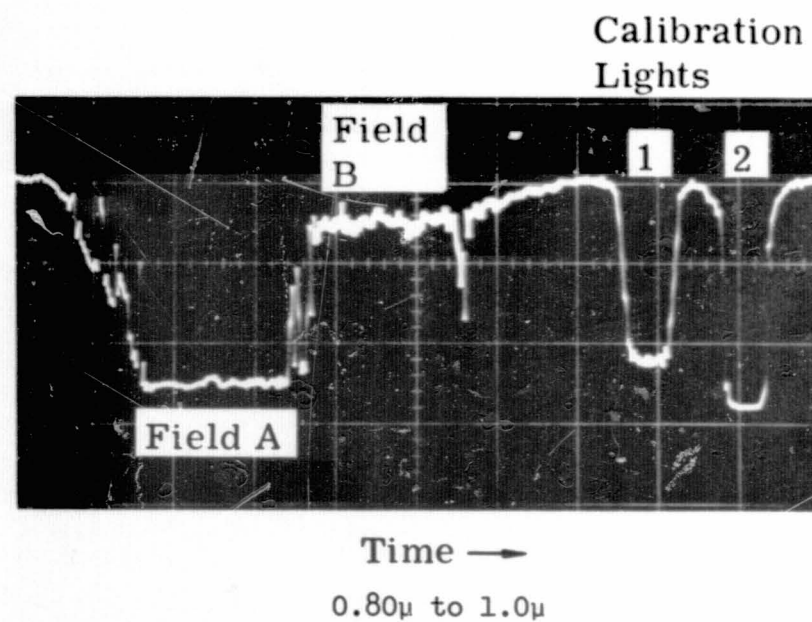
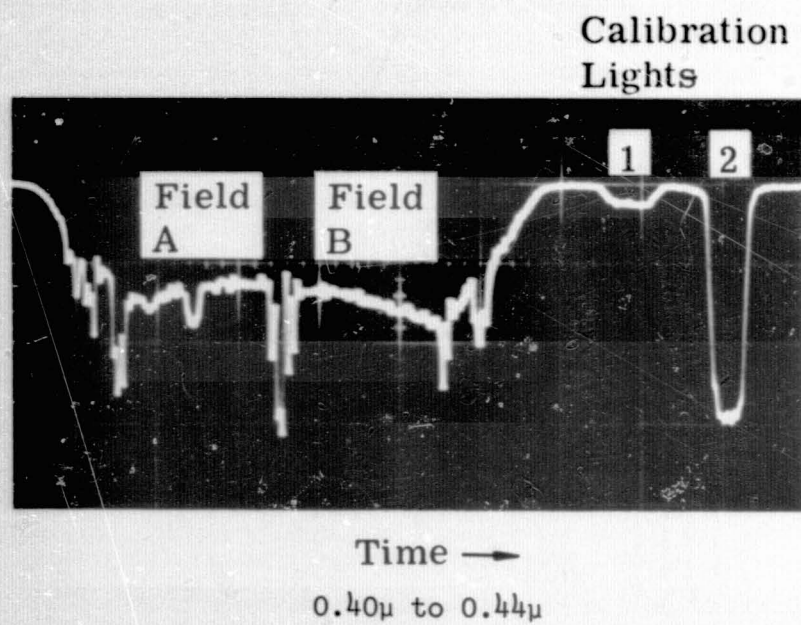


Figure 51-2.- Typical spectrometer video data (U). California Rice Fields 5/26/66 at 1400 hours.

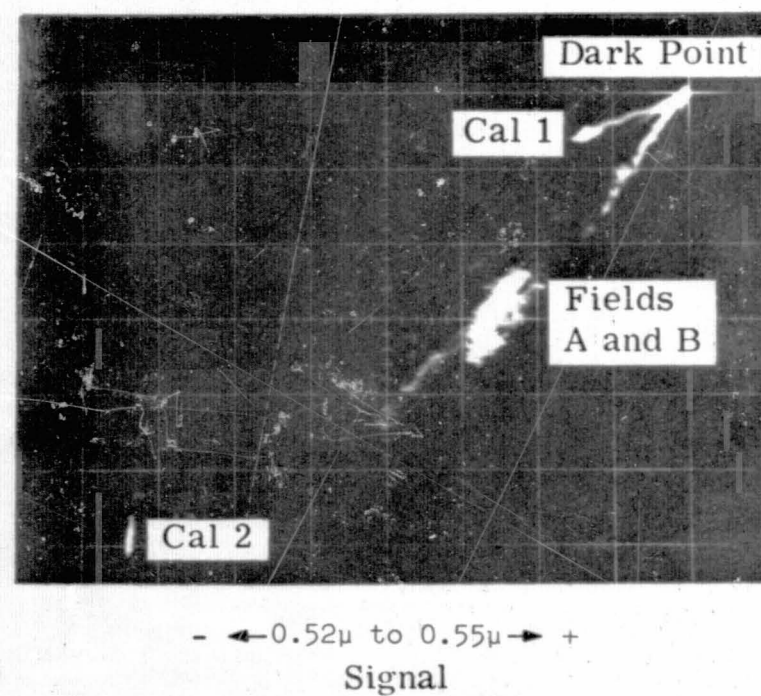
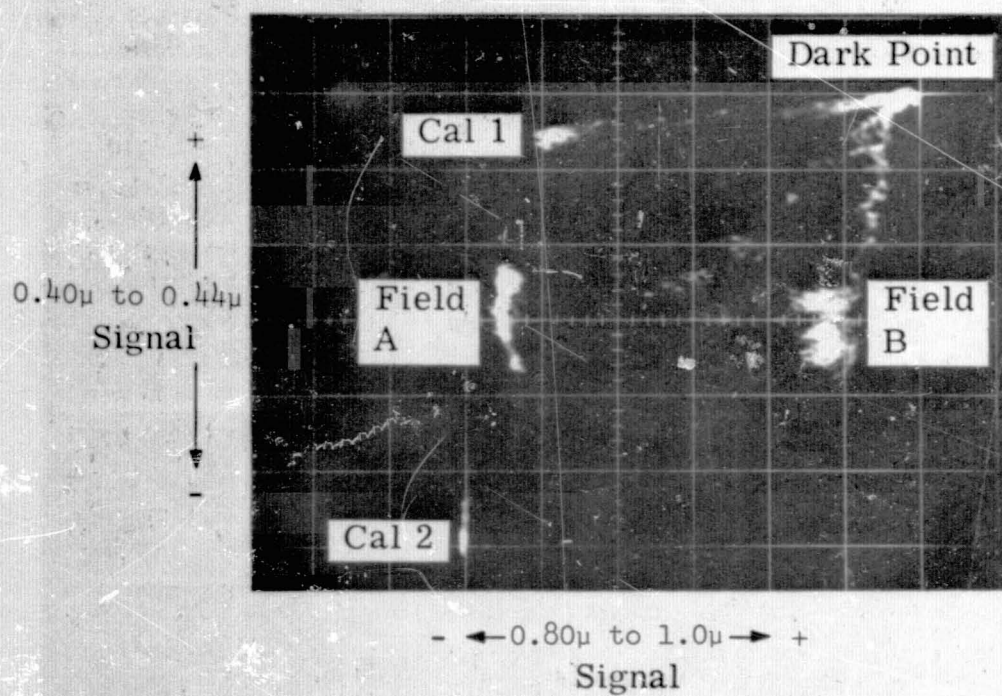


Figure 51-3.- Typical x-y scope pictures (U). California Rice Fields 5/26/66 at 1400 hours.

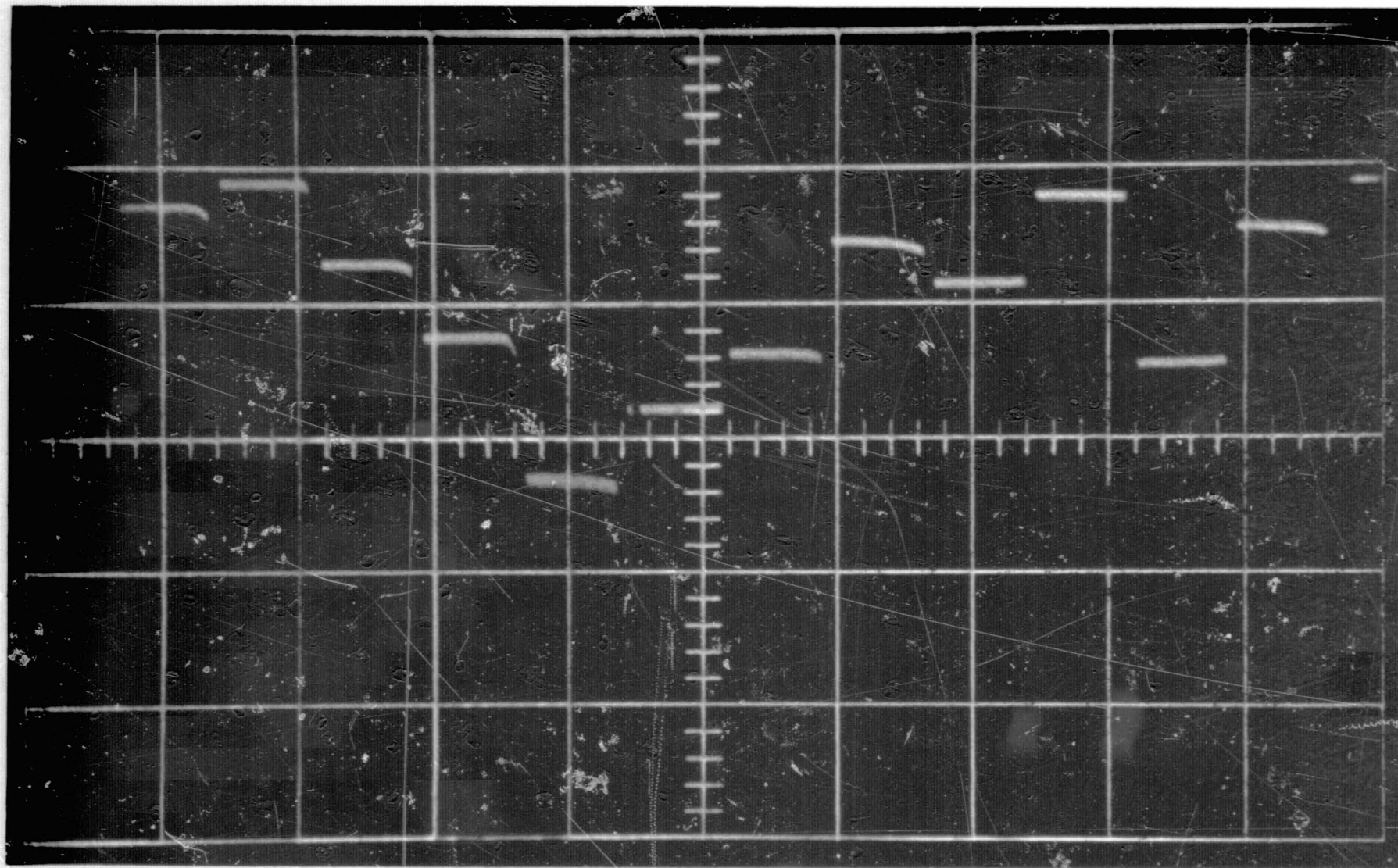


Figure 51-4.- Raw spectrum of green paint.

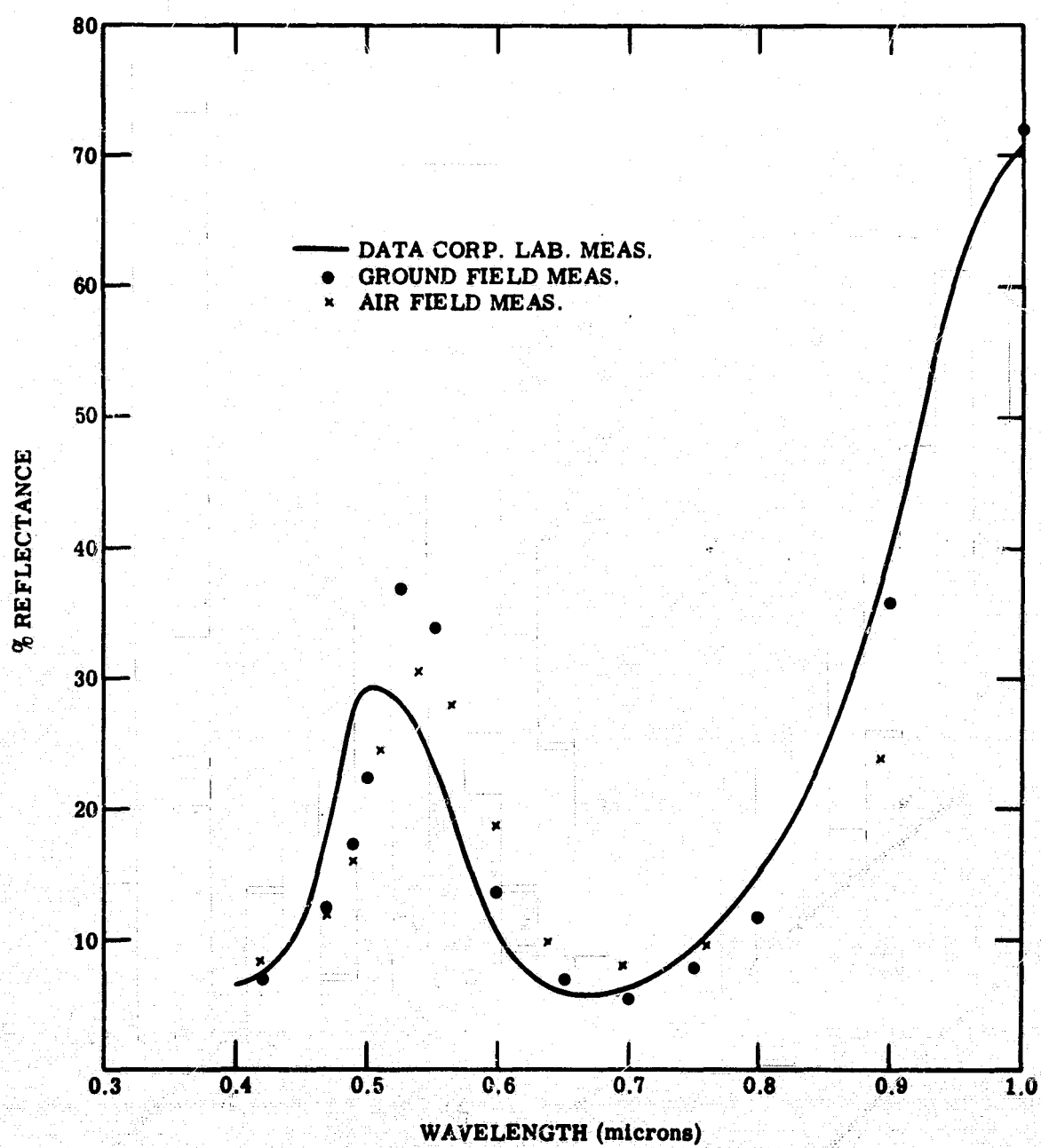


Figure 51-5.- Light-green standard reflectance panel.

51-12

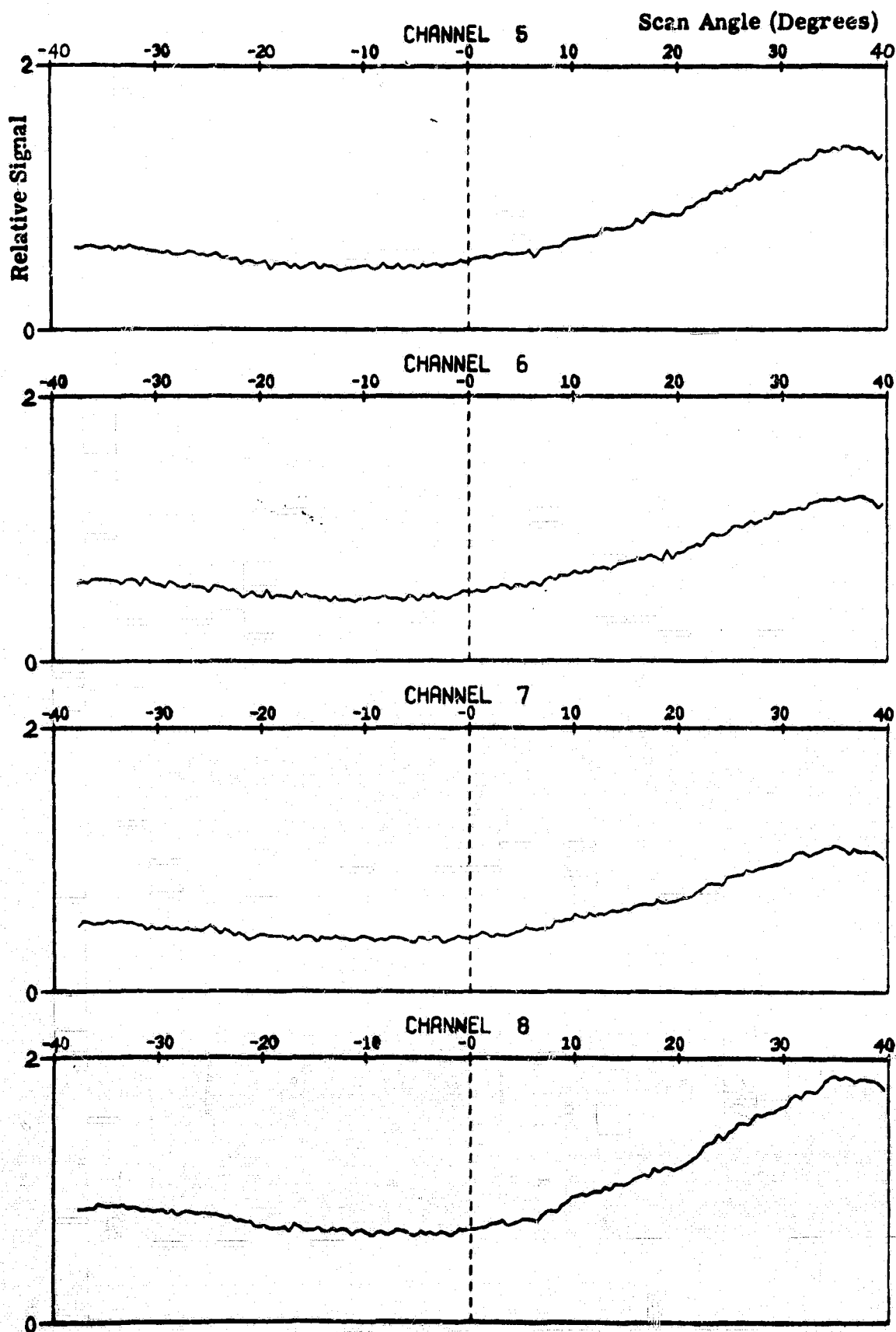


Figure 51-6.- Illustrative plots of relative signal versus scan angle for wheat field; data acquired June 30, 1966, 09:06 hours.

ILLUSTRATION OF EFFECTS OF SCAN ANGLE AND SCAN DIRECTION

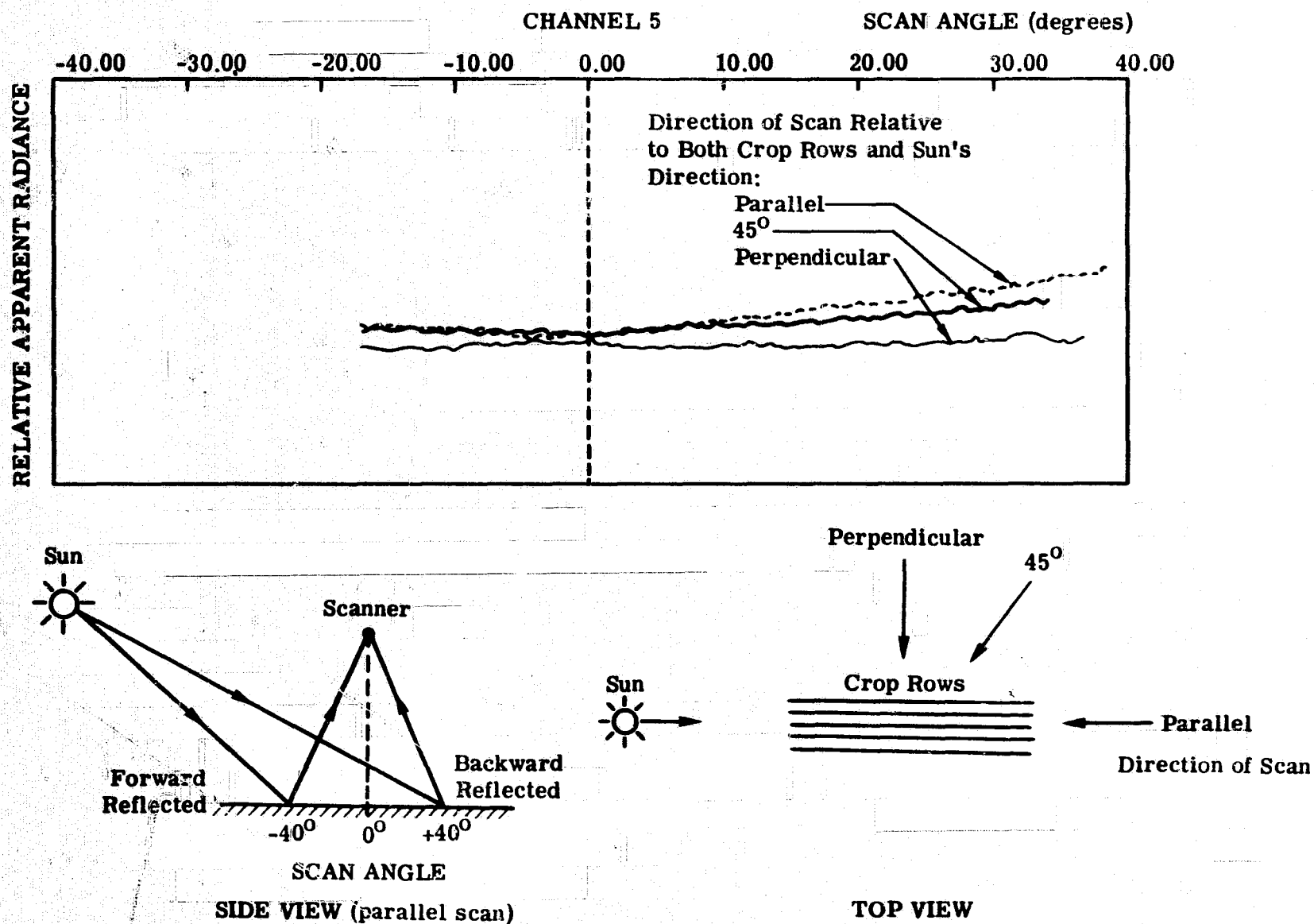


Figure 51-7.- Signal variation as a function of scan angle and direction.

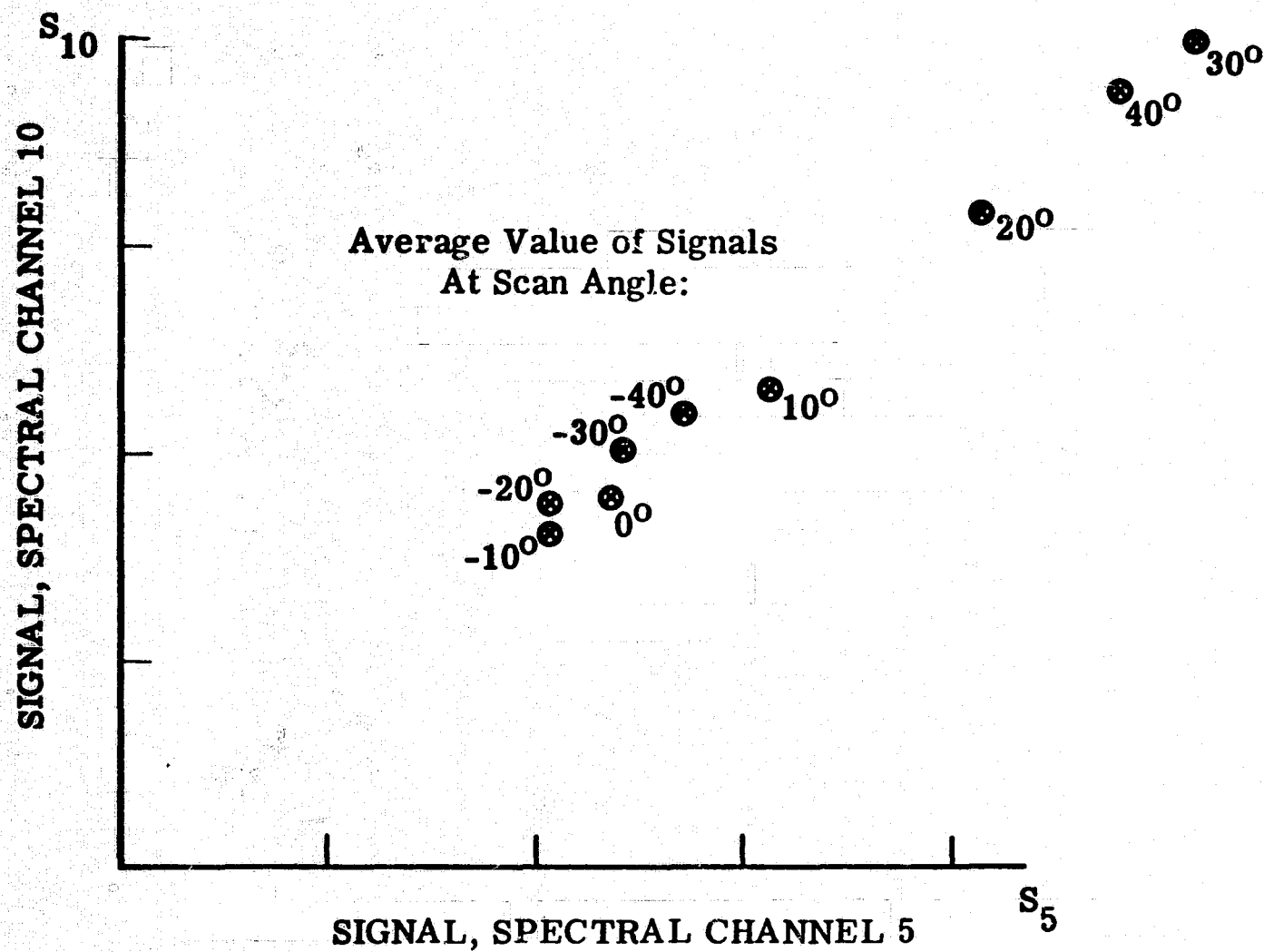


Figure 51-8.- Distribution of wheat-field signals data taken June 30, 1966,
09:06 hours.

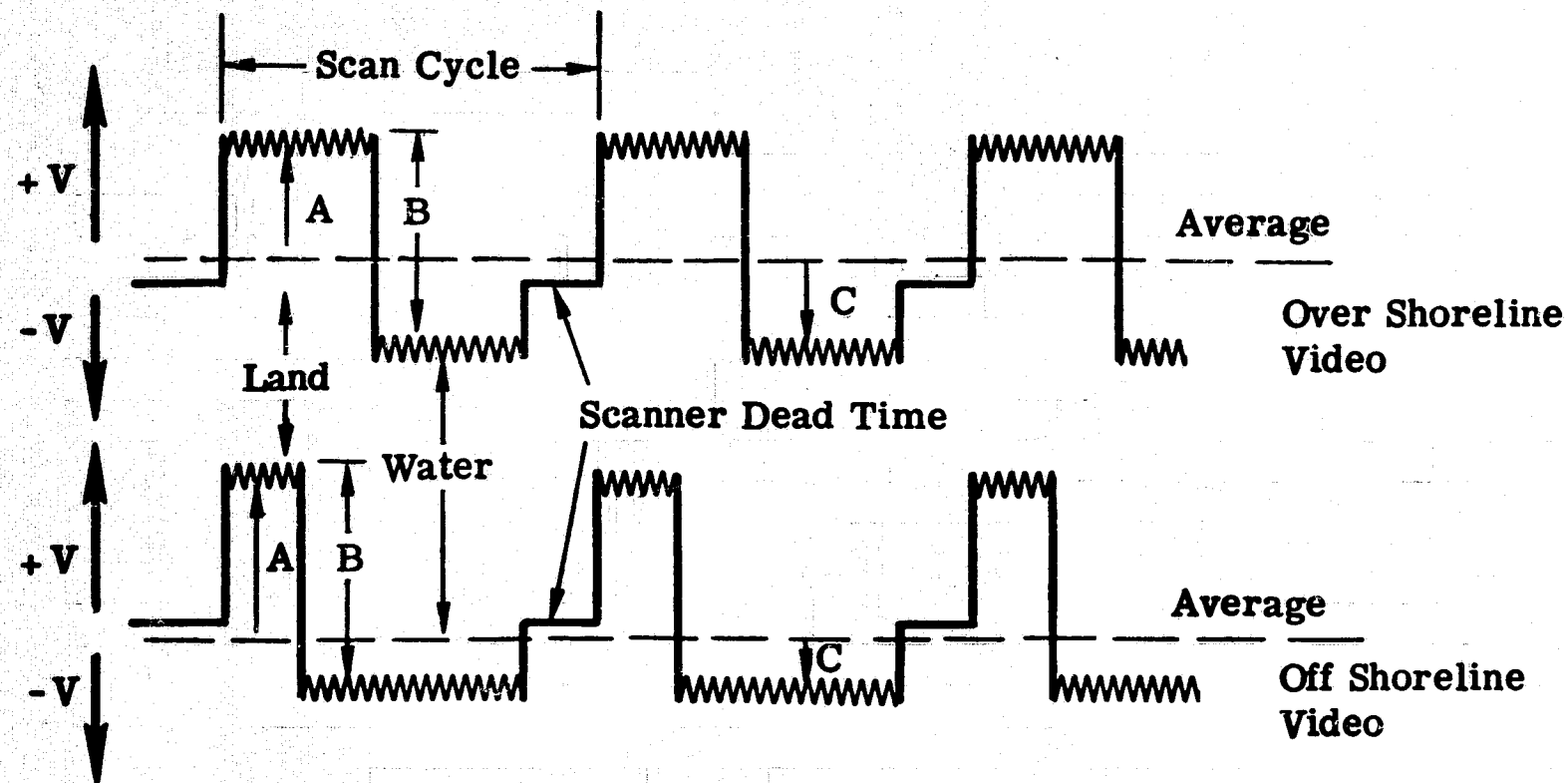


Figure 51-9.- Typical signal relationships of dwell time on land to water changes.

51-16

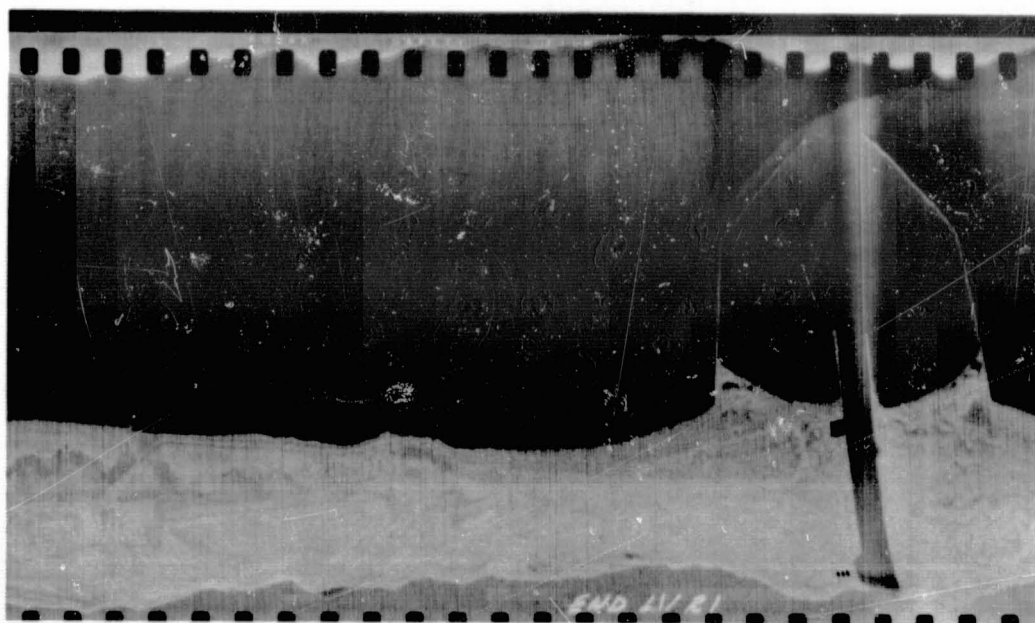


Figure 51-10.- Tonal variations arising from ac coupling.

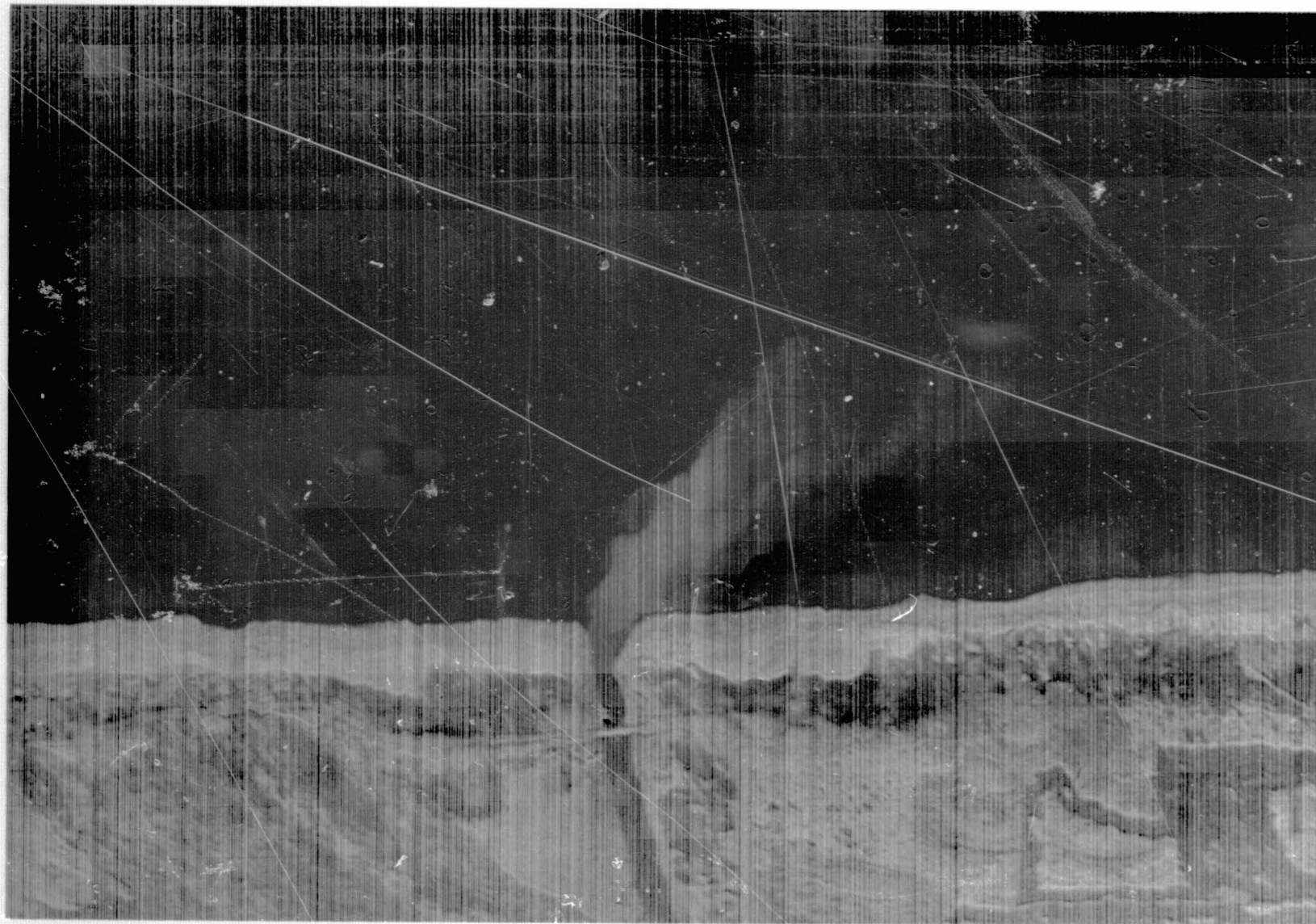


Figure 51-11.- Thermal stripmap with gain set to observe thermal patterns in water.